5-2018

Carbon Dots: Synthesis, Characterization, and Investigation of Optical Properties

Gregory LeCroy
Clemson University, glecroy@g.clemson.edu

Recommended Citation

LeCroy, Gregory, "Carbon Dots: Synthesis, Characterization, and Investigation of Optical Properties" (2018). *All Dissertations*. 2129.
https://tigerprints.clemson.edu/all_dissertations/2129

CARBON DOTS: SYNTHESIS, CHARACTERIZATION, AND INVESTIGATION OF OPTICAL PROPERTIES.

A Dissertation
Presented to
the Graduate School of
Clemson University

In Partial Fulfillment
of the Requirements for the Degree
Doctor of Philosophy
Chemistry

---

by
Gregory Ethan LeCroy
May 2018

Accepted by:
Prof. Ya-Ping Sun, Committee Chair
Prof. Rhett Smith, Co-Chair
Prof. Brian Dominy, Co-Chair
Prof. Leah Casabianca, Co-Chair

ABSTRACT

Recently, carbon nanoparticles have emerged to represent a new class of zero-dimensional carbon nanostructures in contrast to the more beautiful and defined C60-fullerenes. Despite their undefined and seemingly uninspiring properties, surface passivation or functionalization reveals high performance optical properties intrinsic to the carbon nanoparticles, resulting in "core-shell" nanostructures dubbed carbon dots (CDots). Generally defined as small carbon nanoparticles with various surface passivation schemes (i.e. organic or biological molecules), CDots display bright and colorful fluorescence emissions in addition to high performance photoinduced redox, and other properties, rivaling those of the more traditional semiconductor quantum dots (QDs) while retaining the biologically and environmentally benign characteristics of carbon.

In this dissertation, CDots were synthesized through the surface functionalization of carbon nanoparticles with 2,2'-(ethylenedioxy)-bis(ethylamine) (EDA), forming a highly stable aqueous suspension of EDA-CDots. The resulting dispersion could be considered "solution-like", allowing for the analysis and characterization of these CDots with solution phase spectroscopy techniques, and were shown to be highly fluorescent and structurally compact, with the brightest fluorescence emissions occurring over the spectral region covered by popular fluorescent proteins, such as green fluorescent proteins (GFPs).

In terms of photoexcited state properties, photoinduced redox interactions of these CDots with of nitrotoluenes were probed through fluorescence quenching using steady-

state and time-resolved fluorescence spectroscopy techniques. The emission properties of EDA-CDots were efficiently quenched by nitrotoluenes, which, mechanistically, result from highly efficient diffusion-controlled electron-transfer interactions at low quencher concentrations.

Excitation wavelength dependent emission properties of CDots were systematically studied in steady-state and time-resolved fluorescence regimes. CDots were shown to exhibit characteristic emission properties with strong excitation wavelength dependence for fluorescence quantum yields, while the fluorescence lifetimes only exhibited weak excitation wavelength dependencies. In order to better understand CDots fluorescence emissions and a photoexcited state deactivation mechanisms, a model consisting of two sequential processes leading to fluorescence emissions has been constructed, in which one process is primarily responsible for the observed excitation wavelength dependent emissions.

In an effort to specifically tailor the optical properties of carbon dots, core modified CDots have recently been reported, such that red sensitive chromophores, such as Nile blue (NB), are incorporated into the core carbon structure of polyethylene glycol functionalized CDots. The resulting nanostructure exhibits enhanced optical properties beyond what should be expected for the combination of these two species. The modified core structure displays an electronically integrated photoexcited state with excellent optical properties, such as effective visible and near-IR photon-harvesting, corresponding bright fluorescent emissions, and efficient photoninduced electron transfer (PET) serving as both excellent electron donors and acceptors.

DEDICATION

To my parents and my wife, for their love and unwavering support.

ACKNOWLEDGMENTS

First and foremost, I would like to offer my sincere gratitude to my advisor, Prof. Ya-Ping Sun, for giving me a chance and the opportunity to pursue a graduate education under his direction. His unique creativity, breadth of knowledge, and unrelenting determination has been an inspiration in my development as a research scientist. I will forever be indebted for his time, guidance, and patience.

I would like to acknowledge the Air Force Research Laboratory (AFRL) Propulsion Directorate and the University of Dayton Research Institute (UDRI) for allowing me to use their facilities and instruments. A special thanks to Dr. Chris E. Bunker for his mentorship and guidance as well as Dr. K. A. Shiral Fernando and Dr. Will K. Lewis for their insightful discussions of science and life. The lessons I learned while in their company will continue to guide me in my professional and personal life.

The previous and current members of the Sun Research Group deserve immense recognition for they have contributed significantly to the work presented here. Without the years of dedication and diligence necessary to lay a foundation on which this work is based, the construction of this dissertation would not have been possible. A special thanks to Dr. Li Cao, Dr. Jaouad Meziani, Dr. Sumit Sonkar, Dr. Sushant Sahu, Dr. Ankoma Anderson, Ken Tackett, Ping Wang, Fan Yang, and Yamin Liu for their contributions, friendship, and support.

Finally, I would like to thank the members of my committee, Prof. Rhett Smith, Prof. Brian Dominy, and Prof. Leah Casabianca, for their valuable time as well as Clemson University and the Department of Chemistry.

TABLE OF CONTENTS

Table of Contents (Continued)

Page

Table of Contents (Continued)

LIST OF TABLES

Table Page

LIST OF FIGURES

List of Figures (Continued)

List of Figures (Continued)

Figure Page

List of Figures (Continued)

List of Figures (Continued)

Figure Page

List of Figures (Continued)

List of Figures (Continued)

Figure Page

List of Figures (Continued)

CHAPTER ONE

FUNCTIONALIZED CARBON NANOPARTICLES: SYNTHESIS AND APPLICATIONS IN OPTICAL BIOIMAGING AND ENERGY CONVERSION

1.1 Introduction

Quantum dots (QDs) were originally defined as semiconductor nanocrystals of physical dimensions smaller than the exciton Bohr radius for the quantum confinement effect. Because of the quantum confinement, there is a predictable dependence of the energy gap on the nanocrystal dimension in QDs, as manifested by the corresponding variations in optical properties.[1-3]

More specifically, the systematic changes in the beautiful fluorescence emission colors in semiconductor QDs such as CdSe of different sizes have generated much excitement in the research community, with extensive investigations on a variety of potential applications, especially as superior fluorescence probes for imaging and other biomedical applications.[4,5] In fact, the rationale for the use of QDs over organic dyes is now generally accepted in the literature.[4,5] Similarly bright and colorful fluorescence emissions have been found in other nanomaterials containing no conventional semiconductors, and those fluorescent nanomaterials are often referred to, more phenomenologically perhaps, as QDs as well, despite in most cases the absence of any classical quantum confinement effect. Among more popular and promising recent additions to the loosely defined QD family are carbon-based QDs, including carbon dots (Figure 1.1),[6,7] graphene quantum dots,[8,9] nanodiamonds,[10,11] and "carbon nanotube quantum dots" .[12,13] For most of these QD-resembling carbon nanomaterials, surface functionalization is important or critical as in the case of carbon dots.[14] This is also phenomenologically similar to that in conventional semiconductor QDs, such as the surface capping of CdSe with ZnS for substantial performance improvements, despite the obvious mechanistic differences.

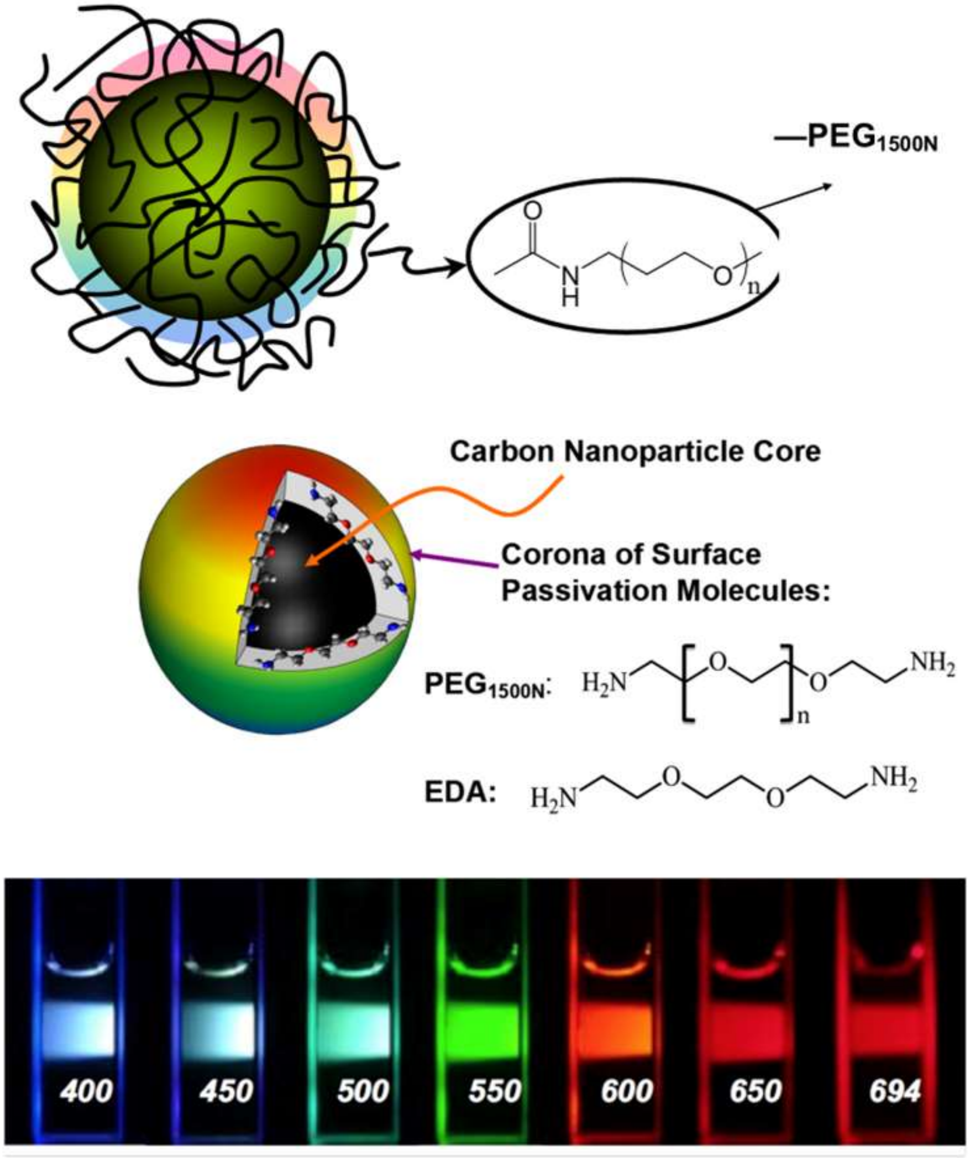

Figure 1.1 Upper and Middle: Cartoon illustrations used in the literature[22,84] on a carbon dot, generally a small carbon nanoparticle core with attached surface passivation molecules (equivalent to a soft corona). Lower: Fluorescence color variations in carbon dots corresponding to the indicated excitation wavelengths.[6]

Carbon dots, generally defined as small carbon nanoparticles with various surface passivation schemes (Figure 1.1)[6,7] have been leading the recent emergence of various carbon-based QDs, and now represent a rapidly advancing and expanding research field.[15-21] As measured by the optical properties of carbon dots, the most effective passivation scheme has been the surface functionalization of carbon nanoparticles with organic or polymeric molecules, corresponding to much brighter fluorescence emissions across the visible spectrum and extending into the near-IR.[22,23] In fact, fluorescence emissions from "naked" (no deliberate surface passivation) carbon nanoparticles in aqueous or organic suspensions have been reported in the literature, but the quantum yields are generally low to very low.[24,25] It may be argued that the surface passivation effect is provided by the solvent molecules in the suspensions.[26] The same dramatic surface passivation effect resulting in substantially enhanced optical properties has also been reported for graphene quantum dots.[27-29] Since passivation is on defects, improving defect-derived or dominated optical properties, it has been suggested that most graphene quantum dots of surface passivation for enhanced fluorescence emissions are essentially carbon dots of a more graphitic carbon core.[14] Therefore, in this article the focus will be on carbon dots that are surface-functionalized carbon nanoparticles, including their representative syntheses and demonstrated properties and their potential uses as high-performance yet nontoxic fluorescence probes for bioimaging *in vitro* and *in vivo* and also as potent photocatalysts in energy conversion applications.

1.2 Carbon Dots: Synthesis and Properties

1.2.1 Functionalization of Carbon Nanoparticles

Carbon dots (Figure 1.1, also referred to in some literature as carbon quantum dots or C-Dots) were found originally for their bright and colorful fluorescence emissions (Figure 1.2).[6,7] Therefore, the fluorescence brightness across the visible and near-IR spectral regions has been a focus of the synthesis to produce carbon dots of the desired performance.

The original synthesis of carbon dots was based on the surface functionalization of small carbon nanoparticles with organic and polymeric molecules in established chemical reactions.[6,7] Such a deliberate functionalization approach with carbon nanoparticles as precursors has yielded some of the best-performing carbon dots in terms of their fluorescence brightness or quantum yields.[22,23] For example, Wang, *et al*. functionalized small carbon nanoparticles from laser ablation production with the oligomeric PEG diamine (PEG1500N) for carbon dots of multicolor fluorescence emissions, particularly bright in the green.[22] The carbon nanoparticles were treated with nitric acid, which introduced oxidative moieties on the particle surface. The surface-bound carboxylic acid groups were targeted for the attachment of PEG1500N molecules under classical amidation reaction conditions. The as-prepared sample mixture was further processed by separation on an aqueous gel column, from which the most fluorescent fraction exhibited a quantum yield close to 60% (excitation at 440 nm and emissions centered around 520 nm, Figure 1.2).[22] The fluorescence performance of the

PEG1500N-carbon dots is competitive to that of the commercially available CdSe/ZnS QDs both in solution and at the individual dot level for the same green spectral region (Figure 1.2).[30] In another study,[31] Sun, *et al*. demonstrated that a combination of surface doping with a wide-bandgap semiconductor such as ZnS or ZnO and PEG1500N functionalization could substantially improve the fluorescence performance of the resulting carbon dots, denoted as CZnS-Dots or CZnO-Dots, respectively. Anilkumar, *et al.* applied the same aqueous gel column separation protocol to the as-prepared CZnS-Dots and CTiO2-Dots samples, and harvested the most fluorescent fractions from the separation that exhibited quantum yields in the same green spectral region (excitation at 440 nm and emissions centered around 520 nm) up to 78%.[23]

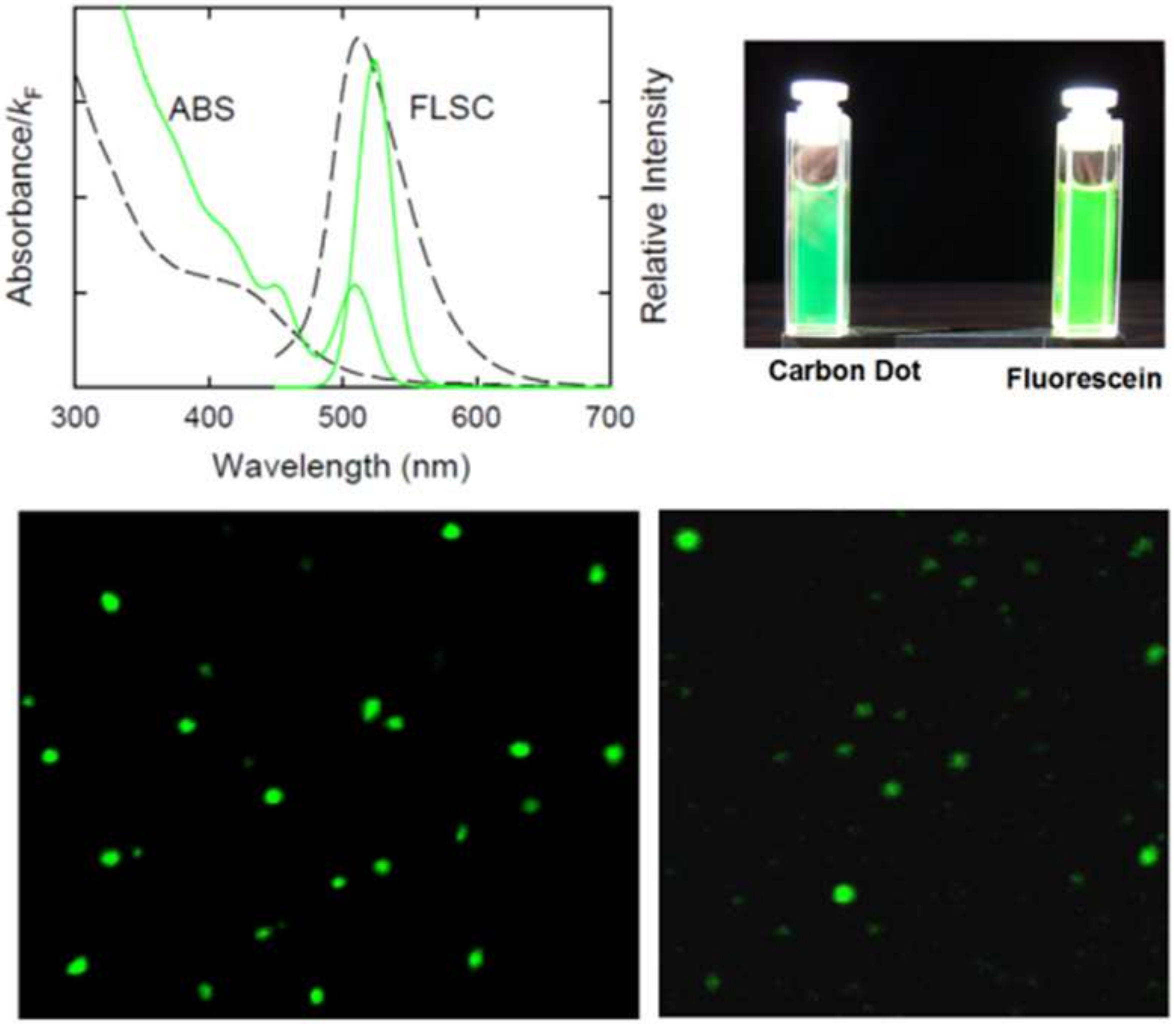

Figure 1.2 Upper-Left: Absorption (ABS) and fluorescence (FLSC) spectra of PEG1500N-carbon dots (- -) are compared with those of Invitrogen "QD525PEG" QDs (─) in aqueous solutions (relative FLSC intensities normalized to per dot).[22] Upper-Right: Photos under sunlight for solutions of the carbon dots and fluorescein (70-90% in fluorescence quantum yield).[22] Lower: Fluorescence microscopy images (458 nm excitation) of individual carbon dots (left) are compared with those of Invitrogen "QD525PEG" QDs (right).[30]

The carbon nanoparticles used in the deliberate functionalization could come from different sources, such as the electrochemical exfoliation of graphite precursors reported by Li, *et al*..[32] The electrolysis was carried out in an amino-terminated ionic liquid, from which carbon dots were harvested. In some studies, carbon nanoparticles were produced from the carbonization of a carbon-rich precursor, followed by surface passivation with organic species.[33-36] For example, Choi, *et al*. carbonized α-cyclodextrin for small carbon nanoparticles, which were functionalized by a PEG diamine and then formic acid. Even with the use of two surface passivation agents, the resulting carbon dots were not very fluorescent, with relatively low quantum yields even in the UV region.[36]

Rednic, *et al.* functionalized pre-selected and processed carbon nanoparticles with poly(*N*-vinylcarbazole) (PVK) thermochemically, which represents essentially a hybrid approach combining the deliberate functionalization discussed above with the carbonization processing detailed in the next section.[37] The PVK-carbon dots thus prepared were used in the fabrication of fluorescent PVK/carbon dots nanocomposites without introducing any unwanted agents or "impurities".

1.2.2 "One-Pot" Carbonization Synthesis

There have been a large number of reports on methods for the preparation or formation of carbon dots that share a common feature: the carbonization of organic or other carbon- rich/containing precursors often in "one-pot" processing.[15-21] These syntheses are generally different from the deliberate functionalization approach such that the carbon core is formed in the carbonization processing, though the use of carbon nanoparticles as precursors in thermochemical functionalization may be considered as a hybrid method in which some features of the one-pot carbonization synthesis are incorporated.[37] An early example for the one-pot synthesis was due to Peng and Travas-Sejdic, who prepared carbon dots by the dehydration of carbohydrates with strong acids and the passivation with 4,7,10-trioxa-1,13-tridecanediamine.[38] The carbonization synthesis has been extremely popular, with hundreds of literature reports on a wide variety of combinations between the carbon precursor, passivation agent, and processing scheme.[15] Particularly stunning has been the use of unusual or even bizarre precursors in the carbonization synthesis, such as hair,[39] goose feathers,[40] shrimp egg,[41] kitchen waste,[42] cow manure,[43] or even human urine.[44] While there is nothing unique about the carbon dots prepared with many of these selected precursors, the diverseness does suggest that carbon dots are not so "picky" with respect to the purity or exact composition of the underlying dot materials beyond the predominating carbon content. This is probably due to the fact that the photoexcited state properties of carbon dots are dictated by defects.[14]

Generally speaking, the one-pot processing is convenient and versatile, but less controllable, yielding carbon dots of widely varying optical properties and performances.[15] Among the primary processing methods have been microwave irradiation, hydrothermal treatment, and thermochemical carbonization, for which some representative literature reports are highlighted as follows.

Microwave irradiation is relatively simple and quick, thus quite popular.[45-48] For example, Zhu, *et al*. made carbon dots by heating a solution of saccharide and PEG in a microwave oven (Figure 1.3).[45] More recently, Liu, *et al.*, synthesized carbon dots of different fluorescence colors by microwave processing of poly(ethylenimine) (PEI) and PEI + glutaraldehyde (Figure 1.3).[47] Experimentally, PEI was microwaved at 200 W (180 °C) for about half an hour to yield blue fluorescent carbon dots (347 nm excitation and 464 nm emission, and quantum yield ~ 10%), while a mixture of PEI and glutaraldehyde (as a cross-linking agent) processed under the same conditions resulted in yellow fluorescent carbon dots (347 nm excitation and 520 nm emission, and quantum yield ~ 8%).[47] Similarly, Lu, *et al*. used a mixture of oxalic acid and urea as precursor for carbonization by microwave (700 W for about 8 min) to obtain blue fluorescent carbon dots of a relatively high quantum yield.[47]

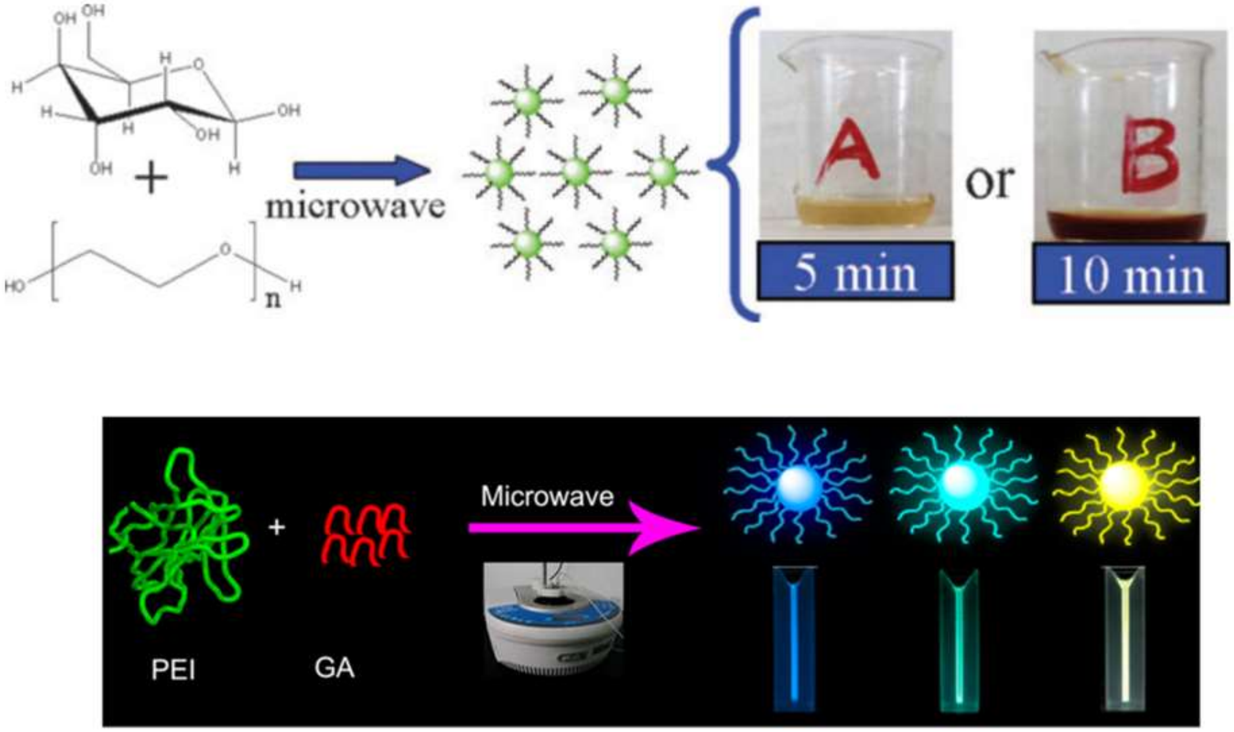

Figure 1.3 Representative schemes for the synthesis of carbon dots with the use of microwave irradiation.[45,47]

In thermochemical processing, thermal energy instead of microwave is used for the carbonization, or more accurately partial carbonization similar to that with microwave irradiation discussed above, with the surviving part of the organic precursor for passivation.[49] In the study by Stan, *et al*. as an example, *N*-hydroxysuccinimide was thermally treated (180 °C for about half an hour) for one-pot formation of carbon dots with blue to green fluorescence emissions.[50] The processing temperature and time were not sufficient for a complete carbonization of the precursor *N*-hydroxysuccinimide, with the remaining organic species to serve the function of passivation, as in many similar syntheses. In other syntheses based on the same thermochemical approach but with a slight yet significant modification to the precursor selection, multiple organic species in a mixture were used as precursor, among which one was selected to be "sacrificed" in the carbonization.[35,51,52] For example, Dong, *et al*. used a mixture of citric acid and branched polyethylenimine as precursor for the one-step carbonization synthesis of carbon dots, where the former was targeted more as the carbon source and the latter for the passivation function.[52]

Hydrothermal syntheses may be considered as a significant variation of the thermal processing discussed above, with the carbonization of organic precursor in an aqueous medium.[53-55] There have been a large number of such syntheses reported in the literature,[56-59] such as the earlier investigation by Yang, *et al*. in which carbon dots were obtained from the hydrothermal carbonization of chitosan,[58] and the more recent study by Wang, *et al*. in which blue fluorescent carbon dots were synthesized by hydrothermal carbonization of milk.[59] There have also been many reports on the use of multiple precursor organic species to divide the roles of being the carbon source and the surviving moieties for passivation in the hydrothermal carbonization processing.[55,60-62]

The one-pot synthesis approach has been popular in the effort on purposely introducing heteroatoms into carbon dots.[63-66] For example, Wang, *et al.* reported on the use of glutathione as nitrogen- and sulfur-containing precursor for the thermal carbonization into "nitrogen and sulfur co-doped carbon dots" (with nitrogen and sulfur contents of 16.1% and 2%, respectively).[66] The processing conditions were largely similar to those in other syntheses, simply heating the solid-state precursor at 260 °C for about an hour. Wang and Zhou prepared "nitrogen-doped carbon dots" from milk.[59] Xu, *et al*. synthesized blue fluorescent "sulfur- doped carbon dots" by hydrothermal treatment of sodium citrate solution and sodium thiosulfate in various ratios. The heteroatom doping of carbon dots apparently shares the same concept with that found in the similar modification of "graphene quantum dots".[54] However, for carbon dots there have been so many syntheses from almost all imaginable organic, biological, and other precursor species containing a variety of heteroatoms as well as metals and other elements, and no systematic property and/or optical performance variations could be identified other than the conclusion that carbon dots are not "picky" at all in terms of elemental compositions. The studies of purposely adding heteroatoms to carbon dots have not produced any significant evidence for altering the not-picky conclusion above.

Beyond microwave and thermal, electrochemical energies have also been applied to the synthesis of carbon dots from various precursor species,[32,67,68] as originally reported by Zhou, *et al*..[25]

1.2.3 Host-Guest Carbon Dots

Carbon dots from deliberate functionalization of small carbon nanoparticles can be made brightly fluorescent in the green spectral region matching that of the green fluorescence proteins, achieving fluorescence quantum yields easily higher than 50% at 400 - 450 nm excitation.[22] They are also fluorescent in the red to near-IR spectral regions, but the corresponding intensities and quantum yields are progressively lower.[6,69] One-pot carbonization syntheses generally yield carbon dots of relatively strong blue fluorescence, corresponding to near-UV excitation.[70-72]

Those from specifically selected precursors can be fluorescent at longer wavelengths, but their quantum yields in the green and red spectral regions are mostly lower to much lower than those of the high-performance carbon dots from the deliberate functionalization approach. Therefore, the preparation of brightly red/near-IR fluorescent carbon dots with quantum yields into double digits in percentage still represents a major challenge, despite the extensive effort already made. Beyond fluorescence quantum yields, the optical absorptivity of carbon dots decreases progressively with increasing wavelength (Figure 1.2), which also limits the performance of the carbon dots as fluorescence probes in the red to near-IR spectral range. As a new strategy towards the desired fluorescence probes with high performance in the biologically significant spectral window, Sun, *et al.* recently proposed and demonstrated the development of host-guest carbon dots, which are conceptually similar to endohedral fullerenes (Figure 1.4), to have red/near-IR fluorescent species enclosed in the dot structure.[73] In the reported study, fluorescent dyes cresyl violet, nile blue, and zinc pthalocyanine were selected as guests.

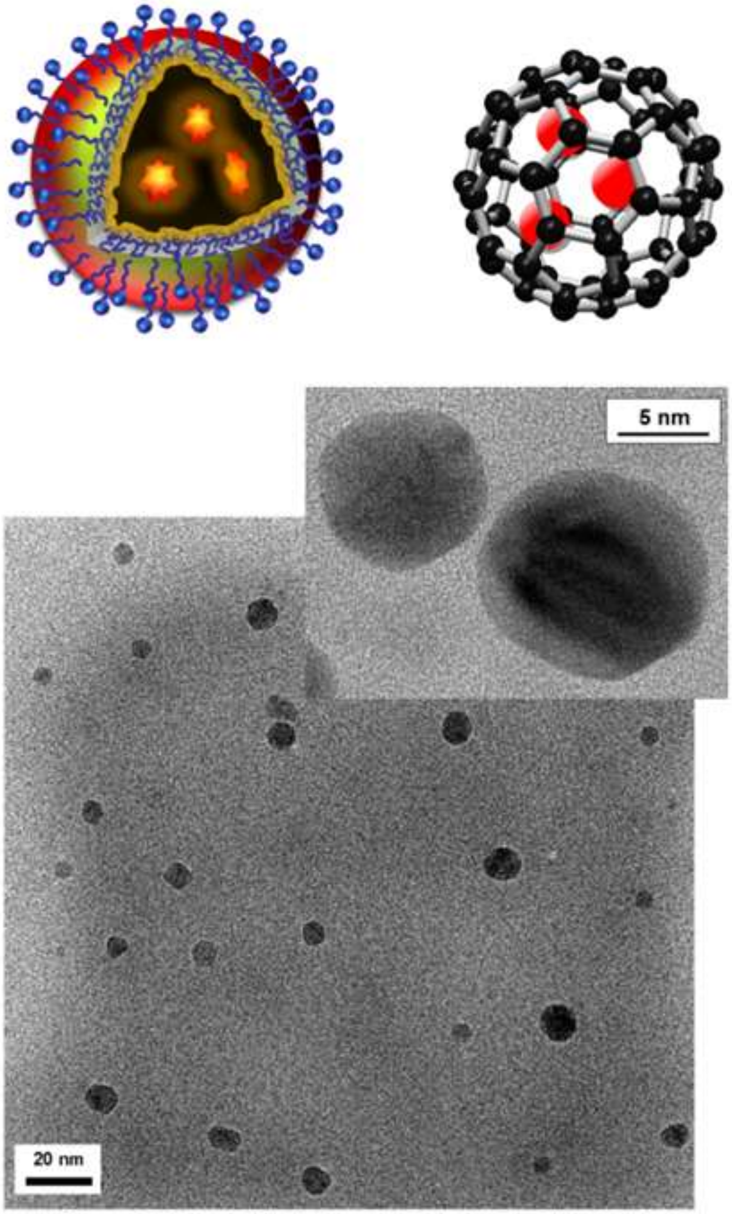

Figure 1.4 Upper: A carbon dot with encapsulated species (host-guest carbon dot, left) *verses* an endofullerene (right). Lower: TEM images (high-resolution in the inset) of NB@CDots on silicon oxide-coated copper grid.[73]

As discussed in the previous section, the thermal carbonization of organic precursors has been a popular approach for carbon dots, in which a portion of the precursor organic species is converted into carbon nanoparticles and the remaining serves the function of surface passivation agents. In the synthesis with microwave irradiation, there is likely the initial creation of carbonized seeds for their subsequent preferential absorption of the microwave energy towards the formation of the targeted dot structure. The microwave processing was used in the one-pot synthesis of the host-guest carbon dots, or G@CDots, where G denotes the guest fluorescent dyes cresyl violet (CV), nile blue (NB), and zinc pthalocyanine (ZnPc).[73] Experimentally for the synthesis of CV@CDots as an example, an ethanol solution of CV was mixed well with oligomeric PEGs, followed by the removal of ethanol. The resulting mixture was irradiated with microwave until the desired carbonization was reached. Since the hosting carbon dots are more transparent in the red/near-IR, the observed absorption spectra are generally suppositions of the host and the guest dye species (Figure 1.5). According to atomic force microscopy (AFM) and transmission electron microscopy (TEM) results, these G@CDots synthesized from thermal carbonization reactions were still relatively narrowly distributed. Most of the dots were small, with their overall size profiles on the order of 10 nm or less (Figure 1.4).[73]

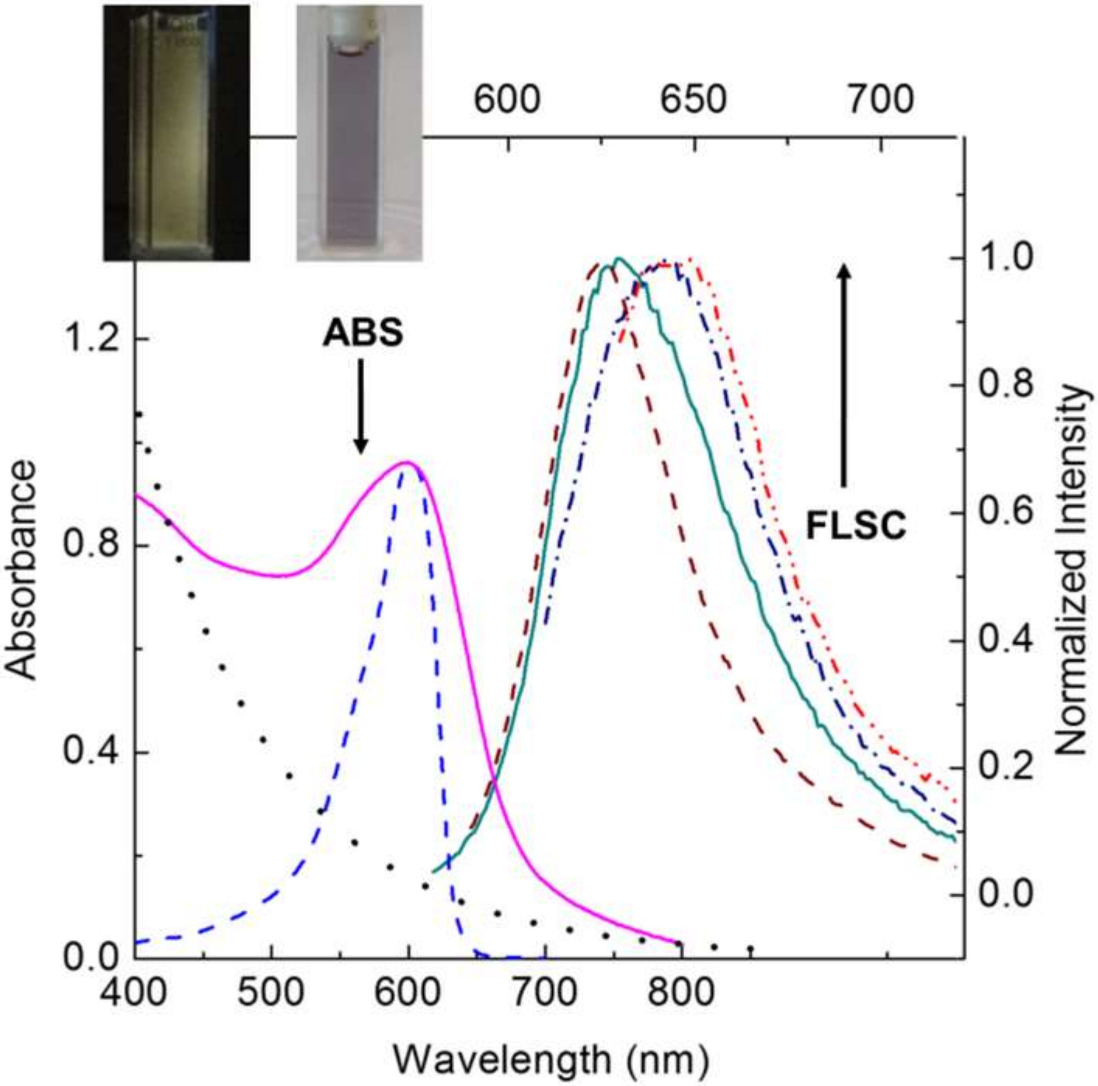

Figure 1.5 The absorption (ABS) spectrum of CV@CDots (—) and corresponding fluorescence (FLSC) spectra (excitation at 570 nm: —, 600 nm: -.-, and 620 nm: -..-) in aqueous solution. The spectra of free CV (- - -) and carbon dots from the carbonization of PEG900 without any encapsulation (. . .) in aqueous solutions are also shown for comparison. Inset: Photographs of an aqueous solution of the sample under UV light in the dark (left) and under natural day light (right). (CV = cresyl violet).[73]

Similar host-guest concept has been used for the encapsulation of magnetic elements in carbon dots.[45,55,74-77] For example, Bourlinos, *et al.* synthesized a hybrid carbon nanostructure doped with gadolinium to be used as fluorescence-MRI dual-modality bioimaging probe.[74] Similarly, Xu, *et al.* synthesized gadolinium-doped carbon dots from the hydrothermal carbonization of citric acid in the presence of ethylene diamine, with citric acid also as a strong chelating agent for gadolinium cations.[55] Gong, *et al.* also prepared gadolinium-containing carbon dots via one-step microwave processing of a mixture of sucrose, sulfuric acid, diethylene glycol, and gadolinium chloride.[45] Kumar, *et al.* applied a sonochemical method to the synthesis of carbon dots with gallium as guest, denoted as Ga@C-dots.[76] Experimentally, granule gallium was mixed with polyethylene glycol and sonicated at 50 °C with an ultrasonic transducer for about 2 hours. The resulting Ga@C-dots were not so fluorescent, with quantum yield ~ 1% at 360 nm excitation, though they were responsive to electron paramagnetic resonance (EPR) for the purpose of photosensitization.[76] Guo, *et al.* synthesized Ni@C-dots in a two-step process, first the hydrothermal carbonization of citric acid for carbon dots and then in the second step the carbon dots were mixed with nickel chloride and ethylene glycol, followed by the addition of hydrazine and sodium borohydride and heating at 60 °C. A characteristic feature of the Ni@C-dots was the nearly complete quenching of fluorescence emissions.[77]

The host-guest carbon dots with a guest list from metal ions to organic dyes represent a highly versatile new platform in the development of carbon dots technology, promising great potential in the design and synthesis of novel dot compositions and configurations for expanded applications.

1.3 Optical Bioimaging

1.3.1 Cell Labeling/Imaging

Carbon dots as brightly fluorescent nanoscale probes have been pursued for their uses in fluorescence imaging *in vitro* and *in vivo*, yielding results that not only serve as the initial demonstration on their widely predicted potential but also reveal some significant challenges for the further development effort.[7,15,16,78]

Carbon dots are nontoxic to cells at concentration levels much higher than those commonly used in fluorescence labeling and imaging.[15,16,30,79] As reported originally by Sun, *et al.*,[6] carbon dots were readily taken up by cells, residing primarily in the cytoplasm, with only minor penetration into the cell nucleus. Many subsequent studies have demonstrated similar cell internalization of carbon dots,[78,80-83] such as the work by Liu, *et al*. in which the imaging results showed efficient uptake of carbon dots by *E. coli* and murine P19 progenitor cells.[80] Chen, *et al.* used carbon dots made from carbonizing sucrose with oil acid in the imaging of 16HBE cells, and they found green fluorescence emissions around the cell membrane and in the cytoplasm, but much weaker fluorescence in the cell nucleus.[81] More recently, Ruan, *et al*. investigated the subcellular distribution of carbon dots, which were synthesized in the hydrothermal processing of spider silk.[82] The dots were found in the cytoplasm of U87 cells, but not in the endosome or mitochondria. In contrast, according to Zhang, *et al*.,[83] a conjugate containing Fe3O4 and carbon dots could be used to image the mitochondria in cells, with an enhanced cellular uptake in a magnetic field.

Carbon dots have extremely large two-photon absorption cross-sections in the near-IR, on the order of at least 40,000 Goeppert-Mayer units (1 GM = 10^{-50} cm^4 s/photon).[7] The two-photon excitation in the near-IR results in bright visible fluorescence emissions, which makes carbon dots excellent two-photon fluorescence probes.[7,84] Following the original report by Cao, *et al*.,[7] Tong, *et al.* used carbon dots with amino molecules as surface passivation agent in the two-photon fluorescence imaging of HeLa cells.[85] In a similar study also on the imaging of HeLa cells, Hu, *et al*. prepared nitrogen-doped carbon dots from alkanolamines and found that the dots internalized in the cells could be excited with two 760 nm photons for green fluorescence emissions.[86]

There have been reports on carbon dots entering into the cell nucleus.[87-89] For example, Shi, *et al.* showed that the carbon dots prepared from the hydrothermal carbonization of flower petals could be endocytosed into the cytoplasm and nucleus of A193 cells.[87] Kong, *et al*. used carbon dots prepared from refluxing PEGs to stain cell nucleoli, suggesting that the performance was competitive to that of commercial DNA-specific dyes.[88] Fan, *et al*. used similarly prepared carbon dots for two-photon fluorescence imaging, showing that the dots could be found around the cell membrane and in the nucleus of MCF-7 cells.[89]

Carbon dots have also found uses in the fluorescence labeling of stem cells. In the more recent study,[74,84] Liu, *et al*. exploited the structural compactness of the short-chain PEG diamine-functionalized carbon dots[69] for the imaging of SD rat mesenchymal stem cells (MSCs). For both live and fixed cells, the carbon dots were found in the cell membrane and cytoplasm, though the labeling efficiency was significantly lower in the live cells (Figure 1.6). The difference was attributed to the cationic surface character of the carbon dots at the biological pH, which might be less favorable to the uptake by the live cells. According to the results, the surface functionalities on carbon dots may play a significant role in determining the cell labeling efficiency.

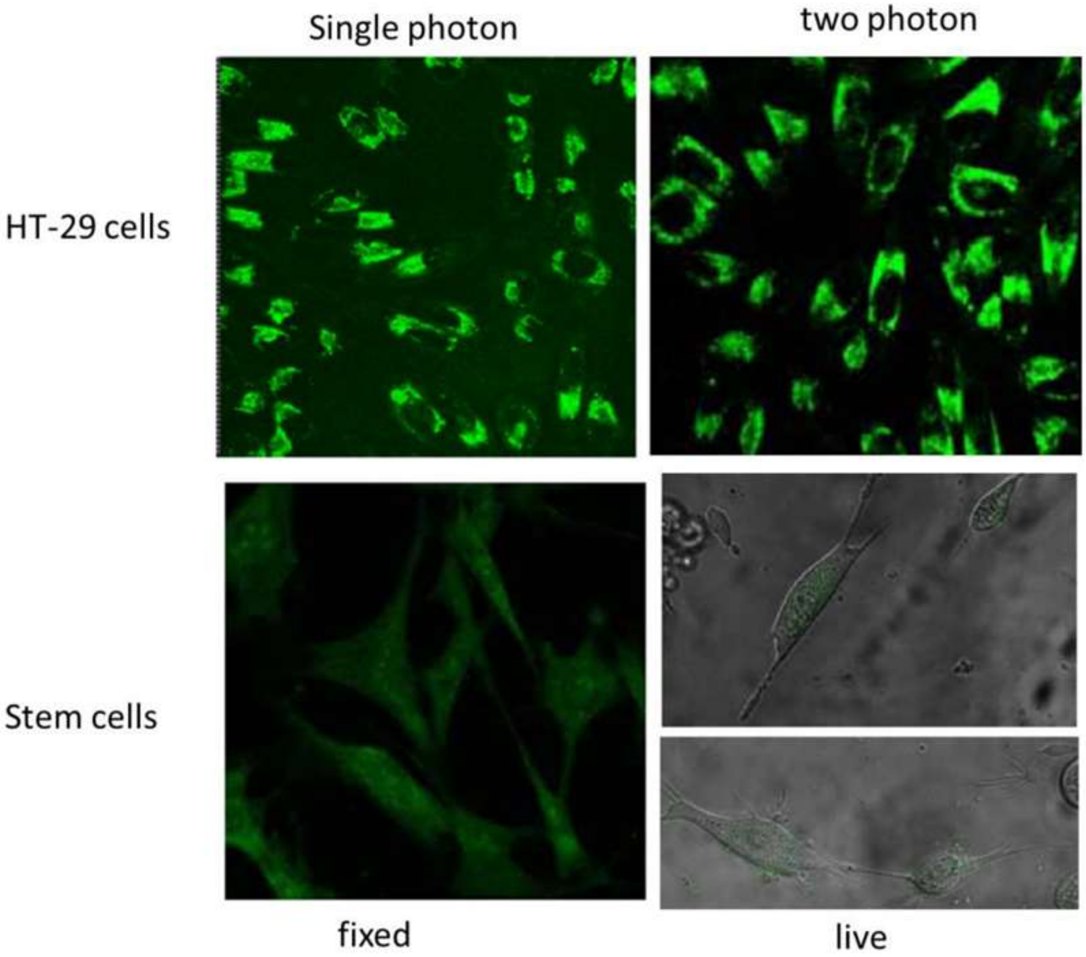

Figure 1.6 (Upper-left) Confocal fluorescence images (458 nm excitation, 470-590 nm emissions) for HT-29 cells with PEG1500N-carbon dots. (Upper-right) Fluorescence images with two- photon excitation (800 nm excitation, 470-590 nm emissions) for HT-29 cells labeled with PEG1500N-carbon dots. (Lower-left) Fluorescence images of fixed stem cells labeled with EDA-carbon dots. (Lower-right) merged (fluorescence + bright-field) images of live stem cells labeled with EDA-carbon dots.[84]

Another important role of the surface functionalities in carbon dots is with their ready conjugation with species for specific targeting purposes.[90-92] For example, Yang, *et al.* conjugated carbon dots with nuclear localization signal (NLS) peptides for fluorescence imaging of MCF-7 and A549 cells.[90] While majority of the dots were found in the cell membrane and cytoplasm, there was some accumulation within the cell nucleus. Li, *et al*. synthesized carbon dots via the hydrothermal carbonization of glucose and sodium polyacrylate, which were designed as turn-on fluorescent probes for cancer cells that over-express folate receptors.[91] In another study of targeting the folate receptors, Yang, *et al*. prepared carbon dots by microwave heating of a folic acid - urea mixture.[92] In a comparison between HeLa cells and normal GES- 1 cells, the carbon dots were largely internalized by the former but not the latter with the same incubation time, and the difference was rationalized by the folic acid species on the dot surface targeting the cancer cells.[92]

In addition to mammalian cells, there have been recent studies on the use of carbon dots for fluorescence labeling and imaging of bacteria, fungi, and plant cells. For example, Nandi, *et al*. used amphiphilic carbon dots to stain and detect bacteria based on fluorescence intensities.[93] Kasibabu, *et al*. showed that carbon dots could stain bacterial (*Bacillus subtilis*) and fungal (*Aspergillus aculeatus*) cells in both green and red fluorescence colors.[94] In similar studies,[95,96] Mehta, *et al*. used carbon dots to stain various bacteria (*E. coli*, *Mycobacterium tuberculosis*, and *Pseudomonas aeruginosa*), yeast (*Saccharomyces cerevisiae*), and fungal (*Magnaporthe oryzae*). Jin, *et al*. also stained fungal cells with carbon dots.[97] For plant cells, Wang, *et al*. prepared oligomeric poly(ethylene glycol)-functionalized carbon dots to stain the onion epidermal cells.[98]

1.3.2. Fluorescence Imaging in Vivo

The nontoxic nature of carbon dots makes them particularly valuable as probes for *in vivo* uses.[15,99] It was demonstrated in the fluorescence imaging experiments with mice that carbon dots are competitive in performance to the commercially supplied CdSe/ZnS QDs.[99,100] The *in vivo* evaluations have included the use of different injection routes. For example, Yang, *et al*. injected carbon dots to the front extremity of mice to monitor their migration toward the axillary lymph node.[99] Following the same concept, Wu, *et al*. used carbon dots prepared from the carbonization of honey in the effort on contrast enhancement in the auxiliary lymph node imaging.[101]

Intravenous injection is important in investigations of pharmacokinetics and biodistribution, crucial to toxicological evaluations and various biomedical applications of carbon dots. In the early investigation,[99] carbon dots were found to be excreted via urine rather efficiently, without any major accumulation in the internal organs, likely due to their small sizes (on the order of 5 nm in diameter) and high solubility. Nevertheless, in a more recent study Li, *et al.* managed to use intravenously injected carbon dots for *ex vivo* fluorescence imaging of the slices from heart, liver, spleen, kidneys, lungs, brain, and small intestine.[78]

Significant effort has been made to tailor carbon dots for targeting tumors *in vivo*. For example, He, *et al*. attached arginyl-glycyl-aspartic acid to carbon dots for the targeting of HeLa tumors in mice.[102] Upon intravenous injection, fluorescence signals could be detected at the tumor site and in the bladder. The results from the imaging of dissected organ specimens were similar, with only weak fluorescence found in liver, heart, spleen, and kidneys, consistent with the finding in the early study using carbon dots without the specific targeting moieties.[99,102] Sharker, *et al.* carbonized hyaluronic acid in a dehydration reaction with sulfuric acid to yield two kinds of carbon dots, denoted as HA-FCN and FCN in which the precursor hyaluronic acid was partially and nearly completed carbonized, respectively, with the former upon intravenous injection exhibiting more accumulation at the tumor site.[103] Wang, *et al*. used carbon dots in the fluorescence imaging of glioma (Figure 1.7).[104] Fu, *et al*. embedded carbon dots in silica nanorattle to be used as fluorescence probes for tumor imaging.[105]

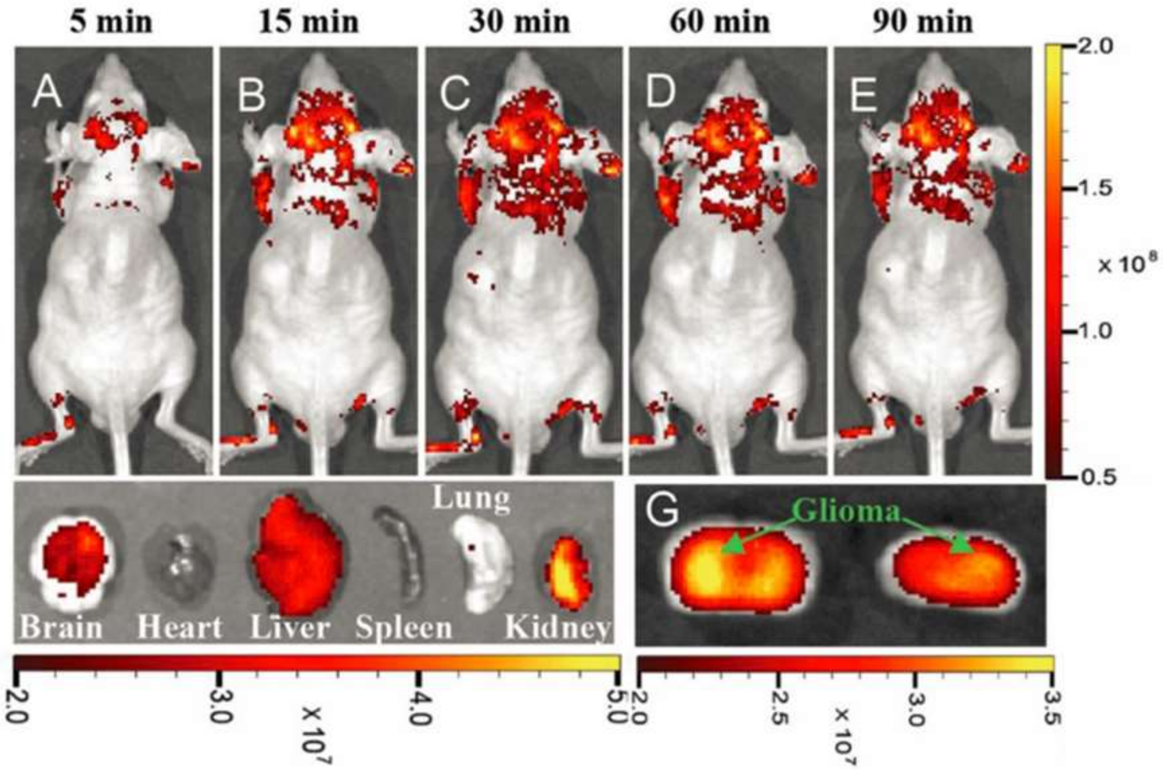

Figure 1.7 In- and ex-vivo imaging of glioma-bearing mice intravenously administered with the pN- CNDs. A–E) Whole body imaging of the pN-CNDs at various time points post-injection. F) Ex-vivo imaging of major organs 90 min after pN-CNDs administration. G) Coronal imaging of the brain 90 min after pN-CNDs administration. Black arrow represents the signal intensity (radiant efficiency) from weak (red) to strong (yellow).[104]

Zhou, *et al*. prepared cholera toxin B conjugated carbon dots (CTB–CDs) as a fluorescent retrograde neural tracer.[106] Upon the injection of CTB–CDs on the back of a mouse, blue fluorescence was recognizable. However, the desired noninvasive *in vivo* imaging was hindered by the strong autofluorescence due to the short excitation and emission wavelengths associated with CTB–CDs. For *ex vivo* imaging, CTB–CDs were injected to the mid-thigh level of the right sciatic nerve, and then the tissues were sliced. Strong fluorescence signals from CTB–CDs were observed in the ipsilateral sciatic nerve and the dorsal root ganglion (DRG) of the spinal segment L5. L4 DRG neurons were also labelled with CTB–CDs. In the longitudinal section of the spinal cord, CTB–CDs-labeled neurons were observed in the spinal segments L3–L5. The transverse section of the spinal cord exhibited the CTB–CDs-labeled afferent terminals in the dorsal horn of the L5 spinal segment and the CTB–CDs-labeled motor neurons in the ventral horn. CTB–CDs could bind with high affinity to monoganglioside GM1, and were retrogradely transported from axonal terminals to neuronal soma within 4 days.[106] Ruan, *et al*. compared "naked" carbon nanoparticles (~122 nm in diameter) and their PEGylated counterparts (~140 nm in diameter) for heart imaging.[107] Upon intravenous injection, the former exhibited a higher accumulation in heart than in other tissues of liver, spleen, kidneys, lungs, and brain. For the latter, the accumulation in heart was lower, but still higher than that in other tissues.[107] Also with the use of large carbon nanoparticles (67 nm) was the work by Mukherjee, *et al*.,[108] in which the particles were incubated with pig skin to visualize the penetration. The 3D light sheet fluorescence images suggested that the particles only penetrated to about 100 μm in depth.

Carbon dots are generally more fluorescent in the green than in the red/near-IR, but the latter is more favorable to tissue transmittance in imaging applications. In the work by Huang, *et al*.,[109] brightly green fluorescent carbon dots were linked with the fluorescence dye ZW800 for its strong emissions in the red/near-IR, and the resulting probes were used for imaging *in vivo* and *ex vivo*. The ZW800-linked carbon dots were efficiently and rapidly excreted from the body after injection in different routes. Post intravenous injection, there were some probes found in liver, spleen, and lungs within an hour, and very bright fluorescence was observed in kidneys and the urine excretion was confirmed. All injection pathways led to meaningful tumor uptakes.[109] For another configuration of the carbon dots - dye FRET probes to extend the emission color to longer wavelengths, Huang, *et al.* attached the fluorescence dye Ce6 to carbon dots to allow blue excitation (430 nm) and red fluorescence emissions (668 nm) via FRET.[110] After intravenous injection, the accumulation of the probes at the tumor site was detected, and the laser excitation of the probes in the mice could significantly suppress the tumor growth.[110]

There have been studies on the conjugation of carbon dots with magnetic species for dual-modality imaging *in vivo*. Srivastava, *et al.* fabricated iron oxide-doped carbogenic nanocomposite (IO-CNC) for fluorescence - magnetic resonance (MR) imaging .[111] After intravenous injection, spleen tissue samples were collected, in which fluorescence signals from IO-CNC were observed. Separately in the MRI imaging, there were enhanced signals in the brain blood vessel under both T1 and T2 models.[111] More recently, Xu, *et al.* used gadolinium-in-carbon dots as probe for MRI study of time-dependent biodistribution in mice.[55]

Kang, *et al*. used zebra fish as a model for the evaluation of carbon dots .[112] Upon soaking for 3 hours, the carbon dots entered into embryos across the chorion and the germ ring. The fluorescence imaging of the dots allowed the visualization of the embryo development. Similarly, Fahmi, *et al.* prepared phenylboronic acid-modified magneto-fluorescent nano-probes, which consisted of MnFe2O4 nanoparticles conjugated to carbon dots, for the imaging of zebra fish.[113] Strong fluorescence emissions from carbon dots were observed in the brain, nervous system, and muscles of the fish embryo. Shi, *et al*. hydrothermally treated petals to produce carbon dots for the imaging of carp fish.[87] Yuan, *et al*. used carbon dots in the fluorescence imaging of Caenorhabditis elegans.[114] After incubation, the *C. elegans* were homogenously labeled by the carbon dots, with blue or green fluorescence emissions corresponding to different excitation wavelengths. Parvin, *et al*. prepared carbon dots that are polyelectrolyte-like for the imaging of Drosophila.[115] Drosophila melanogaster was incubated with the dots for the imaging at different developmental stages (larvae, pupa and adult). At 12 hours' post-incubation, for example, internal organs of larva could be clearly recognized.[115]

1.3.3. Theranostics

Beyond imaging, carbon dots have been studied for potential uses in theranostics, namely for the concurrent effect of imaging and treatment such as drug delivery or photodynamic therapy.[116-126] For example, Lai, *et al*. prepared carbon dots from glycerol inside mesoporous silica nanoparticles for both fluorescence imaging and drug release.[119] Ding, *et al.* synthesized carbon dots in hydrothermal carbonization of DNA, and then loaded the anticancer drug doxorubicin (DOX) through presumably π-π stacking interactions.[120] The drug-loaded carbon dots were incubated with *S. cerevisiae*, and the results from microscopy imaging suggested intracellular drug release. Wang, *et al*. also used carbon dots to carry DOX for both imaging and delivery, with the imaging as a tool for the evaluation of the delivery.[121] Carbon dots were found in the cytoplasm of human breast cancer MCF-7, MDA-MB-231, and BT-549 cells. However, the MTT assay results suggested that the toxicity of the DOX carried by carbon dots was lower than that of free DOX, which was attributed to the slow release of DOX from carbon dots.[121] Matai, *et al*. prepared a hybrid of carbon dots and PAMAM dendrimer for the imaging and delivery of the anticancer drug epirubicin.[122] For both MCF-7 and NIH 3T3 cells, the toxicity of the hybrid carried epirubicin was somewhat lower than that of free epirubicin. Palashuddin, *et al*. prepared carbon dots-like nanoparticles embedded with Cu2+.[123] In HeLa cells, blue fluorescence from the nanoparticles was observed. While the nanoparticles without Cu2+ were nearly nontoxic, they apparently enhanced the toxicity of the embedded Cu2+ to HeLa cells, for which a suggested possible mechanism was such that the nanoparticles up-regulated the sub G1 population of cells and induced apoptosis.[123] More recently, Cheng, *et al.* conjugated carbon dots with polycation-b-polyzwitterion copolymers and used the resulting conjugate as a serum-resistant gene delivery carrier to be compared with the widely used carrier PEI25K.[124] The carrier was loaded with DNA vectors for green fluorescent proteins (GFP) and transfected into COS-7 cells at different serum concentrations. It was found that the carrier was better in performance than PEI25K, especially at high serum concentrations.[124] Wang, *et al*. used carbon dots - polyethyleneimine complexes to deliver siRNA to gastric cancer cells (Figure 1.8),[125] while Hu, *et al*. hydrothermally carbonized polyethyleneimine into carbon dots for gene delivery to take advantage of the dots being positively charged.[126]

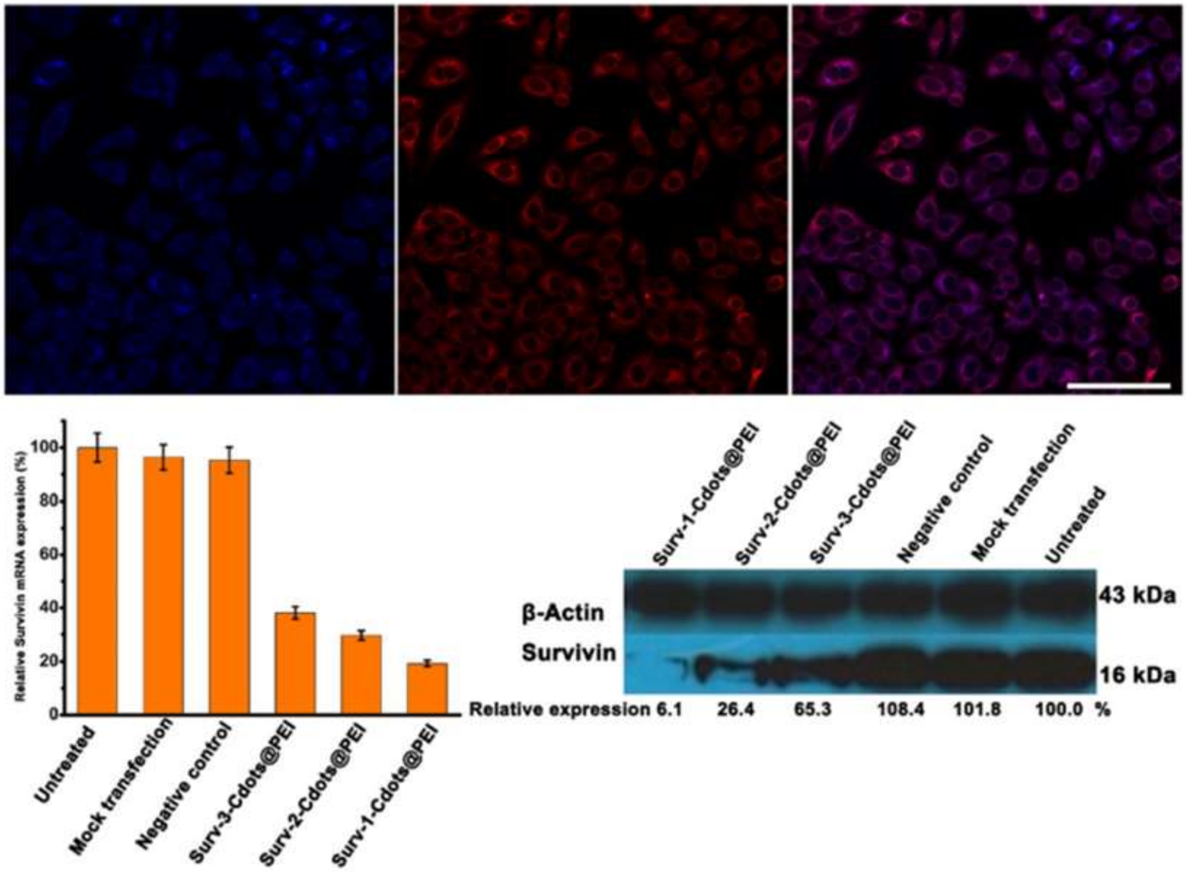

Figure 1.8 (Upper) Confocal laser scanning microscopic images of Cy3-siRNA-Cdots@PEI complexes for 5 h and (lower) gene silencing efficiency of siRNA-Cdots@PEI complexes against Survivin at (a) mRNA and (b) protein expression level.[125]

The photoactive nature of carbon dots makes photodynamic therapy a natural choice for combination with fluorescence imaging, and a number of studies have been reported for such an approach in theranostics.[36,127-129] For example, Choi, *et al.* prepared carbon dots with both PEG diamine and folic acid as surface passivation agents and then loaded with zinc phthalocyanine (ZnPc) for imaging and photodynamic therapy.[36] Upon the incubation with HeLa cells, the ZnPc-loaded carbon dots were internalized, exhibiting blue-green and red fluorescence emissions assigned to the carbon dots and ZnPc at 358 nm and 647 nm excitations, respectively. The cells were irradiated with 660 nm laser light (30 mW/cm^2), which reduced the cell viability to 10%.[36] Kleinauskas, *et al.* demonstrated that the silver-doped carbon dots could serve as sensitizers in photodynamic therapy and radiotherapy.[127] Wang, *et al*. prepared nanoparticles containing carbon dots, Fe_3O_4, and gold for magnetic/near-IR-responsive drug release, multicolor fluorescence imaging, and photothermal therapy.[128] For the nanoparticles in B16F10 cells, blue, green, and red fluorescence emissions could be detected with 405 nm, 488 nm, and 546 nm excitations, respectively, and the emissions were stable under the imaging conditions. When the nanoparticles were used to carry the anticancer drug DOX, the release was enhanced in a magnetic field and by near-IR irradiation. Photothermal effect in the nanoparticles was confirmed, and its combination with the DOX delivery and release resulted in a high toxicity against B16F10 cells.[128] To take advantage of the large two-photon absorption cross-sections of carbon dots, Wang, *et al*. linked porphyrins to carbon dots for the two-photon excitation of the dots at 700 nm and then energy transfer (FRET) to the porphyrins for photodynamic effect.[129]

The use of carbon dots as antioxidant in addition to fluorescence imaging has also been pursued. For example, Das, *et al*. compared the antioxidant functions of carbon dots with those of typical molecular antioxidants such as butylated hydroxytoluene and *L*-ascorbic acid.[130] Similarly, Zhao, *et al*. reported on the free radical scavenging activity of carbon dots, which were prepared by the hydrothermal treatment of garlic.[131] Among the studies on carbon dots for theranostics *in vivo*, Choi, *et al.* prepared PEGylated carbon dots with or without the functionalization of formic acid, and then loaded with zinc pthalocyanine.[36] In the *in vivo* biodistribution and photodynamic therapy experiments with tumor-bearing mice, fluorescence signals from the dots without formic acid were detected mainly in liver, much weaker in kidneys, intestine, and spleen. For the dots with formic acid, the fluorescence results suggested an appreciable accumulation in the tumor. At 12 hours' post- injection, the irradiation with 660 nm laser (0.3 W/cm^2) for 20 minutes resulted in a 4-time reduction in the tumor volume.[36] Ge, *et al*. used carbon dots for fluorescence and photoacoustic detection and thermal theranostics in mice (Figure 1.9).[132] After intravenous injection, fluorescence from the carbon dots could be detected in the tumor area. The imaging *ex vivo* suggested that the dots were mostly in the liver and tumor, very minor in heart, spleen, and lungs. Photoacoustic signals were also found in the tumor area. The tumor site with the dots was illuminated with a near-IR laser for 3 and 10 minutes, resulting in temperature increases at the site to 50.4 °C and 60 °C, respectively. The photothermal therapy induced substantial empyrosis and suppressed the tumor growth.[132]

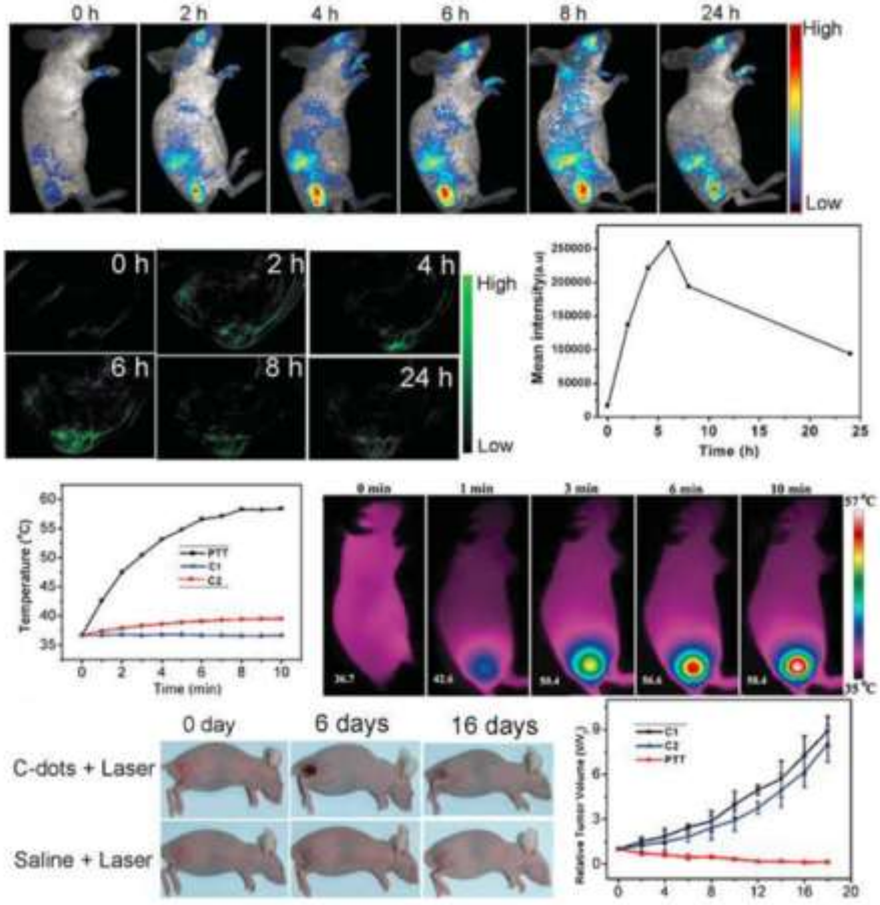

Figure 1.9 (a) Real-time in vivo red FL images after i.v. injection of C-dots in nude mice at different time points. (b) PA images of tumors in mice after i.v. injection with C-dots at different time points and (c) intensities of the mean signal and maximum mean signal of the ROI at different time points (0-24 h) after i.v. injection. (d) PTT change in temperature at the mice tumor sites as a function of irradiation time and (e) IR thermal imaging of intratumoral C-dots injected mice tumor sites at 0, 1, 3, 6, and 10 min after irradiation by 671 nm laser at 2 W cm^{-2}. (f) Photographs of the tumor-bearing mice on different days after different treatments and (g) relative change in the tumor volume of the tumor- bearing mice of the different groups after treatments (n= 5, $P < 0.05$ for each group).[132]

Liu, *et al*. used the conjugate of carbon dots with ribonuclease A for synchronous cancer imaging and therapy.[133] The conjugate could be found in both cell cytoplasm and the nucleus, and it exhibited higher toxicity to MGC803 cancer cells than free ribonuclease A. Upon the intratumoral injection of the conjugate, bright fluorescence was detected at 10 minutes and 4 hours' post-injection, but the signal decreased dramatically after 12 hours.[133] Tang, *et al*. prepared the conjugate of carbon dots with folic acid and the anticancer drug DOX for theranostics.[134] Glomerular tissue incubated with the conjugate was imaged by using a 3D two-photon fluorescence microscope to monitor the release of DOX.

1.4 Photocatalytic Energy Conversion

1.4.1 Photoinduced Redox Processes

Carbon dots resemble conventional semiconductor QDs beyond the similar bright and colorful fluorescence emissions. They also share the characteristic behavior of driving photocatalytic energy conversion processes, such as the photoreduction of CO_2 into small organic molecules.[135-137]

In the presently adopted mechanistic framework, the photoexcitation of carbon dots results in efficient charge separation, with the separated electrons and holes (or radical anions and cations in a different description) trapped at various surface sites that are passivated by the surface functionalization species, and the radiative recombinations of the electrons and holes are responsible for the observed fluorescence emissions (Figure 1.10).[14,138] This is in several respects similar to the photoexcited state mechanism in conventional semiconductor QDs.[4,5] The mechanistic framework for carbon dots has been supported by experimental results,[138-140] including especially those demonstrating that photoexcited carbon dots are both excellent electron donors and acceptors, with fluorescence emissions quenched efficiently by electron acceptor and donor molecules statically and dynamically in a diffusion-controlled fashion (Figure 1.10).[138] Within the mechanistic framework, the fluorescence quenching results could readily be explained in terms of the electron acceptor or donor quenchers scavenging the electrons and holes in carbon dots, respectively, thus disrupting the radiative recombinations (Figure 1.10). In a subsequent investigation using the same electron acceptor and donor quenchers as those in ref. 138 2,4-dinitrotoluene and *N*,*N*-diethylaniline, respectively, Zhang, *et al.* performed fluorescence decay measurements to have the results confirm the redox processes in photoexcited carbon dots.[139] More recently, there was a study based on transient absorption spectroscopy to probe more directly the redox species and processes associated with photoexcited carbon dots.[141] Triethanolamine (TEOA) and methyl viologen (MV2+) were used as electron donor and acceptor, respectively, for redox interactions with the carbon dots.

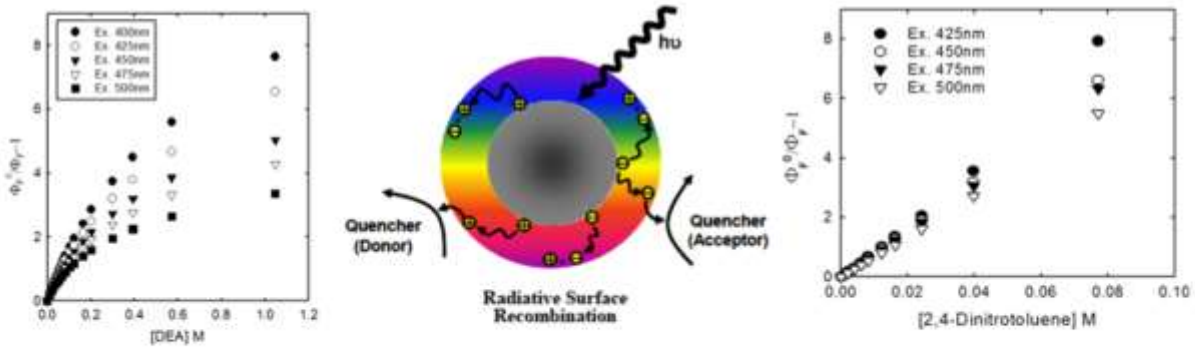

Figure 1.10 Middle: A cartoon illustration of the mechanistic framework on photoexcited state processes in carbon dots (with the rainbow color showing fluorescence from radiative recombinations of the electrons and holes). Left: Stern-Volmer plots for the fluorescence quenching by electron donor *N*,*N*-diethylaniline (DEA); and Right: by acceptor 2,4-dinitrotoluene at different excitation wavelengths.[147]

In other recent studies, Mondal, *et al*. synthesized hydrophobic carbon dots via thermal carbonization of glucose in the presence of dodecylamine, and then loaded cyclometalated complexes of Ir(III) and Rh(III) onto the dot surface in a nonpolar solvent gradient.[142] Upon photoexcitation of the carbon dots loaded with the metal complexes, there was fluorescence quenching, more significant at a higher loading of the metal complexes. The quenching was attributed to electron transfer, or more specifically hot electron injection from the metal complexes into the excited carbon dots.[142] Mondal, *et al*. also used amino acids as precursor for carbon dots, with dot surface protected by surfactants of different chain lengths from 12 to 16 carbons.[143] The fluorescence emissions of these carbon dots were quenched by dimethylaniline as electron donor. A somewhat surprising observation was that the quenching efficiency was higher for carbon dots protected by a longer chain surfactant.[143] In a similar study of photoinduced electron transfer, Gao, *et al*. found that fluorescence emissions of the carbon dots could be quenched by Fe(III).[144]

The surface-bound electrons generated from the photoexcitation of carbon dots could be used to reduce metal ions in solution to result in the coating of the carbon dots with the corresponding metal.[140,145] For example, the photoirradiation of carbon dots in an aqueous solution of gold compound was used to deposit gold metal on the dot surface, which was accompanied by an extremely efficient static quenching of fluorescence emissions.[140] Since the metal is electron affinitive, it takes electrons from the attached carbon dots, thus disrupting the radiative recombinations. The photo-reductive deposition of a noble metal on carbon dots has valuable applications, such as much improved photocatalytic functions.[146,147] Choi, *et al*. also exploited the same processing to decorate the surface of carbon dots with plasmonic silver nanoparticles for hybrid nanostructures of enhanced light harvesting capability in optoelectronic devices (Figure 1.11).[145] The observation on effective quenching of fluorescence in carbon dots by the presence of silver was also reported.[148] Similarly, Mazzier, *et al*. exploited the electron- donating character of photoexcited carbon dots to grow silver nanoparticles on the surface of carbon dots.[149] The results again served as experimental evidence for the availability of photo-generated electrons in carbon dots that could be harvested for reduction or other productive purposes.

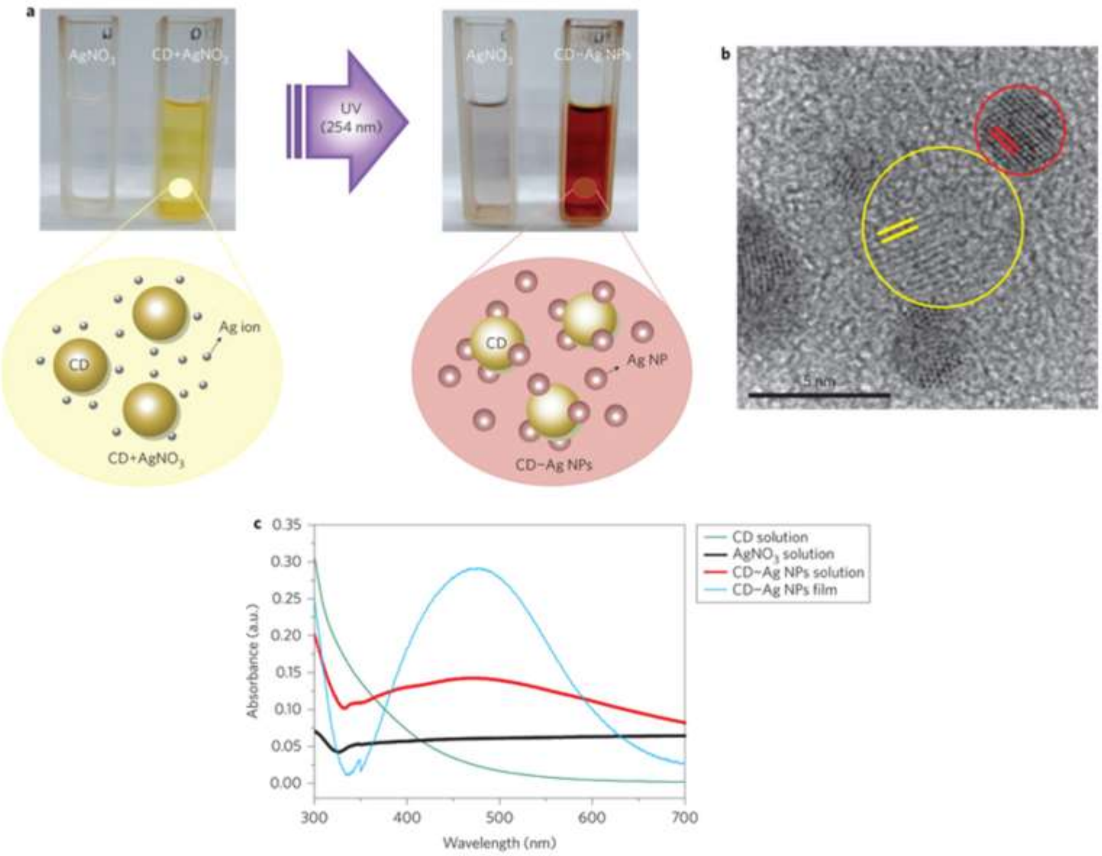

Figure 1.11 Schematic illustration and characterization of CD-Ag nanoparticles. a) Photographs and schematic illustration of AgNO3 and carbon dot (CD) + AgNO3 blend solutions before (left) and after (right) ultraviolet irradiation. b) HR-TEM image of CD–Ag nanoparticles (NPs). Yellow and red circles indicate the presence of carbon dots and silver nanoparticles, respectively. The two parallel lines in yellow and red show the distinguishable lattice fringes (3.2 Å and 2.1 Å) of carbon dots and silver nanoparticles, respectively. Scale bar, 5 nm. c) Comparison of UV–vis absorption spectra of CD–Ag nanoparticles in solution and in a film, and carbon dot and AgNO3 solutions after ultraviolet irradiation.[145]

1.4.2 Photocatalytic Functions

One of the most challenging yet rewarding photocatalytic processes for energy conversion is the reduction of CO_2 into small molecular fuels, with solar radiation in particular. Semiconductor nanomaterials, including especially colloidal TiO_2 have traditionally been employed as photocatalysts in the relevant reactions. However, TiO_2 nanoparticles and other semiconductor QDs for such a purpose are absorptive only or mostly in UV, inefficient in the harvesting of solar photons, so that a number of strategies to extend the absorption into the visible spectrum have been pursued.[150] Carbon dots are broadly absorptive over the UV and visible spectral regions, extending into the near-IR, with a significant overlap with the solar spectrum (Figure 1.12). The photoexcitation in carbon dots drives the excited state redox processes, which are not only responsible for the observed fluorescence emissions but also make the associated electrons and holes available for the catalytic energy conversion reactions, including the CO_2 reduction.[147]

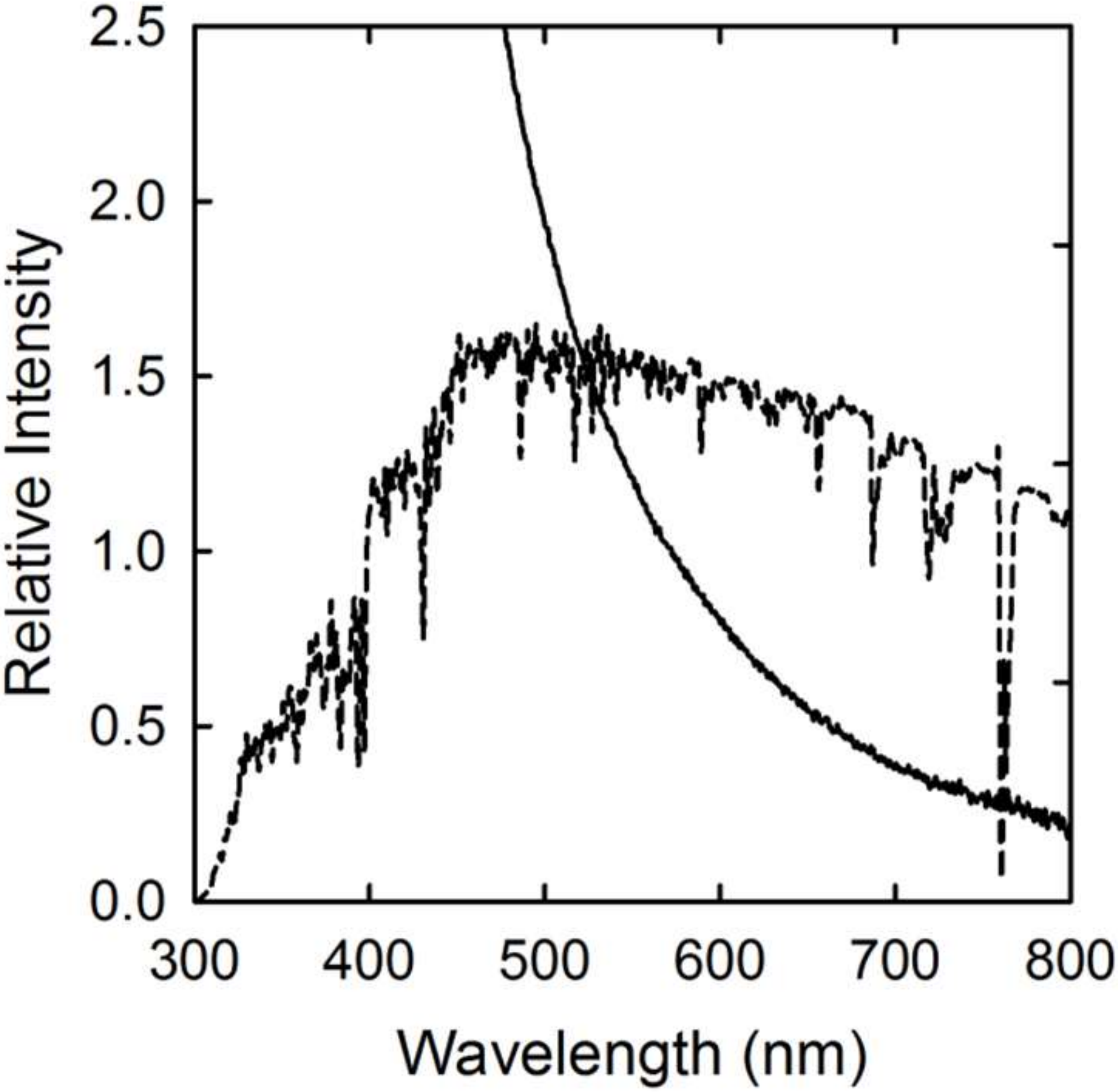

Figure 1.12 The observed absorption spectrum of broadly distributed carbon dots in aqueous solution (solid line) compared with the solar spectrum at the sea level (dashed line).[147]

It has been demonstrated that carbon dots with surface passivation by amino or other molecules are capable of serving as photocatalysts with broad-band visible excitation for CO_2 reduction in aqueous solution (Figure 1.13).[135,137] Experimentally, the carbon dots were irradiated with light over a broad visible spectral range (405 – 720 nm) in an aqueous solution saturated with CO_2 (or $NaHCO_3$ as the CO_2 source), with the reduction monitored by the detection and quantification of formic acid as a major product. The formic acid formation was apparently significant, around 40 μmol g^{-1} h^{-1}, better than the performance with the use of colloidal TiO_2 (Degussa P25) as photocatalyst and UV irradiation.[137] The results of photocatalytic CO_2 conversion have also contributed to the understanding of the mechanistic framework, providing valuable experimental evidence for the photo-generated redox species in carbon dots, as already suggested by the fluorescence quenching results (Figure 1.10).[138,140,145] Similarly of mechanistic values was the much improved photocatalytic performance of the carbon dots after the photo-deposition of gold on the dot surface (Figure 1.13),[33,135,137] which in terms of the mechanistic framework must be due to the concentration of the photo-generated electrons by the gold metal.[150] For the gold-coated carbon dots as photocatalysts in an aqueous solution saturated with CO_2 and the photoirradiation with light over a broad visible spectral range, the estimated quantum yield for the conversion to formic acid was ~0.3%.[135] This likely underestimated the actual overall quantum yield for the CO_2 photocatalytic reduction because there are other photoproducts in addition to formic acid.

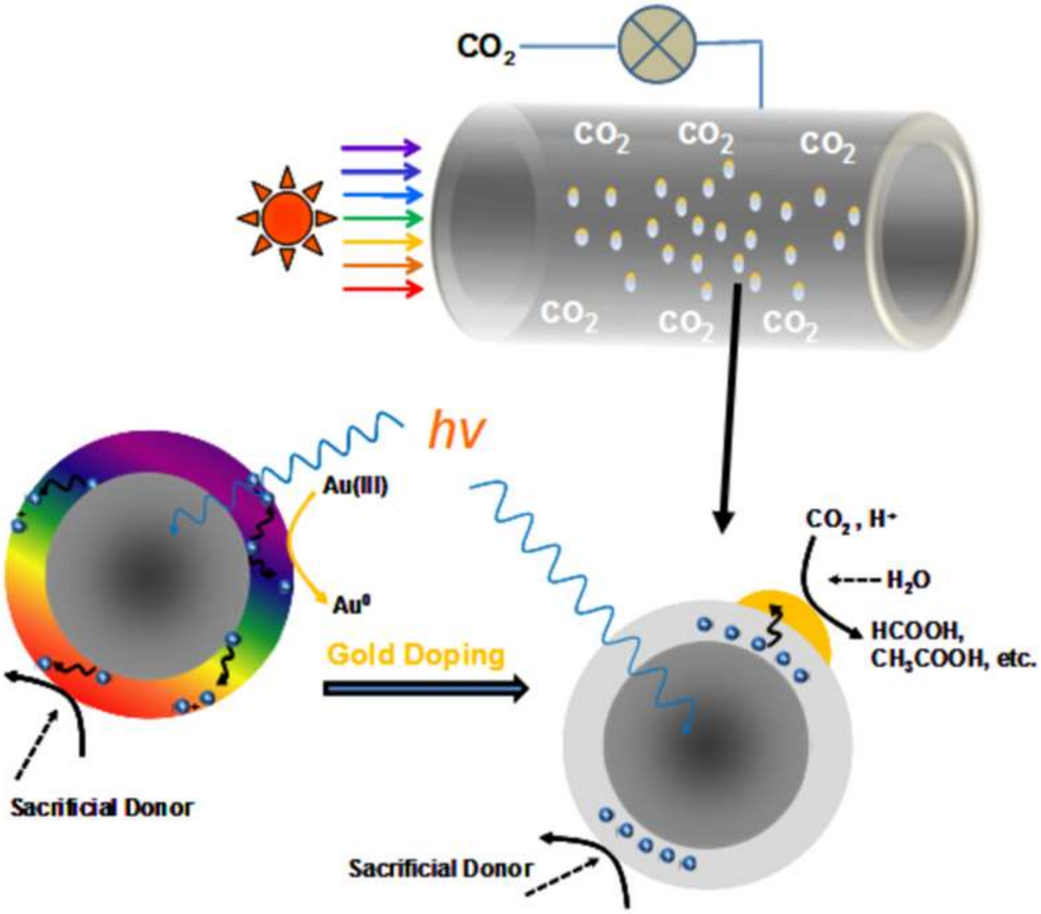

Figure 1.13 Cartoon illustrations on (upper) the high-pressure optical reactor; (lower-left) the photoreductive doping of the carbon dot with gold, completely quenching the dot surface- based fluorescence (illustrated as the change of the dot surface from rainbow to grey); and (lower-right) the gold-doped carbon dot as photocatalyst for CO_2 conversion, where the doped gold (in yellow) was small in quantity, insufficient to form a shell, and likely random in terms of size and shape. The sacrificial electron donor was isopropanol added in some experiments or PEG_{1500N} molecules on the surface of the carbon dots in the absence of isopropanol.[136]

The relatively efficient conversion to formic acid is in itself a reflection on the effectiveness of the metal-coated carbon dots as photocatalysts. Beyond formic acid, other photoproducts have been identified, in which the characterization and quantification of acetic acid are particularly significant ,[136] as the photoreduction of CO_2 to acetic acid requires overall eight electrons, regardless of mechanistic details.[150] In fact, the proposed mechanisms in the literature on the conversion to acetic acid had to invoke the involvement of other small organic molecules as intermediate products, especially methanol.[136,150,152] Therefore, not only the overall CO_2 conversion quantum yields must be higher than that for only the formic acid formation, but also the results on acetic acid and methanol as other significant products in addition to formic acid suggest that carbon dots represent uniquely potent broad-band visible- light photocatalysts for the CO_2 conversion.

Other noble metals have been used to coat carbon dots, and the resulting "hybrid nanostructures" have exhibited similarly potent photocatalytic functions. For example, the results from the use of platinum-coated carbon dots as photocatalysts in the CO_2 conversion were largely the same as those with their gold-coated counterparts.[135] Li, *et al*. prepared nanocomposites of carbon dots with Cu_2O as visible-light photocatalysts for the conversion of CO_2 into methanol.[153] The photoinduced redox properties of the carbon dots/Cu_2O nanocomposites were examined in the fluorescence quenching study with the known electron acceptor 2,4-dinitrotoluene and electron donor *N*,*N*–diethylaniline as redox quenchers.[153] The quenching results suggesting the presence of photo-generated redox species in the carbon dots/Cu_2O nanocomposites were used to justify their photocatalytic functions in the CO_2 conversion. The proposed mechanism was such that the visible-light excitation of Cu_2O produces electron-hole pairs, with the electrons consumed for the CO_2 reduction and the holes transferred to the surface of the carbon dots for the oxidization of H_2O into O_2.[153]

Particularly interesting and consequential results on the use of carbon dots and their metal-coated hybrid nanostructures as photocatalysts for the CO_2 conversion have been the obviously significant dependence on CO_2 concentration in the aqueous solution,[136] which is rather unusual because photocatalytic reactions are generally independent of reactant concentrations. The observation was such that the product yields, the production of formic acid in particular (Figure 1.14), increased substantially with the increasing CO_2 concentration.[136]

Experimentally, the CO_2 concentration variations were achieved with varying CO_2 pressures over an aqueous solution in a high-pressure optical cell, with the gold-doped carbon dots as photocatalysts and broad band visible-light excitation for the photoreduction. The formic acid production obviously increased more significantly with the increasing CO_2 pressure (Figure 1.14) and thus correspondingly increasing CO_2 concentration in the aqueous solution. At 1,900 psia (about 1.37 M CO_2 in the solution), for example, the amount of formic acid was more than an order of magnitude higher than that produced under ambient CO_2 pressure. Since all other experimental conditions of the photoreduction reaction were kept the same except for the CO_2 pressure and corresponding concentration in the aqueous solution, the number of photons harvested by the carbon dots as photocatalysts should be constant. Therefore, the observed increase in formic acid production at the high CO_2 pressure must be a reflection of the same magnitude of increase in the reaction quantum yield for this photoproduct.[136] This would put the performance level of the carbon dots-derived photocatalysts with broad-band visible-light (405 - 720 nm) excitation much beyond the state of the art.[146] The results on the CO_2 concentration dependence also have significant mechanistic implications. Technologically, the aqueous solution under pressurized CO_2 conditions may represent an ideal reaction setting for much more efficient CO_2 photocatalytic conversion into small organic molecules.

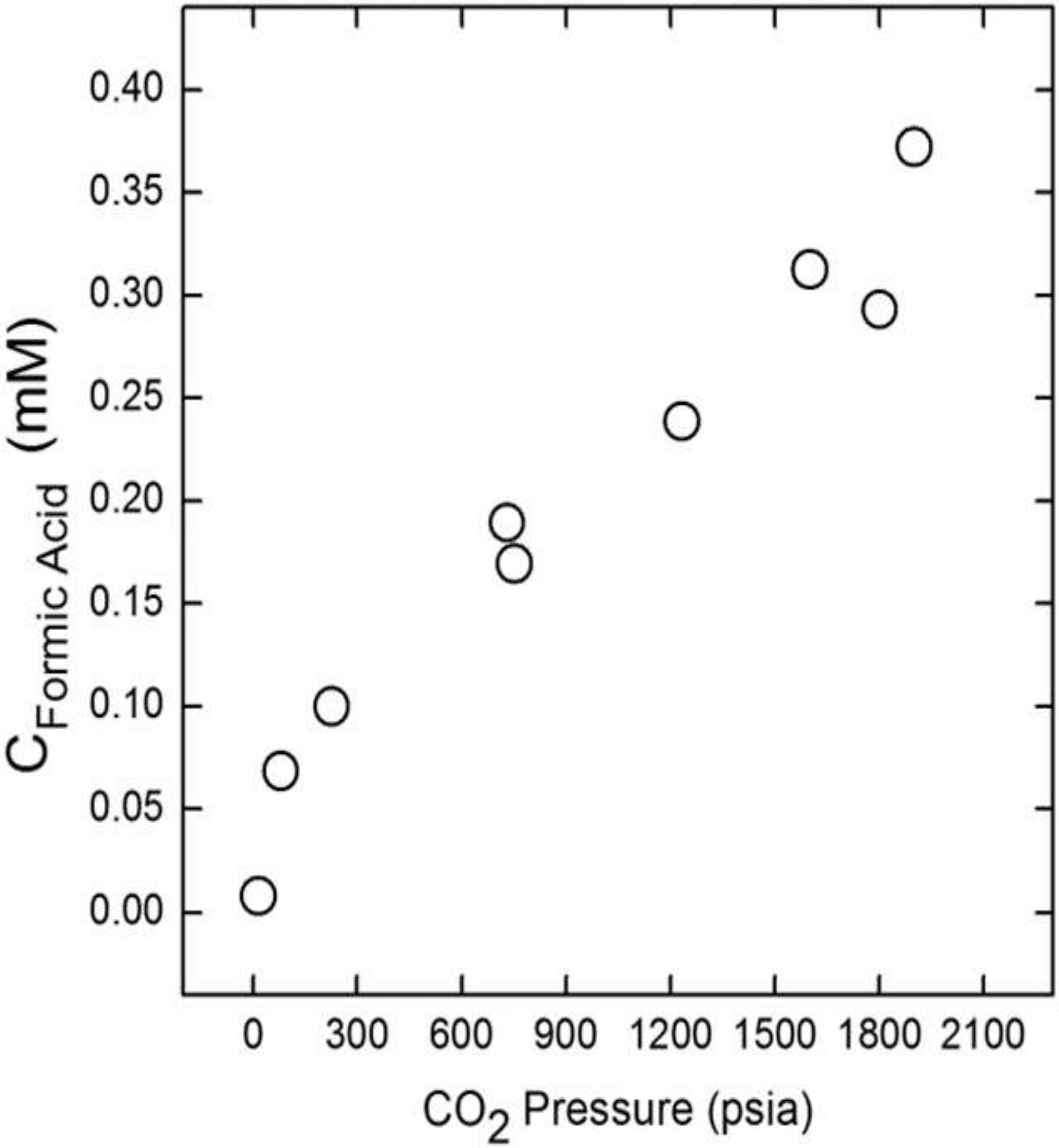

Figure 1.14 Results in terms of formic acid concentrtations in the reaction mixtures from a series of photoconversion reactions in aqueous solution of the carbon dots under different CO_2 pressures (in the long-path optical cell as the high-pressure reactor).[136]

1.5 Summary and Perspectives

Carbon dots, which are generally functionalized carbon nanoparticles, have obviously emerged to represent an important research field that is still experiencing rapid advances, as reflected by an ever increasing number of recent publications. Some characteristics of this research field, recent trends, and possible future directions are summarized as follows.

There have been a disproportionally large number of publications on the synthesis of carbon dots, mostly by a partial carbonization of a variety of carbon-rich or carbon-containing precursors. The relevant methods are generally simple and versatile, but the resulting carbon dots have yet to reach the performance levels achieved by carbon dots obtained from the deliberate functionalization of carbon nanoparticles, and an understanding of the structural details in the dots from the carbonization synthesis still presents a significant challenge. Hybrid approaches that combine the deliberate functionalization concept with the facile carbonization processing may prove valuable in the versatile and efficient preparation of carbon dots with different surface functionalities and in large quantities.

The increasing amount of experimental evidence for the nontoxic nature of carbon dots will have far reaching implications in their further development, stimulating more explorations that target *in vivo* and *ex vivo* uses in biology and medicine. In addition to the fluorescence imaging emphasized in this review, carbon dots have also been explored for their electrochemiluminescence properties[154-156] targeting related imaging applications.[157,158] With the performance benchmarks already achieved, carbon dots are expected to find biomedical applications that have been widely pursued in the research field of semiconductor QDs. Special opportunities are in those imaging-sensing and related uses that require human interactions, *in vivo*, *ex vivo*, food, water, and so on, to take advantage of the unique attributes of carbon dots as being high-performance yet benign and nontoxic. Significant advances in areas such as carbon dots as a new platform for multi-modality imaging agents and for combining imaging with drug delivery and therapy may be envisaged.

Beyond bioimaging and theranostics, there has been increasing recent attention on the photocatalytic functions and related properties of carbon dots. Carbon dots have also been explored for photoelectrochemical[159,160] and optoelectronic applications.[145,161,162] These are hardly surprising considering the fact that carbon dots share some of the key mechanistic steps with conventional semiconductor QDs, namely carbon dots are essentially nanoscale semiconductors in many respects. Therefore, it may be expected that investigations into the relevant photoinduced redox properties of carbon dots and their uses in photocatalytic, photoelectrochemical, and optoelectronic processes and devices will continue and be expanded significantly.

Lastly, there have been some confusions on the relationships between different carbon- based QD-like nanomaterials, carbon dots vs graphene quantum dots in particular.[14,147] While such confusions may take some time to resolve, there is the prospect for a unified and mechanistically consistent understanding of these nanomaterials when more experimental as well as theoretical results become available. As a takeaway from this article, it is the surface functionalization of carbon nanoparticles that makes carbon dots and their associated superior optical and other properties, and the same functionalization effect is apparently evident in the field of graphene quantum dots (and their various structurally heteroatom-doped derivatives),[147] likely a reflection of their shared mechanistic origins. Further investigations are obviously needed.

1.6 Acknowledgements

Chapter one has been published in the literature in collaboration with Prof. Sheng-Tao Yang, Fan Yang, Yamin Liu, Dr. K. A. Shiral Fernando, Dr. Christopher E. Bunker, Yin Hu, Dr. Pengju G. Luo, and Prof. Ya-Ping Sun.[163]

1.7 References

1. Brus. L.E. *J. Chem. Phys.* **1984**, *80,* 4403-4409.
2. Bawendi, M.G.; Steigerwald, M.L.; Brus, L.E. *Annu. Rev. Phys. Chem.* **1990**,*41*, 477- 496.
3. Smith, A.M., Nie, S. *Acc. Chem. Res*. **2010**, *43,* 190-200.
4. Resch-Genger, U.; Grabolle, M.; Cavaliere-Jaricot, S.; Nitschke, R.; Nann, T. *Nat. Meth.* **2008**, *5*, 763-775.
5. Kairdolf, B.A.; Smith, A.M.; Stokes, T.H.; Wang, M.D.; Young, A.N.; Nie, S. *Annu. Rev. Anal. Chem.***2013**, *6*, 143-162.
6. Sun, Y.-P.; Zhou, B.; Lin, Y.; Wang, W.; Fernando, K.A.S.; Pathak, P.; Meziani, M.J.; Harruff, B.A.; Wang, X.; Wang, H.; Luo, P.G.; Yang, H.; Kose, M.E.; Chen, B.; Veca, L.M.; Xie, S.-Y. *J. Am. Chem. Soc.* **2006**, *128,* 7756-7757.
7. Cao, L.; Wang, X.; Meziani, M.J.; Lu, F.; Wang, H.; Luo, P.G.; Lin, Y.; Harruff, B.A.; Veca, L.M.; Murray, D.; Xie, S.-Y.; Sun, Y.-P. *J. Am. Chem. Soc.* **2007**,*129*, 11318-11319.
8. Bacon, M.; Bradley, S.J.; Nann, T. *Part. Part. Syst. Charact.* **2013**, 1-14. 9. Yoo, J.M.; Kang, J.H.; Hong, B.H. *Chem. Soc. Rev*. **2015**, *44*, 4835-4852.
10. Yu, S.J.; Kang, M.W.; Chang, H.C.; Chen, K.M.; Yu, Y.C. *J. Am. Chem. Soc.* **2005**, *127*, 17604-17605.
11. Mochalin, V.N.; Shenderova, O.; Ho, D.; Gogotsi, Y. *Nat. Nanotechnol.* **2012**, *7*, 11-23.

12. Chico, L.; Lopez Sancho, M.P.; Munoz, M.C. *Phys. Rev. Lett.* **1998**, *81*, 1278-1281.

13. Leturcq, R.; Stampfer, C.; Inderbitzin, K.; Durrer, L.; Hierold, C.; Mariani, E.; Schultz, M.G.; von Oppen, F.; Ensslin, K. *Nat. Phys.* **2009**, *5*, 327-331.

14. Cao, L.; Meziani, M.J.; Sahu, S.; Sun, Y.-P. *Acc. Chem. Res.* **2013**, *46*, 171-180.

15. Luo, P.G; Sahu, S.; Yang, S.-T.; Sonkar, S.K.; Wang, J.; Wang, H.; LeCroy, G.E.; Cao, L.; Sun, Y.-P. *J. Mater. Chem. B* **2013**, *1*, 2116-2127.

16. Luo, P.G.; Yang, F.; Yang, S.-T.; Sonkar, S.K.; Yang, L.; Broglie, J.J.; Liu, Y.; Sun, Y.-P. RSC Adv. 4 (2014) 10791-10807.

17. Wang, Y.; Hu, A. *J. Mater. Chem. C* **2014**, *2*, 6921-6939.

18. Lim, S.Y.; Shen, W.; Gao, Z. *Chem. Soc. Rev*. **2015**, *44*, 362-381.

19. Miao, P.; Han, K.; Tang, Y.; Wang, B.; Lin, T.; Cheng, W. *Nanoscale* **2015**, *7*, 1586- 1595.

20. Zhao, A.; Chen, Z.; Zhao, C.; Gao, N.; Ren, J.; Qu, X. *Carbon* **2015**, *85*, 309-327.

21. Hola, K.; Zhang, Y.; Wang, Y.; Giannelis, E.P.; Zboril, R.; Rogach, A. L. *Nano Today* **2014**, *9*, 590-603.

22. Wang, X.; Cao, L.; Yang, S.-T.; Lu, F.; Meziani, M.J.; Tian, L.; Sun, K.W.; Bloodgood, M.A.; Sun, Y.-P. *Angew. Chem. Int. Ed.* **2010,** *49*, 5310-5314.

23. Anilkumar, P.; Wang, X.; Cao, L.; Sahu, S.; Liu, J.-H.; Wang, P.; Korch, K.; Tackett, II, K.N.; Parenzan, A.; Sun, Y.-P. *Nanoscale*, **2011**, *3*, 2023-2027.

24. Ray, S.C.; Saha, A.; Jana, N. R.; Sarkar, R. *J. Phys. Chem. C* **2009**, *113*, 18546-

18551.

25. Zhou, J.; Booker, C.; Li, R.; Zhou, X.; Sham, T.-K.; Sun, X.; Ding, Z. *J. Am. Chem.Soc.* **2007**, *129*, 744-745.

26. Cao, L.; Anilkumar, P.; Wang, X.; Liu, J.-H.; Sahu, S.; Meziani, M.J.; Myers, E.; Sun, Y.-P. *Can. J. Chem.* **2011**, *89*, 104-109.

27. Sun, H.; Gao, N.; Wu, L.; Ren, J.; Wei, W.; Qu, X. *Chem. Eur. J.* **2013**, *19*, 13362-13368.

28. Qian, Z.; Ma, J.; Shan, X.; Shao, L.; Zhou, J.; Chen, J.; Feng, H. *RSC Adv.* **2013**, *3*, 14571-14579.

29. Tetsuka, H.; Asahi, R.; Nagoya, A.; Okamoto, K.; Tajima, I.; Ohta, R.; Okamoto, A. *Adv. Mater.* **2012**, *24*, 5333-5338.

30. Yang, S.-T.; Wang, X.; Wang, H.F.; Lu, F.S.; Luo, P.G.; Cao, L.; Meziani, M.J.; Liu, J.-H.; Liu, Y.; Chen, M.; Huang, Y.; Sun, Y.-P. *J. Phys. Chem. C* **2009**, *113*, 18110-18114.

31. Sun, Y.-P.; Wang, X.; Lu, F.; Cao, L.; Meziani, M.J.; Luo, P.G.; Gu, L.; Veca, L.M. *J. Phys. Chem. C,* **2008**, *112*, 18295-18298.

32. Li, H.; Chen, L.; Wu, H.; He, H.; Jin, Y. *Langmuir* **2014**, *30*, 15016-15021.

33. Wang, J.; Sahu, S.; Sonkar, S.K.; Tackett II, K.N.; Sun, K.W.; Liu, Y.; Maimaiti, H.; Anilkumar, P.; Sun, Y.-P. *RSC Adv.* **2013**, *3*, 15604-15607.

34. Zhang, Z.; Hao, J.; Zhang, J.; Zhang, B.; Tang, J. *RSC Adv.* **2012**, *2*, 8599-8601.

35. Bhunia, S.K.; Saha, A.; Maity, A.R.; Ray, S.C.; Jana, N.R. *Sci. Rep.* **2013**, *3,* 1473.

36. Choi, Y.; Kim, S.; Choi, M.H.; Ryoo, S.R.; Park, J.; Min, D.H.; Kim, B.S. *Adv.*

Funct. Mater. **2014**, *24*, 5781-5789.

37. Rednic, M.I.; Lu, Z.; Wang, P.; LeCroy, G.E.; Yang, F.; Liu, Y.; Qian, H.; Terec, A.; Veca, L.M.; Lu, F.; Sun, Y.-P. *Chem. Phys. Lett.* **2015**, *639*, 109-113.
38. Peng, H.; Sejdic, J.T. *Chem. Mater.* **2009**, *21*, 5563-5565.
39. Liu, S.-S.; Wang, C.-F.; Li, C.-X.; Wang, J.; Mao, L.-H.; Chen, S. *J. Mater. Chem. C* **2014**, *2*, 6477-6483.
40. Liu, R.; Zhang, J.; Gao, M.; Li, Z.; Chen, J.; Wu, D.; Liu, P. *RSC Adv.* **2015**, *5*, 4428- 4433.
41. Lin, P.-Y.; Hsieh, C.-W.; Kung, M.-L.; Chu, L.-Y.; Huang, H.-J.; Chen, H.-T.; Wu, D.-C.; Kuo, C.-H.; Hsieh, S.-L.; Hsieh, S. *J. Biotechnol.* **2014**, *189*, 114-119.
42. Xu, J.; Lai, T.; Feng, Z.; Weng, X.; Huang, C. *Luminescence* **2015**, *30*, 420-424.
43. Barbosa, C.D.E.S.; Corrêa, J.R.; Medeiros, G.A.; Barreto, G.; Magalhães, K.G.; de Oliveira, A.L.; Spencer, J.; Rodrigues, M.O.; Neto, B.A. *Chem. Eur. J.* **2015**, *21*, 5055-5060.
44. Essner, J.B.; Laber, C.H.; Ravula, S.; Polo-Parada, L.; Baker, G.A. *Green Chem*. **2016**, *18*, 243-250.
45. Zhu, H.; Wang, X.; Li, Y.; Wang, Z.; Yang, F. Yang, X. *Chem. Commun.* **2009**, *34*, 5118- 5120.
46. Gong, N.; Wang, H.; Li, S.; Deng, Y.; Chen, X.; Ye, L.; Gu, W. *Langmuir* **2014**, *30*, 10933- 10939.
47. Liu, H.; He, Z.; Jiang, L.-P.; Zhu, J.-J. *ACS Appl. Mater. Interfaces* **2015**, *7*,

4913-4920.

48. Lu, W.; Gong, X.; Yang, Z.; Zhang, Y.; Hu, Q.; Shuang, S.; Dong, C.; Choi, M. M. *RSC Adv.* **2015**, *5*, 16972-16979.

49. Gao, X.; Lu, Y.; Zhang, R.; He, S.; Ju, J.; Liu, M.; Li, L.; Chen, W. *J. Mater. Chem. C* **2015**, *3*, 2302-2309.

50. Stan, C.S.; Albu, C.; Coroaba, A.; Popa, M.; Sutiman, D. *J. Mater. Chem. C* **2015**, *3*, 789- 795.

51. Zhu, S.; Meng, Q.; Wang, L.; Zhang, J.; Song, Y.; Jin, H.; Zhang, K.; Sun, H.; Wang, H.; Yang, B. *Angew. Chem. Int. Ed.* **2013**, *52*, 3953-3957.

52. Dong, Y.; Wang, R.; Li, H.; Shao, J.; Chi, Y.; Lin, X.; Chen, G. *Carbon* **2012**, *50*, 2810-2815.

53. Wang, C.; Xu, Z.; Cheng, H.; Lin, H.; Humphrey, M. G.; Zhang, C. *Carbon* **2015**, *82*, 87-93. 54. Q. Xu, P. Pu, J. Zhao, C. Dong, C. Gao, Y. Chen, J. Chen, Y. Liu, H. Zhou. *J. Mater. Chem. A* **2015**, *3*, 542-546.

55. Xu, Y.; Jia, X.-H.; Yin, X.-B.; He, X.-W.; Zhang, Y.-K. *Anal. Chem.* **2014**, *86*, 12122- 12129.

56. Qu, K.; Wang, J.; Ren, J.; Qu, X. *Chem. Eur. J.* **2013**, *19*, 7243-7249.

57. Li, C.-L.; Huang, C.-C.; Periasamy, A.P.; Roy, P.; Wu, W.-C.; Hsu, C.-L.; Chang, H.-T. *RSC Adv.* **2015**, *5*, 2285-2291.

58. Yang, Y.; Cui, J.; Zheng, M.; Hu, C.; Tan, S.; Xiao, Y.; Yang, Q.; Liu, Y. *Chem. Commun.* **2012**, *48*, 380-382.

59. Wang, L.; Zhou, H.S. *Anal. Chem.* **2014**, *86*, 8902-8905.

60. Yang, Z.-C.; Wang, M.; Yong, A.M.; Wong, S.Y.; Zhang, X.-H.; Tan, H.; Chang, A.Y.; Li, X.; Wang, J. *Chem. Commun.* **2011**, *47*, 11615-11617.

61. Zou, Y.; Yan, F.; Dai, L.; Luo, Y.; Fu, Y.; Yang, N.; Wun, J.; Chen, L. *Carbon* **2014**, *77*, 1148- 1156.

62. Du, F.; Jin, X.; Chen, J.; Hua, Y.; Cao, M.; Zhang, L.; Li, J.; Zhang, L.; Jin, J.; Wu, C.; Gong, A.; Xu, Q.; Shao, Q.; Zhang, M. *J. Nanopart. Res.* **2014**, *16*, 2720-2728.

63. Wu, Z.Z.L.; Zhang, P.; Gao, M.X.; Liu, C.F.; Wang, W.; Leng, F.; Huang, C.Z. *J. Mater. Chem. B* **2013**, *1*, 2868-2873.

64. Ding, H.; Wei, J.-S.; Xiang, H.-M. *Nanoscale* **2014**, *6*, 13817-13823.

65. Fei, H.; Ye, R.; Ye, G.; Gong, Y.; Peng, Z.; Fan, X.; Samuel, E.L.G.; Ajayan, P.M.; Tour, J.M. *ACS Nano* **2014**, *8*, 10837-10843.

66. Wang, W.; Lu, Y.-C. Huang, H.; Wang, A.-J.; Chen, J.-R.; Feng, J.-J. *Sens. Act. B* **2014**, *202*, 741-747.

67. Hou, Y.; Lu, Q.; Deng, J.; Li, H.; Zhang, Y. *Anal. Chim. Acta* **2015**, *866*, 69-74. 68. G. Jiang, T. Jiang, H. Zhou, J. Yao, X. Kong. *RSC Adv.* **2015**, *5*, 9064-9068.

69. LeCroy, G.E.; Sonkar, S.K.; Yang, F.; Veca, L.M.; Wang, P.; Tackett, K.N.; Yu, J.J.; Vasile, E.; Qian, H.J.; Liu, Y.; Luo, P. G.; Sun, Y.-P. *ACS Nano* **2014**, *8*, 4522-4529.

70. Pan, D.; Zhang, J.; Li, Z; Wu, M. *Adv. Mater.* **2010**, *22*, 734-738.

71. Peng, J.; Gao, W.; Gupta, B. K.; Liu, Z.; Romero-Aburto, R.; Ge, L.; Song, L.; Alemany, L.B.; Zhan, W.; Gao, G.; Vithayathil, S. A.; Kaipparettu, B. A.; Marti,

A. A.; Hayashi, T.; Zhu, J.-J.; Ajayan, P.M. *Nano Lett.* **2012**, *12*, 844-849.

72. Li, Y.; Zhao, Y.; Cheng, H.; Hu, Y.; Shi, G.; Dai, L.; Qu, L. *J. Am. Chem. Soc.* **2012**, *134*, 15- 18.

73. Sun, Y.-P.; Wang, P.; Lu, Z.; Yang, F.; Meziani, M.J.; LeCroy, G.E.; Liu, Y.; Qian, H. *Sci. Rep.* **2015**, *5*, 12354.

74. Bourlinos, A.B.; Bakandritsos, A.; Kouloumpis, A.; Gournis, D.; Krysmann, M.; Giannelis, E.P.; Polakova, K.; Safarova, K.; Hola, K.; Zboril, R. *J. Mater. Chem. C* **2012**, *22*, 23327-23330.

75. Chen, H.; Wang, G.D.; Tang, W.; Todd, T.; Zhen, Z.; Tsang, C.; Hekmatyar, K.; Cowger, T.; Hubbard, R.B.; Zhang, W.; Stickney, J.; Shen, B.; Xie, J. *Adv. Mater.* **2014**, *26*, 6761-6766.

76. Kumar, V. B.; Perelshtein, I.; Lipovsky, A.; Porat, Z.; Gedanken, A. *RSC Adv.* **2015**, *5*, 25533-25540.

77. Guo, Y.; Wang, D.; Liu, X.; Wang, X.; Liu, W.; Qin, W. *New J. Chem.* **2014**, 38, 5861-5867.

78 Li, N.; Liang, X.; Wang, L.; Li, Z.; Li, P.; Zhu, Y.; Song, J. *J. Nanopart. Res.* **2012**, *14*, 1177- 1185.

79. Wang, Y.; Anilkumar, P.; Cao, L.; Liu, J.-H.; Luo, P.G.; Tackett, K.N.; Sahu, S.; Wang, P.; Wang, X.; Sun, Y.-P. *Exp. Bio. Med.* **2011**, *236*, 1231-1238.

80. Liu, R.; Wu, D.; Liu, S.; Koynov, K.; Knoll, W.; Li, Q. *Angew. Chem. Int. Ed.* **2009**, *48*, 4598-4601.

81. Chen, B.; Li, F.; Li, S.; Weng, W.; Guo, H.; Guo, T.; Zhang, X.; Chen, Y.; Huang,

T.; Hong, X. *Nanoscale* **2013**, *5*, 1967-1971.

82 Ruan, S.; Zhu, B.; Zhang, H.; Chen, J.; Shen, S.; Qian, J.; He, Q.; Gao, H. *J. Colloid Interface Sci.* **2014**, *422*, 25-29.

83. Zhang, Y.; Shen, Y.; Teng, X.; Yan, M.; Bi, H.; Morais, P.C. *ACS Appl. Mater. Interfaces* **2015**, *7*, 10201-10212.

84. Liu, J.-H.; Cao, L.; LeCroy, G.E.; Wang, P.; Meziani, M.J.; Dong, Y.; Liu, Y.; Luo, P.G.; Sun, Y.-P. *ACS Appl. Mater. Interfaces* **2015**, *7,* 19439-19445.

85. Tong, G.; Wang, J.; Wang, R.; Guo, X.; He, L.; Qiu, F.; Wang, G.; Zhu, B.; Zhu, X.; Liu, T. *J. Mater. Chem. B* **2015**, *3*, 700-706.

86. Hu, Y.; Yang, J.; Tian, J.; Jia, L.; Yu, J.-S. *RSC Adv.* **2015**, *5*, 15366-15373.

87. Shi, L.; Li, L.; Li, X.; Wen, X.; Zhang, G.; Yang, J.; Dong, C.; Shuang, S. *Nanoscale* **2015**, *7*, 7394-7401.

88. Kong, W.; Liu, R.; Li, H.; Liu, J.; Huang, H.; Liu, Y.; Kang, Z. *J. Mater. Chem. B* **2014**, *2*, 5077-5082.

89. Fan, R.-J.; Sun, Q.; Zhang, L.; Zhang, Y.; Lu, A.-H. *Carbon* **2014**, *71,* 87-93.

90. Yang, L.; Jiang, W.; Qiu, L.; Jiang, X.; Zuo, D.; Wang, D.; Yang, L. *Nanoscale* **2015**, *7,* 6104- 6113.

91. Liu, Q.; Xu, S.; Niu, C.; Li, M.; He, D.; Lu, Z.; Ma, L.; Na, N.; Huang, F.; Jiang, H. *Biosens. Bioelectron.* **2015**, 64, 119-125.

92. Yang, X.; Yang, X.; Li, Z.; Li, S.; Han, Y.; Chen, Y.; Bu, X.; Su, C.; Xu, H.; Jiang, Y.; Lin, Q. *J. Colloid Interface Sci.* **2015**, *456*, 1-6.

93. Nandi, S.; Ritenberg, M.; Jelinek, R. *Analyst* **2015**, *140,* 4232-4237.

94. Kasibabu, B.S.; D'Souza, S.L.; Jha, S.; Kailasa, S.K. *J. Fluoresc.* **2015**, *25*, 803-810.

95. Mehta, V.N.; Jha, S.; Kailasa, S.K. *Mater. Sci. Eng. C Mater. Biol. Appl.* **2014**, *38*, 20-27.

96. Mehta, V.N.; Jha, S.; Basu, H.; Singhal, R.K.; Kailasa, S.K. *Sensor Actuat. B-Chem.* **2015**, *213*, 434-443.

97. Jin, X.; Sun, X.; Chen, G.; Ding, L.; Li, Y.; Liu, Z.; Wang, Z.; Pan, W.; Hu, C.; Wang, J. *Carbon* **2015**, 81, 388-395.

98. Wang, Z.; Qu, Y.; Gao, X.; Mu, C.; Bai, J.; Pu, Q. *Mater. Lett.* **2014**, *129*, 122-125.

99. Yang, S.-T.; Cao, L.; Luo, P.G.; Lu, F.; Wang, X.; Wang, H.; Meziani, M.J.; Liu, Y.; Qi, G.; Sun, Y.-P. *J. Am. Chem. Soc.* **2009**, *131*, 11308-11309.

100. Cao, L.; Yang, S.-T.; Wang, X.; Luo, P.G.; Liu, J.-H.; Sahu, S.; Liu, Y.; Sun, Y.-P. *Theranostics* **2012**, 2, 295-301.

101. Wu, L.; Luderer, M.; Yang, X.; Swain, C.; Zhang, H.; Nelson, K.; Stacy, A.J.; Shen, B.; Lanza, G.M.; Pan, D. *Theranostics* **2013**, *3*, 677-686.

102. He, H.; Wang, X.; Feng, Z.; Cheng, T.; Sun, X.; Sun, Y.; Xia, Y.; Wang, S.; Wang, J.; Zhang, X. *J. Mater. Chem. B* **2015**, *3*, 4786-4789.

103. Sharker, S.M.; Kim, S.M.; Lee, J.E.; Jeong, J.H.; In, I.; Lee, K.D.; Lee, H.; Park, S.Y. *Nanoscale* **2015**, *7*, 5468-5475.

104. Wang, Y.; Meng, Y.; Wang, S.; Li, C.; Shi, W.; Chen, J.; Wang, J.; Huang, R. *Small* **2015**, *11*, 3575-3581.

105. Fu, C.; Qiang, L.; Liang, Q.; Chen, X.; Li, L.; Liu, H.; Tan, L.; Liu, T.; Ren, X.;

Meng, X. *RSC Adv.* **2015**, *5*, 46158-46162.

106. Zhou, N.; Hao, Z.; Zhao, X.; Maharjan, S.; Zhu, S.; Song, Y.; Yang, B.; Lu, L. *Nanoscale* **2015**, *7*, 15635-15642.
107. Ruan, S.; Wan, J.; Fu, Y.; Han, K.; Li, X.; Chen, J.; Zhang, Q.; Shen, S.; He, Q.; Gao, H. *Bioconjugate Chem.* **2014**, *25*, 1061-1068.
108. Mukherjee, P.; Misra, S.K.; Gryka, M.C.; Chang, H.H.; Tiwari, S.; Wilson, W.L.; Scott, J.W.; Bhargava, R.; Pan, D. *Small* **2015**, *11*, 4691-4703.
109. Huang, X.; Zhang, F.; Zhu, L.; Choi, K.Y.; Guo, N.; Guo, J.; Tackett, K.N.; Anilkumar, P.; Liu, G.; Quan, Q.; Choi, H.S.; Niu, G.; Sun, Y.-P.; Lee, S.; Chen, X. *ACS Nano* **2013**, *7*, 5684-5693.
110. Huang, P.; Lin, J.; Wang, X.; Wang, Z.; Zhang, C.; He, M.; Wang, K.; Chen, F.; Li, Z.; Shen, G.; Cui, D.; Chen, X. *Adv. Mater.* **2012**, *4*, 5104-5110.
111. Srivastava, S.; Awasthi, R.; Tripathi, D.; Rai, M.K.; Agarwal, V.; Agrawal, V.; Gajbhiye, N.S.; Gupta, R.K. *Small* **2012**, *8*, 1099-1109.
112. Kang, Y.F.; Li, Y.H.; Fang, Y.W.; Xu, Y.; Wei, X.M.; Yin, X.B. *Sci. Rep.* **2015**, *5*, 11835.
113. Fahmi, M.Z.; Chen, J.-K.; Huang, C.-C.; Ling, Y.-C.; Chang, J.-Y. *J. Mater. Chem. B* **2015**, *3*, 5532-5543.
114. Yuan, M.; Zhong, R.; Gao, H.; Li, W.; Yun, X.; Liu, J.; Zhao, X.; Zhao, G.; Zhang, F. *Appl. Surf. Sci.* **2015**, *355*, 1136-1144.
115. Parvin, N.; Mandal, T.K.; Roy, P. *J. Nanosci. Nanotechnol.* **2013**, *13*, 6499-6505.

116. He, Q.; Ma, M.; Wei, C.; Shi, J. *Biomaterials* **2012**, *33*, 4392-4402.

117. Mitra, S.; Chandra, S.; Laha, D.; Patra, P.; Debnath, N.; Pramanik, A.; Pramanik, P.; Goswami, A. *Mater. Res. Bull.* **2012**, *47*, 586-594.

118. Wang, Q.; Huang, X.; Long, Y.; Wang, X.; Zhang, H.; Zhu, R.; Liang, L.; Teng, P.; Zheng, H. *Carbon* **2013**, *59*, 192-199.

119. Lai, C.-W.; Hsiao, Y.-H.; Peng, Y.-K.; Chou, P.-T. *J. Mater. Chem.* **2012**, *22*, 14403-14409.

120. Ding, H.; Du, F.; Liu, P.; Chen, Z.; Shen, J. *ACS Appl. Mater. Interfaces* **2015**, *7*, 6889- 6897.

121. Wang, Z.; Liao, H.; Wu, H.; Wang, B.; Zhao, H.; Tan, M. *Anal. Methods* **2015**, *7*, 8911-8917.

122. Matai, I.; Sachdev, A.; Gopinath. P. *ACS Appl. Mater. Interfaces* **2015**, *7*, 11423-11435. 123. M.P. Sk, U. Goswami, S.S. Ghosh, A. Chattopadhyay. *J. Mater. Chem. B* **2015**, *3*, 5673-5677.

124. Cheng, L.; Li, Y.; Zhai, X.; Xu, B.; Cao, Z.; Liu, W. *ACS Appl. Mater. Interfaces* **2014**, *6*, 20487-20497.

125. Wang, Q.; Zhang, C.; Shen, G.; Liu, H.; Fu, H.; Cui, D. *J. Nanobiotechnology* **2014**, *12*, 58.

126. Hu, L.; Sun, Y.; Li, S.; Wang, X.; Hu, K.; Wang, L.; Liang, X.-J.; Wu, Y. *Carbon* **2014**, *67*, 508-513.

127. Kleinauskas, A.; Rocha, S.; Sahu, S.; Sun, Y.-P.; Juzenas, P. *Nanotechnol.* **2013**, *24*, 325103.

128. Wang, H.; Cao, G.; Gai, Z.; Hong, K.; Banerjee, P.; Zhou, S. *Nanoscale* **2015**, *7*, 7885-7895.

129. Wang, J.; Zhang, Z.; Zha, S.; Zhu, Y.; Wu, P.; Ehrenberg, B.; Chen, J. Y. *Biomaterials* **2014**, *35*, 9372-9381.

130. Das, B.; Dadhich, P.; Pal, P.; Srivas, P.K.; Bankoti, K.; Dhara, S. *J. Mater. Chem. B* **2014**, *2*, 6839-6847.

131. Zhao, S.; Lan, M.; Zhu, X.; Xue, H.; Ng, T.W.; Meng, X.; Lee, C.S.; Wang, P.; Zhang, W. *ACS Appl. Mater. Interfaces* **2015**, *7*, 17054-17060.

132. Ge, J.; Jia, Q.; Liu, W.; Guo, L.; Liu, Q.; Lan, M.; Zhang, H.; Meng, X.; Wang, P. *Adv. Mater.* **2015**, *27*, 4169-4177.

133. Liu, H.; Wang, Q.; Shen, G.; Zhang, C.; Li, C.; Ji, W.; Wang, C.; Cui, D. *Nanoscale Res. Lett.* **2014**, *9*, 1-11.

134. Tang, J.; Kong, B.; Wu, H.; Xu, M.; Wang, Y.; Wang, Y.; Zhao, D.; Zheng, G. *Adv. Mater.* **2013**, *25*, 6569-6574.

135. Cao, L.; Sahu, S.; Anilkumar, P.; Bunker, C.E.; Xu, J.; Fernando, K.A.S.; Wang, P.; Guliants, E.A.; Tackett, K.N.; Sun, Y.-P. *J. Am. Chem. Soc.* **2011**, *133*, 4754-4757.

136. Sahu, S.; Liu, Y.; Wang, P.; Bunker, C.E.; Fernando, K.A.S.; Lewis, W.K.; Guliants, E.A.; Yang, F.; Wang, J.; Sun, Y.-P. *Langmuir* **2014**, *30*, 8631-8636.

137. Sahu, S.; Cao, L.; Meziani, M.J.; Bunker, C.E.; Fernando, K.A.S.; Wang, P.; Sun, Y.-P. *Chem. Phys. Lett.* **2015**, *634*, 122-128.

138. Wang, X.; Cao, L.; Lu, F.; Meziani, M.J.; Li, H.; Qi, G.; Zhou, B.; Harruff, B.A.;

Kermarrec, F.; Sun, Y.-P. *Chem. Commun.* **2009**, 3774-3776.

139. Zhang, H.; Huang, H.; Ming, H.; Li, H.; Zhang, L.; Liu, Y.; Kang, Z. *J. Mater. Chem.* **2012**, *22*, 10501-10506.

140. Xu, J.; Sahu, S.; Cao, L.; Bunker, C.E.; Peng, G.; Liu, Y.M.; Fernando, K.A.S.; Wang, P.; Guliants, E.A.; Meziani, M.J.; Qian, H.J.; Sun, Y.-P. *Langmuir* **2012**, *28*, 16141-16147.

141. Strauss, V.; Margraf, J.T.; Dolle, C.; Butz, B.; Nacken, T.J.; Walter, J.; Bauer, W.; Peukert, W.; Spiecker, E.; Clark, T.; Guldi, D.M. *J. Am. Chem. Soc.* **2014**, *136*, 17308-17316.

142. Mondal, S.; Seth, S.K.; Gupta, P.; Purkayastha, P. *J. Phys. Chem. C* **2015**, *119*, 25122-25128.

143. Mondal, S.; Das, T.; Ghosh, P.; Maity, A.; Mallick, A.; Purkayastha, P. *Mater. Lett.* **2015**, *141*, 252-254.

144. Gao, Z.; Wang, L.; Su, R.; Huang, R.; Qi, W.; He, Z. *Biosens. Bioelectron.* **2015**, *70*, 232- 238.

145. Choi, H.; Ko, S.-J.; Choi, Y.; Joo, P.; Kim, T.; Lee, B.R.; Jung, J.-W.; Choi, H.J.; Cha, M.; Jeong, J.-R.; Hwang, I.-W.; Song, M.H.; Kim, B.-S.; Kim, J.Y. *Nat. Photon.* **2013**, *7*, 732-738.

146. Tu, W.; Zhou, Y.; Zou, Z. *Adv. Mater.* **2014**, *26*, 4607-4626.

147. Fernando, K.A.S.; Sahu, S.; Liu, Y.; Lewis, W.K.; Guliants, E.A.; Jafariyan, A.; Wang, P.; Bunker, C.E.; Sun, Y.-P. *ACS Appl. Mater. Interfaces* **2015**, *7*, 8363-8376.

148. Choi, Y.; Ryu, G.H.; Min, S.H.; Lee, B.R.; Song, M.H.; Lee, Z.; Kim, B.-S. *ACS Nano* **2014**, *8*, 11377-11385.

149. Mazzier, D.; Favaro, M.; Agnoli, S.; Silvestrini, S.; Granozzi, G.; Maggini, M.; Moretto, A. *Chem. Commun.* **2014**, *50*, 6592-6595.

150. Habisreutinger, S.N.; Schmidt-Mende, L.; Stolarczyk, J.K. *Angew. Chem. Int. Ed.* **2013**, *52*, 7372-7408.

150. Hong, J.; Zhang, W.; Ren, J.; Xu, R. *Anal. Methods* **2013**, *5*, 1086-1097.

152. Shkrob, I.A.; Marin, T.W.; He, H.; Zapol. P. *J. Phys. Chem. C* **2012**, *116*, 9450-9460.

153. Li, H.; Zhang, X.; MacFarlane, D.R. *Adv. Energy Mater.* **2015**, *5*, 1401077.

154. Dong, Y.; Zhou, N.; Lin, X.; Lin, J.; Chi, Y.; Chen, G. *Chem. Mater.* **2010**, *22*, 5895-5899.

155. Dong, Y.; Chen, C.; Lin, J.; Zhou, N.; Chi, Y.; Chen, G. *Carbon* **2013**, *56*, 12-17.

156. Wang, L.; Chen, X.; Lu, Y.; Liu, C.; Yang, W. *Carbon* **2015**, *94*, 472-478.

157. Wu, L.; Wang, J.; Ren, J.; Li, W.; Qu, X. *Chem. Commun.* **2013**, *49*, 5675-5677.

158. Su, M.; Liu, H.; Ge, L.; Wang, Y.; Ge, S.; Yu, J.; Yan, M. *Electrochim. Acta* **2014**, *146*, 262-269.

159. Xie, S.; Su, H.; Wei, W.; Li, M.; Tong, Y.; Mao, Z. *J. Mater. Chem. A* **2014**, *2*, 16365-16368.

160. Nan, F.; Kang, Z. H.; Wang, J. L.; Shen, M. R.; Fang, L. *Appl. Phys. Lett.* **2015**, *106*, 153901-153905.

161. Wang, F.; Chen, Y.-H.; Liu, C.-Y.; Ma, D.-G. *Chem. Commun.* **2011**, *47*, 3502-

3504.

162. Veca, L. M.; Diac, A.; Mihalache, I.; Wang, P.; LeCroy, G. E.; Pavelescu, E. M.; Gavrila, R.; Vasile, E.; Terec, A.; Sun, Y.-P. *Chem. Phys. Lett.* **2014**, *613*, 40-44.

163. LeCroy, G. E.; Yang, S.-T.; Yang, F.; Liu, Y.; Fernando, K. A. S.; Bunker, C. E. Hu, Y.; Luo, P. G.; Sun, Y.-P. *Coord. Chem. Rev.* **2016**, *320*, 66-81.

CHAPTER TWO

TOWARDS STRUCTURALLY DEFINED CARBON DOTS AS ULTRA-COMPACT FLUORESCENT PROBES

2.1 Introduction

Fluorescent semiconductor nanocrystals, generally referred to as quantum dots (QDs) for the quantum confinement effect in these nanomaterials, have attracted much attention for their serving as optical probes in biomedical and other applications.[1,2] Among the most popular QDs, some of which are now commercially available, are those based on cadmium salts, especially CdSe/ZnS core-shell nanostructures with various surface coatings for organic or aqueous compatibilities.[3-5] Strong cases have been made in the literature on using QDs to replace organic dyes and in some applications genetically encoded fluorescent tags.[1,2,6] Among many widely considered advantageous properties of conventional semiconductor QDs, a unique feature due to the quantum confinement effect is the beautiful display of different fluorescence colors for QDs of different sizes. However, the defined color-size dependence also limits any dot size variation for a specific fluorescence color. For the more established CdSe/ZnS QDs with the necessary surface coating (for solubility and/or compatibility needs) as fluorescence probes, the probe size profiles are typically on the order of 10 nm in diameter.[6-8] Therefore, there has been increasing interest in a reduction of the probe size, targeting similar size profiles to those of many commonly used fluorescent proteins (green fluorescent protein, or GFP, for example),[9] for which strategies such as the use of a thinner coating on the QD surface have been pursued.[1,10-12]

In terms of application potential, ultra-compact probes (referring to structurally compact and very small in the overall probe size) offer additional and sometimes unique opportunities, with specific biologically relevant examples including their less interference with or perturbation to the biological events in the cells being probed[13-15] and more favorable renal clearance, for which a threshold probe size around 5.5 nm was determined.[16] There were also studies in which issues with the use of larger nanoparticles were identified, such as their accumulation in leaky vasculature or in solid tumors, thus potentially inhibiting clearance and increasing the likelihood of long-term toxicity effect.[17-19] Most of the recently pursued ultra-compact probes were based on metal or metal oxide nanoparticles, especially sub-5 nm gold nanoparticles[20,21] and gadolinium or iron oxide nanoparticles for MRI tracking applications.[22,23] As a demonstration on the critical effect of probe size, gold nanoparticles of 2.4 nm in diameter were found in the cell nucleus, 5.5-8.2 nm in the cytoplasm, and 16 nm or larger mostly outside the cell.[21]

Carbon dots have emerged as a new platform of QD-like fluorescent nanomaterials,[24] with competitive optical performance under one- and multiphoton excitation conditions and their being generally nontoxic in nature.[25-39] Presently more fluorescent carbon dots are those of small carbon nanoparticles with the particle surface passivated by chemical functionalization with oligomeric or polymeric species. For example, with the oligomeric poly(ethylene glycol) diamine (PEG_{1500N}) as surface passivation agent, the PEG_{1500N} carbon dots exhibited fluorescence quantum yields of more than 50%.[34] Mechanistically, both the optical absorption and fluorescence emissions in carbon dots are not band gap in origin, due instead to π-plasmon and radiative recombination of the surface-confined electrons and holes, respectively,[39,40] different from those in conventional semiconductor QDs. The absence of any theoretically defined fluorescence color dot size relationships in carbon dots may actually be exploited as a unique advantage in the size reduction toward having carbon dots serve as ultra-compact QD-like fluorescence probes. More specifically, there has been extensive recent discussion on the push to reduce the sizes of fluorescence probes (mostly those based on conventional semiconductor QDs with the necessary surface coating) to less than 5 nm in diameter.[9] In this regard, the PEG_{1500N}-carbon dots referred to above had an average core carbon nanoparticle size of about 3 nm,[34] but the overall dot profiles were on average significantly larger due to the use of the relatively large PEG_{1500N} molecules (average molecular weight ∼1500) for carbon particle surface passivation via chemical functionalization. The expectation was such that a reduction in the size of the surface functionalization molecules would not only add less to the overall profile (the core carbon nanoparticle surface passivation layer) of each carbon dot but also be more selective toward the solubilization of smaller carbon nanoparticles in the dot synthesis, resulting in smaller carbon dots and their corresponding fluorescence probes.

Here we report on carbon dots of less than 5 nm in overall dot diameter with the use of 2,2'-(ethylenedioxy)-bis(ethylamine) (EDA, $H_2NCH_2CH_2OCH_2CH_2OCH_2CH_2NH_2$) molecules for carbon particle surface functionalization passivation (Figure 2.1). The EDA-carbon dots were found to be brightly fluorescent, especially over the GFP spectral range. These aqueous soluble smaller carbon dots also enabled more quantitative characterizations, including the use of solution-phase NMR techniques, and the results suggested that the dot structures were relatively simple and better defined. The potential for these smaller carbon dots to serve as fluorescence probes of overall sizes comparable to those of fluorescent proteins (Figure 2.1) [41-43] is also discussed.

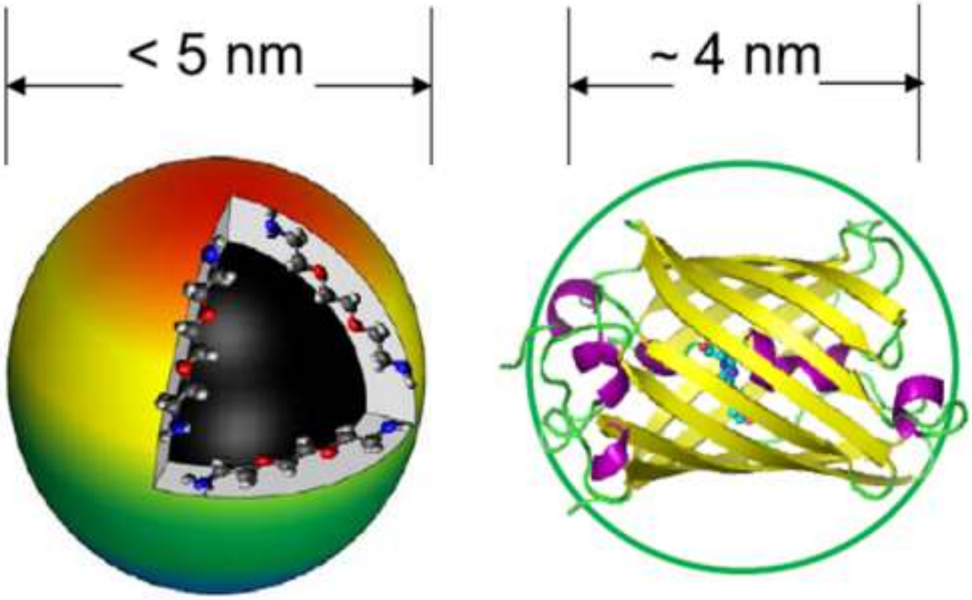

Figure 2.1 Cartoon illustration (left) of and EDA-carbon dot, which is essentially a special "core-shell" nanostructure with a small carbon nanoparticle as the core and a soft shell of tethered EDA molecules, and (right) green fluorescent protein with the size profile highlighted.

2.1 Experimental

Materials. Carbon nanopowder (<50 nm, purity 99+%), 13C powders (isotopic purity 99%), and 2,2’-(ethylenedioxy)bis- (ethylamine) were purchased from Sigma-Aldrich, and fine extruded graphite rods (carbon content 99+%) from Graphite store, Inc. Thionyl chloride (>99%) was obtained from Alfa Aesar, nitric acid from VWR, and Sephadex G-100 gel from GE Healthcare. Dialysis membrane tubing (cutoff molecular weight 500) was supplied by Spectrum Laboratories. Water was deionized and purified by being passed through a Labconco Water- Pros water purification system.

Measurements. Optical absorption spectra were recorded on a Shimadzu UV2501-PC spectrophotometer. Fluorescence spectra were measured on a Jobin-Yvon emission spectrometer equipped with a 450 W xenon source, Gemini-180 excitation and Tirax-550 emission monochromators, and a photoncounting detector (Hamamatsu R928P PMT at 950 V). The nonlinear instrumental responses at both excitation and emission sides of the spectrometer were corrected by using separately determined correction factors with respect to different excitation and emission wavelengths.48 Raman spectra were obtained on a Jobin-Yvon T64000 Raman spectrometer equipped with a Melles-Griot He-Ne laser (35 mW) for 632.8 nm excitation, a triple monochromator, a liquid-nitrogen- cooled symphony detector, and an Olympus BX-41 microscopy for sampling. FT-IR spectra were collected on a Thermo- Nicolet Nexus 670 FT-IR/NIR spectrometer, with the samples for analysis deposited on the surface of a KBr crystal pellet. NMR measurements were performed on a Bruker Avance 500 NMR spectrometer. Atomic force microscopy images were acquired in the acoustic ac mode on a Molecular Imaging

PicoPlus AFM system equipped with a multipurpose scanner and a Nano-World point probe NCH sensor. The height profile analysis was assisted by using the SjPIP software distributed by Image Metrology. Transmission electron microscopy images were obtained on a Hitachi H9500 TEM system.

^{13}C-Enriched Carbon Nanoparticles. The carbon soot containing the nanoparticles was obtained in the arc-discharge production, as reported previously.[31] A graphite rod was made hollow and then filled with a mixture of the commercially supplied 13C powders and graphite cement. The discharge chamber was purged with helium and then stabilized to 1 atm (101.325 kPa) in a helium atmosphere. The rods were vaporized with a direct current of 70 A (28 V). The as-produced carbon soot was collected and dispersed in dimethylformamide (DMF) with ultrasonication (Crest Ultrasonics, model 950 DA, 50-60 Hz) for 24 h. The DMF was removed by evaporation, and the carbon particles were recovered. The ^{13}C content in the sample was estimated in terms of Raman spectral shifts, as validated previously.[31]

EDA-Carbon Dots. The precursor carbon nanoparticles were refluxed in an aqueous nitric acid solution (2.6 M) for 12 h, dialyzed against fresh water, and then centrifuged at 1000g to retain the supernatant. The recovered sample was refluxed in neat thionyl chloride for 12 h. Upon the removal of excess thionyl chloride, the sample (50 mg) was mixed well with carefully dried EDA liquid (600 mg) in a round-bottom flask, heated to 120 ^{o}C, and vigorously stirred under nitrogen protection for 3 days. The reaction mixture back at room temperature was dispersed in water and then centrifuged at 20800g to retain the supernatant. The solution was filtrated through a Sephadex G-100 column (packed in house with commercially supplied gel sample),[39,44] and the colored section with high fluorescence quantum yields was collected, followed by dialysis against fresh water (dialysis tubing cutoff molecular weight 500) to yield an aqueous solution of the EDA-carbon dots. 1H NMR (500 MHz, D2O) δ 3.67 (m, br), 3.54 (m, br), 3.17 (m, br), 3.07 (m, br), 3.03 (m, br) ppm; 13C NMR (125 MHz, D2O) δ 164.76, 71.78, 70.33, 69.69, 67.85, 40.93, 39.45 ppm. The 13C-enriched EDA-carbon dots were prepared from the 13C-enriched precursor carbon nanoparticles by following the same experimental procedures. 1H NMR (500 MHz, D2O) δ 3.65 (m, br), 3.53 (m, br), 3.17 (m, br), 2.98 (m, br), 2.91 (m, br) ppm; 13C NMR (125 MHz, D2O) δ 171.12, 164.81, 164.63, 161.56, 71.75, 70.34, 69.65, 69.61, 68.81, 40.98, 39.64 ppm. For the gold metal doping of the EDA-carbon dots (for TEM imaging), an aqueous dispersion of the EDA-carbon dots was mixed with an aqueous solution of the Au(III) compound $HAuCl_4$, and the mixture was irradiated with visible light.[46] The doping level was kept relatively low, as monitored in terms of the gold plasmon absorption band.

2.3 Results and Discussion

Precursor carbon nanoparticles were obtained from the commercially supplied sample of carbon nanopowders in a procedure that included refluxing the as-supplied sample in an aqueous nitric acid solution, dialysis, centrifuging to retain the supernatant (with a higher population of smaller particles), and then the removal of water.[34] The nanoparticles were functionalized with EDA molecules under amidation reaction conditions. Briefly, the sample of carbon nanoparticles was first refluxed in neat thionyl chloride and then mixed well with carefully dried EDA (liquid at ambient temperature). The mixture was heated to 120 °C and vigorously stirred for the reaction under nitrogen protection. The reaction mixture was dispersed in water for centrifugation to retain the supernatant, followed by purification through a gel column (packed in-house by using commercially supplied Sephadex G-100 gel)[44] to isolate the targeted carbon dots (EDA-functionalized carbon nanoparticles, Figure 2.1) of bright fluorescence emissions. The carbon dots sample was further purified in dialysis against fresh water to remove residual small molecular species including free EDA molecules, yielding a clean aqueous solution of the purified carbon dots (designated as EDA-carbon dots). According to results from the quantitative optical absorption measurement of the EDA-carbon dots (Figure 2.2), in which the amount of core carbon nanoparticles was calculated with the separately determined molar absorptivity values[45] and the amount was compared to that of the precursor carbon nanoparticles, the estimated overall reaction yield was around 10% (the percentage of the precursor carbon nanoparticles converted to the core carbon nanoparticles in the final purified EDA-carbon dots).

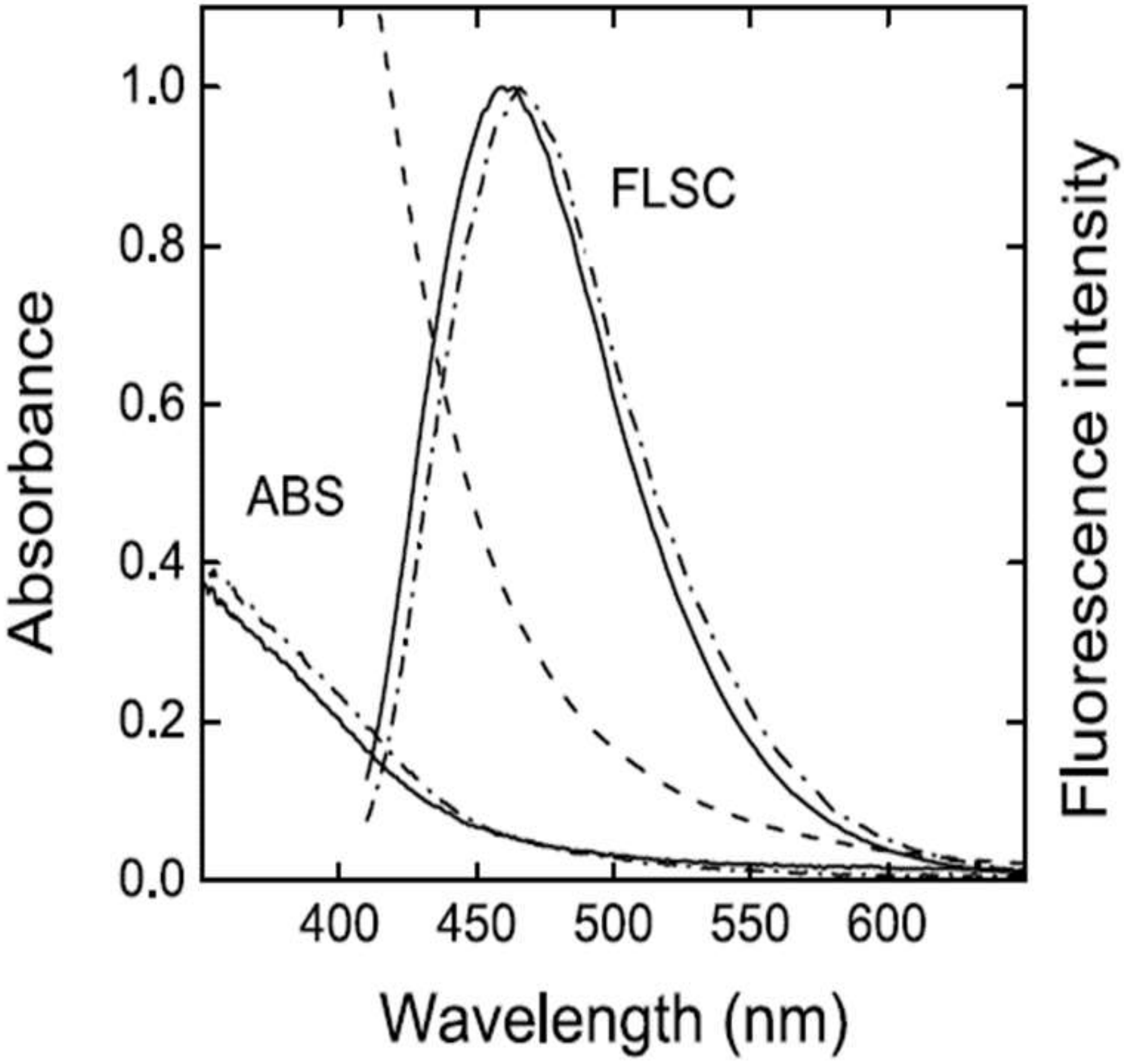

Figure 2.2 Absorption (ABS) and fluorescence (FLSC, 400 nm excitation) spectra of the EDA-carbon dots (- and - - - for ABS of a concentrated solution) and the ^{13}C-enriched EDA-carbon dots (-·-·-).

The EDA-carbon dots were characterized by using atomic force microscopy (AFM) for the determination of overall dot sizes. The AFM specimen was prepared by dropping an aqueous solution of a selected dot concentration onto the mica surface, followed by the evaporation of water. Shown in Figure 2.3 are representative AFM imaging results for the EDA-carbon dots, in which according to height analyses an overwhelming majority of the dots were less than 5 nm in diameter. Multiple AFM images were used in the same height analyses to produce a data set for about 280 dots, and as also shown in Figure 2.3, the statistical analysis with a simple Gaussian function yielded an average dot size of 4.1 nm. The results are consistent with the expectation that the EDA-carbon dots should be smaller than the PEG_{1500N}-carbon dots, which averaged around 5 nm in diameter according to previous investigations.[34,39] The conclusion is also supported by the results from transmission electron microscopy (TEM) imaging experiments.

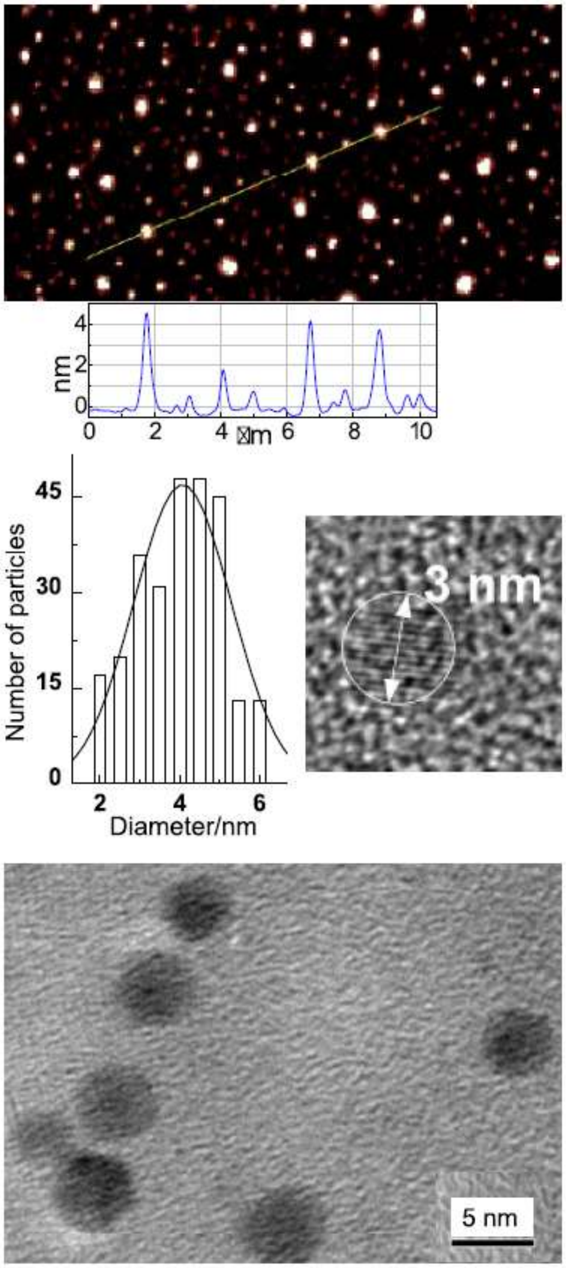

Figure 2.3 (Top) AFM imaging results for the EDA-carbon dots on mica substrate, with height profiles of some dots along the line highlighted. (Middle) (left) Size distribution based on height analyses of multiple AFM images, fitted with the Gaussian distribution curve, and (right) a high-resolution TEM image illustrating the carbon core in a carbon dot.[34] (Bottom) TEM image of the gold-doped EDA-carbon dots.

For the PEG_{1500N}-carbon dots reported previously, the TEM imaging enabled the size characterization of the core carbon nanoparticles, averaging 3 nm in diameter,[34] as the organic surface functionalization molecules (PEG_{1500N}) were largely transparent in contrast with the carbon core. For some dots in which the core carbon nanoparticles were more crystalline, the size measurements could also benefit from the more defined lattice fringes (Figure 2.3). However, in order to apply the TEM imaging to the determination of overall size profiles that include the surface passivation layer in carbon dots (Figure 2.1), the approach of doping the dots with materials of high electron density has found some success.[46] In this work the EDA-carbon dots were doped with gold metal in a simple photolysis procedure, with visible-light photoirradiation of the dots in an aqueous solution of the Au(III) compound $HAuCl_4$.[46] The gold-doped dots were readily detected in TEM imaging for the improved dispersion into individual dots on the TEM grid, in addition to the increased electron densities. The TEM images (Figure 2.3) thus obtained were consistent with the AFM results (Figure 2.3), which suggested that the EDA-carbon dots should be mostly less than 5 nm in diameter for the overall dot profiles including the surface passivation layer of tethered EDA molecules.

The optical transitions in carbon dots are due to the π-plasmon absorption of the core carbon nanoparticles, namely, the "chromophores" in the dots.[45] The absorption (Figure 2.2) is relatively strong, with the observed per-carbon molar absorptivities of 50-100 $M_{C\ atom}^{-1}$ cm^{-1} in the 400-450 nm region, where $M_{C\ atom}$ denotes molar concentration in terms of carbon atoms in the core carbon nanoparticles (assuming no other elements) for the carbon dots in a solution. For a carbon core size of 3 nm in diameter, the number of carbon atoms in the core was estimated to be around 1700, thus per-dot molar absorptivities of approximately 85 000-170 000 $M_{C\text{-particle}}^{-1}$ cm^{-1} for the same wavelength region, where $M_{C\text{-particle}}$ refers to the molar concentration of the carbon dots with 3 nm diameter carbon cores. The per-dot molar absorptivities should obviously be sensitive to the dot diameter. For example, the EDA-carbon dots with a carbon core of 3.5 nm in diameter would have absorptivities up to approximately 250 000 $M_{C\text{-particle}}^{-1}$ cm^{-1}. These estimates accounted for only carbons in the nanoparticle cores (again the visible chromophores) in the carbon dots, with the carbons in EDA molecules excluded for their being non-absorptive in the visible spectral region.

The fluorescence spectrum of the EDA-carbon dots in aqueous solution, with excitation at 400 nm, is also shown in Figure 2.2. It is relatively broad, similar to those of carbon dots with other surface-functionalization molecules. The green fluorescence emissions are associated with quantum yields around 30%, determined in reference to 9,10-bis(phenylethynyl)anthracene as a standard (quantum yield of unity, calibrated against the quinine sulfate standard).[47,48] The fluorescence properties of the EDA-carbon dots were apparently stable with respect to further sample purification effort on removing any loosely attached EDA molecules from the carbon dots in vigorous dialysis. Both the fluorescence spectrum and quantum yield remained the same after the repeated dialysis procedures, suggesting that the aqueous dispersed EDA-carbon dots were structurally robust, with the EDA functionalization on the dot surface being either covalent or associated with bonding-like strong interactions. More generally, the EDA-carbon dots are similar to the more extensively studied PEG_{1500N}-carbon dots in terms of excellent chemical and photochemical stabilities.

In molecular imaging and related uses, the performance of fluorescence probes is often measured in terms of the relative brightness, expressed as (molar absorptivity) X (fluorescence quantum yield). For the EDA-carbon dots of the carbon core at 3 nm in diameter, the corresponding fluorescence robes of less than 5 nm in diameter and with green fluorescence emissions could have a relative brightness as high as 50 000. As a rough comparison, the relative brightness values quoted in the literature on the commonly used GFP and derivatives are on the order of 30 000.[49]

Structurally an EDA-carbon dot is simply a small carbon nanoparticle with a thin layer of tethered EDA molecules on the particle surface (Figure 2.1). The aqueous dispersion of EDA-carbon dots is solution equivalent in appearance and in properties, suitable for solution-phase NMR characterizations. The ^{1}H NMR spectrum of the EDA-carbon dots (Figure 2.4), due to the tethered EDA molecules on the dot surface, shows broader signals than those in the spectrum of free EDA, consistent with the reduced mobility of the EDA molecules attached to carbon nanoparticles. Also consistent with the attachment is the lower symmetry for the particle-bound EDA species, with ^{1}H NMR signals for the three sets of protons in free EDA (Figure 2.4, γ: singlet, β: triplet, and α: triplet) split into multiple peaks in two groups, one for γ and β protons and the other for α protons (Figure 2.4). The relative integrations between $\gamma+\beta$ and α proton signals are about 2.3 to 1, larger than the theoretical ratio of 2 to 1. A question was then on the assignment of the signal around 3.5 ppm, namely, the possibility for its being due to α protons. Such a possibility could be eliminated on the basis of correlation spectroscopy (COSY) results, which clearly identified the coupling of the broad 3.5 ppm signal with those of the α protons. Therefore, an alternative explanation is such that the NMR signal integration for the α protons is distorted by these protons being closer to the core carbon nanoparticles in the carbon dots. The ^{13}C NMR spectrum of the EDA-carbon dots (Figure 2.4) shows similarly two groups of peaks, again one for γ and β carbons and the other for α carbons, but no meaningful peaks that could be assigned to the core carbon nanoparticles. Results from the FT-IR characterization (Figure 2.5) were generally consistent with the NMR results. The carbon nanoparticles before the EDA functionalization exhibited only weak absorptions in the 1550-1750 cm^{-1} region, suggesting the presence but low population of oxygen-containing moieties (such as carboxylic acids). These absorption features could still be identified in the spectrum of the EDA-carbon dots, although only to a rather limited extent due to their overlapping with the more substantial absorption of EDA over the same spectral region (1400-1700 cm^{-1}).[50,51] Overall the FT-IR spectrum of the EDA-carbon dots is similar to that of EDA molecules in terms of major spectral features, but with some peak broadening probably due to the association of EDA with carbon nanoparticles in the carbon dots. Therefore, the FT-IR results were not as useful as desired in the elucidation of structural details, but overall did seem to suggest that there were no significant changes to the EDA chemical structure, such as those that might create visible chromophores, as a result of the functionalization chemistry (probably as expected for the rather mild reaction conditions).

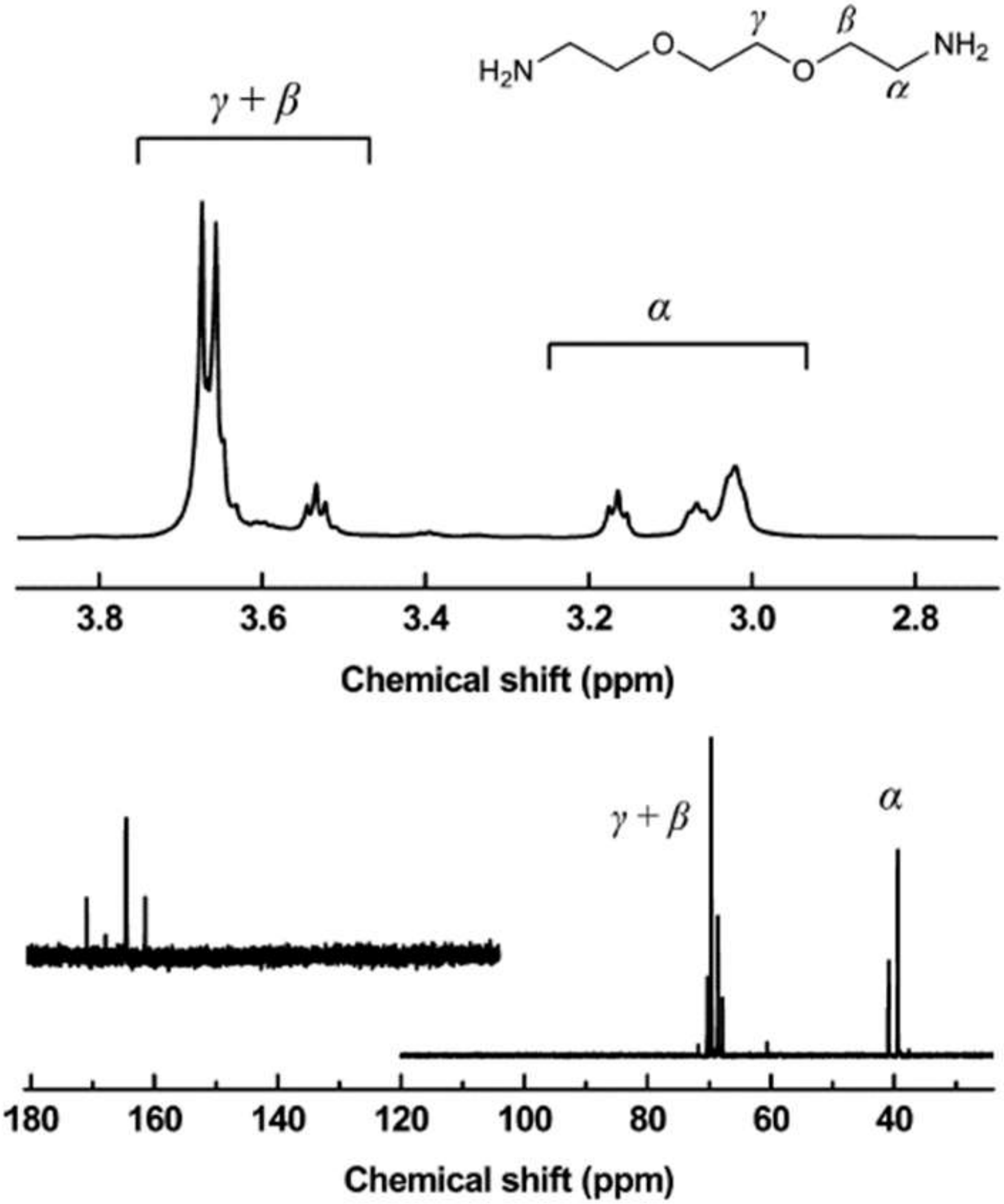

Figure 2.4 (Top) ^{1}H NMR spectrum of the EDA-carbon dots. (Bottom) ^{13}C NMR spectrum of the EDA-carbon dots and (inset on the left) the lower-field portion of the spectrum for the ^{13}C-enriched EDA-carbon dots.

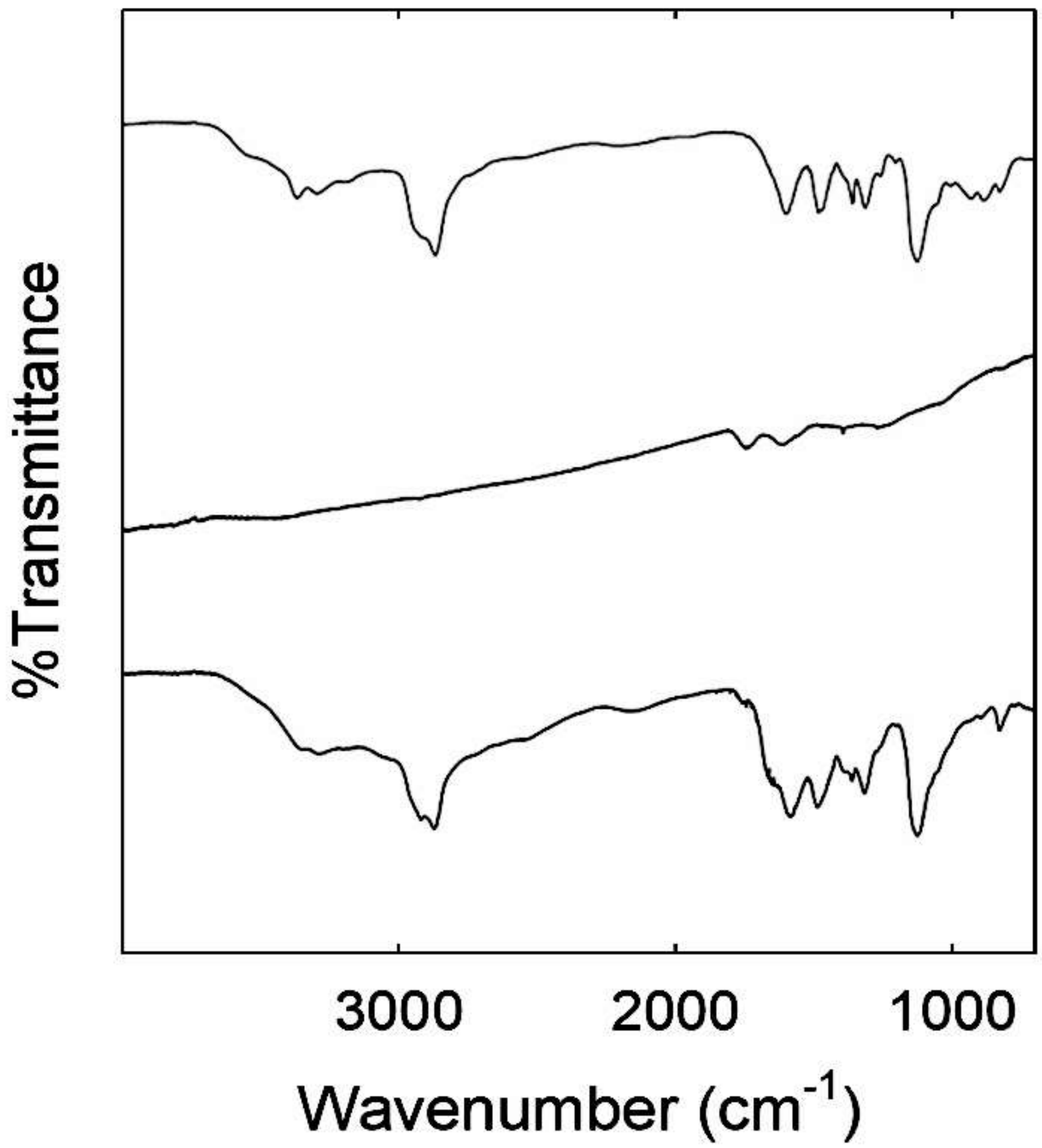

Figure 2.5 FT-IR spectra of EDA-carbon dots (bottom) in comparison to pre-selected and purified carbon nanoparticles (middle) and monomeric EDA (top). Spectra for EDA-carbon dots and monomeric EDA were collected on CaF_2 salt plate, while the spectrum for carbon nanoparticles were collected by pressing into KBr salt pellet.

Further ^{13}C NMR characterization was on the similarly prepared EDA-carbon dots with the core carbon nanoparticles ^{13}C-enriched. Experimentally, the carbon soot sample containing ^{13}C-enriched carbon nanoparticles was produced in the arc-discharge of two graphite rods, one of which was made hollow and then filled with a mixture of commercially supplied ^{13}C powders and graphite cement.[31] According to quantitative Raman spectral shift measurements, the precursor carbon nanoparticles for the functionalization with EDA molecules had a ^{13}C content of 10-15%, and the same ^{13}C enrichment in the resulting carbon dots should be expected. As compared in Figure 2.2, the absorption and fluorescence spectra of the ^{13}C-enriched EDA-carbon dots are rather similar to those without the ^{13}C enrichment. For the ^{13}C NMR results of the ^{13}C-enriched EDA-carbon dots, there are no additional peaks in the aliphatic region nor any detectable aromatic signals (Figure 2.4). The relatively weak but meaningful peaks in the 175-160 ppm region (Figure 2.4) may be assigned to carbonyl carbons on the core carbon nanoparticles. However, since smaller carbon nanoparticles are expected to have more diverse surface defects or carbon sites, the ^{13}C NMR signals of the EDA-carbon dots, whose carbon cores are definitely at the smaller side, are subject to more significant broadening effects. Therefore, the observed carbonyl signals likely represent only some in the minority that could be detected. The results are informative in the sense that they are consistent with the expected diverse carbon environment on the core carbon nanoparticle surface.

It is interesting that the functionalization results for the precursor carbon nanoparticles without and with the ^{13}C-enrichment were rather similar, as the nanoparticles were from different production methods, laser processing for the commercially supplied sample vs arc-discharge for the ^{13}C-enriched sample. The former is generally somewhat more crystalline than the latter. Therefore, the nearly identical optical properties of their resulting EDA-carbon dots suggest stability with the synthesis method for more consistent production of the carbon dots from different sources of precursor carbon nanoparticles.

The EDA-carbon dots as ultra-compact fluorescence probes, with overall size profiles of less than 5 nm in diameter, are not limited to green fluorescence only, with emissions also observed in other colors at different excitation wavelengths (Figure 2.6). Again for a rough comparison, the fluorescent protein mCherry, whose spectrum is also included in the figure, has a similar size profile of around 4 nm.[52] Previous results suggested that the same carbon dots could be used for fluorescence imaging at different colors, though not with the same sensitivities.[39] Further investigations targeting color variations of bright fluorescence emissions over the visible spectrum, such as the exploration of other carbon nanoparticle surface passivation schemes, while maintaining the overall size profiles of the carbon dots are warranted, thus to take full advantage of their different fluorescence emission mechanism from that in conventional semiconductor QDs.

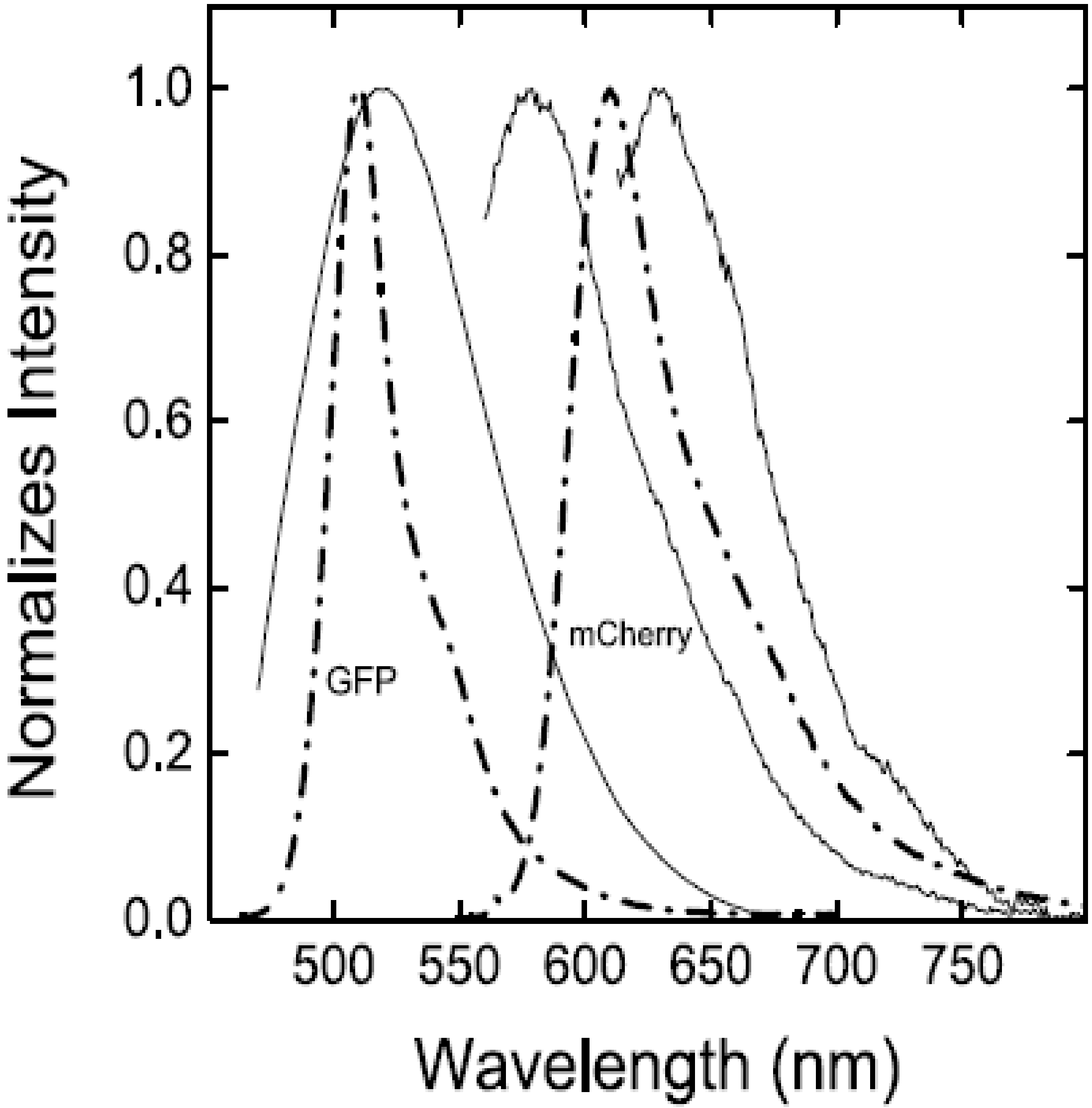

Figure 2.6 Fluorescence spectra of the EDA-carbon dots excited at (from left to right, -) 440 nm (fluorescence quantum yield $\Phi_F \approx 30\%$), 550 nm ($\Phi_F \approx 7\%$), and 600 nm ($\Phi_F \approx 3.7\%$), with spectra of the fluorescent proteins GFP and mCherry also shown for comparison.

The development of ultra-compact fluorescence probes based on carbon dots offers significant values both fundamentally and technologically. On the fundamental side, the experimental confirmation on the preparation of the very small carbon dots of multiple fluorescence colors in the visible spectrum serves to support the existing mechanistic framework for carbon dots, namely, that the fluorescence emissions are due to the radiative recombination of the trapped or confined electrons and holes from the initial charge separation following the photoexcitation. The emission colors may be affected by changes in the core carbon nanoparticle size, with associated changes in the particle surface properties such as the surface curvature, trapping sites, different passivation effects, etc., but not limited by any defined relationships as in conventional semiconductor QDs. Therefore, it seems reasonable to argue that the reduction of carbon dot size profile in this work may represent just the beginning, with more room for further miniaturization through the production or harvesting from mixtures of even smaller carbon nanoparticles for surface passivation by a thinner layer of organic materials. Technologically, the fluorescence probes of size profiles comparable to or eventually smaller than those of the genetically encoded fluorescent tags may open up many new application opportunities, which should also benefit from the other known properties of carbon dots, such as physicochemical and photochemical stabilities, non-blinking, and the intrinsically available organic functional groups on the probe surface amenable to bio-conjugations and other purposes.

One of the applications targeted in the literature for small fluorescence probes is in cell imaging.[1,9] Previous investigations demonstrated that carbon dots with the surface passivation molecules containing abundant amino moieties were readily taken up by cells, enabling fluorescence imaging of the cells by using confocal or multiphoton fluorescence microscopy techniques.[39] Similar cellular uptake of the EDA-carbon dots may be expected, and evaluations related to their potential uses in fluorescence cell imaging will be pursued.

2.4 Acknowledgements

This work has been published in the literature in collaboration with Prof. Sumit Sonkar, Fan Yang, Dr. Monica L. Veca, Ping, Wang, Ken Tackett, Dr. Jing-Jiang Yu, Dr. Eugeniu Vasile, Dr. Haijun Qian, Yamin Liu, Dr. Pengju G. Luo, and Prof. Ya-Ping Sun, whom are all gratefully acknowledged.[53]

2.5 References

1. Kairdolf, B. A.; Smith, A. M.; Stokes, T. H.; Wang, M. D.; Young, A. N.; Nie, S. *Annu. Rev. Anal. Chem.* **2013**, 6, 143.
2. Freeman, R.; Willner, I. *Chem. Soc. Rev.* **2012**, 41, 4067–4085.
3. Hines, M. A.; Philippe, G.-S. *J. Phys. Chem.* **1996**, 100, 468–471.
4. Uyeda, H. T.; Medintz, I. L.; Jaiswal, J. K.; Simon, S. M.; Mattoussi, H. *J. Am. Chem. Soc.* **2005**, 127, 3870–3878.
5. Dorokhin, D.; Tomczak, N.; Han, M. Y.; Reinhoudt, D. N.; Velders, A. H.; Vancso, G. J. *ACS Nano* **2009**, 3, 661–667.
6. Medintz, I. L.; Uyeda, H. T.; Goldman, E. R.; Mattoussi, H. *Nat. Mater.* **2005**, 4, 435–446.
7. Sperling, R. A.; Liedl, T.; Duhr, S.; Kudera, S.; Zanella, M.; Lin, J.; Chang, W. H.; Braun, D.; Parak, W. J. *J. Phys. Chem. C* **2007**, 111, 11552–11559.
8. Zhang, Y.; Clapp, A. *Sensors* **2011**, 11, 11036–11055.
9. Baker, M. *Nat. Methods* **2010**, 7, 957–962.
10. Pinaud, F.; Clarke, S.; Sittner, A.; Dahan, M. *Nat. Methods* **2010**, 7, 275–285.
11. Gerion, D.; Pinaud, F.; Williams, S. C.; Parak, W. J.; Zanchet, D.; Weiss, S.; Alivisatos, A. P. *J. Phys. Chem. B* **2001**, 105, 8861–8871.
12. Yoffe, A. D. *Adv. Phys*. **2001**, 50, 1–208.
13. Groc, L.; Lafourcade, M.; Heine, M.; Renner, M.; Racine, V.; Sibarita, J.-B.; Lounis, B.; Choquet, D.; Cognet, L. *J. Neurosci.* **2007**, 27, 12433–12437.

14. Howarth, M.; Liu, W.; Puthenveetil, S.; Zheng, Y.; Marshall, L. F.; Schmidt, M. M.; Wittrup, K. D.; Bawendi, M. G.; Ting, A. Y. *Nat. Methods* **2008**, 5, 397–399.

15. Kim, Y.; Kim, S. H.; Tanyeri, M.; Katzenellenbogen, J. A.; Schroeder, C. M. Dendrimer *Biophys. J.* **2013**, 104, 1566–1575.

16. Choi, H. S.; Liu, W.; Misra, P.; Tanaka, E.; Zimmer, J. P.; Ipe, B. I.; Bawendi, M. G.; Frangioni, J. V. *Nat. Biotechnol.* **2007**, 25, 1165–1170.

17. Maeda, H.; Wu, J.; Sawa, T.; Matsumura, Y.; Hori, K. *J. Controlled Release* **2000**, 65, 271–284.

18. Jain, R. K.; Stylianopoulos, T. *Nat. Rev. Clin. Oncol.* **2010**, 7, 653–664.

19. Cheng, Y.; Meyers, J. D.; Broome, A. M.; Kenney, M. E.; Basilion, J. P.; Burda, C. *J. Am. Chem. Soc.* **2011**, 133, 2583–2591.

20. Wu, X.; He, X.; Wang, K.; Xie, C.; Zhou, B.; Qing, Z. *Nanoscale* **2010**, 2, 2244–2249.

21. Oh, E.; Delehanty, J. B.; Sapsford, K. E.; Susumu, K.; Goswami, R.; Blance-Canosa, J. B.; Dawson, P. E.; Granek, J.; Shoff, M.; Zhang, Q.; Goering, P. L.; Huston, A.; Medintz, I. L. *ACS Nano* **2011**, 5, 6434–6448.

22. Faucher, L.; Tremblay, M.; Lagueux, J.; Gossuin, Y.; Fortin, M.-A. *ACS Appl. Mater. Interfaces* **2012**, 4, 4506–4515.

23. Zeng, L.; Ren, W.; Zheng, L.; Cui, P.; Wu, A. *Phys. Chem. Chem. Phys.* **2012**, 14, 2631–2636.

24. Sun, Y.-P.; Zhou, B.; Lin, Y.; Wang, W.; Fernando, K. A. S.; Pathak, P.; Meziani, M. J.; Harruff, B. A.; Wang, X.; Wang, H.; et al. *J. Am. Chem. Soc.* **2006**, 128, 7756–7757.

25. Cao, L.; Wang, X.; Meziani, M. J.; Lu, F.; Wang, H.; Luo, P. G.; Lin, Y.; Harruff, B. A.; Veca, L. M.; Murray, D.; et al *J. Am. Chem. Soc.* **2007**, 129, 11318–11319.

26. Bourlinos, A. B.; Stassinopoulos, A.; Anglos, D.; Zboril, R.; Karakassides, M.; Giannelis, E. P. *Small* **2008**, 4, 455–458.

27. Bourlinos, A. B.; Stassinopoulos, A.; Anglos, D.; Zboril, R.; Georgakilas, V.; Giannelis, E. P. *Chem. Mater.* **2008**, 20, 4539–4541.

28. Peng, H.; Travas-Sejdic, J. *Chem. Mater.* **2009**, 21, 5563–5565.

29. Mochalin, V. N.; Gogotsi, Y. *J. Am. Chem. Soc.* **2009**, 131, 4594–4595.

30. Yang, S.-T.; Cao, L.; Luo, P. G.; Lu, F.; Wang, X.; Wang, H.; Meziani, M. J.; Liu, Y.; Qi, G.; Sun, Y.-P. *J. Am. Chem. Soc.* **2009**, 131, 11308–11309.

31. Yang, S.-T.; Wang, X.; Wang, H.; Lu, F.; Luo, P. G.; Cao, L.; Meziani, M. J.; Liu, J.-H.; Liu, Y.; Chen, M.; et al. *J. Phys. Chem. C* **2009**, 113, 18110–18114.

32. Li, Q.; Ohulchanskyy, T. Y.; Liu, R.; Koynov, K.; Wu, D.; Best, A.; Kumar, R.; Bonoiu, A.; Prasad, P. N. *J. Phys. Chem. C* **2010**, 114, 12062–12068.

33. Li, H.; He, X.; Kang, Z.; Huang, H.; Liu, Y.; Liu, J.; Lian, S.; Tsang, C. H. A.; Yang, X.; Lee, S.-T. *Angew. Chem., Int. Ed.* **2010**, 49, 4430–4434.

34. Wang, X.; Cao, L.; Yang, S.-T.; Lu, F.; Meziani, M. J.; Tian, L.; Sun, K. W.; Bloodgood, M. A.; Sun, Y.-P. *Angew. Chem., Int. Ed.* **2010**, 49, 5310–5314.

35. Chandra, S.; Das, P.; Bag, S.; Laha, D.; Pramanik, P. *Nanoscale* **2011**, 3, 1533–1540.

36. Bourlinos, A. B.; Zboril, R.; Petr, J.; Bakandritsos, A.; Krysmann, M.;Giannelis, E. P. *Chem. Mater*. **2012**, 24, 6–8.

37. Tao, H.; Yang, K.; Ma, Z.; Wan, J.; Zhang, Y.; Kang, Z.; Liu, Z. *Small* **2012**, 8, 281–290.

38. Li, H.; Kang, Z.; Liu, Y.; Lee, S.-T. *J. Mater. Chem.* **2012**, 22, 24230–24253.

39. Luo, P. G.; Sahu, S.; Yang, S.-T.; Sonkar, S. K.; Wang, J.; Wang, H.; LeCroy, G. E.; Cao, L.; Sun, Y.-P. *J. Mater. Chem. B* **2013**, 1, 2116–2127.

40. Cao, L.; Meziani, M. J.; Sahu, S.; Sun, Y.-P. *Acc. Chem. Res.* **2013**, 46, 171–180.

41. Liu, Z.; Zu, Y.; Fu, Y.; Zhang, Z.; Meng, R. *Microsc. Res. Technol.* **2008**, 71, 802–809.

42. Yang, F.; Moss, L. G.; Phillips, G. N. *Nat. Biotechnol.* **1996**, 14, 1246–1251.

43. Prachayasittikul, V.; Isarankura-Na-Ayudhya, C.; Hilterhaus, L.; Hinz, A.; Tantimongcolwat, T.; Galla, H. *J. Biochem. Biophys. Res. Commun.* **2005**, 327, 174–182.

44. Andrews, P. *Biochem. J.* **1964**, 91, 222–233.

45. Xu, J.; Sahu, S.; Cao, L.; Anilkumar, P.; Tackett, K. N., II; Qian, H.; Bunker, C. E.; Guliants, E. A.; Parenzan, A.; Sun, Y.-P. *ChemPhysChem* **2011**, 12, 3604–3608.

46. Xu, J.; Sahu, S.;Cao, L.; Bunker,C.E.;Peng,G.; Liu,Y.; Fernando, K. A. S.; Wang, P.; Guliants, E. A.;Meziani, M. J.; et al. *Langmuir* **2012**, 28, 16141–16147.

47. Bunker, C. E.; Sun, Y.-P. *J. Am. Chem. Soc.* **1995**, 117, 10865–10870.

48. Lakowicz, J. R. Principles of Fluorescence Spectroscopy; Springer: NJ, 2006.

49. Patterson, G.; Day, R. N.; Piston, D. *J. Cell Sci*. **2001**, 114, 837–838.

50. Spectral Database for Organic Compounds. National Institute of Advanced Industrial Science and Technology (AIST), Japan (http://sdbs.db.aist.go.jp/sdbs/cgi-bin/cre_index.cgi).

51. Sadtler Infrared Spectral Database, Bio-Rad, USA (http:// www.bio-rad.com/en-us/category/ir).

52. Day, N. R.; Davidson, M. W. T. *Chem. Soc. Rev*. **2009**, 38, 2887–2921.

53. LeCroy, G. E.; Sonkar, S.; Yang, F.; Veca, M. L.; Wang, P.; Tackett II, K. N.; Yu, J.-J.; Vasile, E.; Qian, H.; Liu, Y.; Luo, P. G.; Sun, Y.-P. *ACS Nano* **2014**, *8*, 4522-4529.

CHAPTER THREE

STEADY-STATE AND TIME-RESOLVED FLUORESCENCE STUDIES ON INTERACTION OF CARBON “QUANTUM” DOTS WITH NITROTOLUENES

3.1 Introduction

Carbon "quantum" dots or more appropriately referred to as carbon dots (CDots) [1] for a lack of the classical quantum confinement effect have emerged to represent a rapidly advancing and expanding research field.[2-10] Among many unique and/or advantageous properties of CDots, which are generally defined as small carbon nanoparticles with various surface passivation schemes (Figure 3.1),[10-13] bright and colorful fluorescence emissions have captured more attention since the original finding of CDots.[1] The core carbon nanoparticles in CDots are strongly absorptive over the visible spectrum, extending into the near-IR, due to transitions associated with the π plasmon. Because of the surface passivation CDots are readily soluble in water and other solvents to form solutions of little optical scattering effect. As observed experimentally, the excitation into the absorption spectrum of CDots at different wavelengths results in fluorescence emissions of different colors, with varying quantum yields. The more intense fluorescence emissions from CDots are often found in the green spectral region (overlapping with that covered by the green fluorescent protein), reaching quantum yields of more than 50% in CDots of more effective surface passivation.[10-14] Thus, while CDots have been widely pursued as fluorescence probes for imaging and sensing applications in general, the sensing uses that do not require high optical absorption and bright fluorescence emissions in the more tissue transparent red/near-IR spectral region have been much more popular.[8,15-29] In fact, a quick survey of the literature would reveal that

CDots from various syntheses, corresponding to different structural configurations, have been used for a wide variety of sensing targets,[8,15-33] including metal ions (Hg^{2+}, Cd^{2+}, Cu^{2+}, etc.),[15-21,33] biologically significant species,[22-27] and explosives or their associated signature substances.[28-32]

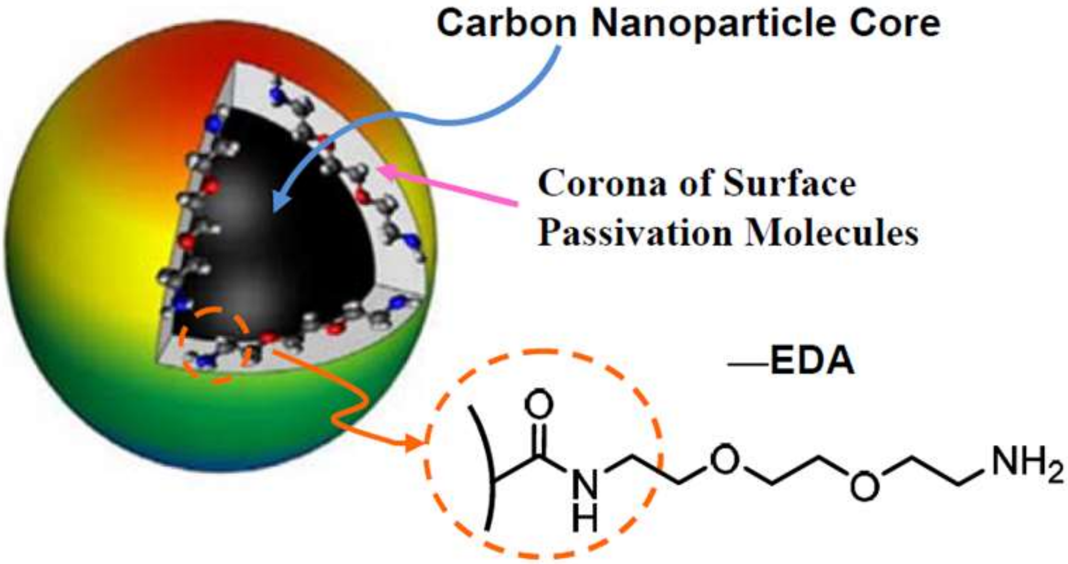

Figure 3.1 A cartoon illustration on carbon dot, which is generally a small carbon nanoparticle core with attached and strongly adsorbed surface passivation molecules (a configuration similar to a soft corona).

More specifically on the use of CDots in the detection of TNT and more broadly nitroaromatic compounds, Sun and coworkers borrowed the concept from the study of using fluorescent carbon nanotubes for the detection of nitrotoluenes,[34] demonstrating that fluorescence emission intensities of CDots surface-functionalized with large oligomeric organic molecules were highly sensitive to the presence of nitrotoluenes, which were attributed mechanistically to charge transfers.[31] The same fluorescence quenching was subsequently studied in terms of fluorescence decay measurements.[32] More recently, sensing protocols on using CDots for the detection of TNT and signature molecules were developed by taking advantage of the charge transfer quenching associated with the electron deficient nature of these molecules.[28-30] For example, Zhang, *et al.* reported that the quenching of the fluorescence emission intensities of CDots by TNT could enable the detection of TNT down to 1 nM level.[28] Campos, *et al*. used CDots with poly(amidoamine) dendrimer on the surface for the detection of 4-chloro-2,6-dinitroaniline down to 2 μM.[29] Sun, *et al.* found that the quenching of CDots fluorescence emission intensities by picric acid was extraordinarily efficient, with an observed Stern-Volmer quenching constant K_{SV} of 31,800 M^{-1}.[30] Similarly off-the-charts large K_{SV} values have been observed and reported in the literature from many other studies on using CDots as sensors based on fluorescence quenching, such as the enormously large K_{SV} of 130,000 M^{-1} obtained in the sensing of mercury ions.[33] However, these K_{SV} values, while derived from experimentally measured quenching data, are obviously contradictory to the basic principle behind the Stern-Volmer quenching behavior in solution, as the diffusion rate constants inferred by these large K_{SV} values are beyond or orders of magnitude beyond the diffusion control limit in Stern-Volmer quenching.[35,36] In reality, therefore, the Stern-Volmer equation, which models only dynamic quenching in solution, is not applicable to the behavior found in the fluorescence quenching of CDots by the nitroaromatic molecules and some of the other sensing targets. Other interactions between CDots and the quenchers that involve no or minimal diffusion processes, broadly defined as static quenching,[35,36] must have contributed to the seemingly extraordinarily large K_{SV} values derived from experimental quenching data. Systematic investigations that combine steady-state and time-resolved fluorescence techniques are required to dissect the complicated quenching behavior, thus to improve the design and implementation of the fluorescence sensing with CDots.

In the study reported here, structurally compact and defined and brightly fluorescent CDots were used in steady-state and time-resolved measurements of fluorescence quenching by 4-nitrotoluene and 2,4-dinitrotoluene, which are commonly used as signature compounds for nitroaromatic explosives. The observed fluorescence quenching behaviors reflecting mechanistically interactions of the photoexcited CDots with the quenchers in different concentration regions could be understood as being primarily dynamic in nature, with some static quenching contributions due to near-neighbor charge transfer interactions at high quencher concentrations, especially for the more electron deficient 2,4-dinitrotoluene. The implications of the results and conclusions to the use of CDots as fluorescence sensors for nitroaromatics and related explosives are discussed.

3.2 Experimental Section

Materials. Carbon nanopowder (US1074) was purchased from US Research Nanomaterials, Inc., 2,2'-(ethylenedioxy)bis(ethylamine) (EDA), 4-nitrotoluene, 2,4-dinitrotoluene, and anhydrous methanol from Sigma-Aldrich, thionyl chloride (>99%) from Alfa Aesar, and nitric acid from VWR. Dialysis membrane tubing (molecular weight cut-off ~ 500) was acquired from Spectrum Laboratories, and Spehadex G-100 gel from GE Healthcare Life Sciences. Water was deionized and purified by being passed through a Barnstead Nanopure II water purification system.

Measurements UV/Vis absorption spectra were obtained on a Perkin Elmer Lambda 900 absorption spectrophotometer. Fluorescence spectra were recorded on a Horiba Jobin-Yvon Fluorolog-3 FL3-22 spectrophotometer equipped with a 450 W xenon XBO short arc lamp and a Hamamatsu T928P PMT photon counting detector operated at 950 V. The spectra were collected in the ratio mode, and corrected for the non-linear instrument response by using the separately determined correction factors. Fluorescence quantum yields were determined with 9,10-bis(phenylethynyl)-anthracene in cyclohexane as a fluorescence reference, calibrated against the quinine sulfate standard. Fluorescence decays were measured in terms of the time-correlated single photon counting (TCSPC) on a Horibia Ultima Extreme spectrometer equipped with a SuperK Extreme supercontinuum laser source pulsed at 5 MHz, TDM-800 excitation and TDM-1200 emission monochromators, a R3809-50 MCP-PMT detector operated at 3.0 KV in a thermoelectrically cooled housing, and FluoroHub A+ timing electronics. The deconvolution fits of experimental decay curves were performed with the use of the Das6 fluorescence decay analysis software.

Carbon Nanoparticles. Small carbon nanoparticles were harvested from the commercially supplied carbon nanopowder sample in a procedure similar to what has been reported previously.[11-13] Briefly, the carbon nanopowder sample (2 g) was refluxed in 8 M nitric acid (200 mL) for 48 h. The acid solution was cooled to room temperature, and then centrifuged at 1,000 g to discard the supernatant. The residue was re-dispersed in water and dialyzed (molecular weight cut-off ~ 500) against fresh water. The resulting solution was centrifuged at 1,000 g to retain the supernatant, which resembled a highly coloured and transparent solution. Upon evaporation to remove water, surface-oxidized small carbon nanoparticles were obtained for functionalization reactions.

EDA-Carbon Dots. EDA-CDots were synthesized by the functionalization of the carbon nanoparticles obtained from the above procedure with EDA molecules under amidation reaction conditions.[11,12,14] In a typical experiment, a sample of the carbon nanoparticles (50 mg) was refluxed in neat thionyl chloride for 12 h for the acylation of the particle surface-bound carboxylic moieties. Then, excess thionyl chloride was removed via evaporation, and the treated carbon nanoparticles were carefully mixed with EDA (1 g). The mixture was heated to 120 °C and stirred vigorously at that temperature under nitrogen protection for 3 days. Post reaction, the mixture was cooled back to ambient temperature and dispersed in water, followed by centrifugation at 20,000 g to retain the supernatant. The aqueous solution thus obtained was dialyzed (molecular weight cutoff ~ 500) against fresh water to remove unreacted EDA molecules and other small molecular species. The resulting aqueous solution of the as-synthesized EDA-CDots was concentrated and then separated on a Sephadex G-100 gel column to harvest the more fluorescent fractions.[11,14] These fractions were combined for the EDA-CDots sample used in the subsequent characterization and spectroscopic experiments.

Fluorescence Quenching. A solution of the EDA-CDots in methanol was prepared for all fluorescence quenching measurements. The solution was used for the preparation of solutions with the two different quenchers (4-nitrotoluene and 2,4-dinitrotoluene) at different quencher concentrations up to 0.1 M, and in all these solutions the concentration of the EDA-CDots was kept the same. Fluorescence spectra and decays of the solutions were collected at room temperature with excitation at 425 nm, 450 nm, and 475 nm, and for the decays the fluorescence emissions were monitored at 480 nm, 515 nm, and 545 nm, respectively, and also at 600 nm for all three excitation wavelengths.

3.3 Results and Discussion

In previous studies it was demonstrated that CDots from the chemical functionalization of small carbon nanoparticles with 2,2'-(ethylenedioxy)bis(ethylamine) (EDA, Figure 3.1) are ultracompact in overall dot profile and structurally simple and defined, yet still brightly fluorescent.[11] Briefly in the same synthetic scheme, commercially supplied carbon nanopowder sample was processed in procedures involving oxidative acid treatments to impact carboxylic acid moieties on the particle surface. From the processed sample small carbon nanoparticles were harvested and used in the functionalization reaction based on the amidation of the particle surface-bound carboxylic acids with EDA molecules.[11] The as-synthesized sample of EDA-CDots was cleaned via dialysis to remove unreacted EDA and other small molecular species, followed by separation on an aqueous gel column (SephadexTM G-100) to collect the more fluorescent fractions. The fractionation has been rationalized such that better functionalized CDots, corresponding to more effective surface passivation of the core carbon nanoparticles in the dots and different elution behavior on the gel column, are generally correlated with those of higher fluorescence quantum yields.[14] The more fluorescent fractions were combined into one sample of about 20% in fluorescence quantum yield (400 nm excitation), whose absorption and fluorescence spectra are shown in Figure 3.2. According to TEM results, the EDA-CDots were on the order of 5 nm in average diameter, consistent with the results reported previously.[11]

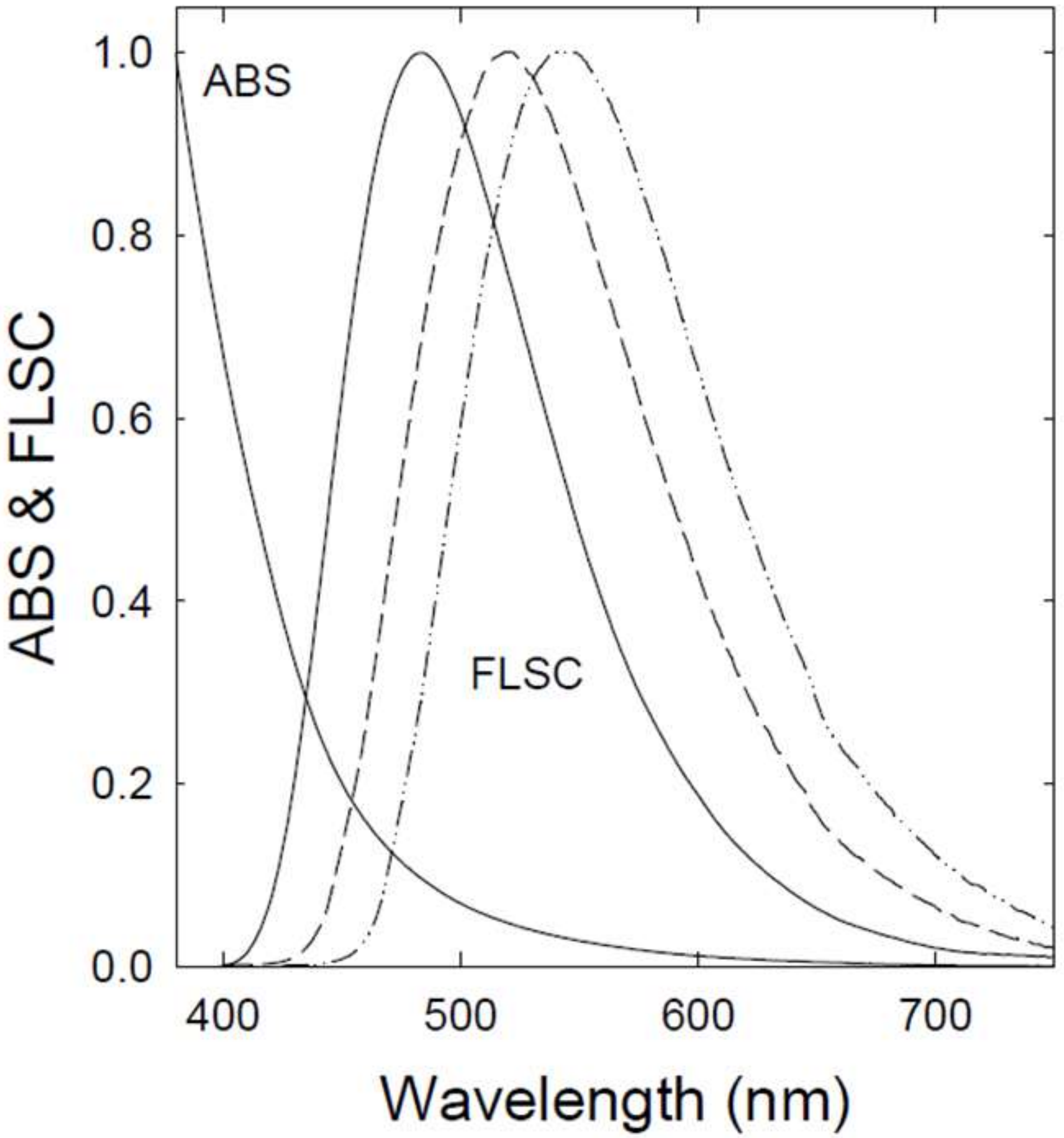

Figure 3.2 UV/vis absorption (ABS) and normalized fluorescence (FLSC) spectra of the EDA-CDots in methanol solution without any quenchers excited at 425 nm (——), 450 nm (····), and 475 nm (- - -).

4-Nitrotoluene (NT) and 2,4-dinitrotoluene (DNT) as fluorescence quenchers are both colorless, with absorption cutoff shorter than 400 nm, thus no interference to the absorption of the EDA-CDots in the visible spectral region. The possibility of any reactions between the quenchers and the EDA-CDots was examined by comparing the absorption spectra and fluorescence spectral profiles of the dot solutions without and with the quenchers, and no differences were observed. However, the fluorescence emission intensities of the EDA-CDots were quenched effectively by the nitrotoluenes, and the quenching was obviously dependent on quencher concentrations (Figure 3.3). Interestingly, despite the fact that fluorescence spectra of CDots are generally excitation wavelength dependent, suggesting a distribution of emissions in an observed fluorescence spectrum, there were no changes in the fluorescence spectral profiles when the emission intensities were decreased progressively and substantially with increasing quencher concentrations (Figure 3.3 and insets). Thus, while each observed fluorescence spectrum could still be a distribution of multiple emissions, the quenching of these emissions must be essentially the same to result in no meaningful changes in the spectral profiles even though the intensities became substantially lower (down to about 20% at the highest quencher concentration used, Figure 3.3).

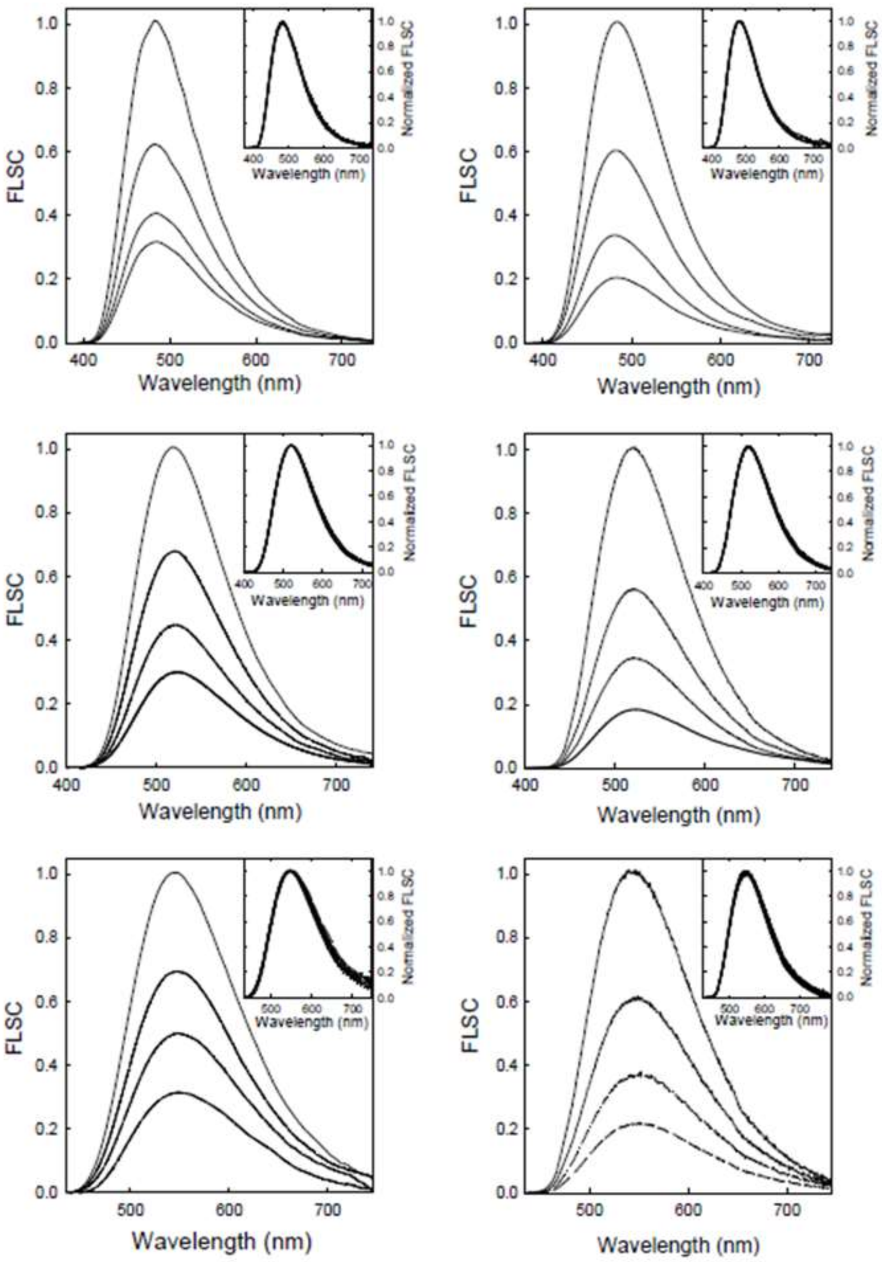

Figure 3.3 The quenching of fluorescence intensities of the EDA-CDots by NT (left column) and DNT (right column) in methanol solution at 425 nm (top), 450 nm (middle), and 475 nm (bottom) excitation. In each figure the spectra with decreasing intensities correspond to quencher concentrations of 0 to 0.05 M for the 425 nm excitation (top) and 0 to 0.1 M for the other two excitation wavelengths (middle and bottom). Shown in the insets are the corresponding normalized spectra.

Shown in Figure 3.4 are plots of observed fluorescence quantum yield ratios (Φ_F°/Φ_F, where Φ_F° and Φ_F are the yields without quencher and at a given quencher concentration, respectively) against the corresponding quencher concentrations. The plots are close to linear initially at low quencher concentrations for both NT and DNT at all three excitation wavelengths (Figure 3.4 insets), to which applications of the Stern-Volmer equation yield quenching constant K_{SV} values of 39 - 54 M^{-1} for NT and 59 - 89 M^{-1} for DNT (Table 3.1). With the estimated average fluorescence lifetime of around 6 ns for the EDA-CDots in the absence of any quenchers (τ_F°, Table 3.1), the corresponding diffusion rate constants (k_d) derived from the K_{SV} values ($k_d = K_{SV}/\tau_F$°) are rather large, up to 1×10^{10} $M^{-1}s^{-1}$ for NT and 1.6×10^{10} $M^{-1}s^{-1}$ for DNT, but likely still at the very upper boundary of dynamic quenching processes involving emissive species of large sizes [36]. The difference between NT and DNT might be rationalized such that even with both at the diffusion-controlled limit, the latter is a stronger quencher (a better electron acceptor, see more discussion below), thus probably corresponding to a larger average quenching radius, which is manifested in the derivation of the experimental data as a shorter diffusion length or equivalently a larger apparent diffusion rate constant. The predominantly dynamic nature of the quenching with both NT and DNT is further supported by the results from fluorescence decay measurements of the EDA-CDots in solutions with different quencher concentrations.

Table 3.1 Fluorescence decay parameters of the CDots without quenchers at different excitation wavelengths and the corresponding quenching constants from Stern-Volmer plots in the linear low quencher concentration region.

λ_{ex} (nm)	A_1^o (%)	A_2^o (%)	τ_{F1}^o (ns)	τ_{F2}^o (ns)	$<\tau_F^o>$ (ns)	NT K_{SV} (M^{-1})	DNT K_{SV} (M^{-1})
425	29	71	2.1	6.0	5.5	54	89
450	35	65	2.1	6.9	6.2	47	62
475	32	68	1.9	6.9	6.1	39	59

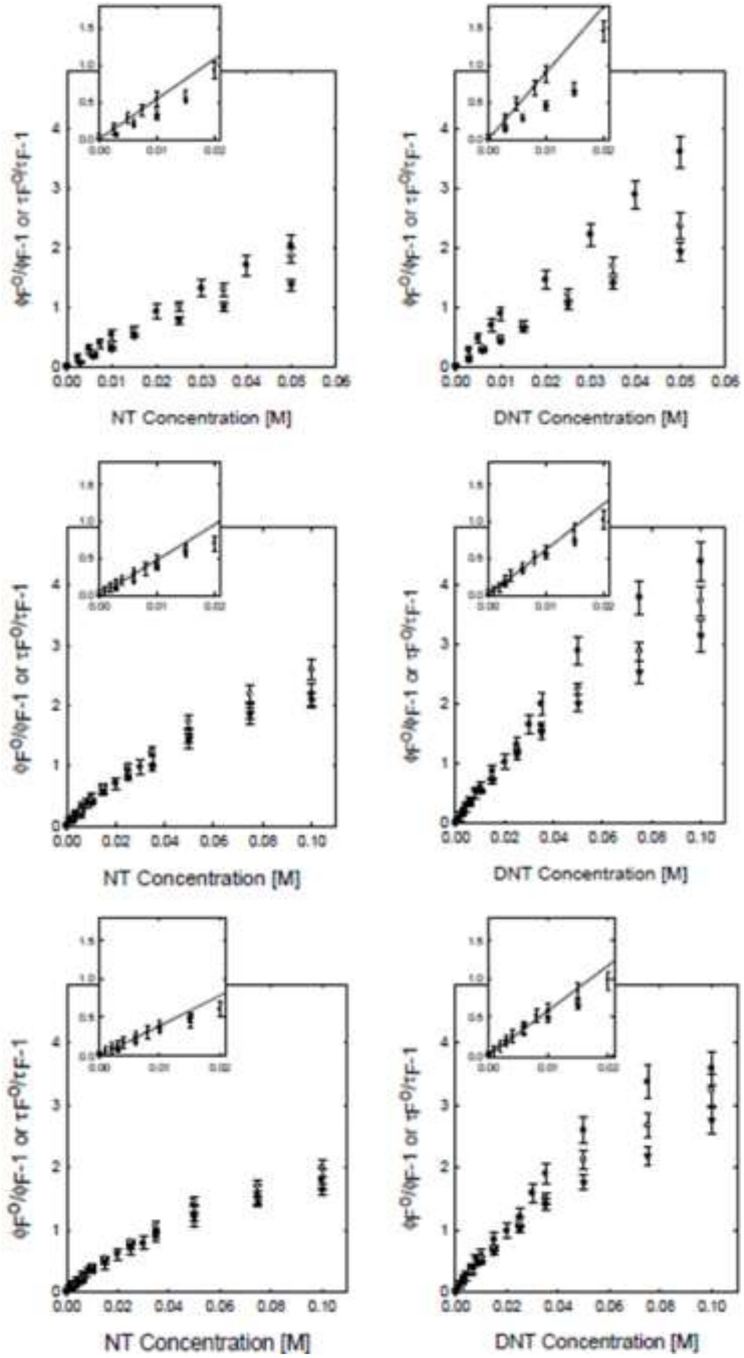

Figure 3.4 Stern-Volmer plots for the quenching of fluorescence intensities (●) and average fluorescence lifetimes (with emissions monitored at the spectral peak: ○, and at 600 nm: ▼) of the EDA-CDots in methanol solutions with difference concentrations of NT (left column) and DNT (right column), with excitation at 425 nm (top), 450 nm (middle), and 475 nm (bottom).

Fluorescence decays of the EDA-CDots in methanol solutions without and with the quenchers under similar experimental conditions were measured in terms of the time-correlated single photon counting (TCSPC) technique (Figure 3.5). Even in the absence of any quenchers, the decays could not be reconvoluted with a mono-exponential function, similar to what have been found for other CDots. The deconvolution fits became acceptable with the use of a biexponential function, though the good fits probably only suggest that the likely more complex fluorescence decays of the CDots could be represented on average by two components, for which the corresponding pre-exponential factors ($A_1°$ and $A_2°$) and lifetimes ($\tau_{F1}°$ and $\tau_{F2}°$) are shown in Table 3.1. These parameters could be used in the further averaging to estimate the average fluorescence lifetime, $<\tau_F°>=A_1°(\tau_{F1}°)^2+A_2°(\tau_{F2}°)^2]/(A_1°\tau_{F1}°+A_2°\tau_{F2}°)$,[35] and the results thus obtained are also shown in Table 3.1. As discussed above, with these average lifetimes and the K_{SV} values derived experimentally (Figure 3.4 insets, Table 3.1), the calculated diffusion rate constants are rather large but still not extraordinary by not being significantly above the limit of diffusion control in predominantly dynamic quenching.

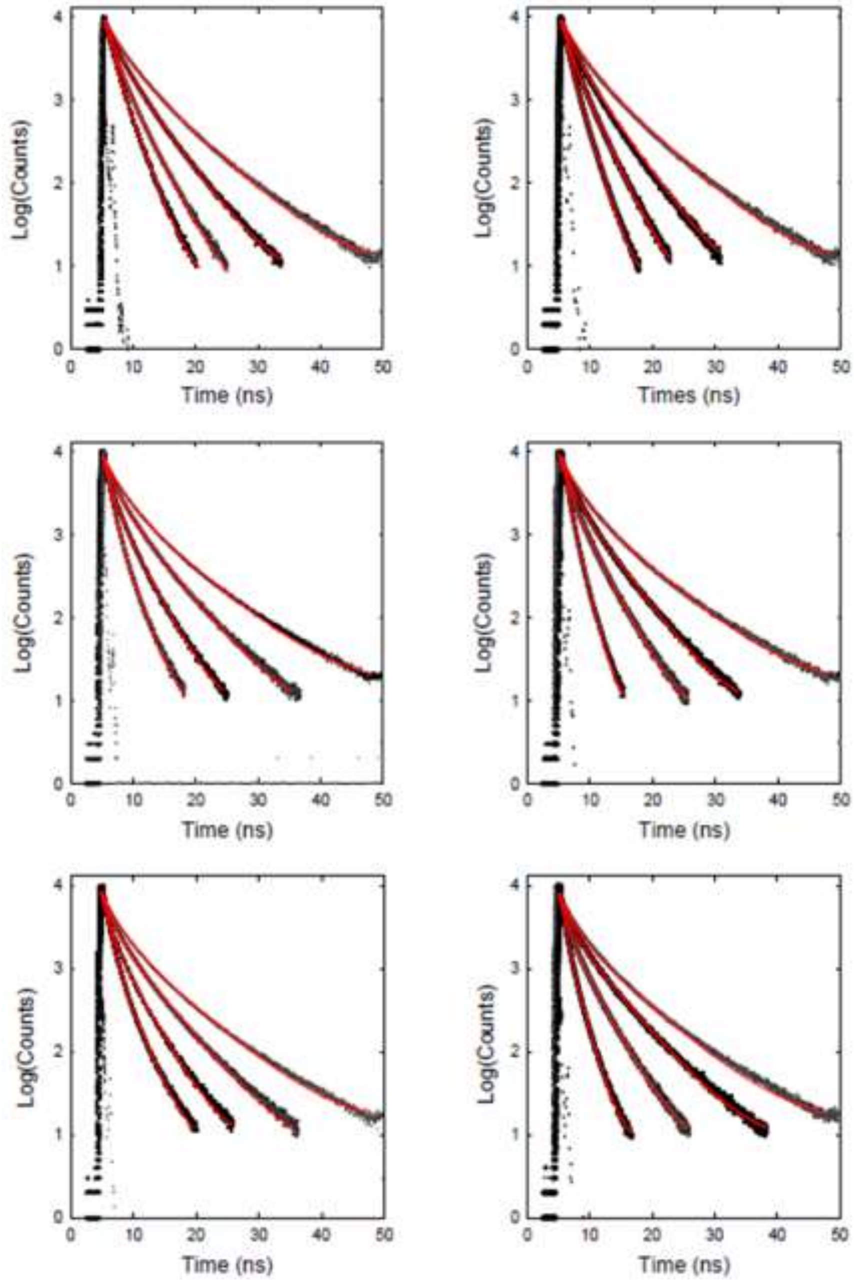

Figure 3.5 Observed fluorescence decay curves and two-exponential deconvolution fits for the EDA-CDots in methanol solutions with NT (left column) and DNT (right column) as quenchers. For excitation at 425 nm (top), the quencher concentrations were 0, 0.01, 0.025, and 0.05 M; and for excitation at 450 nm (middle) and 475 nm (bottom), the quencher concentrations were 0, 0.01, 0.025, and 0.1 M.

The same data treatments were applied to the fluorescence decays at different excitation wavelengths and varying quencher concentrations to obtain average lifetime $<\tau_F>$ values. At each excitation wavelength, the $<\tau_F>$ decreases monotonically with the increasing quencher concentration. The quenching plots based on average lifetime results, $<\tau_F^\circ>/<\tau_F>$ against the quencher concentration, are also shown in Figure 3.4. At low quencher concentrations (Figure 3.4 insets), the plots based on the lifetime quenching are mostly consistent with those based on the quantum yield quenching, which further supports the notion that the quenching results are associated primarily with dynamic processes that are at or close to the diffusion-controlled limit.[36] While the diffusion rate constants derived from the quenching results of NT and DNT are both large, those with DNT are larger, which as discussed above may be rationalized by DNT being a stronger quencher toward the photoexcited CDots (again a larger average quenching radius, equivalently a shorter diffusion length manifested as a larger apparent diffusion rate constant).[31,37,38]

Beyond the initial region of low quencher concentrations (Figure 3.4 insets), the plots for the fluorescence lifetime quenching obviously diverge from those for the fluorescence quantum yield quenching, and all of the deviations are downward from the initial linear relationships (Figure 3.4). The divergence may be attributed to a gradually increasing deviation from the predominantly dynamic quenching behavior found at low quencher concentrations, namely that the fluorescence quantum yield quenching was subject to an increasing contribution of static quenching effect[36] at a higher quencher concentration, as the fluorescence lifetime quenching could only account for the dynamic processes.[35,36] Mechanistically, photoexcited CDots are known as strong electron donors,[31] so that their charge transfer interactions with the electron deficient NT and DNT are responsible for the observed efficient fluorescence quenching. Static quenching is in many cases associated with the formation of excited state complexes, those between the emissive species and the quencher molecules.[35,36] In this case, however, there are no experimental evidence for the formation of such complexes, with no changes in the observed absorption and fluorescence spectra of the dot solutions at all of the quencher concentrations used. It may thus be argued that the relatively small static quenching contributions are due to the large quenching radius (associated with the emissive species being large and the quenchers being strong, as discussed above) being manifested somewhat differently in the fluorescence quantum yield and lifetime quenching processes, though a more detailed mechanistic picture on the difference is beyond the reach of the fluorescence spectroscopy techniques used in this study.

In the extensive investigation of sensing based on the fluorescence quenching of CDots by a variety of analytes, extraordinarily efficient quenching reflected by extremely large quenching constants derived from empirical Stern-Volmer plots has been a common observation,[8] especially with respect to the sensing of various metal cations.[33] While such quenching behaviors offer opportunities for potentially highly sensitive sensing applications, mechanistically and practically, the obviously substantial static (near-neighbor and more likely complexation) quenching contributions may present challenges in some of the desired quantitative analyses, as the linear relationships commonly used for such purposes are very sensitive to local dot - quencher configurations. In the case of sensing nitroaromatics and related explosives based on fluorescence quenching, results from the study reported here suggest that the brightly fluorescent CDots are indeed excellent probes, not only extremely sensitive but also predominantly dynamic quenching in nature for at least the low analyte concentrations, thus mechanistically valid and experimentally reproducible. Unlike some of the metal cations as quenchers widely investigated in the literature, which probably form complexes or the like with the photoexcited CDots (especially those with surface amino moieties), there is no evidence for any similar complexation in the quenching with NT and DNT. Therefore, as fluorescence sensors, the CDots are ideally suited for the sensitive detection and quantitative analyses of low concentration nitroaromatics.

The results reported here suggest that the structurally compact and defined EDA-CDots are excellent fluorescence probes for the sensitive, quantitative, and reproducible analysis of the low-concentration nitrotoluenes as signature compounds for nitroaromatic explosives. Mechanistically, the fluorescence quenching of the EDA-CDots by the nitrotoluenes due to charge transfer interactions is predominately dynamic in nature, not only confirming earlier observations associated with structurally more complex CDots[31] but also offering more insights into the fluorescence quenching behavior in an experimentally more systematic and consistent fashion. Further investigations on the interactions of photoexcited CDots with various targeted analytes as quenchers by using other techniques in addition to fluorescence spectroscopy will prove valuable to the development of CDots into highly sensitive and quantitative fluorescence sensors for broad applications.

3.4 Acknowledgements

Chapter three has been published in in the literature in collaboration with Dr. K. A. Shiral Fernando, Dr. Christopher E. Bunker, Ping Wang, Nicholas Tomlinson, and Prof. Ya-Ping Sun.[39]

3.5 References

1. Sun, Y.-P.; Zhou, B.; Lin, Y.; Wang, W.; Fernando, K. A. S.; Pathak, P.; Meziani, M. J.; Harruff, B. A.; Wang, X.; Wang, H.; et al. *J. Am. Chem. Soc.* **2006**, 128, 7756-7757.

2. Luo, P. G.; Sahu, S.; Yang, S.-T.; Sonkar, S. K.; Wang, J.; Wang, H.; LeCroy, G. E.; Cao, L.; Sun, Y.-P. *J. Mater. Chem. C* **2013**, 1, 2116-2127.

3. Luo, P. G.; Yang, F.; Yang, S.-T.; Sonkar, S. K.; Yang, L.; Broglie, J. J.; Liu, Y.; Sun, Y.-P. *RSC Adv.* **2014**, 4, 10791−10807.

4. Hola, K.; Zhang, Y.; Wang, Y.; Giannelis, E. P.; Zboril, R.; Rogach, A. L. *Nano Today* **2014**, 9, 590−603.

5. Wang, Y.; Hu, A. *J. Mater. Chem. C* **2014**, 2, 6921−6939.

6. Lim, S. Y.; Shen, W.; Gao, Z. *Chem. Soc. Rev.* **2015**, 44, 362−381.

7. Fernando, K. A. S.; Sahu, S.; Liu, Y.; Lewis, W. K.; Guliants, E. A.; Jafariyan, A.; Wang, P.; Bunker, C. E.; Sun, Y.-P. *ACS Appl. Mater. Interfaces* **2015**, 7, 8363−8376.

8. Baptista, F. R.; Belhout, S. A.; Giordani, S.; Quinn, S. J. *Chem. Soc. Rev.* **2015**, 44, 4433-4453.

9. Du, Y.; Guo, S. *Nanoscale* **2016**, 8, 2532−2543.

10. LeCroy, G. E.; Yang, S.-T.; Yang, F.; Liu, Y.; Fernando, K. A. S.; Bunker, C. E.; Hu, Y.; Luo, P. G.; Sun, Y.-P. *Coord. Chem. Rev.* **2016**, 320, 66 -81.

11. LeCroy, G. E.; Sonkar, S. K.; Yang, F.; Veca, L. M.; Wang, P.; Tackett, K. N., II; Yu, J.-J.; Vasile, E.; Qian, H.; Liu, Y.; et al. *ACS Nano* **2014**, 8, 4522−4529.

12. Yang, F.; LeCroy, G. E.; Wang, P.; Liang, W.; Chen, J.; Fernando, K. A. S.; Bunker, C. E.; Qian, H.; Sun, Y.-P. *J. Phys. Chem. C* **2016**, 120, 25604-25611.

13. Hu, Y.; Al Awak, M. M.; Yang, F.; Yan, S.; Xiong, Q.; Wang, P.; Tang, Y.; Yang, L.; LeCroy, G. E.; Hou, X.; et al. *J. Mater. Chem. C* **2016**, 4, 10554-10561.

14. Wang, X.; Cao, L.; Yang, S.-T.; Lu, F.; Meziani, M. J.; Tian, L.; Sun, K. W.; Bloodgood, M. A.; Sun, Y.-P. *Angew. Chem. Int. Ed.* **2010**, 122, 5438-5442.

15. Lu, W.; Qin, X.; Liu, S.; Chang, G.; Zhang, Y.; Luo, Y.; Asiri, A.; M.; Al-Youbi, A.; O.; Sun, X. *Anal. Chem.* **2012**, 84, 5351-5357.

16. Karfa, P.; Roy, E.; Patra, S.; Kumar, S.; Tarafdar, A.; Madhuri, R.; Sharma, P. K. *RSC Adv.* **2015**, 5, 58141-58153.

17. Niu, X.; Liu, G.; Li, L.; Fu, Z.; Xu, H.; Cui, F. *RSC Adv.* **2015**, 5, 95223-95229.

18. Shen, C.; Sun, Y.; Wang, J.; Lu, Y. *Nanoscale* **2014**, 6, 9139-9147.

19. Kong, D.; Yan, F.; Han, Z.; Xu, J.; Guo, X.; Chen, L. *RSC Adv.* **2016**, 6, 57481-57487.

20. Sharma, V.; Saini, A. K.; Mobin, S. M. *J. Mater. Chem. B* **2016**, 4, 2466-2476.

21. Zheng, M.; Xie, Z.; Qu, D.; Li, D.; Du, P.; Jing, X.; Sun, Z. *ACS Appl. Mater. Interfaces* **2013**, 5, 13242-13247.

22. Gao, X.; Du, C.; Zhuang, Z.; Chen, W. *J. Mater. Chem. C* **2016**, 4, 6927-6945.

23. Li, H. L.; Zhang, Y. W.; Wang, L.; Tian, J. Q.; Sun, X. P. *Chem. Commun.* **2011**, 47, 961-963.

24. Shi, Y. P.; Pan, Y.; Zhang, H.; Zhang, Z. M.; Li, M.-J.; Yi, C. Q.; Yang, M. S. *Biosens. Bioelectron.* **2014**, 56, 39-45.

25. Wang, Y. H.; Gao, D. Y.; Zhang, P. F.; Gong, P.; Chen, C.; Gao, G. H.; Cai, L. T. *Chem. Commun.* **2014**, 50, 811-813

26. Shen, P.; Xia, Y. *Anal. Chem.* **2014**, 86, 5323-5329.

27. Chai, L.; Zhou, J.; Feng, H.; Tang, C.; Huang, Y.; Qian, Z. *ACS Appl. Mater. Interfaces* **2015**, 7, 23564-23574.

28. Zhang, L.; Han, Y.; Zhu, J.; Zhai, Y.; Dong, Y. *Anal. Chem.* **2015**, 87, 2033-2036.

29. Campos, B.; Contreras, R.; Bandosz, T. J.; Jimenez-Jimenez, J.; Rodriguez-Castellon, E.; Esteves da Silva, J. C. G.; Algarra, M. *Carbon* **2016**, 106, 171-178.

30. Sun, X.; He, J.; Meng, Y.; Zhang, L.; Zhang, S.; Ma, X.; Det, S.; Zhao, J.; Lei, Y. *J. Mater. Chem. A* **2016**, 4, 4161-4171.

31. Wang, X.; Cao, L.; Lu, F.; Meziani, M. J.; Li, H.; Qi, G.; Zhou, B.; Harruff, B. A.; Sun, Y.-P. *Chem. Commun.* **2009**, 3774-3776.

32. Zhang, H.; Huang, H.; Ming, H.; Li, H.; Zhang, L.; Liu, Y.; Kang, Z.; *J. Mater. Chem.* **2012**, 22, 10501-10506.

33. Goncalves, H.; Jorge, P. A. S.; Fernandes, J. R. A.; Esteves da Silva, J. C. G. *Sens. Actuators, B* **2010**, 145, 702-107.

34. Kose, M. K.; Harruff, B. A.; Lin, Y.; Veca, L. M.; Lu, F.; Sun, Y.-P. *J. Phys. Chem. B* **2006**, 110, 14032-14034.

35. Lakowicz, J. R. Principles of Fluorescence Spectroscopy, 2nd ed.; Kluwer Academic/Plenum Publishers: New York, 1999.

36. Birks, J. B. Photophysics of Aromatic Molecules. Wiley-Interscience: London, 1970.

37. Rehm, J. M.; Mclendon G. L.; Fauchet, P. M. *J. Am. Chem. Soc.* **1996**, 118, 4490-4491.

38. Sohn, H.; Calhoun, R. M.; Sailor, M. J.; Trogler, W. C. *Angew. Chem., Int. Ed.* **2001**, 40, 2104-2105.

39. LeCroy, G. E.; Fernando, K. A. S.; Bunker, C. E.; Wang, P.; Tomlinson, N.; Sun, Y.-P. *Inorg. Chim. Acta.* **2017**, *468,* 300-307.

CHAPTER FOUR

CHARACTERISTIC EXCITATION WAVELENGTH DEPENDENCES OF FLUORESCENCE EMISSION IN CARBON "QUANTUM" DOTS

4.1 Introduction

Optical properties of carbon-based nanomaterials have garnered much attention and excitement in the research community for their wide variety of potential applications from optoelectronics to bioimaging.[1–6] More extensively pursued among these nanomaterials have been carbon "quantum" dots, or more accurately referred to as carbon dots (CDots) for the lack of a classical quantum confinement effect, whose high performance yet generally benign and nontoxic characteristics have made them competitive alternatives to the well-established semiconductor quantum dots (QDs).[1,7,8] In fact, the research and development of CDots and related technologies now represent a rapidly advancing and expanding field, as made evident by the large number of recent publications.[9–15]

CDots are generally defined as small carbon nanoparticles with various surface passivation schemes (Figure 4.1),[8,9,16] with their optical properties characterized by strong UV/vis absorptions and bright and colorful fluorescence emissions.[17–19] Despite a certain variability of CDots' structure and optical properties depending on the synthesis route "prototypical" CDots, such as those obtained by deliberate chemical functionalization of preprocessed and selected small carbon nanoparticles, typically display broad and unstructured UV/vis absorption spectra. Their absorption transitions have been assigned to π plasma transitions in the carbon nanoparticles, and the emissions are attributed to radiative recombinations of radical cations and anions that are likely generated via photoinduced charge separation occurring after photoexcitation. These photogenerated charges are trapped at diverse surface defect sites and stabilized by the surface passivation with organic molecules and other species.[2,4,18] In particular, the concept of spontaneous surface trapping of electrons upon photoexcitation of CDots has been clearly demonstrated by their participation in various types of electron transfer reactions.[20–22]

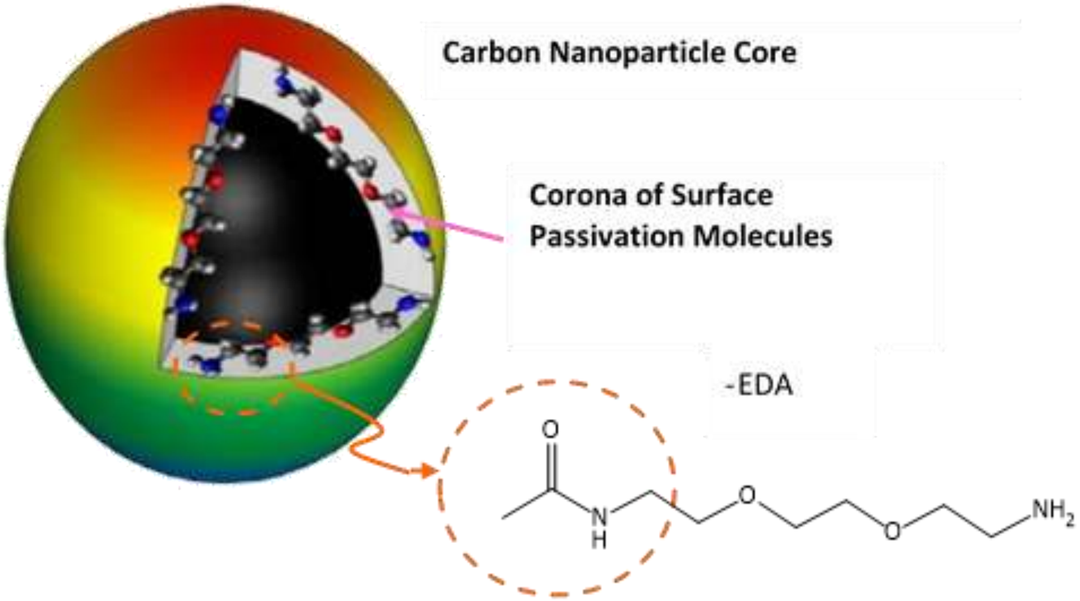

Figure 4.1 A cartoon illustration on EDA-CDots.

As in the CDots originally reported[17] and a general experimental observation ever since, the fluorescence emissions of CDots are excitation wavelength dependent, and the dependence follows a rather characteristic pattern, as found in many independent studies.[17−19,23−27] Mechanistically, however, little effort has been made to understand the characteristic excitation wavelength dependence, even though it may serve as a window through which more insights can be gained into the origins of fluorescence properties in CDots.[28,29] We explored in this work the mechanistic implications of the excitation wavelength-dependent fluorescence properties in terms of their correlation with their optical absorptions, and thus electronic transitions and probabilities, and the exploration was based on the structurally better defined and characterized CDots with 2,2′-(ethylenedioxy)bis(ethylamine) (EDA) for surface functionalization and passivation (EDA-CDots, Figure 4.1).[19]

Ever since the finding of CDots,[17] there have been extensive investigations on the synthesis of CDots, resulting in a large variety of proposed routes.[8,18,30−33] Among the more popular synthetic techniques have been the deliberate chemical functionalization of small carbon nanoparticles and the carbonization of organic precursors, often in “one-pot”, where the precursor acts as both the source for the carbonized nanoparticle core and surface functional groups for the required passivation. The former was applied to the synthesis of the EDA-CDots, whereby preprocessed and selected small carbon nanoparticles were functionalized by EDA molecules via simple amidation chemistry.[19] Such a synthesis, including the reaction and associated configuration of reactants, adheres closely to the structural definition of CDots without any ambiguity and thus is ideally suited for the investigation of the characteristic excitation wavelength dependence in fluorescence properties without any unnecessary complications arising from the involvement of different types of electronic transitions associated with unusual or more complex dot structures. Both steady-state and time-resolved fluorescence techniques were used in the investigation of the EDA-CDots. The results suggest that the excitation wavelength dependence in observed fluorescence quantum yields is essentially decoupled from that in fluorescence lifetimes, implying that the quantum yield follows the changes in the fluorescence radiative rate constants. Furthermore, these wavelength-dependent radiative rates appear to correlate also to the shape of the absorption spectrum of CDots. Potential origins for this behavior are explored, and the broad mechanistic implications are discussed.

4.2 Experimental Section

Materials. Carbon nanopowder (US1074) was purchased from US Research Nanomaterials, Inc., 2,2'-(ethylenedioxy)bis(ethylamine) (EDA) and *N*,*N*-diethylaniline (DEA) from Sigma-Aldrich, thionyl chloride (>99%) from Alfa Aesar, and nitric acid from VWR. Dialysis membrane tubing (molecular weight cut-off 100-500) was purchased from Spectrum Laboratories and Spehadex G-100 aqueous gel column powder from GE Healthcare Life Sciences. Water was deionized and purified by passing through nanopure water purification system.

Measurements. UV/Vis absorption were measured with a Perkin Elmer Lambda 900 absorption spectrophotometer. Steady-state fluorescence spectra were recorded on a Horiba Jobin-Yvon Fluorolog-3 FL3-22 spectrophotometer equipped XBO 450 W Xe short arc-lamp and Hamamatsu T928P PMT photon counting detector operated at 950 V. Reported photoluminescence spectra were collected in ratio mode and have been corrected for non-linear instrument response by applying separately determined correction factor. Fluorescence quantum yields were calculated against 9,10-Bis(phenylethynyl)-anthracene in cyclohexane as a standard with quantum yield of unity measured against quinine sulfate. Fluorescence decays were collected via time-correlated single photon counting (TCSPC) technique on a Horibia Ultima Extreme spectrometer equipped with a SuperK Extreme supercontinuum laser source pulsed at 5 MHz, TDM-800 excitation and TDM-1200 emission monochromators, a R3809-50 MCP-PMT detector operated at 3.0 KV in a thermoelectrically cooled housing, and FluoroHub A+ timing electronics. The time resolution of these measurements, as characterized by the instrumental response function (IRF) of the setup, is 100-200 ps (depending on excitation wavelength). Experimental decay curves were fitted on Das6 fluorescence decay analysis software. Atomic force microscopy (AFM) images were acquired in the acoustic AC mode on a Molecular Imaging PicoPlus AFM system equipped with a multipurpose scanner and a NanoWorld point probe NCH sensor. The height profile analysis was assisted by using the SjPIP software distributed by Image Metrology.

Carbon Nanoparticles. Small carbon nanoparticles were harvested from commercially supplied carbon nanopowder with procedure preciously reported.[23,24] Carbon nanopowder (2 g) was refluxed in 8 M nitric acid (200 mL) for 48 hours. The acidic solution was cooled to room temperature then centrifuged at 1,000 *g*. The residue was redispersed in nanopure water and dialyzed (100-500 MWCO) against fresh water until pH of wash solution was ~4. The dialyzed solution was centrifuged at 1000 *g* to retain small oxidized carbon nanoparticles in the supernatant, which resembled a highly coloured solution while remaining transparent. The carbon nanoparticles were recovered from the supernatant via evaporation then saved for future use in functionalization reactions.

EDA-Carbon Dots. EDA-carbon dots were synthesized by deliberate surface functionalization of oxidized carbon nanoparticles with EDA monomers in a two-step reaction, activation of the carboxylic moieties on the carbon nanoparticles followed by nucleophilic acyl substitution by EDA. Detailed experimental procedures have been previously reported in the literature.[19] In a typical experimental procedure, nitric-acid treated carbon nanoparticles (50 mg) was refluxed in excess neat thionyl chloride for 12

h. Upon removal of excess thionyl chloride via evaporation, acyl chloride activated carbon nanoparticles were carefully mixed with EDA (1 g) heated to 120 ^{o}C and stirred vigorously under nitrogen protection for 3 days. The reaction mixture was cooled to room temperature and dispersed in water then centrifuged at 20,000 *g* for 1 hour to retain the supernatant. The aqueous solution was dialyzed against fresh water (100-500 MWCO) to remove unreacted EDA monomers and other small molecular species, resulting in a transparent aqueous solution of EDA-carbon dots. The as-prepared EDA-carbon dots were then separated on a Sephadex G-100 gel column to retain the most brightly fluorescent fractions. Detailed separation procedures already reported in the literature.[24]

Fluorescence Quenching. A solution of EDA-CDots in methanol was prepared for fluorescence quenching studies. This solution was used for the preparation of solutions with the quencher diethylaniline (DEA) at quencher concentrations up to 0.05 M. Fluorescence spectra and decays were collected at room temperature with excitations of 400 nm and 425 nm while monitoring the decay kinetics of the emission at 480 nm.

4.3 Results and Discussion

Commercially supplied carbon nanopowder sample was processed in a procedure involving oxidative acid treatment for the harvesting of small carbon nanoparticles in an aqueous dispersion. The nanoparticles were recovered from the dispersion and used in the functionalization with 2,2'-(ethylenedioxy)bis(ethylamine) (EDA) under amidation reaction conditions, yielding EDA-CDots, as previously reported.[19] The synthesis is often referred to as the deliberate chemical functionalization method in the preparation of CDots.[8,9] According to TEM imaging results, the EDA-CDots are on average around 6-7 nm in diameter (Figure 4.2), and they are quasi-spherical with essentially amorphous core structure.

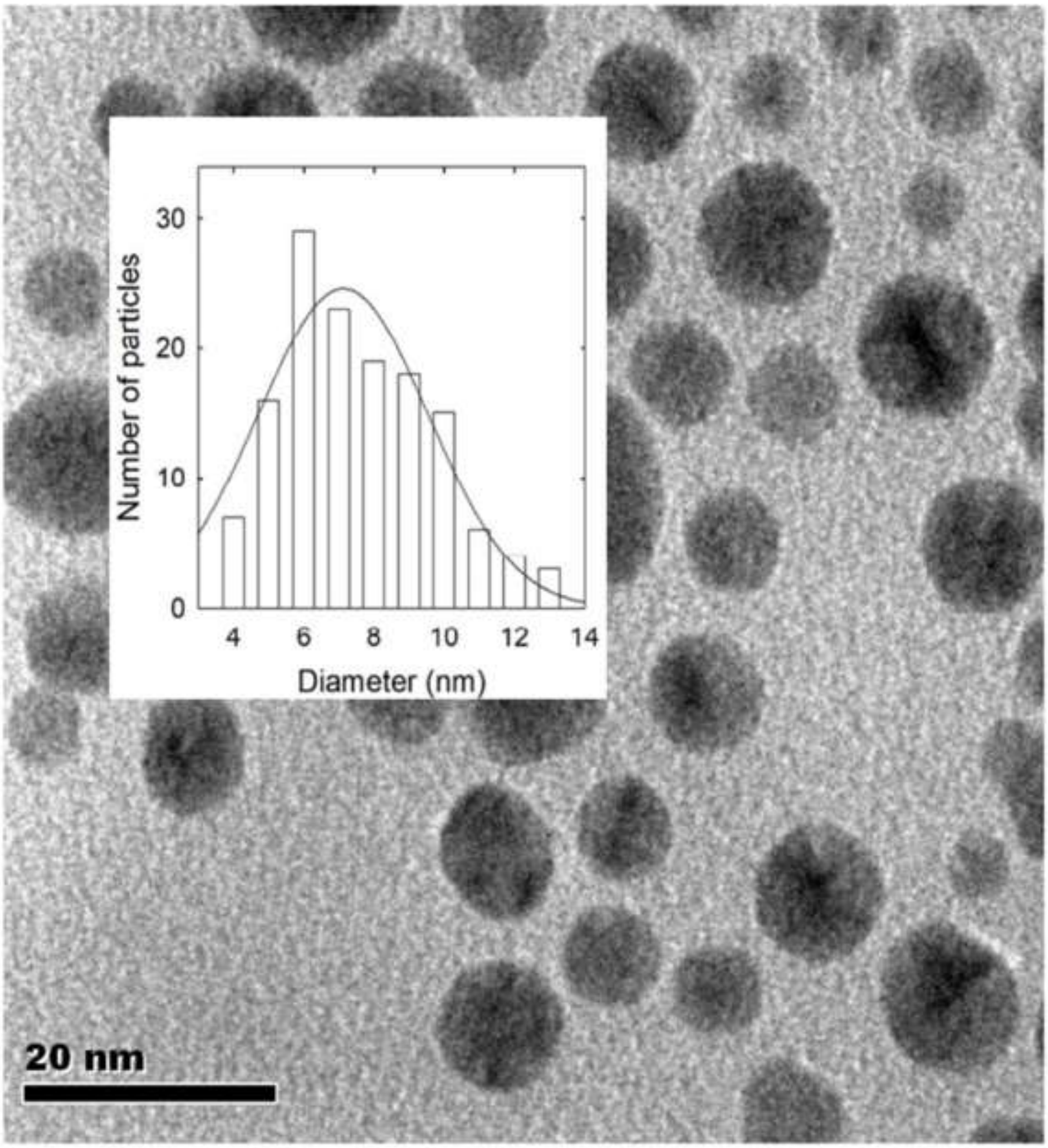

Figure 4.2 A TEM image of the EDA-CDots, with the size distribution based on multiple images shown in the inset.

UV/vis absorption spectra of the EDA-CDots and the aqueous dispersed carbon nanoparticles are almost identical (Figure 4.3), except for the latter being subject to more significant light scattering effect. The results support the notion that the optical absorption in the CDots is dominated by the core carbon nanoparticles, with the organic surface functional moieties in the CDots (Figure 1) optically transparent. However, the functionalization affects the fluorescence emissions significantly, as made evident by the comparison in Figure 4.3. In fact, the functionalization causes a large increase in the fluorescence intensities (more than an order of magnitude),[25] accompanied by a red-shift and change of shape of the emission band, suggesting that the inherent nature of the emissive state is not the same in the two systems.

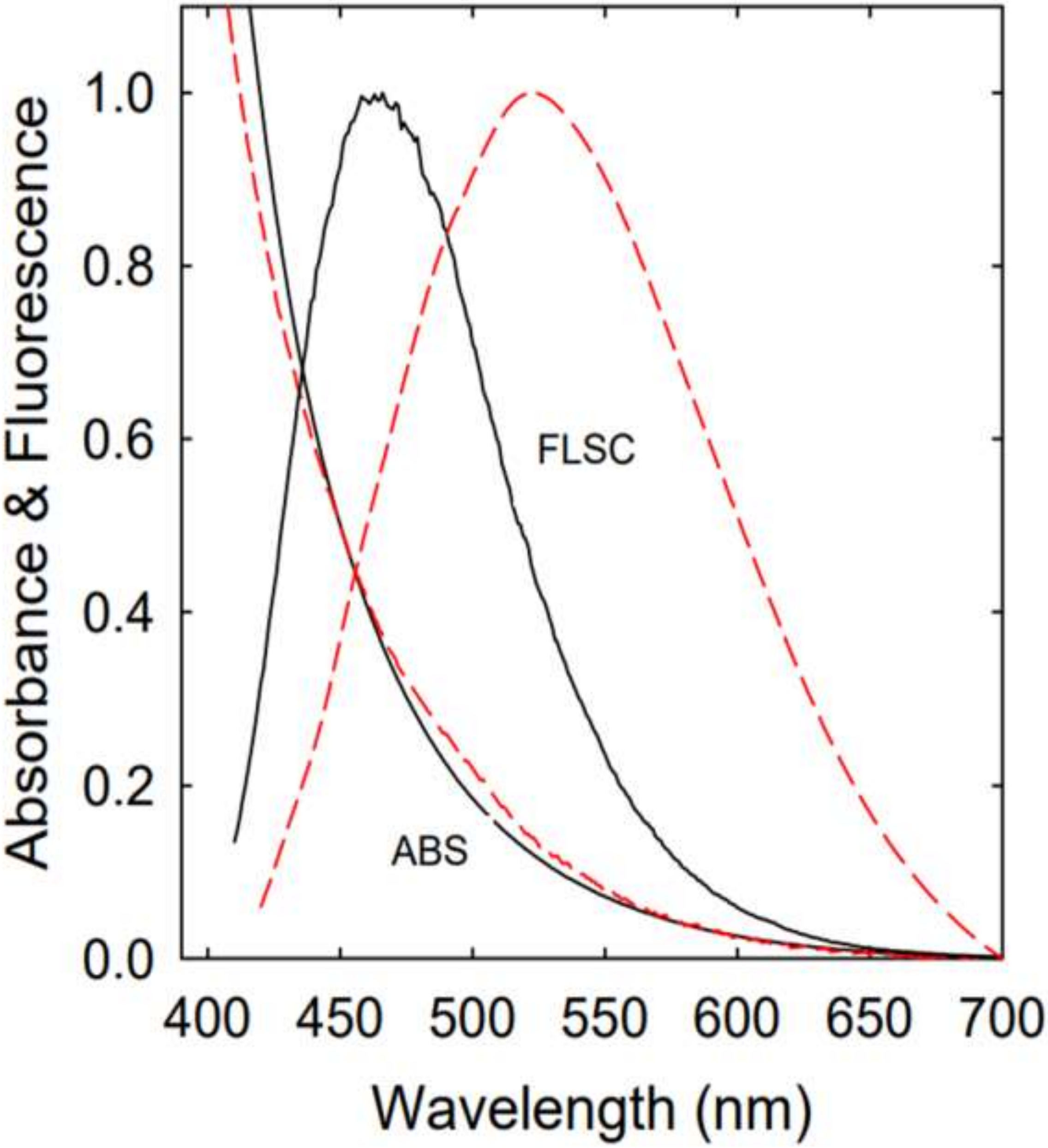

Figure 4.3 Absorption (ABS) and fluorescence (FLSC, 400 nm excitation) spectra of the EDA-CDots in aqueous solution (solid line) and aqueous dispersed carbon nanoparticles (dashed line).

Fluorescence spectra of the EDA-CDots at a series of excitation wavelengths are shown in Figure 4.4 in both relative intensities and a normalized scale. The emissions are obviously excitation wavelength dependent, with the fluorescence band maximum shifting progressively with the excitation toward longer wavelengths, accompanied by progressive narrowing of the emission band width and decreasing of emission intensities (Figure 4.4). These dramatic changes of the emission color as a function of the excitation wavelength are a rather common finding for CDots, likely reflecting the availability of surface traps at different energies, probably variable from dot to dot as a consequence of structural inhomogeneity. The fluorescence quantum yields Φ_F at a series of excitation wavelengths were determined accurately by careful corrections of nonlinear instrumental responses with respect to different excitation and emission wavelengths.[34] The Φ_F values are obviously excitation wavelength dependent, and more interestingly the dependence (higher quantum yields in the blue and progressively lower at longer excitation wavelengths) tracks closely the absorption spectral profile (Figure 4.5). Even more interesting and mechanistically significant is that the excitation wavelength dependence of fluorescence quantum yields in the CDots is decoupled from that of observed fluorescence decays and lifetimes presented as follows.

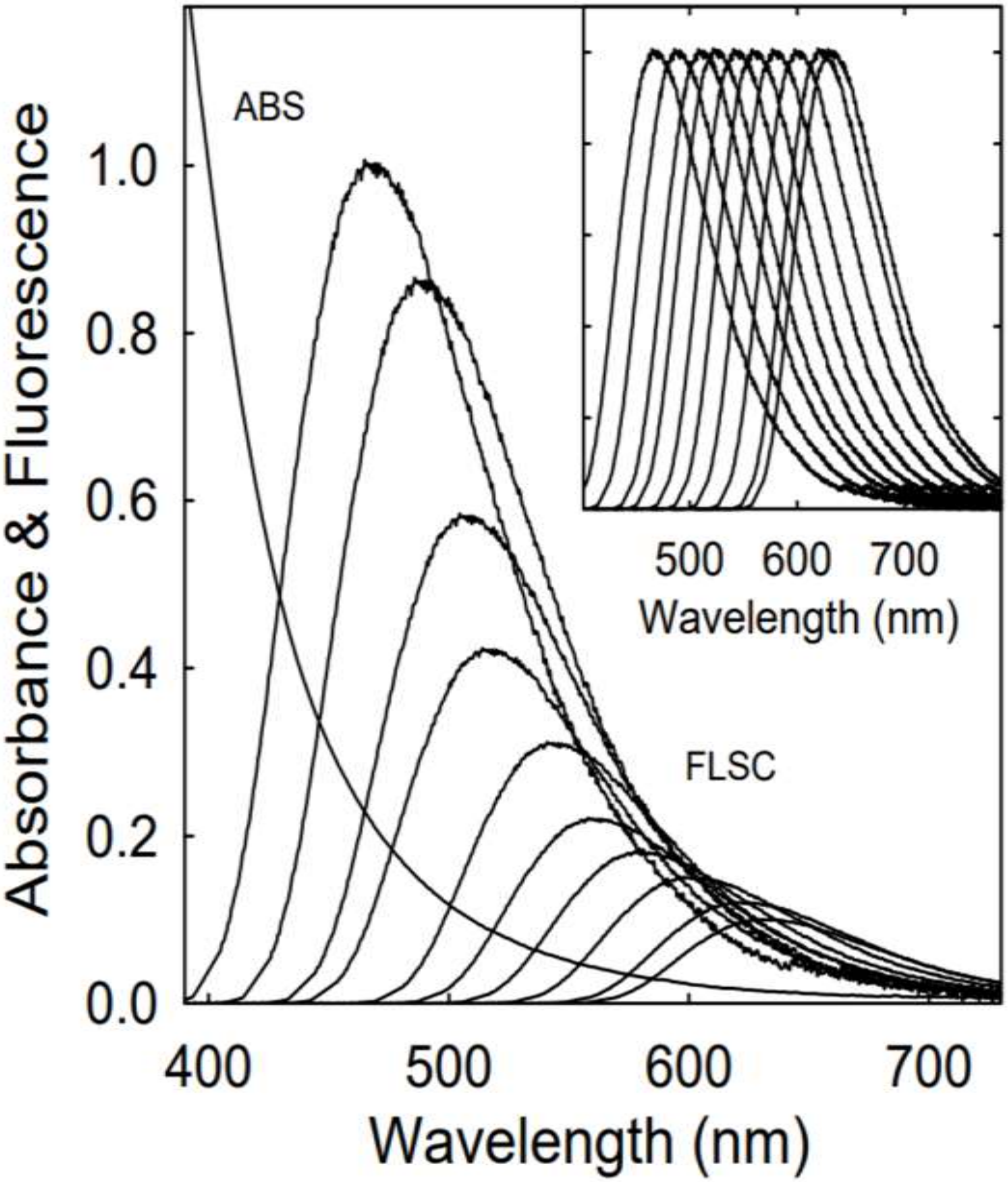

Figure 4.4 Fluorescence (FLSC) spectra of the EDA-CDots in aqueous solution excited at (in the order of progressively lower peak intensity) 400 nm to 580 nm in 20 nm increment. The corresponding normalized spectra are shown in the inset.

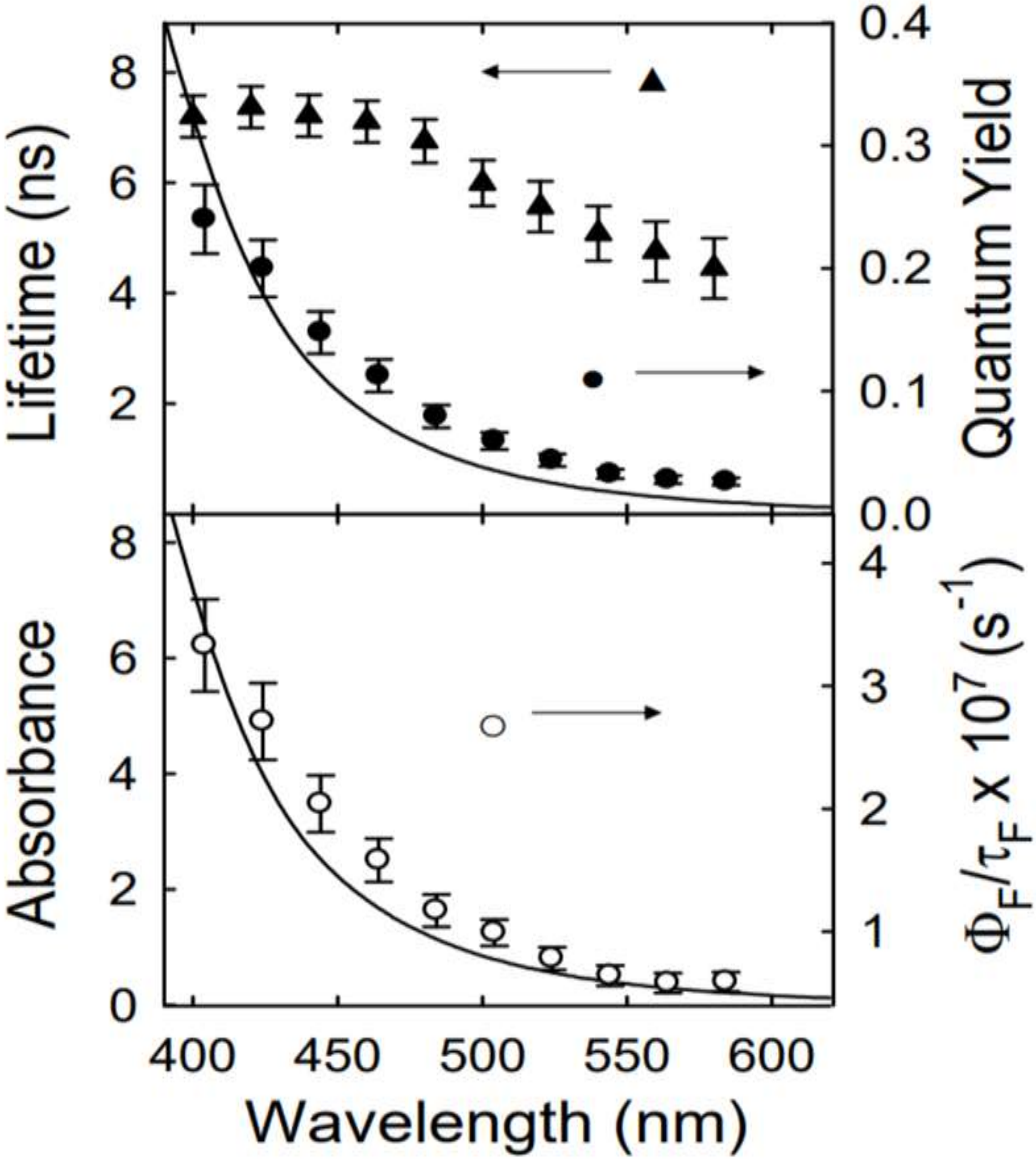

Figure 4.5 Upper: Observed fluorescence quantum yields (Φ_F, solid circle) and averaged fluorescence lifetimes (τ_F, solid triangle) of the EDA-CDots in aqueous solution at different excitation wavelengths. Lower: Φ_F/τ_F ratios for the different excitation wavelengths.

Nanosecond fluorescence decays of the EDA-CDots were measured by using the time-correlated single photon counting (TCSPC) technique. As illustrated in Figure 4.6, the decays at different excitation wavelengths are similar, suggesting no dramatic changes in the depopulation processes of the emissive excited states that are populated by excitation at the series of wavelengths, again decoupled from what are found in fluorescence quantum yields (Figure 4.5). The decays are all non-exponential, but could be satisfactorily fitted with the use of a bi-exponential decay function.[23,24,35] The good data fits provide a way of averaging the overall fluorescence decay processes in the EDA-CDots. The fluorescence lifetime (τ_{F1} and τ_{F2}) and pre-exponential factor (A_1 and A_2) values from the fits are shown in Table 1. In a further averaging, the τ and A values were used to calculate the average fluorescence lifetime for each excitation wavelength, $<\tau_F> = (A_1\tau_{F1}^2+A_2\tau_{F2}^2)/(A_1\tau_{F1}+A_2\tau_{F2})$,[34] and the $<\tau_F>$ values thus calculated are also shown in Table 4.1. As compared in Figure 4.5, the average fluorescence lifetimes are only weakly dependent on excitation wavelengths, clearly decoupled from fluorescence quantum yields. In fact, the average lifetime changes less than twofold across the entire excitation wavelength range, in contrast to the quantum yield, which decreases almost tenfold in the same interval.

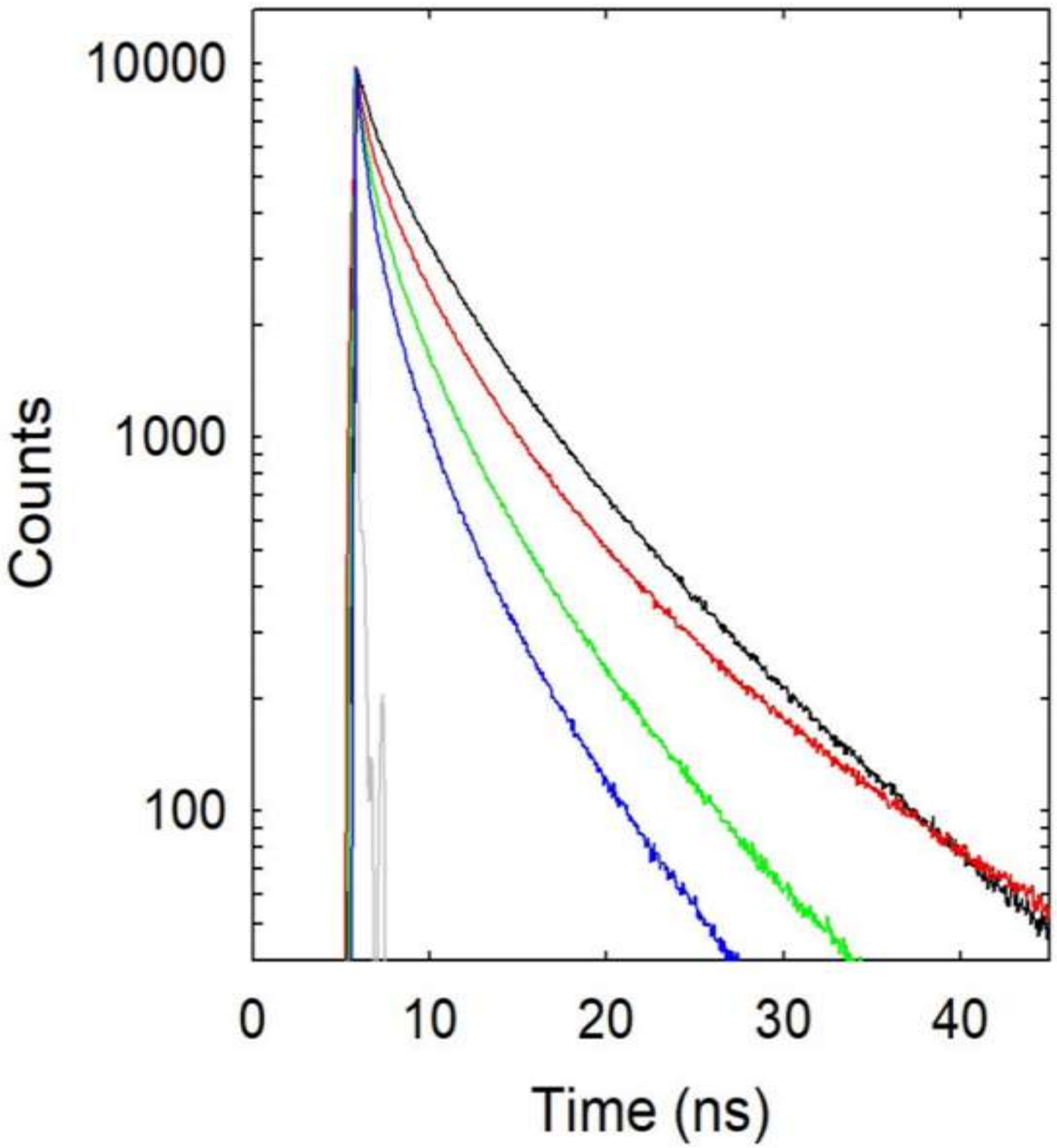

Figure 4.6 Observed decay curves of the EDA-CDots in aqueous solution at different excitation wavelengths.

Table 4.1 Fluorescence Decay Kinetics of the EDA-CDots Deconvoluted with a Biexponential Decay Function

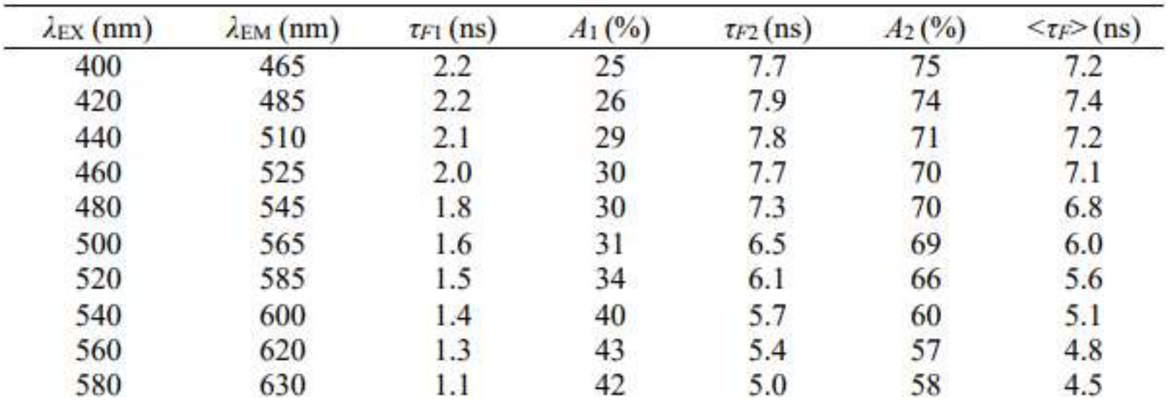

λ_{EX} (nm)	λ_{EM} (nm)	τ_{F1} (ns)	A_1 (%)	τ_{F2} (ns)	A_2 (%)	$<\tau_F>$ (ns)
400	465	2.2	25	7.7	75	7.2
420	485	2.2	26	7.9	74	7.4
440	510	2.1	29	7.8	71	7.2
460	525	2.0	30	7.7	70	7.1
480	545	1.8	30	7.3	70	6.8
500	565	1.6	31	6.5	69	6.0
520	585	1.5	34	6.1	66	5.6
540	600	1.4	40	5.7	60	5.1
560	620	1.3	43	5.4	57	4.8
580	630	1.1	42	5.0	58	4.5

On the two parameters Φ_F and τ_F describing the same emissions, the determination of each Φ_F value was based on the total fluorescence (the integration of the area under the observed fluorescence spectrum), while the measurement of fluorescence decay at each excitation wavelength covered only a portion of the emission spectrum, namely a potential issue that the observed fluorescence emissions could have different average lifetimes at different emission wavelengths. The issue was examined by comparing fluorescence decays at the same excitation wavelength but monitored at different spectral positions within the overall emission band, and no meaningful difference was found in the observed decays. The homogeneity of the fluorescence spectrum in terms of the same decay at different emission wavelengths was further confirmed by the fluorescence quenching results described below. In fact, the emissions of the EDA-CDots could be quenched efficiently by both electron donors and acceptors, such as *N*,*N*-diethylaniline (DEA) and 2,4-dinitrotoluene (DNT),[35] respectively. For DEA as quencher, low quencher concentrations were used to avoid any static quenching contributions and also the potential quenching of any shorter-lived transient species and/or faster transient processes that feed the emissive excited states responsible for the observed fluorescence emissions. As shown in Figure 4.7, the quenching is extremely efficient, at the upper limit of diffusion control, and more relevant and important to the discussion above the fluorescence intensities are reduced due to the quenching uniformly across the entire emission spectrum, suggesting again homogeneity in the time profiles of emissions at different wavelengths.

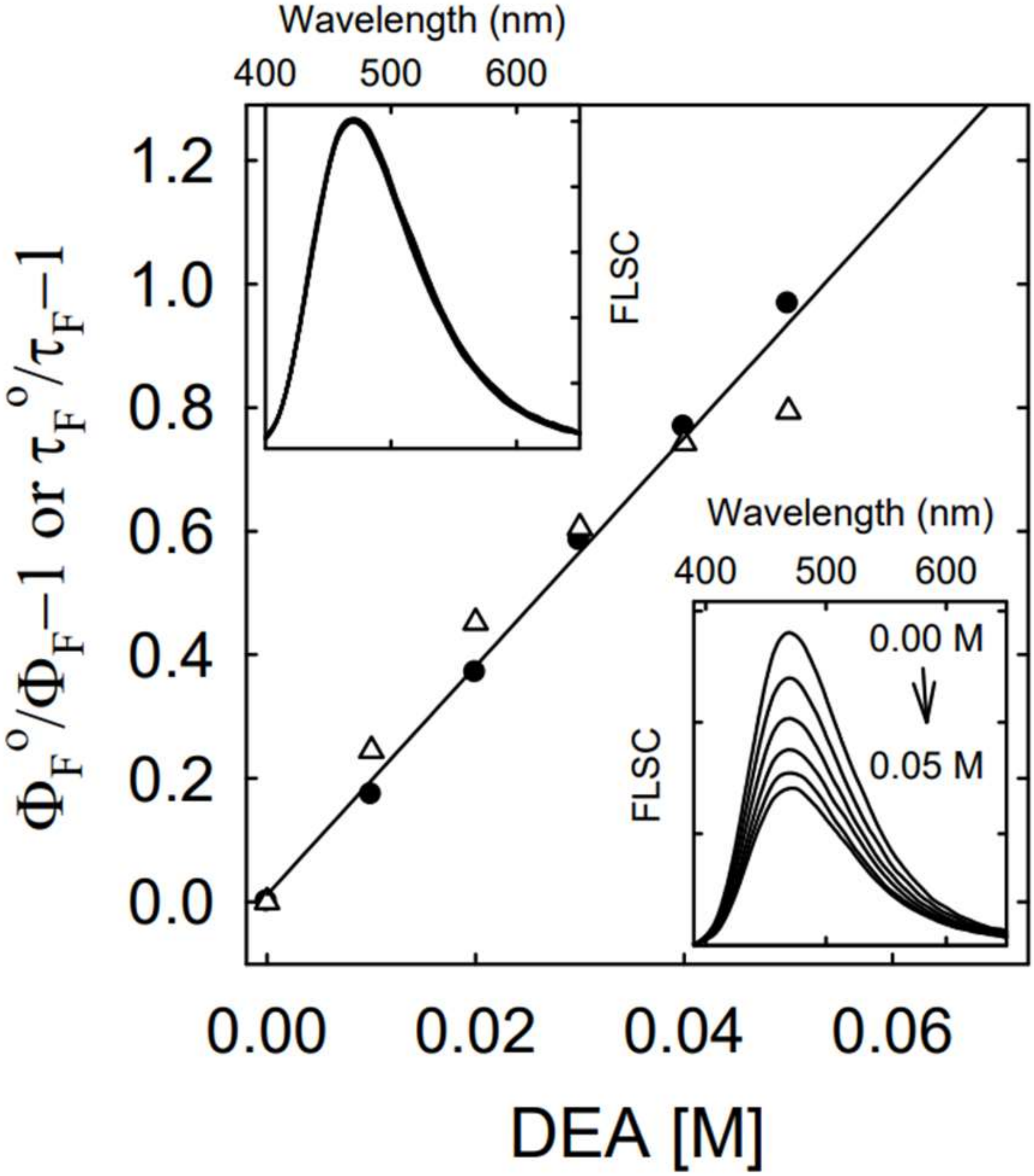

Figure 4.7 Stern-Volmer quenching plots for fluorescence quantum yields (open triangle) and lifetimes (solid circle) of the EDA-CDots in methanol with *N*,*N*-diethylaniline (DEA) as quencher. Shown in the insets are the corresponding fluorescence spectra at different EDA concentrations (lower, normalized in upper).

Beside the excitation-dependence of the emission color, what is most surprising and mechanistically significant in Figure 4.5 is the energy dependence of the Φ_F/τ_F ratios, which, for a molecular fluorophore, typically express the radiative rate constant. In fact, the Φ_F/τ_F ratios display a pronounced excitation-energy dependence, rapidly decreasing towards the red; additionally, their excitation dependence appears to closely track the absorption profile. These observations probably subtend important information about the underlying CDots photophysics, as discussed in the following.

In CDots, the optical absorptions reflecting electronic transitions are associated with the core carbon nanoparticles, with likely multiple transitions in a distribution over the absorption wavelengths. Their absorption profile has been rationalized as being superposition from diverse state transitions, in which more strongly absorptive species exist in the blue region of the visible spectrum. It is therefore no surprise for the excitation wavelength dependent emissions in the EDA-CDots and other CDots reported in the literature.[17-19,23-27] Mechanistically, the observed fluorescence properties may be explained in terms of two distinct photophysical processes and their efficiencies: **(i)** the population of an emissive excited state (Φ_1), proceeding through spontaneous charge separation and trapping at surface sites, occurring after absorption, and **(ii)** the radiative recombination of charge carriers after trapping (Φ_2). The observed fluorescence quantum yield can then be viewed as a product of these two efficiencies such that $\Phi_F = \Phi_1\Phi_2$. Based on previous findings, the surface passivation in CDots mainly acts on the first term (Φ_1) in populating the emissive excited state, on which mechanistic reasons might include an improved stabilization of the trapping sites (consistent with the fluorescence red shift upon passivation, as from Figure 4.3) and/or a more effective electronic coupling between the core structure and surface moieties.[23,25] The dramatic fluorescence enhancement effect produced on CDots by a proper passivation, together with the very large Φ_F values reported for many types of CDots, and the marked redox capabilities of photoexcited CDots strongly suggest that Φ_1 approaches unity, that is, no significant losses are expected in EDA-CDots during the formation of the emissive state. The latter process (Φ_2), as discussed herein, is primarily governed by radiative rate constants in competition with other deactivation pathways, specifically derived from inherent optical transitions in which the transition strengths are strongly correlated with brightness of fluorescent emissions. Even though the population of the emissive states and radiative recombinations can be categorically distinguished, they do not occur in isolation. However, several findings have suggested there to be a specific surface interaction between the carbon core and surface passivation agent that leads to a select wavelength region of increased optical transition strength, leading to enhanced fluorescence emission brightness. The specific nature of this interaction is not well understood and will require more investigation to shed light on the specific mechanistic origin of the selective enhancement in fluorescence emissions.

The population of the emissive state from the earliest excited one (that is Φ_1) is likely driven by an excited-state reorganization expected to occur on the picosecond and sub-picosecond range, which can only be experimentally addressed by femtosecond spectroscopies, still very rare in the literature.[22] Although it may be possible in principle that the excitation-dependence of Φ_F partially reflects changes of Φ_1, the simplest working assumption for the present purposes is the absence of losses during this step: (1) Φ_1 is excitation-independent and possibly close to unity, and (2) the excited-state relaxation and subsequent formation of the emissive state occurs with no significant decreases in the optical strength of the transition (namely, emission and absorption efficiencies), which would tend to lower the quantum yield.

In this scenario, the dependence of the quantum yield entirely arises from Φ_2 and for the same fluorescence emissions the observed quantum yield of the emitting state (Φ_F) is related to lifetime (τ_F) by the equation,

$$\Phi_F \approx \Phi_2 = k_F \tau_F \qquad (1)$$

where k_F is the fluorescence radiative rate constant. Therefore, the Φ_F/τ_F ratios plotted in Figure 4.5 essentially express the radiative efficiency of the fluorescent transitions. While in molecular spectroscopy,[34,36-38] the radiative rate constant k_F for a molecular fluorophore is generally excitation wavelength independent, Figure 4.5 shows that this is not the case for CDots. Our data rather suggest that the optical transitions of CDots form a continuous distribution in which lower-energy emissive transitions are less and less allowed, as reflected by their progressively smaller radiative rates.

Furthermore, the radiative rate can be generally correlated with the electronic transition probabilities reflected by the corresponding optical absorption band,

$$k_F = 3\text{x}10^{-9}\nu_o^2 \int \varepsilon d\nu \qquad (2)$$

where ε is the extinction coefficient and ν_o is the energy corresponding to the maximum transition energy (in wavenumbers).[36] Therefore, the changes of the radiative rate are expected to reflect in corresponding changes of the absorption strength.

Indeed, across the investigated spectral range (a relatively narrow one in absolute terms), the term ν_o^2 in equation (2) changes slower than either the absorption coefficient or k_F, whose wavelength-dependence is very steep, and thus plays a relatively minor role. Considering this, a similarity between the radiative rate and the absorption profile (Figure 4.5) suggests that the shape of the absorption spectrum largely reflects the different absorption strengths of the diverse transitions contributing to the overall spectrum. Although many transitions are involved and superimposed in the broad visible absorption, the absorption curve does not seem to be dictated only by the different abundance of CDots absorbing at different wavelengths, which would be the simplest assumption to make. On the contrary, the fundamental optical properties of CDots seem to be largely governed by the corresponding strengths of optical transitions, rather than inherent abundance. This can most clearly be illustrated by the tracing of the radiative rates, and, consequently, the fluorescence quantum yield of each occupied state.

While equation (2) cannot be strictly applied in a case where the optical absorption spectrum results from the superposition of many transitions, and therefore cannot be used to calculate the radiative rates, it still represents a framework to understand the photophysical relationship between the transition strengths and radiative rate constants. Equation (2) essentially states a proportionality between the radiative rate of an electronic transition and the allowedness of its optical absorption, hence the strength of the corresponding absorption band. Thus, the data in Figures 4.4 and 4.5 suggest that the optical absorption spectrum of CDots consists of an inhomogeneous distribution of transitions at different energies having different degrees of allowedness, systematically decreasing in the red, therefore producing emissions with similarly decreasing radiative rates and quantum yields.

Further investigations will certainly be needed to concretely track down this inhomogeneous distribution to the underlying structural differences responsible for it. Because of the absence of quantum confinement effects, the size of the dots is expected to play no role here. In contrast, we expect that the variable surface structure of different dots is entirely responsible for their different emission features. Because the degree of allowdness of an electronic transition is mostly decided by the (squared) transition dipole moment, a way to interpret our results would be hypothesising that the CDots capable of lower energy emissions are characterized by surface structures having such characteristics that the charge separation induced by photoexcitation is more pronounced. In fact, a higher degree of charge separation would correlate with stronger energy relaxation (because of solvent interactions)[21] thereby redder emissions, as well as with a smaller oscillator strength and radiative rates, due to the smaller wavefunction overlap hindering radiative recombination. We believe present results may trigger ab-initio quantum chemical studies aimed at testing these speculations or proposing alternative ones.

4.4 Conclusion

The EDA-CDots synthesized by the more controllable deliberate functionalization of pre-processed and selected small carbon nanoparticles, thus structurally simple and better defined, were studied by using steady-state and time-resolved fluorescence methods. The observed fluorescence quantum yields are strongly excitation wavelength dependent, and the dependence apparently tracks closely the observed absorption profile of the CDots, whereas the excitation wavelength dependence of observed fluorescence decays or average lifetimes is much weaker, obviously decoupled from the quantum yields. Mechanistically, the presence of two sequential processes immediately following photoexcitation leading to fluorescence is used to rationalize the observed characteristic excitation wavelength dependence, with the first process (Φ_1) for the formation of the emissive excited state, and the second process (Φ_2) for the competition between radiative and non-radiative deactivations. The experimental results seem better explained by attributing the latter to be primarily responsible for the characteristic excitation wavelength dependence. A strong case is also made for further experimental investigations, especially those based on femtosecond spectroscopy techniques, as well as theoretical and computational efforts, towards a more detailed mechanistic understanding of the rather characteristic dependence and the fluorescence properties of CDots in general.

4.5 Acknowledgements

This work has been previously published in the literature in collaboration with Prof. Fabrizio Messina, Alice Sciortino, Dr. Christopher E. Bunker, Ping Wang, Dr. K. A. Shiral Fernando, and Prof. Ya-Ping Sun, all of whom I gratefully acknowledge.[39]

4.6 References

1. Luo, P. G.; Sahu, S.; Yang, S.-T.; Sonkar, S. K.; Wang, J.; Wang, H.; LeCroy, G. E.; Cao, L.; Sun, Y.-P. *J. Mater. Chem. B* **2013**, 1, 2116-2127.
2. Hola, K.; Zhang, Y.; Wang, Y.; Giannelis, E. P.; Zboril, R.; Rogach, A. L. *Nano Today* **2014**, 9, 590−603.
3. Du, Y.; Guo, S. *Nanoscale* **2016**, 8, 2532−2543.
4. Wang, F.; Chen, Y. H.; Liu, C. Y.; Ma, D. G. *Chem. Commun.* **2011**, 47, 3502-3504
5. Veca, L. M.; Diac, A.; Mihalache, I.; Wang, P.; LeCroy, G. E.; Pavelescu, E. M.; Gavrila, R.; Vasile, E.; Terec, A.; Sun, Y.-P. *Chem. Phys. Lett.* **2014**, 613, 40-44
6. Li, X.; Rui, M.; Song, H.; Shen, Z.; Zeng, H. *Adv. Funct. Mater.* **2015**, 25, 4929-4947.
7. Lim, S. Y.; Shen, W.; Gao, Z. *Chem. Soc. Rev*. **2015**, 44, 362−381.
8. LeCroy, G. E.; Yang, S.-T.; Yang, F.; Liu, Y.; Fernando, K. A. S.; Bunker, C. E.; Hu, Y.; Luo, P. G.; Sun, Y.-P. *Coord. Chem. Rev*. **2016**, 320, 66-81.
9. Fernando, K. A. S.; Sahu, S.; Liu, Y.; Lewis, W. K.; Guliants, E. A.; Jafariyan, A.; Wang, P.; Bunker, C. E.; Sun, Y.-P. *ACS Appl. Mater. Interfaces* **2015**, 7, 8363−8376.
10. Wang, Y.; Hu, A. *J. Mater. Chem. C* **2014**, 2, 6921−6939.
11. Miao, P.; Han, K.; Tang, Y.; Wang, B.; Lin, T.; Cheng, W. *Nanoscale* **2015**, 7, 1586−1595.
12. Zhao, A.; Chen, Z.; Zhao, C.; Gao, N.; Ren, J.; Qu, X. *Carbon* **2015**, 85, 309-327.

13. Luo, P. G.; Yang, F.; Yang, S.-T.; Sonkar, S. K.; Yang, L.; Broglie, J. J.; Liu, Y.; Sun, Y.-P. *RSC Adv*. **2014**, 4, 10791−10807.

14. Hu, C.; Yu, C.; Li, M.; Wang, X.; Yang, J.; Zhao, Z.; Eychmuller, A.; Sun, Y.-P.; Qiu, J. *Small* **2014**, 4926-4933.

15. Konstantinos, D. *Curr. Org. Chem.* **2016**, 20, 682-695.

16. Cao, L.; Meziani, M. J.; Sahu, S.; Sun, Y.-P. *Acc. Chem. Res.* **2013**, 46, 171−180.

17. Sun, Y.-P.; Zhou, B.; Lin, Y.; Wang, W.; Fernando, K. A. S.; Pathak, P.; Meziani, M. J.; Harruff, B. A.; Wang, X.; Wang, H.; et al. *J. Am. Chem. Soc*. **2006**, 128, 7756−7757.

18. Wang, X.; Cao, L.; Yang, S.-T.; Lu, F.; Meziani, M. J.; Tian, L.; Sun, K. W.; Bloodgood, M. A.; Sun, Y.-P. *Angew. Chem., Int. Ed*., **2010**, 49, 5310–5314.

19. LeCroy, G.E.; Sonkar, S. K.; Yang, F.; Veca, L. M.; Wang, P.; Tackett II, K. N.; Yu, J.-J.; Vasile, E.; Qian, H.; Liu, Y.; Luo, P. G.; Sun, Y.-P. *ACS Nano* **2014**, 8, 4522-4529.

20. Wang, X.; Cao, L.; Lu, F.; Meziani, M.; Li, H.; Qi, G.; Zhou, B.; Harruff, B. A.; Kermarrec, F.; Sun, Y.-P. *Chem. Commun.* **2009**, 3774-3776.

21. Sciortino, A.; Marino, E.; van Dam, B.; Schall, P.; Cannas, M.; Messian, F. *J. Phys. Chem. Lett.* **2016**, 7, 3419-3423.

22. Sciortino, A.; Madonia, A.; Gazzetto, M.; Sciortino, L.; Rohwer, E. J.; Feurer, T.; Gelardi, F. M.; Cannas, M.; Cannizzo, A.; Messina, F. *Nanoscale* **2017**, 9, 11902-11911.

23. Yang F.; LeCroy, G. E.; Wang, P.; Liang, W.; Chen, J.; Fernando, K. A. S.; Bunker, C. E.; Qian, H.; Sun, Y.-P. *J. Phys. Chem. C* **2016**, 120, 25604-25611.

24. Hu, Y.; Al Awak, M. M.; Yang, F.; Yan, S.; Xiong, Q.; Wang, P.; Tang, Y.; Yang, L.; LeCroy, G. E.; Hou, X.; Bunker, C. E.; Xu, L.; Tomlinson, N.; Sun, Y.-P. *J. Mater. Chem. C* **2016**, 4, 10554-10561.

25. Liu, Y.; Wang, P.; Fernando, K. A. S.; LeCroy, G. E.; Maimaiti, H.; Harruff-Miller, B. A.; Lewis, W. K.; Bunker, C. E.; Hou, Z.-L.; Sun, Y.-P. *J. Mater. Chem. B* **2016**, 29, 1-8.

26. Anilkumar, P.; Wang, X.; Cao, L.; Sahu, S.; Jiu, J.-H.; Wang, P.; Korch, K.; Tackett, K. N. II; Parenzan, A.; Sun, Y.-P. *Nanoscale* **2011**, 3, 2023-2027.

27. Wang, L.; Zhu, S.-J.; Wang, H.-Y.; Qu, S.-N.; Zhang, Y.-L.; Chen, Q.-D.; Xu, H.-L.; Han, W.; Yang, B.; Sun, H.-B. *ACS Nano* **2014**, 8, 2541-2547.

28. Ghosh, S.; Chizhik, A. M.; Karedla, N.; Dekaliuk, M. O.; Gregor, I.; Schuhmann, H.; Seibt, M.; Bodensiek, K.; Schaap, I. A. T.; Schulz, O.; Demchenko, A. P.; Enderlein, J.; Chizhik, A. I. *Nano Lett.* **2014**, 14, 5656-5661.

29. Khan, S.; Gupta, A.; Verma, N. C.; Nandi, C. K. *Nano Lett.* **2015**, 15, 8300-8305.

30. Anilkumar, P.; Wang, X.; Cao, L.; Sahu, S.; Liu, J.-H.; Wang, P.; Korch, K.; Tackett II, K. N.; Parenzan, A.; Sun, Y.-P. *Nanoscale* **2011**, 3, 2023-2027.

31. Zhai, X.; Zhang, P.; Liu, C.; Bai, T.; Li, W.; Dai, L.; Liu, W. *Chem. Comm.* **2012**, 48, 7955-7957.

32. Stan, C. S.; Albu, C.; Coroaba, A.; Popa, M.; Sutiman, D. *J. Mater. Chem. C* **2015**, 3, 789-795.

33. Hou, X.; Hu, Y.; Wang, P.; Yang, L.; Al Awak, M. M.; Tang, Y.; Twara, F. K.; Qian, H.; Sun, Y.-P. *Carbon* **2017**, 122, 389-394.

34. Lakowicz, J. R. Kluwer Academic/Plenum Publishers: New York, 1999.

35. LeCroy, G. E.; Fernando, K. A. S.; Bunker, C. E.; Wang, P.; Tomlinson, N.; Sun, Y.-P. *Inorg. Chim. Acta* **2017**, *468*, 300-307.

36. Turro, J. N.; Ramaurthy, V.; Scaiano, J. C. University Science Books: Sausalito, 2009.

37. Birks, J. B. Wiley-Interscience: London, 1970.

38. Strickler, S. J.; Berg, R. A. *J. Chem. Phys*. **1962**, 37, 814-822.

39. LeCroy, G. E.; Messina, F.; Sciortino, A.; Bunker, C. E.; Wang, P.; Fernando, K. A. S.; Sun, Y.-P. *J. Phys. Chem. C* **2017**, *121*, 28180-18186.

CHAPTER FIVE

TOWARDS PROPERTY-BY-DESIGN THROUGH MODIFICATION OF CARBON-BASED “QUANTUM” DOTS

5.1 Introduction

In the extensive pursuit of nanoscale carbon allotropes, from fullerenes at the zero-dimension to one-dimensional carbon nanotubes and more recently two-dimensional graphenes, carbon nanoparticles have largely been excluded probably for their apparent lack of the kind of structural beauty found in the other carbon allotropes and/or seemingly uninspiring properties. However, small carbon nanoparticles, with sizes on the order of a few nanometers, should in fact be classified as another zero-dimensional carbon allotrope, in addition to fullerenes, for their unique and many superior optical, redox, and other characteristics, which have been made evident with the particle surface passivation in the nanoscale configuration now widely recognized as carbon “quantum” dots or carbon dots (CDots).[1-7]

CDots are defined generally as small carbon nanoparticles with various surface passivation schemes (Figure 5.1),[1,2,6] including the deliberate chemical functionalization of pre-processed and selected carbon nanoparticles with organic molecules [8,9] or the surface passivation by the remaining organic species following "one-pot" carbonization processing of organic precursors.[10-13] There have been a large number of reported studies on all aspects of CDots, from syntheses and structural and property characterizations[5-7] to a variety of potential applications in bioimaging and sensing,[3] optoelectronics and energy conversions,[5,7] biocidal functions,[14,15] and others.[5-7,16-18] In fact, the study and development of CDots have emerged to become a rapidly advancing and expanding research field.

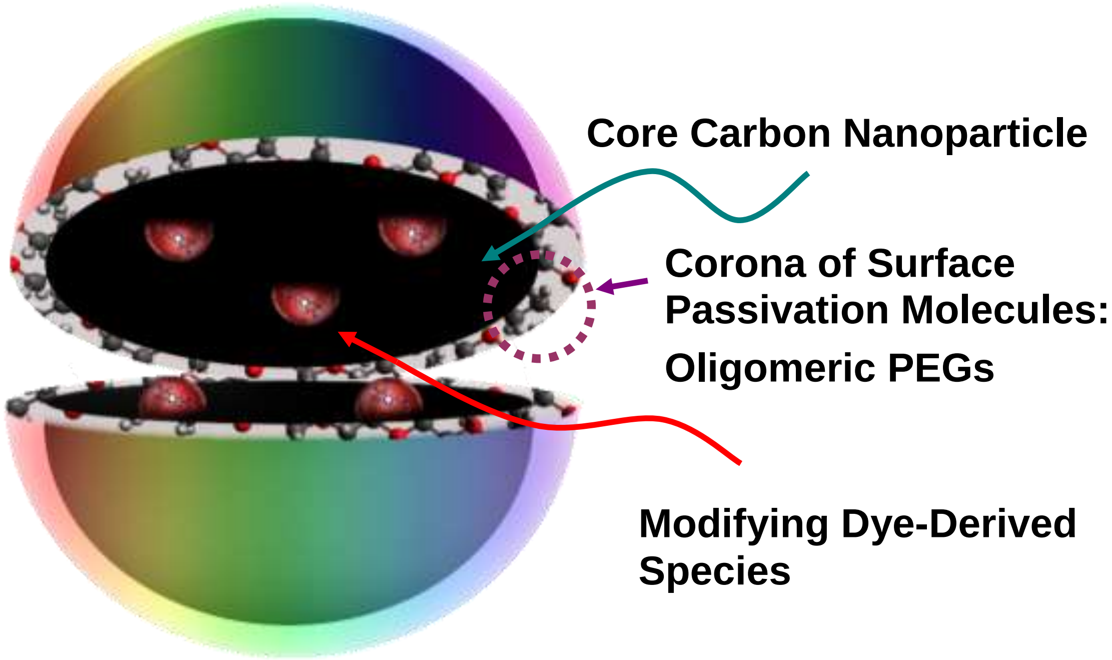

Figure 5.1 A carton illustration on the general configuration of CDots and the modifying dye-derived species incorporated in the core carbon nanoparticle structure.

On the optical properties of CDots, the observed UV/vis absorptions are dictated by the core carbon nanoparticles, which are progressively weaker toward longer wavelengths,[19] with correspondingly weaker fluorescence emissions.[20] Despite the great interest in CDots of enhanced absorption and emissions over the red/near-IR spectral region, the effort on altering the intrinsic electronic transitions in carbon nanoparticles has yielded little success. In an alternative approach, small carbon nanoparticles are apparently compatible with their modification by organic chromophores, with the incorporation of red/near-IR dyes into the nanoparticle structure resulting in the desired spectroscopic enhancements at the targeted longer wavelengths.[21,22] As found in this work, the CDots with the dye modification in the core carbon nanoparticle structure adopt most of the dye's absorption and fluorescence emission features yet retain the unique photoinduced redox characteristics intrinsic to non-modified CDots as both highly effective electron acceptors and donors.[23,24] Hence, it sets the stage for being able to prepare CDots of desired optical and redox properties by design.

5.2 Experimental Section

Materials. Nile blue sulfate salt was purchased from Chem-Impex International, and oligomeric polyethylene glycol (PEG, average molecular weight ~1,000) from Alfa Aesar. *N*,*N*-diethylaniline (DEA), 2,4-dinitrotoluene (DNT), and methanol (spectroscopy grade) were acquired from Sigma-Aldrich. Dialysis membrane tubing (molecular weight cut-off ~ 1,000) was supplied by Spectrum Laboratories, and Sephadex G-100 gel by GE Healthcare Life Sciences. Water was deionized and purified in a NANOpure Water Purification System.

Measurement. UV/vis absorption spectra were recorded with a Perkin-Elmer Lamba 900 spectrophotometer. Steady-state fluorescence measurements were performed on a Horiba Jobin-Yvon Fluorolog-3 (FL3-22) emission spectrometer equipped with a XBO 450 W xenon short-arc lamp and Hamamatsu T928P PMT photon counting detector operated at 950 V. Fluorescence spectra were collected in the ratio mode on the instrument and corrected for nonlinear instrument responses by applying separately determined correction factors. Fluorescence quantum yields were determined by using the relative method in cross reference to three established fluorescence dyes: 9,10-bis(phenylethynyl)-anthracene in cyclohexane, rhodamine 6G in ethanol, and nile blue in methanol with the quantum yields of unity, 95%, and 27%, respectively. Fluorescence decays were measured by using the time-correlated single photon counting (TCSPC) technique on a Horibia Ultima Extreme spectrometer equipped with a SuperK Extreme supercontinuum laser source pulsed at 10 MHz, TDM-800 excitation and TDM-1200 emission monochromators, a R3809-50-MCP-PMT detector operated at 3 kV in a thermoelectrically cooled housing, and FluoroHub A+ timing electronics. The time resolution of the setup in terms of the instrument response function (IRF) is 100-250 ps, depending on excitation wavelengths. Experimental decay curves were deconvoluted by using the Das6 decay analysis software. Transmission electron microscopy (TEM) images were obtained on a Hitachi H9500 high-resolution TEM system.

PEG-NB@CDots. Nile blue (100 mg) was dissolved in ethanol (2 mL), and to the solution was added the oligomeric PEG (1 g). The resulting mixture was sonicated in a bath sonicator (VWR 250D) at 40 °C for 30 min, followed by the removal of ethanol via evaporation to obtain the reactant mixture in a small glass container. For the carbonization processing, SiC powders (170 g) in a silica crucible casting dish were heated in a conventional microwave oven at 500 W for 3 min. The small glass container with the reactant mixture was buried in the preheated SiC powders in the silica crucible casting dish for processing in the same microwave oven at 1,000 W. The initial microwave heating time was 2 min, and additional time was added in accordance with the carbonization outcome. The degree of carbonization was monitored by taking out a small quantity of the sample from the microwave oven, dispersing the sample in water, and measuring the absorbances at 400 nm ($A_{400\mathrm{nm}}$) and 550 nm ($A_{550\mathrm{nm}}$). The $A_{400\mathrm{nm}}/A_{550\mathrm{nm}}$ ratio of about one was targeted as the end point for the microwave processing. Post-processing, the reaction mixture back at ambient temperature was dispersed in deionized water (10 mL) with sonication in a bath sonicator, and the dispersion was centrifuged at 20,000 *g* to keep the supernatant. The aqueous solution thus obtained was concentrated for fractionation on an aqueous Sephadex G-100 gel column to harvest the desired PEG-

NB@CDots.[22] For electron microscopy characterization only, the dots were very lightly coated with silver by visible-light irradiation of the aqueous solution with a silver salt for a few minutes.[19]

Fluorescence Quenching. A solution of the dot sample in methanol was prepared. It was diluted to make solutions of the same PEG-NB@CDots concentration but varying concentrations of the quencher (DEA or DNT). Fluorescence spectra were measured with excitations at 480 nm, 530 nm, and 560 nm for relative quantum yields ($\Phi_F°/\Phi_F$) at different quencher concentrations. Fluorescence decays were collected with excitation wavelengths of 480 nm, 530 nm, and 560 nm and monitored emission wavelengths of 625 nm, 630 nm, and 635 nm, respectively, for the lifetime quenching ($\tau_F°/\tau_F$) at different quencher concentrations. The quantum yield and lifetime quenching data were used for the Stern-Volmer plots.

5.3 Results and Discussion

In the thermal carbonization synthesis of CDots from selected organic precursors, nile blue (NB) could be added as a modifying organic dye to yield NB@CDots, where "@" denotes broadly, in addition to the encapsulation of NB-derived species in the core carbon nanoparticles,[21] a defined modification in the nanoparticle structure by the NB-derived species in various possible modes (such as doping, trapping, composition, internal structural functionalization, etc.). In this work, the NB@CDots with oligomeric polyethylene glycol (PEG) for surface passivation, namely PEG-NB@CDots (Figure 5.1), were synthesized in the microwave-assisted carbonization processing by following a previously reported protocol.[22] Experimentally, a mixture of NB and the oligomeric PEG in large excess was prepared and used as precursor for carbonation processing via microwave irradiation. In the processing the degree of carbonization was assessed and controlled by monitoring the relative optical absorptions at 400 nm and 550 nm, which are dominated by the carbon nanoparticles and the modifying NB-derived species, respectively. Post processing the reaction mixture was cleaned and separated on an aqueous gel column to obtain the desired PEG-NB@CDots in an aqueous solution. According to transmission electron microscopy (TEM) imaging results, these dots are about 5 nm in average diameter.[22]

Optical absorption spectra of the PEG-NB@CDots are obviously different from that of the PEG-CDots without the NB modification (Figure 5.2), and in the former the NB-derived species must be responsible for the extra absorptions at longer wavelengths. When excited into those wavelengths, 530 nm for example, bright red fluorescence emissions from the PEG-NB@CDots were observed (Figure 5.2). The quantum yields for the red emissions were found to be very high, 85-90% in a methanol solution determined by cross-referencing to three fluorescence standards, one of which was free NB in methanol with a known fluorescence quantum yield of 27%.[26] The corresponding fluorescence lifetime of the PEG-NB@CDots is also long, 3.6 ns vs 1.25 ns in free NB. Such an ultrahigh fluorescence emission performance is likely beyond a simple explanation such that the NB-derived species become more fluorescent when confined in the more restrictive core carbon nanoparticle structure. More likely, in the modified CDots the carbon nanoparticles and the modifying dye species are not only physically mixed or incorporated, but also accompanied by strong electronic interactions to result in altered or new electronic states and transitions, namely that the core carbon nanoparticle with the modifying dye species incorporated in the particle structure should be considered as one integrated entity in terms of electronic and photophysical characteristics, rather than two separate entities in a simple host-guest arrangement. Consistent with such a mechanistic picture are the negative outcomes highlighted below from experiments aimed at probing the possible presence of intra-dot host-to-guest excited state energy transfers.

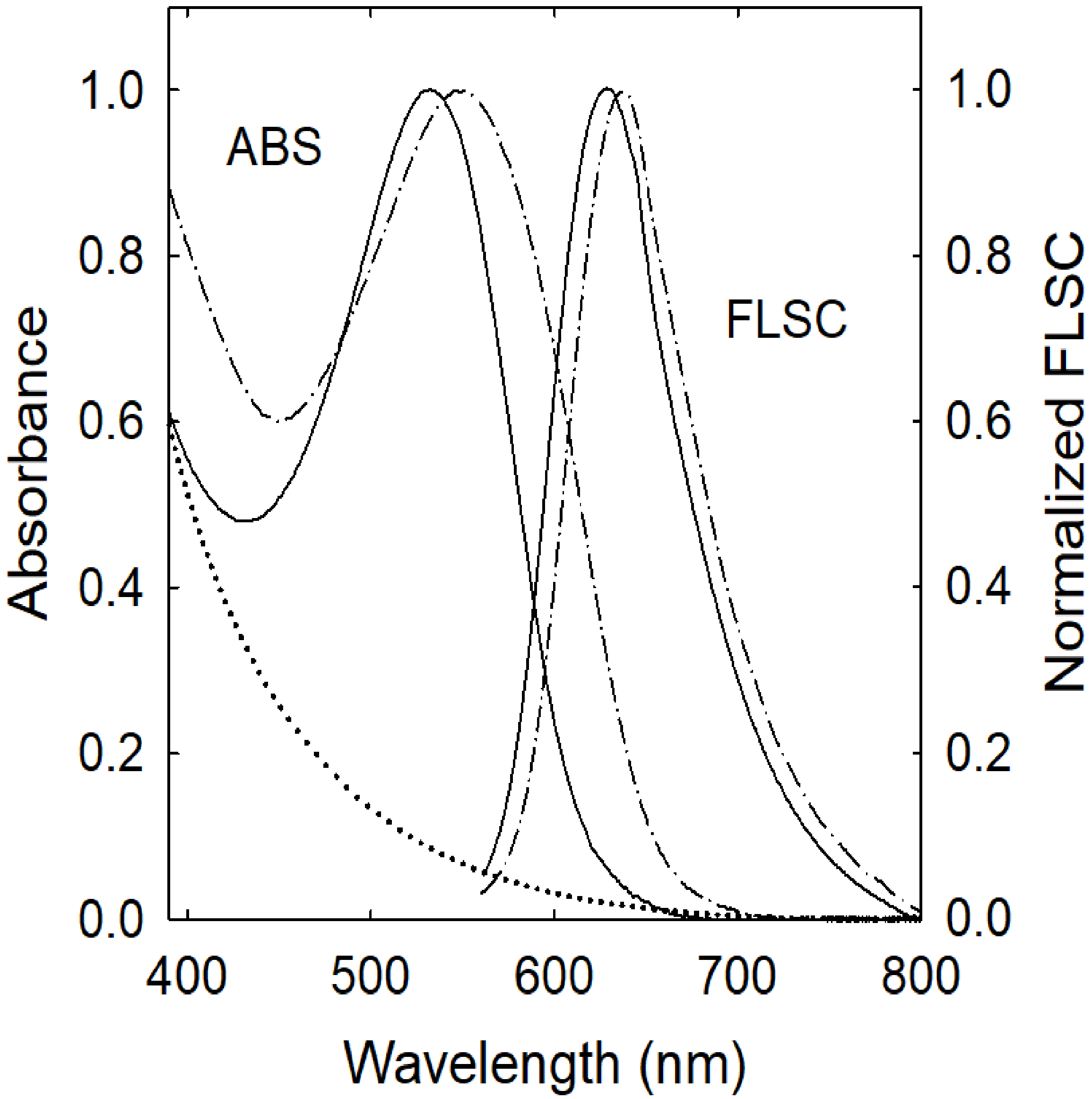

Figure 5.2 Absorption (ABS) and fluorescence (FLSC, 530 nm excitation) spectra of the PEG-NB@CDots in methanol (solid) and aqueous (dash-dot) solutions, and for comparison ABS of the PEG-CDots in methanol (dot).

For the red emission band (centered around 630 nm, Figure 5.2) of the PEG-NB@CDots, observed quantum yields at a series of different excitation wavelengths are shown in Figure 5.3. The results suggest no significant energy transfers from the excited carbon nanoparticles (with dominating absorptions in the blue/green) to the emissive excited states of the modifying NB-derived species, which would otherwise be expected if the two entities (nanoscale carbon and incorporated dye species) in each core carbon nanoparticle were physically in contact or mixed yet electronically independent. As a relevant comparison, in a different configuration of CDots with surface tethered organic dyes, substantial fluorescence resonance energy transfers (FRET) have been observed and reported,[27] because in those systems the neat dots as donor and dyes as acceptor of the excited state energies are two separate entitles.

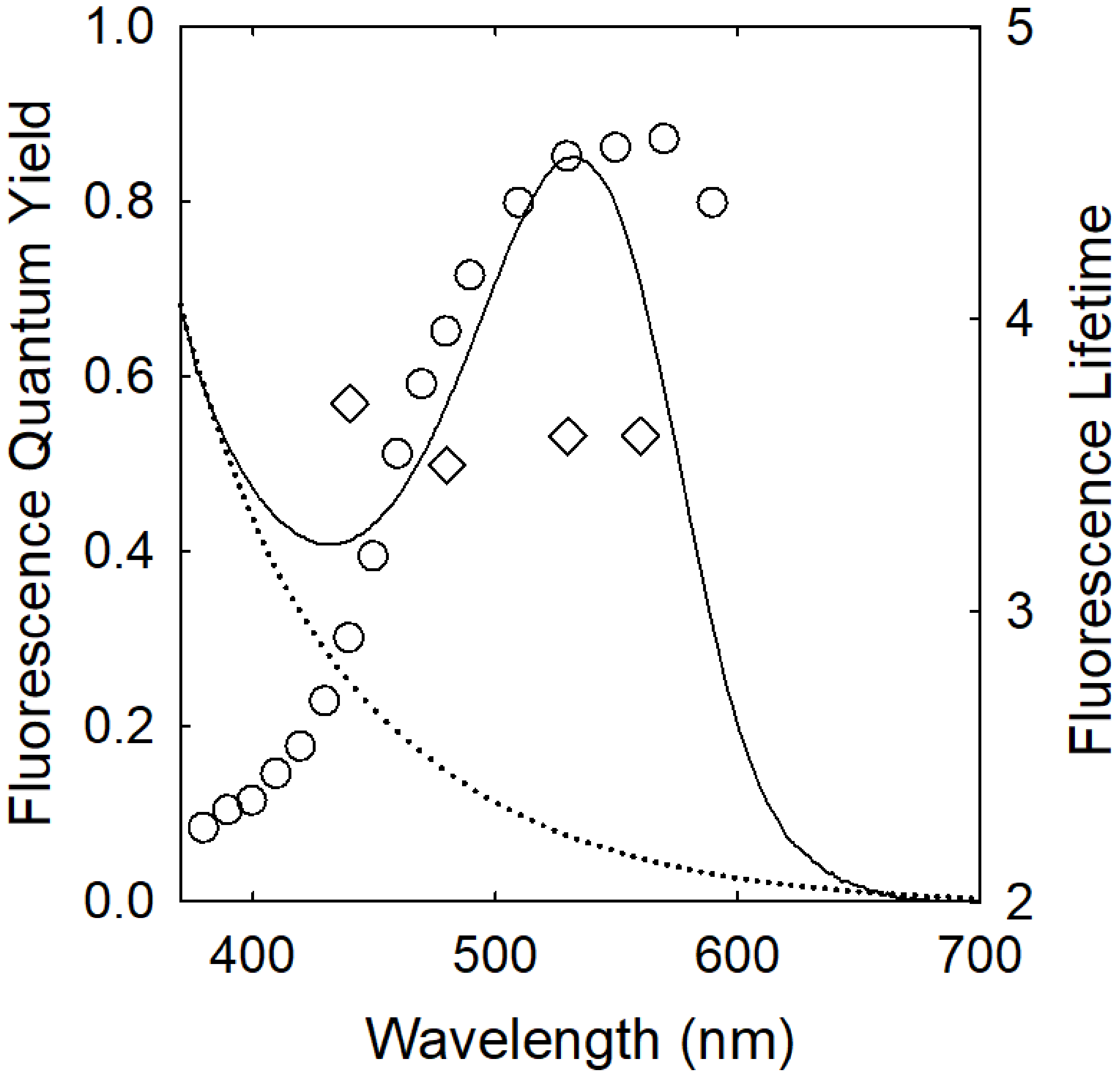

Figure 5.3 Fluorescence quantum yields (circle, left axis) and lifetimes (diamond, right axis) of the PEG-NB@CDots in methanol at different excitation wavelengths, and for referencing absorption spectra of the solution (solid line) and the PEG-CDots in methanol (dot line).

The modified CDots as one electronically integrated entity become more evident in accordance with their photoinduced redox characteristics. As already established in the literature,[5,23,24] photoexcited CDots without dye or any other modification are in general both excellent electron acceptors and donors, with their fluorescence emissions quenched very efficiently by electron donating and accepting molecules, respectively. Mechanistically, the characteristic redox quenchings are attributed to the disruption of radiative recombinations of the separated elections and holes, which are generated in the ultrafast charge separation following photoexcitation of the core carbon nanoparticles in CDots.[5,16] Here in the PEG-NB@CDots, when excited into the absorption region dominated by the NB-derived species (530 nm, for example), the red emissions could also be quenched efficiently by both electron acceptor 2,4-dinitrotoluene (DNT) and donor *N*,*N*-diethylaniline (DEA), for which the Stern-Volmer plots are shown in Figure 5.4. The slight divergence of the quenching on fluorescence quantum yields from that on fluorescence lifetimes at DNT and DEA concentrations higher than 0.02 M (Figure 5.4) is likely a result of static quenching contributions even at these rather low quencher concentrations, suggesting highly effective and efficient redox interactions.[28] The Stern-Volmer constants (K_{SV}) obtained from a linear fit on a combination of the quantum yield quenching data at quencher concentrations of 0.02 M and lower and all of the lifetime quenching data are 25 M^{-1} for DNT and 34 M^{-1} for DEA. The corresponding diffusion rate constants ($k_q = K_{SV}/\tau_F°$) are 7 x 10^9 $M^{-1}s^{-1}$ for DNT and 1 x 10^{10} $M^{-1}s^{-1}$ for DEA, both at the upper limit of diffusion control. For comparison, fluorescence emissions of free NB could be quenched by DEA, but not DNT. Thus, even with the photon-harvesting due almost exclusively to the NB-derived species at the longer wavelengths, the photoinduced redox characteristics of the PEG-NB@CDots is still clearly dictated by what is intrinsic to carbon nanoparticles without any modifications, largely the same as that in non-modified neat CDots. Again, the PEG-NB@CDots obviously behaves as a single electronically integrated entity in the response to external electron acceptors and donors.

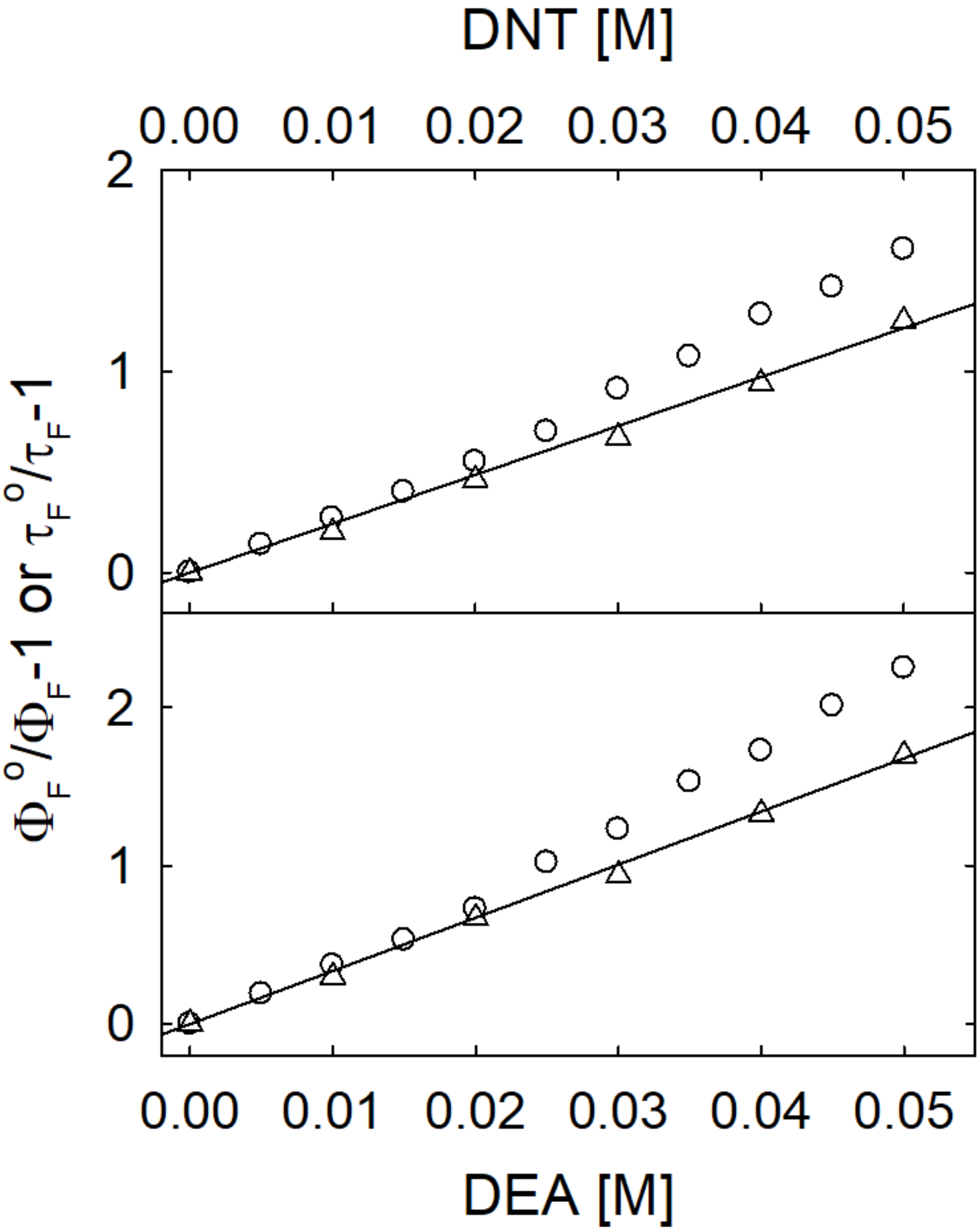

Figure 5.4. Stern-Volmer plots for fluorescence quantum yields (circle) and lifetimes (triangle) of the PEG-NB@CDots in methanol with DNT (top) and DEA (bottom) as quenchers. The lines are from linear least square fits of the quantum yield quenching data at low quencher concentrations (0.02 M and less) and lifetime quenching data combined.

The results presented above demonstrate that the core carbon nanoparticles in CDots could readily be modified with a selected organic chromophore in the carbonization synthesis, yielding integrated electronic structures and associated processes that are significantly different from those without the modification. With the selection of a red/near-IR dye, specifically nile blue (NB) for the PEG-NB@CDots in this work, the optical absorption for photon-harvesting is enhanced substantially over the longer wavelength spectral region in comparison with that of the neat CDots without modification (Figure 5.2), as desired and designed. The photon energies thus harvested are apparently shared by the modified CDots as a whole, not just localized in the NB-derived species, as reflected clearly in the redox quenching of the excited state energies, with the observed fluorescence quenching behavior in the PEG-NB@CDots resembling that intrinsic to non-modified neat CDots.

While photoexcited CDots are known as both excellent electron acceptors and donors, their donor function is generally better, as reflected in the more efficient fluorescence quenching by electron acceptors such as DNT.[23,28] For free nile blue, on the other hand, fluorescence emissions could be quenched by the electron donor DEA but only marginally by the acceptor DNT, suggesting the emissive excited state of an electron deficient character. Such a character could apparently be incorporated into the NB-modified CDots, with the PEG-NB@CDots exhibiting Stern-Volmer constants actually somewhat smaller for DNT than for DEA (Figure 5.4). Nevertheless, the intrinsic redox characteristics of surface-passivated carbon nanoparticles still play a dominating role to have the modified CDots remain as both highly effective electron acceptors and donors.

The photoinduced redox properties of CDots are valuable to optoelectronics and related applications, as already demonstrated in some reported studies.[7,29,30] In fact, CDots may serve similar functions to those of fullerenes, the prettier and more famous zero-dimensional carbon nanostructures,[31,32] and some more. For example, many uses of fullerenes in optoelectronic systems exploit their intrinsic electron acceptor characteristics and also their modifications in redox dyads and triads. CDots are equally capable electron acceptors, and electron donors as well, and they are generally more effective than fullerenes in photon-harvesting in terms of higher absorptivities on a per carbon basis. The results from this work show that the core carbon nanoparticles could be modified by a selected chromophore to obtain modified CDots of the targeted optical absorption profiles for considerably more effective photon-harvesting yet preserving the intrinsic redox characteristics, which are now associated with all of the photon energies harvested by the modified CDots as a single electronically integrated entity. Since there is a wide variety of choices for modifying chromophores, the modified CDots represent a highly versatile and effective platform for the design and preparation of zero-dimensional carbon nanostructures with specifically targeted optical, redox, and other properties.

5.4 Acknowledgements

This chapter has been submitted for publication to Chemical Communications in collaboration with Ping Wang, Dr. Christopher E. Bunker, Dr. K. A. Shiral Fernando, McIver Reibold, Yamin Liu, and Prof. Ya-Ping Sun.

5.5 References

1. Sun, Y.-P.; Zhou, B.; Lin, Y.; Wang, W.; Fernando, K. A. S.; Pathak, P.; Meziani, M. J.; Harruff, B. A.; Wang, X.; Wang, H.; et al. *J. Am. Chem. Soc*. **2006**, *128*, 7756−7757.
2. Cao, L.; Meziani, M. J.; Sahu, S.; Sun, Y.-P. *Acc. Chem. Res.* **2013**, *46*, 171−180.
3. Luo, P. G.; Sonkar, S. K.; Yang, S.-T.; Yang, F.; Yang, L.; Broglie, J. J.; Sun, Y.-P. *RSC Adv*. **2014**, *4*, 10791-10807.
4. Lim, S. Y.; Shen, W.; Gao, Z. *Chem. Soc. Rev*. **2015**, *44*, 362−381.
5. Fernando, K. A. S.; Sahu, S.; Liu, Y.; Lewis, W. K.; Guliants, E. A.; Jafariyan, A.; Wang, P.; Bunker, C. E.; Sun, Y.-P. *ACS Appl. Mater. Interfaces* **2015**, *7*, 8363−8376.
6. LeCroy, G. E.; Yang, S.-T.; Yang, F.; Liu, Y.; Fernando, K. A. S.; Bunker, C. E.; Hu, Y.; Luo, P. G.; Sun, Y.-P. *Coord. Chem. Rev*. **2016**, *320*, 66-81.
7. Essner, J. B.; Baker, A. G. *Environ. Sci. Nano* **2017**, *4*, 1216-1263.
8. Wang, X.; Cao, L.; Yang, S.-T.; Lu, F.; Meziani, M. J.; Tian, L.; Sun, K. W.; Bloodgood, M. A.; Sun, Y.-P. *Angew. Chem., Int. Ed*. **2010**, *49,* 5310–5314.
9. LeCroy, G. E.; Sonkar, S. K.; Yang, F.; Veca, L. M.; Wang, P.; Tackett II, K. N.; Yu, J.-J.; Vasile, E.; Qian, H.; Liu, Y.; et al. *ACS Nano* **2014**, *8*, 4522-4529.

10 Zhai, X.; Zhang, P.; Liu, C.; Bai, T.; Li, W.; Dai, L.; Liu, W. *Chem. Comm.* **2012**, *48*, 7955-7957.

11. Stan, C. S.; Albu, C.; Coroaba, A.; Popa, M.; Sutiman, D. *J. Mater. Chem. C* **2015**, *3*, 789-795.

12. Essner, J. B.; Laber, C. H.; Ravula, S.; Polo-Parada, L.; Baker, G. A. *Green Chem.* **2016**, *18*, 243-250.

13. Hou, X.; Hu, Y.; Wang, P.; Yang, L.; Al Awak, M. M.; Tang, Y.; Twara, F. K.; Qian, H.; Sun, Y.-P. *Carbon* **2017**, *122*, 389-394.

14. Meziani, M. J.; Dong, X.; Zhu, L.; Jones, L. P.; LeCroy, G. E.; Yang, F.; Wang, S.; Wang, P.; Zhao, Y.; Yang, L.; et al. *ACS Appl. Mater. Interfaces* **2016**, *8*, 10761-10766.

15. Dong, X.; Moyer, M. M.; Yang, F.; Sun, Y.-P.; Yang, L. *Sci. Rep.* **2017**, *7*, 519.

16. Cao, L.; Sahu, S.; Anilkumar, P.; Bunker, C. E.; Xu, J.; Fernando, K. A. S.; Wang, P.; Guliants, E. A.; Tackett, K. N., II; Sun, Y.-P. *J. Am. Chem. Soc.* **2011**, *133*, 4754−4757.

17. Peng, Z.; Han, X.; Li, S.; Al-Youbi, A. O.; Bashammakh, A. S.; El-Shahawi, M. S.; Leblanc, R. M. *Coord. Chem. Rev.* **2017**, *343*, 256-277.

18. Hutton, G. A. M.; Martindale, B. C. M.; Reisner, E. *Chem. Soc. Rev.* **2017**, *46*, 6111-6123.

19. Xu, J.; Sahu, S.; Cao, L.; Anilkumar, P.; Tackett, K. N., II; Qian, H.; Bunker, C. E.; Guliants, E. A.; Parenzan, A.; Sun, Y.-P. *ChemPhysChem* **2011**, *12*, 3604-3608.

20. LeCroy, G. E.; Messina, F.; Sciortino, A.; Bunker, C. E.; Wang, P.; Fernando, K. A. S.; Sun, Y.-P. *J. Phys. Chem. C* **2017**, *121*, 28180-28186.

21. Sun, Y.-P.; Wang, P.; Lu, Z.; Yang, F.; Meziani, M. J. LeCroy, G. E.; Liu, Y.; Qian, H. *Sci. Rep.* **2015**¸ *5*, 12354.

22. Wang, P.; Liu, J.-H.; Gao, H.; Hu, Y.; Hou, X.; LeCroy, G. E.; Bunker, C. E.; Liu, Y.; Sun, Y.-P. *J. Mater. Chem. C* **2017**, *5*, 6328-6335.

23. Wang, X.; Cao, L.; Lu, F.; Meziani, M. J.; Li, H.; Qi, G.; Zhou, B.; Harruff, B. A.; Kermarrec, F.; Sun, Y.-P. *Chem. Commun.* **2009**, *0*, 3774-3776.

24. Sciortino, A.; Madonia, A.; Gazzetto, M.; Sciortino, L.; Rohwer, E. J.; Feurer, T.; Gelardi, F. M.; Cannas, M.; Cannizzo, A.; Messina, F. *Nanoscale* **2017**, *9*, 11902-11911.

25. Jaiswal, A.; Ghosh, S. S.; Chattopadhyay, A. *Chem. Commun.* **2012**, *48*, 407–409.

26. Sens, R.; Drexhage, K. H. *J. Lumin.* **1981**, *24-25*, 709-712.

27. Huang, X.; Zhang, F.; Zhu, L.; Choi, K. Y.; Guo, N.; Guo, J.; Tackett, K.; Anilkumar, P.; Liu, G.; Quan, Q.; et al. *ACS Nano* **2013**, *7*, 5684-5693.

28. LeCroy, G. E.; Fernando, K. A. S.; Bunker, C. E.; Wang, P.; Tomlinson, N.; Sun, Y.-P. *Inorg. Chim. Acta* **2017**, *468*, 300-307.

29. Lin, X.; Yang, Y.; Nian, L.; Su, H.; Ou, J.; Yuan, Z.; Xie, F.; Hong, W.; Yu, D.; Zhang, M.; et al. *Nano Energy* **2016**, *26*, 216-223.

30. (a) Zhang, X.; Zhang, Y.; Wang, Y.; Kalytchuk, S.; Kershaw, S. V.; Wang, Y.; Wang, P.; Zhang, T.; Zhao, Y.; Zhang, H.; et al. *ACS Nano* **2013**, *7*, 11234-11241. (b) Luo, Z.; Qu, G.; Chen, K.; Zou, M.; Yuwen, L.; Zhang, X.; Huang, W.; Wang, L. *Adv. Mater.* **2016**, *26*, 2739-2744.

31. You, J.; Hong, Z.; Yang, Y.; Chen, Q.; Cai, M.; Song, T.-B.; Chen, C.-C.; Lu, S.; Liu, Y.; Zhou, H.; et al. *ACS Nano* **2014**, *8*, 1674-1680.

32. Li, C.-Z.; Yip, H.-L.; Jen, A. K.-Y. *J. Mater. Chem. C* **2012**, *22*, 4161-4177.

APPENDICES

Appendix A

Coauthored Publications

1. Yang, F.; LeCroy, G. E.; Wang, P.; Liang, W.; Chen, J.; Fernando, K. A. S.; Bunker, C. E.; Qian, H.; Sun, Y.-P. *J. Phys. Chem. C* **2016**, *120*, 25604-25611.
2. Liu, Y.; Wang, P.; Fernando, K. A. S.; LeCroy, G. E.; Maimaiti, H.; Harruff-Miller, B. A.; Lewis, W. K.; Bunker, C. E.; Hou, Z.-L.; Sun, Y.-P. *J. Mater. Chem. C* **2016**, *4*, 6967-6974.
3. Liu, J.-H.; Cao, L.; LeCroy, G. E.; Wang, P.; Meziani, M. J.; Dong, Y.; Liu, Y.; Luo, P. G.; Sun, Y.-P. *ACS Appl. Mater. Interfaces* **2015**, *7*, 19439-19445.
4. Sun, Y.-P.; Wang, P.; Lu, Z.; Yang, F.; Meziani, M. J.; LeCroy, G. E.; Liu, Y.; Qian, H. *Sci. Rep.* **2015**, *5*, 12354.
5. Wang, P.; Liu, J.-H.; Gao, H.; Hu, Y.; Hou, X.; LeCroy, G. E.; Bunker, C. E.; Liu, Y.; Sun, Y.-P. *J. Mater. Chem. C* **2017**, *5*, 6328-6335.
6. Meziani, M. J.; Dong, X.; Zhu, L.; Jones, L. P.; LeCroy, G. E.; Yang, F.; Wang, S.; Wang, P.; Zhao, Y.; Yang, L.; Tripp, R. A.; Sun, Y.-P. *ACS Appl. Mater. Interfaces* **2016**, *8*, 10761-10766.
7. Wang, S.; LeCroy, G. E.; Yang, F.; Dong, X.; Sun, Y.-P. Yang, L. *RSC Adv.* **2015**, *5*, 91246-91253.
8. Veca, L. M.; Diac, A.; Mihalache, I.; Wang, P.; LeCroy, G. E.; Pavelescu, E. M.; Gavrila, R.; Vasile, E.; Terec, A.; Sun, Y.-P. *Chem. Phys. Lett.* **2014**, *613*, 40-44.
9. Rednic, M. I.; Lu, Z.; Wang, P.; LeCroy, G. E.; Yang, F.; Liu, Y.; Qian, H.; Terec, A.; Veca, L. M.; Lu, F.; Sun, Y.-P. *Chem. Phys. Lett.* **2015**, *639*, 109-113.

10. Hu, Y.; Al Awak, M. M.; Yang, F.; Yan, S.; Xiong, Q.; Wang, P.; Tang, Y.; Yang, L.; LeCroy, G. E.; Hou, X.; Bunker, C. E.; Xu, L.; Tomlinson, N.; Sun, Y.-P. *J. Mater. Chem. C* **2016**, *4*, 10554-10561.
11. Hou, Z.-L.; Song, W.-L.; Wang, P.; Meziani, M. J.; Kong, C. Y.; Anderson, A.; Maimaiti, H.; LeCroy, G. E.; Qian, H.; Sun, Y.-P. *ACS Appl. Mater. Interfaces* **2014**, *6*, 15026-15032.
12. Luo, P. G.; Sahu, S.; Yang, S.-T.; Sonkar, S. K.; Wang, J.; Wang, H.; LeCroy, G. E.; Cao, L.; Sun, Y.-P. *J. Mater. Chem. B* **2013**, *1*, 2116-2127.

THE JOURNAL OF PHYSICAL CHEMISTRY C
Article
pubs.acs.org/JPCC

Functionalization of Carbon Nanoparticles and Defunctionalization—Toward Structural and Mechanistic Elucidation of Carbon "Quantum" Dots

Fan Yang,[†] Gregory E. LeCroy,[†] Ping Wang,[†] Weixiong Liang,[†] Jijie Chen,[†] K. A. Shiral Fernando,[‡] Christopher E. Bunker,*[,§] Haijun Qian,[†] and Ya-Ping Sun*[,†]

[†]Department of Chemistry and Laboratory for Emerging Materials and Technology, Clemson University, Clemson, South Carolina 29634, United States

[‡]University of Dayton Research Institute, Sensors Technology Office, Dayton, Ohio 45469, United States

[§]Air Force Research Laboratory, Propulsion Directorate, Wright-Patterson Air Force Base, Ohio 45433, United States

S *Supporting Information*

ABSTRACT: Small carbon nanoparticles were functionalized by low-molecular weight amino compound 3-ethoxypropylamine (EPA) for ultracompact carbon dots of bright fluorescence emissions. The results from solution-phase NMR characterization support the expected dot structure of carbon nanoparticles surface-attached with EPA species. The optical properties of the EPA-carbon dots share many features with those found in carbon dots of other surface functionalities, but there is an extra absorption shoulder in the blue spectral region, into which the excitation results in much enhanced green fluorescence emissions. The EPA-carbon dots were defunctionalized by gradually removing the EPA species from the carbon nanoparticles, along with spectroscopic characterizations on the samples of different degrees of defunctionalization. The outcomes further confirm the critical role of surface functionalization in the superior optical properties of carbon dots. Results from systematic measurements of fluorescence quantum yields and decays at different excitation wavelengths for the EPA-carbon dots and their gradually defunctionalized samples are presented, and their mechanistic implications are discussed.

INTRODUCTION

Semiconductor nanocrystals, commonly referred to as quantum dots (QDs), exhibit strong size dependence of optical properties when the nanocrystal sizes are smaller than the Bohr exciton radius.[1−6] Compared with organic dyes and fluorescent proteins, QDs are known for their strong optical absorption, high fluorescence emission quantum yields, large Stokes shifts, and excellent resistance to photobleaching.[7,8] However, high-performance QDs are mostly those containing heavy metals such as cadmium and lead, whose known toxicity has raised significant concerns and may ultimately prove prohibitive for many desired applications.[9,10] Much effort has been made in the search for QD-like optical nanomaterials derived from benign elements, among which carbon-based QDs,[11,12] especially carbon dots,[13] have attracted widespread attention. In fact, carbon dots research now represents a rapidly advancing and expanding field, as reflected by the large number of recent publications in the literature.[11,14−20]

Carbon dots are generally defined as small carbon nanoparticles with various particle surface passivation schemes.[13,18,20] As a new class of QD-like fluorescent nanomaterials, carbon dots have been shown to possess many advantageous properties amenable to their serving as bright optical probes for a variety of imaging and sensing applications,[11,17,20−23] including being readily aqueous soluble, having high optical performance and nonblinking, physicochemical, and photochemical stabilities, and being benign and nontoxic to cells and in animals according to available cytotoxicity and in vivo toxicity assays.[11,16,17,20,24] The surface passivation in carbon dots apparently plays a critical role in their optical performance, especially the fluorescence brightness and associated properties.[12,20,25] While fluorescence emissions have been observed from seemingly "naked" carbon nanoparticles, including those of a more defined graphitic structure or from partially reduced graphene oxides that are commonly referred to as "graphene quantum dots", in aqueous or other suspensions,[26−34] the emission intensities are relatively low in general and mostly centered in the UV/blue spectral region. The surface passivation has been shown to substantially enhance the fluorescence performance, with the most effective being chemical functionalization of the carbon nanoparticle surface by organic molecules (Figure 1).[12,20,25] For example,

Received: August 12, 2016
Revised: October 20, 2016
Published: October 21, 2016

DOI: 10.1021/acs.jpcc.6b08171
J. Phys. Chem. C 2016, 120, 25604−25611

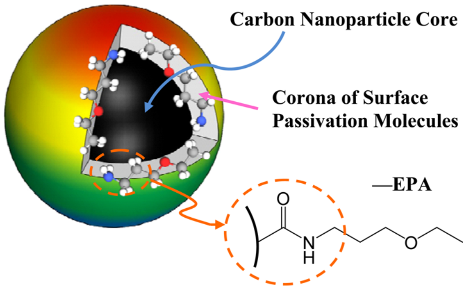

Figure 1. Illustration of the carbon dot, which is generally a small carbon nanoparticle core with attached and strongly adsorbed surface passivation molecules (a configuration similar to a soft corona).

carbon dots with the oligomeric poly(ethylene glycol) diamine (PEG_{1500N}, Figure 1) for surface functionalization exhibited fluorescence quantum yields of up to 60%.[25]

More recently, smaller amino molecules such as 2,2′-(ethylenedioxy)bis(ethylamine) (EDA, molecular weight 148) were used successfully in the functionalization of carbon nanoparticles for brightly fluorescent carbon dots, which are structurally ultracompact and of a relatively simpler surface passivation layer (Figure 1).[35] As a result, more traditional solution-phase characterization techniques such as proton and carbon-13 NMR methods could be applied to the structural elucidation of the carbon dots. In the study reported here, we used another small amino molecule, 3-ethoxypropylamine (EPA, molecular weight 103, Figure 1), for the functionalization of small carbon nanoparticles to obtain carbon dots of significantly higher fluorescence performance than that of EDA-carbon dots. The similarly ultracompact EPA-carbon dots exhibited enhanced optical absorption that could be correlated with the observed high fluorescence quantum yields, and the correlation was investigated systematically via the defunctionalization of the EPA-carbon dots. The combination of functionalization and defunctionalization experiments and outcomes provided valuable insight into the critical role of surface passivation in carbon dots, contributing to an improved mechanistic understanding of carbon dots for their optical properties and other related functions.

EXPERIMENTAL SECTION

Materials. Carbon nanopowders (US1074) were supplied by U.S. Research Nanomaterials, Inc. 3-Ethoxypropylamine (EPA) was purchased from TCI, thionyl chloride (>99%) from Alfa Aesar, and nitric acid and sodium hydroxide from Fisher Scientific. Deuterated water for NMR experiments was obtained from Cambridge Isotope Laboratories, and dialysis membrane tubing (molecular weight cutoff 100–500) from Spectrum Laboratories. Water was deionized and purified by being passed through a Labconco WaterPros water purification system.

Measurements. UV/vis absorption spectra were recorded on a Shimadzu UV2501-PC spectrophotometer. Fluorescence spectra were acquired on a Jobin–Yvon emission spectrometer equipped with a 450 W xenon source, Gemini-180 excitation and Tirax-550 emission monochromators, and a photon counting detector (Hamamatsu R928P PMT at 950 V). 9,10-Bis(phenylethynyl)anthracene in cyclohexane was used as a standard in the determination of fluorescence quantum yields by the relative method (matching the absorbance at the excitation wavelength between the sample and standard solutions and comparing their corresponding integrated total fluorescence intensities). Fluorescence decays were measured in terms of the time-correlated single photon counting (TCSPC) technique on a Horiba Ultima Extreme spectrometer. The spectrometer is equipped with a SuperK Extreme supercontinuum laser source operated at 3.894 MHz repetition rate, TDM-800 excitation and TDM-1200 emission monochromators, a R3809–50 MCP-PMT detector operated at 3.0 kV in a thermoelectrically cooled housing, and FluoroHub A+ timing electronics. Analyses of the decay curves were performed by using the Horiba Das6 fluorescence decay analysis software. NMR measurements were carried out on a Bruker Advance 500 NMR spectrometer. Atomic force microscopy (AFM) images were acquired in the acoustic AC mode on a Molecular Imaging PicoPlus AFM system equipped with a multipurpose scanner and a NanoWorld point probe NCH sensor. The height profile analysis was assisted by using the SjPIP software distributed by Image Metrology. Transmission electron microscopy (TEM) images were obtained on a Hitachi H-9500 high-resolution TEM system.

Carbon Dots. Small carbon nanoparticles were harvested from the commercially acquired carbon nanopowders in procedures similar to those reported previously.[35] In a typical experiment, a sample of carbon nanopowders (2 g) was refluxed in aqueous nitric acid (8 M, 200 mL) for 48 h. The reaction mixture was cooled to room temperature and centrifuged at 1000 *g* to discard the supernatant. The residue was redispersed in deionized water, dialyzed in a membrane tubing (molecular weight cutoff ~500) against fresh water for 48 h, and then centrifuged at 1000 *g* to retain the supernatant. Upon the removal of water, small carbon nanoparticles were recovered for their use in the functionalization reaction.

The carbon nanoparticles obtained above were dispersed in neat thionyl chloride and then refluxed for 12 h. The excess thionyl chloride was removed, and the treated sample (50 mg) was mixed well with 3-ethoxypropylamine (EPA, 1 g) in a round-bottom flask, heated to 110 °C, and vigorously stirred under nitrogen protection for 72 h. The reaction mixture was cooled to room temperature, dispersed in water, and then centrifuged at 20 000 *g* to retain the supernatant, followed by dialysis in a membrane tubing (molecular weight cutoff ~500) against fresh water to yield the EPA-carbon dots in an aqueous solution. ^1H NMR (500 MHz, D_2O) δ 3.46 (m, br), 2.93 (m, br), 1.79 (m, br), 1.04 (m, br) ppm; ^{13}C NMR (125 MHz, D_2O) δ 67.48, 66.42, 37.53, 26.85, 14.08 ppm.

Some of the EPA-carbon dots were doped with a small amount of gold via photolysis for the TEM imaging purpose. In a typical experiment, an aqueous solution of the EPA-carbon dots was mixed with an aqueous solution of $HAuCl_4$, and the mixture was irradiated with visible light.[36] The doping level was kept very low, as monitored in terms of the initial emergence of the gold plasmon absorption band.

The progressive defunctionalization of the EPA-carbon dots was carried out under base-catalyzed hydrolysis conditions. Experimentally, to an aqueous solution of the EPA-carbon dots (0.5 mg/mL, 20 mL) was added sodium hydroxide (0.4 g, 0.5 M), and the solution was heated to 80 °C. After 4 h, the temperature was increased to 100 °C, along with an increase of the base concentration (0.75 M). After another 4 h, the temperature was further increased to 120 °C, and so was the base concentration (1.0 M), and the reaction was allowed to proceed for 4 h more. Finally, the temperature was increased to 130 °C, and the mixture was reacted for 8 h. During the

DOI: 10.1021/acs.jpcc.6b08171
J. Phys. Chem. C 2016, 120, 25604–25611

reaction period (a total of 20 h), a portion of the reaction mixture was collected in 2 h intervals for spectroscopic and other characterizations.

■ RESULTS AND DISCUSSION

Commercially acquired carbon nanopowders were refluxed in aqueous nitric acid for purification and also for the introduction of oxygen-containing functionalities such as carboxylic acids on the particle surface, followed by dialysis and centrifugation to harvest mostly smaller carbon nanoparticles in an aqueous suspension.[35] The carbon nanoparticles thus obtained were functionalized with EPA molecules for EPA-carbon dots in a typical amidation reaction scheme involving the use of thionyl chloride for the acylation of the particle surface-bound carboxylic acid moieties for amide linkages with EPA molecules. Free EPA and other small molecular impurities were removed via dialysis to obtain the EPA-carbon dots sample as a colored aqueous solution (Figure 2).

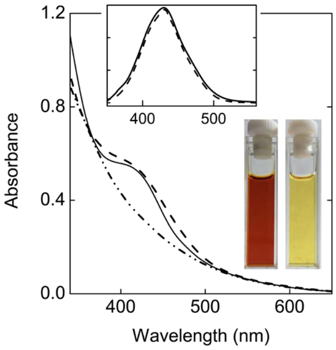

Figure 2. Absorption spectrum of the EPA-carbon dots in aqueous solution (—) compared with those of the aqueous suspended carbon nanoparticles (−···−) and the PEG_{1500N}-carbon dots (− −).[25] The photos are for concentrated (left) and dilute (right) aqueous solutions of the EPA-carbon dots. The other inset shows a comparison of two spectra corresponding to the extra absorption shoulder, obtained by subtracting the spectrum of the carbon nanoparticles (− −) or the final defunctionalized sample (—) from that of the EPA-carbon dots.

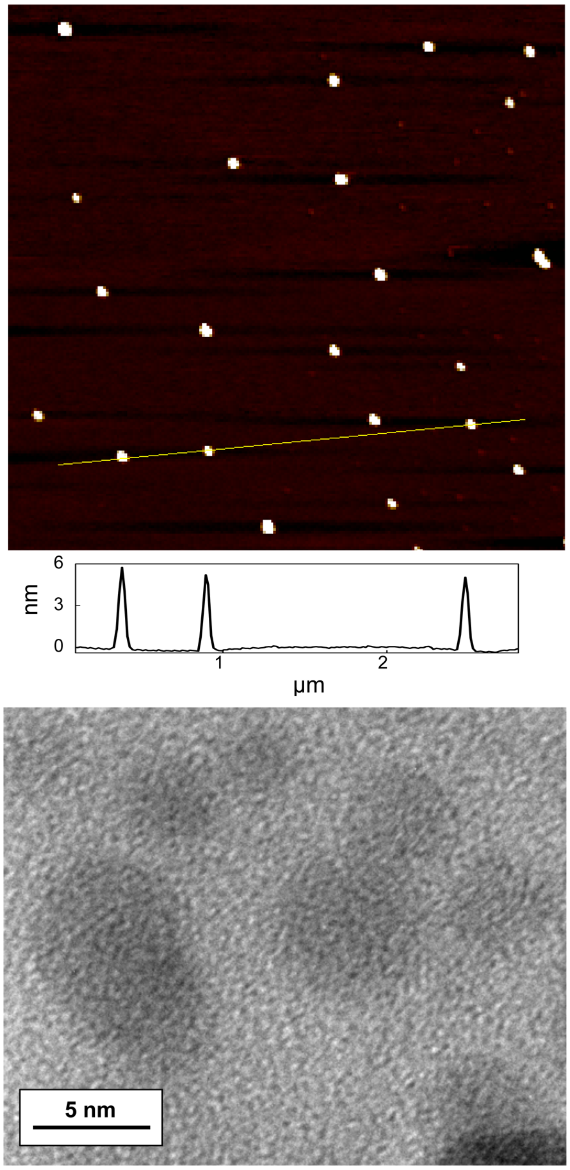

Figure 3. Results from AFM (top) and TEM (bottom) imaging of the EPA-carbon dots.

For atomic force microscopy (AFM) analyses, aqueous solution of the EPA-carbon dots was diluted, from which a few drops were deposited onto a piece of mica, followed by the removal of water via evaporation. As shown in Figure 3, the EPA-carbon dots are relatively well-defined, with the height analysis results of multiple AFM images suggesting an average dot size of 4.5 nm and size distribution standard deviation of 0.9 nm in diameter. For the transmission electron microscopy (TEM) imaging, the EPA-carbon dots in aqueous solution were coated with a small amount of gold in simple photolysis to increase the imaging contrast.[36] Shown in Figure 3 is a representative TEM image, where the dot profiles are generally comparable with those found in the AFM analysis. According to the microscopy results, the EPA-carbon dots are similarly compact in comparison with the previously reported EDA-carbon dots.[35]

The UV/vis absorption spectrum of the EPA-carbon dots in aqueous solution is shown in Figure 2. Generally, the absorption of carbon dots is due primarily to the core carbon nanoparticles (Figure 1), with the particle surface functionalization by colorless molecules playing a rather minor role. For the EPA functionalization, however, there are apparently significant new features in the absorption spectrum of EPA-carbon dots, specifically the shoulder in the blue region that is in addition to the absorption of the core carbon nanoparticles (Figure 2). Similar absorption features were previously found in carbon dots with the oligomeric poly(ethylene glycol) diamine (PEG_{1500N}) functionalization, as also shown in Figure 2 for comparison.[25] These significant absorption spectral changes suggest that upon the surface functionalization of carbon nanoparticles with the selected organic molecules, there could be significant effect associated with the functionalization to alter the electronic transitions of the core carbon nanoparticles in the resulting carbon dots, corresponding to the enhanced absorption in the blue as reflected by the additional absorption shoulder (Figure 2). Since the mode of functionalization was the formation of amide linkages between the carbon nanoparticle surface-bound carboxylic acid moieties and EPA molecules,[20,25] as targeted by the amidation reaction conditions for the functionalization, the effect on the optical absorption of the resulting carbon dots seems unusually significant, for which a mechanistic elucidation remains a challenge. Apparently, the altered electronic transitions reflected in the observed

DOI: 10.1021/acs.jpcc.6b08171
J. Phys. Chem. C 2016, 120, 25604−25611

absorption spectra were also consequential to the observed fluorescence emission properties.

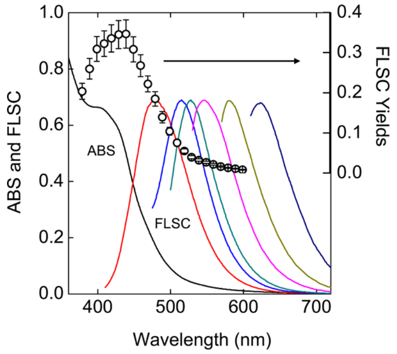

Figure 4. Absorption (ABS) and fluorescence (FLSC) spectra at different excitation wavelengths (from left to right: 400, 440, 480, 520, 560, and 600 nm) of the EPA-carbon dots in aqueous solution. Also shown is the excitation wavelength dependence of the observed fluorescence quantum yields (○).

Fluorescence spectra of the EPA-carbon dots in aqueous solution are dependent on excitation wavelengths (Figure 4), similar to those of carbon dots with other surface functional molecules. Correspondingly, the observed fluorescence quantum yields, determined in reference to 9,10-bis(phenylethynyl)-anthracene as a standard (quantum yield of unity, calibrated against the quinine sulfate standard), are also excitation wavelength dependent (Figure 4). The peak fluorescence quantum yield was found at around 440 nm excitation, coinciding with the shoulder in the absorption spectrum (Figure 4). Therefore, the above-discussed enhancement in optical transitions due to the specific effect associated with the carbon nanoparticle surface functionalization by EPA molecules is apparently correlated with significantly brighter fluorescence emissions, likely sharing the same mechanistic origin. It is probably no coincidence that the PEG_{1500N}-carbon dots with the enhanced optical absorption (a similar absorption shoulder in the blue spectral region, Figure 2) also exhibited significantly higher fluorescence quantum yields when excited into the absorption shoulder around 440 nm.[25] In terms of photophysical principles, fluorescence quantum yield (Φ_F) is a function of lifetime (τ_F) and radiative rate constant (k_F) of the emissive excited state, $\Phi_F = k_F\tau_F$, where k_F is proportional to the transition probabilities or approximately the optical absorptivities.[37,38] Therefore, the absorption and fluorescence emission results presented above suggest that the observed higher fluorescence quantum yields when excited into the additional shoulder of the absorption spectrum (Figure 2) may have been contributed in a significant part by larger k_F values, again reflecting the enhanced optical transitions (specifically radiative transitions from the corresponding emissive excited states to the ground state).[38] Such an assessment was supported by the results from fluorescence decay measurements.

The time-correlated single photon counting (TCSPC) technique was employed for determining the fluorescence decay profiles of the EPA-carbon dots in aqueous solution at different excitation wavelengths. Shown in Figure 5 is the decay curve at 440 nm excitation, and those at other excitation wavelengths are only slightly different. The decays could not be deconvoluted quantitatively with a monoexponential function, but reasonably well with a biexponential function (Table 1). Despite the good deconvolution fits, however, it would be an oversimplification to assume only two emission contributions at all of these different excitation wavelengths. The excited states and processes in carbon dots are likely more complicated, so that the good deconvolution fits were probably just a result of phenomenological biexponential averaging of the likely multicomponent decays. A further averaging was made by using the pre-exponential factors (A_1 and A_2) and lifetimes (τ_{F1} and τ_{F2}) from the deconvolution fits, $\langle\tau_F\rangle = (A_1\tau_{F1}^2 + A_2\tau_{F2}^2)/(A_1\tau_{F1} + A_2\tau_{F2})$,[37] and the average fluorescence lifetime $\langle\tau\rangle$ values thus calculated are also shown in Table 1. These averages provide a rough estimate of the relative time constants for the observed decay curves at different excitation wavelengths. While still somewhat excitation wavelength dependent (Table 1), their variations are not as pronounced as those in the corresponding fluorescence quantum yields (Figure 4). The results again suggest that some of the changes in observed fluorescence quantum yields over different excitation wavelengths are due to similar changes in the fluorescence radiative rate constant (k_F, Table 1), which are correlated with the changes in optical absorptivities.[38]

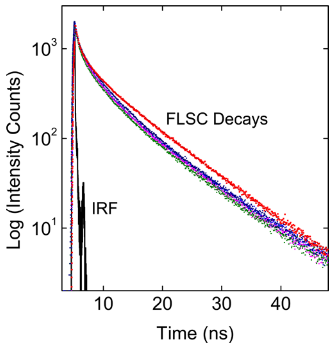

Figure 5. Observed fluorescence decays of the EPA-carbon dots (red) and the four samples with different degrees of defunctionalization listed in Table 2 (D_1, blue; D_2, magenta; D_3, olive; and D_4, navy), all at 440 nm excitation and the monitored emission centered at 510 nm. The biexponential fitting curves for all of the decays are also shown (black), and the same fitting results plotted separately for individual decays are provided in the Supporting Information.

On the structure of carbon dots (Figure 1), the amidation reaction targets specifically the carboxylic acid moieties on the carbon nanoparticle surface, which are known as being generated in the oxidative acid treatment of the nanoparticles.[12,20,25] The reaction conditions are much too mild for anything other than the formation of amide linkages, far from those required for any structural modification or heteroatom replacement of the surface carbons in the carbon nanoparticles. In this regard, the issue for structural analyses was whether the amidation reaction did result in the attachment of EPA molecules to the carbon nanoparticles. Thus, the EPA-carbon dots were characterized in solution by using proton and carbon-13 NMR techniques. Shown in Figure 6 are the proton NMR results of the EPA-carbon dots in deuterated water. The signals for all protons in the dot-attached EPA moieties are significantly broadened in comparison with those in free EPA molecules, where the broadening effect is consistent with the attachment of EPA to carbon nanoparticles as larger species of lower mobility (thus slower isotropic averaging),[39] and also the inhomogeneous distribution of sites for the functionalization on the carbon nanoparticle surface.[40] Similar effect is established in the literature for other surface functionalization of nanoscale species, such as in chemically functionalized carbon nano-

Table 1. Results from the Deconvolution of the Observed Fluorescence Decays

		exponential fit		exponential fit					
λ_{EX} (nm)	λ_{EM} (nm)	τ_F (ns)	χ^2	A_1 (%)	A_2 (%)	τ_{F1} (ns)	τ_{F2} (ns)	χ^2	$\langle\tau\rangle$ (ns)[a]
400	475	4.7(0.9)	2.5−3.5	7(1)	93(1)	1(0.2)	6.2(0.3)	1.0−1.1	6.1(0.3)
440	510	6.8(0.4)	2.2−2.8	5(2)	95(2)	1(0.2)	8.3(0.3)	1.0−1.05	8.3(0.3)
480	520	6.3(0.6)	2.3−3.2	7(1)	93(1)	1.3(0.2)	8.3(0.3)	1.0−1.1	8.2(0.3)
520	560	3.2(0.9)	1.5−3.2	6(2)	94(2)	0.5(0.3)	4.1(0.5)	1.0−1.1	4.1(0.4)

[a] The average fluorescence lifetime $\langle\tau_F\rangle = (A_1\tau_{F1}^2 + A_2\tau_{F2}^2)/(A_1\tau_{F1} + A_2\tau_{F2})$ (see ref 37).

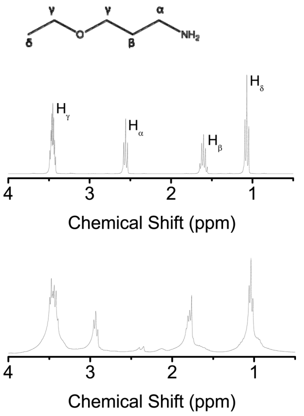

Figure 6. Proton NMR spectra of free EPA molecules (top) and the EPA-carbon dots (bottom) in deuterated water.

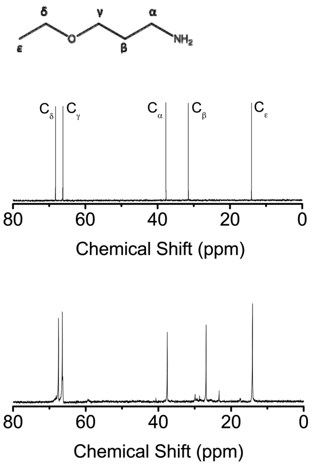

Figure 7. Carbon-13 NMR spectra of free EPA molecules (top) and the EPA-carbon dots (bottom) in deuterated water.

tubes[41] and inorganic nanoparticles.[42] In addition to the signal broadening, the changes in chemical shift are also consistent with the attachment of EPA to carbon nanoparticles. The α proton signal is downfield-shifted to 2.93 ppm (vs 2.56 ppm in free EPA), which may be attributed to deshielding effect as a result of the amidation. The β proton signal is also downfield-shifted, but to a lesser extent, while the other proton signals are unchanged in chemical shifts (Figure 6). The signal integrations are largely unchanged from free EPA molecules to their attachment to carbon nanoparticles, suggesting that other than the functionalization affecting the chemical environments of the α and β protons, the EPA molecular structure is intact, as one would expect. The carbon-13 NMR results are generally consistent with the proton NMR results, with also the signal broadening effect. As often observed,[43−45] the shifts in carbon-13 NMR signals due to chemical environment changes following the functionalization are not as pronounced as those in proton NMR signals (Figure 7).

The NMR and other results described above are in support of or consistent with the dot structure of a small carbon nanoparticle core functionalized by EPA molecules (Figure 1). Further structural elucidation was pursued by chemically defunctionalizing the EPA-carbon dots to gradually remove the attached EPA molecules from the surface passivation layer, coupled with the monitoring of progressive spectroscopic changes in the samples associated with different levels of defunctionalization.

Since the functionalization in the synthesis of the EPA-carbon dots was by amidation chemistry, the chemical defunctionalization was carried out under base-catalyzed hydrolysis reaction conditions.[46,47] In order to be able to monitor the gradual defunctionalization process, the hydrolysis reaction conditions were controlled by starting at a lower base concentration and also a lower reaction temperature and then increasing stepwise both the base concentration and reaction temperature until the formation of substantial precipitation due to nearly completely defunctionalized carbon nanoparticles. As the reaction progressed, a portion of the reaction mixture was collected at different reaction time points for spectroscopic analyses. Proton NMR results of the sample solutions exhibited no significant changes, which should be expected as the defunctionalization merely decreased the population of the carbon nanoparticle surface-bound EPA species. The UV/vis absorption spectra for the samples collected at different reaction time points are shown in Figure 8. The absorption shoulder in the blue spectral region obviously decreased progressively and largely diminished at the conclusion of the

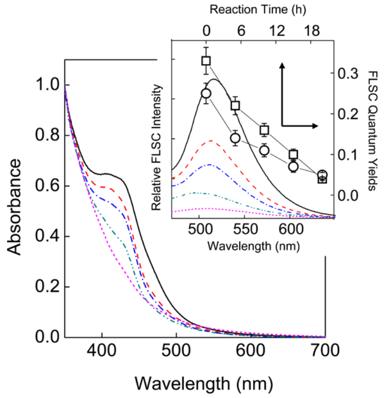

Figure 8. Absorption and fluorescence (FLSC, 440 excitation, in the inset) spectra of the EPA-carbon dots (—) and the four samples with different degrees of defunctionalization listed in Table 2 (D_1, ——; D_2, —·—·—; D_3, —··—··—; and D_4: — — —). Also shown in the inset are the changes in fluorescence quantum yield with the defunctionalization at 400 nm (○) and 440 nm (□) excitations.

Table 2. Fluorescence Decay Results for the Defunctionalization[a]

sample[b]	A_1 (%)	A_2 (%)	τ_{F1} (ns)	τ_{F2} (ns)	χ^2	$\langle\tau_F\rangle$ (ns)
original	8(1)	92(1)	0.8(0.2)	6.9(0.4)	1.0−1.05	6.8(0.3)
D_1	12(2)	88(2)	0.7(0.2)	4.7(0.4)	1.0−1.1	4.6(0.4)
D_2	10(2)	90(2)	0.8(0.2)	4.9(0.4)	1.0−1.1	4.8(0.4)
D_3	9(2)	91(2)	0.7(0.2)	4.8(0.4)	1.0−1.1	4.7(0.4)
D_4	9(2)	91(2)	0.8(0.2)	5(0.4)	1.0−1.1	4.9(0.4)

[a] Excitation at 440 nm and the monitored emission centered at 510 nm, with the deconvolution based on biexponential fit. [b] Original is the EPA-carbon dots before defunctionalization, and the others are samples with different degrees of defunctionalization collected at different time points in the reaction (D_1, 2 h; D_2, 6 h; D_3, 12 h; and D_4, 20 h and the final defunctionalized sample).

reaction, with the resulting absorption spectrum similar to that of the "naked" carbon nanoparticles before the functionalization (Figure 8). These results serve to confirm that the enhanced optical transitions reflected by the additional absorption shoulder (Figure 2) are due to the EPA functionalization of carbon nanoparticles.

Fluorescence spectra of the same samples collected at different defunctionalization reaction points are also shown in Figure 8. The spectral profiles are similar between different samples, but the emission intensities are progressively lower, and so are the observed fluorescence quantum yields (Figure 8). However, the decrease in yields at 440 nm excitation is relatively more rapid than that at 400 nm excitation, likely due to the fact that upon defunctionalization the absorption shoulder responsible for the enhanced fluorescence emissions in the original EPA-carbon dots disappears quickly (Figure 8). For the sample collected at the end of the defunctionalization reaction, namely the remaining solution without the precipitate, the fluorescence quantum yields are around 4% for both 400 and 440 nm excitations, getting close to those of suspended carbon nanoparticles without deliberate surface functionalization by organic molecules.[48−55] Thus, these results provide unambiguous evidence for the notion that the surface functionalization of carbon nanoparticles by otherwise colorless organic molecules like EPA is responsible for the observed bright and colorful fluorescence emissions of carbon dots, reaffirming the definition of carbon dots as surface-passivated (functionalized) small carbon nanoparticles.[12,13,20] More specifically with the EPA functionalization, the fluorescence emissions can be further enhanced when the dots are excited into the additional absorption shoulder in the blue spectral region (Figure 2).

The samples with different degrees of defunctionalization were also evaluated by fluorescence decay measurements. As compared in Figure 5, there are no major changes in the fluorescence decay curves between the samples, suggesting that the dynamic processes in the emissive excited states are decoupled from the dramatic decreases in fluorescence quantum yields upon defunctionalization (Figure 8). The decay curves could again be deconvoluted well with a biexponential function, and the results are shown in Table 2. The averaging of the two lifetime values allows the calculation of fluorescence radiative rate constants, $k_F = \Phi_F/\tau_F$, where Φ_F and τ_F are observed fluorescence quantum yield and average fluorescence lifetime, respectively. Apparently, in the defunctionalization the fluorescence quantum yield decrease is correlated with the decrease in k_F (Table 2), consistent with the disappearance of the extra absorption shoulder, as k_F and optical absorptivity are correlated and both serve as measures for electronic transition probabilities.[38]

The functionalization and defunctionalization results presented above clearly show the critical role of carbon nanoparticle surface passivation in determining the optical properties of carbon dots. Mechanistically, the fluorescence emissions are attributed to radiative recombinations of photogenerated electrons and holes trapped at diverse surface defect sites.[12,55,56] The observed fluorescence properties including quantum yields and decays may be explained in terms of two sequential processes following photoexcitation, the first for the formation of the emissive excited states (quantum yield Φ_1) and then the other from the emissive states for fluorescence (quantum yield Φ_2) and competing nonradiative decay pathways. Thus, the observed fluorescence quantum yields (Φ_F) reflect a combination of the two processes, $\Phi_F = \Phi_1\Phi_2$. The obvious decoupling between the observed fluorescence quantum yields and decays in the defunctionalization experiments indicates that the beneficial effect of surface passivation for observed higher fluorescence quantum yields is primarily through Φ_1, probably the stabilization of the surface defect sites to facilitate more effective radiative recombinations. Specific to EPA-carbon dots, however, the extra absorption shoulder in the blue (Figure 2) as a result of the functionalization may also contribute to a larger Φ_2 through enhanced transition probabilities (larger k_F values). Overall, the results reported here are not only consistent with the presently adopted mechanistic framework for the optical properties of carbon dots but also provide more details that are valuable to an improved mechanistic understanding. In further investigations, a more systematic evaluation on other similar small amino molecules for functionalization in the preparation of carbon dots will prove interesting and rewarding.

■ CONCLUSION

Small carbon nanoparticles were functionalized with EPA molecules for the EPA-carbon dots of bright fluorescence emissions. With EPA of a low molecular weight, these carbon dots are ultracompact (averaging less than 5 nm in diameter). The solution-phase NMR results support the expected dot structure of carbon nanoparticles surface-attached with EPA species. It should again be emphasized that the amidation reaction used in this study for the functionalization of carbon nanoparticles is specific, with the reaction conditions impossible to cause any "heteroatom doping" in the resulting carbon dots, thus very different from the carbonization reactions or the like used in the synthesis of "graphene quantum dots" without or with surface passivation (the latter being essentially carbon dots of a more graphitic carbon core).[57−60] As related, the hydrolysis reaction for the defunctionalization is also impossible to reverse any heteroatom doping or structural modifications if there were such doping or modifications in the original functionalization. Thus, none of the observed optical properties in this study

DOI: 10.1021/acs.jpcc.6b08171
J. Phys. Chem. C 2016, 120, 25604−25611

could be attributed to effects associated with any doping or structural modifications of the carbon nanoparticles used in the amidation reaction.

On the optical properties, while the EPA-carbon dots share many features found in carbon dots of other surface functionalities, there is an extra absorption shoulder in the blue spectral region into which the excitation results in enhanced green fluorescence emissions. The EPA-carbon dots were defunctionalized by gradually removing the EPA species from the carbon nanoparticles, along with spectroscopic characterizations. The results further confirm the critical role of surface functionalization in the bright fluorescence emissions of carbon dots. According to systematic measurements of fluorescence quantum yields and decays for the EPA-carbon dots and their gradually defunctionalized samples, two mechanistic conclusions can be made. One is that the enhanced green fluorescence emissions corresponding to the extra blue absorption shoulder are due to significant contributions of larger fluorescence radiative constants, associated with enhanced transition probabilities. The other is that after taking out the special effect discussed in the first conclusion above, the observed fluorescence properties of carbon dots in general can be explained by a combination of two sequential processes following photoexcitation: the formation of the emissive excited states and the decays from these states. Further investigations by using ultrafast spectroscopy techniques are needed.

■ ASSOCIATED CONTENT

Ⓢ Supporting Information

The Supporting Information is available free of charge on the ACS Publications website at DOI: 10.1021/acs.jpcc.6b08171.

> The same biexponential fitting results for all of the fluorescence decay curves in Figure 5 presented separately for individual decays (PDF)

■ AUTHOR INFORMATION

Corresponding Authors

*E-mail: christopher.bunker@us.af.mil. Tel.: 937-255-6935.
*E-mail: syaping@clemson.edu. Tel.: 864-656-5026.

Notes

The authors declare no competing financial interest.

■ ACKNOWLEDGMENTS

Financial support from the Air Force Office of Scientific Research through Dr. Charles Lee (Y.-P.S.) and Dr. Michael Berman (C.E.B.), NIH (Y.-P.S.), and the Air Force Research Laboratory (C.E.B.) is gratefully acknowledged. W.L. and J.C. were visiting students from Prof. Fushen Lu's program at Shantou University in China, supported by NSFC (51272152).

■ REFERENCES

(1) Ekimov, A. I.; Efros, Al. L.; Onushchenko, A. A. Quantum Size Effect in Semiconductor Microcrystals. *Solid State Commun.* **1985**, *56*, 921−924.

(2) Henglein, A. Small-Particle Research—Physicochemical Properties of Extremely Small Colloidal Metal and Semiconductor Particles. *Chem. Rev.* **1989**, *89*, 1861−1873.

(3) Bawendi, M. G.; Steigerwald, M. L.; Brus, L. E. The Quantum-Mechanics of Larger Semiconductor Clusters (Quantum Dots). *Annu. Rev. Phys. Chem.* **1990**, *41*, 477−496.

(4) Brus, L. E. Quantum Crystallites and Nonlinear Optics. *Appl. Phys. A: Solids Surf.* **1991**, *53*, 465−474.

(5) Alivisatos, A. P. Perspectives on the Physical Chemistry of Semiconductor Nanocrystals. *J. Phys. Chem.* **1996**, *100*, 13226−13239.

(6) Kamat, P. V. Quantum Dot Solar Cells. Semiconductor Nanocrystals as Light Harvesters. *J. Phys. Chem. C* **2008**, *112*, 18737−18753.

(7) Michalet, X.; Pinaud, F. F.; Bentolila, L. A.; Tsay, J. M.; Doose, S.; Li, J. J.; Sundaresan, G.; Wu, A. M.; Gambhir, S. S.; Weiss, S. Quantum Dots for Live Cells, in Vivo Imaging, and Diagnostics. *Science* **2005**, *307*, 538−544.

(8) Kairdolf, B. A.; Smith, A. M.; Stokes, T. H.; Wang, M. D.; Young, A. N.; Nie, S. Semiconductor Quantum Dots for Bioimaging and Biodiagnostic Applications. *Annu. Rev. Anal. Chem.* **2013**, *6*, 143−162.

(9) Hardman, R. A Toxicologic Review of Quantum Dots: Toxicity Depends on Physicochemical and Environmental Factors. *Environ. Health Perspect.* **2006**, *114*, 165−172.

(10) Geys, J.; Nemmar, A.; Verbeken, E.; Smolders, E.; Ratoi, M.; Hoylaerts, M. F.; Nemery, B.; Hoet, P. H. M. Acute Toxicity and Prothrombotic Effects of Quantum Dots: Impact of Surface Charge. *Environ. Health Perspect.* **2008**, *116*, 1607−1613.

(11) Luo, P. G.; Yang, F.; Yang, S.-T.; Sonkar, S. K.; Yang, L.; Broglie, J. J.; Liu, Y.; Sun, Y.-P. Carbon-Based Quantum Dots for Fluorescence Imaging of Cells and Tissues. *RSC Adv.* **2014**, *4*, 10791−10807.

(12) Cao, L.; Meziani, M. J.; Sahu, S.; Sun, Y.-P. Photoluminescence Properties of Graphene versus Other Carbon Nanomaterials. *Acc. Chem. Res.* **2013**, *46*, 171−180.

(13) Sun, Y.-P.; Zhou, B.; Lin, Y.; Wang, W.; Fernando, K. A. S.; Pathak, P.; Meziani, M. J.; Harruff, B. A.; Wang, X.; Wang, H.; et al. Quantum-Sized Carbon Dots for Bright and Colorful Photoluminescence. *J. Am. Chem. Soc.* **2006**, *128*, 7756−7757.

(14) Hola, K.; Zhang, Y.; Wang, Y.; Giannelis, E. P.; Zboril, R.; Rogach, A. L. Carbon Dots-Emerging Light Emitters for Bioimaging, Cancer Therapy, and Optoelectronics. *Nano Today* **2014**, *9*, 590−603.

(15) Wang, Y.; Hu, A. Carbon Quantum Dots: Synthesis, Properties, and Applications. *J. Mater. Chem. C* **2014**, *2*, 6921−6939.

(16) Miao, P.; Han, K.; Tang, Y.; Wang, B.; Lin, T.; Cheng, W. Recent Advances in Carbon Nanodots: Synthesis, Properties, and Biomedical Applications. *Nanoscale* **2015**, *7*, 1586−1595.

(17) Lim, S. Y.; Shen, W.; Gao, Z. Carbon Quantum Dots and Their Applications. *Chem. Soc. Rev.* **2015**, *44*, 362−381.

(18) Fernando, K. A. S.; Sahu, S.; Liu, Y.; Lewis, W. K.; Guliants, E. A.; Jafariyan, A.; Wang, P.; Bunker, C. E.; Sun, Y.-P. Carbon Quantum Dots and Applications in Photocatalytic Energy Conversion. *ACS Appl. Mater. Interfaces* **2015**, *7*, 8363−8376.

(19) Du, Y.; Guo, S. Chemically Doped Fluorescent Carbon and Graphene Quantum Dots for Bioimaging, Sensor, Catalytic and Photoelectronic Applications. *Nanoscale* **2016**, *8*, 2532−2543.

(20) LeCroy, G. E.; Yang, S.-T.; Yang, F.; Liu, Y.; Fernando, K. A. S.; Bunker, C. E.; Hu, Y.; Luo, P. G.; Sun, Y.-P. Functionalized Carbon Nanoparticles: Syntheses and Applications in Optical Bioimaging and Energy Conversion. *Coord. Chem. Rev.* **2016**, *320*, 66−81.

(21) Yang, S.-T.; Cao, L.; Luo, P. G.; Lu, F.; Wang, X.; Wang, H.; Meziani, M. J.; Liu, Y.; Qi, G.; Sun, Y.-P. Carbon Dots for Optical Imaging in Vivo. *J. Am. Chem. Soc.* **2009**, *131*, 11308−11309.

(22) Dong, Y.; Wang, R.; Li, G.; Chen, C.; Chi, Y.; Chen, G. Polyamine-Functionalized Carbon Quantum Dots as Fluorescent Probes for Selective and Sensitive Detection of Copper Ions. *Anal. Chem.* **2012**, *84*, 6220−6224.

(23) Zhu, S.; Meng, Q.; Wang, L.; Zhang, J.; Song, Y.; Jin, H.; Zhang, K.; Sun, H.; Wang, H.; Yang, B. Highly Photoluminescent Carbon Dots for Multicolor Patterning, Sensors, and Bioimaging. *Angew. Chem., Int. Ed.* **2013**, *52*, 3953−3957.

(24) Yang, S.-T.; Wang, X.; Wang, H.; Lu, F.; Luo, P. G.; Cao, L.; Meziani, M. J.; Liu, J.-H.; Liu, Y.; Chen, M.; et al. Carbon Dots as Nontoxic and High-Performance Fluorescence Imaging Agents. *J. Phys. Chem. C* **2009**, *113*, 18110−18114.

(25) Wang, X.; Cao, L.; Yang, S.-T.; Lu, F.; Meziani, M. J.; Tian, L.; Sun, K. W.; Bloodgood, M. A.; Sun, Y.-P. Bandgap-Like Strong Fluorescence in Functionalized Carbon Nanoparticles. *Angew. Chem., Int. Ed.* **2010**, *49*, 5310−5314.

(26) Li, L.-S.; Yan, X. Colloidal Graphene Quantum Dots. *J. Phys. Chem. Lett.* **2010**, *1*, 2572−2576.

(27) Peng, J.; Gao, W.; Gupta, B. K.; Liu, Z.; Romero-Aburto, R.; Ge, L.; Song, L.; Alemany, L. B.; Zhan, X.; Gao, G.; et al. Graphene Quantum Dots Derived from Carbon Fibers. *Nano Lett.* **2012**, *12*, 844−849.

(28) Yan, X.; Li, B.; Cui, X.; Wei, Q.; Tajima, K.; Li, L.-S. Independent Tuning of the Band Gap and Redox Potential of Graphene Quantum Dots. *J. Phys. Chem. Lett.* **2011**, *2*, 1119−1124.

(29) Li, Q.; Zhang, S.; Dai, L.; Li, L.-S. Nitrogen-Doped Colloidal Graphene Quantum Dots and Their Size-Dependent Electrocatalytic Activity for the Oxygen Reduction Reaction. *J. Am. Chem. Soc.* **2012**, *134*, 18932−18935.

(30) Li, L.; Wu, G.; Yang, G.; Peng, J.; Zhao, J.; Zhu, J.-J. Focusing on Luminescent Graphene Quantum Dots: Current Status and Future Perspectives. *Nanoscale* **2013**, *5*, 4015−4039.

(31) Sun, H.; Wu, L.; Wei, W.; Qu, X. Recent Advances in Graphene Quantum Dots for Sensing. *Mater. Today* **2013**, *16*, 433−442.

(32) Wang, Z.; Zeng, H.; Sun, L. Graphene Quantum Dots: Versatile Photoluminescence for Energy, Biomedical, and Environmental Applications. *J. Mater. Chem. C* **2015**, *3*, 1157−1165.

(33) Zheng, X.; Ananthanarayanan, A.; Luo, K.; Chen, P. Glowing Graphene Quantum Dots and Carbon Dots: Properties, Syntheses, and Biological Applications. *Small* **2015**, *11*, 1620−1636.

(34) Wang, J.; Qiu, J. Luminescent Graphene Quantum Dots: As Emerging Fluorescent Materials for Biological Application. *Sci. Adv. Mater.* **2015**, *7*, 1979−1989.

(35) LeCroy, G. E.; Sonkar, S. K.; Yang, F.; Veca, L. M.; Wang, P.; Tackett, K. N., II; Yu, J.-J.; Vasile, E.; Qian, H.; Liu, Y.; et al. Toward Structurally Defined Carbon Dots as Ultracompact Fluorescent Probes. *ACS Nano* **2014**, *8*, 4522−4529.

(36) Xu, J.; Sahu, S.; Cao, L.; Bunker, C. E.; Peng, G.; Liu, Y.; Fernando, K. A. S.; Wang, P.; Guliants, E. A.; Meziani, M. J.; et al. Efficient Fluorescence Quenching in Carbon Dots by Surface-Doped Metals—Disruption of Excited State Redox Processes and Mechanistic Implications. *Langmuir* **2012**, *28*, 16141−16147.

(37) Lakowicz, J. R. *Principles of Fluorescence Spectroscopy*, 2nd ed.; Kluwer Academic/Plenum Publishers: New York, 1999.

(38) Turro, N. J.; Ramamurthy, V.; Scaiano, J. C. *Principles of Molecular Photochemistry: An Introduction*; University Science Books: Sausalito, CA, 2009.

(39) Terrill, R. H.; Postlethwaite, T. A.; Chen, C. H.; Poon, C. D.; Terzis, A.; Chen, A. D.; Hutchison, J. E.; Clark, M. R.; Wignall, G.; Londono, J. D.; et al. Monolayers in Three Dimensions: NMR, SAXS, Thermal, and Electron Hopping Studies of Alkanethiol Stabilized Gold Clusters. *J. Am. Chem. Soc.* **1995**, *117*, 12537−12548.

(40) Marega, R.; Aroulmoji, V.; Dinon, F.; Vaccari, L.; Giordani, S.; Bianco, A.; Murano, E.; Prato, M. Diffusion-Ordered NMR Spectroscopy in the Structural Characterization of Functionalized Carbon Nanotubes. *J. Am. Chem. Soc.* **2009**, *131*, 9086−9093.

(41) Sun, Y.-P.; Huang, W.; Lin, Y.; Fu, K.; Kitaygorodskiy, A.; Riddle, L. A.; Yu, Y.; Carroll, D. L. Soluble Dendron-Functionalized Carbon Nanotubes: Preparation, Characterization, and Properties. *Chem. Mater.* **2001**, *13*, 2864−2869.

(42) Holland, G. P.; Sharma, R.; Agola, J. O.; Amin, S.; Solomon, V. C.; Singh, P.; Buttry, D. A.; Yarger, J. L. NMR Characterization of Phosphonic Acid Capped SnO_2 Nanoparticles. *Chem. Mater.* **2007**, *19*, 2519−2526.

(43) Ruther, M. G.; Frehill, F.; O'Brien, J. E.; Minett, A. I.; Blau, W. J.; Vos, J. G.; Panhuis, M. I. H. Characterization of Covalent Functionalized Carbon Nanotubes. *J. Phys. Chem. B* **2004**, *108*, 9665−9668.

(44) Panzella, L.; Melone, L.; Pezzella, A.; Rossi, B.; Pastori, N.; Perfetti, M.; D'Errico, G.; Punta, C.; d'Ischia, M. Surface-Functionalization of Nanostructured Cellulose Aerogels by Solid State Eumelanin Coating. *Biomacromolecules* **2016**, *17*, 564−571.

(45) Cao, Z.; Kim, D.; Hong, D.; Yu, Y.; Xu, J.; Lin, S.; Wen, X.; Nichols, E. M.; Jeong, K.; Reimer, J. A.; et al. A Molecular Surface Functionalization Approach to Tuning Nanoparticle Electrocatalysts for Carbon Dioxide Reduction. *J. Am. Chem. Soc.* **2016**, *138*, 8120−8125.

(46) Gassman, P. G.; Hodgson, P. K. G.; Balchunis, R. J. Base-Promoted Hydrolysis of Amides at Ambient-Temperatures. *J. Am. Chem. Soc.* **1976**, *98*, 1275−1276.

(47) Lamparth, I.; Hirsch, A. Water-Soluble Malonic-Acid Derivatives of C-60 with a Defined 3-Dimensional Structure. *J. Chem. Soc., Chem. Commun.* **1994**, 1727−1728.

(48) Ray, S. C.; Saha, A.; Jana, N. R.; Sarkar, R. Fluorescent Carbon Nanoparticles: Synthesis, Characterization, and Bioimaging Application. *J. Phys. Chem. C* **2009**, *113*, 18546−18551.

(49) Cao, L.; Anilkumar, P.; Wang, X.; Liu, J.-H.; Sahu, S.; Meziani, M. J.; Myers, E.; Sun, Y.-P. Reverse Stern-Volmer Behavior for Luminescence Quenching in Carbon Nanoparticles. *Can. J. Chem.* **2011**, *89*, 104−109.

(50) Yu, P.; Wen, X.; Toh, Y.-R.; Tang, J. Temperature-Dependent Fluorescence in Carbon Dots. *J. Phys. Chem. C* **2012**, *116*, 25552−25557.

(51) Kozak, O.; Datta, K. K. R.; Greplova, M.; Ranc, V.; Kaslik, J.; Zboril, R. Surfactant-Derived Amphiphilic Carbon Dots with Tunable Photoluminescence. *J. Phys. Chem. C* **2013**, *117*, 24991−24996.

(52) Wang, J.; Wei, J.; Su, S.; Qiu, J. Novel Fluorescence Resonance Energy Transfer Optical Sensors for Vitamin B-12 Detection Using Thermally Reduced Carbon Dots. *New J. Chem.* **2015**, *39*, 501−507.

(53) Wang, D.; Zhu, L.; McCleese, C.; Burda, C.; Chen, J.; Dai, L. Fluorescent Carbon Dots from Milk by Microwave Cooking. *RSC Adv.* **2016**, *6*, 41516−41521.

(54) Messina, F.; Sciortino, L.; Popescu, R.; Venezia, A. M.; Sciortino, A.; Buscarino, G.; Agnello, S.; Schneider, R.; Gerthsen, D.; Cannas, M.; et al. Fluorescent Nitrogen-Rich Carbon Nanodots with an Unexpected β-C_3N_4 Nanocrystalline Structure. *J. Mater. Chem. C* **2016**, *4*, 2598−2605.

(55) Cao, L.; Sahu, S.; Anilkumar, P.; Bunker, C. E.; Xu, J.; Fernando, K. A. S.; Wang, P.; Guliants, E. A.; Tackett, K. N., II; Sun, Y.-P. Carbon Nanoparticles as Visible-Light Photocatalysts for Efficient CO_2 Conversion and Beyond. *J. Am. Chem. Soc.* **2011**, *133*, 4754−4757.

(56) Wang, X.; Cao, L.; Lu, F.; Meziani, M. J.; Li, H.; Qi, G.; Zhou, B.; Harruff, B. A.; Kermarrec, F.; Sun, Y.-P. Photoinduced Electron Transfers with Carbon Dots. *Chem. Commun.* **2009**, 3774−3776.

(57) Reckmeier, C. J.; Wang, Y.; Zboril, R.; Rogach, A. L. Influence of Doping and Temperature on Solvatochromic Shifts in Optical Spectra of Carbon Dots. *J. Phys. Chem. C* **2016**, *120*, 10591−10604.

(58) Qian, Z.; Ma, J.; Shan, X.; Feng, H.; Shao, L.; Chen, J. Highly Luminescent N-Doped Carbon Quantum Dots as an Effective Multifunctional Fluorescence Sensing Platform. *Chem. - Eur. J.* **2014**, *20*, 2254−2263.

(59) Wu, Z.-L.; Gao, M.-X.; Wang, T.-T.; Wan, X.-Y.; Zheng, L.-L.; Huang, C.-Z. A General Quantitative pH Sensor Developed with Dicyandiamide N-Doped High Quantum Yield Graphene Quantum Dots. *Nanoscale* **2014**, *6*, 3868−3874.

(60) Tang, L.; Ji, R.; Li, X.; Bai, G.; Liu, C.-P.; Hao, J.; Lin, J.; Jiang, H.; Teng, K.-S.; Yang, Z.; Lau, S.-P. Deep Ultraviolet to Near-Infrared Emission and Photoresponse in Layered N-Doped Graphene Quantum Dots. *ACS Nano* **2014**, *8*, 6312−6320.

DOI: 10.1021/acs.jpcc.6b08171
J. Phys. Chem. C 2016, 120, 25604−25611

Volume 4 | Number 29 | 7 August 2016 | Pages 6917–7166

Journal of Materials Chemistry C

Materials for optical, magnetic and electronic devices

www.rsc.org/MaterialsC

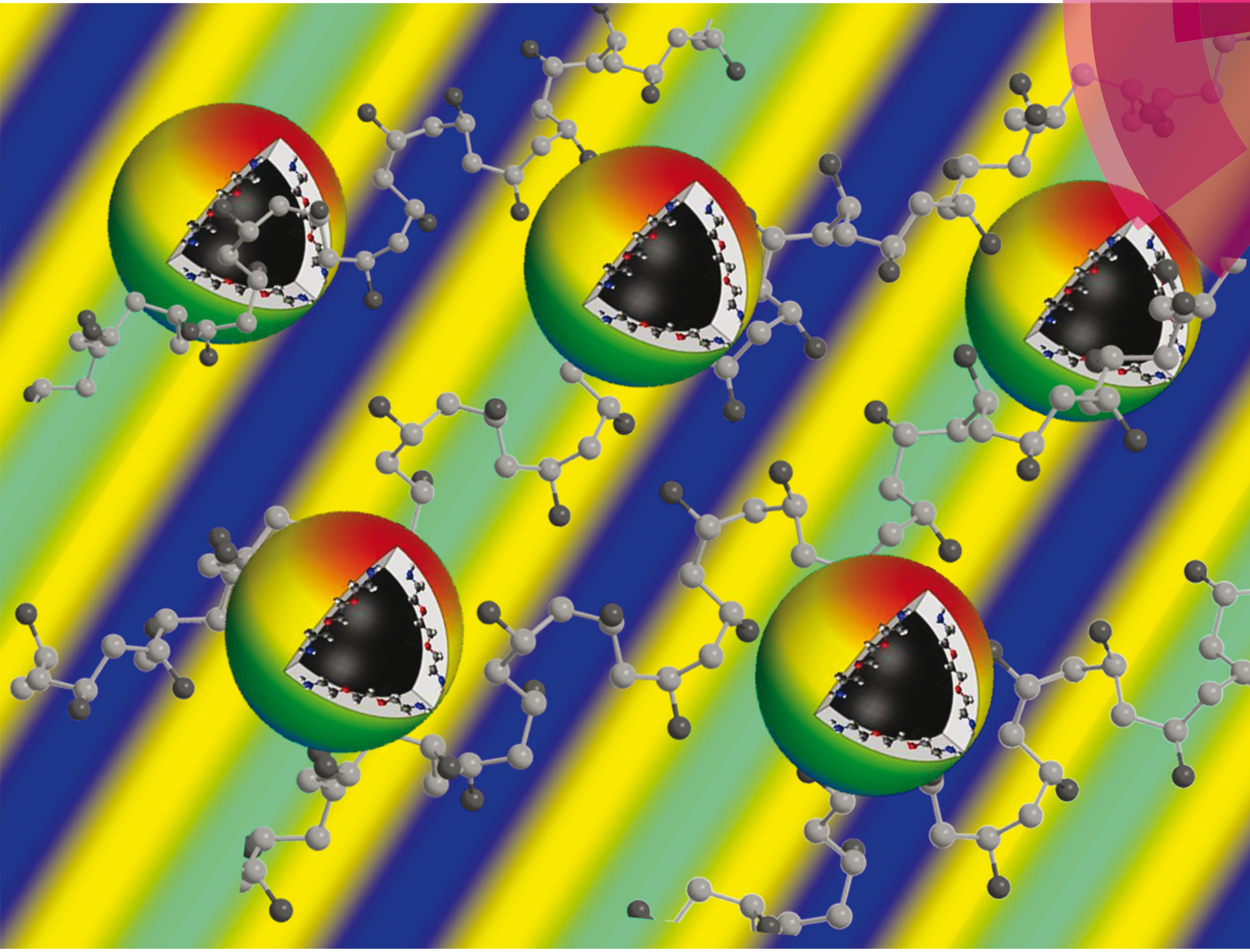

ISSN 2050-7526

ROYAL SOCIETY OF CHEMISTRY

PAPER
K. A. Shiral Fernando, Christopher E. Bunker, Ya-Ping Sun *et al.*
Enhanced fluorescence properties of carbon dots in polymer films

175 YEARS

Journal of
Materials Chemistry C

PAPER

View Article Online
View Journal | View Issue

Cite this: *J. Mater. Chem. C*, 2016, 4, 6967

Enhanced fluorescence properties of carbon dots in polymer films†

Yamin Liu,[a] Ping Wang,[a] K. A. Shiral Fernando,*[b] Gregory E. LeCroy,[a] Halidan Maimaiti,[a] Barbara A. Harruff-Miller,[b] William K. Lewis,[c] Christopher E. Bunker,*[c] Zhi-Ling Hou[a] and Ya-Ping Sun*[a]

Received 11th May 2016,
Accepted 13th June 2016

DOI: 10.1039/c6tc01932c

www.rsc.org/MaterialsC

Carbon dots of small carbon nanoparticles surface-functionalized with 2,2′-(ethylenedioxy)bis(ethylamine) (EDA) were synthesized, and the as-synthesized sample was separated on an aqueous gel column to obtain fractions of the EDA–carbon dots with different fluorescence quantum yields. As already discussed in the literature, the variations in fluorescence performance among the fractions were attributed to the different levels and/or effectiveness of the surface functionalization–passivation in the carbon dots. These fractions, as well as carbon nanoparticles without any deliberate surface functionalization, were dispersed into poly(vinyl alcohol) (PVA) for composite films. In the PVA film matrix, the carbon dots and nanoparticles exhibited much enhanced fluorescence emissions in comparison with their corresponding aqueous solutions. The increased fluorescence quantum yields in the films were determined quantitatively by using a specifically designed and constructed film sample holder in the emission spectrometer. The observed fluorescence decays of the EDA–carbon dots in the films and in the solution were essentially the same, suggesting that the significant enhancement in fluorescence quantum yields from the solution to films is static in nature. Mechanistic implications of the results, including a rationalization in terms of the compression effect on the surface passivation layer (similar to a soft corona) in carbon dots when embedded in the more restrictive film environment resulting in more favorable radiative recombinations of the carbon particle surface-trapped electrons and holes, and also potential technological applications of the brightly fluorescent composite films are highlighted and discussed.

Introduction

Optical properties of carbon nanomaterials have attracted much recent attention because of their variety of potential technological applications, from optoelectronics, bioimaging and sensing, to photocatalysis for energy conversion. Most of these materials are fluorescent over the visible spectrum, extending into the near-IR. More specifically, carbon "quantum" dots or carbon dots were found and developed as a new class of brightly fluorescent nanomaterials,[1,2] with their performance competitive to that of conventional semiconductor quantum dots (QDs) yet nontoxic and environmentally benign.[3–5] In fact, carbon dots have emerged to represent now a rapidly advancing and expanding research field, as reflected by the large number of recent publications in the literature, with extensive investigations looking into many aspects of carbon dots for both fundamental and technological purposes.[3–16]

Carbon dots are generally defined as small carbon nanoparticles with various surface passivation schemes, including especially the surface functionalization by organic and bio-molecular species (Fig. 1).[1,6,14,17,18] While fluorescence emissions from "naked" carbon nanoparticles (without any deliberate surface functionalization) in aqueous or other suspensions have been observed and reported,[19–23] their intensities are low, with observed quantum yields generally on the order of 1–2% or less. Therefore, effective surface passivation in carbon dots is necessary for bright fluorescence emissions.[3,4,6,14] For example, Wang *et al.* reported that for carbon dots with oligomeric poly(ethylene glycol) diamine (PEG_{1500N}) as the surface passivation agent, the as-synthesized sample exhibited fluorescence quantum yields around 20%, from which more fluorescent fractions corresponding to carbon dots of more effective surface functionalization and passivation could be isolated to achieve fluorescence quantum yields of more than 50%.[24] A number of other studies have also confirmed the critical role of surface

---

[a] *Department of Chemistry and Laboratory for Emerging Materials and Technology, Clemson University, Clemson, South Carolina 29634, USA. E-mail: yaping@clemson.edu*

[b] *University of Dayton Research Institute, Sensors Technology Office, Dayton, Ohio 45469, USA. E-mail: KAShiral.Fernando@udri.udayton.edu*

[c] *Air Force Research Laboratory, Propulsion Directorate, Wright-Patterson Air Force Base, Ohio 45433, USA. E-mail: christopher.bunker@wpafb.af.mil*

† Electronic supplementary information (ESI) available. See DOI: 10.1039/c6tc01932c

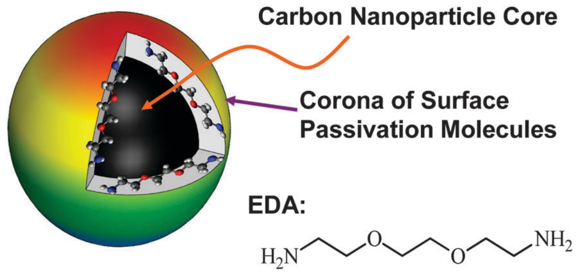

Fig. 1 A cartoon illustration of EDA–carbon dots, generally a small carbon nanoparticle core with attached and strongly adsorbed EDA molecules for surface passivation (a configuration similar to a soft corona).

passivation in determining the fluorescence brightness of the resulting carbon dots.[6,14,25] The mechanistic origin and implications of the surface passivation in carbon dots have also been explored.[6,12,26]

The widely cited mechanistic framework for carbon dots is such that the abundant surface defects in the small carbon nanoparticles must be playing an important role in the observed optical properties of carbon dots.[6,12,27–29] Upon photoexcitation there must be rapid charge separation in the carbon nanoparticles for the formation of electrons and holes, which are "trapped" at various surface sites, and radiative recombinations of the electrons and holes are responsible for the observed fluorescence emissions (Fig. 1).[6,12,29] The more effective passivation in carbon dots might have stabilized the surface sites for the electrons and holes, enabling more efficient radiative recombinations to result in higher fluorescence quantum yields. Within such a mechanistic framework, the weak fluorescence emissions from naked carbon nanoparticles in aqueous or organic suspensions may be understood in terms of the surface passivation effect provided by the solvation.[12,23] Organic solvents are apparently more effective than water in this regard, and the presence of amino molecules in the carbon nanoparticle solutions enhances the passivation effect and therefore the fluorescence performance.[23] It may be expected in the same mechanistic framework that a compression of the surface passivation layer in carbon dots (Fig. 1) could also enhance the passivation effect for brighter fluorescence emissions, as hinted by the results obtained from carbon dots in a more restrictive environment.[30] A more systematic examination of such an enhancement effect is in demand for significant mechanistic implications and also for the relevance to various technological applications of carbon dots, such as their use in polymeric composites for fluorescence displays and/or the like.[31,32]

In the work reported here we dispersed carbon dots of different levels of surface functionalization (thus different fluorescence quantum yields), as well as carbon nanoparticles without any deliberate functionalization, into poly(vinyl alcohol) (PVA, a polymer widely employed in optical spectroscopic investigations) for composite films. In the PVA matrix, the carbon dots and nanoparticles exhibited much enhanced fluorescence emissions in comparison with their corresponding aqueous solutions. The increased fluorescence quantum yields in the films were determined quantitatively by using a specifically designed and constructed film sample holder in the emission spectrometer. Since the fluorescence decays of the carbon dots in the films and in the solution are essentially the same, the significant enhancement in fluorescence quantum yields from the solution to films is static in nature, rationalized as a result of enhanced surface passivation for the carbon dots in a more confined environment in the PVA matrix. The mechanistic and technological implications of the results are discussed.

Experimental section

Materials

Carbon nanopowder samples (99%), 2,2′-(ethylenedioxy)bis-(ethylamine) (EDA), and poly(vinyl alcohol) (PVA, $M_W \sim 90\,000$) were purchased from Sigma-Aldrich, thionyl chloride (>99%) from Alfa Aesar, nitric acid from VWR, and sulfuric acid (98%) from Fisher Scientific. Dialysis membrane tubing (cutoff molecular weight ~500) was supplied by Spectrum Laboratories. Water was deionized and purified by being passed through a Labconco-WaterPros water purification system.

Measurements

An Eppendorf centrifuge (model 5417 R) was used for centrifugation at various *g* values. Transmission electron microscopy (TEM) images were obtained on a Hitachi H-7600 instrument operated at 100–120 kV. Atomic force microscopy (AFM) analysis was carried out in the acoustic AC mode on a Molecular Imaging PicoPlus AFM system equipped with a multipurpose scanner and a NanoWorldPointprobe NCH sensor. The height profile analysis was assisted by using the SjPIP software distributed by Image Metrology.

Optical absorption spectra were recorded on a Shimadzu UV2501-PC spectrophotometer. Fluorescence spectra were recorded on a Jobin-Yvon emission spectrometer equipped with a 450 W xenon source, Gemini-180 excitation and Tirax-550 emission monochromators, and a photon-counting detector (Hamamatsu R928P PMT at 950 V). Fluorescence decays were measured on a time-correlated single photon counting (TCSPC) setup with a Hamamatsu stabilized picosecond light pulser (PLP-02) for 407 nm excitation (<100 ps pulses at 1 MHz repetition rate), coupled with a Phillips XP2254/B PMT in a thermoelectrically cooled housing as a detector for an overall instrument time resolution of 500 ps or better.

A specifically designed film sample holder for being used in the emission spectrometer was made by using 3D printing in house (see also ESI†). The physical dimensions of the holder match exactly those of a standard 1 cm cuvette, so that the holder is fully compatible with the sample chamber in the emission spectrometer. The outer piece of the holder is equivalent to a typical plastic cuvette, except for large openings at all four sides. Inside the outer piece is fitted precisely in the diagonal geometry a pair of composite plates, both of which have a matching large opening in the center. The function of the plates is to sandwich a film specimen for fluorescence measurements in such a geometry that the film is excited in the back with a

45° angle to the excitation light, and the emissions are collected in the front of the film also in a 45° angle to the detector. The performance of the sample holder in terms of reproducibility and reliability in the measurement of film samples against fluorescence film standard (rhodamine 6G in PVA films) was evaluated by repeated measurements of sample and/or standard films, and in each measurement the selected film was reloaded into the holder. The variations in measurement results were around 5% or less, which were considered as being sufficient for the validation of the sample holder.

Carbon nanoparticles and EDA–carbon dots

The commercially acquired carbon nanopowder sample was refluxed in aqueous nitric acid (2.6 M) for 24 h, washed with deionized water repeatedly, and then dried under nitrogen. The treated sample (200 mg) was further treated in the mixed acid of concentrated sulfuric acid and nitric acid (3/1 v/v, 10 mL) at 60 °C with sonication for 1 h and then refluxing for 2 h. To the resulting mixture was added deionized water (100 mL) for centrifugation at 20 000*g* for 30 min to keep the supernatant. It was dialyzed in a membrane tubing (cutoff molecular weight ~500) against fresh water for 3 days to yield a stable dispersion of carbon nanoparticles.

For the synthesis of EDA–carbon dots, the nitric acid treated carbon nanopowder sample discussed above was dialyzed in a membrane tubing (cutoff molecular weight ~500) against fresh water, followed by centrifugation at 1000*g* to retain the supernatant as a suspension of carbon nanoparticles. The nanoparticles were recovered by the removal of water *via* evaporation, and then refluxed in neat thionyl chloride for 12 h. Upon the removal of excess thionyl chloride, the treated sample (50 mg) was mixed well with carefully dried (vacuum oven at ~60 °C for 4 h) EDA liquid in a round-bottom flask, heated to 120 °C, and vigorously stirred under nitrogen protection for 3 days. The reaction mixture back at room temperature was dispersed in water and then centrifuged at 20 000*g* to retain the supernatant. It was dialyzed in a membrane tubing (cutoff molecular weight ~500) against fresh water to remove unreacted EDA and other small molecular species to obtain an aqueous solution of the as-synthesized EDA–carbon dots. A Sephadex™ G-100 gel column (packed in house with a commercially supplied gel sample) was used for the fractionation of the as-synthesized sample by following the experimental protocol already reported in the literature.[24]

PVA films

A PVA polymer (M_W ~ 90 000, 750 mg) was dissolved in deionized water (10 mL) at 80 °C. Separately, aqueous solution with known concentration of a selected sample of EDA–carbon dots was prepared, and a quantitatively measured amount of the solution was mixed with the PVA solution under vigorous stirring. The resulting solution was degassed, concentrated by the evaporation of water until it becomes viscous, and then drop-cast onto a clean glass slide. The film thickness was controlled by controlling the amount of material used for casting and the film dimensions on the slide. After drying, the PVA/carbon dot composite film was peeled off the slide to be free-standing. The same procedure was applied to the fabrication of PVA films embedded with carbon nanoparticles or rhodamine 6G as the fluorescence standard.

Results and discussion

Carbon nanoparticles were harvested from the commercially supplied carbon nanopowder sample using procedures including the sample being subjected to several acid treatment steps involving aqueous nitric acid and the mixed acid composed of concentrated sulfuric acid and nitric acid.[22] The acid treated sample was dialyzed against fresh water, and centrifuged to keep the supernatant as an aqueous dispersion of carbon nanoparticles, which appeared transparent and solution-like (Fig. 2). The treatment with the mixed acid was apparently a necessary step in the processing to make the resulting dispersion relatively more stable without any meaningful precipitation. The dispersed carbon nanoparticles were small, as desired, on average around 4.5 nm according to results from the transmission electron microscopy (TEM) characterization (Fig. 3). The broad optical absorption spectrum of the aqueous dispersed carbon nanoparticles is also shown in Fig. 2.

The carbon nanoparticles in aqueous dispersion were found to be weakly fluorescent (Fig. 2), with observed quantum yields on the order of 1–2%, and somewhat different at different excitation wavelengths. The results are in general agreement with those already reported in the literature.[19–23] It has been argued that even without the deliberate surface passivation *via* the kind of organic functionalization in carbon dots, the solvation of the carbon nanoparticles in an aqueous medium may provide some passivation effect to result in the observed relatively weak fluorescence emissions.[6,21]

The carbon nanoparticles were functionalized with 2,2′-(ethylenedioxy)bis(ethylamine) (EDA) under amidation reaction conditions to obtain EDA–carbon dots, as reported previously.[33] The as-synthesized sample was readily soluble in water, thus cleaned in dialysis (through membrane tubing with cutoff molecular weight ~500) to remove unreacted EDA and other small molecular species. Results from atomic force microscopy (AFM) characterization (Fig. 4) suggested that the carbon dots

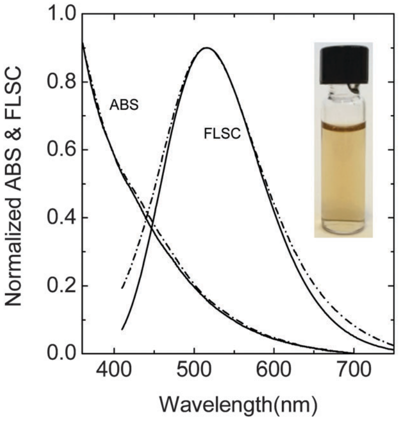

Fig. 2 Absorption (ABS) and fluorescence (FLSC, 400 nm excitation) spectra of carbon nanoparticles in aqueous dispersion (—, with a photograph of the dispersion in the inset) and in PVA films (–·–·–).

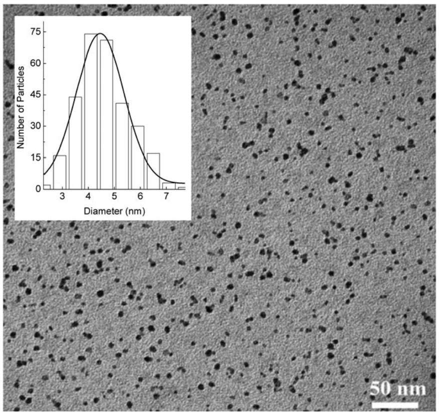

Fig. 3 A representative TEM image of the carbon nanoparticles, with the size distribution analysis in the inset.

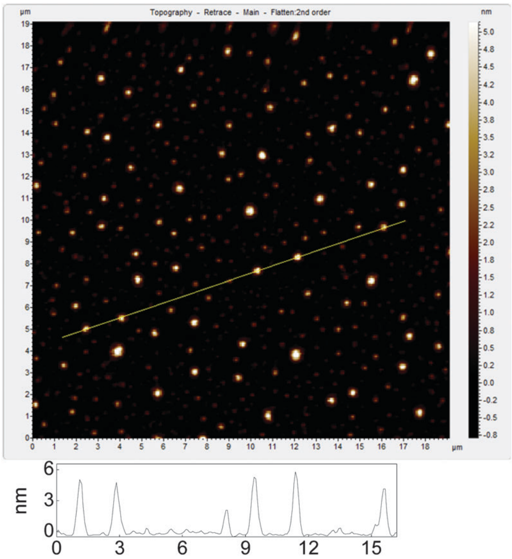

Fig. 4 Results from AFM imaging of the EDA–carbon dots on mica, with height analyses on selected dots for estimating their sizes.

were on the order of 5 nm in diameter, consistent with the TEM results on the sizes of precursor carbon nanoparticles (Fig. 3).

Absorption and fluorescence spectra of the as-synthesized sample of EDA–carbon dots in aqueous solution are shown in Fig. 5. The observed fluorescence quantum yields were much higher than those of the aqueous dispersed carbon nanoparticles, 15–20% (varying from batch to batch in duplicating syntheses) at 400 nm excitation. Since the as-synthesized sample was generally known as a mixture of EDA–carbon dots of different fluorescence quantum yields,[33] an aqueous gel column (Sephadex™ G-100) was used for the fractionation of the sample,[24] yielding fractions of fluorescence quantum yields higher or lower than the pre-fractionation average (Fig. 5). As discussed in the literature, the difference in fluorescence brightness between different fractions reflects upon the effectiveness of surface passivation in the corresponding carbon dots.[24,34] Therefore, fractions of the carbon dots exhibiting lower fluorescence quantum yields due to relatively less effective surface passivation should be expected to benefit more

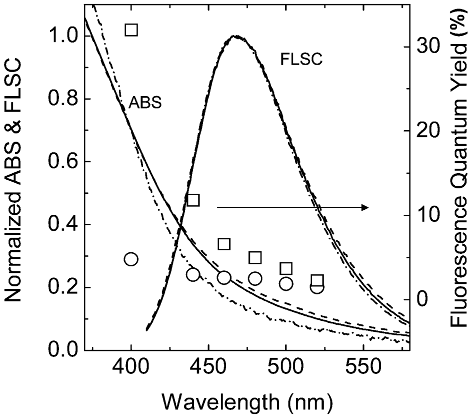

Fig. 5 Absorption (ABS) and fluorescence (FLSC, 400 nm excitation) spectra of the EDA–carbon dots in aqueous solution (the as-prepared sample: —; the separated fractions with fluorescence quantum yields at 400 nm excitation of around 5%: – – – and 32%: –·–·–), and observed fluorescence quantum yields of the two fractions at different excitation wavelengths (the lower-yield fraction: circles, and the higher-yield fraction: squares).

significantly from any external effect that would improve the surface passivation, such as the expected compression effect experienced by the carbon dots embedded in a polymer film matrix. This was confirmed in the film study in which a fraction combining the EDA–carbon dots of fluorescence quantum yields of around 5% at 400 nm excitation was used as the starting point.

Poly(vinyl alcohol) (PVA) was selected as the polymer host because of its known high optical quality and desirable film properties.[35–37] In the fabrication of polymeric nanocomposite films with embedded EDA–carbon dots, the selected sample solution was added dropwise to a separately prepared aqueous solution of PVA with stirring to obtain a homogeneous mixture. The mixture was degassed thoroughly (centrifuged vigorously and then sonicated in the degas mode), concentrated until it becomes viscous, and drop-cast onto a clean glass slide. Upon drying, the PVA/EDA–carbon dot film was peeled off the slide to be free-standing (Fig. 6). A blank PVA film without carbon dots was prepared using the same procedure. The film thickness was controlled in the fabrication by using the same amount of PVA and by keeping the film dimensions as constant as possible.

The PVA/carbon dot composite films appeared colored, but optically transparent (Fig. 6). The observed absorption spectra of the EDA–carbon dots in PVA films (as blank films have no absorption in the same spectral region) are largely the same as those in solution (Fig. 5 and 6). Since the optical absorption of carbon dots is due to transitions associated with the π-plasmon in the core carbon nanoparticles, the results suggest that the film environment has no significant effect on the transitions. The observed fluorescence spectra of the EDA–carbon dots in PVA films are also similar to those in solution at the same excitation wavelengths, except for slight blue shifts due to the film environment (Fig. 6). The composite films were visually brightly fluorescent under light illumination, suggesting substantial fluorescence quantum yields.

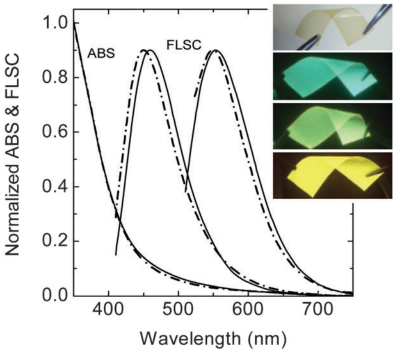

Fig. 6 Absorption (ABS) and fluorescence (FLSC, 400 nm excitation on the left and 500 nm excitation on the right) spectra of the EDA–carbon dots in aqueous solution (—) and in PVA films (–·–·–). Inset: photographs of the PVA/carbon dot composite films (from top to bottom) under ambient light and exposed to a UV lamp (350–400 nm, with the three photos taken through 405 nm, 475 nm, and 525 nm cutoff filters).

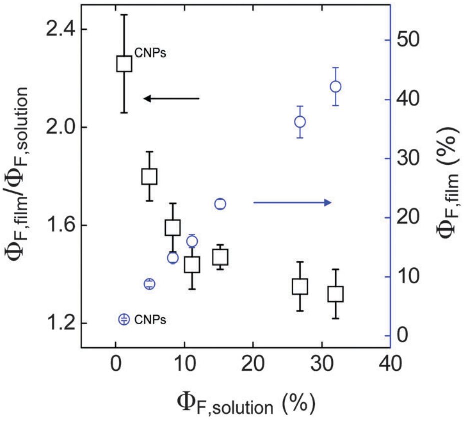

Fig. 7 Fluorescence quantum yields of the separated fractions of the EDA–carbon dots (including naked carbon nanoparticles or CNPs) in PVA films ($\Phi_{F,film}$) *vs.* in solution ($\Phi_{F,solution}$): circles; and a plot of the enhancement factor $\Phi_{F,film}/\Phi_{F,solution}$ *vs.* $\Phi_{F,solution}$: squares.

Fluorescence quantum yields of the EDA–carbon dots in PVA films were determined quantitatively by using the relative method with a film of rhodamine 6G in PVA as the fluorescence standard, for which the assumed no effect on the fluorescence quantum yield of the dye by PVA was justified by the experimental results such that in a comparison of rhodamine 6G in aqueous solutions without and with high concentrations of PVA (up to 200 mg mL^{-1}, with the solution becoming viscous to mimic conditions in films), no meaningful changes in fluorescence intensities were observed. However, because of the implicit assumptions behind the relative method,[38] an absolute requirement is for the sample and the standard to have the same configuration (film *vs.* film) and also the same measurement geometry in the fluorescence spectrometer.[38,39] The latter is intrinsically more difficult for film specimens, requiring special efforts in terms of the instrumental setup and measurements. Therefore, a film sample holder was specifically designed and constructed (details in Experimental section) for the fluorescence spectrometer to ensure the same measurement geometry for the films and thus the reproducibility in the measurement of their fluorescence intensities. As a calibration to evaluate and demonstrate the reproducibility, several PVA/rhodamine 6G films were used for multiple independent (films remounted in the holder each time) measurements, equivalent to multiple independent determinations of the fluorescence quantum yield of a PVA/rhodamine 6G film by using itself or another film of the same kind as the fluorescence standard. The results suggested that the variation over multiple films, each with multiple independent measurements, was around 5%, an error margin not so different from that in the use of the relative method for fluorescence quantum yield determination in general. Therefore, the same film sample holder and measurement protocol were used in the determination of fluorescence quantum yields of all PVA/carbon dot films in reference to the PVA/rhodamine 6G film standard. For the same sample film over multiple independent measurements, the variation in the resulting fluorescence quantum yield values was also on the order of 5%. As shown in Fig. 7, the fraction of EDA–carbon dots with the solution-phase fluorescence quantum yield of 5% (400 nm excitation) exhibited nearly a doubling in the yield upon being incorporated into the PVA film matrix (Fig. 7).

The enhancement in fluorescence quantum yields from the solution to films was apparently more dramatic relatively (in terms of the percentage increase) for less fluorescent fractions of the EDA–carbon dots. For example, the fraction from the gel column separation with a fluorescence quantum yield of around 15% in aqueous solution (400 nm excitation) was used in the fabrication of PVA/carbon dot composite films, and the fluorescence quantum yields in films were also determined in reference to the PVA/rhodamine 6G film standard by using the same film sample holder and measurement protocol. The enhancement from the solution to films was significant, with the observed fluorescence quantum yield increased to more than 20% in films, though seemingly less dramatic in the percentage term (a 50% increase from the solution to films, Fig. 7). A similar enhancement from solutions to films was confirmed with films fabricated by using other fractions of the EDA–carbon dots of different solution-phase fluorescence quantum yields, as also illustrated in Fig. 7. In control experiments, fluorescence quantum yields of EDA–carbon dots in aqueous solutions were measured in the presence of PVA in various concentrations (up to 200 mg mL^{-1}), no meaningful changes were observed.

For carbon dots of the same surface functional molecules, the gel-column separated fractions of different observed fluorescence quantum yields have generally been correlated with different levels of surface functionalization–passivation in the corresponding carbon dots, those less well functionalized–passivated exhibiting lower fluorescence quantum yields.[24,34] In this regard, at the limit is the aqueous dispersed carbon nanoparticles without surface functionalization (depending on solvation for a relatively weak surface passivation effect).[23] Therefore, the particle dispersion was also used for the fabrication of PVA/carbon nanoparticles composite films, and their fluorescence quantum yields were similarly determined. The results suggested the most significant percentage increase in fluorescence quantum yields from the aqueous dispersion to composite films (Fig. 7).

Within the mechanistic framework discussed in the introduction section, the observed substantial increase in fluorescence quantum yields of carbon dots from solutions to PVA films are attributed primarily to significantly enhanced surface passivation effects on the carbon nanoparticles in carbon dots in the film environment. Similar observations in the literature on the solid-state matrix effect on the embedded carbon dots may be understood in terms of the same mechanistic origins.[30,40] In the PVA/carbon dot composite films, while PVA may not add directly to the surface passivation layer in carbon dots (Fig. 1), the film environment may compress the existing EDA functionalization to enhance the surface passivation effect to result in brighter fluorescence emissions across all fractions of the EDA–carbon dots with different solution-phase fluorescence quantum yields (Fig. 7). Similarly, it may be argued that such a film environment-induced effect is more significant relatively on the less fluorescent factions. At the extreme for "naked" carbon nanoparticles in the PVA film matrix, the matrix polymers are apparently able to provide more effective surface passivation than water molecules in aqueous dispersion of the nanoparticles for the largest percentage increase in the observed fluorescence quantum yield. Nevertheless, in absolute terms the incorporation of the most fluorescent fraction of EDA–carbon dots into PVA films resulted in the substantial improvement to push the fluorescence quantum yield over 40% (Fig. 7).

The film environment-induced fluorescence quantum yield enhancement (or the "negative quenching effect" in a different description)[23] must be mostly static in nature, generally manifested in terms of a decoupling between fluorescence intensity quenching and fluorescence lifetime quenching.[38] This was confirmed by the results from fluorescence decay measurements based on the time-correlated single photon counting (TCSPC). As compared in Fig. 8, the decay curve of the EDA–carbon dots in PVA films is essentially the same as that in solution, despite the substantially higher fluorescence quantum yield observed in the same film sample. Both decay curves could not be deconvoluted with a mono- or bi-exponential function, suggesting a distribution of fluorescence lifetimes.

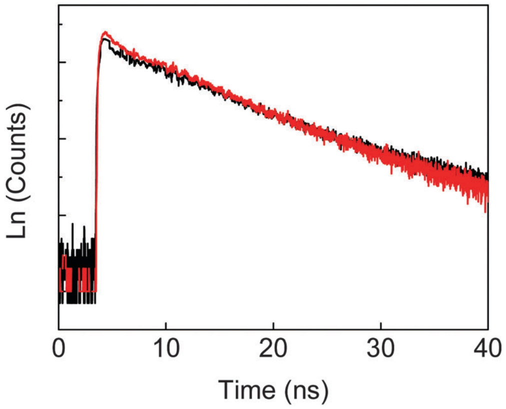

Fig. 8 A comparison between fluorescence decay curves of the EDA–carbon dots in aqueous solution (black) and in PVA films (red).

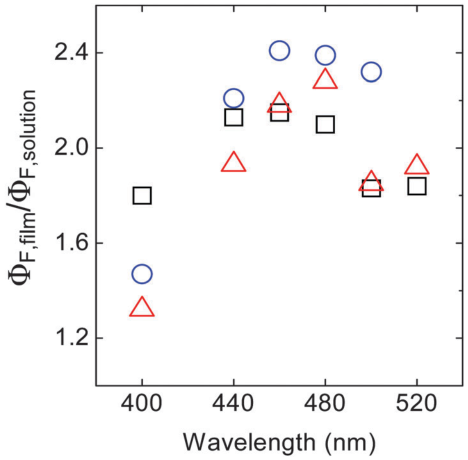

Fig. 9 Excitation wavelength dependencies of the fluorescence quantum yield enhancements from the aqueous solution to PVA films (as measured by $\Phi_{F,film}/\Phi_{F,solution}$) for different EDA–carbon dot fractions with solution-phase quantum yields at 400 nm excitation of around 5% (squares), 15% (circles), and 32% (triangles).

In addition to the results shown in Fig. 7 for 400 nm excitation, enhanced fluorescence quantum yields in representative sample films at other excitation wavelengths were determined and compared. Shown in Fig. 9 are the results for the films corresponding to the fractions of EDA–carbon dots with solution-phase fluorescence quantum yields of around 5%, 15%, and 32% at 400 nm excitation. Across all of the excitation wavelengths, there are significant increases in the observed fluorescence quantum yields from the solution to films, with the film-to-solution ($\Phi_{F,film}/\Phi_{F,solution}$) ratio varying with the excitation wavelength (Fig. 9). The variation is such that the enhancements at longer excitation wavelengths are more pronounced than at 400 nm excitation. For the more fluorescent film (Fig. 9), the $\Phi_{F,film}/\Phi_{F,solution}$ ratios at 480 nm and 520 nm excitations are 2.3 and 1.9, corresponding to absolute fluorescence quantum yield values in the film of 10% and 4%, respectively. The results suggest that the incorporation of carbon dots into polymer films or other optically transparent matrices may be further explored as a strategy for the general need to increase the fluorescence brightness of carbon dots at longer excitation wavelengths.

In addition to mechanistic implications of the results presented above for enhanced surface passivation effects with carbon dots embedded in a more confined environment in a polymer matrix, technologically an improved understanding of polymeric composites with brightly fluorescent carbon dots is relevant to the increasing interest in using carbon dots for optoelectronic devices, light emitting diodes (LEDs) in particular.[41,42] A potentially more direct use of the polymer/carbon dot composite films is to take advantage of their bright fluorescence emissions for displays, signs, or other luminescence-based devices.

Conclusions

Carbon dots are small carbon nanoparticles with various surface passivation schemes, among which the most effective has been the particle surface functionalization. As a result, the fluorescence properties of carbon dots, the brightness or quantum yields in particular, are sensitive to the level and effectiveness of the surface functionalization–passivation, as reflected by the different performances of the fractions from separating the as-synthesized sample of EDA–carbon dots. Demonstrated in this work is that in all fractions the passivation effect could be enhanced significantly upon dispersing the carbon dots into a polymer (PVA) film matrix, corresponding to the observed higher fluorescence quantum yields. The fluorescence decay results suggest that the enhanced passivation effect is static in nature. Mechanistically the enhancement may be rationalized as being associated with the compression of the surface passivation layer (similar to a soft corona) in carbon dots embedded in the more restrictive film environment, which must have provided a stabilization effect on the trapped electrons and holes for more efficient radiative recombinations. Technologically, the brightly fluorescent polymer/carbon dot composite films with multiple emission colors may find direct or indirect applications in various optical or optoelectronic devices, from fluorescent displays to LEDs.

Acknowledgements

Financial support from NSF and NIH (Y.-P. S.), the Air Force Office of Scientific Research through Dr Michael Berman (C. E. B.), and the Air Force Research Laboratory (C. E. B.) is gratefully acknowledged. H. M. was on leave from Xinjiang University in Urumqi, China and Z.-L. H. on leave from Beijing University of Chemical Technology in Beijing, China, both with visiting scholarships provided by the China Scholarship Council.

Notes and references

1 Y.-P. Sun, B. Zhou, Y. Lin, W. Wang, K. A. S. Fernando, P. Pathak, M. J. Meziani, B. A. Harruff, X. Wang, H. F. Wang, P. J. G. Luo, H. Yang, M. E. Kose, B. L. Chen, L. M. Veca and S. Y. Xie, *J. Am. Chem. Soc.*, 2006, **128**, 7756–7757.

2 L. Cao, X. Wang, M. J. Meziani, F. Lu, H. Wang, P. G. Luo, Y. Lin, B. A. Harruff, L. M. Veca, D. Murray, S. Y. Xie and Y.-P. Sun, *J. Am. Chem. Soc.*, 2007, **129**, 11318–11319.

3 P. G. Luo, S. Sahu, S.-T. Yang, S. K. Sonkar, J. Wang, H. Wang, G. E. LeCroy, L. Cao and Y.-P. Sun, *J. Mater. Chem. B*, 2013, **1**, 2116–2127.

4 P. G. Luo, S. K. Sonkar, S. T. Yang, F. Yang, L. Yang, J. J. Broglie and Y.-P. Sun, *RSC Adv.*, 2014, **4**, 10791–10807.

5 P. Miao, K. Han, Y. Tang, B. Wang, T. Lin and W. Cheng, *Nanoscale*, 2015, **7**, 1586–1595.

6 L. Cao, M. J. Meziani, S. Sahu and Y.-P. Sun, *Acc. Chem. Res.*, 2013, **46**, 171–180.

7 Y. Wang and A. Hu, *J. Mater. Chem. C*, 2014, **2**, 6921–6939.

8 K. Hola, Y. Zhang, Y. Wang, E. P. Giannelis, R. Zboril and A. L. Rogach, *Nano Today*, 2014, **9**, 590–603.

9 S. Y. Lim, W. Shen and Z. Gao, *Chem. Soc. Rev.*, 2015, **44**, 362–381.

10 A. Zhao, Z. Chen, C. Zhao, N. Gao, J. Ren and X. Qu, *Carbon*, 2015, **85**, 309–327.

11 J. Wang and J. Qiu, *J. Mater. Sci.*, 2016, **51**, 4728–4738.

12 K. A. S. Fernando, S. Sahu, Y. Liu, W. K. Lewis, E. A. Guliants, A. Jafariyan, P. Wang, C. E. Bunker and Y.-P. Sun, *ACS Appl. Mater. Interfaces*, 2015, **7**, 8363–8376.

13 Y. Du and S. Guo, *Nanoscale*, 2016, **8**, 2532–2543.

14 D. Konstantinos, *Curr. Org. Chem.*, 2016, **20**, 682–695.

15 C. Hu, C. Yu, M. Li, X. Wang, J. Yang, Z. Zhao, A. Eychmüller, Y. P. Sun and J. Qiu, *Small*, 2014, **10**, 4926–4933.

16 C. Hu, C. Yu, M. Li, X. Wang, Q. Dong, G. Wang and J. Qiu, *Chem. Commun.*, 2015, **51**, 3419–3422.

17 M. Wu, Y. Wang, W. Wu, C. Hu, X. Wang, J. Zheng, Z. Li, B. Jiang and J. Qiu, *Carbon*, 2014, **78**, 480–489.

18 M. Li, C. Hu, C. Yu, S. Wang, P. Zhang and J. Qiu, *Carbon*, 2015, **91**, 291–297.

19 S. C. Ray, A. Saha, N. R. Jana and R. Sarkar, *J. Phys. Chem. C*, 2009, **113**, 18546–18551.

20 J. Lu, J.-x. Yang, J. Wang, A. Lim, S. Wang and K. P. Loh, *ACS Nano*, 2009, **3**, 2367–2375.

21 S. Ciftan Hens, W. G. Lawrence, A. S. Kumbhar and O. Shenderova, *J. Phys. Chem. C*, 2012, **116**, 20015–20022.

22 J.-H. Liu, S.-T. Yang, X. Wang, H. Wang, Y. Liu, P. G. Luo, Y. Liu and Y.-P. Sun, *ACS Appl. Mater. Interfaces*, 2014, **6**, 14672–14678.

23 L. Cao, P. Anilkumar, X. Wang, J.-H. Liu, S. Sahu, M. J. Meziani, E. Myers and Y.-P. Sun, *Can. J. Chem.*, 2011, **89**, 104–109.

24 X. Wang, L. Cao, S.-T. Yang, F. Lu, M. J. Meziani, L. Tian, K. W. Sun, M. A. Bloodgood and Y.-P. Sun, *Angew. Chem., Int. Ed.*, 2010, **49**, 5310–5314.

25 Y. Dong, R. Wang, H. Li, J. Shao, Y. Chi, X. Lin and G. Chen, *Carbon*, 2012, **50**, 2810–2815.

26 X. Li, S. Zhang, S. A. Kulinich, Y. Liu and H. Zeng, *Sci. Rep.*, 2014, **4**, 4976–4984.

27 L. Bao, C. Liu, Z.-L. Zhang and D.-W. Pang, *Adv. Mater.*, 2015, **27**, 1663–1667.

28 S. Chandra, S. H. Pathan, S. Mitra, B. H. Modha, A. Goswami and P. Pramanik, *RSC Adv.*, 2012, **2**, 3602–3606.

29 L. Cao, S. Sahu, P. Anilkumar, C. E. Bunker, J. Xu, K. A. S. Fernando, P. Wang, E. A. Guliants, K. N. Tackett and Y.-P. Sun, *J. Am. Chem. Soc.*, 2011, **133**, 4754–4757.

30 Z. Xie, F. Wang and C.-y. Liu, *Adv. Mater.*, 2012, **24**, 1716–1721.

31 L. Zhou, B. He and J. Huang, *Chem. Commun.*, 2013, **49**, 8078–8080.

32 Y. Hao, Z. Gan, J. Xu, X. Wu and P. K. Chu, *Appl. Surf. Sci.*, 2014, **311**, 490–497.

33 G. E. LeCroy, S. K. Sonkar, F. Yang, L. M. Veca, P. Wang, K. N. Tackett, J.-J. Yu, E. Vasile, H. Qian, Y. Liu, P. Luo and Y.-P. Sun, *ACS Nano*, 2014, **8**, 4522–4529.

34 P. Anilkumar, X. Wang, L. Cao, S. Sahu, J.-H. Liu, P. Wang, K. Korch, K. N. Tackett Ii, A. Parenzan and Y.-P. Sun, *Nanoscale*, 2011, **3**, 2023–2027.

35 J. Michl and V. Bonacic-Koutechy, *Electronic Aspects of Organic Photochemistry*, John Wiley & Sons, New York, 1990.

36 B. Zhou, Y. Lin, L. M. Veca, K. A. S. Fernando, B. A. Harruff and Y.-P. Sun, *J. Phys. Chem. B*, 2006, **110**, 3001–3006.

37 A. C. Hourd, R. T. Baker and A. Abdolvand, *Nanoscale*, 2015, **7**, 13537–13546.

38 R. J. Lakowicz, *Principles of Fluorescence Spectroscopy*, Kluwer Academic/Plenum Publisher, New York, 1999, 2nd edn.

39 C. Würth, M. Grabolle, J. Pauli, M. Spieles and U. Resch-Genger, *Nat. Protoc.*, 2013, **8**, 1535–1550.

40 M. Müller, M. Kaiser, G. M. Stachowski, U. Resch-Genger, N. Gaponik and A. Eychmüller, *Chem. Mater.*, 2014, **26**, 3231–3237.

41 L.-H. Mao, W.-Q. Tang, Z.-Y. Deng, S.-S. Liu, C.-F. Wang and S. Chen, *Ind. Eng. Chem. Res.*, 2014, **53**, 6417–6425.

42 P. K. Sarswat and M. L. Free, *Phys. Chem. Chem. Phys.*, 2015, **17**, 27642–27652.

ACS APPLIED MATERIALS & INTERFACES
Research Article
www.acsami.org

Carbon "Quantum" Dots for Fluorescence Labeling of Cells

Jia-Hui Liu,[†,‡,#] Li Cao,[‡,#] Gregory E. LeCroy,[‡] Ping Wang,[‡] Mohammed J. Meziani,[‡] Yiyang Dong,[†] Yuanfang Liu,[§,¶] Pengju G. Luo,[‡] and Ya-Ping Sun*[,‡]

[†]Beijing Key Laboratory of Bioprocess, College of Life Science and Technology, Beijing University of Chemical Technology, Beijing 100029, China

[‡]Department of Chemistry and Laboratory for Emerging Materials and Technology, Clemson University, Clemson, South Carolina 29634, United States

[§]Beijing National Laboratory for Molecular Sciences, College of Chemistry and Molecular Engineering, Peking University, Beijing 100871, China

[¶]Institute of Nanochemistry and Nanobiology, Shanghai University, Shanghai 200444, China

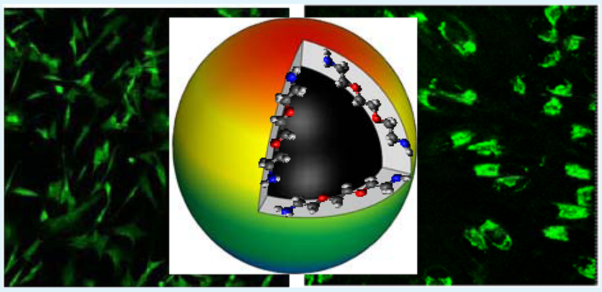

ABSTRACT: The specifically synthesized and selected carbon dots of relatively high fluorescence quantum yields were evaluated in their fluorescence labeling of cells. For the cancer cell lines, the cellular uptake of the carbon dots was generally efficient, resulting in the labeling of the cells with bright fluorescence emissions for both one- and two-photon excitations from predominantly the cell membrane and cytoplasm. In the exploration on labeling the live stem cells, the cellular uptake of the carbon dots was relatively less efficient, though fluorescence emissions could still be adequately detected in the labeled cells, with the emissions again predominantly from the cell membrane and cytoplasm. This combined with the observed more efficient internalization of the same carbon dots by the fixed stem cells might suggest some significant selectivity of the stem cells toward surface functionalities of the carbon dots. The needs and possible strategies for more systematic and comparative studies on the fluorescence labeling of different cells, including especially live stem cells, by carbon dots as a new class of brightly fluorescent probes are discussed.

KEYWORDS: *carbon dots, fluorescence labeling, cell imaging, stem cells, two-photon fluorescence, quantum dots*

INTRODUCTION

Fluorescent semiconductor nanocrystals, commonly referred to as quantum dots (QDs), have attracted much attention for serving as probes in cell imaging and other biomedical applications.[1,2] Strong cases have been made in the literature for using QDs to replace organic dyes and in some applications genetically encoded fluorescent tags due to their advantages such as the fluorescence brightness at the individual dot level, photostability, and so on.[1−3] With a growing demand on high-performance fluorescence tags and probes for cell labeling and imaging purposes, much effort has been made to expand the offering of QD-like fluorescent nanomaterials beyond those based on conventional semiconductors. Among more significant recent successes have been the finding and subsequent development of carbon "quantum" dots or more appropriately called carbon dots (for the lack of the classical quantum confinement effect in these nanomaterials),[4−11] which have played a leading role in an emerging and rapidly expanding research field centered on the design, preparation, and potential biomedical uses of various carbon-based QDs.[12−25]

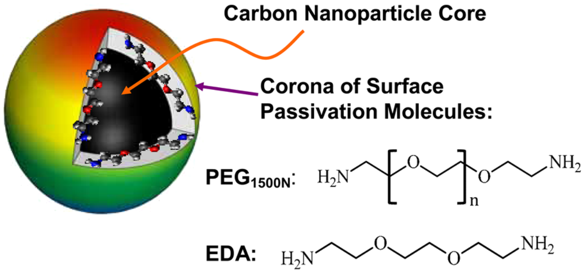

PEG_{1500N}: H_2N–[CH₂CH₂O]ₙ–…–NH_2

Figure 1. Cartoon illustration on carbon dot, which is generally a small carbon nanoparticle core with attached and strongly adsorbed surface passivation molecules (a configuration similar to a soft corona).

Carbon dots are generally small carbon nanoparticles with various surface passivation schemes by organic or biomolecules (Figure 1),[4,6,7,12] where the more effective surface passivation has been correlated with brighter fluorescence emissions from the corresponding dots. The optical absorption of carbon dots is assigned to π-plasmon transitions in the carbon nanoparticle core of the dots, while the fluorescence emissions in the visible to near-IR are attributed to photogenerated electrons and holes trapped at diverse surface sites and their associated radiative recombinations.[4,12] Carbon dots also have relatively very large

Received: June 26, 2015
Accepted: August 11, 2015
Published: August 11, 2015

two-photon excitation cross sections in the near-IR (800−900 nm), with the resulting fluorescence emissions reported in the literature comparable roughly to those associated with the regular excitation into the optical absorption spectrum.[5,26−28] Nevertheless, for specimens of carbon dots on a substrate, colocalization experiments in which the same specimen was imaged with both one- and two-photon excitations on the same platform did confirm that the observed fluorescence emissions were associated with the same nanoscale entity.[5] Carbon dots have been found to be highly photochemically stable, without the optical blinking commonly observed in semiconductor QDs.[4] It is now generally acknowledged that carbon dots represent a new class of high-performance one- and two-photon fluorescence imaging agents.

According to results from various cytotoxicity assays, carbon dots in terms of the intrinsic material configuration are nontoxic to cells at concentration levels much higher than those commonly used for fluorescence labeling and imaging purposes.[6,7,29,30] Even at high concentrations, the effect of carbon dots on cells is mostly associated with the surface passivation agents, and interestingly, such agents in carbon dots are less cytotoxic than their free counterparts.[29,30] Therefore, there have been a number of experiments reported in the literature on carbon dots for fluorescence labeling and imaging of cells.[6−11] For example, Cao et al. used PEGylated carbon dots for the fluorescence imaging of human breast cancer MCF-7 cells with one- and two-photon excitations.[5] Zhang et al. prepared carbon dots from polydopamine for cell imaging. At 405 and 458 nm excitations, green and yellow fluorescence emissions, respectively, were observed in the cytoplasm but not in the cell nucleus.[31] Chen et al. prepared carbon dots by carbonizing sucrose with oil acid for imaging 16HBE cells. Green fluorescence emissions were observed around the cell membrane, in addition to the cytoplasm, though only much weaker fluorescence was detected in the cell nucleus.[32] More recently, Yang et al. conjugated hydrothermally synthesized carbon dots with nuclear localization signal (NLS) peptides for the fluorescence imaging of MCF-7 and A549 cells.[33] While some accumulation within the cell nucleus was detected, the majority of the carbon dots were found to be residing in the cytoplasm and cell membrane.[33] However, most of the reported studies might be considered as being exploratory in nature, and more experiments based on carbon dots of more desirable properties (very bright fluorescence emissions, compactness, etc.) are still needed, especially for broader applications to include stem cells and other special cell lines. In the work reported here, we evaluated the specifically selected carbon dots of relatively high fluorescence quantum yields (with respect to one-photon excitation in the visible spectral region) in their labeling of cancer cell lines under one- and two-photon excitation conditions, and we also explored the labeling of stem cells with the carbon dots. For the latter especially, the results concerning the effect of surface functionalities in carbon dots on the cell labeling efficiency are highlighted and discussed.

■ EXPERIMENTAL SECTION

Materials. Carbon nanopowder (<50 nm, purity >99%) and 2,2′-(ethylenedioxy)bis(ethylamine) (EDA) were purchased from Sigma-Aldrich, and bis(3-aminopropyl)-terminated oligomeric poly(ethylene glycol) of average molecular weight ~1500 (PEG_{1500N}) was from Anvia Chemicals. Thionyl chloride (>99%) was obtained from Alfa Aesar, nitric acid from VWR, and Sephadex G-100 gel from GE Healthcare. Dialysis membrane tubing of various cutoff molecular weights was supplied by Spectrum Laboratories. Water was deionized and purified by being passed through a Labconco WaterPros water purification system.

Measurement. Baxter Megafuge (model 2630), Eppendorf (model 5417 R), and Beckman-Coulter ultracentrifuge (Optima L90K with a type 90 Ti fixed-angle rotor) were used for centrifugation at various *g* values. Optical absorption spectra were recorded on a Shimadzu UV2501-PC spectrophotometer. Fluorescence spectra were measured on a Jobin-Yvon emission spectrometer equipped with a 450 W xenon source, Gemini-180 excitation and Tirax-550 emission monochromators, and a photon counting detector (Hamamatsu R928P PMT at 950 V). Fluorescence quantum yields were measured in reference to 9,10-bis(phenylethynyl)-anthracene as a standard (quantum yield of unity, calibrated against the quinine sulfate standard). NMR measurements were performed on a Bruker Avance 500 NMR spectrometer. Transmission electron microscopy (TEM) images were obtained on a Hitachi H9500 TEM system. A Leica laser scanning confocal fluorescence microscope (DM IRE2, with Leica TCS SP2 SE scanning system) equipped with an argon ion laser (JDS Uniphase) and a femtosecond pulsed Ti:sapphire laser (Spectra-Physics Tsunami with a 5 W Millennia pump) was used in the imaging experiments, so was a Zeiss LSM 700 laser scanning microscope. On both microscopes, a plan apochromat 100× oil immersion objective was used. The images were processed and analyzed with the NIH ImageJ software.

Carbon Dots. For carbon nanoparticles as the precursor for carbon dots, an as-supplied carbon nanopowder sample (1 g) was refluxed in an aqueous nitric acid solution (5 M, 90 mL) for 48 h. The reaction mixture was cooled back to ambient temperature and then dialyzed against fresh water for up to 3 days. The postdialysis mixture was centrifuged at 1000*g* to retain the supernatant, followed by the removal of water to obtain the desired carbon nanoparticle sample.

In the synthesis of PEG_{1500N}-carbon dots, the carbon nanoparticle sample obtained from the processing above was refluxed in neat thionyl chloride for 12 h, followed by the removal of excess thionyl chloride under nitrogen. The post-treatment carbon nanoparticle sample (100 mg) was mixed well with carefully dried PEG_{1500N} (1 g) in a flask, heated to 110 °C, and stirred at the constant temperature under nitrogen for 72 h. The reaction mixture was cooled to ambient temperature, dispersed in water, and then centrifuged at 20 000*g* to retain the dark supernatant as an aqueous solution of the as-prepared PEG_{1500N}-carbon dots.

The EDA-carbon dots were synthesized in largely the same experimental procedures as those described above. The post-thionyl chloride treatment carbon nanoparticle sample (50 mg) was mixed well with carefully dried EDA liquid (600 mg) in a round-bottom flask, heated to 120 °C, and vigorously stirred under nitrogen protection for 3 days. The reaction mixture was cooled back to ambient temperature, dispersed in water, and then centrifuged at 20 800*g* to retain the supernatant as an aqueous solution of the as-prepared EDA-carbon dots.

The as-prepared PEG_{1500N}-carbon dots and EDA-carbon dots samples were filtrated through a Sephadex G-100 gel column for fractionation. The gel column was packed in house with commercially supplied gel sample and evaluated according to protocols already reported in the literature.[34] For PEG_{1500N}-carbon dots, more fluorescent fractions eluted from the gel column were collected and combined to have the resulting sample in sufficient quantity and a fluorescence quantum yield of ~40% at 440 nm excitation. For EDA-carbon dots, the colored section on the gel column with high fluorescence quantum yields was collected, followed by dialysis against fresh water (dialysis tubing cutoff molecular weight ~500) to obtain the desired sample, whose ^1H and ^{13}C NMR spectra were similar to those reported previously.[20]

Cells and Imaging. The human breast cancer cell line MCF-7 (ATCC) and human colon adenocarcinoma grade II cell line HT-29 (ATCC) were grown at 37 °C with 5% CO_2 in EMEM medium (ATCC, with nonessential amino-acids, 1 mM sodium pyruvate, 2 mM L-glutamine, and 1.5 g/L sodium bicarbonate) supplemented with 10% (v/v) fetal bovine serum (ATCC) and 1% of penicillin/streptomycin

(Cambrex Bio Science). The cells were plated on a four-chambered Lab-Tek cover-glass system (Nalge Nunc) at 50 000 cells per chamber for 24 h. Separately, the selected carbon dots in aqueous solutions were diluted to the desired concentrations with fresh culture medium and sterilized with a 0.2 μm Acrodisc syringe filter just prior to the cell exposure, and the samples were introduced to the cells. Cells cultured in the free medium were taken as the control. Upon incubation for up to 24 h, the cells were washed three times with PBS (500 μL each time) and kept in PBS for fluorescence imaging. The confocal fluorescence images were obtained with 405 or 458 nm excitation, and the two-photon images were acquired with femtosecond pulsed laser excitation at 800−900 nm.

The SD rat mesenchymal stem cells (MSCs) from passage 2 (OriCell Sprague−Dawley rat MSCs, Cyagen) were expanded in SD rat MSC basal media with 10% fetal bovine serum and 1% v/v penicillin/streptomycin. The MSCs within passage 8 were used in all experiments. For the viability assay, the cells were plated in 96-well plates at an initial density of 1×10^4 cells per well in 200 μL of growth medium for incubation. The EDA-carbon dots were diluted with fresh culture medium to the exposure concentrations, and the solutions were introduced to the cells. The cells cultured in the free medium were taken as the control. Upon the exposure for 24 h, the cell viability was determined by using the Cell Counting Kit-8 (CCK-8, Dojindo Laboratory) assay.

For the labeling, the stem cells were plated on a four-chambered Lab-Tek cover-glass system (Nalge Nunc) at 50 000 cells per chamber for 24 h, followed by their being mixed with the separately prepared carbon dots sample. For the EDA-carbon dots, the sample preparation included the treatment with aqueous HCl for the pH to be neutral before the sample solution was used for labeling the MSCs. In another set of experiments, the MSCs were plated on a four-chambered Lab-Tek cover-glass system for 24 h and fixed by 4% formaldehyde, followed by being mixed with the separately prepared carbon dots sample. Upon incubation for up to 24 h, the live or fixed cells were washed carefully with PBS for a complete removal of unattached carbon dots, and the cells postwashing were kept in PBS for the imaging experiments. The confocal fluorescence images were obtained with 405 nm excitation. For a more quantitative comparison of the signal intensities in the images, the as-acquired color fluorescence images were converted to the grayscale by using the ImageJ software (NIH). The images were then mapped digitally for a determination of the corresponding fluorescence intensities.

■ RESULTS AND DISCUSSION

The $\mathrm{PEG}_{1500\mathrm{N}}$-carbon dots and EDA-carbon dots were synthesized as reported previously.[19,20,34] The as-synthesized samples were separated on an aqueous Sephadex G-100 gel column, from which more fluorescent fractions were collected. Shown in Figure 2 are absorption and fluorescence spectra of the $\mathrm{PEG}_{1500\mathrm{N}}$-carbon dots and EDA-carbon dots that were used in cell imaging experiments, with the fluorescence quantum yields of the two samples at 440 nm excitation of ~40% and ~30%, respectively. These carbon dots are generally small in size, as confirmed by results from microscopy analyses (Figure 3),[20,34] especially so for the EDA-carbon dots characterized as being "ultracompact" due to the much shorter PEG chain in EDA than that in $\mathrm{PEG}_{1500\mathrm{N}}$.[20]

The carbon dots in aqueous solution were progressively diluted for being deposited onto a substrate (glass slide) to have them individually dispersed for fluorescence imaging under single-dot conditions. The fluorescence of the specimen could readily be detected under a confocal microscope, with the observed images confirming the desired dispersion of the carbon dots (Figure 4).

The specimens of $\mathrm{PEG}_{1500\mathrm{N}}$-carbon dots were also imaged with two-photon excitation at 800 nm, in which fluorescence emissions were readily detected, again confirming the desired dispersion of carbon dots on the substrate (Figure 5). The fluorescence spectra corresponding to the individualized dot images were collected on the microscope for comparison with the solution-phase spectra of the carbon dots measured on a conventional emission spectrometer at corresponding excitation wavelengths (800 nm two-photon vs 400 nm one-photon). The results suggested that the spectra were comparable qualitatively (Figure 5), reflecting not only their likelihood of being from the same emissive excited states but also the comparability between the fluorescence properties of the carbon dots in solution and when dispersed on a substrate under single-dot conditions.

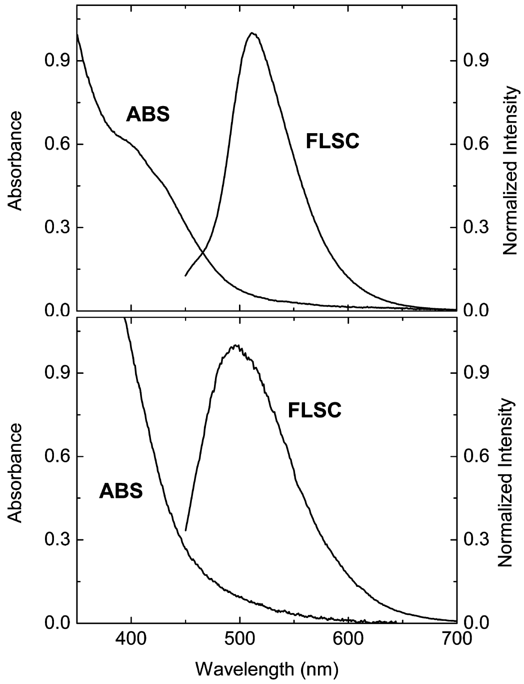

Figure 2. Absorption (ABS) and fluorescence (FLSC, 440 nm excitation) spectra of the $\mathrm{PEG}_{1500\mathrm{N}}$-carbon dots (top) and EDA-carbon dots (bottom) in aqueous solutions.

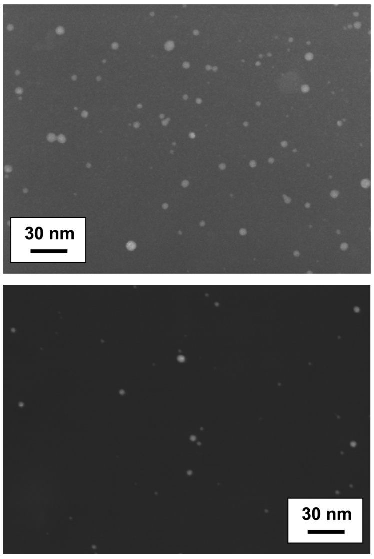

Figure 3. TEM images of the $\mathrm{PEG}_{1500\mathrm{N}}$-carbon dots (top) and EDA-carbon dots (bottom).

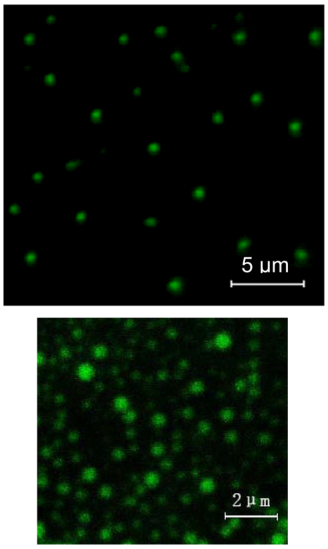

Figure 4. Confocal fluorescence images of the PEG$_{1500N}$-carbon dots (top) and EDA-carbon dots (bottom) well-dispersed on a glass substrate.

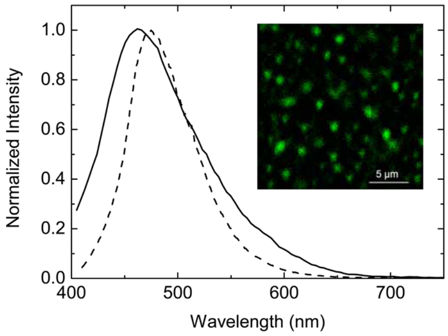

Figure 5. Comparison of the fluorescence spectrum (two-photon excitation at 800 nm) of an individually dispersed PEG$_{1500N}$-carbon dot on a glass substrate (solid line) with that (regular fluorescence spectrometer at 400 nm excitation) of the corresponding dots in aqueous solution (dashed line). Inset: Two-photon fluorescence images (800 nm excitation) of the PEG$_{1500N}$-carbon dots.

The results highlighted above for the PEG$_{1500N}$-carbon dots and EDA-carbon dots of relatively high fluorescence quantum yields suggest that these are well-behaved fluorescence probes in the visible spectral region for both one- and two-photon excitations. These probes are generally stable in their optical absorption and fluorescence properties in various aqueous buffers, amenable to cell labeling and imaging applications.

The human breast cancer MCF-7 and human colon adenocarcinoma HT-29 cells were selected for the labeling by the PEG$_{1500N}$-carbon dots. Both MCF-7 and HT-29 cells were cultured by following established protocols.[29,30] For the cell imaging experiments, the cells were incubated with the PEG$_{1500N}$-carbon dots in an aqueous buffer at 37 °C for up to 24 h and then washed to remove carbon dots that were not associated with the cells. Since the dot concentrations were significantly lower than those that could cause cell damage,[30] the cells were close to completely viable under the experimental conditions.

For both cell lines, the fluorescence images acquired with 458 nm excitation (argon ion laser line) suggested significant uptake of the carbon dots by the cells, with the dots mostly residing in the cell membrane and cytoplasm and without any meaningful presence in the cell nucleus (Figure 6). There were no major differences between the two cell lines in terms of their fluorescence labeling by the carbon dots. The contrast between the emissive carbon dots and the background (somewhat fluorescent in general) was very good, due likely to the high fluorescence quantum yields of the carbon dots used for the cell labeling. For an estimate of the fluorescence brightness in the labeled cells, while using an established standard as intensity reference was rather difficult in our setup and therefore not pursued, qualitatively the brightness in the fluorescence images of the cells was comparable with that in the images of the carbon dots without cells. It suggests that the fluorescence properties of the carbon dots were not degraded in any significant fashion upon their being taken up by the cells. In fact, there is experimental evidence from unrelated studies on the carbon dots in polymer films indicating enhanced fluorescence intensities for the dots in a more confined environment. The possibility for similar effects on carbon dots in various cellular domains will be evaluated in further investigations.

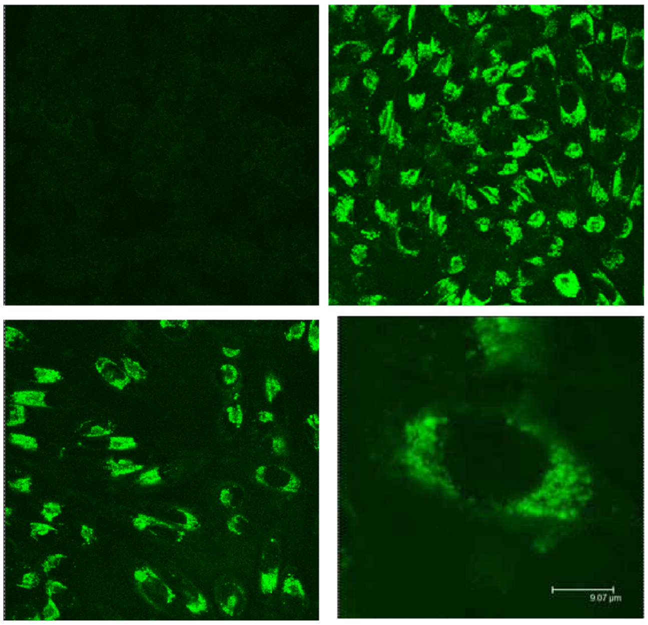

Figure 6. Confocal fluorescence images (458 nm excitation, 470−590 nm emissions) for MCF-7 cells without (top left) and with the PEG$_{1500N}$-carbon dots (top right) and for HT-29 cells with the PEG$_{1500N}$-carbon dots at different resolutions (bottom left and right).

The same cells labeled with the PEG$_{1500N}$-carbon dots were imaged by using the fluorescence microscope with two-photon excitation (femtosecond pulsed laser at 800−900 nm) under otherwise the same experimental conditions. Green fluorescence emissions from the PEG$_{1500N}$-carbon dots in both cell lines could readily be detected, with the results again suggesting that the dots resided mostly in the cell membrane and cytoplasm and no major differences between the two cell lines (Figure 7). Two-photon fluorescence imaging has been widely acknowledged as being particularly advantageous in terms of minimizing background fluorescence interferences, though in this case the advantage was not so obvious. The imaging contrast appeared not so different from that found in one-photon (regular confocal, Figure 6) experiments, as both were

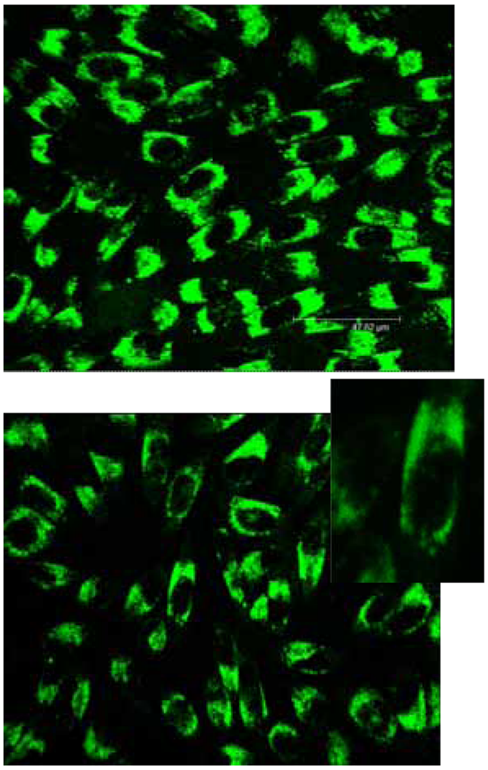

Figure 7. Fluorescence images with two-photon excitation (800 nm excitation, 470−590 nm emissions) for MCF-7 (top) and HT-29 (bottom, and the inset) cells, both labeled with the PEG_{1500N}-carbon dots.

relatively high, again due likely to the high fluorescence quantum yields of the carbon dots used for the cell labeling. There was more experimental evidence supporting the dependence of labeling and imaging outcomes on the quality of the carbon dots. For example, when another PEG_{1500N}-carbon dots sample of a lower fluorescence quantum yield (∼6% at 440 nm excitation, a fraction from the aqueous gel column separation of the as-synthesized sample) was used for labeling the same cells under otherwise the same experimental conditions, the fluorescence intensities in the resulting images were obviously lower, as expected.

In the fluorescence labeling of cells with the carbon dots, the efficiency as reflected by the brightness and contrast in the images obtained with one- and two-photon excitations was clearly dependent on incubation conditions, especially the length of time in which the cells were exposed to the carbon dots. Under otherwise the same experimental conditions, the longer incubation time (24 h vs 6 h, for example) resulted in more effective fluorescence labeling of the cells, corresponding to significantly brighter and higher-contrast images of the resulting cell specimens. The cellular uptake of the carbon dots was essentially absent when the incubation was at low temperature (4 °C), as reported previously.[5]

Beyond the human cancer cells, the carbon dots were also explored for their labeling of mesenchymal stem cells (MSCs). As a justification, stem cells are widely considered as holding the promise for a variety of *in vivo* tracking applications. Fluorescence probes are in demand for labeling stem cells[35] due to some advantageous attributes over those of other labels, such as magnetic and Raman probes.[36−38] In addition to the high sensitivity associated with bright fluorescence emissions in the probes for stem cells, these probes are also required to minimally affect the subcellular structure and have no or little toxic effect.[39,40] For conventional semiconductor QDs as fluorescence probes, it was found that those functionalized with long ligands were more cytotoxic than those with short ligands.[41] The EDA-carbon dots in this work were developed specifically as bright fluorescence probes of an ultracompact configuration for related purposes,[20] and they were used in the labeling of MSCs.

Experimentally, the SD rat MSCs within passage 8 were used in the cell labeling experiments with the EDA-carbon dots. The results from the cell viability assay suggested that the stem cells were completely viable upon being exposed to the EDA-carbon dots at concentrations much higher than those used in the fluorescence labeling under otherwise the same experimental conditions. In the labeling evaluation, postexposure of the stem cells to the separately prepared EDA-carbon dots, the cells were imaged under a confocal fluorescence microscope with 405 nm excitation. The fluorescence images thus obtained confirmed the labeling of the stem cells by the carbon dots (Figure 8), suggesting that the dots in the live cells were again mostly in the cell membrane and cytoplasm, not in the nucleus, similar in general to the cellular distribution of the other PEGylated carbon dots in human cancer cells MCF-7 and HT-29 described above. However, the labeling efficiency for the stem cells by the EDA-carbon dots was significantly lower, as reflected in the low cellular uptake of the carbon dots and

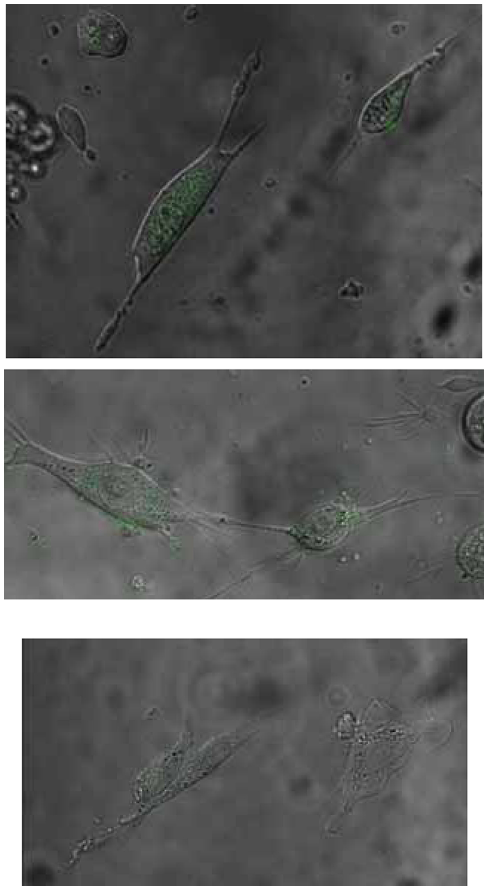

Figure 8. Merged (fluorescence + bright-field) images of the live stem cells labeled with the EDA-carbon dots (top and middle) and the control (without the dots, bottom).

weaker fluorescence emissions in the images. One possible cause might be related to the chemical structures of EDA-carbon dots, which are rather basic (pH ~ 13) due to a relatively large population of amino groups on the dot surface (Figure 1). Consequently, aqueous EDA-carbon dots sample had to be neutralized with an acid (aqueous HCl) before the stem cell labeling. The acid treatment protonated the amino groups to result in a similarly large population of cationic moieties on the dot surface, which were probably not favorable to the desired efficient uptake by the live cells. In a follow-up exploration on this issue, the MSCs were fixed by the treatment with 4% formaldehyde. The labeling of the fixed MSCs by the EDA-carbon dots was much more efficient, corresponding to much brighter fluorescence images and with the hyperchromatic nucleolus brighter than the other regions (Figure 9). Here, a quantification of the fluorescence brightness was accomplished by converting the as-acquired color images into the grayscale (NIH ImageJ software), followed by mapping the resulting images digitally to determine the spatially resolved fluorescence intensities.

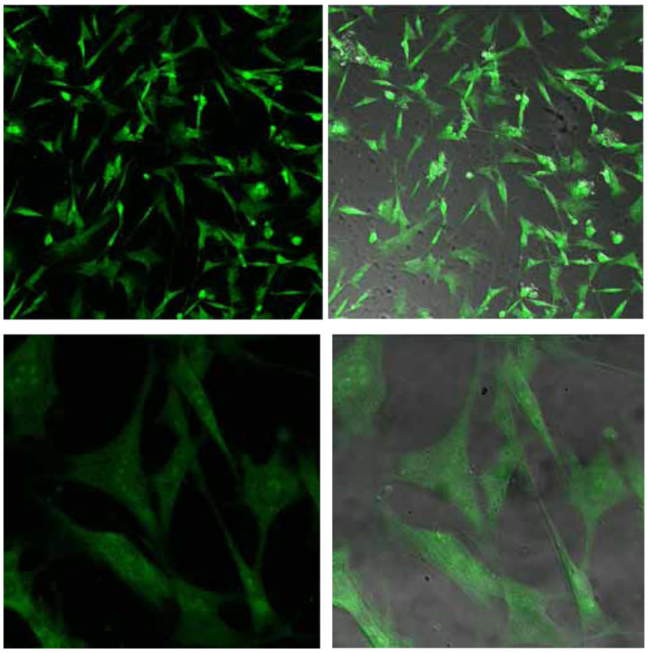

Figure 9. Fluorescence (left) and merged (fluorescence + bright-field, right) images of the fixed stem cells labeled with the EDA-carbon dots.

The results described above suggested that the live MSCs could be labeled by the EDA-carbon dots, but the labeling efficiency was relatively low, insufficient for being used in following the cell divisions (such as in the 20 day cell division or differentiation culture). Further investigations with the design and synthesis of brightly fluorescent and compact carbon dots of surface functionalities more favorable to the uptake by live stem cells will be pursued. Also, a comparison between stem cells and commonly studied cancer cell lines (those used in this study and others such as Hela cells) with respect to carbon dots of the same surface functionalities will be investigated. It seems that stem cells are more "picky" about surface functionalities when taking up the carbon dots, as cancer and other cell lines often used in the literature on carbon dots have not exhibited in general the kind of issues with a high population of amino moieties on the dot surface affecting cellular uptake. This presents both challenges and opportunities in the use of carbon dots as a new class of fluorescence probes for the labeling of stem cells, with the latter enabling potentially the exploitation of selectivity in the uptake of the probes by stem cells vs other cell lines.

■ CONCLUSION

The carbon dots of bright fluorescence emissions can be synthesized in a relatively facile fashion, and they can be imaged down to the individual dot level on a substrate by using both one- and two-photon excitations. The uptake of the carbon dots by cancer cells is generally efficient, resulting in the labeling of the cells with bright fluorescence from predominantly the cell membrane and cytoplasm, again with both one- and two-photon excitations. In the use of the ultracompact EDA-carbon dots for labeling live stem cells, the cellular uptake is relatively less efficient, though the fluorescence emissions can still be adequately detected and they are again predominantly from the cell membrane and cytoplasm. This combined with the observed more efficient internalization of the same carbon dots by the fixed stem cells may suggest selectivity of the live stem cells toward the dot surface functionalities. More systematic and comparative studies on the fluorescence labeling of different cell lines by carbon dots, including more specific design and synthesis of carbon dots that are more suitable for the labeling of stem cells, are needed and will be pursued.

■ AUTHOR INFORMATION

Corresponding Author

*E-mail: syaping@clemson.edu.

Author Contributions

$^{\#}$J.-H.L. and L.C. contributed equally.

Notes

The authors declare no competing financial interest.

■ ACKNOWLEDGMENTS

J.-H.L. acknowledges financial support by China Natural Science Foundation (No. 21301015), and Y.-P.S. acknowledges support from NIH and NSF. L.C. was funded by a *Susan G. Komen for the Cure* Postdoctoral Fellowship, and M.J.M. was on leave from Department of Chemistry and Physics, Northwest Missouri State University with support provided by the South Carolina Space Grant Consortium.

■ REFERENCES

(1) Kairdolf, B. A.; Smith, A. M.; Stokes, T. H.; Wang, M. D.; Young, A. N.; Nie, S. Semiconductor Quantum Dots for Bioimaging and Biodiagnostic Applications. *Annu. Rev. Anal. Chem.* **2013**, *6*, 143−162.

(2) Freeman, R.; Willner, I. Optical Molecular Sensing with Semiconductor Quantum Dots (QDs). *Chem. Soc. Rev.* **2012**, *41*, 4067−4085.

(3) Medintz, I. L.; Uyeda, H. T.; Goldman, E. R.; Mattoussi, H. Quantum Dot Bioconjugates for Imaging, Labelling and Sensing. *Nat. Mater.* **2005**, *4*, 435−546.

(4) Sun, Y.-P.; Zhou, B.; Lin, Y.; Wang, W.; Fernando, K. A. S.; Pathak, P.; Meziani, M. J.; Harruff, B. A.; Wang, X.; Wang, H.; Luo, P. G.; Yang, H.; Kose, M. E.; Chen, B.; Veca, M.; Xie, S. Y. Quantum-Sized Carbon Dots for Bright and Colorful Photoluminescence. *J. Am. Chem. Soc.* **2006**, *128*, 7756−7757.

(5) Cao, L.; Wang, X.; Meziani, M. J.; Lu, F.; Wang, H.; Luo, P. G.; Lin, Y.; Harruff, B. A.; Veca, L. M.; Murray, D.; Xie, S. Y.; Sun, Y.-P. Carbon Dots for Multiphoton Bioimaging. *J. Am. Chem. Soc.* **2007**, *129*, 11318−11319.

(6) Luo, P. G.; Sahu, S.; Yang, S.-T.; Sonkar, S. K.; Wang, J.; Wang, H.; LeCroy, G. E.; Cao, L.; Sun, Y.-P. Carbon "Quantum" Dots for Optical Bioimaging. *J. Mater. Chem. B* **2013**, *1*, 2116–2127.

(7) Luo, P. G.; Sonkar, S. K.; Yang, S.-T.; Yang, F.; Yang, L.; Broglie, J. J.; Liu, Y.; Sun, Y.-P. Carbon-Based Quantum Dots for Fluorescence Imaging of Cells and Tissues. *RSC Adv.* **2014**, *4*, 10791–10807.

(8) Wang, Y.; Hu, A. Carbon Quantum Dots: Synthesis, Properties and Applications. *J. Mater. Chem. C* **2014**, *2*, 6921–6939.

(9) Lim, S. Y.; Shen, W.; Gao, Z. Carbon Quantum Dots and Their Applications. *Chem. Soc. Rev.* **2015**, *44*, 362–381.

(10) Miao, P.; Han, K.; Tang, Y.; Wang, B.; Lin, T.; Cheng, W. Recent Advances in Carbon Nanodots: Synthesis, Properties and Biomedical Applications. *Nanoscale* **2015**, *7*, 1586–1595.

(11) Zhao, A.; Chen, Z.; Zhao, C.; Gao, N.; Ren, J.; Qu, X. Recent Advances in Bioapplications of C-dots. *Carbon* **2015**, *85*, 309–327.

(12) Cao, L.; Meziani, M. J.; Sahu, S.; Sun, Y.-P. Photoluminescence Properties of Graphene versus Other Carbon Nanomaterials. *Acc. Chem. Res.* **2013**, *46*, 171–180.

(13) Hola, K.; Zhang, Y.; Wang, Y.; Giannelis, E. P.; Zboril, R.; Rogach, A. L. Carbon Dots-Emerging Light Emitters for Bioimaging, Cancer Therapy and Optoelectronics. *Nano Today* **2014**, *9*, 590–603.

(14) Yang, S.-T.; Cao, L.; Luo, P. G.; Lu, F.; Wang, X.; Wang, H.; Meziani, M. J.; Liu, Y.; Qi, G.; Sun, Y.-P. Carbon Dots for Optical Imaging in Vivo. *J. Am. Chem. Soc.* **2009**, *131*, 11308–11309.

(15) Zhang, J.; Shen, W.; Pan, D.; Zhang, Z.; Fang, Y.; Wu, M. Controlled Synthesis of Green and Blue Luminescent Carbon Nanoparticles with High Yields by the Carbonization of Sucrose. *New J. Chem.* **2010**, *34*, 591–593.

(16) Anilkumar, P.; Wang, X.; Cao, L.; Sahu, S.; Liu, J.-H.; Wang, P.; Korch, K.; Tackett, K. N.; Parenzan, A.; Sun, Y.-P. Toward Quantitatively Fluorescent Carbon-Based "Quantum" Dots. *Nanoscale* **2011**, *3*, 2023–2027.

(17) Wang, F.; Xie, Z.; Zhang, H.; Liu, C. Y.; Zhang, Y. G. Highly Luminescent Organosilane-Functionalized Carbon Dots. *Adv. Funct. Mater.* **2011**, *21*, 1027–1031.

(18) Cao, L.; Yang, S.-T.; Wang, X.; Luo, P. G.; Liu, J.-H.; Sahu, S.; Liu, Y.; Sun, Y.-P. Competitive Performance of Carbon "Quantum" Dots in Optical Bioimaging. *Theranostics* **2012**, *2*, 295–301.

(19) Anilkumar, P.; Cao, L.; Yu, J. J.; Tackett, K. N.; Wang, P.; Meziani, M. J.; Sun, Y.-P. Crosslinked Carbon Dots as Ultra-Bright Fluorescence Probes. *Small* **2013**, *9*, 545–551.

(20) LeCroy, G. E.; Sonkar, S. K.; Yang, F.; Veca, L. M.; Wang, P.; Tackett, K. N.; Yu, J. J.; Vasile, E.; Qian, H. J.; Liu, Y. M.; Luo, P.; Sun, Y.-P. Toward Structurally Defined Carbon Dots as Ultracompact Fluorescent Probes. *ACS Nano* **2014**, *8*, 4522–4529.

(21) Ding, C.; Zhu, A.; Tian, Y. Functional Surface Engineering of C-Dots for Fluorescent Biosensing and in Vivo Bioimaging. *Acc. Chem. Res.* **2014**, *47*, 20–30.

(22) Lemenager, G.; de Luca, E.; Sun, Y.-P.; Pompa, P. P. Super-Resolution Fluorescence Imaging of Biocompatible Carbon Dots. *Nanoscale* **2014**, *6*, 8617–8626.

(23) Weng, C. I.; Chang, H. T.; Lin, C. H.; Shen, Y. W.; Unnikrishnan, B.; Li, Y. J.; Huang, C. C. One-Step Synthesis of Biofunctional Carbon Quantum Dots for Bacterial Labeling. *Biosens. Bioelectron.* **2015**, *68*, 1–6.

(24) Bao, L.; Liu, C.; Zhang, Z. L.; Pang, D. W. Photoluminescence-Tunable Carbon Nanodots: Surface-State Energy-Gap Tuning. *Adv. Mater.* **2015**, *27*, 1663–1667.

(25) Pei, S.; Zhang, J.; Gao, M.; Wu, D.; Yang, Y.; Liu, R. A Facial Hydrothermal Approach towards Photoluminescent Carbon Dots from Amino Acids. *J. Colloid Interface Sci.* **2015**, *439*, 129–133.

(26) Kong, B.; Zhu, A.; Ding, C.; Zhao, X.; Li, B.; Tian, Y. Carbon Dot-Based Inorganic-Organic Nanosystem for Two-Photon Imaging and Biosensing of pH Variation in Living Cells and Tissues. *Adv. Mater.* **2012**, *24*, 5844–5848.

(27) Zhu, A.; Luo, Z.; Ding, C.; Li, B.; Zhou, S.; Wang, R.; Tian, Y. A Two-Photon ″Turn-on″ Fluorescent Probe Based on Carbon Nanodots for Imaging and Selective Biosensing of Hydrogen Sulfide in Live Cells and Tissues. *Analyst* **2014**, *139*, 1945–1952.

(28) Tong, G.; Wang, J.; Wang, R.; Guo, X.; He, L.; Qiu, F.; Wang, G.; Zhu, B.; Zhu, X.; Liu, T. Amorphous Carbon Dots with High Two-Photon Fluorescence for Cellular Imaging Passivated by Hyper-branched Poly(amino amine). *J. Mater. Chem. B* **2015**, *3*, 700–706.

(29) Yang, S.-T.; Wang, X.; Wang, H.; Lu, F.; Luo, P. G.; Cao, L.; Meziani, M. J.; Liu, J.-H.; Liu, Y.; Chen, M.; Huang, Y.; Sun, Y.-P. Carbon Dots as Nontoxic and High-Performance Fluorescence Imaging Agents. *J. Phys. Chem. C* **2009**, *113*, 18110–18114.

(30) Wang, Y.; Anilkumar, P.; Cao, L.; Liu, J.-H.; Luo, P. G.; Tackett, K. N.; Sahu, S.; Wang, P.; Wang, X.; Sun, Y.-P. Carbon Dots of Different Composition and Surface Functionalization - Cytotoxicity Issues Relevant to Fluorescence Imaging of Cells. *Exp. Biol. Med. (London, U. K.)* **2011**, *236*, 1231–1238.

(31) Zhang, X.; Wang, S.; Xu, L.; Ji, Y.; Feng, L.; Tao, L.; Li, S.; Wei, Y. Biocompatible Polydopamine Fluorescent Organic Nanoparticles: Facile Preparation and Cell Imaging. *Nanoscale* **2012**, *4*, 5581–5584.

(32) Chen, B.; Li, F.; Li, S.; Weng, W.; Guo, H.; Guo, T.; Zhang, H.; Chen, Y.; Huang, T.; Hong, X.; You, S.; Lin, Y.; Zeng, K.; Chen, S. Large Scale Synthesis of Photoluminescent Carbon Nanodots and Their Application for Bioimaging. *Nanoscale* **2013**, *5*, 1967–1971.

(33) Yang, L.; Jiang, W.; Qiu, L.; Jiang, X.; Zuo, D.; Wang, D.; Yang, L. One Pot Synthesis of Highly Luminescent Polyethylene Glycol Anchored Carbon Dots Functionalized with a Nuclear Localization Signal Peptide for Cell Nucleus Imaging. *Nanoscale* **2015**, *7*, 6104–6113.

(34) Wang, X.; Cao, L.; Yang, S.-T.; Lu, F.; Meziani, M. J.; Tian, L.; Sun, K. W.; Bloodgood, M. A.; Sun, Y.-P. Bandgap-Like Strong Fluorescent in Functionalized Carbon Nanoparticles. *Angew. Chem., Int. Ed.* **2010**, *49*, 5310–5314.

(35) Zhang, M.; Bai, L.; Shang, W.; Xie, W.; Ma, H.; Fu, Y.; Fang, D.; Sun, H.; Fan, L.; Han, M.; Liu, C.; Yang, S. Paper Facile Synthesis of Water-Soluble, Highly Fluorescent Graphene Quantum Dots as a Robust Biological Label for Stem Cells. *J. Mater. Chem.* **2012**, *22*, 7461–7467.

(36) Michalet, X.; Pinaud, F. F.; Bentolila, L. A.; Tsay, J. M.; Doose, S.; Li, J. J.; Sundaresan, G.; Wu, A. M.; Gambhir, S. S.; Weiss, S. Quantum Dots for Live Cells, in Vivo Imaging, and Diagnostics. *Science* **2005**, *307*, 538–544.

(37) Zhang, S. J.; Wu, J. C. Comparison of Different Imaging Techniques for Tracking Cardiac Stem Cell Therapy. *J. Nucl. Med.* **2007**, *48*, 1916–1919.

(38) Wang, Y.; Xu, C. J.; Ow, H. W. Commercial Nanoparticles for Stem Cell Labeling and Tracking. *Theranostics* **2013**, *3*, 544–560.

(39) Liang, C.; Wang, C.; Liu, Z. Stem Cell Labeling and Tracking with Nanoparticles. *Part. Part. Syst. Charact.* **2013**, *30*, 1006–1017.

(40) Shang, W. H.; Zhang, X. Y.; Zhang, M.; Fan, Z.; Sun, Y.; Han, M.; Fan, L. Z. The Uptake Mechanism and Biocompatibility of Graphene Quantum Dots with Human Neural Stem Cells. *Nanoscale* **2014**, *6*, 5799–5806.

(41) Nagy, A.; Steinbruck, A.; Gao, J.; Doggett, N.; Hollingsworth, J. A.; Iyer, R. Comprehensive Analysis of the Effects of CdSe Quantum Dot Size, Surface Charge, and Functionalization on Primary Human Lung Cells. *ACS Nano* **2012**, *6*, 4748–4762.

SCIENTIFIC REPORTS

OPEN

Host-Guest Carbon Dots for Enhanced Optical Properties and Beyond

Received: 10 March 2015
Accepted: 26 June 2015
Published: 21 July 2015

Ya-Ping Sun, Ping Wang, Zhuomin Lu, Fan Yang, Mohammed J. Meziani, Gregory E. LeCroy, Yun Liu & Haijun Qian

Carbon dots, generally small carbon nanoparticles with various forms of surface passivation, have achieved the performance level of semiconductor quantum dots in the green spectral region, but their absorption and fluorescence in red/near-IR are relatively weaker. Conceptually similar to endofullerenes, host-guest carbon dots were designed and prepared with red/near-IR dyes encapsulated as guest in the carbon nanoparticle core. Beyond the desired enhancement in optical properties, the host-guest configuration may significantly broaden the field of carbon dots.

Carbon dots (also called carbon quantum dots in some literature reports despite the absence of classically defined quantum confinement) have emerged as a new class of photoactive nanomaterials[1–4], with their fluorescence properties resembling those typically found in conventional semiconductor nanocrystals or quantum dots (QDs)[5]. The structure of a carbon dot is relatively simple, generally a small carbon nanoparticle with various forms of surface passivation, among which the more effective has been the chemical functionalization with organic or polymeric species (Fig. 1) for carbon dots of bright fluorescence emissions[4]. In the green over the spectral region covered by green fluorescent protein (GFP), for example, the performance of existing carbon dots in terms of fluorescence quantum yields in solution or the image brightness at the individual dot level on a substrate has been found to be competitive to that of the presently dominating CdSe/ZnS QDs[6]. According to available experimental results, carbon dots are nontoxic[2–4,7], certainly without the toxicity concerns associated with the heavy metal-containing semiconductor QDs. Therefore, there has been a growing interest in potential applications of carbon dots for fluorescence bioimaging *in vitro* and *in vivo*[2–4,7–12]. However, despite the extensive effort in the relevant research community, the development of carbon dots of high fluorescence quantum yields in the biologically more significant near-IR spectral region has found only limited success. This, combined with the generally lower absorptivity of carbon nanoparticles in the red/near-IR, suggests that new strategies are necessary in order to use the carbon dots platform for fluorescence probes of the desired red/near-IR performance.

In the work reported here we "borrowed" the concept from the field of endofullerenes[13] by considering the core carbon nanoparticle in a carbon dot as a "solid-state pool" (*versus* the cavity in a fullerene) to trap or encapsulate chromophoric species of strong red/near-IR absorption and emissions. This host-guest configuration takes advantage of the small carbon nanoparticle as host being optically largely transparent in the corresponding spectral regions, which has actually been identified above as a shortcoming of currently available carbon dots in their serving as red/near-IR probes. The resulting host-guest carbon dots, denoted as G@CDots (Fig. 1), exhibited the desired absorption and fluorescence properties, as designed and expected.

Department of Chemistry and Laboratory for Emerging Materials and Technology, Clemson University, Clemson, South Carolina 29634-0973, USA. Correspondence and requests for materials should be addressed to Y.-P.S. (email: syaping@clemson.edu)

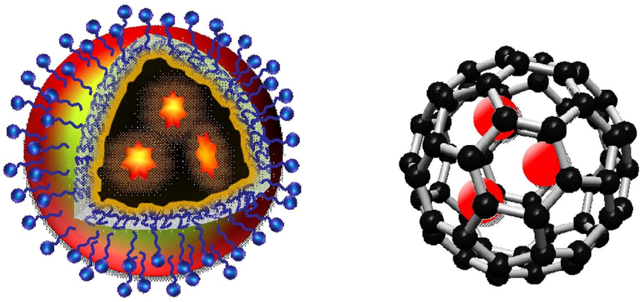

Figure 1. A carbon dot with encapsulated species (host-guest carbon dot, left) *verses* an endofullerene (right).

Results and Discussion

The thermal carbonization of organic precursors has been a popular approach for the synthesis of carbon dots[2–4], in which a portion of the precursor organic species is converted into carbon nanoparticles and the remaining serves the function of surface passivation agents. Among various thermal processing options is the use of microwave irradiation[14–21], which in principle creates carbonized seeds for their preferential absorption of the subsequent microwave energy towards the formation of the targeted carbon dot structure of a carbon nanoparticle with organic species on the surface for passivation. The microwave processing was adopted in this work for the "one-pot" synthesis of the G@CDots, with G denoting the selected fluorescent dyes of cresyl violet (CV), nile blue (NB), and zinc phthalocyanine (ZnPc).

Experimentally for the synthesis of CV@CDots, CV (20 mg) in an ethanol solution was mixed well with oligomeric polyethylene glycol of molecular weight ~900 (PEG_{900}, 2 g), followed by the removal of ethanol via purging with nitrogen gas. The resulting mixture was placed in a commercial microwave oven and irradiated at 300 W for 20 min. Then, water was added to the reaction mixture with sonication to obtain a dark colored aqueous solution. The solution was centrifuged at 20,000 *g*, from which only a negligible amount of precipitate was observed and discarded. The supernatant was dialyzed in a membrane tubing (cutoff molecular weight ~1,000) against fresh water to remove unreacted starting materials and other small molecular species, yielding CV@CDots in an aqueous solution. The same processing protocol was applied to the preparation of NB@CDots and ZnPc@CDots, except that for the latter a 1:1 mixture of PEG_{900} and oligomeric polypropionylethyleneimine instead of neat PEG_{900} was in the mixture with ZnPc for microwave irradiation. The sample solutions were used for optical spectroscopy measurements and microscopy characterization.

For all three host-guest carbon dots, the absorption spectra in aqueous solutions exhibited contributions from carbon nanoparticles (more significantly in the blue/green spectral region, comparable with the absorption of carbon dots from the carbonization of PEG_{900} without the dye encapsulation, Fig. 2) and the guest dye molecules (Figs 2 and 3). However, the absorption bands of the encapsulated dyes are somewhat different from those of their corresponding free molecules, likely reflecting effects of the different environment in the hosting carbon nanoparticles. For example, the absorption of the CV in CV@CDots is much broader in comparison with that of the free dye molecules, both in aqueous solutions (Fig. 2). Similar encapsulation effects were observed in fluorescence spectra of the host-guest carbon dots. The spectra were found to be excitation wavelength dependent, as shown in Fig. 2 for example, which might be as expected considering the solid-like environment around the guest dye molecules in the hosting carbon nanoparticles (namely the molecules are each in a slightly different surrounding in a "solid-state solution", a classical case for excitation wavelength dependent fluorescence emissions). Similarly for ZnPc@CDots in aqueous solution excited at its absorption peak, the fluorescence band is broader and red-shifted from that of the free ZnPc molecules (Fig. 3).

The aqueous solutions of the host-guest carbon dots were diluted for the preparation of specimens on mica substrate for atomic force microscopy (AFM) characterization. Shown in Fig. 4 are the results for CV@CDots, NB@CDots, and ZnPc@CDots. According to image height analyses, these host-guest carbon dots synthesized from thermal carbonization reactions are not as uniform in size as those from the surface chemical functionalization of pre-processed carbon nanoparticles reported previously[6,22], though still relatively narrowly distributed. Most of these host-guest carbon dots are small, with their overall size profiles on the order of 10 nm or less (Fig. 4).

The carbon nanoparticle cores in the host-guest carbon dots are likely somewhat smaller than the overall dot profiles estimated from the height analysis of AFM images, as the latter may also include contributions of the organic species on carbon particle surface that survived the thermal carbonization processing. The expected significant contrast between the carbon core and surface organic species was exploited in the probing of the carbon nanoparticles by using transmission electron microscopy (TEM). For NB@CDots as an example, the TEM specimen was prepared such that a few drops of a dilute sample solution were deposited onto a silicon oxide-coated copper grid, followed by careful evaporation of the solvent. The imaging experiments were performed on a high-resolution TEM instrument (Hitachi

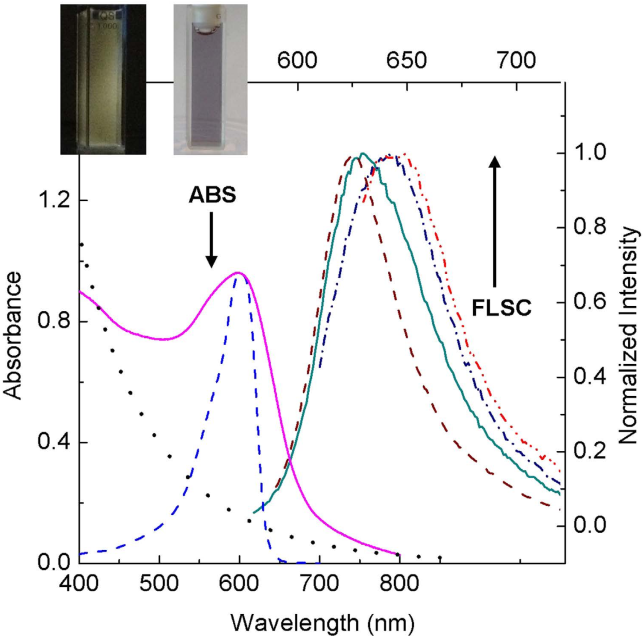

Figure 2. The absorption (ABS) spectrum of CV@CDots (—) and corresponding fluorescence (FLSC) spectra (excitation at 570 nm: —, 600 nm: -.-, and 620 nm: -..-) in aqueous solution. The spectra of free CV (- - -) and carbon dots from the carbonization of PEG$_{900}$ without any encapsulation (…) in aqueous solutions are also shown for comparison. Inset: Photographs of an aqueous solution of the sample under UV light in the dark (left) and under natural day light (right).

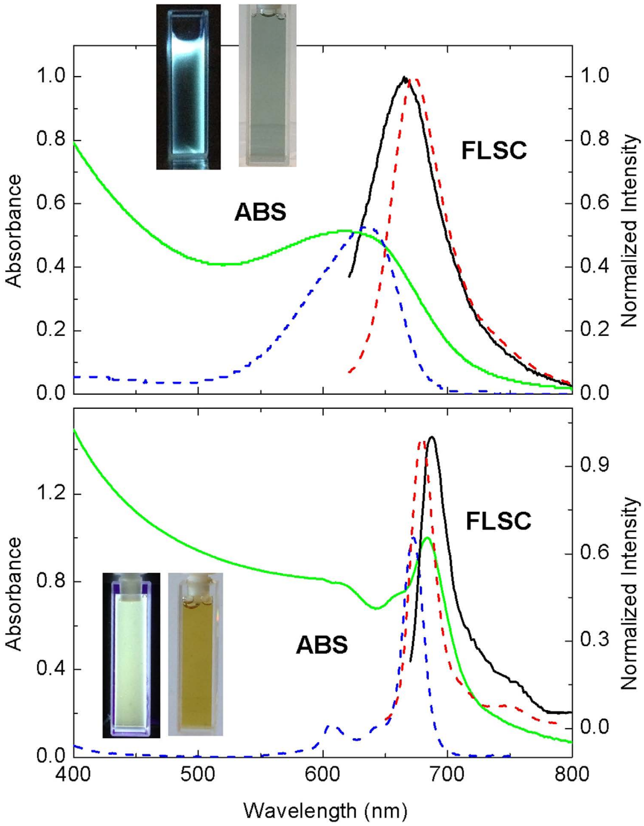

Figure 3. Absorption (ABS) and fluorescence (FLSC) spectra of NB@CDots (top, —) and ZnPc@CDots (bottom, —) and the corresponding free dyes (- - -) in aqueous solutions (except for free ZnPc in DMSO). Insets: Photographs of aqueous solutions of the corresponding samples under UV in the dark (left) and under natural day light (right).

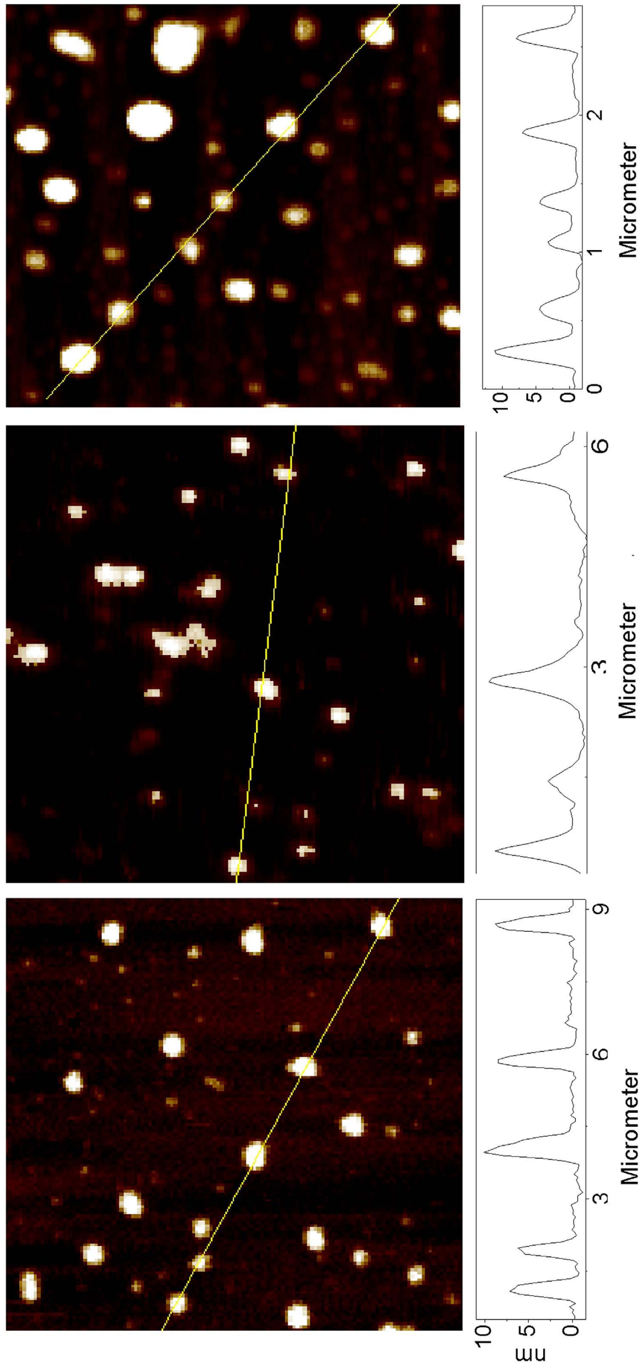

Figure 4. AFM images of CV@CDots (top), NB@CDots (middle), and ZnPc@CDots (bottom).

H-9500). The results shown in Fig. 5 suggest that the NB-encapsulated carbon dots with residual PEG molecules as surface passivation moieties (confirmed by the significant PEG carbon peaks in ^{13}C NMR analyses) are well-dispersed and that the carbon nanoparticle cores are size-wise small and relatively narrowly distributed.

For the host-guest carbon dots in aqueous solutions, the fluorescence quantum yields of the encapsulated dyes were evaluated against those of their free counterparts. Mechanistically, the observed fluorescence emissions from the guest dyes were due to their intrinsic electronic transition properties, not induced by the host carbon dots. However, the carbon pool environment in the hosting carbon dots could have meaningful effects on the fluorescence properties of the guest dyes. Among the three selected dyes, CV is soluble in water[23], NB less so and only weakly fluorescent in an aqueous environment[24], and ZnPc soluble in organic solvents[23]. Generally the results suggested that the fluorescence quantum yields of CV and NB as guests in the host-guest carbon dots were similar to those of free CV and NB molecules, respectively, all in aqueous solutions. More specifically for CV, it is known in the literature that

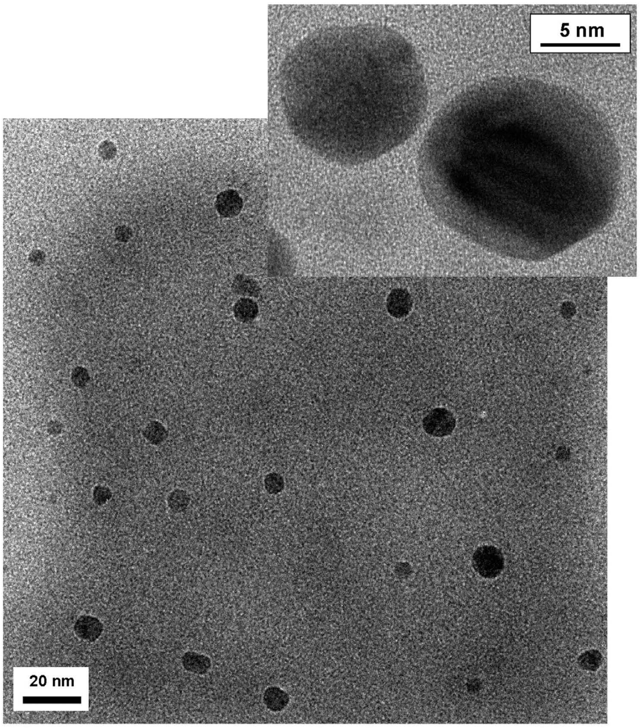

Figure 5. TEM images (high-resolution in the inset) of NB@CDots on silicon oxide-coated copper grid.

its fluorescence quantum yields in aqueous solutions are somewhat concentration dependent, higher in a more dilute solution, yet overall about 40% lower than the yields in methanol[25]. The observed similar fluorescence quantum yields between the encapsulated and free CV molecules might be due to the opposing effects of a relatively higher CV concentration and more non-aqueous environment in CV@CDots, which decreases and enhances the quantum yields, respectively. However, for NB@CDots in an aqueous solution, the estimated fluorescence quantum yields of the guest NB were higher than that of free NB molecules in water (on the order of 0.01)[24] but still significantly lower than that in ethanol (around 0.27)[23], probably suggesting that the environment for the encapsulated NB is not entirely free from water. Similarly, the fluorescence quantum yields of ZnPc as guest in the host-guest carbon dots in an aqueous solution were also significantly lower than those of free ZnPc molecules in organic solvents, likely also due to the exposure of the encapsulated ZnPc to water (because the ZnPc fluorescence in a polar organic solvent is apparently quenched efficiently by the addition of water). Therefore, in further investigations the fluorescence properties of these water-sensitive dyes may be used to study the local environment in the core carbon nanoparticles in the host-guest carbon dots. Experimentally, more effort is needed to correct the light scattering effect in aqueous solutions of the host-guest carbon dots for a more accurate determination of the fluorescence quantum yields of the encapsulated dyes.

Conceptually similar to endofullerenes that have expanded the horizons of the fullerene field[13], the host-guest carbon dots represent a new QD-like nanoarchitecture for materials properties and functions beyond those achieved with the original carbon dots. The extension of absorption and fluorescence coverage of carbon dots into the red/near-IR spectral regions with the relevant dyes as guest in this work serves as a representative example for the potential and versatile nature of the host-guest carbon dots platform. Such a new platform is expected to significantly broaden the reach of the already rapidly advancing carbon dots research and development.

References

1. Sun, Y.-P. *et al.* Quantum-sized carbon dots for bright and colorful photoluminescence. *J. Am. Chem. Soc.* **128,** 7756–7757 (2006).
2. Luo, P. G. *et al.* Carbon "quantum" dots for optical bioimaging. *J. Mater. Chem. B* **1,** 2116–2127 (2013).
3. Wang, Y. & Hu, A. Carbon quantum dots: synthesis, properties and applications. *J. Mater. Chem. C* **2,** 6921–6939 (2014).
4. Luo, P. G. *et al.* Carbon-based quantum dots for fluorescence imaging of cells and tissues. *RSC Adv.* **4,** 10731–10807 (2014).
5. Kairdolf, B. A. *et al.* Semiconductor Quantum Dots for Bioimaging and Biodiagnostic Applications. *Annu. Rev. Anal. Chem.* **6,** 143–162 (2013).
6. Wang, X. *et al.* Bandgap-Like Strong Fluorescence in Functionalized Carbon Nanoparticles. *Angew. Chem. Int. Ed.* **49,** 5310–5314 (2010).
7. Yang, S.-T. *et al.* Carbon Dots as Nontoxic and High-Performance Fluorescence Imaging Agents. *J. Phys. Chem. C* **113,** 18110–18114 (2009).
8. Yang, S.-T. *et al.* Carbon Dots for Optical Imaging *in vivo*. *J. Am. Chem. Soc.* **131,** 11308–11309 (2009).

9. Ding, C., Zhu, A. & Tian, Y. Functional surface engineering of C-dots for fluorescent Biosensing and *in vivo* bioimaging. *Acc. Chem. Res.* **47,** 20–30 (2014).
10. Cao, L. *et al.* Competitive Performance of Carbon "Quantum" Dots in Optical Bioimaging. *Theranostics* **2,** 295–301 (2012).
11. Tao, H. *et al.* In Vivo NIR Fluorescence Imaging, Biodistribution, and Toxicology of Photoluminescent Carbon Dots Produced from Carbon Nanotubes and Graphite. *Small* **8,** 281–290 (2012).
12. Huang, X. *et al.* Effect of Injection Routes on the Biodistribution, Clearance, and Tumor Uptake of Carbon Dots. *ACS Nano* **7,** 5684–5693 (2013).
13. Popov, A. A., Yang, S. & Dunsch. L. Endohedral fullerenes. *Chem. Rev.* **113,** 5989–6113 (2013).
14. Zhu, H. *et al.* Microwave synthesis of fluorescent carbon nanoparticles with electrochemiluminescence properties. *Chem. Commun.* **45,** 5118–5120 (2009).
15. Liu, C. *et al.* One-step synthesis of surface passivated carbon nanodots by microwave assisted pyrolysis for enhanced multicolor photoluminescence and bioimaging. *J. Mater. Chem.* **21,** 13163–13167 (2011).
16. Jaisawl, A., Ghosh, S. S. & Chattopadhyay, A. One step synthesis of C-dots by microwave mediated caramelization of poly (ethylene glycol). *Chem. Commun.* **48,** 7955–7957 (2012).
17. Zhai, X. *et al.* Highly luminescent carbon nanodots by microwave-assisted pyrolysis. *Chem. Commun.* **48,** 7955–7957 (2012).
18. Chandra, S., Das, P., Bag, S., Laha, D. & Pramanik. P. Synthesis, functionalization and bioimaging applications of highly fluorescent carbon nanoparticles. *Nanoscale* **3,** 1533–1540 (2012).
19. Chandra, S. *et al.* Tuning of photoluminescence on different surface functionalized carbon quantum dots. *RSC Adv*. **2,** 3602–3606 (2012).
20. Sachdev, A. *et al.* A novel one-step synthesis of PEG passivated multicolour fluorescent carbon dots for potential biolabeling application. *RSC Adv*. **3,** 16958–16961 (2013).
21. Liu, C. *et al.* Nano-carrier for gene delivery and bioimaging based on carbon dots with PEI-passivation enhanced fluorescence. *Biomaterials* **33,** 3604–3613 (2012).
22. LeCroy, G. E. *et al.* Toward Structurally Defined Carbon Dots as Ultracompact Fluorescent Probes. *ACS Nano* **8,** 4522–4529 (2014).
23. Brouwer, A. M. Standards for photoluminescence quantum yield measurements in solution. *Pure Appl. Chem.* **83,** 2213–2228 (2011).
24. Jose, J., Ueno, Y. & Burgess, K. Water-Soluble Nile Blue Derivatives: Syntheses and Photophysical Properties. *Chem. Euro. J.* **15,** 418–425 (2009).
25. Isak, S. & Eyring, E. M. Fluorescence quantum yield of cresyl violet in methanol and water as a function of concentration. *J. Phys. Chem.* **96,** 1738–1742 (1992).

Acknowledgments

The support from Air Force Office of Scientific Research (AFOSR, through the program of Dr. Charles Lee) is gratefully acknowledged. Z.L. was a visiting student from Prof. Fushen Lu's group at Shantou University in China, M.J.M. a visiting professor from Northwest Missouri State University supported by the South Carolina Space Grant Consortium, and Y.L. on leave from Technical Institute of Physics and Chemistry in Beijing, China with a visiting scholarship provided by Chinese Academy of Sciences.

Author Contributions

Y.-P.S. came up with the idea and supervised the performance of the work; P.W., Z.L. and F.Y. performed various tasks of the work; M.J.M. and H.Q. contributed to the sample analyses; and G.E.L. and Y.L. assisted the performance of the work.

Additional Information

Supplementary information accompanies this paper at http://www.nature.com/srep

Competing financial interests: The authors declare no competing financial interests.

How to cite this article: Sun, Y.-P. *et al.* Host-Guest Carbon Dots for Enhanced Optical Properties and Beyond. *Sci. Rep.* **5**, 12354; doi: 10.1038/srep12354 (2015).

Journal of
Materials Chemistry C

PAPER

View Article Online
View Journal | View Issue

Cite this: *J. Mater. Chem. C*, 2017, 5, 6328

Host–guest carbon dots as high-performance fluorescence probes†

Ping Wang,[a] Jia-Hui Liu,*[b] Haidi Gao,[b] Yin Hu,[a] Xiaofang Hou,[a] Gregory E. LeCroy,[a] Christopher E. Bunker,[c] Yuanfang Liu[de] and Ya-Ping Sun*[a]

Received 11th April 2017,
Accepted 5th June 2017

DOI: 10.1039/c7tc01574g

rsc.li/materials-c

Host–guest carbon dots (G@CDots) represent a new platform in the rapidly advancing and expanding research field of carbon "quantum" dots or carbon dots, enabling the development of novel carbon hybrid nanostructures of unique and/or advantageous properties and capabilities beyond those of conventional carbon dots. In this study, the red/near-IR emissive dye nile blue (NB) was selected as the guest, and NB@CDots were prepared in a microwave-assisted one-pot thermal carbonization synthesis with oligomeric polyethylene glycols (PEGs) as the precursor and also surface passivation species in the resulting host–guest dots. The NB@CDots exhibited unique and/or favorable characteristics, including especially the bright red/near-IR fluorescence emissions, with the observed fluorescence quantum yield due to the guest nile blue species more than an order of magnitude higher than that of free nile blue molecules, all in aqueous solutions. The higher fluorescence intensities were coupled with a longer fluorescence lifetime, and also accompanied by excellent photochemical stability, making the NB@CDots high-performance fluorescence probes for bioimaging-sensing and related applications. Indeed, their potential in this regard was explored and demonstrated in the fluorescence imaging of live stem cells. The NB@CDots were also evaluated in cytotoxicity assays, and the results suggested their being nontoxic. Excellent opportunities in further development of the host–guest carbon dots platform for high-performance yet nontoxic fluorescence probes are discussed.

Introduction

Carbon "quantum" dots or carbon dots (CDots)[1,2] are defined generally as small carbon nanoparticles with various surface passivation schemes, including the deliberate chemical functionalization with selected organic molecules (Fig. 1)[1–8] or the passivation by the remaining organic species following "one-pot" carbonization processing of organic precursors.[5–12] The deliberate functionalization synthesis has produced some of the best-performing CDots in terms of bright and colorful fluorescence emissions, with observed fluorescence quantum yields of more than 50%.[3] These CDots, as well as some of those

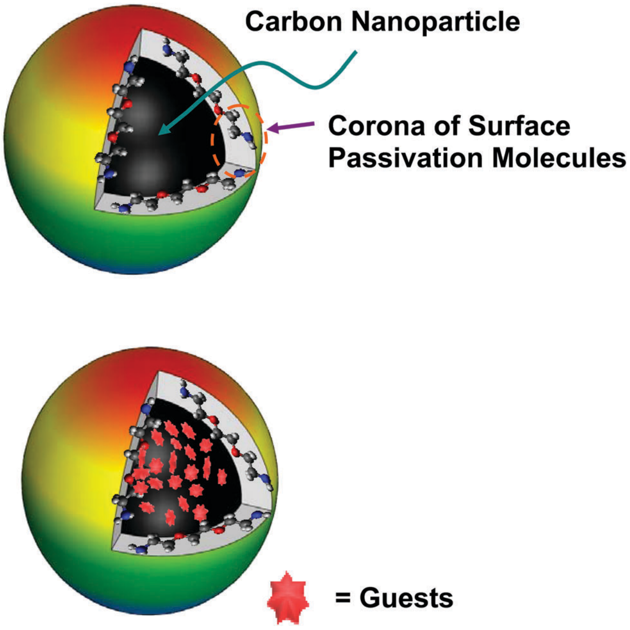

Fig. 1 Cartoon illustration on a neat CDot (upper), which is a carbon nanoparticle with attached surface passivation molecules in a configuration similar to a soft corona, and a corresponding host–guest CDot (lower).

---

[a] Department of Chemistry and Laboratory for Emerging Materials and Technology, Clemson University, Clemson, South Carolina 29634, USA. E-mail: syaping@clemson.edu

[b] Beijing Key Laboratory of Bioprocess, College of Life Science and Technology, Beijing University of Chemical Technology, Beijing 100029, China. E-mail: jhliu@mail.buct.edu.cn

[c] Air Force Research Laboratory, Propulsion Directorate, Wright-Patterson Air Force Base, Ohio 45433, USA

[d] Beijing National Laboratory for Molecular Sciences, College of Chemistry and Molecular Engineering, Peking University, Beijing 100871, China

[e] Institute of Nanochemistry and Nanobiology, Shanghai University, Shanghai 200444, China

† Electronic supplementary information (ESI) available. See DOI: 10.1039/c7tc01574g

prepared from the carbonization of organic precursors, have been evaluated as nanoscale probes for the fluorescence imaging of cells and also *in vivo* with various injection modes, from which the results have suggested competitive performance to that of the comparable semiconductor QDs (specifically CdSe/ZnS core/shell nanoparticles that are surface modified for aqueous solubility) now available commercially.[13–20]

CDots from different syntheses are mostly fluorescent over the entire visible spectrum, depending on excitation wavelengths,[1,5–8] and the observed emissions are generally much stronger in blue/green than in red/near-IR.[5–8,16–20] In fact, the best-performing CDots so far have exhibited bright fluorescence emissions in the same spectral region as that covered by the green fluorescent protein (GFP).[3,4] According to results from recent studies,[12] the absorption spectra of CDots from different synthetic schemes are rather similar, generally with weaker absorptivities at longer wavelengths (500 nm and longer, for example), which are likely correlated with the relatively much weaker red/near-IR fluorescence emissions of the available CDots from different syntheses. The apparent insensitivity of the optical absorption in the visible spectrum to the structural details of CDots may be considered as being beneficial in some of their intended applications, but it may prove negative or limiting to the effort on enhancing the fluorescence performance of CDots in different spectral regions *via* their structural manipulations, such as by varying the surface passivation schemes in CDots. In the quest for CDots-derived fluorescence probes of much enhanced red/near-IR performance, Sun, *et al.* recently developed an alternative approach based on the preparation of host–guest CDots (Fig. 1),[21] which are conceptually analogous and structurally similar to endofullerenes[22] in terms of the encapsulation or embedding of dye molecules or species in small carbon nanoparticles. These host–guest configurations are new and interesting carbon-based hybrid nanostructures, on which systematic investigations of the optical and other properties are needed.

In the study reported here, we focused on the potential use of host–guest CDots as brightly red/near-IR emissive fluorescence probes in bioimaging-sensing. Organic dye nile blue (NB) was selected as the guest, and oligomeric polyethylene glycols (PEGs) as surface passivation species. In the resulting host–guest CDots, denoted as NB@CDots, the guest nile blue species exhibited several favorable characteristics, including significantly enhanced red/near-IR fluorescence emission intensities that were coupled with a longer average fluorescence lifetime, and excellent photochemical stability under conditions beyond those required for fluorescence bioimaging-sensing. The NB@CDots were found to be nontoxic to the selected cancer cells and stem cells, and their performance as red/near-IR emissive probes in the fluorescence imaging of cells was excellent. The potential of host–guest CDots as a new platform for high-performance yet nontoxic fluorescence probes is discussed.

Results and discussion

The host–guest CDots with red/near-IR fluorescent nile blue (NB) as the guest dye, NB@CDots, was prepared by carbonizing oligomeric PEGs (molecular weight ~900) in the presence of nile blue molecules. Experimentally, nile blue in a small amount of ethanol and PEGs in large excess were mixed *via* sonication at above ambient temperature, followed by evaporation to remove the ethanol. The resulting solid-state mixture was placed in a conventional microwave oven for the carbonization processing with microwave irradiation.[21,23–25] The degree of carbonization in correlation with the processing time was assessed by monitoring the relative absorbances at 400 nm and 550 nm, which are dominated by the nanoscale carbon absorption and contributed substantially by the guest nile blue, respectively. The ratio of about unity between the two absorbances was targeted as the end point for the carbonization processing. The reaction mixture thus obtained was cooled to ambient temperature and then dispersed in deionized water, followed by vigorous centrifugation to retain the supernatant for further processing *via* gel column separation, for which a Sephadex G-100 gel column packed in house was used, with water as eluent. In the separation, the later fractions corresponding to relatively higher observed fluorescence quantum yields were harvested, combined, and concentrated to obtain a sample of the desired NB@CDots in aqueous solution (Fig. 2).

The optical absorption spectrum of the NB@CDots is a combination of absorption contributions from the surface-PEGylated carbon nanoparticles and the embedded nile blue species (Fig. 2), with the spectrum of the latter shifted and broadened from that of free nile blue molecules due probably to effects such as the varying local environment in the carbon host. These absorption spectral features are mostly consistent with the host–guest configuration (Fig. 1), so are the results from solution-phase NMR characterization and FT-IR spectral measurements. The observed NMR spectra of the NB@CDots exhibited only signals associated with the surface PEG moieties

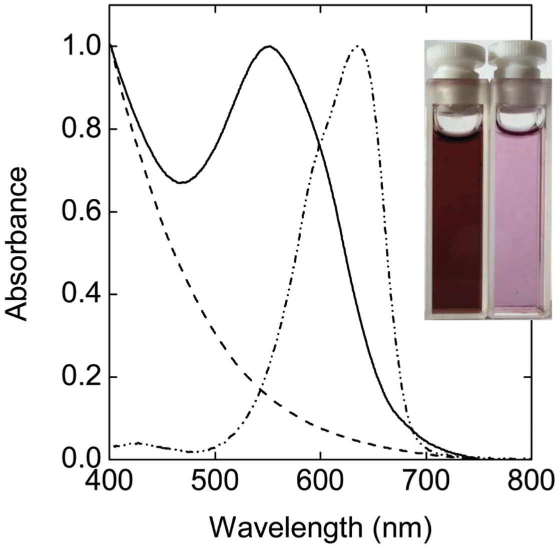

Fig. 2 Optical absorption spectra of the NB@CDots (—) and free nile blue (-..-..-) in aqueous solutions and the aqueous suspended small carbon nanoparticles (- - -). Inset: Photos of more concentrated (left) and dilute (right) solutions of the NB@CDots.

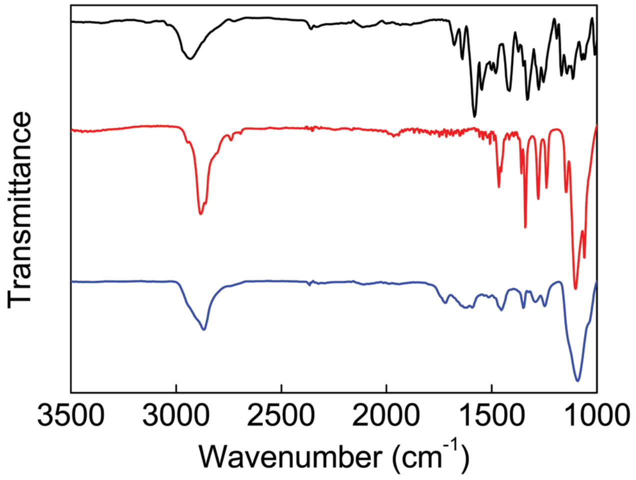

Fig. 3 The FT-IR spectrum of the NB@CDots (lower) is compared with those of the neat precursor PEGs used in the dot synthesis (middle) and free nile blue (upper).

slightly shifted and broadened from those of free PEGs used as precursor in the carbonization processing. The FT-IR spectrum of the NB@CDots is dominated by the surface PEG species, with the absorption bands exhibiting features found in the spectrum of the precursor PEGs used in the carbonization processing, but broader, and also with some contributions from the guest species (Fig. 3), largely as expected. While providing not much structural information on the NB@CDots, these results do suggest the absence of other materials and/or complications, as the abundant surface PEGs are understandably the dominating species more detectable by these experimental techniques.

The NB@CDots were characterized by using transmission electron microscopy (TEM). For the TEM imaging, the specimen was prepared such that a few drops of a dilute sample solution were deposited onto a silicon oxide-coated copper grid, followed by careful evaporation to remove the solvent. As shown in Fig. 4, most of these host–guest CDots are small, with their overall size profiles on the order of 5 nm in average diameter (and the size distribution standard deviation of 0.8 nm, Fig. 4).

As already illustrated in Fig. 2 and discussed above, the absorption spectrum of the NB@CDots in aqueous solution is a combination of contributions by the nanoscale carbon host and the guest nile blue species. In the solution, while the dot as a whole was in water, the environment surrounding the guest dye species in the carbon host must be very different from aqueous, as reflected by the substantial spectral shift in the absorption band corresponding to nile blue (Fig. 2). In fact, the spectral shift was beyond those found for free nile blue molecules from aqueous (peak at 634 nm)[26] to polar organic solvents, such as ethanol (peak at 629 nm)[26,27] and ethyl acetate (peak at 624 nm).[28] Thus, it may be argued that the local environment surrounding guest nile blue species in the carbon host must be more like that in a nonpolar solvent, even though absorption spectral shifts are probably associated with multiple factors, more than just polarity. Nevertheless, the expected non-aqueous environment inside the carbon host, which may be considered as being similar to carbon cement, has significant effects on the guest nile blue species in terms of their fluorescence emission properties important to the NB@CDots serving as high-performance fluorescence probes.

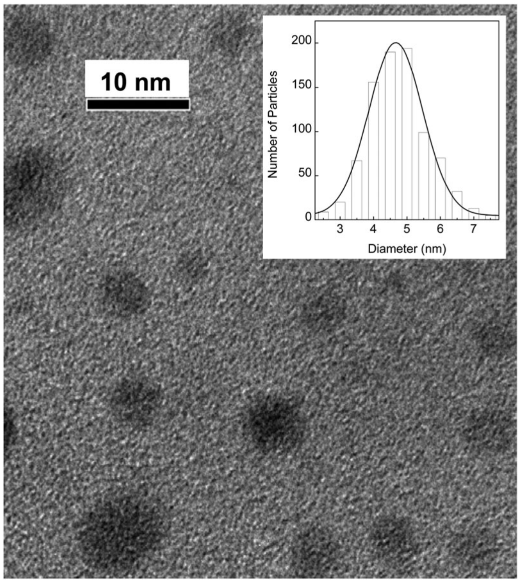

Fig. 4 Representative TEM images of the NB@CDots. Inset: A statistical size analysis based on multiple image sets.

For the host environment effect on the guest in NB@CDots, there were similarly substantial fluorescence spectral shift (Fig. 5) and much enhanced fluorescence intensities in comparison with those of free nile blue molecules, all in aqueous solutions. Since free nile blue is known to be considerably more fluorescent in an organic solvent than in water,[29,30] the observed much brighter fluorescence emissions when exciting into the absorption spectral region dominated by the guest nile blue species again suggest

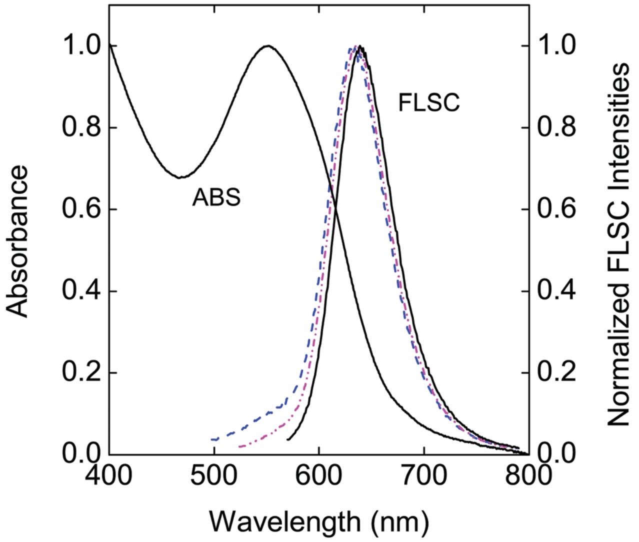

Fig. 5 Absorption (ABS, peak wavelength 550 nm) and fluorescence (FLSC, with excitation at 550 nm: —, emission peak 639 nm; 514 nm: -..-, emission peak 635 nm; and 488 nm: - - -, emission peak 632 nm) spectra of the NB@CDots in aqueous solution.

that the host environment in the NB@CDots is non-aqueous, as expected. Quantitatively in the determination of fluorescence quantum yields, special effort was made to correct the effect of the carbon host absorption at the excitation wavelength (Fig. 2 and 5). By considering the observed absorption spectrum of NB@CDots as a superposition of the absorptions by the guest nile blue species and the carbon host, with the latter being close to that of aqueous dispersed small carbon nanoparticles, an aqueous mixture of free nile blue molecules and carbon nanoparticles was prepared as a reference (matching the superposition at the excitation wavelength) in the fluorescence quantum yield measurements. According to the results thus obtained, the fluorescence quantum yield of the guest nile blue species in the NB@CDots at 550 nm excitation is about 20 times that of free nile blue (about 1%),[29] both in aqueous solutions. The much enhanced fluorescence quantum yield is obviously consistent with the corresponding nile blue species being guests in the host environment that is very different from aqueous. In the absolute term with Rhodamine 6G as a fluorescence standard,[30] the fluorescence quantum yield of the guest nile blue in the NB@CDots is 18 ± 2% (530 nm excitation), sufficiently bright for the NB@CDots as fluorescence probes in the red/near-IR spectral region. For the NB@CDots as a whole probe, the observed fluorescence quantum yield at 550 nm excitation is ∼16%.

The substantial increase in fluorescence quantum yield from free nile blue molecules to their being guests in the NB@CDots is accompanied by a similar increase in fluorescence lifetime. Shown in Fig. 6 is a comparison between fluorescence decays of the NB@CDots and free nile blue molecules in aqueous solutions measured by using the time-correlated single photon counting (TCSPC) technique. The emissions in the former are obviously much longer lived, even longer than those of free nile blue in methanol (Fig. 6). The decays of free nile blue in water and methanol could be deconvoluted by fitting with a mono-exponential function, yielding fluorescence lifetime values of 0.5 ns and 1.2 ns, respectively. On the other hand, the decay of the NB@CDots in aqueous solution is not mono-exponential, but could be fitted by using a bi-exponential function in the deconvolution with the two lifetimes $\tau_{F1} = 1.4$ ns and $\tau_{F2} = 2.5$ ns and their associated relative pre-exponential factors $A_1 = 43\%$ and $A_2 = 57\%$. Despite the good deconvolution fit, however, the results should probably not be considered as evidence for the presence of only two discrete emitting entities, but more likely reflect an averaging of the emissions from a distribution of guest nile blue species in various local environments. A further averaging could be made by using the pre-exponential factors (A_1 and A_2) and lifetimes (τ_{F1} and τ_{F2}) from the bi-exponential deconvolution fit, $\langle\tau_F\rangle = (A_1\tau_{F1}{}^2 + A_2\tau_{F2}{}^2)/(A_1\tau_{F1} + A_2\tau_{F2})$,[31] and the average fluorescence lifetime $\langle\tau_F\rangle$ thus calculated is 2.2 ns. It is much longer than that of free nile blue molecules in water and also longer than that of the molecules in methanol, consistent with the fluorescence quantum yield results.

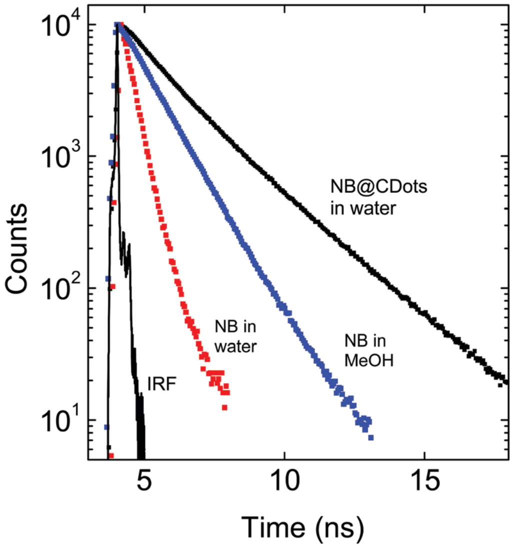

Fig. 6 Fluorescence decays of the NB@CDots in aqueous solution and free nile blue in aqueous and methanol solutions.

The guest nile blue species in the NB@CDots were found to be photochemically much more stable than their free counterparts in aqueous solutions. In the comparison, concentrations of the guest nile blue in the NB@CDots and free nile blue, both in aqueous solutions, were matched by using their respective peak absorptions. The solutions were irradiated with broadband visible light (405–720 nm) in a photochemistry setup (consisting of a xenon arc lamp coupled with optical filters) for up to 30 min. At various time points, absorption spectra of the solutions were measured. There were progressive absorption decreases in the solution of free nile blue, by 30% at the end of the 30 min photoirradiation, whereas the absorption spectra of the aqueous NB@CDots solution photoirradiated under the same conditions were essentially unchanged. The photostability in addition to the bright red/near-IR emissions makes the NB@CDots excellent fluorescence probes for potential bioimaging-sensing and other biomedical applications. In such applications biocompatibility is always a major consideration. Nevertheless, the NB@CDots, similar to other CDots in general,[16,32,33] were found to be biocompatible according to results from the cytotoxicity evaluation described as follows.

The cytotoxicity evaluation of the NB@CDots was based on the CCK-8 assay with the widely used cervical cancer HeLa cells and the rat mesenchymal stem cells (MSCs). Experimentally on the use of MSCs for example, a suspension of 10^5 cells per mL in the MSC basal medium was prepared and seeded in a 96-well plate. After culturing for 24 h, the cells were exposed to the NB@CDots of different concentrations up to 0.5 μM of the dots. Upon another 24 h of culturing, CCK-8 was added to each well to determine the cell viability. Shown in Fig. 7 are the viability results for HeLa cells and MSCs. Apparently, the NB@CDots are nontoxic to these cells, and the non-toxicity might have been expected because to the cells the host–guest CDots would essentially be the same as typical PEGylated CDots without any guests, whose generally benign nature toward various cell lines has been established in the literature.[7,16,32,33]

The NB@CDots were used as probes in the fluorescence imaging of the similarly cultured MSCs. In a typical experiment, MSCs were plated on a four-chambered Lab-Tek coverglass

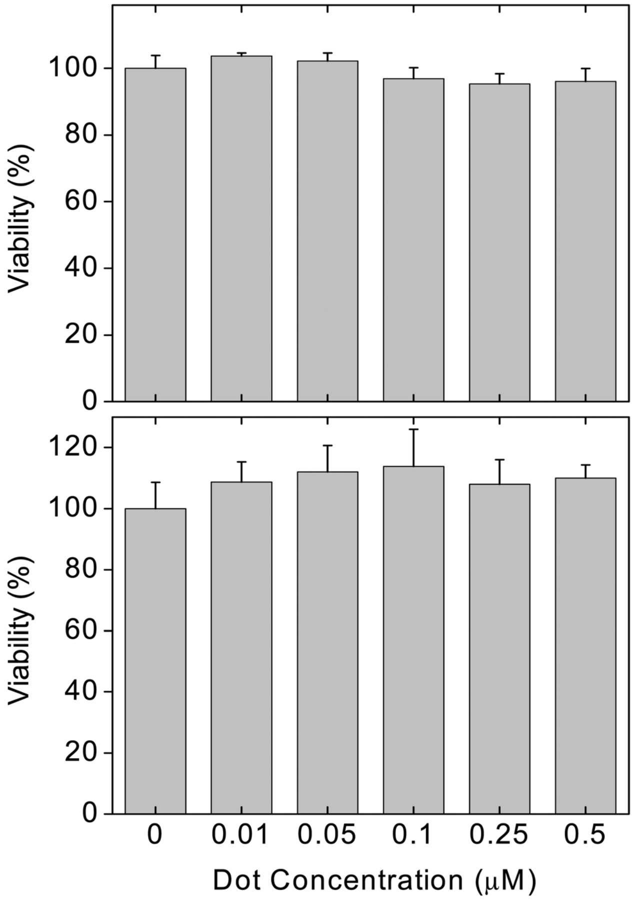

Fig. 7 Results from the cytotoxicity evaluation with HeLa cells (upper) and MSCs (lower). Data presented as the mean ± SD (n = 6).

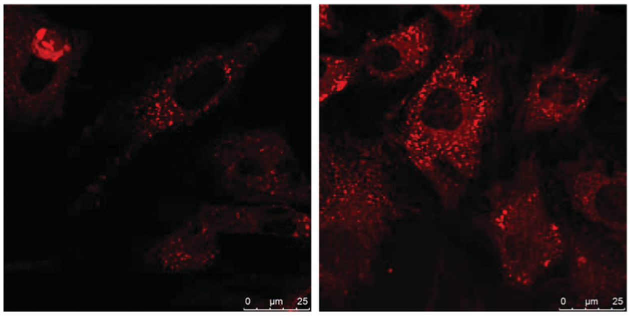

Fig. 8 Confocal fluorescence images (excitation at 488 nm, and emissions monitored at 608–720 nm) for live MSCs labeled with the NB@CDots at dot concentrations of 0.25 μM (left) and 0.5 μM (right).

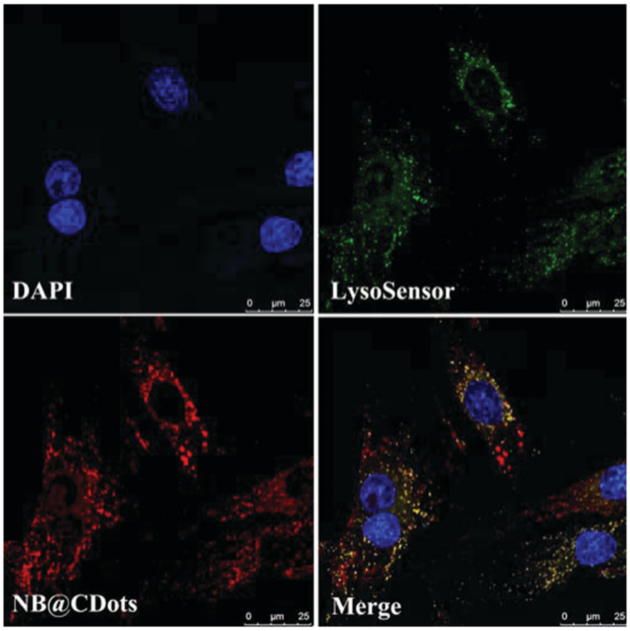

Fig. 9 Confocal fluorescence images of live MSCs with NB@CDots, LysoSensor™ Green DND-189, and DAPI obtained under different conditions. Upper-left: Excitation at 405 nm for DAPI, and emissions monitored at 424–469 nm; upper-right: excitation at 488 nm for LysoSensor™ Green DND-189, and emissions monitored at 490–539 nm; lower-left: excitation at 488 nm for NB@CDots, and emissions monitored at 608–720 nm; and lower-right: the merged three images.

system at a density of 10^5 cells per mL in the MSC basal medium for 24 h. Then, the medium was replaced by the fresh basal medium with the NB@CDots of different concentrations or without any dots as control. After 24 h, the cells were carefully washed for a complete removal of unattached NB@CDots. The cleaned live cells were imaged under a laser scanning confocal microscope by the excitation of argon ion laser lines at 488 nm and 514 nm for red/near-IR fluorescence emissions (longer than 608 nm). For the live cell imaging results corresponding to the NB@CDots concentrations of 0.25 μM and 0.5 μM (Fig. 8) used in the cell labeling experiments, those with the higher dot concentration are obviously brighter. The results also suggest that the NB@CDots in the live MSCs were mostly in the cell cytoplasm, not in the nucleus, similar to what have been observed for conventional CDots without guests in terms of their cellular distributions in general.[16,18] In the cytoplasm, it seems that the NB@CDots are concentrated in one or some specific types of organelle, which might be explored in further investigations on potentially using these probes in the live cell imaging at the sub-cellular level.

The live MSCs labeled with the NB@CDots could be stained by the established lysosome staining agent LysoSensor™ Green DND-189 for their being co-localized in the fluorescence imaging, with observations in the red and green emission windows, respectively. As shown in Fig. 9, the yellow spots in the merged images are due to the overlapping of the red and green signals, indicating the lysosomal co-localization of the NB@CDots with the specific lysosome staining agent. In addition, there are also intracellular areas with red signals only, suggesting that some of the NB@CDots could escape from the endosomes into the cytoplasm, a phenomenon that has been observed in the cell imaging with other nanoparticles.[34] According to these results on the fluorescence labeling of stem cells, the host–guest CDots can apparently not only be taken up by cells like their neat counterparts, but also offer much enhanced performance in the red/near-IR, which is widely acknowledged as being more desirable in terms of suppressing background signals in cell imaging and eventually for the labeled cells to be used for *in vivo* tracking and other relevant applications.

The results presented above suggest that the host–guest CDots could be prepared in a relatively facile synthetic procedure for them to serve as high-performance red/near-IR emissive fluorescence probes. The synthesis may be rationalized such that in the microwave-assisted thermal carbonization of organic precursors, oligomeric PEGs in large excess specifically in this study, a portion of the precursor organic species is converted into carbon nanoparticles and the remaining serves the function of surface passivation agents, a structural configuration consistent with the general definition of CDots (Fig. 1) and essentially the same as that of neat CDots prepared from the deliberate chemical functionalization of small carbon nanoparticles with oligomeric PEGs (though of course there is the difference with the encapsulation of the guest dye in the host–guest CDots). Here in the microwave-assisted processing the PEGs in large excess could apparently protect the selected dye molecules, facilitating their encapsulation in the nanoscale carbon host for the desired host–guest configuration. The dye encapsulation, while not possible to be defined in nanoscopic structural details by using the available experimental techniques, is supported indirectly yet strongly by the observed substantial changes in spectroscopic properties of the guest dye species from those of their free counterparts in solution, especially with respect to the order-of-magnitude enhancement in fluorescence quantum yields. The red/near-IR emissive dye nile blue is only weakly fluorescent in aqueous media, but becomes brightly fluorescent upon being incorporated into the carbon host in NB@CDots, excellent for fluorescence imaging in the red/near-IR spectral region, as made evident by the imaging results on the live stem cells (Fig. 8 and 9). More investigations to take advantage of these probes in cell imaging, especially at sub-cellular level, and also imaging *in vivo* are needed and planned.

Conclusions

Host–guest CDots represent a new platform in the rapidly advancing and expanding research field of CDots, enabling the development of novel carbon hybrid nanostructures of unique and/or advantageous properties and capabilities beyond those of conventional CDots. In addition to the use of the platform for fluorescence probes reported here, other applications including those widely pursued on the basis of endofullerenes may be explored and will likely prove rewarding.

Experimental section

Materials

Nile blue (sulfate salt) was purchased from Chem-Impex International, and polyethylene glycol (PEG, average molecular weight ~900) from Fluka. The dialysis membrane tubing (molecular weight cut-off ~500) was supplied by Spectrum Laboratories, and Sephadex G-100 gel by GE Healthcare Life Sciences. Water was deionized and purified by passing through a Labconco WaterPro water purification system.

Measurement

UV/vis absorption spectra were recorded on a Shimadzu UV2501-PC spectrophotometer, and fluorescence spectra on a Jobin-Yvon emission spectrometer equipped with a 450 W xenon source, Gemini-180 excitation and Triax-550 emission monochromators, and a photon counting detector (Hamamatsu R928P PMT at 950 V). Rhodamine 6G in ethanol was used as a standard in the determination of fluorescence quantum yields by the relative method (matching the absorbance at the excitation wavelength between the sample and standard solutions and comparing their corresponding integrated total fluorescence intensities). Fluorescence decays were measured by using the time-correlated single photon counting (TCSPC) technique on a Horiba Ultima Extreme spectrometer, equipped with a SuperK Extreme supercontinuum laser source operating at 3.894 MHz repetition rate, TDM-800 excitation and TDM-1200 emission monochromators, a R3809-50 MCP-PMT detector operated at 3.0 kV in a thermoelectrically cooled housing, and FluoroHub A+ timing electronics. Analyses of the decay curves were performed by using Horiba Das6 fluorescence decay analysis software. NMR measurements were carried out on a Bruker Advance 500 NMR spectrometer. Transmission electron microscopy (TEM) imaging was performed on a Hitachi H-9500 high-resolution TEM system. Fluorescence images were obtained on a Leica TCS SP8 laser-scanning confocal microscope.

NB@CDots

Nile blue (100 mg) was dissolved in ethanol (2 mL) for a clear and colored solution, and the solution was mixed with the wax-like PEG sample (1 g). The resulting mixture was sonicated in a bath sonicator (VWR 250D) at 40 °C for 30 min. Then, ethanol in the mixture was removed by purging the mixture with nitrogen gas. In the preparation for carbonization processing, SiC powders (170 g) in a silica crucible casting dish were heated in a conventional microwave oven at 500 W for 3 min. Separately, the above-described reactant mixture already prepared was placed in a small glass container. The container with the reactant mixture was buried in the preheated SiC powders in the silica crucible casting dish. The dish containing the preheated SiC powders with the buried reactant container was placed in the conventional microwave oven. The oven power was set at 1000 W. The initial microwave processing time was 2 min, and additional processing time was added based on the carbonization outcome (generally less than 1 min). The degree of carbonization was monitored by taking out a small quantity of the sample from the microwave oven, dispersing the sample in water, and measuring the absorbances at 400 nm ($A_{400\mathrm{nm}}$) and 550 nm ($A_{550\mathrm{nm}}$). The $A_{400\mathrm{nm}}/A_{550\mathrm{nm}}$ ratio of about one was targeted as the end point for the microwave processing. The processed sample was allowed to cool back to room temperature, and then it was dispersed in deionized water (10 mL) with sonication in a bath sonicator for 30 min. The aqueous dispersion thus obtained was centrifuged at 20 000*g* to keep the supernatant as the reaction mixture in aqueous solution. The mixture was separated on an aqueous gel column to harvest the desired NB@CDots.

The gel column was prepared in house by using the commercially supplied Sephadex G-100 gel. The gel (15 g) was soaked in water for 3 days, and the supernatant (including the suspended ultrafine gel) was discarded. The remaining gel was washed until no gel was suspended in the supernatant. Air bubbles were removed under vacuum. Separately, a glass column (25 mm inner diameter) was filled with water to remove air bubbles, and then closed. The gel suspension described above was poured into the column until it reached about 2 cm in height, and then the column was opened for continuous addition of the gel suspension. The gel-filled column was washed until no change in height (36 cm) was observed, followed by the testing and calibration of the column. In the separation, the reaction mixture in aqueous solution was added to the gel column and eluted with water. The later eluted fractions corresponding to higher observed fluorescence quantum yields were collected and combined, as the sample of NB@CDots for characterization and studies. For electron microscopy characterization only, the NB@CDots were very lightly coated with silver by visible-light irradiation of the aqueous solution with a silver salt for a few minutes.[35]

Cytotoxicity evaluation

The Sprague-Dawle (SD) rat mesenchymal stem cells (MSCs) (OriCellTM Cyagen Biosciences, Santa Clara, CA) were resuspended in the Wistar rat MSC basal medium (OriCellTM Cyagen Biosciences, Santa Clara, CA) for a concentration of 10^5 cells per mL, and then seeded in a 96-well plate. After culturing at 37 °C in a humidified atmosphere of 5% CO_2 and 95% air for 24 h, the cells were exposed to different concentrations of the NB@CDots, followed by another 24 h of the culturing. In the CCK-8 assay for cytotoxicity evaluation, CCK-8 assay was added to each well, followed by additional incubation at 37 °C for 3 h. The optical density (OD) of each well at 450 nm was recorded on a MD ELx800 Microplate Reader. The cell viability of the MSCs was expressed as the percentage of $(OD_{test} - OD_{blank})/(OD_{control} - OD_{blank})$, where OD_{test} is for the cells exposed to the dots, $OD_{control}$ for the control, and OD_{blank} for wells without cells.

HeLa cells (FuDan IBS Cell Center, Shanghai, China) were cultured at 37 °C in a humidified atmosphere of 5% CO_2 and 95% air in DMEM medium (Gibco, USA) supplemented with 10% (v/v) fetal bovine serum (Gibco, USA). Cells were seeded in a 96-well plate at a concentration of 10^5 cells per mL. After 24 h culturing, the cells were exposed to different concentrations of the NB@CDots. Cells cultured in the medium without any dots were taken as the control. After another 24 h of the culturing, CCK-8 assay was added to each well, and the cell viability was determined after incubation for 3 h. The optical density (OD) of formazan at 450 nm was recorded on a MD ELx800 Microplate Reader for the calculation of the viability.

Cell imaging

The suspended MSCs prepared the same as above were seeded at 10^5 cells per mL until the cell density reached about 80% to maintain continually exponential growth, and those within the 8th passage were used for all experiments. In the preparation for imaging, the MSCs were plated on a four-chambered Lab-Tek coverglass system (Nalge Nunc) at a density of 10^5 cells per mL in the Wistar rat MSC basal medium for 24 h. For the imaging of live cells, the medium was replaced by fresh basal medium containing the NB@CDots (with the dot concentration up to 0.5 μM) or without the dots as control. After 24 h, the cells were carefully washed with PBS for a complete removal of unattached NB@CDots. The cleaned live cells were imaged under the Leica TCS SP8 laser-scanning confocal microscope.

LysoSensor™ Green DND-189 was used as a lysosome staining agent for co-localization with NB@CDots and for their being viewed in the green and red channels, respectively. Experimentally, the MSCs labeled with NB@CDots described above were stained with LysoSensor™ Green DND-189 (2 μM, Molecular Probes™) and DAPI (50 mg mL^{-1}, Sigma) for 45 min. The treated MSCs were imaged under the Leica TCS SP8 laser-scanning confocal microscope with 405 nm excitation for DAPI (424–469 nm emission window), 488 nm excitation for LysoSensor™ Green DND-189 (490–539 nm emission window), and 488 nm excitation for NB@CDots (608–720 nm emission window).

Acknowledgements

Financial support from the Air Force Office of Scientific Research through the program of Dr Charles Lee and Dr Kenneth Caster (Y.-P. S.), Natural Science Foundation of China (NSFC No. 21301015, J.-H. L.), and South Carolina Space Grant Consortium (Y.-P. S.) is gratefully acknowledged. Y. H. was a visiting student from Beijing Jiaotong University (China) sponsored by the China Scholarship Council, and X. H. was a visiting scholar on leave from Xi'an Jiaotong University (China).

References

1 Y.-P. Sun, B. Zhou, Y. Lin, W. Wang, K. A. S. Fernando, P. Pathak, M. J. Meziani, B. A. Harruff, X. Wang, H. F. Wang, P. G. Luo, H. Yang, M. E. Kose, B. L. Chen, L. M. Veca and S.-Y. Xie, *J. Am. Chem. Soc.*, 2006, **128**, 7756–7757.
2 Y.-P. Sun, *Fluorescent Carbon Nanoparticles, U.S. Pat.*, 7829772, 2010.
3 X. Wang, L. Cao, S.-T. Yang, F. Lu, M. J. Meziani, L. Tian, K. W. Sun, M. A. Bloodgood and Y.-P. Sun, *Angew. Chem., Int. Ed.*, 2010, **122**, 5438–5442.
4 G. E. LeCroy, S. K. Sonkar, F. Yang, L. M. Veca, P. Wang, K. N. Tackett II, J.-J. Yu, E. Vasile, H. Qian, Y. Liu, P. G. Luo and Y.-P. Sun, *ACS Nano*, 2014, **8**, 4522–4529.
5 Y. Wang and A. Hu, *J. Mater. Chem. C*, 2014, **2**, 6921–6939.
6 K. A. S. Fernando, S. Sahu, Y. Liu, W. K. Lewis, E. A. Guliants, A. Jafariyan, P. Wang, C. E. Bunker and Y.-P. Sun, *ACS Appl. Mater. Interfaces*, 2015, **7**, 8363–8376.
7 S. Y. Lim, W. Shen and Z. Gao, *Chem. Soc. Rev.*, 2015, **44**, 362–381.
8 G. E. LeCroy, S.-T. Yang, F. Yang, Y. Liu, K. A. S. Fernando, C. E. Bunker, Y. Hu, P. G. Luo and Y.-P. Sun, *Coord. Chem. Rev.*, 2016, **320**, 66–81.

9 C. Liu, P. Zhang, F. Tian, W. Li, F. Li and W. Liu, *J. Mater. Chem.*, 2011, **21**, 13163–13167.

10 H. Liu, Z. He, L. P. Jiang and J. J. Zhu, *ACS Appl. Mater. Interfaces*, 2015, **7**, 4913–4920.

11 J. Gu, D. Hu, J. Huang, X. Huang, Q. Zhang, X. Jia and K. Xi, *Nanoscale*, 2016, **8**, 3973–3981.

12 Y. Hu, M. M. Al Awak, F. Yang, S. Yan, Q. Xiong, P. Wang, Y. Tang, L. Yang, G. E. LeCroy, X. Hou, C. E. Bunker, L. Xu, N. Tomlinson and Y.-P. Sun, *J. Mater. Chem. C*, 2016, **4**, 10554–10560.

13 S.-T. Yang, L. Cao, P. G. Luo, F. Lu, X. Wang, H. F. Wang, M. J. Meziani, Y. Liu, G. Qi and Y.-P. Sun, *J. Am. Chem. Soc.*, 2009, **131**, 11308–11309.

14 L. Cao, S.-T. Yang, X. Wang, P. G. Luo, J.-H. Liu, S. Sahu, Y. Liu and Y.-P. Sun, *Theranostics*, 2012, **2**, 295–301.

15 X. Huang, F. Zhang, L. Zhu, K. Y. Choi, N. Guo, J. Guo, K. Tackett, P. Anilkumar, G. Liu, Q. Quan, H. S. Choi, G. Niu, Y.-P. Sun, S. Lee and X. Chen, *ACS Nano*, 2013, **7**, 5684–5693.

16 P. G. Luo, S. Sahu, S.-T. Yang, S. K. Sonkar, J. Wang, H. F. Wang, G. E. LeCroy, L. Cao and Y.-P. Sun, *J. Mater. Chem. B*, 2013, **1**, 2116–2127.

17 H. Shi, J. Wei, L. Qiang, X. Chen and X. Meng, *J. Biomed. Nanotechnol.*, 2014, **10**, 2677–2699.

18 P. G. Luo, F. Yang, S.-T. Yang, S. K. Sonkar, L. Yang, J. J. Broglie, Y. Liu and Y.-P. Sun, *RSC Adv.*, 2014, **4**, 10791–10807.

19 K. Hola, Y. Zhang, Y. Wang, E. P. Giannelis, R. Zboril and A. L. Rogach, *Nano Today*, 2014, **9**, 590–603.

20 P. Miao, K. Han, Y. Tang, B. Wang, T. Lin and W. Cheng, *Nanoscale*, 2015, **7**, 1586–1595.

21 Y.-P. Sun, P. Wang, Z. Lu, F. Yang, M. J. Meziani, G. E. LeCroy, Y. Liu and H. Qian, *Sci. Rep.*, 2015, **5**, 12354.

22 A. A. Popov, S. Yang and L. Dunsch, *Chem. Rev.*, 2013, **113**, 5989–6113.

23 H. Zhu, X. Wang, Y. Li, Z. Wang, F. Yang and X. Yang, *Chem. Commun.*, 2009, 5118–5120.

24 A. Jaiswal, S. S. Ghosh and A. Chattopadhyay, *Chem. Commun.*, 2012, **48**, 407–409.

25 X. Zhai, P. Zhang, C. Liu, T. Bai, W. Li, L. Dai and W. Liu, *Chem. Commun.*, 2012, **48**, 7955–7957.

26 H. Tajalli, A. G. Gilani, M. S. Zakerhamidi and P. Tajalli, *Dyes Pigm.*, 2008, **78**, 15–24.

27 S. Basu, S. Panigrahi, S. Praharaj, S. K. Ghosh, S. Pande, S. Jana, A. Pal and T. Pal, *J. Phys. Chem. A*, 2007, **111**, 578–583.

28 D. M. Fox, P. C. Trulove, H. C. De Long, J. Gilman and P. H. Maupin, *ECS Trans.*, 2009, **16**, 141–149.

29 J. Jose, Y. Ueno and K. Burgess, *Chem. – Eur. J.*, 2009, **15**, 418–423.

30 A. M. Brouwer, *Pure Appl. Chem.*, 2011, **83**, 2213–2228.

31 J. R. Lakowicz, *Principles of Fluorescence Spectroscopy*, Kluwer Academic/Plenum Publishers, New York, 2nd edn, 1999.

32 Y. Wang, P. Anilkumar, L. Cao, J.-H. Liu, P. G. Luo, K. N. Tackett II, S. Sahu, P. Wang, X. Wang and Y.-P. Sun, *Exp. Biol. Med.*, 2011, **236**, 1231–1238.

33 J.-H. Liu, L. Cao, G. E. LeCroy, P. Wang, M. J. Meziani, Y. Dong, Y. Liu, P. G. Luo and Y.-P. Sun, *ACS Appl. Mater. Interfaces*, 2015, **7**, 19439–19445.

34 Y. Zhang, Y. Shen, X. Teng, M. Yan, H. Bi and P. C. Morais, *ACS Appl. Mater. Interfaces*, 2015, **7**, 10201–10212.

35 J. Xu, S. Sahu, L. Cao, C. E. Bunker, G. Peng, K. A. S. Fernando, P. Wang, E. A. Guliants, M. J. Meziani, H. Qian and Y.-P. Sun, *Langmuir*, 2012, **28**, 16141–16147.

ACS APPLIED MATERIALS & INTERFACES

Research Article

www.acsami.org

Visible-Light-Activated Bactericidal Functions of Carbon "Quantum" Dots

Mohammed J. Meziani,[†,∥] Xiuli Dong,[‡,∥] Lu Zhu,[§,∥] Les P. Jones,[¶] Gregory E. LeCroy,[†] Fan Yang,[†] Shengyuan Wang,[‡] Ping Wang,[†] Yiping Zhao,[*,⊥] Liju Yang,[*,‡] Ralph A. Tripp,[*,¶] and Ya-Ping Sun[*,†]

[†]Department of Chemistry and Laboratory for Emerging Materials and Technology, Clemson University, Clemson, South Carolina 29634, United States

[‡]Department of Pharmaceutical Sciences, Biomanufacturing Research Institute and Technology Enterprise, North Carolina Central University, Durham, North Carolina 27707, United States

[§]College of Engineering, [¶]Department of Infectious Diseases, and [⊥]Department of Physics and Astronomy and Nanoscale Science and Engineering Center, University of Georgia, Athens, Georgia 30602, United States

Ⓢ *Supporting Information*

ABSTRACT: Carbon dots, generally defined as small carbon nanoparticles with various surface passivation schemes, have emerged as a new class of quantum-dot-like nanomaterials, with their optical properties and photocatalytic functions resembling those typically found in conventional nanoscale semiconductors. In this work, carbon dots were evaluated for their photoinduced bactericidal functions, with the results suggesting that the dots were highly effective in bacteria-killing with visible-light illumination. In fact, the inhibition effect could be observed even simply under ambient room lighting conditions. Mechanistic implications of the results are discussed and so are opportunities in the further development of carbon dots into a new class of effective visible/natural light-responsive bactericidal agents for a variety of bacteria control applications.

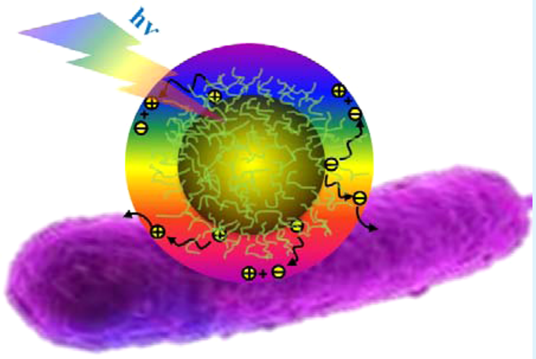

KEYWORDS: *carbon dots, bactericidal functions, light activation, photodynamic effect, E. coli, colloidal TiO_2*

INTRODUCTION

Bacterial infections present a major healthcare challenge, especially with the increasing bacterial resistance to antibiotics,[1,2] demanding the development of alternative antimicrobial strategies. Among the most effective alternatives is the use of photoactivated antimicrobial nanomaterials and nanotechnology, for which the recent rapid advances offer some unique opportunities. Nanoscale semiconductors have been a popular choice for their photoinduced redox properties and associated bactericidal functions. For example, colloidal TiO_2 has been widely employed as a photocatalyst for antibacterial and general disinfection purposes.[3] However, a significant limitation with TiO_2 nanostructures is the large band gap (3.2 eV), requiring UV activation. Therefore, there has been much effort on the modification of TiO_2 via doping or coupling with dyes or narrower-band-gap materials to extend photoexcitation into the visible spectrum.[3−6] Alternative semiconductors and other nanomaterials for visible-light-responsive antibacterial activities have been pursued.[7−9] Visible-light activation considerably broadens the reach of the photochemical antimicrobial agents, potentially enabling their uses under solar irradiation or natural-light exposure to inhibit the growth of pathogens and other infectious agents. Our focus has been on exploring the newly developed carbon "quantum" dots, or more appropriately called carbon dots for their lack of classical quantum confinement behavior,[10] for their visible-light-activated bactericidal functions.

Carbon dots (Figure 1),[10] generally defined as small carbon nanoparticles with various surface passivation schemes,[11] have emerged as a new class of quantum-dot-like nanomaterials, with their optical properties and photocatalytic functions resembling those found in conventional nanoscale semiconductors.[11−17] For example, in addition to their bright and colorful fluorescence emissions, carbon dots have been demonstrated as effective visible-light photocatalysts for oxidation and reduction reactions.[17,18] The same photoinduced redox processes responsible for the photocatalytic activities should make carbon dots excellent candidates as antibacterial agents, for which a major advantage is the broad and strong optical absorption of carbon dots over the visible spectral region, extending into the near-IR. Here we report the experimental confirmation on the bactericidal functions of photoexcited carbon dots. 2,2′-(Ethylenedioxy)bis(ethylamine) (EDA) carbon dots were selected for being compact in structure and well-

Received: February 10, 2016
Accepted: April 11, 2016
Published: April 11, 2016

DOI: 10.1021/acsami.6b01765
ACS Appl. Mater. Interfaces 2016, 8, 10761−10766

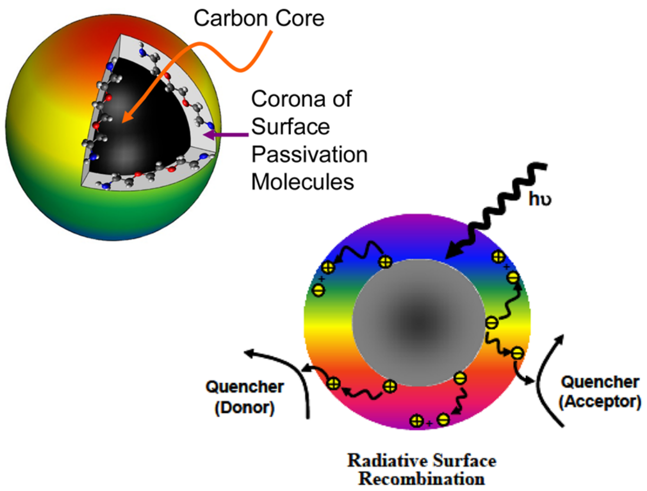

Figure 1. Cartoon illustrations of (left) a carbon dot, with a small carbon nanoparticle core and the surface functionalization molecules forming a soft shell, and (right) the photoexcited-state species and processes, with the rainbow color showing fluorescence from the dot surface.

characterized in a previously reported study.[19] The evaluation experiments were performed under household LED lighting or ambient laboratory light conditions, and the carbon dots inhibited *Escherichia coli* cells in all of the experimental settings. These results and their mechanistic implications are discussed.

■ RESULTS AND DISCUSSION

Carbon nanoparticles as precursors to carbon dots were obtained from the commercially supplied carbon nanopowder sample by following an established protocol including the refluxing of the as-supplied sample in an aqueous nitric acid solution, dialysis, centrifuging to retain the supernatant, and then drying to recover the carbon nanoparticles. The nanoparticles were surface-functionalized with EDA under amidation reaction conditions to yield EDA carbon dots.[19,20] Briefly, the carbon nanoparticles were refluxed in neat thionyl chloride, followed by the removal of excess thionyl chloride, and then the sample was mixed well with carefully dried EDA. The mixture was heated and stirred at 120 °C with nitrogen protection in the experimental setup designed for reactions under refluxing conditions. The reaction mixture was dispersed in water and centrifuged to retain the supernatant as the as-synthesized sample, which was further purified by removing residual small molecular species including free EDA in dialysis against deionized water to obtain EDA carbon dots in an aqueous solution. The solution appeared optically transparent (Figure 2), stable without any precipitation over an extended period of time (many months). The solubility and solution stability may be expected for these dots, being small carbon nanoparticles with the surface well-functionalized by hydrophilic molecules (Figure 1). According to results from atomic force microscopy (AFM) and transmission electron microscopy (TEM) characterization, the EDA carbon dots were on the order of 5 nm diameter (Figure 3).

The optical absorption of carbon dots is due to a π-plasmon transition in the carbon nanoparticle core, with a broad absorption spectrum covering most of the visible region (Figure 2). The carbon dots in aqueous solution are brightly fluorescent, with the emission colors dependent on the excitation wavelengths (Figure 2), which along with the broad fluorescence spectra suggests a distribution of emissive excited states. It is known in the literature that the fluorescence emissions of carbon dots could be quenched effectively with either electron donors or acceptors, supporting the notion that the redox characteristics in the photoexcited states of carbon dots are responsible for their observed photocatalytic activities.[11,21,22] The same characteristics were exploited in this study for their visible-light-activated bactericidal functions.

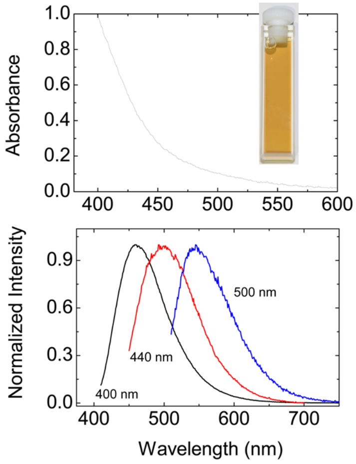

Figure 2. Top: Absorption spectrum of the EDA carbon dots in an aqueous solution (photograph in the inset). Bottom: Fluorescence spectra of the EDA carbon dots in an aqueous solution excited at the indicated wavelengths.

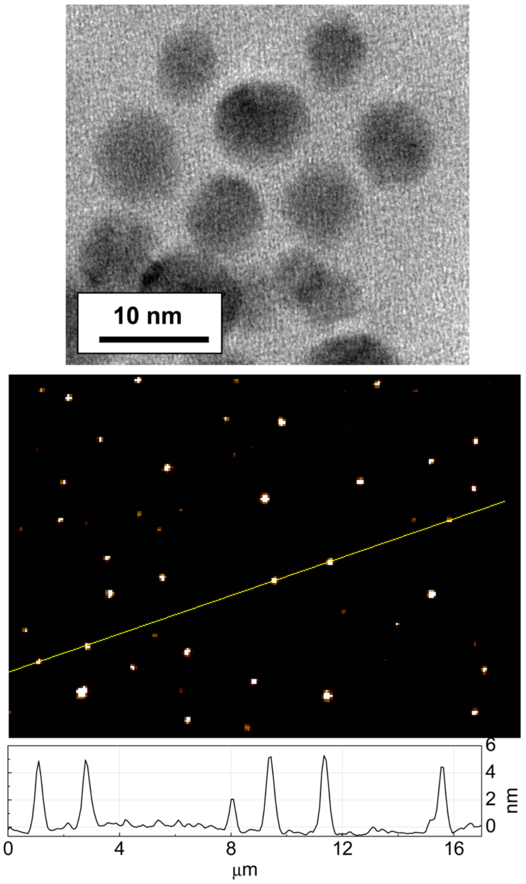

Figure 3. TEM (top) and AFM (bottom) images of the EDA carbon dots on commercial TEM grid and mica, respectively.

E. coli (K12) cells were used in the experiments to evaluate the antibacterial activities of photoexcited carbon dots, with the cell growth measurements based on the optical density (OD) at 600 nm (OD600) and/or the viable cell number determined by the plating method. Experimentally, the *E. coli* cells were inoculated in a 12-well plate at 0.2 OD/mL per well, treated with the EDA carbon dots of different concentrations, and exposed to ambient light for an hour in a safety cabinet. Then, the plate was incubated for 21 h, followed by the measurement of OD600. As shown in Figure 4, the results clearly suggest that there were substantial effects of the EDA carbon dots with light exposure on the *E. coli* cells. In the literature, there was a report on some antibacterial activities of the carbon dots obtained from carbonization of glucose and poly(ethylenimine), with the dots quaternized with benzyl bromide before bacteria experiments.[23] While no deliberate light exposure was mentioned in that report, the ambient experimental conditions could have contributed to the reported observations.

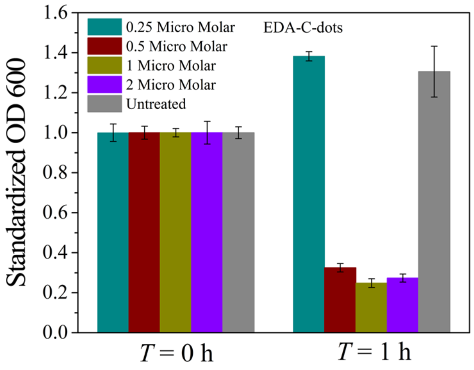

Figure 4. Photoinduced bacteria inactivation measured by OD600 for the EDA carbon dots (presented as mean ± standard deviation of quadruplicate experimental results).

Similarly, the *E. coli* cells in aqueous suspension were mixed with an aqueous solution of EDA carbon dots, and the resulting mixture containing ~10^7 colony-forming units per milliliter (CFU/mL) *E. coli* was incubated for 30 min at room temperature under visible-light illumination (12 V, 36 W bulb in a light box) or in the dark as the control. Then, the growth of *E. coli* cells after treatment with and without light exposure was monitored. Shown in Figure 5 are the growth curves of *E. coil* in a brain heart infusion medium post-treatment with EDA carbon dots, along with the control (untreated cells), based on OD measurements at 595 nm (OD595). The treated cells exhibited much prolonged lag phases (7−8 h) compared to the control, indicating that the EDA carbon dots inhibited/inactivated the growth of bacterial cells. The effect was somewhat more pronounced (the lag phase was longer by 1 h) when the treatment included exposure to visible light (Figure 5), but the light versus dark inhibition difference was not as obvious as that shown in Figure 4 (for which the experiments were performed in different laboratories at different times). Therefore, to address the inconsistency issue at the quantitative level for the OD measurement method, separate experiments with the same parameters and conditions were performed for the inhibition effect probed by the more quantitative method of determining the viable cell numbers post-treatment.

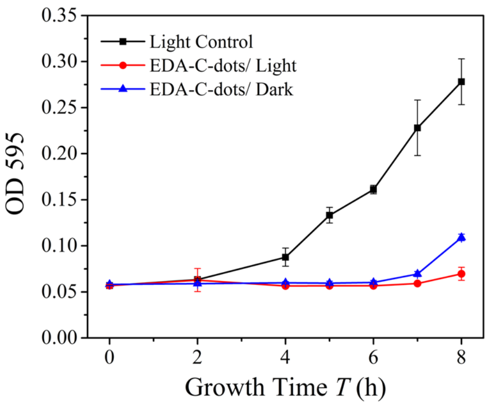

Figure 5. Growth curves of *E. coli* cells post-treatment with the EDA carbon dots for 30 min with or without light, in terms of measuring the OD595 values.

Again the samples of *E. coli* with and without (control) carbon dots were treated in the light box or in the dark for 30 min. The viable cell numbers in the treated samples were determined, and according to the results (Figure 6), the EDA carbon dots treatment coupled with visible-light illumination was obviously effective for bacteria killing, with about 4 logs of *E. coli* cells killed. Compared to the results shown in Figure 4, the bacteria-killing effect seemed more dramatic in these experiments. A significant contributing factor might be the use of a lamp instead of ambient light for the photoexcitation of carbon dots, although more systematic and quantitative experiments are needed in further investigation. Nevertheless, the results are all consistent in terms of confirming the visible-light-activated bactericidal functions of EDA carbon dots.

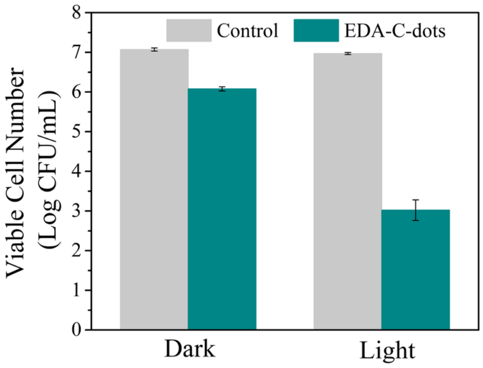

Figure 6. Reductions in the viable cell number after *E. coli* cells were treated with the EDA carbon dots for 30 min with or without light (presented as mean ± standard deviation of triplicate experimental results, and the data were also analyzed using the Student *t* test with $P < 0.05$ as a significant difference; see also Supporting Information).

A different experimental configuration was employed for further evaluation on the bactericidal activities of EDA carbon dots, in which the dots were plated on the trypticase soy agar (TSA) plates with bacteria cells during visible-light exposure. In a typical experiment, an *E. coli* (TOP10) suspension of 1.3 × 10^3 CFU/mL concentration was mixed with an aqueous solution of EDA carbon dots, and the mixture was spread onto the TSA plates. Upon exposure of the plates to visible light (Osram Sylvania LED A19 lamp, ~10 mW/cm^2) for up to 6 h, there were obvious differences between the treated plate and controls (Figure 7), again suggesting a substantial bactericidal effect of carbon dots with visible-light illumination. The plates were read for CFU counts, and according to the results, the

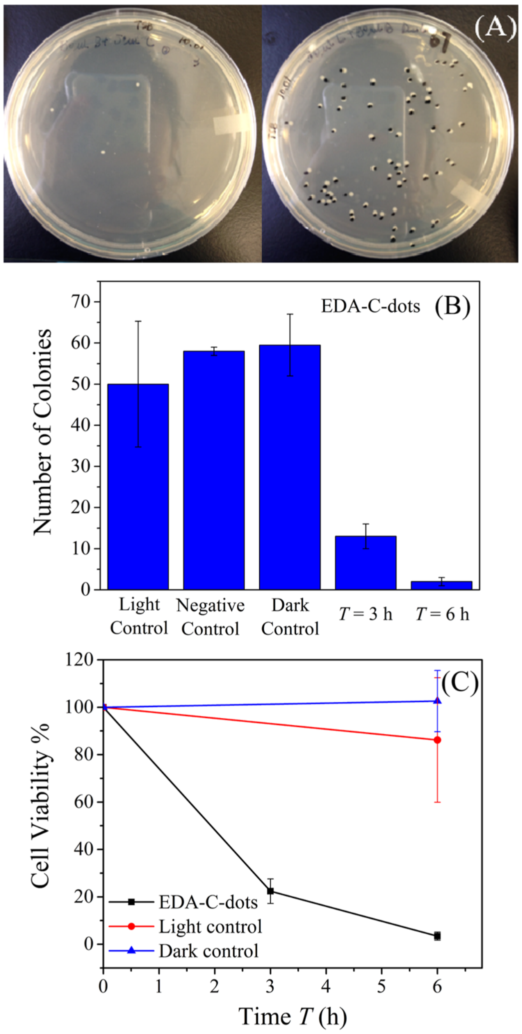

Figure 7. Photoinduced bacteria inactivation by the EDA carbon dots: (A) photographs showing colonies on TSA plates (left, 6 h treatment; right, dark control); (B) *E. coli* colony numbers; (C) cell viability ratio. The carbon dots were presented in the dark control.

photoexcited carbon dots were very effective in inactivating the growth of bacteria cells (Figure 7).

The results presented above, which were obtained in different laboratories of the participating research groups under various experimental settings, provide consistent and unambiguous evidence for the highly effective bactericidal functions of carbon dots under visible-light illumination, including even the common household lighting conditions. Mechanistically, carbon dots have been demonstrated for photodynamic effects on cancer cells,[24,25] and similar effects on bacterial cells might be a logical extension. The current mechanistic framework for the known optical properties of carbon dots is such that upon photoexcitation there are efficient charge separations for the formation of radical anions and cations (electrons and holes in a somewhat different description), which are "trapped" at various passivated surface sites. The radiative recombination of redox pairs is responsible for the observed fluorescence emissions, with their associated emissive excited states of lifetimes on the order of a few nanoseconds.[26−28] The redox species and emissive excited states could, in principle, be responsible for the observed bactericidal functions. However, in the fluorescence decay measurements, the rise time for the fluorescence was generally within the instrumental response function (1 ns or less), suggesting rather fast radiative recombination and short lifetimes of the radical-ion species. Therefore, the emissive excited states are more likely responsible for the photodynamic effects.

There have been no reports in the literature that explicitly describe the apparently effective bactericidal functions of photoexcited carbon dots. As related, there have been a few studies of using "graphene quantum dots" as photodynamic agents.[9,29,30] In the study by Ristic et al.,[9] antibacterial activities were observed with 470 nm light irradiation of the graphene quantum dots obtained from the electrochemical method. Those dots are essentially graphitic nanoparticles, which share optical properties similar to those of the precursor carbon nanoparticles for carbon dots.[16] However, the surface passivation of the carbon nanoparticles in carbon dots (or similarly in surface-passivated graphene quantum dots) substantially improves the optical properties, as is often reflected in the much enhanced fluorescence emissions.[11,16,17] Because the emissive excited states are likely responsible for the observed bactericidal functions, carbon dots with the more effective surface passivation and correspondingly more fluorescence are likely more desirable in serving as visible-light-activated bactericidal agents for a variety of bacteria control applications. In further investigations, steady-state and kinetic studies that correlate the optical properties of carbon dots, such as different fluorescence quantum yields and average lifetimes at various emission colors, with their antibacterial performance will be pursued.

CONCLUSION

The results obtained in this work, while somewhat more qualitative than quantitative in some of the experiments, demonstrate unambiguously that carbon dots can readily be activated by visible light (or even under ambient room lighting conditions) for significant bactericidal functions. The light sensitivity of carbon dots is apparently rather high to the degree that would require unusually stringent experimental conditions for the dark control, an issue (such as that in Figure 5) to be examined more closely and quantitatively in further investigations, although the determination of viable cell numbers (Figure 6) should remain a more favorable method in general. Also investigated will be the issues important to the quantification of the light-activated biocidal functions, including their correlations with the properties of carbon dots in various structural and surface configurations.

EXPERIMENTAL SECTION

Materials. Carbon nanopowder (purity >99%) and 2,2′-(ethylenedioxy)bis(ethylamine) (EDA) were purchased from Sigma-Aldrich. Thionyl chloride (>99%) was obtained from Alfa Aesar and nitric acid from VWR. Dialysis membrane tubing of various cutoff molecular weights was supplied by Spectrum Laboratories. Water was deionized and purified by being passed through a Labconco WaterPros water purification system.

Measurement. Baxter Megafuge (model 2630), Eppendorf (model 5417 R), and Beckman-Coulter (Optima L90K with a type 90 Ti fixed-angle rotor) ultracentrifuges were used for centrifugation at various g values. Optical absorption spectra were recorded on a Shimadzu UB2501-PC spectrophotometer. Fluorescence spectra were measured on a Jobin-Yvon emission spectrometer equipped with a 450 W xenon excitation source, Gemini-180 excitation and Tirax-550 emission monochromators, and a Hamamatsu R928P PMT photoncounting detector operated at 950 V. AFM images were acquired in the acoustic AC mode on a Molecular Imaging PicoPlus AFM system equipped with a multipurpose scanner and a NanoWorld point probe NCH sensor. Height profile analysis was assisted by using the *SjPIP* software distributed by Image Metrology. TEM images were obtained on a Hitachi H9500 high-resolution TEM system.

Carbon Dots. For carbon nanoparticles as the precursors for carbon dots, an as-supplied carbon nanopowder sample (1 g) was refluxed in an aqueous nitric acid solution (5 M, 90 mL) for 48 h. The reaction mixture was cooled to ambient temperature and then dialyzed against fresh water for up to 3 days. The postdialysis mixture was centrifuged at 1000*g* to retain the supernatant, followed by the removal of water to obtain the desired carbon nanoparticle sample.

In the synthesis of EDA carbon dots using a previously reported procedure,[19] the carbon nanoparticle sample obtained from the processing above was refluxed in neat thionyl chloride for 12 h, followed by the removal of excess thionyl chloride under nitrogen. The post-treatment carbon nanoparticle sample (50 mg) was mixed well with carefully dried EDA (500 mg) in a flask, heated to 120 °C, and stirred vigorously under nitrogen protection for 3 days. The reaction mixture was cooled to ambient temperature, dispersed in water, and then centrifuged at 20000*g* to retain the dark supernatant as an aqueous solution of the as-synthesized sample. The solution was dialyzed in membrane tubing (cutoff molecular weight ~500) against fresh water to remove free EDA and other impurities to obtain the EDA carbon dots in aqueous solution. For microscopy characterization only, the EDA carbon dots were very lightly coated with gold by visible-light irradiation of the solution with $HAuCl_4$ for a few minutes.[31]

Light-Activated Bactericidal Functions. For one set of experiments, *E. coli* (K12) cells were cultured in fresh nutrient broth overnight, and OD600 values of these cultures were measured and then standardized to 1 OD/mL. The bacteria suspension at 0.2 OD/mL per well was inoculated in a 12-well plate. Four treatment groups with different concentrations of carbon dots at 0.25, 0.50, 1, and 2 μM were exposed under light in a safety cabinet for T = 0, 15, 30, and 60 min, respectively. Then, the 12-well plate was incubated at 37 °C for 21 h. The OD600 value of each well was recorded, and the readings were standardized to that of the T = 0 control plate.

For another set of experiments, fresh grown *E. coli* (K12) cells in nutrient broth (Fisher Scientific, Pittsburgh, PA) were washed three times and then resuspended in deionized water. With the use of 96-well plates, to a well was added a bacteria−carbon dots mixture (150 μL), in which the bacteria concentration was fixed at 1.0×10^6 CFU/mL and the concentration of carbon dots was varied (triplicate for each concentration). The plates were either exposed to visible light (12 V, 36 W light bulb) or kept in the dark for 30 min. The solutions in the wells were then transferred to 1.5 mL centrifuge tubes, followed by centrifugation at 8000 rpm for 5 min. The supernatants were discarded, and the bacterial pellets were washed twice with deionized water. The cells were resuspended in 500 μL of nutrient broth, with 150 μL distributed into the wells of a 96-well plate for incubation at 37 °C. The growth of carbon-dot-treated bacterial cells and untreated cells (as controls) were monitored by measuring the OD595 values at various time points on a Spectra Max M5 spectrophotometer (Molecular Devices, LLC, Sunnyvale, CA).

For the viable cell number determination by using the traditional plating method, the suspended *E. coli* cells post-treatment with various concentrations of carbon dots were centrifuged and washed twice. The cells were resuspended in phosphate-buffered saline (PBS), and a series of dilutions were made with PBS. Aliquots of 100 μL appropriate dilutions were surface-plated on Luria−Bertani agar plates (Fisher Scientific, Pittsburgh, PA), and the plates were incubated at 37 °C for 24 h. The number of colonies was counted, and the viable cell numbers of the treated samples and controls were calculated in colony-forming units per milliliter.

In the use of the direct plating method for evaluation of the light-activated bactericidal functions, an *E. coli* (TOP10) stock culture was activated in fresh tryptic soy broth at 37 °C overnight. The bacteria culture (1 mL) was washed twice by a combination of centrifuging at 4000 rpm and resuspending in sterile PBS. The resulting cell suspension was 10-fold serially diluted in PBS. For detection of the cell concentration, aliquots of 100 μL dilutions were plated onto TSA plates and incubated at 37 °C overnight before counting. Separately, the *E. coli* suspension (50 μL) at a concentration of 1.3×10^3 CFU/mL was mixed with aqueous solution of EDA carbon dots (50 μL) at a concentration of 1 mg/mL. The mixture was then plated onto TSA plates, which were exposed to LED light (Osram Sylvania LED A19 lamp, ~10 mW/cm^2) for up to 6 h, along with the dark control (without light exposure), light control (without carbon dots), and negative control (without carbon dots and light). The carbon-dot-treated plates with light exposure and all control plates were incubated at 37 °C for 24 h before counting to determine the viable cell numbers.

All experiments were performed in triplicate or more. Statistical analysis of the experimental results was performed using the Student *t* test, with $P < 0.05$ considered as a significant difference.

■ ASSOCIATED CONTENT

Supporting Information

The Supporting Information is available free of charge on the ACS Publications website at DOI: 10.1021/acsami.6b01765.

> Available experimental results for the visible-light-activated bactericidal effect of carbon dots on two other bacteria (Gram-positive and Gram-negative) (PDF)

■ AUTHOR INFORMATION

Corresponding Authors

*E-mail: zhaoy@physast.uga.edu.
*E-mail: lyang@nccu.edu.
*E-mail: ratripp@uga.edu.
*E-mail: syaping@clemson.edu.

Author Contributions

‖Authors contributed equally.

Notes

The authors declare no competing financial interest.

■ ACKNOWLEDGMENTS

The authors thank Dr. Rene Alvarez and Dr. Kranti Yemmireddy for their help throughout the project. Financial support from NIH Grant R15GM114752 (to L.Y. and Y.-P.S.) and Agriculture and Food Research Initiative Grant 2011-68003-30012 by the USDA National Institute of Food and Agriculture (to L.Z. and Y.Z.) is gratefully acknowledged. M.J.M. was a visiting faculty on leave from Department of Natural Sciences, Northwest Missouri State University, with support provided by the NSF and South Carolina Space Grant Consortium.

■ REFERENCES

(1) Rodriguez-Rojas, A.; Rodriguez-Beltran, J.; Couce, A.; Blazquez, J. Antibiotics and Antibiotic Resistance: A Bitter Fight Against Evolution. *Int. J. Med. Microbiol.* **2013**, *303*, 293−297.

(2) Laxminarayan, R.; Duse, A.; Wattal, C.; Zaidi, A. K. M.; Wertheim, H. F.; Sumpradit, N.; Vlieghe, E.; Hara, G. L.; Gould, I. M.; Goossens, H.; Greko, S.; So, A. D.; Bigdeli, M.; Tomson, G.; Woodhouse, W.; Ombaka, E.; Peralta, A. Q.; Qamar, F. N.; Mir, F.; Kariuki, S.; Bhutta, Z. A.; Coates, A.; Bergstrom, R.; Wright, G. D.; Brown, E. D.; Cars, O. Antibiotic Resistance − The Need for Global Solutions. *Lancet Infect. Dis.* **2013**, *13*, 1057−1098.

(3) Liou, J. W.; Chang, H. H. Bactericidal Effects and Mechanisms of Visible Light-Responsive Titanium Dioxide Photocatalysts on Pathogenic Bacteria. *Arch. Immunol. Ther. Exp.* **2012**, *60*, 267−275.

(4) Cheng, C. L.; Sun, D. S.; Chu, W. C.; Tseng, Y. H.; Ho, H. C.; Wang, J. B.; Chung, P. H.; Chen, J. H.; Tsai, P. J.; Lin, N. T.; Yu, M. S.; Chang, H. H. The Effects of the Bacterial Interaction with Visible-Light Responsive Titania Photocatalyst on the Bactericidal Performance. *J. Biomed. Sci.* **2009**, *16*, 7.

(5) Chen, Y. L.; Chen, Y. S.; Chan, H.; Tseng, Y. H.; Yang, S. R.; Tsai, H. Y.; Liu, H. Y.; Sun, D. S.; Chang, H. H. The Use of Nanoscale Visible Light-Responsive Photocatalyst TiO2-Pt for the Elimination of Soil-Borne Pathogens. *PLoS One* **2012**, *7*, e31212.

(6) Anehosur, G. V.; Kulkarni, R. D.; Naik, M. G.; Nadiger, R. K. Synthesis and Determination of Antimicrobial Activity of Visible Light Activated TiO_2 Nanoparticles with Polymethyl Methacrylate Denture Base Resin Against Staphylococcus Aureus. *J. Gerontol Geriat. Res.* **2012**, *1*, 1000103.

(7) Foster, H. A.; Ditta, I. B.; Varghese, S.; Steele, A. Photocatalytic Disinfection Using Titanium Dioxide: Spectrum and Mechanism of Antimicrobial Activity. *Appl. Microbiol. Biotechnol.* **2011**, *90*, 1847−1868.

(8) Applerot, G.; Lipovsky, A.; Dror, R.; Perkas, N.; Nitzan, Y.; Lubart, R.; Gedanken, A. Enhanced Antibacterial Activity of Nanocrystalline ZnO Due to Increased ROS-Mediated Cell Injury. *Adv. Funct. Mater.* **2009**, *19*, 842−852.

(9) Ristic, B. Z.; Milenkovic, M. M.; Dakic, I. R.; Todorovic-Markovic, B. M.; Milosavljevic, M. S.; Budimir, M. D.; Paunovic, V. G.; Dramicanin, M. D.; Markovic, Z. M.; Trajkovic, V. S. Photodynamic Antibacterial Effect of Graphene Quantum Dots. *Biomaterials* **2014**, *35*, 4428−4435.

(10) Sun, Y.-P.; Zhou, B.; Lin, Y.; Wang, W.; Fernando, K. A. S.; Pathak, P.; Meziani, M. J.; Harruff, B. A.; Wang, X.; Wang, H.; Luo, P. G.; Yang, H.; Kose, M. E.; Chen, B.; Veca, L. M.; Xie, S.-Y. Quantum-Sized Carbon Dots for Bright and Colorful Photoluminescence. *J. Am. Chem. Soc.* **2006**, *128*, 7756−7757.

(11) Luo, P. G.; Sonkar, S. K.; Yang, S.-T.; Yang, F.; Yang, L.; Broglie, J. J.; Liu, Y.; Sun, Y.-P. Carbon-Based Quantum Dots for Fluorescence Imaging of Cells and Tissues. *RSC Adv.* **2014**, *4*, 10791−10807.

(12) Wang, Y.; Hu, A. Carbon Quantum Dots: Synthesis, Properties and Applications. *J. Mater. Chem. C* **2014**, *2*, 6921−6939.

(13) Lim, S. Y.; Shen, W.; Gao, Z. Carbon Quantum Dots and Their Applications. *Chem. Soc. Rev.* **2015**, *44*, 362−381.

(14) Miao, P.; Han, K.; Tang, Y.; Wang, B.; Lin, T.; Cheng, W. Recent Advances in Carbon Nanodots: Synthesis, Properties and Biomedical Applications. *Nanoscale* **2015**, *7*, 1586−1595.

(15) Zhao, A.; Chen, Z.; Zhao, C.; Gao, N.; Ren, J.; Qu, X. Recent Advances in Bioapplications of Carbon Dots. *Carbon* **2015**, *85*, 309−327.

(16) Cao, L.; Meziani, M. J.; Sahu, S.; Sun, Y.-P. Photoluminescent Properties of Graphene versus Other Carbon Nanomaterials. *Acc. Chem. Res.* **2013**, *46*, 171−180.

(17) Fernando, K. A. S.; Sahu, S.; Liu, Y.; Lewis, W. K.; Guliants, E. A.; Jafariyan, A.; Wang, P.; Bunker, C. E.; Sun, Y.-P. Carbon Quantum Dots and Applications in Photocatalytic Energy Conversion. *ACS Appl. Mater. Interfaces* **2015**, *7*, 8363−8376.

(18) Cao, L.; Sahu, S.; Anilkumar, P.; Bunker, C. E.; Xu, J.; Fernando, K. A. S.; Wang, P.; Guliants, E. A.; Tackett, K. N., II; Sun, Y.-P. Carbon Nanoparticles as Visible-Light Photocatalysts for Efficient CO_2 Conversion and Beyond. *J. Am. Chem. Soc.* **2011**, *133*, 4754−4757.

(19) LeCroy, G. E.; Sonkar, S. K.; Yang, F.; Veca, L. M.; Wang, P.; Tackett, K. N., II; Yu, J.-J.; Vasile, E.; Qian, H.; Liu, Y.; Luo, P. G.; Sun, Y.-P. Toward Structurally Defined Carbon Dots as Ultracompact Fluorescent Probes. *ACS Nano* **2014**, *8*, 4522−4529.

(20) Wang, Y.; Anilkumar, P.; Cao, L.; Liu, J.-H.; Luo, P. G.; Tackett, K. N.; Sahu, S.; Wang, P.; Wang, X.; Sun, Y.-P. Carbon Dots of Different Composition and Surface Functionalization: Cytotoxicity Issues Relevant to Fluorescence Cell Imaging. *Exp. Biol. Med.* **2011**, *236*, 1231−1238.

(21) Wang, X.; Cao, L.; Lu, F.; Meziani, M. J.; Li, H.; Qi, G.; Zhou, B.; Harruff, B. A.; Sun, Y.-P.; Kermarrec, F. Photoinduced Electron Transfer with Carbon Dots. *Chem. Commun.* **2009**, 3774−3776.

(22) Zhang, H.; Huang, H.; Ming, H.; Li, H.; Zhang, L.; Liu, Y.; Kang, Z. Carbon Quantum Dots/Ag_3PO_4 Complex Photocatalysts with Enhanced Photocatalytic Activity and Stability Under Visible Light. *J. Mater. Chem.* **2012**, *22*, 10501−10506.

(23) Dou, Q.; Fang, X.; Jiang, S.; Chee, P. L.; Lee, T.-C.; Loh, X. J. Multi-Functional Fluorescent Carbon Dots with Antibacterial and Gene Delivery Properties. *RSC Adv.* **2015**, *5*, 46817−46822.

(24) Kleinauskas, A.; Rocha, S.; Sahu, S.; Sun, Y.-P.; Juzenas, P. Carbon-Core Silver-Shell Nanodots as Sensitizers for Phototherapy and Radiotherapy. *Nanotechnology* **2013**, *24*, 325103.

(25) Juzenas, P.; Kleinauskas, A.; Luo, P. G.; Sun, Y.-P. Photoactivatable Carbon Nanodots for Cancer Therapy. *Appl. Phys. Lett.* **2013**, *103*, 063701.

(26) Wang, X.; Cao, L.; Yang, S.-T.; Lu, F.; Meziani, M. J.; Tian, L.; Sun, K. W.; Bloodgood, M. A.; Sun, Y.-P. Bandgap-Like Strong Fluorescence in Functionalized Carbon Nanoparticles. *Angew. Chem., Int. Ed.* **2010**, *49*, 5310−5314.

(27) Strauss, V.; Margraf, J. T.; Dolle, C.; Butz, B.; Nacken, T. J.; Walter, J.; Bauer, W.; Peukert, W.; Spiecker, E.; Clark, T.; Guldi, D. M. Carbon Nanodots: Toward a Comprehensive Understanding of Their Photoluminescence. *J. Am. Chem. Soc.* **2014**, *136*, 17308−17316.

(28) Wang, L.; Zhu, S.-J.; Wang, H.-Y.; Qu, S.-N; Zhang, Y.-L.; Zhang, J.-H.; Chen, Q.-D.; Xu, H.-L.; Han, W.; Yang, B.; Sun, H.-B. Common Origin of Green Luminescence in Carbon Nanodots and Graphene Quantum Dots. *ACS Nano* **2014**, *8*, 2541−2547.

(29) Markovic, Z. M.; Ristic, B. Z.; Arsikin, K. M.; Klisic, D. G.; Harhaji-Trajkovic, L. M.; Todorovic-Markovic, B. M.; Kepic, D. P.; Kravic-Stevovic, T. K.; Jovanovic, S. P.; Milenkovic, M. M.; Milivojevic, D. D.; Bumbasirevic, V. Z.; Dramicanin, M. D.; Trajkovic, V. S. Graphene Quantum Dots as Autophagy-Inducing Photodynamic Agents. *Biomaterials* **2012**, *33*, 7084−7092.

(30) Ge, J.; Lan, M.; Zhou, B.; Liu, W.; Guo, L.; Wang, H.; Jia, Q.; Niu, G.; Huang, X.; Zhou, H.; Meng, X.; Wang, P.; Lee, C.-S.; Zhang, W.; Han, X. A Graphene Quantum Dot Photodynamic Therapy Agent with High Singlet Oxygen Generation. *Nat. Commun.* **2014**, *5*, 4596.

(31) Xu, J.; Sahu, S.; Cao, L.; Bunker, C. E.; Peng, G.; Liu, Y.; Fernando, K. A. S.; Wang, P.; Guliants, E. A.; Meziani, M. J.; Qian, H.; Sun, Y.-P. Efficient Fluorescence Quenching in Carbon Dots by Surface-Doped Metals - Disruption of Excited State Redox Processes and Mechanistic Implications. *Langmuir* **2012**, *28*, 16141−16147.

RSC Advances

PAPER

View Article Online
View Journal | View Issue

Cite this: *RSC Adv.*, 2015, **5**, 91246

Carbon nanotube-assisted capturing of bacterial pathogens

Shengyuan Wang,[a] Gregory E. LeCroy,[b] Fan Yang,[b] Xiuli Dong,[a] Ya-Ping Sun*[b] and Liju Yang*[a]

Received 18th August 2015
Accepted 20th October 2015

DOI: 10.1039/c5ra16684e

www.rsc.org/advances

This study explored the use of co-polymer poly(propionylethyleneimine-*co*-ethyleneimine (PPEI-EI) functionalized multi-walled carbon nanotubes (MWNTs) as a coating material on filters for capturing of bacterial pathogens from aqueous solutions. Polycarbonate membranes with pore sizes of 1.2 and 3.0 μm were coated with different PPEI-EI-MWNTs and cross-linked PPEI-EI-MWNTs samples at various coating densities, and then evaluated for capturing of *E. coli* cells at flow rates of 0.25 and 0.5 mL min^{-1}. With a good combination of PPEI-EI-MWNTs sample, coating density, appropriate filter pore size and flow rate, a capture efficiency of higher than 4 log (up to 6 log or larger) of bacterial cells was achieved. The filters coated with the cross-linked PPEI-EI-MWNTs were unexpectedly less efficient than those with the other PPEI-EI-MWNTs samples, likely due to the poorer dispersibility of the cross-linked sample and consequently the less homogeneous coating on filters. The results of this study demonstrated the feasibility of PPEI-EI-MWNTs as a coating material on filters for highly effective capturing of bacterial pathogens, and also presented both challenges and opportunities for further investigations in controlling the coating material synthesis to improve performance in capturing bacterial cells.

Introduction

Foodborne illness is recognized as a common and costly public health problem around the world. The Centers for Disease Control and Prevention (CDC) estimates that, in the United States alone, each year, foodborne outbreaks cause sickness in 48 million people, accounting for 128 000 hospitalizations and 3000 deaths.[1] A variety of foodborne pathogens, including bacteria, viruses, and parasites, have been known for causing more than 250 different foodborne diseases.[1] However, these foodborne diseases are preventable through effective strategies for pathogen detection, isolation/removal, or inactivation. A major challenge for both preventing and responding to the contamination of pathogens is that the numbers of the pathogens in most food and related samples are relatively low, so that their isolation and concentration are necessary to enable rapid detection and analyses. In the technological development for such a purpose, there have been some significant advances in new or improved methods for capturing and concentrating pathogens, such as microfluidic filtration, nanoparticle-based immuno-separation, and isoelectric focusing.[2–7] Membrane-based separation represents a class of methods that can be incorporated into a range of devices for the isolation or concentrating of pathogens for subsequent detection.[8–10] In practice, these methods are still challenged in dealing with multiple pathogens in various matrices in addition to other technical issues, therefore new approaches for effective yet low-cost methods are in demand.

The development of nanotechnology and its successful integration with biotechnology offer excellent opportunities in addressing the pathogen isolation or concentrating issues. In this regard, carbon nanotubes (CNTs) have been shown as being particularly promising.[11,12] CNTs are well-ordered, hollow carbon fibers with a high aspect ratio [lengths from several hundred nanometers to several micrometers; diameters of 0.4–2 nm for single-walled carbon nanotubes (SWNTs), and 2–30 nm for coaxial multiple-walled carbon nanotubes (MWNTs)].[13] CNTs possess remarkable properties that have been explored for a wide range of biological applications.[14,15] Particularly, research results obtained in our laboratories and by others have demonstrated two major promising properties of CNTs that are applicable in the microbiology field: the high absorptivity for removing biological contaminants and the strong antimicrobial activity for inactivation of bacterial cells. These properties have afforded CNTs the potential to make important advancements in dealing with foodborne bacterial pathogens. Especially, their microbial absorption capacities are proven to be higher than any other commercially available adsorbent media.[16]

CNTs are insoluble, which makes their dispersion and processing a major challenge.[17] The chemical modification or

---

[a] *Biomanufacturing Research Institute and Technology Enterprises (BRITE), Department of Pharmaceutical Sciences, North Carolina Central University, Durham, NC 27707, USA. E-mail: lyang@nccu.edu; Tel: +1-919-530-6704*

[b] *Department of Chemistry and Laboratory for Emerging Materials and Technology, Clemson University, Clemson, SC 29634, USA. E-mail: syaping@clemson.edu; Tel: +1-864-5026*

functionalization has become an effective strategy in the solubilization and dispersion of CNTs for various purposes.[11,18,19] For example, it has been demonstrated that CNTs could be functionalized covalently or non-covalently with a series of biologically significant oligomers or polymers,[11,20–22] including poly(ethylene glycol) (or PEG), proteins (bovine serum albumin or BSA) for further conjugation with antibody[23,24] to target specific pathogens,[25,26] and various carbohydrates for cell adhesion and related applications.[23–25,27–35] The surface functional moieties coupled with the intrinsic high absorptivity of CNTs have found these functionalized nanotube samples in applications such as the removal, concentration and/or detection of pathogens.[33,35]

In the work reported here, we designed and synthesized several configurations of polymer functionalized MWNTs, and used them in the coating of filters for their capturing of bacterial cells. We used an inexpensive co-polymer poly(propionylethyleneimine-*co*-ethyleneimine (PPEI-EI) for the nanotube functionalization. The variations in the functionalized MWNT samples included PPEI-EI of two different molecular weights (5000 and 50 000), different functionalization chemistries and processing conditions (amidation and thermochemical methods), and different post-functionalization sample selections (gravimetric fractionation and cross-linking to yield samples containing networked species for more filter-coating options). We evaluated the efficiencies of filters coated with different PPEI-EI-MWNTs samples and also cross-linked PPEI-EI-MWNTs samples for capturing of *Escherichia coli* K12 cells, from which the results confirmed the feasibility of using polymer-functionalized CNTs in the development of rapid, low-cost, and efficient methods for capturing/isolation of pathogens.

Experimental

Materials

The multiple-walled carbon nanotube (MWNT, 95% purity, 10–20 nm in diameter and ~15 μm in average length) sample was supplied by Nanostructured and Amorphous Materials, Inc, and poly(2-ethyl-2-oxazoline) (PPEI, average $M_W \sim 5000$ and 50 000) from Polysciences, Inc. Nitric acid (70%) and chloroform (99.9%) were purchased from Fisher Scientific, hydrochloric acid (38%) from EMD, sodium hydroxide (98%) from Sigma Aldrich, thionyl chloride (99%) from Alfa Aesar, and methanol (99.8%) from Mallinckrodt Chemicals. Deuterated chloroform with TMS internal standard for NMR measurements was acquired from Cambridge Isotope Laboratories. Dialysis membrane tubing was obtained from Spectrum Laboratories. Water was deionized and purified by being passed through a Labconco WaterPros water purification system.

Measurements

Desktop centrifuges (Fisher Scientific Model 228 and Eppendorf Centrifuge 5417R) and sonicator (VWR Model 250D) were used in purification and functionalization experiments. Thermal gravimetric analysis (TGA) was performed on a TA Instruments SDT-Q600 system. NMR measurements were carried out on a Bruker Avance 500 spectrometer. Scanning electron microscopic (SEM) images were taken using the FEI XL30 microscope (Netherlands) at the Shared Materials and Instrumentations Facility (SMIF) at Duke University. Uncoated filters and PPEI-EI-MWNTs coated filters with and without bacterial filtration were examined under SEM to determine the distribution of PPEI-EI-MWNTs on the filters and the interactions between bacterial cells and the coated filters. For filters with bacterial cells, the cells were first fixed in bacterial fixative (4% formaldehyde and 2% glutaraldehyde in 1× PBS) for 6 h at room temperature. After washing with DI water, the samples were air dried. Filters without bacterial cells did not need the fixing step. Before SEM imaging, all filters were coated with gold using Denton Vacuum Desk IV (Czech Republic) as previously described.[36]

PPEI-EI-MWNT

The as-supplied MWNT sample was purified to remove carbon impurities and catalysts by following a protocol reported previously.[27] Briefly, the sample (1 g) was refluxed in aqueous nitric acid (2.6 M, 200 mL) for 48 h, followed by centrifugation and washing repeatedly with deionized water to retain the residue and then drying under vacuum. The PPEI polymer with M_W of either 5000 or 50 000 was partially hydrolyzed to obtain random copolymer poly(propionylethylenimine-*co*-ethylenimine) (PPEI-EI).[37] In a typical reaction, PPEI (5 g) was dissolved in methanol (15 mL), and the solution was transferred to deionized water (250 mL), followed by evaporation to remove methanol. To the resulting aqueous dispersion of the polymer was added aqueous HCl (1 M, 2 mL), and the acidified dispersion was refluxed with stirring for 12 h. The reaction mixture was cooled to ambient, and then aqueous NaOH (1 M) was added to adjust pH to ~10. The mixture was concentrated by removing water and extracted with chloroform to obtain PPEI-EI. The copolymer was further purified by repeated precipitation from the concentrated chloroform solution into hexanes. Upon the removal of solvents and drying in vacuum at 50 °C, PPEI-EI was recovered as a glassy solid sample. ^{1}H NMR (500 MHz, $CDCl_3$) δ 3.45 (broad, $NC\mathbf{H_2}$), 2.78 (broad, $NHC\mathbf{H_2}$), 2.4 (broad, $CO\mathbf{CH_2}CH_3$), 1.12 (broad, $COCH_2\mathbf{CH_3}$) ppm. The NMR signal integrations were used to estimate the EI fraction in PPEI-EI, which was generally 15–20% among different precursor PPEI samples and different batches.

MWNTs were functionalized with PPEI-EI under classical amidation reaction conditions.[27,38] In a typical experiment, the purified MWNT sample (50 mg) was acylated by refluxing in neat thionyl chloride for 12 h. Upon removal of excess thionyl chloride, the acylated nanotubes were mixed with carefully dried PPEI-EI (500 mg), heated to 200 °C, and vigorously stirred under nitrogen for 72 h. The reaction mixture was cooled to ambient, and extracted with water for the PPEI-EI-functionalized MWNTs (PPEI-EI-MWNT) in an aqueous dispersion. Cross-linking of the functionalized nanotubes was performed by hydrothermal processing in a sealed reactor.

PPEI-EI-MCNT coated filters

In the coating of commercially supplied membrane filters, a selected PPEI-EI-MCNT sample in aqueous dispersion was diluted with deionized water to the desired concentration. Aliquots of 450 μL of the aqueous dispersed nanotube sample at different concentrations were deposited on either 3.0 μm pore sized TSTP hydrophilic polycarbonate membranes or 1.2 μm pore sized RTTP hydrophilic polycarbonate membranes (both membranes of a diameter of 25 mm) (EMD Millipore, Billerica, MA) to attain a PPEI-EI-MWNT loading ranging from 0.095 μg mm^{-2} to 1.25 μg mm^{-2} on the base filter. The filter membranes were held in a filter holder (EMD Millipore, Billerica, MA), and were dried in a fume hood overnight.

Bacteria culture

Escherichia coli K12 was grown in 10 mL nutrient broth by inoculating the broth with a single colony of a plated culture on a Luria–Bertani (LB) agar plate, and incubated overnight at 37 °C to reach 10^8 CFU mL^{-1} to 10^9 CFU mL^{-1}. The actual bacterial cell concentration was determined by the traditional surface plating of appropriate serial dilutions on LB agar plates. The plates were incubated at 37 °C overnight, and the colonies were counted to calculate the bacterial cell concentration in the original culture as colony forming unit per milliliter (CFU mL^{-1}). For the use in further filtration experiments, *E. coli* cells were diluted with DI water to a concentration of $\sim 2.5 \times 10^6$ CFU mL^{-1}.

Bacterial sample filtration

Aliquots of 2.5 mL *E. coli* suspension in DI water were filtered by uncoated and PPEI-EI-MWNT coated filters through a syringe and a syringe pump (Harvard Apparatus PHD 2000 Infuse/Withdraw) with flow rate at 0.5 mL min^{-1} or 0.25 mL min^{-1}. Filtrates were collected in centrifuge tubes, and *E. coli* concentrations in the filtrates were determined by the traditional surface plating with the same procedure described above. The reduction in logarithmic value of *E. coli* cell number before and filtration was used to determine the efficiency of various coated filters for bacterial capture.

Statistical analysis

Statistical analysis was performed using the Student's *t*-test. Differences were considered to be significant at the level of $P < 0.05$.

Results and discussion

MWNTs are in general difficult to be dispersed in water or other solvents, which limits their further processing or being incorporated into various devices such as the coated filters targeted in this study. A common approach for much improved dispersibility has been the functionalization of MWNTs with oligomeric and polymeric species.[38] The aminopolymer poly(propionylethylenimine-*co*-ethylenimine) (PPEI-EI, Scheme 1) was used for the functionalization. It is well-known that MWNTs purified in processing with oxidative acid such as nitric acid contain surface sites that are populated with carboxylic acid moieties.[27] These were targeted for the attachment of PPEI-EI in functionalization under classical amidation reaction conditions, where the EI moieties in PPEI-EI copolymers (Scheme 1) were used to form amide linkages to the nanotubes.[27] Beyond the desired dispersibility, the polymer functionalization could also improve the adhesion of the nanotubes to the membrane filters to be used for capturing bacterial cells in the filtration of the cell solution, and/or possibly influence the capture of bacterial cells by adjusting the molecular weight of the polymer. PPEI-EI copolymers of average molecular weight 5000 and 50 000 were used for the amidation reactions, yielding their functionalized MWNT samples denoted as PPEI-EI(5000)-MWNT and PPEI-EI(50 000)-MWNT, respectively.

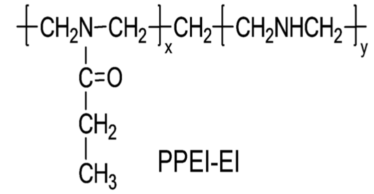

Scheme 1 Chemical structure of PPEI-EI.

The functionalized MWNTs were obtained in aqueous dispersions. The nanotube concentrations in the dispersions were determined by taking out accurately measured aliquots for the removal of water, drying, and then thermal gravimetric analysis (TGA). The TGA under inert gas purging allowed the selective removal of PPEI-EI, thus the determination of nanotube contents in the samples.[27,38] The concentrations used in this study are referred to the nanotube contents determined by TGA.

Commercially acquired hydrophilic polycarbonate filters were coated with the PPEI-EI-functionalized MWNTs, for which the protocol to evaluate the efficiency in capturing bacterial cells was based on the enumeration of viable cell number in the filtrate using the traditional surface plating method, with the results compared to those in unfiltered samples and/or those in filtrate using uncoated filters.

We first examined the effect of molecular weight of PPEI-EI on the bacterial capture efficiency by using PPEI-EI(5000)-MWNT and PPEI-EI(50 000)-MWNT samples to coat filters (3.0 μm pore size) for the purpose of capturing bacterial cells from solutions. Fig. 1 shows the efficiency of the coated filters for capturing of *E. coli* cells. The uncoated filters were unable to capture *E. coli* cells from solutions, as the cells were easily passing through the pores on the filters. The coating with PPEI-EI-MWNT enabled the filters to capture *E. coli* cells. The results indicated that the filters coated with PPEI-EI(5000)-MWNT were able to capture approximately 1.79 log of cells from a solution containing 1.88×10^6 CFU mL^{-1} *E. coli* cells, whereas those with PPEI-EI(50 000)-MWNT were somewhat less efficient, capturing approximately 0.91 log of cells. The ability of the coated filters to capture bacterial cells may be attributed to a combination of bacterial cells being physically blocked from

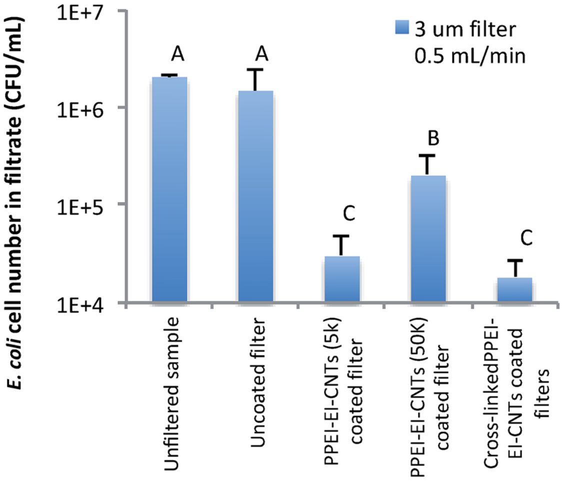

Fig. 1 The capture efficiencies of PPEI-EI(5000)-MWNTs, PPEI-EI(50 000)-MWNTs, and cross-linked PPEI-EI-MWNTs coated filters for the filtration of *E. coli* cells from aqueous solutions containing ~10^6 CFU mL^{-1} cells. Filters: polycarbonate, $d = 25$ mm, pore size 3.0 μm; both PPEI-EI-MWNT samples were coated on the filters at the same density of 1.01 μg mm^{-2}; flow rate: 0.5 mL min^{-1}. Statistical analysis was performed among all the samples, different letters on the columns indicate a statistical difference ($P < 0.05$), while the same letters indicate no statistical difference ($P > 0.05$).

passing through the pores and the known absorptivity of CNTs to bacterial cells.[39,40] The same combination of effects might also be responsible for the observed different efficiencies between filters coated with PPEI-EI(5000)-MWNT and PPEI-EI(50 000)-MWNT in capturing *E. coli* cells.

The pore sizes (3.0 μm) of the filters used in the experiments above were much larger than the average dimension of the *E. coli* cells, so that the observed retention of the cells on the coated filters must be due to the presence of the nanotube coating. The functionalized MWNTs were of a large aspect ratio, but the overall size profiles were not significantly larger than the filter pore sizes. It was assumed that a more desirable configuration for capturing bacterial cells might be for the functionalized MWNTs to form a network on top of the pores to reduce the effective pore sizes for the passing cells during the filtration and to facilitate more effective nanotube–cell interactions.

Therefore, the cross-linked PPEI-EI-MWNT samples (designed for such a purpose and prepared with a cross-linking protocol after the functionalization reaction) were used to coat the filters (3.0 μm) at the same density. These filters were evaluated by using the same experimental protocol in their capturing *E. coli* cells, and the results suggested significant capturing efficiency, with the best of 2.1 log (shown in Fig. 1), and down to 1.1 log, but still not meaningfully better than the filters coated with the nanotube samples without cross-linking.

SEM examination of PPEI-EI(5000)-MWNT, PPEI-EI(50 000)-MWNT found that the two nanotube samples appeared morphologically similar (Fig. 2A and B). However, the size profiles for individual functionalized carbon nanotubes in the two samples might still be different, and the different PPEI-EI molecular weights could also affect the way in their wrapping MWNTs and consequently the availability and nanoscale details of the exposed areas on the nanotubes (not wrapped by PPEI-EI), thus altering the absorptivity to bacterial cells, resulting in different efficiency for capturing bacteria on those coated filters. Fig. 2C shows a representative SEM image of a cross-linked sample, where less individual nanotubes and more conjugates with polymers can be seen. It is true that the cross-linked samples had poorer dispersibility, which made the coating more difficult and resulted in coated filters on which the distribution of the nanotubes was less homogeneous. And this is the likely cause of unimproved capture efficiency of filters coated with cross-linked samples.

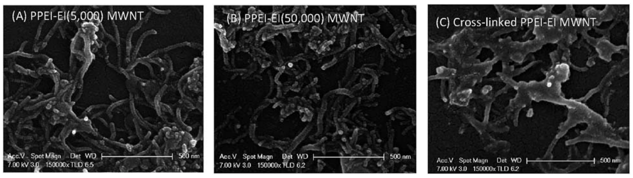

Fig. 2 SEM images of PPEI-EI co-polymer functionalized MWTs, (A) PPEI-EI(5000)-MWNTs, (B) PPEI-EI(50 000)-MWNTs, and (C) cross-linked PPEI-EI-MWNTs.

Based on the above results, filters coated with PPEI-EI(5000)-MWNTs and the cross-linked samples showed better capture efficiencies. Next, we examined the effect of reduced pore size of the filters on the coating for capturing of bacterial cells. Filters of a smaller pore size (1.2 μm) were coated with the PPEI-EI(5000) MWNT samples and the cross-linked samples, and the coated filters were examined for their capturing bacterial cells by filtration of *E. coli* suspensions containing 10^6 to 10^7 CFU mL^{-1} at a flow rate of 0.5 mL min^{-1}. Fig. 3 shows the efficiencies of capturing *E. coli* cells with these filters, along with the uncoated filters and the unfiltered suspensions as

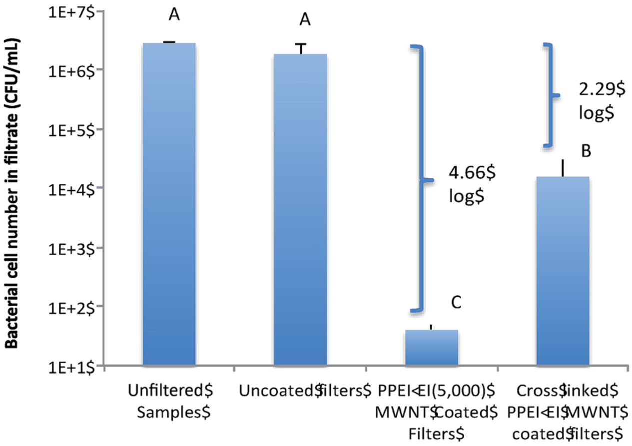

Fig. 3 The capture efficiencies of PPEI-EI-MWNTs and cross linked PPEI-EI-MWNTs coated filters for capturing of *E. coli* cells from aqueous solution containing ~10^6 CFU mL^{-1} cells. Filters: polycarbonate, $d = 25$ mm, pore size 1.2 μm; all PPEI-EI-MWNT samples were coated on the filters at the same density of 0.75 μg mm^{-2}. Statistical analysis was performed among all the samples, different letters on the columns indicate a statistical difference ($P < 0.05$), while the same letters indicate no statistical difference ($P > 0.05$).

controls. The uncoated filters were generally incapable of capturing bacterial cells, as the cell number in the filtrate was not significantly different from that in the unfiltered suspensions. Obviously, all PPEI-EI-MWNT-coated filters were able to retain a significant number of *E. coli* cells in general. The capturing efficiency was up to 4.66 log with a well-coated filter (Fig. 3).

However, the performance of the coated filters varied with the functionalized nanotube samples synthesized in different batches, which might be associated with slightly different material properties, especially in terms of solubility or dispersibility of the samples. These properties could affect the distribution of the nanotubes on the coated filters, resulting in somewhat different efficiencies in capturing bacterial cells, down to 2.73 log in the worst case, which were still significantly better than the coated filters of 3.0 μm pores. The results from the use of filters coated with the cross-linked sample were consistent with such an assessment, with the observed capturing efficiency up to 2.29 log as shown in Fig. 3, and down to 1.1 log in the worst case.

Since the cross-linked samples were more difficult to disperse, making the coating on the filters less homogeneous, as discussed above, the reduced pore size did not improve the coating homogeneity and the capturing efficiency. The microscopy imaging results were consistent with such an explanation as quite amount of large aggregates of cross-linked nanotubes were presented on the coated filter (Fig. 4A). The filters coated with PPEI-EI(5000)-MWNT were also examined directly under SEM, and representative results are shown in Fig. 4. On the PPEI-EI(5000) coated filters (Fig. 4B), the distribution of the functionalized MWNTs was not even, with small aggregates of the nanotubes found in some parts of the filter, and some pores, especially those adjunct pores, left uncovered in other parts of the filter. The uncoated hydrophilic polycarbonate filters clearly showed that the pores were distributed unevenly with some of them adjunct to each other, resulting in larger actual pore size (Fig. 4C). These observations present both challenges and opportunities for further investigations. The challenges would be to control the material synthesis for samples that are more compatible with the coating process for filters of more homogenous distribution of coated nanotubes, thus improved performance in capturing bacterial cells. On the other hand, the opportunities are such that there are still much room for improvements from the mostly proof-of-concept results in this study.

Similar SEM imaging conditions were applied to a direct examination on the coated filters with captured bacterial cells. Shown in Fig. 5 are representative SEM images of *E. coli* cells captured on PPEI-EI-MWNT-coated filters, which suggest that the functionalized MWNTs retained bacterial cells in several possible ways. For the first way, Fig. 5A indicates that *E. coli* cells could be trapped by their mostly sitting on top of the nanotubes, similar to what was observed in some previously reported studies on using CNTs coated filters for filtration of bacterial cells.[41] The nanotubes on the filter apparently blocked the pores, so that the cells approaching the filter in a flow were trapped and retained on top of the coated filter. For the second way, Fig. 5B shows that *E. coli* cells were wrapped by PPEI-EI-MWNT species, and the wrapped cells were retained on the filters. Similar wrapping was observed when bacterial cells interacted with CNTs in solutions.[31,42] The nanotubes coated on the filter were probably stirred up during the filtration process, so that the cells approaching the filter could be "mixed" with the nanotubes to result in the wrapping. The wrapped cells were thus aggregated and retained on the filter. The seemingly more complex way depicted in Fig. 5C might be considered as something deviated from the second way shown in Fig. 5B. This observation also brought up an attention that some of the PPEI-EI-MWNT samples may not adhere well to the filters by direct coating. As expected, the loss of polymer-coated MWNTs during the filtration was observed, and it mostly happened during the first 1 mL of filtration. It was estimated that on a 3.0 μm filter, at a filtration rate of 0.5 mL min^{-1}, the loss of non-cross-linked PPEI-EI-MWNTs and cross-linked PPEI-EI-MWNTs was about 0.7–10% and 5.9–14.9%, respectively, when a total of 0.345 to 0.575 mg (approximately 1.25 to 0.75 μg mm^{-2}) MWNTs was coated on the filters. On the 1.2 μm pore sized filters, the average loss was 0.1–3% less than on the 3.0 μm pore sized filters. Again, these observations indicated that an improvement in the coating for stable adhesion and a more homogeneous distribution of nanotubes on the filter should be pursued in further investigation.

The capturing efficiency of the coated filters was found to be dependent on the coating density of PPEI-EI-MWNT on the filters, as well as the flow rate of bacterial solution in the filtration process (Fig. 6). For example, when the coating density of PPEI-EI-MWNT on the filters increased from 0.095 to 0.25 and to 0.75 μg mm^{-2}, the efficiency in terms of log reduction improved from 0.73 log to 2.04 log and to 4.66 log, respectively, at the constant flow rate of 0.5 mL min^{-1}. With the same coated

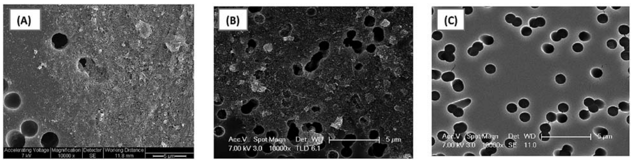

Fig. 4 Representative SEM images of coated and un-coated filters, (A) a filter coated with cross linked PPEI-EI(5000)-MWNTs, (B) a filter coated with PPEI-EI(5000)-MWNTs, and (C) an un-coated filter. (A) A 3 μm pore sized filter and (B and C) 1.2 μm pore sized filters.

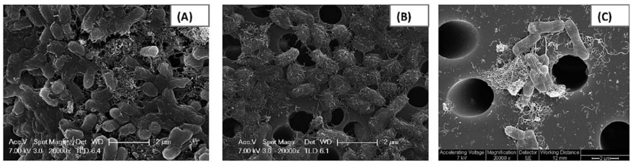

Fig. 5 SEM images of *E. coli* cells captured on filters coated with PPEI-EI-MWNTs. (A) and (B) PPEI-EI(5000)-MWNTs coated filters with 1.2 μm pores, and (C) cross-linked PPEI-EI-MWNTs coated filters with 3.0 μm pore.

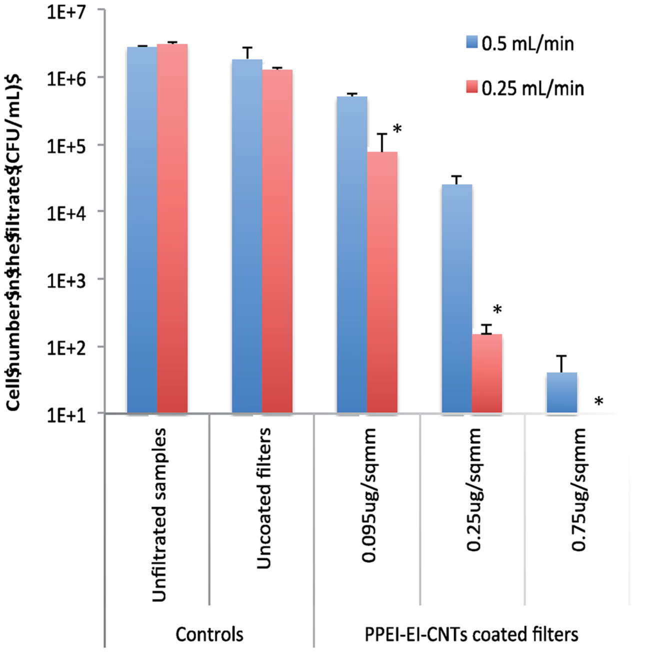

Fig. 6 The coating density- and the flow rate-dependent bacterial capture efficiencies of PPEI-EI(5000)-MWNTs coated filters. The coating density ranged from 0.095 to 0.75 μg mm^{-2} on 1.2 μm pore sized polycarbonate filters and the flow rate varied from 0.25 to 0.5 mL min^{-1}. Statistical analysis was performed only between the efficiencies from the two flow rates: 0.25 mL min^{-1} and 0.5 mL min^{-1} at the same coating density, * indicates a significant difference ($P < 0.05$).

filters, when the flow rate decreased to 0.25 mL min^{-1}, the efficiency increased significantly to 1.61 to 4.32 and to >6 log, respectively. The results demonstrated that the coating of PPEI-EI-MWNT on filters could be tuned to alter the number of bacterial cells be captured, including also the possibility to select and optimize the coating parameters and filtration conditions to capture all bacterial cells from its original solution. However, the dependency of capture efficiency to coating density and flow rate for the cross-linked PPEI-EI-MWNT coated filters was not obvious. This again suggested that the coating inhomogeneity of the cross-linked samples on the filter rather than the density affected more significantly the capture efficiency. Certainly, besides the factors examined here, there are other factors that would affect the capture efficiency of the coated filter, which in general would include the factors related to the coating of PPEI-EI-MWNTs to the filters and the factors related to the interactions between the coated PPEI-EI-MWNTs and bacterial cells. The former may include, but not limited to the material nature of filters, the synthesis process of PPEI-EI-MWNTs, and the coating methods; whereas the latter may include the nature of PPEI-EI-MWNTs, bacterial species, bacterial shape, pH and salinity of the medium, and the presence/absence of other inorganic/organic compounds. Detailed investigations on the effect of these factors on the filtration efficiency would be necessary in further studies.

In the filtration through filters of pores larger than the bacterial cell dimension, the coating with functionalized MWNTs apparently served the desired function of capturing the bacterial cells. The functionalization and associated dispersibility of the nanotubes in solvent systems not only enabled the processing for the filter-coating but also facilitated the formation of nanotube networks on the filters, as designed to modify the large filter pores for cell retention. The results reported here have validated the approach, though the performance has not been improved substantially from those from the previously reported uses of un-modified MWNTs, SWNTs, or SWNTs-MWNTs hybrid coated filters.[41,43,44] Nevertheless, the results have indeed revealed the potential of using filters coated with CNTs for capturing bacterial cells in simple filtration processing. For further performance improvements towards quantitatively and selectively capturing bacterial cells, the functionalized nanotube samples will have to be prepared such that they are sufficiently large in individual species yet still dispersible to be compatible with the coating processing. Again, the coating should be nanotube networks microscopically, for which the challenge would be an improved dispersion during and after the coating. The wetting characteristics of the filter surface might be an important issue, as it could have contributed to the observed inhomogeneous distribution of the nanotubes on the filter. In fact, it was noted in our tests that the hydrophobic filters (PTFE fluorophore filters from EMD Millipore) were not suitable for coating with the hydrophilic PPEI-EI-MWNTs. No reproducible results were achieved even with the aid of vacuum for the coating of PPEI-EI-MWNTs on PTFE filters. Other coating protocols will be explored in further investigations.

As reported previously, filters coated with mostly naked CNTs (without surface functionalization) served a noticeable function in inactivating pathogens. Here the polymer-functionalized CNTs and their coated filters may not have such a function, rather just retaining the status of the bacterial cells for their being separated from the samples/matrixes. Therefore, there may be opportunities for these filters as a good platform to be incorporated into subsequent detection methods designed for efficient screening of bacterial pathogens.

Conclusions

This study evaluated several PPEI-EI-MWNTs samples as coating materials on commercial hydrophilic polycarbonate membranes for capturing of bacterial pathogens in aqueous solution. The results demonstrated that the coating of PPEI-EI-MWNTs on the filters effectively enhanced the efficiency of bacterial capture compared with un-coated filters. Bacterial capture efficiencies of >4 log, up to 6 log or larger in some experimental configurations, were achieved by the combination of coating density of PPEI-EI-MWNTs and the flow rate, which is comparable to or better than the performance of existing capture methods. The cross-linked PPEI-EI-MWNTs coated filters were unexpectedly less efficient than those with PPEI-EI-MWNT samples without the cross-linking, likely due to the poorer dispersibility of the cross-linked samples and thus their less homogeneous coating on filters. It was found that the bacterial capture efficiency of the PPEI-EI-MWNTs coated filters depended significantly on the properties of the PPEI-EI-MWNTs coating, as the dispersibility, absorptivity, and nanoscale details of the PPEI-EI-MWNTs were obvious factors that affected the distribution of nanotubes on the filter, the tightness of the coating nanotubes on the filter, and the interactions between the nanotubes and bacterial cells. This study has demonstrated that the coating of filters with functionalized carbon nanotubes represents a promising approach for effective capture of bacterial pathogens, and the capture step can potentially be incorporated into detection schemes to improve pathogen detection, especially for samples with low pathogen concentrations.

Acknowledgements

This research was supported by USDA grant #2014-67017-21706.

References

1 CDC, CDC Estimates of Foodborne Illness in the United States: Centers for Disease Control and Prevention, 2011, updated April 17, 2014, http://www.cdc.gov/foodborneburden/estimates-overview.html.

2 M. M. Meighan, S. J. R. Staton and M. A. Hayes, Bioanalytical separations using electric field gradient techniques, *Electrophoresis*, 2009, **30**(5), 852–865.

3 Y. J. Sung, H.-J. Suk, H. Y. Sung, T. Li, H. Poo and M.-G. Kim, Novel antibody/gold nanoparticle/magnetic nanoparticle nanocomposites for immunomagnetic separation and rapid colorimetric detection of Staphylococcus aureus in milk, *Biosens. Bioelectron.*, 2013, **43**, 432–439.

4 F. Dai, M. Zhang, B. Hu, Y. Sun, Q. Tang, M. Du, *et al.*, Immunomagnetic nanoparticles based on a hydrophilic polymer coating for sensitive detection of Salmonella in raw milk by polymerase chain reaction, *RSC Adv.*, 2015, **5**(5), 3574–3580.

5 Sub-Microfluidic Devices to Optimize Removal of Pathogens from Drinking Water using Sand Filtration, *18th International Conference on Miniaturized Systems for Chemistry and Life Sciences (microTAS 2014)*, ed. N. Tandogan, Y. A. Zhu, K. T. Wan and E. D. Goluch, San Antonio, TX, 2014.

6 L. Clime, X. Hoa, N. Corneau, K. Morton, C. Luebbert, M. Mounier, *et al.*, Microfluidic filtration and extraction of pathogens from food samples by hydrodynamic focusing and inertial lateral migration, *Biomed. Microdevices*, 2015, **17**(1), 1–14.

7 W. Lee, D. Kwon, W. Choi, G. Y. Jung, A. K. Au, A. Folch, *et al.*, 3D-Printed Microfluidic Device for the Detection of Pathogenic Bacteria Using Size-based Separation in Helical Channel with Trapezoid Cross-Section, *Sci. Rep.*, 2015, **5**, 7717.

8 T. Murakami, Filter-Based Pathogen Enrichment Technology for Detection of Multiple Viable Foodborne Pathogens in 1 Day, *J. Food Prot.*, 2012, **75**(9), 1603–1610.

9 R. J. Isaacs, K. Debelak, P. R. Norris, J. M. Jenkins, J. C. Rooks, T. R. Young, *et al.*, Non-invasive detection of pulmonary pathogens in ventilator-circuit filters by PCR, *Am. J. Transl. Res.*, 2012, **4**(1), 72–82.

10 K. A. Lampel, P. A. Orlandi and L. Kornegay, Improved template preparation for PCR-based assays for detection of food-borne bacterial pathogens, *Appl. Environ. Microbiol.*, 2000, **66**(10), 4539–4542.

11 Y. P. Sun, K. Fu, Y. Lin and W. Huang, Functionalized carbon nanotubes: properties and applications, *Acc. Chem. Res.*, 2002, **35**(12), 1096–1104.

12 T. Akasaka and F. Watari, Capture of bacteria by flexible carbon nanotubes, *Acta Biomater.*, 2009, **5**(2), 607–612.

13 P. M. Ajayan, Nanotubes from Carbon, *Chem. Rev.*, 1999, **99**(7), 1787–1800.

14 R. H. Baughman, C. Cui, A. A. Zakhidov, Z. Iqbal, J. N. Barisci, G. M. Spinks, *et al.*, Carbon Nanotube Actuators, *Science*, 1999, **284**(5418), 1340–1344.

15 G. M. Spinks, G. G. Wallace, L. S. Fifield, L. R. Dalton, A. Mazzoldi, D. De Rossi, *et al.*, Pneumatic carbon nanotube actuators, *Adv. Mater.*, 2002, **14**(23), 1728.

16 V. K. K. Upadhyayula, S. Deng, M. C. Mitchell and G. B. Smith, Application of carbon nanotube technology for removal of contaminants in drinking water: A review, *Sci. Total Environ.*, 2009, **408**(1), 1–13.

17 O. V. Kharissova, B. I. Kharisov and E. G. de Casas Ortiz, Dispersion of carbon nanotubes in water and non-aqueous solvents, *RSC Adv.*, 2013, **3**(47), 24812–24852.

18 Y.-P. Sun, W. Huang, Y. Lin, K. Fu, A. Kitaygorodskiy, L. A. Riddle, *et al.*, Soluble Dendron-Functionalized Carbon Nanotubes: Preparation, Characterization, and Properties, *Chem. Mater.*, 2001, **13**(9), 2864–2869.

19 P.-C. Ma, N. A. Siddiqui, G. Marom and J.-K. Kim, Dispersion and functionalization of carbon nanotubes for polymer-based nanocomposites: A review, *Composites, Part A*, 2010, **41**(10), 1345–1367.

20 A. Parambath, N. T. Kenneth, L. Fushen, G. L. Pengju, G. Lingrong and A. Ankoma, *et al.*, Sugar-Functionalized Carbon Nanotubes: Unique Properties and Interactions with Biological Species, *Petite and Sweet: Glyco-Nanotechnology as a Bridge to New Medicines. ACS Symposium Series. 1091*, American Chemical Society, 2011, pp. 123–141.

21 F. S. Lu, L. R. Gu, M. J. Meziani, X. Wang, P. G. Luo, L. M. Veca, *et al.*, Advances in Bioapplications of Carbon Nanotubes, *Adv. Mater.*, 2009, **21**(2), 139–152.

22 Y. Lin, S. Taylor, H. Li, K. A. S. Fernando, L. Qu, W. Wang, *et al.*, Advances toward bioapplications of carbon nanotubes, *J. Mater. Chem.*, 2004, **14**(4), 527–541.

23 W. Huang, S. Taylor, K. Fu, Y. Lin, D. Zhang, T. W. Hanks, *et al.*, Attaching Proteins to Carbon Nanotubes via Diimide-Activated Amidation, *Nano Lett.*, 2002, **2**(4), 311–314.

24 K. Fu, W. Huang, Y. Lin, D. Zhang, T. W. Hanks, A. M. Rao, *et al.*, Functionalization of Carbon Nanotubes with Bovine Serum Albumin in Homogeneous Aqueous Solution, *J. Nanosci. Nanotechnol.*, 2002, **2**(5), 457–461.

25 Y. Lin, X. Jiang, T. Elkin, K. A. Fernando, L. Gu, S. Taylor, *et al.*, Carbon nanotubes for immunomagnetic separation of Escherichia coli O157: H7, *J. Nanosci. Nanotechnol.*, 2006, **6**(3), 868–871.

26 Y. Lin, T. Elkin, S. Taylor, L. Gu, B. Chen, L. M. Veca, *et al.*, Preparation, Characterization, and Evaluation of Immuno Carbon Nanotubes, *Microchim. Acta*, 2006, **152**(3–4), 249–254.

27 Y. Lin, A. M. Rao, B. Sadanadan, E. A. Kenik and Y.-P. Sun, Functionalizing Multiple-Walled Carbon Nanotubes with Aminopolymers, *J. Phys. Chem. B*, 2002, **106**(6), 1294–1298.

28 W. Huang, Y. Lin, S. Taylor, J. Gaillard, A. M. Rao and Y.-P. Sun, Sonication-Assisted Functionalization and Solubilization of Carbon Nanotubes, *Nano Lett.*, 2002, **2**(3), 231–234.

29 W. Huang, S. Fernando, L. F. Allard and Y.-P. Sun, Solubilization of Single-Walled Carbon Nanotubes with Diamine-Terminated Oligomeric Poly(ethylene Glycol) in Different Functionalization Reactions, *Nano Lett.*, 2003, **3**(4), 565–568.

30 S. Taylor, L. Qu, A. Kitaygorodskiy, J. Teske, R. A. Latour and Y.-P. Sun, Synthesis and Characterization of Peptide-Functionalized Polymeric Nanoparticles, *Biomacromolecules*, 2004, **5**(1), 245–248.

31 L. Gu, T. Elkin, X. Jiang, H. Li, Y. Lin, L. Qu, *et al.*, Single-walled carbon nanotubes displaying multivalent ligands for capturing pathogens, *Chem. Commun.*, 2005, (7), 874–876.

32 L. Gu, Y. Lin, L. Qu and Y.-P. Sun, Carbon Nanotubes as a Scaffold to Display Paired Sugars in Solution, *Biomacromolecules*, 2006, **7**(1), 400–402.

33 H. Wang, L. Gu, Y. Lin, F. Lu, M. J. Meziani, P. G. Luo, *et al.*, Unique Aggregation of Anthrax (Bacillus anthracis) Spores by Sugar-Coated Single-Walled Carbon Nanotubes, *J. Am. Chem. Soc.*, 2006, **128**(41), 13364–13365.

34 L. Gu, P. G. Luo, H. Wang, M. J. Meziani, Y. Lin, L. M. Veca, *et al.*, Single-Walled Carbon Nanotube as a Unique Scaffold for the Multivalent Display of Sugars, *Biomacromolecules*, 2008, **9**(9), 2408–2418.

35 P. G. Luo, H. Wang, L. Gu, F. Lu, Y. Lin, K. A. Christensen, *et al.*, Selective Interactions of Sugar-Functionalized Single-Walled Carbon Nanotubes with Bacillus Spores, *ACS Nano*, 2009, **3**(12), 3909–3916.

36 K. Aferchich, M. Lilly and L. Yang, Effect of single-walled carbon nanotubes on Bacillus anthracis cell growth, sporulation, and spore germination, *J. Nanosci. Nanotechnol.*, 2012, **12**(5), 3821–3830.

37 Y.-P. Sun, G. E. Lawson, W. Huang, A. D. Wright and D. K. Moton, Preparation and Characterization of Highly Water-Soluble Pendant Fullerene Polymers, *Macromolecules*, 1999, **32**(26), 8747–8752.

38 Y. Lin, M. J. Meziani and Y.-P. Sun, Functionalized carbon nanotubes for polymeric nanocomposites, *J. Mater. Chem.*, 2007, **17**(12), 1143–1148.

39 A. Srivastava, O. N. Srivastava, S. Talapatra, R. Vajtai and P. M. Ajayan, Carbon nanotube filters, *Nat. Mater.*, 2004, **3**(9), 610–614.

40 C. D. Vecitis, M. H. Schnoor, M. S. Rahaman, J. D. Schiffman and M. Elimelech, Electrochemical Multiwalled Carbon Nanotube Filter for Viral and Bacterial Removal and Inactivation, *Environ. Sci. Technol.*, 2011, **45**(8), 3672–3679.

41 A. S. Brady-Estévez, S. Kang and M. Elimelech, A Single-Walled-Carbon-Nanotube Filter for Removal of Viral and Bacterial Pathogens, *Small*, 2008, **4**(4), 481–484.

42 L. R. Arias, C. A. Perry and L. Yang, Real-time electrical impedance detection of cellular activities of oral cancer cells, *Biosens. Bioelectron.*, 2010, **25**(10), 2225–2231.

43 A. S. Brady-Estévez, M. H. Schnoor, S. Kang and M. Elimelech, SWNT–MWNT Hybrid Filter Attains High Viral Removal and Bacterial Inactivation, *Langmuir*, 2010, **26**(24), 19153–19158.

44 A. S. Brady-Estévez, M. H. Schnoor, C. D. Vecitis, N. B. Saleh and M. Elimelech, Multiwalled Carbon Nanotube Filter: Improving Viral Removal at Low Pressure, *Langmuir*, 2010, **26**(18), 14975–14982.

Chemical Physics Letters 613 (2014) 40–44

Contents lists available at ScienceDirect

Chemical Physics Letters

journal homepage: www.elsevier.com/locate/cplett

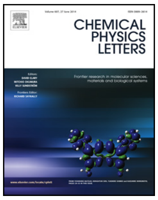

Electroluminescence of carbon ‘quantum’ dots – From materials to devices

L. Monica Veca[a,*], Andreea Diac[b], Iuliana Mihalache[a], Ping Wang[c], Gregory E. LeCroy[c], Emil Mihai Pavelescu[a], Raluca Gavrila[a], Eugeniu Vasile[d], Anamaria Terec[b], Ya-Ping Sun[c]

[a] National Institute for Research and Development in Microtechnologies, IMT-Bucharest, Bucharest 077190, Romania
[b] Faculty of Chemistry and Chemical Engineering, Babes-Bolyai University, Cluj-Napoca 400084, Romania
[c] Department of Chemistry and Laboratory for Emerging Materials and Technology, Clemson University, Clemson, SC 29634, USA
[d] Faculty of Applied Chemistry and Material Science, Department of Oxide Materials and Nanomaterials, University Politehnica of Bucharest, Bucharest, Romania

ARTICLE INFO

Article history:
Received 20 June 2014
In final form 24 August 2014
Available online 28 August 2014

ABSTRACT

Carbon ‘quantum’ dots or carbon dots have emerged as a new class of luminescent nanomaterials. While photoluminescence properties of carbon dots had targeted optical imaging and related usage, their unique excited state redox processes responsible for the luminescence emissions may find potentially significant optoelectronic applications. In this regard, we investigated the electroluminescence properties of the carbon dots integrated into multilayer light emitting diode devices. The devices emitted white light with a slight blue color, visible to naked eyes, thus validating the expectation that carbon dots may potentially serve as a new platform for electroluminescent nanomaterials.

1. Introduction

Since 2006, photoluminescent carbon nanoparticles, dubbed as carbon ‘quantum’ dots or carbon dots, have emerged as a new class of optically active nanomaterials for biological and energy conversion applications [1–12]. A simple passivation of surface defects on the carbon nanoparticles with organic molecules or polymers was found to induce fiercely photoluminescent properties of carbon dots, competitive to those in conventional semiconductor quantum dots (QDs) [13–17]. These carbon nanomaterials are photoluminescent in an aqueous solution as well as in the solid state, such as a polymeric matrix, thus opening up new avenues to broader applications [18].

Beyond photoluminescence, there have been studies on the chemiluminescence and electroluminescence properties of carbon dots. For instance, the radiative recombination of the electrons from the ‘chemical reduction’ of carbon dots with thermally generated holes has allowed Zhao et al. to observe the chemiluminescence of carbon dots in strong alkaline solution [19]. In addition, carbon dots containing amorphous carbon nanoparticles from the thermal carbonization of citric acid in hot octadecene, with 1-hexadecylamine as the surface passivation agent, were found to be electroluminescent when sandwiched between an organic hole transport layer and an organic or inorganic electron transport layer [20,21].

However, most of the light emitting applications of carbon dots reported thus far has been on their uses to convert the blue light of a commercial LED into white light [22–25]. For example, Guo et al. prepared multicolor luminescent carbon dots by chemically unzipping epoxy-enriched polystyrene – PGMA (glycidylmethacrylate) microspheres; these were then encased in superglue and subsequently coated on the prototype solid-state lighting unit comprised of a 370 nm excitation light emitting chip [22]. The resulting devices exhibited different colors for the carbon dots of different sizes [22]. More recently, Chen et al. combined blue GaN-based LED chips with carbon dots of broad yellow emissions (under stimulation with blue light) to fabricate a warm white light device [23], while Luck et al. demonstrated that the coating of a commercial blue emitting LED with carbon dot – agar composite could produce white light emissions [24]. The luminous efficiency and light conversion efficiency of the white LED were 42.2 lm W^{-1} and 61.1%, respectively [24].

In this study we investigated the electroluminescence properties of carbon dots in a LED device (Figure 1), in which the wide-bandgap polymer poly(9-vinylcarbazole) (PVK) was used as the hole transport layer. As in classical OLED [26] and QDs-based LED [27,28] devices, the presence of the PVK layer favors energy transfer to the carbon dots layer due to spectral overlap between

---

* Corresponding author.
E-mail address: monica.veca@imt.ro (L.M. Veca).

http://dx.doi.org/10.1016/j.cplett.2014.08.059

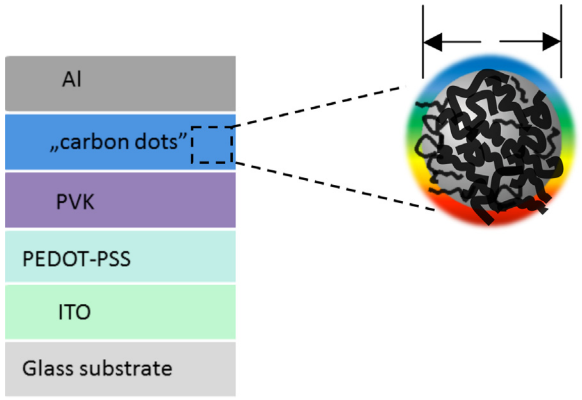

Figure 1. Carbon quantum dot diode – the architecture of the device with the ITO (anode), PEDOT:PSS (HIL), PVK (HTL), carbon quantum dots (EL), Al (cathode).

the PVK emission and the absorption of the carbon dots, as well as the direct charge injection from the valance band of the polymer into the carbon dots layer. The results suggest that carbon dots with their excellent luminescence emission properties are of great potential as lumophores in LEDs for solid-state light sources.

2. Experimental

2.1. Materials

Carbon nano-powder samples (>99%), oligomeric poly(ethylene glycol) diamine (PEG_{1500N}), poly(propionylethyleneimine) (PPEI), poly(9-vinylcarbazole) (PVK), and poly(ethylenedioxythiophene): polystyrene sulfonate (PEDOT:PSS) were purchased from Sigma–Aldrich. Thionyl chloride (>99%) was acquired from Alfa Aesar and nitric acid from VWR. Dialysis membrane tubing (molecular weight cut off 1000) was supplied by Spectrum Laboratories.

2.2. Measurements

Optical absorption spectra were recorded on a Shimadzu UV2501-PC spectrophotometer. Photoluminescence and electroluminescence spectra were measured on a Jobin-Yvon emission spectrometer equipped with a 450 W xenon source, Gemini-180 excitation and Tirax-550 emission monochromators, and a photon counting detector (Hamamatsu R928P PMT at 950 V). Transmission electron microscopy (TEM) images were obtained on a Tecnai^{TM} G^2F30 S-TWIN transmission electron microscope operated at 300 kV. The TEM specimens were prepared by placing a drop of a dilute carbon dots solution on a holey-carbon grid, and the images were analyzed with Digital Micrograph software. The AFM characterization was performed on a Scanning Probe Microscope Ntegra (Nt-MDT), operated in soft-tapping regime of the semicontact mode (tapping mode), and equipped with a standard silicon cantilever with 7.5 N/m nominal spring constant, and 160 kHz resonance frequency and 10 nm nominal tip radius. All data were processed by using first order line flattening algorithm.

2.3. Carbon dots

The synthesis of carbon dots was based on the previously reported procedures [13]. Briefly, the carbon nano-powder sample was refluxed in aqueous nitric acid solution (2.6 M) for 15 h, dialyzed against fresh water, and then centrifuged at 1000 × g to retain the supernatant. The recovered sample was refluxed in neat $SOCl_2$ for 12 h. Upon the removal of excess $SOCl_2$, the sample (50 mg) was mixed well with carefully dried 500 mg of PEG_{1500N} in a round bottom flask, heated to 120 °C, and vigorously stirred under nitrogen atmosphere for 3 days. The reaction mixture brought back at room temperature was dispersed in water, centrifuged at 25 000 × g to retain the supernatant. The colored fraction was further dialyzed with the dialysis membrane tubing (1000 molecular weight cut off) against fresh water for two days to eliminate the free and loosely bonded functionalization molecules.

The synthetic procedures for the PPEI-EI-carbon dots were largely the same, where the PPEI-EI was obtained from the commercially supplied PPEI in simple hydrolysis reactions.

2.4. Device fabrication

The architecture of the device comprised an indium tin oxide (ITO) glass substrate (with the sheet resistance of 20 Ω/□, and thickness of 100 nm) and cleaned in an ultrasonic bath with extran, water, acetone, isopropanol, followed by 10 min of UV-ozone exposure. Subsequently the PEDOT:PSS solution was spin-coated from the water solution at 5000 rpm for 60 s, followed by 15 min of thermal treatment at 150 °C in air to obtain a PEDOT:PSS layer of around 50 nm. The PVK solution was spin-coated from a solution of 1,2-dichlorobenzene/chloroform mixture at 1500 rpm for 30 s onto the PEDOT:PSS layer, followed by 2 h of thermal treatment in vacuum at 100 °C to form a PVK thin layer of around 40 nm. The carbon dots layer (thickness around 10 nm) was deposited from an aqueous solution by spin-coating onto the PVK film at 1500 rpm for 30 s, followed by thermal treatment under vacuum at 80 °C for 1 h. The 100 nm thick aluminum cathode was deposited on top of the carbon dots layer under vacuum (6×10^{-7} Torr) through a shadow mask that defined a 3 mm × 1.5 mm active area.

3. Results and discussion

The carbon nanoparticles, supplied commercially, were processed via refluxing in an aqueous nitric acid solution, followed by the adjustment of pH, dialysis and then centrifugation to retain the supernatant (Figure 2). Upon being recovered from the aqueous solution, the nanoparticles were refluxed in neat thionyl chloride for the subsequent amidation reaction with oligomeric poly(ethylene glycol) diamine (PEG_{1500N}) or the aminopolymer poly(propionylethyleneimine-*co*-ethyleneimine) (PPEI-EI). The PEG_{1500N}-carbon dots and PPEI-EI-carbon dots were obtained as colored aqueous solutions.

For the morphological characterization with high-resolution transmission electron microscopy (HR-TEM), the carbon dots were deposited onto a holey-carbon TEM grid. Representative HR-TEM images are shown in Figure 3 (with the fast Fourier transform FFT in the inset), where the graphitic structures of 2–3 nm in diameter are identified. The observed lattice fringes of 0.215 nm and 0.19 nm correspond to the (1 0 0) and (1 0 1) diffraction planes of graphitic carbons, similar to the crystalline plane found in the FFT image (80-0004 ICDD file) (Figure 3).

The optical absorption spectrum of the carbon dots is shown in Figure 4, depicting the typical π-plasmon transitions in the core carbon nanoparticle. Photoluminescence emissions of the carbon dots were obviously excitation wavelength dependent, as also shown in Figure 4, similar to what were reported previously in the literature [13]. At longer excitation wavelengths, the emission spectra were progressively red-shifted, with the spectral bandwidth becoming narrower. Nevertheless, the observed emission spectra corresponding to multiple excitation wavelengths covered the entire visible spectral region (Figure 4). The photoluminescence quantum yields of the carbon dots in aqueous solutions were around 10% (400–450 nm excitation, in reference to the quinine

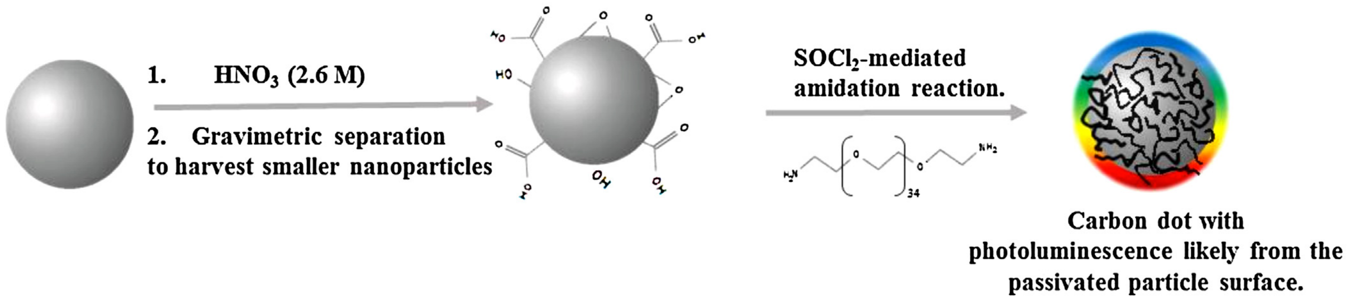

Figure 2. Scheme on the synthesis of the PEGylated carbon dots.

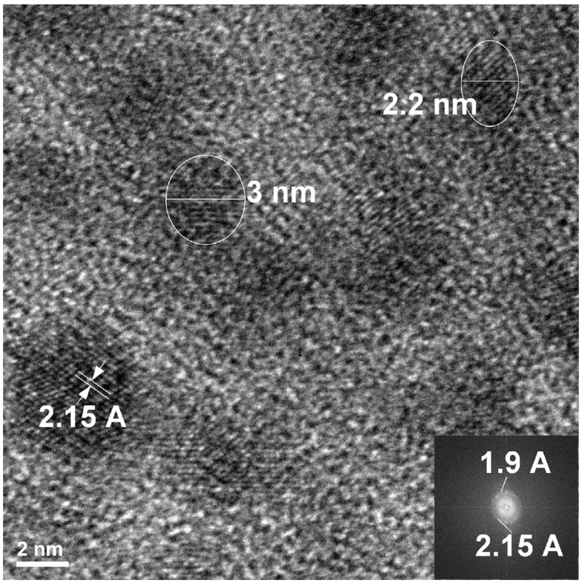

Figure 3. TEM image with the FFT in the inset of the PEGylated carbon quantum dots.

sulfate standard), similar to those found in as-synthesized samples of carbon dots in previous studies.

The LED device of a multilayer structure (ITO/PEDOT:PSS/PVK/carbon dots/Al, Figure 1) was fabricated by sequentially spin-coating each layer from orthogonal solvents on top of the ITO substrate, with the Al cathode as the final layer deposited by thermal evaporation method through a shadow mask. Experimentally, the clean ITO substrate was first coated with PEDOT:PSS as the hole injecting layer for an improved charge injection efficiency. The PEDOT:PSS coating is also known to decrease the roughness of the ITO electrode, an additional advantage. PVK polymer was subsequently coated as the hole transporting layer (also referred to as buffer layer), taking advantage of the polymer being photoconductive, emissive in the violet-blue spectral region, and transporting positive charges. Then, the substrate already coated with the polymer layers was spin-coated with the PEG$_{1500N}$-carbon dots by using an aqueous dispersed sample. The carbon dots deposited on top of the PVK layer formed a thin (on the order of 10 nm in thickness) continuous layer according to the atomic force microscopy (AFM) imaging result (Figure 5). In the AFM images, the carbon dots layer (Figure 5b) on top of the PVK film (Figure 5a) appears to be a relatively even and complete layer, with a kurtosis parameter (Sku) of unity for the carbon dots film in comparison with the 0.3 Sku value for the control film (the PVK film on top of the PEDOT:PSS layer), and a carbon dots film roughness of 0.67 nm. The resulting device of three coated layers on the ITO substrate was then transferred to a thermal evaporator for the deposition of Al (about 100 nm in thickness) as the metal cathode (Figure 1)

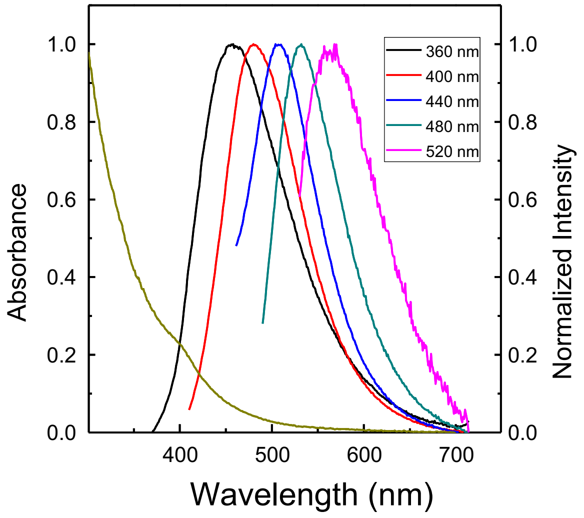

Figure 4. Absorption and normalized photoluminescence spectra (at different excitation wavelengths as listed) of the PEGylated carbon dots in aqueous solution.

The LED device with the carbon dots layer sandwiched between the PVK (as the hole transport layer or HTL) and the low work function Al cathode was evaluated by applying a forward bias on the hole-injecting contact (HIL, ITO/PEDOT:PSS). With the external bias, electrons and holes were injected to result in the formation of excitons, from which the positive and negative polarons could radiatively recombine in the carbon dots layer for luminescence emissions. In addition to the direct charge injection, the large bandgap of PVK layer might also be in favor of charge transfer to the emissive carbon dots layer.

The electroluminescence from the device was visible to naked eyes, white light with a bluish color (Figure 6). The corresponding electroluminescence spectrum was found to be broad, covering a wide range of the visible spectral region. Shown in Figure 7 is a comparison of the electroluminescence spectrum with the photoluminescence spectra (obtained with multiple excitation wavelengths) of the corresponding carbon dots. Apparently the electronic excitation could generate the emissive excited states that would require photoexcitations at multiple wavelengths. While the comparison is rather rough without any quantitative value, the general overlap between the electroluminescence spectrum and the collection of multiple photoluminescence spectra seems to suggest that the recombination zone is within the carbon dots layer, with the PVK layer serving primarily the function of hole-transport. The electroluminescence spectra were not sensitive to variations in the applied voltage (11–15 V), as also shown in Figure 6. From the electroluminescence spectrum, the chromaticity CIE coordinate (0.25, 0.24) for 15 V applied biases was calculated (Figure 6).

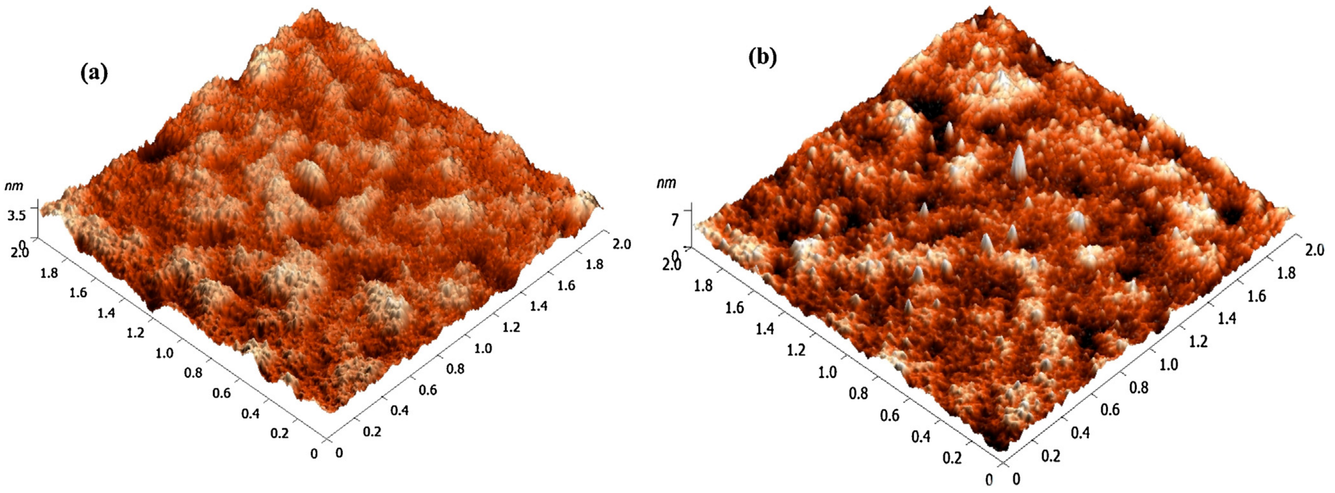

Figure 5. AFM images of the (a) HTL – PVK layer (ITO/PEDOT:PSS/PVK) and (b) EL – PEGylated carbon quantum dots layer in the device (the carbon quantum dot layer on top of PVK actually it is the device without the aluminum electrode).

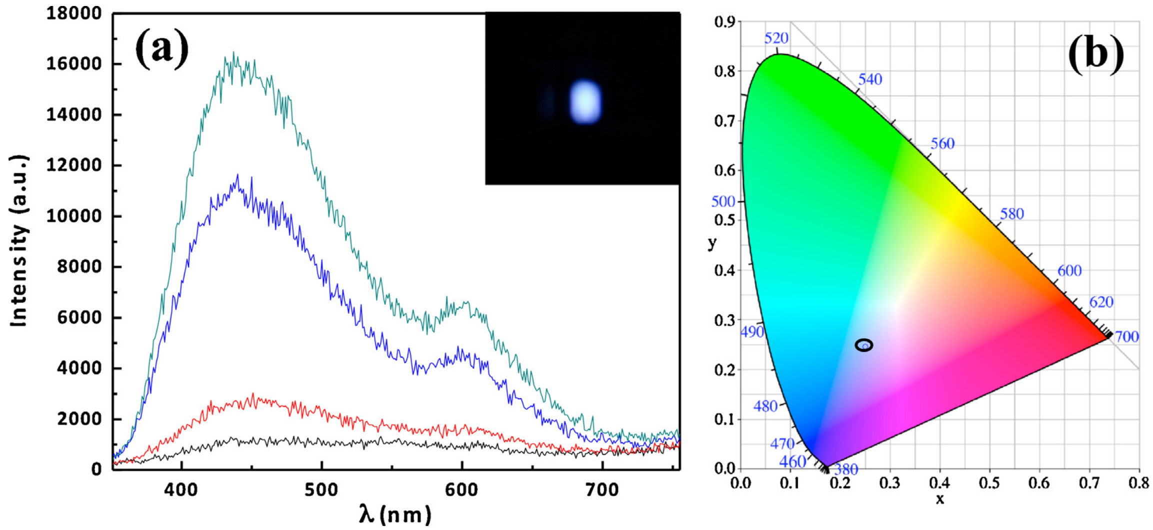

Figure 6. (a) Electroluminescence spectra of the device from Fig. 1 at 10 V, 11 V, 13 V, and 15 V applied bias and (b) the CIE coordinates of the LED with carbon quantum dots as the active layer, operated at 15 V and 5 mA. The inset shows a picture of the device at 20 V applied bias.

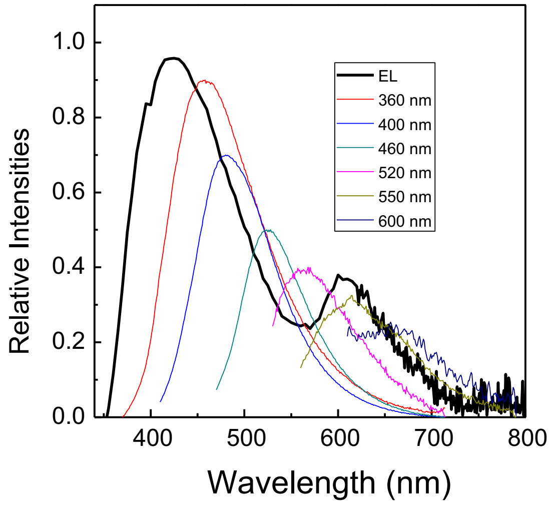

Figure 7. A comparison between the electroluminescence (EL) spectrum from the LED device with the PEGylated carbon dots and the corresponding photoluminescence spectra at the listed excitation wavelengths.

In quantum efficiency measurements, the emission signal was maximized by minimizing the distance between the emitting surface and a large area detector (detector active area 100 mm^2 Ophir silicon photodiode type PD300 – 3W). The LED device was operated at 15 V (current up to 5 mA), and the recorded power at 440 nm was 130 nW. Thus, the 'wall-plug efficiency' of the LED device was estimated (as the ratio of the measured power to the input power) to be 1.73×10^{-6}. The luminescence from the device operated at 15 V was about 2×10^{-6} lm [calculated from the total power output measured at room temperature under ambient atmosphere with the following equation: $PQ = 683\,\mathrm{lm/W} \int (SPQ)_\lambda \cdot V(\lambda) \cdot d\lambda$, where PQ is the photometric quantity, SPQ the matching radiometric quantity in W, $V(\lambda)$ the response of the 'standard' light adapted eye – photopic vision] and a luminance of 0.14 cd/m^2.

The electroluminescence was not specific to the PEG_{1500N}-carbon dots, as it was similarly observed in devices containing carbon dots of other surface passivation molecules. For example, the use of PPEI-EI-carbon dots sample for the carbon dots layer in the LED device of the same configuration yielded similar electroluminescence spectra. The estimated wall-plug quantum efficiency was somewhat lower, which might be attributed to the larger size of PPEI-EI for surface passivation in the carbon dots (thus a thicker passivation layer on the dot surface). In this regard, it may be expected that the development of carbon dots with a shorter-chain surface passivation molecule would lead to an increased LED efficiency at a lower operating voltage for the corresponding devices. In fact, this has been found true in the studies of LED devices based on conventional semiconductor nanoparticles [29].

In summary, we fabricated LED devices with carbon dots as the active layer. The devices emitted white light with a slight blue color, visible to naked eyes, suggesting that the carbon dots may potentially serve as a new platform for electroluminescent nanomaterials. The agreement between the observed electroluminescence and photoluminescence spectra is valuable to the mechanistic understanding of excited state redox processes and charge recombination in carbon dots, providing important evidence for the notion that carbon dots are at least phenomenologically very similar to conventional nanoscale semiconductors [30]. While these first-generation devices are still somewhat rough with relatively low efficiencies, they do serve the purpose for proof of concept and point to significant opportunities for further improvements. For example, with the observed agreement between the electroluminescence and photoluminescence spectra, the use of more photoluminescent samples of carbon dots should lead to significantly enhanced performance. Among other improvements in further investigations include the addition of an electron transport layer in the device design and better controlled device fabrication. Some of these efforts are already in progress.

Acknowledgments

This work was supported by a grant from the Romanian National Authority for Scientific Research, CNCS-UEFISCDI, project number PNII-ID-PCCE-2011-2-0069. Partial support from the US National Science Foundation (Y.-P.S.) is also gratefully acknowledged.

References

[1] L. Cao, et al., J. Am. Chem. Soc. 129 (2007) 11318.
[2] S.-T. Yang, et al., J. Am. Chem. Soc. 131 (2009) 11308.
[3] S.-T. Yang, et al., J. Phys. Chem. C 113 (2009) 18110.
[4] S.C. Ray, A. Saha, N.R. Jana, R. Sarkar, J. Phys. Chem. C 113 (2009) 18546.
[5] C.Q. Ding, A.W. Zhu, Y. Tian, Acc. Chem. Res. 47 (2014) 20.
[6] X. Wang, et al., Chem. Commun. 25 (2009) 3774.
[7] Q. Li, et al., J. Phys. Chem. C 114 (2010) 12062.
[8] Z.Q. Xu, et al., Carbon 66 (2014) 351.
[9] A. Prasannan, T. Imae, Ind. Eng. Chem. Res. 52 (2013) 15673.
[10] X.L. Yu, R.J. Liu, G.J. Zhang, H.B. Cao, Nanotechnology 24 (2013) 335401.
[11] Z.P. Zhang, J. Zhang, N. Chen, L.T. Qu, Energy Environ. Sci. 5 (2012) 8869.
[12] (a) L. Cao, et al., J. Am. Chem. Soc. 133 (2011) 4754;
(b) L. Cao, et al., Theranostics 2 (2012) 295.
[13] Y.-P. Sun, et al., J. Am. Chem. Soc. 128 (2006) 7756.
[14] A.B. Bourlinos, A. Stassinopoulos, D. Anglos, R. Zboril, M. Karakassides, E.P. Giannelis, Small 4 (2008) 455.
[15] H. Peng, J. Travas-Sejdic, J. Chem. Mater. 21 (2009) 5563.
[16] P. Luo, Z. Ji, C. Li, G. Shi, Nanoscale 5 (2013) 7361.
[17] A. Khanam, S.K. Tripathi, D. Roy, M. Nasim, Colloids Surf. B 102 (2013) 63.
[18] S. Zhu, et al., Angew. Chem. Int. Ed. 52 (2013) 3953.
[19] L. Zhao, F. Di, D. Wang, L.H. Guo, Z. Zang, B. Wan, H. Zhang, Nanoscale 5 (2013) 2655.
[20] F. Wang, Y.H. Chen, C.Y. Liu, D.G. Ma, Chem. Commun. 47 (2011) 3502.
[21] X. Zhang, et al., ACS Nano 7 (2013) 11234.
[22] X. Guo, C.-F. Wang, Z.-Y. Yu, L. Chen, S. Chen, Chem. Commun. 48 (2012) 2692.
[23] Q.-L. Chen, C.-F. Wang, S. Chen, J. Mater. Sci. 48 (2013) 2352.
[24] C.M. Luk, L.B. Tang, W.F. Zhang, S.F. Yu, K.S. Teng, S.P. Lau, J. Mater. Chem. 22 (2012) 22378.
[25] W. Kwon, S. Do, J. Lee, S. Hwang, J.K. Kim, S.-W. Rhee, Chem. Mater. 25 (2013) 1893.
[26] H.B. Wu, et al., Adv. Mater. 20 (2008) 696.
[27] B.O. Dabbousi, M.G. Bawendi, O. Onitsuka, M.F. Rubner, Appl. Phys. Lett. 66 (1995) 1316.
[28] M. Molaei, M. Marandi, E. Saievar-Iranizad, N. Taghavinia, B. Liu, H.D. Sun, X.W. Sun, J. Lumin. 132 (2012) 467.
[29] Y. Liu, M. Gibbs, J. Puthyssery, S. Gaik, R. Ihly, H. Hillhouse, M. Law, Nano Lett. 10 (2010) 1960.
[30] L. Cao, M.J. Meziani, S. Sahu, Y.-P. Sun, Acc. Chem. Res. 46 (2013) 171.

Chemical Physics Letters 639 (2015) 109–113

Contents lists available at ScienceDirect

Chemical Physics Letters

journal homepage: www.elsevier.com/locate/cplett

Fluorescent carbon 'quantum' dots from thermochemical functionalization of carbon nanoparticles

Monica I. Rednic[a,b], Zhuomin Lu[a,c], Ping Wang[a], Gregory E. LeCroy[a], Fan Yang[a], Yun Liu[a], Haijun Qian[a], Anamaria Terec[b], L. Monica Veca[d], Fushen Lu[c], Ya-Ping Sun[a,*]

[a] Department of Chemistry and Laboratory for Emerging Materials and Technology, Clemson University, Clemson, SC 29634, USA
[b] Faculty of Chemistry and Chemical Engineering, Babes-Bolyai University, Cluj-Napoca 400084, Romania
[c] Department of Chemistry, Shantou University, Shantou, Guangdong 515063, China
[d] National Institute for Research and Development in Microtechnologies, IMT-Bucharest, Bucharest 077190, Romania

ARTICLE INFO

Article history:
Received 26 June 2015
In final form 29 August 2015
Available online 9 September 2015

ABSTRACT

Fluorescent carbon 'quantum' dots are generally obtained by deliberate chemical functionalization of carbon nanoparticles or by 'one-pot' carbonization processing. For brightly fluorescent carbon dots with optoelectronic polymers, a hybrid approach was developed to use pre-processed and selected carbon nanoparticles as precursor for surface passivation by poly(9-vinylcarbazole) (PVK) in one-pot thermochemical processing, thus taking advantage of the more controllable feature from the deliberate functionalization and also the versatility associated with the one-pot synthesis. The PVK-carbon dots were characterized by optical spectroscopy, microscopy, and other techniques. The broad applicability of the hybrid approach is discussed.

1. Introduction

Carbon 'quantum' dots or more appropriately called carbon dots for a lack of the classical quantum confinement effect in these nanomaterials were found and have since been developed as a competitive alternative to conventional semiconductor quantum dots (QDs) [1–4]. Generally carbon dots are defined as small carbon nanoparticles with various surface passivation via modification or functionalization [1–4]. Ever since the inception [1], these new fluorescent carbon nanomaterials have been investigated extensively, from the development of synthetic strategies to structural and mechanistic understandings and to the exploration on a variety of potential applications [2–4]. For the effort on using carbon dots in optoelectronics as an example, Wang et al. synthesized non-aqueous carbon dots with hexadecylamine as the surface passivation agent for their electroluminescence in light emitting diodes (LEDs) [5]. Similar approach and dot samples were employed in the fabrication of LEDs with switchable emission colors [6]. Guo et al. also pursued the preparation of carbon dots that are fluorescent at different colors with poly(styrene-*co*-glycidylmethacrylate) particles as precursor for processing under various selected conditions and used the resulting carbon dots in the emissive layer of LEDs [7]. In more recent studies, carbon dots from different syntheses were demonstrated as being amenable to uses in white-light LEDs [8–12]. These light emitting devices are generally designed such that the emissive layer containing the carbon dots is sandwiched by other layered components for charge injection and transport purposes, such as the optically transparent and electrically conductive PEDOT:PSS layer found in all of these devices [5–9]. Polymers such as the wide-bandgap poly(9-vinylcarbazole) (PVK) are often used for hole transport, enabling more favorable energy transfer to the electroluminescent materials like carbon dots in the devices [9,13,14].

Among more popular syntheses of carbon dots, there have been the approach of deliberate chemical functionalization of small carbon nanoparticles and the method of 'one-pot' carbonization processing of organic or other precursors [2–4]. The former has been more controllable, yielding carbon dots of high fluorescence quantum yields (more than 50% in some configurations) [15], but the synthesis is more tedious with some limitation in the selection of functionalization molecules or species. The latter is more versatile with respect to the introduction of desired functional groups on the resulting dot surface, but less controllable, among other processing issues [16–20]. For carbon dots in optoelectronic and related applications, their improved coupling or compatibility with the polymeric materials commonly employed in various devices may play a significant role for enhanced performance. In this work on preparing brightly fluorescent carbon dots with

---

* Corresponding author.
E-mail address: syaping@clemson.edu (Y.-P. Sun).

http://dx.doi.org/10.1016/j.cplett.2015.08.069

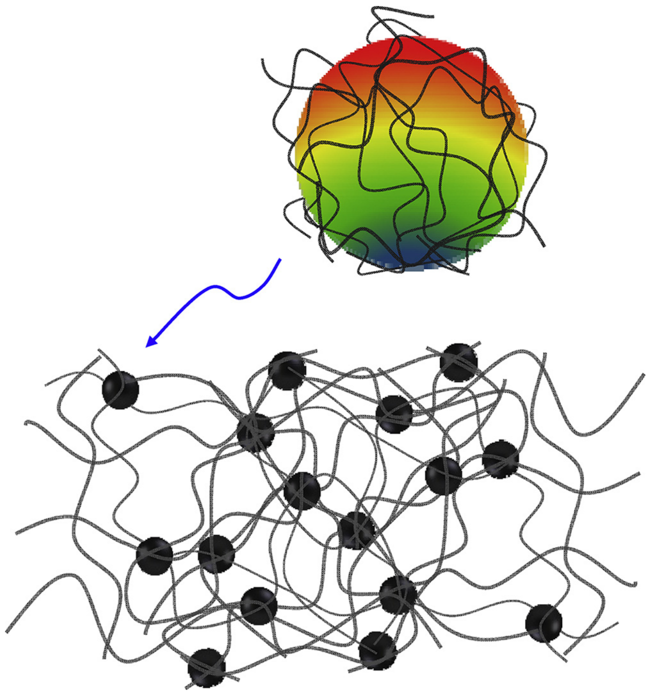

Figure 1. A cartoon illustration on the PVK-carbon dots, whose primary configuration may be characterized as being a number of fluorescent dots (carbon nanoparticles surface-passivated with PVK) connected by polymer networks.

polymers relevant to optoelectronic uses [9–14], we developed a hybrid approach to use pre-processed and selected small carbon nanoparticles as the precursor for surface passivation by PVK in one-pot thermochemical processing into carbon dots, thus to take advantage of the more controllable feature from the deliberate functionalization approach and also the versatility associated with the one-pot thermochemical synthesis. According to results from optical spectroscopy, microscopy, and other characterizations, the structural and fluorescence properties of the samples thus prepared were typical of carbon dots, except for some special features (Figure 1). The broad applicability of the hybrid approach in the synthesis of carbon dots with specifically targeted surface functional moieties is discussed.

2. Experimental

2.1. Materials

The carbon nanopowder sample (<50 nm in particle size, carbon purity 99+%) was purchased from Sigma–Aldrich, and poly(*N*-vinylcarbazole) (PVK, $M_W \sim 90\,000$) from Acros Organics. Nitric acid (70%), *N*,*N*-dimethylformamide (DMF), tetrahydrofuran (THF), chloroform, chlorobenzene, and 1,2-dichlorobenzene were obtained from VWR, and deuterated chloroform for NMR measurements from Cambridge Isotope Laboratories. Dialysis membrane tubing (cutoff molecular weight ~ 500) was supplied by Spectrum Laboratories. Water was deionized and purified by being passed through a Labconco WaterPros water purification system.

2.2. Measurements

Optical absorption spectra were recorded on a Shimadzu UV2501-PC spectrophotometer. Fluorescence spectra were measured on a Jobin-Yvon emission spectrometer equipped with a 450 W xenon source, Gemini-180 excitation and Tirax-550 emission monochromators, and a photon counting detector (Hamamatsu R928P PMT at 950 V). The correction for nonlinear instrumental response of the spectrometer was accomplished by using separately determined correction factors with respect to different emission wavelengths. NMR measurements were performed on a Bruker Avance 500 NMR spectrometer. AFM images were acquired in the acoustic AC mode on a Molecular Imaging PicoPlus AFM system equipped with a multipurpose scanner and a NanoWorld point probe NCH sensor. The height profile analysis was assisted by using the SjPIP software distributed by Image Metrology.

SEM imaging was carried out in the SE mode on a Hitachi HD-2000 S-TEM system, and TEM imaging on a Hitachi H-9500 TEM system, coupled with the use of carbon- or holey carbon-coated copper grids. For TEM specimen prepared via microtoming, a solid sample was embedded in acrylic resin, followed by the use of a Reichert–Jung Ultracut E microtome with a 45° angle diamond knife at room temperature to obtain thin slices of less than 100 nm in thickness.

2.3. Carbon nanoparticles and carbon dots

The as-supplied nanopowder sample was refluxed in aqueous nitric acid (2.6 M) for 24 h. Upon being cooled to ambient, the acidic suspension was centrifuged at $3500 \times g$ to collect the supernatant, which was then neutralized with sodium carbonate. The suspension was dialyzed in a membrane tubing (cutoff molecular weight ~ 500) against fresh deionized water for 3 days, followed by vigorous centrifugation at $20\,000 \times g$ to obtain a stable dispersion of the carbon nanoparticles.

The PVK-carbon dots were prepared by thermochemical processing with microwave irradiation. The reactor was a small container (about 8 cm in diameter and 2.5 cm in height) filled with silicon carbide powder as solid bath in a commercial microwave oven. In a typical experiment, the carbon nanoparticles (20 mg) were mixed well with PVK (1 g) in a vial, and with the vial immersed in the pre-heated (microwave irradiation at 500 W for 3 min) silicon carbide bath, the solid-state mixture was irradiated in the microwave oven at 300 W for 25 min. The reacted sample cooled to room temperature under ambient conditions was dispersed in THF, and the resulting dispersion was centrifuged at $20\,000 \times g$ for 60 min to collect the supernatant as a solution of the PVK-carbon dots.

2.4. PVK/carbon dots composite films

In a typical fabrication experiment, solutions of the PVK-carbon dots and neat PVK in the solvent mixture chlorobenzene/chloroform (3/1, v/v) were prepared separately and then mixed well, followed by a gradual evaporation of the solvent until the mixture becoming viscous. The viscous solution was drop-cast onto a pre-cleaned glass substrate. A polymer film was formed after slow solvent evaporation under ambient conditions for 12 h, and the film could readily be peeled off the glass slide to be free standing (thickness on the order of 5 μm).

3. Results and discussion

The commercially supplied carbon nanopowder sample was wet-processed in procedures involving the refluxing in nitric acid solution and various combinations of dispersion and vigorous centrifugation for the purpose of harvesting small carbon nanoparticles [21,22]. The nanoparticles thus obtained were generally on the order of 10 nm or less, as reported previously with the same processing and also confirmed by results from microscopy analyses (Figure 2).

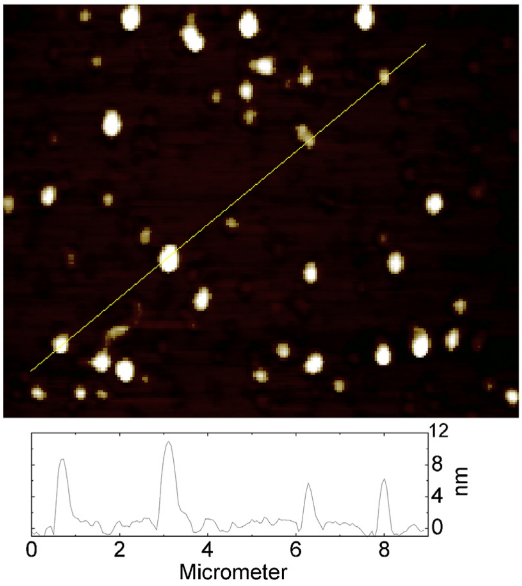

Figure 2. Representative AFM images of the carbon nanoparticles as precursor for carbon dots on mica substrate.

The carbon nanoparticles were mixed well with commercially supplied PVK to obtain a solid blend for subsequent thermochemical processing. The one-pot processing was accomplished with microwave irradiation [23–30], in which the preferential absorption of microwave energy by the carbon nanoparticles was expected, which likely resulted in the thermochemical functionalization of the nanoparticles by the surrounding PVK moieties. After the microwave processing, the PVK-functionalized carbon nanoparticles were dispersed in THF, followed by vigorous centrifugation to yield the soluble fraction designated as the carbon dots of PVK as the surface passivation agent (PVK-carbon dots). A solution of PVK-carbon dots appeared brightly colored (Figure 3), in contrast to the colorless appearance of neat PVK solution. The color must be associated predominantly with the core carbon nanoparticles in the carbon dots sample, with the observed broad optical absorption spectrum characteristic of π–plasmon transitions in nanoscale carbon particles (Figure 3) [21,31].

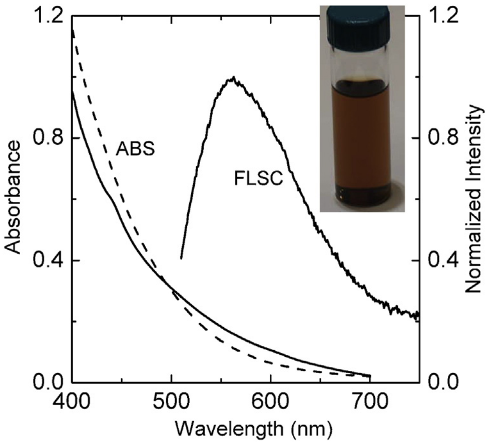

Figure 3. Absorption (ABS) and fluorescence (FLSC, 500 nm excitation, corrected for nonlinear instrumental response of the spectrometer) spectra of the PVK-carbon dots in THF solution (——), with the absorption spectrum of aqueous suspended precursor carbon nanoparticles (----) also shown for comparison. Inset: photograph for a typical THF solution of the PVK-carbon dots.

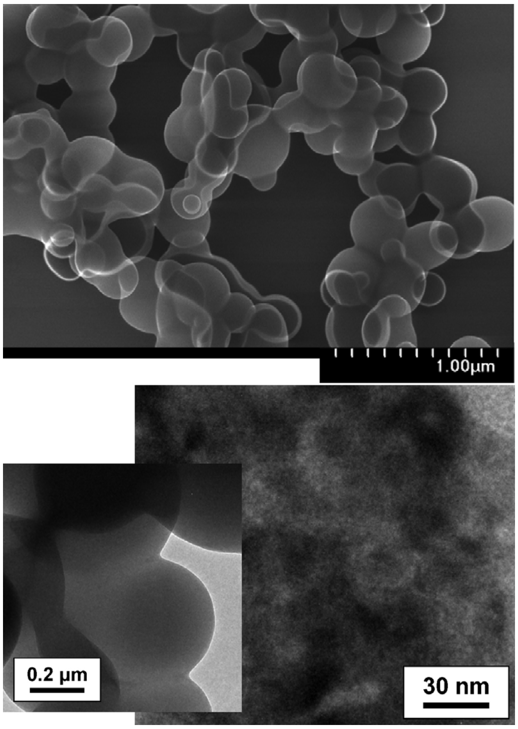

Figure 4. SEM images (upper) and TEM images at low (lower left) and high (lower right) resolution for a specimen of the PVK-carbon dots.

Fluorescence emissions of the PVK-carbon dots were obviously excitation wavelength dependent, with the measured fluorescence spectra progressively red-shifted corresponding to longer excitation wavelengths, similar to those found in other carbon dots already reported in the literature [2–4,22]. PVK is known as being colorless, as confirmed by the observation that the polymer sample used in this work had the absorption edge well into the UV spectral region. Therefore, the fluorescence emissions corresponding to visible excitations, such as 500 nm (Figure 3), could not be associated with PVK moieties. In terms of the presently adopted mechanistic framework on carbon dots [31], the observed bright and colorful fluorescence emissions must be from the PVK-passivated carbon nanoparticle surface (Figure 1).

The fluorescence quantum yields of the PVK-carbon dots in THF solution were measured in reference to 9,10-bis(phenylethynyl)anthracene as a standard, which has a quantum yield of unity as determined by calibration against the quinine sulfate standard [32,33]. At 440 nm excitation, the fluorescence quantum yield of the solution was found to be around 13%, which is comparable to results for other more extensively studied carbon dots from the deliberate functionalization syntheses, such as those with the oligomeric poly(ethylene glycol) diamine (PEG_{1500N}) as the surface passivation agent (corresponding fluorescence quantum yields of 10–20% for the as-synthesized samples in aqueous solution) [15,33]. The quantum yields of the PVK-carbon dots were lower at longer excitation wavelengths, also similar to what were observed in carbon dots of other surface functional groups [15].

Morphologically, the PVK-carbon dots are not discrete individual dots (namely that the carbon nanoparticles would each be functionalized by one or more PVK molecules), rather composite-like with the functionalized carbon nanoparticles embedded in PVK polymer networks (Figure 1), consistent with the results from scanning electron microscopy (SEM) and transmission electron microscopy (TEM) characterizations. Experimentally, the specimen for microscopy analyses was prepared by dropping a THF solution of the PVK-carbon dots onto a carbon-coated copper grid, followed by the evaporation of the solvent. As shown in Figure 4, the SEM images (obtained in the SE mode on a scanning-transmission

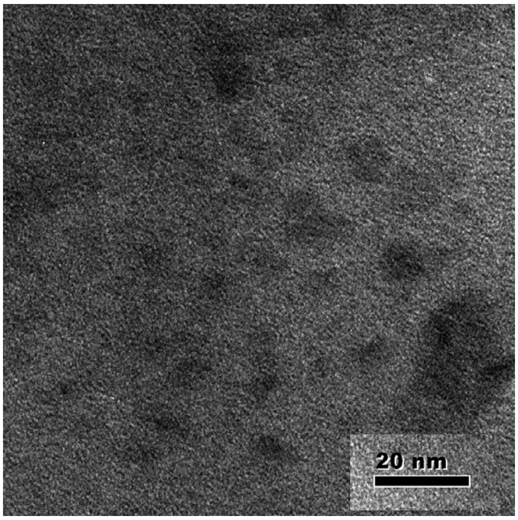

Figure 5. TEM images for the microtome-prepared specimen of the PVK-carbon dots.

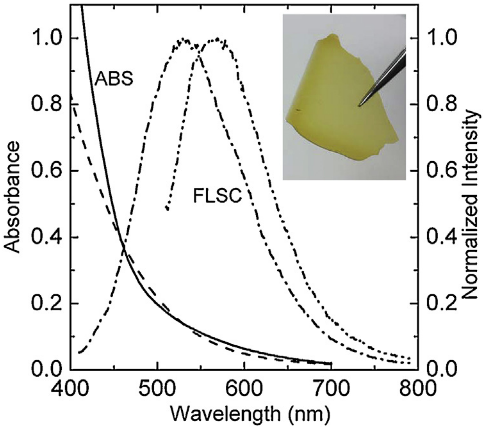

Figure 7. Absorption (ABS, ——) and fluorescence (FLSC, with excitation at 400 nm: -.-.-, and 500 nm: -..-..-) spectra for the film of PVK-carbon dots + PVK, with the absorption of aqueous suspended carbon nanoparticles also shown for comparison. Inset: photograph for a typical film.

electron microscopy or S-TEM instrument) are dominated by large particle-like features commonly found in the imaging of polymeric nanocomposites. The same specimen was analyzed by TEM at different resolutions, with the results also shown in Figure 4. The lower magnification images are similar to those from SEM, while those at high resolution suggest the embedding of carbon nanoparticles, again morphologically similar to what are typically observed in the TEM imaging of polymeric nanoparticles.

For a more detailed TEM characterization, a specimen of the PVK-carbon dots was prepared by dispersing the sample into acrylic resin for being microtomed into thin slices of less than 100 nm in thickness. As shown in Figure 5, carbon nanoparticles in the PVK-carbon dots are more clearly identified in the TEM images of the specimen prepared via microtoming, further confirming the composite-like structural feature (Figure 1).

The PVK-carbon dots in a solution of deuterated solvent were characterized in NMR measurements, with the results compared with those of the corresponding neat PVK. As shown in Figure 6, the solution-phase ^{1}H NMR signals in the spectrum of the PVK-carbon dots are similar to those of the neat PVK, without any fundamental changes in terms of their chemical shifts or the broadness in the signals. Within the proposed structural framework (Figure 1) such that the carbon dots (carbon nanoparticles functionalized by PVK polymers for the observed bright fluorescence emissions in the visible spectral region) are composited with the polymers (Figures 4 and 5), the NMR results suggest that the presence of carbon dot domains in the overall composite-like sample structures do not significantly change the already diverse environments for the PVK protons. Therefore, the primary effect of the thermochemical synthesis seems to be only the introduction of the pre-processed and selected carbon nanoparticles into the PVK network for being surface-passivated to enable bright and colorful fluorescence emissions that are essentially the same as those from the ‘conventional’ carbon dots already reported in the literature [1–4].

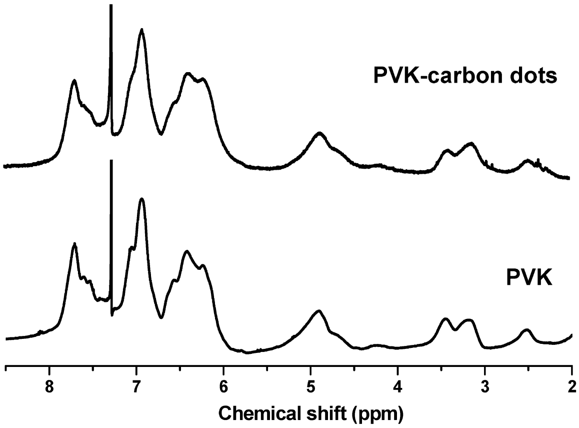

Figure 6. The proton NMR spectrum of the PVK-carbon dots in $CDCl_3$ is compared with that of the free PVK.

The already composite-like nature of the as-synthesized PVK-carbon dots samples made them ideal precursors in solution-phase processing for the fabrication of optically transparent PVK films dispersed with fluorescent carbon dots (Figure 7). In a typical fabrication protocol, a carbon dots sample was mixed well with a selected amount of neat PVK in solution, and the mixture was concentrated for wet-casting onto a clean glass slide. The PVK/carbon dots composite film thus formed could be peeled off to be free-standing (Figure 7). The film, special in terms of being free from any other materials or reagents besides the nanoscale carbon particles and PVK, exhibited largely similar optical absorption and fluorescence emissions to those of the PVK-carbon dots in solution (Figure 7).

The hybrid approach in this work that combines the more controllable feature of functionalizing pre-processed and selected carbon nanoparticles with the advantage of thermochemical synthesis enables highly versatile access to carbon dots of a variety of surface passivation agents. In comparison with the deliberate and specific chemical functionalization method, the hybrid approach is subject to much less constraints (including those that might be prohibitive), considerably more efficient, especially with the use of microwave processing. On the other hand, the use of pre-processed and selected carbon nanoparticles as precursor not only removes the limitation of relying on the direct carbonization to form size-wise homogeneously distributed carbon nanoparticles, which is generally speaking difficult or unlikely. In addition, there are abundant and inexpensive carbon sources from which the precursor carbon nanoparticles could be processed and selected for specific needs or configurations of the final carbon dots.

The carbon dots from the thermochemical functionalization of pre-processed and selected carbon nanoparticles were apparently very stable, probably due to the expected functionalization mode of PVK moieties being ‘melted’ onto the carbon nanoparticles. The samples and sample solutions of the PVK-carbon dots exhibited similar optical properties over a significant period of time, such as being stored under ambient conditions for several months.

4. Conclusion

As demonstrated in this work, the hybrid approach is more useful to the preparation of polymer-functionalized carbon dots for strongly absorptive and fluorescent nanocomposites without any unwanted foreign materials (such as the surface passivation agents in the 'conventional' carbon dots), thus with improved properties and performance. This is particularly valuable to nanocomposite materials targeted for optoelectronic devices, in which the presence of any foreign materials (essentially 'impurities') might have significant negative effects, such as those due to potentially microscopic phase separation.

The optical properties of the carbon dots from thermochemical synthesis reported here, including the fluorescence brightness, are in line with those from the deliberate chemical functionalization method, though somewhat toward the lower end. Therefore, further investigations on the hybrid approach for significant performance improvements of the resulting carbon dots, especially for higher fluorescence quantum yields across the visible spectrum, represent both challenges and opportunities.

Acknowledgments

The work at Clemson University (CU) was funded by U.S. National Science Foundation (Y.-P.S.). M.I.R. was a visiting student at CU supported by a grant from the Romanian National Authority for Scientific Research, CNCS-UEFISCDI, project number PNII-ID-PCCE-2011-2-0069 (A.T. and L.M.V.), and Z.L. also a visiting student at CU supported by Shantou University. Y.L. was on leave from Technical Institute of Physics and Chemistry in Beijing, China with a visiting scholarship provided by Chinese Academy of Sciences.

References

[1] Y.-P. Sun, et al., J. Am. Chem. Soc. 128 (2006) 7756, http://dx.doi.org/10.1021/ja062677d.

[2] H. Li, et al., Angew. Chem. Int. Ed. 49 (2010) 4430, http://dx.doi.org/10.1002/anie.200906154.

[3] P.G. Luo, F. Yang, S.-T. Yang, S.K. Sonkar, L. Yang, J.J. Broglie, Y. Liu, Y.-P. Sun, RSC Adv. 4 (2014) 10791, http://dx.doi.org/10.1039/C3RA47683A.

[4] Y. Wang, A. Hu, J. Mater. Chem. C 2 (2010) 6921, http://dx.doi.org/10.1039/C4TC00988F.

[5] F. Wang, Y.-H. Chen, C.-Y. Liu, D.-G. Ma, Chem. Commun. 47 (2011) 3502, http://dx.doi.org/10.1039/C0CC05391K.

[6] X. Zhang, et al., ACS Nano 7 (2013) 11234, http://dx.doi.org/10.1021/NN405017Q.

[7] X. Guo, C.-F. Wang, Z.-Y. Yi, L. Chen, S. Chen, Chem. Commun. 48 (2012) 2692, http://dx.doi.org/10.1039/C2CC17769B.

[8] L.-H. Mao, W.-Q. Tang, Z.-Y. Deng, S.-S. Liu, C.-F. Wang, S. Chen, Ind. Eng. Chem. Res. 53 (2014) 6417, http://dx.doi.org/10.1021/IE500602N.

[9] L.M. Veca, et al., Chem. Phys. Lett. 613 (2014) 40, http://dx.doi.org/10.1016/J.CPLET.T.059 201408.

[10] Q.-L. Chen, C.-F. Wang, S. Chen, J. Mater. Sci. 48 (2013) 2352, http://dx.doi.org/10.1007/s10853-012-7016-8.

[11] Q. Zhang, C.-F. Wang, L.-T. Ling, S. Chen, J. Mater. Chem. C 2 (2014) 4358, http://dx.doi.org/10.1039/C4TC00048J.

[12] Y. Wang, S. Kalytchuk, L. Wang, O. Zhovtiuk, K. Cepe, R. Zboril, A.L. Rogach, Chem. Commun. 51 (2015) 2950, http://dx.doi.org/10.1039/C4CC09589H.

[13] H.B. Wu, J.H. Zou, F. Liu, L. Wang, A. Mikhailovsky, G.C. Bazan, W. Yang, Y. Cao, Adv. Mater. 20 (2008) 696, http://dx.doi.org/10.1002/ADMA. 200701329.

[14] M. Molaei, M. Marandi, E. Saievar-Iranizad, N. Taghavinia, B. Liu, H.D. Sun, X.W. Sun, J. Lumin. 132 (2012) 467, http://dx.doi.org/10.1016/J.JLUMIN.201108.038.

[15] X. Wang, L. Cao, S.-T. Yang, F. Lu, M.J. Meziani, L. Tian, K.W. Sun, M.A. Bloodgood, Y.-P. Sun, Angew. Chem. Int. Ed. 49 (2010) 5310, http://dx.doi.org/10.1002/ANIE. 201000982.

[16] Z.-C. Yang, M. Wang, A.M. Yong, S.Y. Wong, X.-H. Zhang, H. Tang, A.Y. Chang, X. Li, J. Wang, Chem. Commun. 47 (2011) 11615, http://dx.doi.org/10.1039/C1CC14860E.

[17] Z. Zhang, J. Hao, J. Zhang, B. Zhang, J. Tang, RSC Adv. 2 (2012) 8599, http://dx.doi.org/10.1039/C2RA21217J.

[18] S. Sahu, B. Behera, T.K. Maiti, S. Mohapatra, Chem. Commun. 48 (2012) 8835, http://dx.doi.org/10.1039/C2CC33796G.

[19] S. Zhu, et al., Angew. Chem. Int. Ed. 52 (2013) 3953, http://dx.doi.org/10.1002/ANIE. 201300519.

[20] S.K. Bhunia, A. Saha, A.R. Maity, S.C. Ray, N.R. Jana, Sci. Rep. 3 (2013) 1473, http://dx.doi.org/10.1038/SREP01473.

[21] J. Xu, et al., ChemPhysChem 12 (2011) 3604, http://dx.doi.org/10.1002/CPHC. 201100640.

[22] G.E. LeCroy, et al., ACS Nano 8 (2014) 4522, http://dx.doi.org/10.1021/NN406628S.

[23] H. Zhu, X. Wang, Y. Li, Z. Wang, F. Yang, X. Yang, Chem. Commun. 5118 (2009), http://dx.doi.org/10.1039/B907612C.

[24] C. Liu, P. Zhang, F. Tian, W. Li, F. Li, W. Liu, J. Mater. Chem. 21 (2011) 13163, http://dx.doi.org/10.1039/C1JM12744F.

[25] A. Jaiswal, S.S. Ghosh, A. Chattopadhyay, Chem. Commun. 48 (2012) 407, http://dx.doi.org/10.1039/C1CC15988G.

[26] X. Zhai, P. Zhang, C. Liu, T. Bai, W. Li, L. Dai, W. Liu, Chem. Commun. 48 (2012) 7955, http://dx.doi.org/10.1039/C2CC33869F.

[27] S. Chandra, P. Das, S. Bag, D. Laha, P. Pramanik, Nanoscale 3 (2012) 1533, http://dx.doi.org/10.1039/C0NR00735H.

[28] S. Chandra, S.H. Pathan, S. Mitra, B.H. Modha, A. Goswami, P. Pramanik, RSC Adv. 2 (2012) 3602, http://dx.doi.org/10.1039/C2RA00030J.

[29] C. Liu, et al., Biomaterials 33 (2012) 3604, http://dx.doi.org/10.1016/J.BIOMATERIALS.052.201201.

[30] A. Sachdev, I. Matai, S.U. Kumar, B. Bhushan, P. Dubey, P. Gopinath, RSC Adv. 3 (2013) 16958, http://dx.doi.org/10.1039/C3RA42415D.

[31] L. Cao, M.J. Meziani, S. Sahu, Y.-P. Sun, Acc. Chem. Res. 46 (2013) 171, http://dx.doi.org/10.1021/AR300128J.

[32] C.E. Bunker, Y.-P. Sun, J. Am. Chem. Soc. 117 (1995) 10865, http://dx.doi.org/10.1021/JA00149A009.

[33] J.R. Lakowicz, Principles of Fluorescence Spectroscopy, Springer, 2006, http://dx.doi.org/10.1007/978-0-387-46312-4.

Journal of
Materials Chemistry C

PAPER

View Article Online
View Journal | View Issue

Cite this: *J. Mater. Chem. C*, 2016, **4**, 10554

Photoexcited state properties of carbon dots from thermally induced functionalization of carbon nanoparticles

Yin Hu,[a] Mohamad M. Al Awak,[b] Fan Yang,[a] Sijia Yan,[a] Qingwu Xiong,[a] Ping Wang,[a] Yongan Tang,[c] Liju Yang,*[b] Gregory E. LeCroy,[a] Xiaofang Hou,[a] Christopher E. Bunker,[d] Linxi Xu,[a] Nicholas Tomlinson[a] and Ya-Ping Sun*[a]

Carbon dots are small carbon nanoparticles with various surface passivation schemes, in which more effective has been the deliberate chemical functionalization of the nanoparticles for brighter fluorescence emissions, even though the synthesis method is more tedious and subject to some limitations in the selection of functionalization molecules. Another more popular synthesis method has been the carbonization of organic species, with the method being more efficient and versatile, but less controllable regarding synthesis and achieving the desired dot structure and performance. In this work, a hybrid approach combining the advantageous characteristics of the two synthesis methods was applied to the preparation of carbon dots using polyethyleneimine (PEI) for surface passivation, where pre-processed and selected small carbon nanoparticles were functionalized with PEI by microwave-induced thermal reactions. Their optical absorption and fluorescence emission properties were evaluated, and the results suggested that the carbon dots thus prepared shared the same photoexcited state characteristics with those from the deliberate chemical functionalization, including comparable fluorescence colors and other properties. A further demonstration of the similarity in photoexcited state properties was based on the same visible light-activated bactericidal functions of the PEI-carbon dots as those found in carbon dots from the deliberate chemical functionalization method. The advantages and potential limitations of the hybrid approach for more controllable yet versatile and efficient syntheses of carbon dots are highlighted and discussed.

Received 24th August 2016,
Accepted 18th October 2016

DOI: 10.1039/c6tc03666j

www.rsc.org/MaterialsC

Introduction

Carbon "quantum" dots or more appropriately named carbon dots (for the lack of classical quantum confinement in these fluorescent carbon nanomaterials)[1–3] have attracted much recent attention,[2–9] from simple curiosity or fascination on the fact that any "carbon dirt" could be made to exhibit colorful fluorescence emissions[8–15] to the exploration of their various potential technological applications.[2–4,8,16–20] In fact, with a quick search of recent literature one would conclude that research on carbon dots has emerged as a highly active and rapidly expanding field, whose broad impacts similar to or even beyond those already derived from conventional semiconductor quantum dots (QDs)[21–26] may be envisaged.

Carbon dots are generally small carbon nanoparticles with various surface passivation schemes (Fig. 1),[1–3] in which more effective has been surface functionalization of the nanoparticles by organic molecules or biological species for more intense fluorescence emissions in the visible spectrum, extending to the near-IR.[2–4,27] Among the more popular approaches for the synthesis of carbon dots have been the deliberate chemical functionalization of small carbon nanoparticles[1,27–29] and carbonization (often in "one-pot") of organic or other carbon-containing precursors.[2,8,30,31] The deliberate functionalization approach has been successful in terms of producing structurally well-defined carbon dots of high fluorescence quantum yields (more than 50% in some configurations),[27] but the synthesis is more tedious and subject to some limitations in the selection of molecules for functionalization. The carbonization approach is more efficient and versatile, compatible with a diverse selection

---

[a] *Department of Chemistry and Laboratory for Emerging Materials and Technology, Clemson University, Clemson, South Carolina 29634, USA. E-mail: syaping@clemson.edu*

[b] *Department of Pharmaceutical Sciences, Biomanufacturing Research Institute and Technology Enterprise, North Carolina Central University, Durham, NC 27707, USA. E-mail: lyang@nccu.edu*

[c] *Department of Mathematics and Physics, North Carolina Central University, Durham, NC 27707, USA*

[d] *Air Force Research Laboratory, Propulsion Directorate, Wright-Patterson Air Force Base, Ohio 45433, USA*

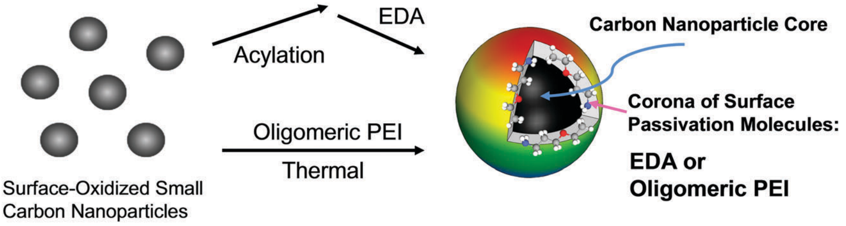

Fig. 1 A cartoon illustration of reaction schemes based on chemical functionalization (amidation with 2,2′-(ethylenedioxy)bis(ethylamine) or EDA,[29] as an example) and thermally induced functionalization with oligomeric polyethyleneimine (PEI). Regarding the cartoon on a carbon dot, it is generally a small carbon nanoparticle core with attached and strongly adsorbed surface passivation molecules (a configuration similar to a soft corona).

of precursors and functionalization molecules or species, but less controllable both in the synthesis and for the desired structures of produced carbon dots, among other processing and performance issues.[2–4,6,8] Thus, an interesting and useful strategy is to combine the advantageous characteristics of the two synthetic approaches for more controllable yet efficient and versatile preparations of carbon dots. Specifically for such a hybrid approach,[32] the pre-processed and selected small carbon nanoparticles are used as a precursor, but instead of chemical functionalization reactions, the molecules or species designed for surface passivation are "attached to" (or more like "welded onto") the carbon nanoparticles in thermally induced reactions, in which the molecules for passivation may also be slightly or partially carbonized in the reactions (Fig. 1). Nevertheless, the hybrid approach still adheres closely to the definition of carbon dots as surface-passivated small carbon nanoparticles.

In this work, the hybrid approach was applied to the preparation of carbon dots using polyethyleneimine (PEI) for surface passivation (Fig. 1), where small carbon nanoparticles from the processing of a commercially supplied carbon nanopowder sample were functionalized with PEI in microwave-induced thermal reactions. The optical absorption and fluorescence emission properties were evaluated, and the results suggested that the carbon dots thus prepared shared the same photoexcited state characteristics with those synthesized by the deliberate chemical functionalization approach (such as the carbon dots with EDA for surface functionalization, Fig. 1), including comparable fluorescence colors and other properties. A further demonstration on the similarity in photoexcited state properties was based on the same visible light-activated bactericidal functions of the PEI-carbon dots as those found in carbon dots synthesized by the deliberate chemical functionalization approach. The advantages and potential limitations of the hybrid approach for more controllable yet versatile and efficient syntheses of carbon dots with desired photoexcited state properties are highlighted and discussed.

Results and discussion

A commercially acquired carbon nanopowder sample was used as a precursor in the processing employed to harvest small carbon nanoparticles. Briefly, the as-supplied carbon nanopowder sample was refluxed in nitric acid, followed by dialysis and centrifugation to obtain mostly smaller carbon nanoparticles in an aqueous suspension,[29] which appeared transparent and solution-like. The observed absorption spectrum of the suspension was similar to those of similarly processed carbon nanoparticles reported previously, so were the relatively weak fluorescence emission spectra.[33–35] According to atomic force microscopy (AFM) results, these particles were on the order of 5 nm in diameter, also similar to those reported previously.

An oligomeric polyethylenimine (PEI) of a more branched structure, which contains a significant number of primary amine moieties and is structurally more compact, was used for the functionalization of the carbon nanoparticles. Experimentally, carbon nanoparticles were mixed with PEI and a small amount of ethanol *via* vigorous sonication at a temperature slightly above the ambient temperature, followed by the removal of ethanol *via* evaporation. The resulting mixture was heated in a conventional microwave oven following a multiple-cycle regimen such that the sample was heated until smoke started to appear, then cooled in the ambient temperature for a short period of time, and the same heating and cooling processes were repeated for a total of up to 30 heating–cooling cycles. Post-processing, the sample again at ambient temperature was dispersed in water with vigorous sonication. The resulting aqueous dispersion was centrifuged at 20 000*g* to collect the supernatant, followed by dialysis in a membrane tubing against fresh water to remove unreacted PEI and other small molecular impurities to obtain the PEI-carbon dots as a clear solution (Fig. 2). The results of AFM analyses of the PEI-carbon dot sample suggest that these dots are size-wise relatively narrowly distributed, on average are 6.5 nm in diameter with the size distribution standard deviation a little more than 1 nm (Fig. 3).

The absorption spectrum of the PEI-carbon dots in aqueous solution is shown in Fig. 2, which is similar to those of the precursor carbon nanoparticles and also carbon dots prepared from deliberate chemical functionalization (such as EDA-carbon dots, Fig. 2),[29] supporting the notion that the optical absorption in carbon dots is due to electronic transitions in the core carbon nanoparticles.[36] Also shown in Fig. 2 is the fluorescence spectrum of the PEI-carbon dots in an aqueous solution at 400 nm excitation, which is again comparable with that of the EDA-carbon dots.[29]

The PEI-carbon dots in solution were characterized by using a solution-phase NMR technique, and the results were compared with those of free PEI used in the functionalization reaction.

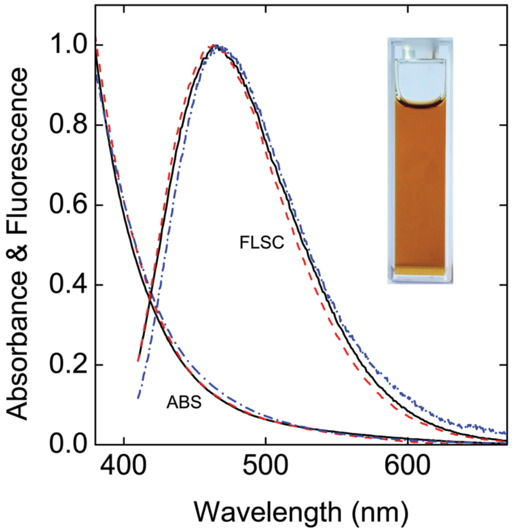

Fig. 2 Absorption (ABS) and fluorescence (FLSC, 400 nm excitation) spectra of PEI-carbon dots in aqueous solutions (solid line: as-synthesized; dash line: the more fluorescent sample from fractionation), and the spectra of the EDA-carbon dots (dash-dotted line)[29] also shown for comparison. Inset: photo of an aqueous solution of the PEI-carbon dots.

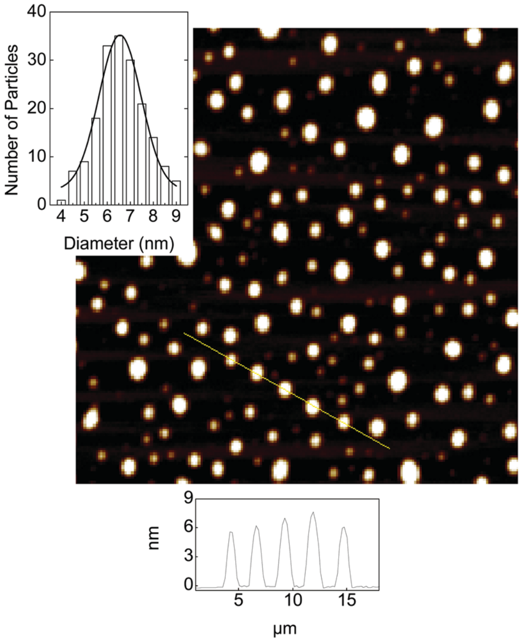

Fig. 3 An AFM image of the PEI-carbon dots on a mica surface, with height analyses of the selected dots. Inset: statistical analysis of the size data from height analyses of more than 150 dots in multiple AFM images.

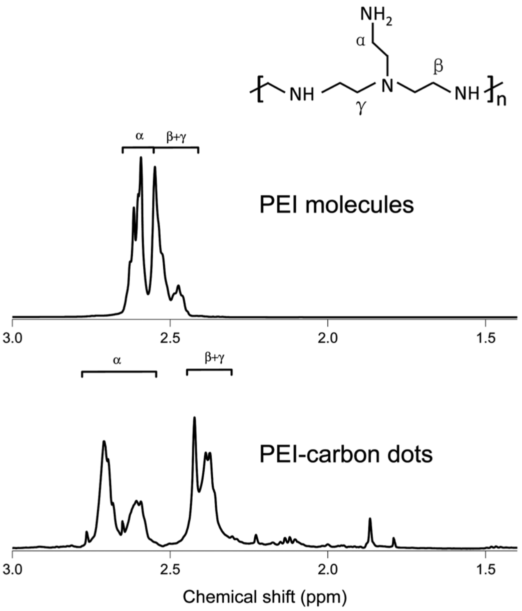

Fig. 4 The proton NMR spectra of neat PEI (top, with different groups of protons marked in the chemical structure) and the PEI-carbon dots (bottom) in deuterated water.

As shown in Fig. 4, the proton NMR signals of the PEI-carbon dots in deuterated water are significantly broader than those of free PEI, consistent with the expected lower mobility of the PEI species attached to carbon nanoparticles.[37] A similar broadening effect was observed in carbon dots prepared by deliberate chemical functionalization with small organic molecules, such as in the EDA-carbon dots,[29] though to a somewhat lesser extent, because signals of the free PEI are already broad (Fig. 4). Overall, the proton NMR signals of the PEI-carbon dots in reference to those of free PEI could be assigned to two groups, one for the α protons, which is downfield-shifted from that of free PEI (Fig. 4), and might be attributed to some de-shielding effect that resulted from the binding and/or strong interactions of the amino groups with carbon nanoparticles, and the other for the β and γ protons (Fig. 4). The relative integrations between the α and β + γ proton signals (1-to-1.1) are unchanged from free PEI to the PEI-carbon dots, suggesting no major structural changes in the particle-bound PEI species.

Fluorescence spectra of the PEI-carbon dots in aqueous solution were also measured more systematically as a function of excitation wavelengths. Similar to those found in carbon dots from other syntheses (again the EDA-carbon dots, for example),[29] the excitation wavelength dependence exhibited progressive red shifts and a narrowing of the emission band width with excitation at longer wavelengths (Fig. 5). The excitation wavelength dependence of fluorescence quantum yields followed a similar pattern, as also shown in Fig. 5, again similar to those of carbon dots obtained from other syntheses.[1,29,35] The dependencies of fluorescence spectra and quantum yields on excitation wavelengths have been rationalized previously as being associated with the selective access of different collections of emissive excited states, with less states accessed at longer wavelength excitations.[1,36]

Fluorescence decays of the PEI-carbon dots were measured by using the time-correlated single photon counting (TCSPC) technique (Fig. 6). The observed decays at both 400 nm and 440 nm excitations could be deconvoluted with a bi-exponential function, and the results are shown in Table 1. It should be pointed out that despite the good deconvolution fits, the excited states and processes in the carbon dots are likely more complicated than

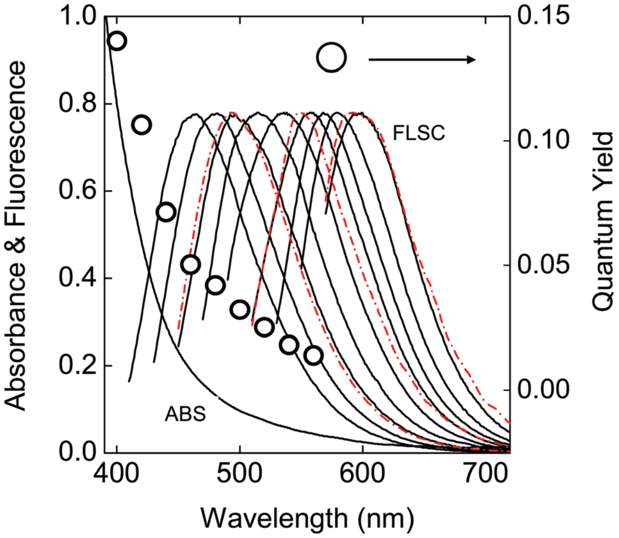

Fig. 5 Absorption (ABS) and fluorescence (FLSC) spectra and quantum yields of the PEI-carbon dots at different excitation wavelengths (spectra shown as solid lines from left to right corresponding to excitation wavelengths from 400 nm to 560 nm in 20 nm increment). The spectra of the EDA-carbon dots (dashed lines)[29] at 440 nm, 500 nm, and 560 nm excitations are also shown for comparison.

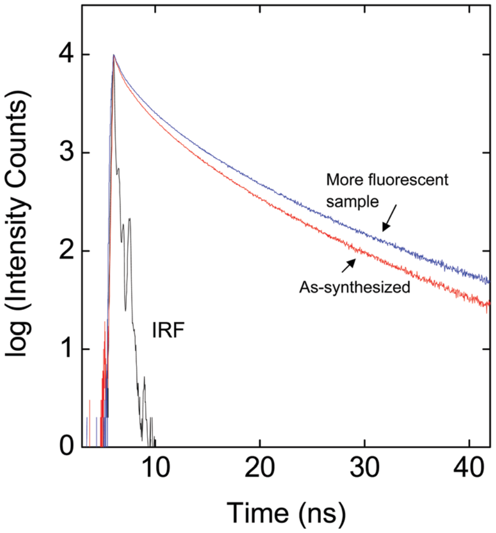

Fig. 6 Observed fluorescence decays of the as-synthesized PEI-carbon dots and the more fluorescent sample from fractionation (400 nm excitation).

only two emission contributions. Nevertheless, the phenomenological bi-exponential fits provide a reasonable averaging for the likely multi-component decay processes in these carbon dots. For the purpose of a more direct comparison, further averaging was made by using the pre-exponential factors (A_1 and A_2) and lifetimes (τ_{F1} and τ_{F2}) from the deconvolution fits, $\langle\tau_F\rangle = (A_1\tau_{F1}^2 + A_2\tau_{F2}^2)/(A_1\tau_{F1} + A_2\tau_{F2})$,[38] and the average fluorescence lifetime $\langle\tau\rangle$ values thus calculated are also shown in Table 1. These lifetime results are roughly comparable with those of the carbon dots from deliberate chemical functionalization syntheses.[27,35]

The spectroscopic results presented above suggest that the PEI-carbon dots obtained from thermally induced functionalization of small carbon nanoparticles by the PEI molecules are similar to carbon dots from more controlled chemical functionalization syntheses in terms of their optical transitions and fluorescence emissions, which reflect upon their associated excited state properties. From a somewhat different angle, the photoexcited state properties of carbon dots have been investigated by examining their photodynamic effects,[4] including, for example, the use of carbon dots for photoinduced killing of cancer cells[39–41] and also more recently for the visible light-driven bactericidal functions of the EDA-carbon dots.[42] Thus, the PEI-carbon dots obtained from the thermally induced functionalization were also evaluated for their ability to inhibit bacterial growth upon visible light activation.

Bacillus subtilis, a Gram-positive bacterium, has been a popular laboratory model organism and often considered as the Gram-positive equivalent of *Escherichia coli*, an extensively studied Gram-negative bacterium.[43–45] It was used in the evaluation of the visible light-activated antibacterial function of the PEI-carbon dots. Experimentally, a suspension of the cultured bacterial cells and an aqueous solution of the PEI-carbon dots were added to multiple-well plates, with the final bacterial cell concentration in each well about 10^6 CFU mL^{-1} and the concentration of the PEI-carbon dots was varied as needed (triplicates for each concentration). The plates were either exposed to visible light or kept in the dark for a pre-determined period of time. Immediately after treatment, the treated samples and the controls were serially diluted for the determination of the viable cell numbers by using the traditional plating method. The reduction in the viable cell number in the samples treated with the PEI-carbon dots and light in comparison to the controls was used as a measure of the efficiency of the light-activated bactericidal function. As shown in Fig. 7, for the sample treated with 0.02 mg mL^{-1} PEI-carbon dots, there were ~2.5 log viable cell reductions upon 1 h of light illumination, *versus* about 0.5 log reductions in the dark controls, indicating the substantial effect of visible light activation. The results are generally consistent with those from similar studies in which carbon dots from other syntheses were used.[42] However, the apparently somewhat

Table 1 Results of the deconvolution of observed fluorescence decays with a bi-exponential function

Sample	λ_{EX} (nm)	λ_{EM} (nm)	τ_{F1} (ns)	A_1 (%)	τ_{F2} (ns)	A_2 (%)	$\langle\tau_F\rangle^a$ (ns)	Φ_F
As-synthesized	400	480	0.7	9	3.3	91	3.2	0.12
	440	520	0.6	7	2.9	93	2.9	0.07
More fluorescent sample from the fractionation	400	480	0.9	8	4.4	92	4.3	0.22
	440	520	0.7	8	3.7	92	3.7	0.12

[a] The average fluorescence lifetime $\langle\tau_F\rangle = (A_1\tau_{F1}^2 + A_2\tau_{F2}^2)/(A_1\tau_{F1} + A_2\tau_{F2})$ (see ref. 38).

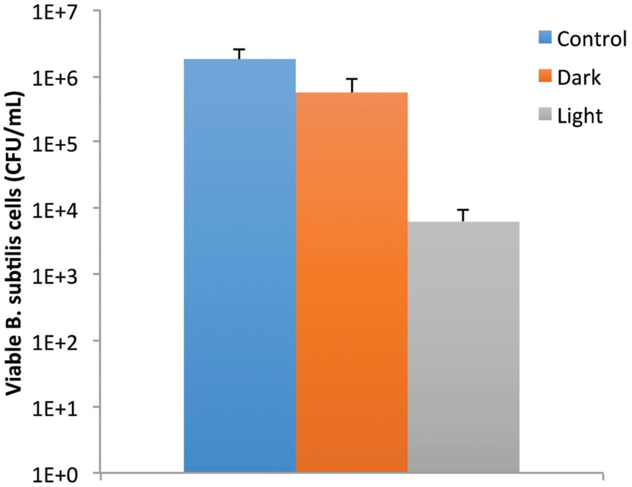

Fig. 7 Results on the viable cell number reduction after *B. subtilis* cells were treated with PEI-carbon dots (0.02 mg mL^{-1}) in the dark and upon 1 h of visible light illumination. Data are shown as mean ± standard deviation from triplicate tests.

significant antibacterial effect of the PEI-carbon dots even in the absence of light activation is puzzling. In addition to experimental factors such as the high sensitivity of the bactericidal function of carbon dots to even minimal ambient light exposure,[42] the carbon nanoparticle-bound PEI species might have some surfactant-like properties, slightly inhibitive to the bacterial cell growth in the dark controls. Nevertheless, the visible light activation obviously made the PEI-carbon dots orders of magnitude more effective in the inhibition of *B. subtilis*. The bacterial inhibition may be attributed to the photodynamic effect,[42] similar to what has been reported on the use of conventional semiconductor nanomaterials.[46–49]

Similar to carbon dots from other syntheses,[27,29] the sample of PEI-carbon dots from the thermally induced functionalization in this work contained a mixture of various fractions with different fluorescence performances. The more fluorescent fractions could be harvested *via* separation on an aqueous gel column, as similarly practiced and reported previously.[27,29] The aqueous gel column was packed in-house by using a commercially acquired Sephadex™ G-100 gel. In the fractionation, the sample of PEI-carbon dots was added to the column and eluted with water, and colored fractions were collected and characterized. The more fluorescent fractions (fluorescence quantum yields around 20% at 400 nm excitation) were combined into one sample, as the observed absorption and fluorescence spectra of the fractions were rather similar. For the more fluorescent sample thus obtained, its absorption and fluorescence spectra are similar to those of the as-synthesized sample pre-fractionation (Fig. 2). Interestingly, however, despite the significantly higher fluorescence quantum yields (Table 1), the more fluorescent sample from the fractionation exhibited fluorescence decays similar to those of the as-synthesized sample pre-fractionation (Fig. 6 and Table 1). Such a decoupling between changes in fluorescence quantum yields and decays (or average fluorescence lifetimes, Table 1) reflects upon the likely more complicated photoexcited state properties and processes in carbon dots, with significant mechanistic implications.

Mechanistically, the fluorescence emissions in carbon dots are attributed to radiative recombinations of photo-generated electrons and holes trapped at diverse surface defect sites.[17,35,50] Experimental evidence for the involvement of electrons and holes included the results on highly efficient fluorescence quenching of carbon dots by both electron donors and acceptors,[50] and the harvesting of the photo-generated electrons for various reactions such as the reduction of carbon dioxide into small organic molecules.[2,17,51] Within such a mechanistic framework, the apparent decoupling between the observed fluorescence quantum yields and decays may be rationalized by the presence of two primary excited state processes following the initial photoexcitation, one for the formation (or populating) of the emissive excited states and the other for the deactivation of these states *via* fluorescence emissions and competing nonradiative pathways.[38] Thus, with quantum yields for the former denoted as Φ_1 and those for the radiative process in the latter as Φ_2, the observed fluorescence quantum yields (Φ_F) must be reflecting a combination of the two processes, $\Phi_F = \Phi_1\Phi_2$. The first process represented by Φ_1 was apparently too fast to be captured in the fluorescence decay measurements, where the time resolution in terms of the instrument response function was on the order of 100–200 ps, so that the observed fluorescence decays were associated only with the deactivation process of the emissive excited states. Thus, the average fluorescence lifetimes (Table 1) are coupled with the quantum yields Φ_2 for the radiative pathway in the second process. In general, carbon dots with more effective surface passivation exhibited brighter fluorescence emissions and correspondingly higher fluorescence quantum yields.[3,27,35] As such, the more fluorescent sample from the gel column fractionation was likely composed of carbon dots with more effective passivation by the surface-bound PEI species. Based on the discussion above, we can say that such enhanced fluorescence emissions and quantum yields must be primarily due to larger Φ_1 values. However, mechanistic details on how the improved surface passivation in carbon dots makes the Φ_1 process more efficient are yet to be probed and understood.

Conclusions

Thermally induced functionalization of pre-processed and selected small carbon nanoparticles with the oligomeric PEI yielded carbon dots with optical absorption and fluorescence properties similar to those of the dots synthesized by the deliberate chemical functionalization method. The similarity in the photoexcited state properties is also reflected in the observed visible light-activated bactericidal functions of the PEI-carbon dots. The results provide a clear validation of the hybrid approach employed for the preparation of carbon dots that combines the advantageous characteristics of the method of deliberate chemical functionalization synthesis and those of the method based on the carbonization of organic and other carbon-containing precursors. Carbon dots prepared by the deliberate chemical functionalization method are generally nontoxic according to the results available from cytotoxicity and *in vivo* toxicity studies.[3,4,16,52–54] Similar investigation on the PEI-carbon dots will be pursued.

Experimental section

Materials

The carbon nanopowder sample was purchased from US Research Nanomaterials, Inc., polyethyleneimine (PEI, branched, average molecular weight ∼ 1200) was obtained from Polyscience, Inc., and silicon carbide (120 grit) was from Panadyne Abrasives. Nitric acid was obtained from Fisher Scientific and deuterated water for NMR experiments was from Cambridge Isotope Laboratories. The dialysis membrane tubes (molecular weight cut-off ∼ 500 and ∼ 1000) were supplied by Spectrum Laboratories. Water was deionized and purified by passing through a Labconco WaterPros water purification system.

Measurements

UV/vis absorption spectra were recorded on a Shimadzu UV2501-PC spectrophotometer. Fluorescence spectra were acquired on a Jobin-Yvon emission spectrometer equipped with a 450 W xenon source, Gemini-180 excitation and Tirax-550 emission monochromators, and a photon counting detector (Hamamatsu R928P PMT at 950 V). 9,10-Bis(phenylethynyl)-anthracene in cyclohexane was used as a standard in the determination of fluorescence quantum yields by the relative method (matching the absorbance at the excitation wavelength between the sample and standard solutions and comparing their corresponding integrated total fluorescence intensities). Fluorescence decays were measured in terms of the time-correlated single photon counting (TCSPC) technique on a Horiba Ultima Extreme spectrometer. The spectrometer is equipped with a SuperK Extreme supercontinuum laser source operating at 3.894 MHz repetition rate, TDM-800 excitation and TDM-1200 emission monochromators, a R3809-50 MCP-PMT detector operated at 3.0 kV in a thermoelectrically cooled housing, and FluoroHub A+ timing electronics. Analyses of the decay curves were performed by using Horiba Das6 fluorescence decay analysis software. NMR measurements were carried out on a Bruker Advance 500 NMR spectrometer. Atomic force microscopy (AFM) images were acquired in the acoustic AC mode on a Molecular Imaging PicoPlus AFM system equipped with a multipurpose scanner and a NanoWorld point probe NCH sensor. The height profile analysis was assisted by using SjPIP software distributed by Image Metrology.

Carbon dots

Small carbon nanoparticles were harvested from the commercially acquired carbon nanopowder sample in a procedure similar to those reported previously.[29,35] In a typical experiment, the carbon nanopowder sample (2 g) was refluxed in aqueous nitric acid (8 M, 200 mL) for 48 h. The reaction mixture was cooled to room temperature and centrifuged at 1000*g* to discard the supernatant. The residue was re-dispersed in deionized water, dialyzed in a membrane tubing (molecular weight cut-off ∼ 500) against fresh water for 48 h, and then centrifuged at 1000*g* to retain the supernatant. Upon the removal of water, carbon nanoparticles were recovered.

Carbon nanoparticles obtained from the above processing (100 mg) were mixed with PEI (2 g) and ethanol (1 mL) in a scintillation vial, and the mixture was sonicated (ultrasonic cleaner, VWR 250D) at 40 °C for 1 h, followed by the removal of ethanol *via* evaporation. Separately, a silicon carbide bath was prepared by placing silicon carbide (170 g) in a silica crucible casting dish (about 8 cm in diameter and 2.5 cm in height). The bath was pre-heated in a conventional microwave oven at 500 W for 3 min, and then the vial containing the mixture of carbon nanoparticles and PEI was immersed in the bath, followed by the microwave treatment in multiple cycles. In each cycle, the mixture in the bath was irradiated at 400 W until smoke started to appear. Upon irradiation for another 30 s, the vial containing the mixture was taken out of the bath for 1 min in the ambient temperature, and then immersed in the bath again for the next treatment cycle. After the microwave treatment of up to 30 heating–cooling cycles, the reaction mixture was cooled to the ambient temperature and dispersed in deionized water (10 mL) with vigorous sonication. The resulting aqueous dispersion was centrifuged at 20 000*g* for 30 min to collect the supernatant, followed by dialysis against fresh water for 24 h. The as-synthesized sample of the PEI-carbon dots was obtained as a colored aqueous solution. ^{1}H NMR (500 MHz, D_2O): δ 2.71 (m, br), 2.60 (m, br), 2.42 (m, br), 2.38 (m, br) ppm.

For more fluorescent PEI-carbon dots, the as-synthesized sample was separated in an aqueous gel column. The column was packed with the commercially supplied Sephadex™ G-100 gel by following the previously reported protocol.[27] Briefly, the gel (15 g) was soaked in water for 3 days, and the supernatant (including the suspended ultrafine gel) was discarded. The remaining gel was washed until no gel was suspended in the supernatant. Air bubbles were removed under vacuum. Separately, a glass column (25 mm inner diameter) was filled with water to remove air bubbles, and then closed. The gel suspension described above was poured into the column until reaching about 2 cm in height, and then the column was opened for the continuous addition of the gel suspension. The gel column was washed with water until no change in the height, followed by the testing and calibration.[27] In the fractionation of the as-synthesized PEI-carbon dot sample, a concentrated solution of the sample was added to the gel column and eluted with water. Colored fractions (80 drops per fraction) were collected for characterization and further investigation.

Light-activated bactericidal functions

Fresh grown *B. subtilis* cells in nutrient broth (Fisher Scientific, Pittsburgh, PA) were washed three times with PBS and then re-suspended in PBS. 96-well plates were utilized, to each well was added 150 μL of bacterial cell suspension and 50 μL of PEI-carbon dot solution. The final bacterial cell concentration in each well was about 10^6 CFU mL^{-1} and the concentration of the carbon dots was varied as needed (triplicates for each concentration). The plates were either exposed to visible light (12 V 36 W light bulb) or kept in the dark for 1 h. Immediately after the treatments, the samples were serially diluted in PBS. The viable cell numbers in the control and treated samples were determined by the traditional plating method. For each sample, aliquots of 100 μL appropriate dilutions were surface-plated on Luria-Bertani agar plates (Fisher Scientific, Pittsburgh, PA). After 24 h of incubation at 37 °C, the number of colonies was counted and the viable cell number was calculated in colony forming units per milliliter (CFU mL^{-1}) for all treated samples and the control. The reduction in the viable cell number in the carbon dots-treated samples in comparison to the control was used to evaluate the efficiency of bactericidal function of the PEI-carbon dots.

Acknowledgements

Financial support from NIH (R15GM114752) and the Air Force Office of Scientific Research through the program of Dr Charles Lee (Y.-P. S.) is gratefully acknowledged. Y. H. was a visiting student from Beijing Jiaotong University (China) and S. Y. and Q. X. were visiting students from Shantou University (China), with the visits sponsored by the China Scholarship Council and NSFC (51272152 and 21671127), respectively, and L. X. and N. T. were participants of the Palmetto Academy funded and managed by the South Carolina Space Grant Consortium.

References

1 Y.-P. Sun, B. Zhou, Y. Lin, W. Wang, K. A. S. Fernando, P. Pathak, M. J. Meziani, B. A. Harruff, X. Wang, H. F. Wang, P. G. Luo, H. Yang, M. E. Kose, B. L. Chen, L. M. Veca and S.-Y. Xie, *J. Am. Chem. Soc.*, 2006, **128**, 7756–7757.
2 K. A. S. Fernando, S. Sahu, Y. Liu, W. K. Lewis, E. A. Guliants, A. Jafariyan, P. Wang, C. E. Bunker and Y.-P. Sun, *ACS Appl. Mater. Interfaces*, 2015, **7**, 8363–8376.
3 G. E. LeCroy, S.-T. Yang, F. Yang, Y. Liu, K. A. S. Fernando, C. E. Bunker, Y. Hu, P. G. Luo and Y.-P. Sun, *Coord. Chem. Rev.*, 2016, **320**, 66–81.
4 P. G. Luo, F. Yang, S.-T. Yang, S. K. Sonkar, L. Yang, J. J. Broglie, Y. Liu and Y.-P. Sun, *RSC Adv.*, 2014, **4**, 10791–10807.
5 K. Hola, Y. Zhang, Y. Wang, E. P. Giannelis, R. Zboril and A. L. Rogach, *Nano Today*, 2014, **9**, 590–603.
6 Y. Wang and A. Hu, *J. Mater. Chem. C*, 2014, **2**, 6921–6939.
7 P. Miao, K. Han, Y. Tang, B. Wang, T. Lin and W. Cheng, *Nanoscale*, 2015, **7**, 1586–1595.
8 S. Y. Lim, W. Shen and Z. Gao, *Chem. Soc. Rev.*, 2015, **44**, 362–381.
9 Y. Du and S. Guo, *Nanoscale*, 2016, **8**, 2532–2543.
10 S.-S. Liu, C.-F. Wang, C.-X. Li, J. Wang, L.-H. Mao and S. Chen, *J. Mater. Chem. C*, 2014, **2**, 6477–6483.
11 P.-Y. Lin, C.-W. Hsieh, M.-L. Kung, L.-Y. Chu, H.-J. Huang, H.-T. Chen, D.-C. Wu, C.-H. Kuo, S.-L. Hsieh and S. Hsieh, *J. Biotechnol.*, 2014, **189**, 114–119.
12 R. Liu, J. Zhang, M. Gao, Z. Li, J. Chen, D. Wu and P. Liu, *RSC Adv.*, 2015, **5**, 4428–4433.
13 J. Xu, T. Lai, Z. Feng, X. Weng and C. Huang, *Luminescence*, 2015, **30**, 420–424.
14 B. D'Angelis do ES, J. R. Corrêa, G. A. Medeiros, G. Barreto, K. G. Magalhães, A. L. de Oliveira, J. Spencer, M. O. Rodrigues and B. A. Neto, *Chem. – Eur. J.*, 2015, **21**, 5055–5060.
15 J. B. Essner, C. H. Laber, S. Ravula, L. Polo-Parada and G. A. Baker, *Green Chem.*, 2016, **18**, 243–250.
16 S.-T. Yang, L. Cao, P. G. Luo, F. Lu, X. Wang, H. Wang, M. J. Meziani, Y. Liu, G. Qi and Y.-P. Sun, *J. Am. Chem. Soc.*, 2009, **131**, 11308–11309.
17 L. Cao, S. Sahu, P. Anilkumar, C. E. Bunker, J. Xu, K. A. S. Fernando, P. Wang, E. A. Guliants, K. N. Tackett and Y.-P. Sun, *J. Am. Chem. Soc.*, 2011, **133**, 4754–4757.18.
18 Y. Dong, R. Wang, G. Li, C. Chen, Y. Chi and G. Chen, *Anal. Chem.*, 2012, **84**, 6220–6224.
19 S. Zhu, Q. Meng, L. Wang, J. Zhang, Y. Song, H. Jin, K. Zhang, H. Sun, H. Wang and B. Yang, *Angew. Chem., Int. Ed.*, 2013, **52**, 3953–3957.
20 A. Zhao, Z. Chen, C. Zhao, N. Gao, J. Ren and X. Qu, *Carbon*, 2015, **85**, 309–327.
21 J. D. Holmes, K. J. Ziegler, R. C. Doty, L. E. Pell, K. P. Johnston and B. A. Korgel, *J. Am. Chem. Soc.*, 2001, **123**, 3743–3748.
22 Z. Li and E. Ruckenstein, *Nano Lett.*, 2004, **4**, 1463–1467.
23 T. N. Lambert, N. L. Andrews, H. Gerung, T. J. Boyle, J. M. Oliver, B. S. Wilson and S. M. Han, *Small*, 2007, **3**, 691–699.
24 F. Erogbogbo, K.-T. Yong, I. Roy, G. Xu, P. N. Prasad and M. T. Swihart, *ACS Nano*, 2008, **2**, 873–878.
25 S. Prabakar, A. Shiohara, S. Hanada, K. Fujioka, K. Yamamoto and R. D. Tilley, *Chem. Mater.*, 2009, **22**, 482–486.
26 Z. Kang, Y. Liu and S.-T. Lee, *Nanoscale*, 2011, **3**, 777–791.
27 X. Wang, L. Cao, S.-T. Yang, F. Lu, M. J. Meziani, L. Tian, K. W. Sun, M. A. Bloodgood and Y.-P. Sun, *Angew. Chem., Int. Ed.*, 2010, **122**, 5438–5442.
28 P. Anilkumar, X. Wang, L. Cao, S. Sahu, J.-H. Liu, P. Wang, K. Korch, K. N. Tackett II, A. Parenzan and Y.-P. Sun, *Nanoscale*, 2011, **3**, 2023–2027.
29 G. E. LeCroy, S. K. Sonkar, F. Yang, L. M. Veca, P. Wang, K. N. Tackett II, J.-J. Yu, E. Vasile, H. Qian, Y. Liu, P. G. Luo and Y.-P. Sun, *ACS Nano*, 2014, **8**, 4522–4529.
30 P.-C. Hsu and H.-T. Chang, *Chem. Commun.*, 2012, **48**, 3984–3986.
31 C. Stan, C. Albu, A. Coroaba, M. Popa and D. Sutiman, *J. Mater. Chem. C*, 2015, **3**, 789–795.
32 M. I. Rednic, Z. Lu, P. Wang, G. E. LeCroy, F. Yang, Y. Liu, H. Qian, A. Terec, L. M. Veca, F. Lu and Y.-P. Sun, *Chem. Phys. Lett.*, 2015, **639**, 109–113.
33 S. C. Ray, A. Saha, N. R. Jana and R. Sarkar, *J. Phys. Chem. C*, 2009, **113**, 18546–18551.
34 L. Cao, P. Anilkumar, X. Wang, J.-H. Liu, S. Sahu, M. J. Meziani, E. Myers and Y.-P. Sun, *Can. J. Chem.*, 2010, **89**, 104–109.
35 Y. Liu, P. Wang, K. A. S. Fernando, G. E. LeCroy, H. Maimaiti, B. A. Harruff-Miller, W. K. Lewis, C. E. Bunker, Z.-L. Hou and Y.-P. Sun, *J. Mater. Chem. C*, 2016, **4**, 6967–6974.
36 L. Cao, M. J. Meziani, S. Sahu and Y.-P. Sun, *Acc. Chem. Res.*, 2013, **46**, 171–180.

37 R. H. Terrill, T. A. Postlethwaite, C.-h. Chen, C.-D. Poon, A. Terzis, A. Chen, J. E. Hutchison, M. R. Clark and G. Wignall, *J. Am. Chem. Soc.*, 1995, **117**, 12537–12548.

38 R. J. Lakowicz, *Principles of fluorescence spectroscopy*, Kluwer Academic/Plenum Publisher, New York, 2nd edn, 1999.

39 A. Kleinauskas, S. Rocha, S. Sahu, Y.-P. Sun and P. Juzenas, *Nanotechnology*, 2013, **24**, 325103.

40 Y. Choi, S. Kim, M. H. Choi, S. R. Ryoo, J. Park, D. H. Min and B. S. Kim, *Adv. Funct. Mater.*, 2014, **24**, 5781–5789.

41 H. Wang, G. Cao, Z. Gai, K. Hong, P. Banerjee and S. Zhou, *Nanoscale*, 2015, **7**, 7885–7895.

42 M. J. Meziani, X. Dong, L. Zhu, L. P. Jones, G. E. LeCroy, F. Yang, S. Wang, P. Wang, Y. Zhao, L. Yang, R. A. Tripp and Y.-P. Sun, *ACS Appl. Mater. Interfaces*, 2016, **8**, 10761–10766.

43 P. Graumann, *Bacillus: Cellular and Molecular Biology*, Horizon Scientific Press, Germany, 2nd edn, 2012.

44 P. Govind, *Int. Res. J. Pharm.*, 2011, **2911**, 62–65.

45 S. Mukherjee and D. B. Kearns, *Annu. Rev. Genet.*, 2014, **48**, 319–340.

46 T. Matsunaga, R. Tomoda, T. Nakajima, N. Nakamura and T. Komine, *Appl. Environ. Microbiol.*, 1988, **54**, 1330–1333.

47 K. Sunada, T. Watanabe and K. Hashimoto, *J. Photochem. Photobiol., A*, 2003, **156**, 227–233.

48 M. Cho, H. Chung, W. Choi and J. Yoon, *Appl. Environ. Microbiol.*, 2005, **71**, 270–275.

49 A. S. Garcez, S. C. Núñez, M. S. Baptista, N. A. Daghastanli, R. Itri, M. R. Hamblin and M. S. Ribeiro, *Photochem. Photobiol. Sci.*, 2011, **10**, 483–490.

50 X. Wang, L. Cao, F. Lu, M. J. Meziani, H. Li, G. Qi, B. Zhou, B. A. Harruff, F. Kermarrec and Y.-P. Sun, *Chem. Commun.*, 2009, 3774–3776.

51 S. Sahu, Y. Liu, P. Wang, C. E. Bunker, K. A. S. Fernando, W. K. Lewis, E. A. Guliants, F. Yang, J. Wang and Y.-P. Sun, *Langmuir*, 2014, **30**, 8631–8636.

52 S.-T. Yang, X. Wang, H. Wang, F. Lu, P. G. Luo, L. Cao, M. J. Meziani, J.-H. Liu, Y. Liu, M. Chen, Y. Huang and Y.-P. Sun, *J. Phys. Chem. C*, 2009, **113**, 18110–18114.

53 Y. Wang, P. Anilkumar, L. Cao, J.-H. Liu, P. G. Luo, K. N. Tackett, S. Sahu, P. Wang, X. Wang and Y.-P. Sun, *Exp. Biol. Med.*, 2011, **236**, 1231–1238.

54 J.-H. Liu, L. Cao, G. E. LeCroy, P. Wang, M. J. Meziani, Y. Dong, Y. Liu, P. G. Luo and Y.-P. Sun, *ACS Appl. Mater. Interfaces*, 2015, **7**, 19439–19445.

ACS APPLIED MATERIALS & INTERFACES

Research Article

www.acsami.org

Flexible Graphene–Graphene Composites of Superior Thermal and Electrical Transport Properties

Zhi-Ling Hou,[†] Wei-Li Song,*[,‡] Ping Wang,[†] Mohammed J. Meziani,*[,§] Chang Yi Kong,[†] Ankoma Anderson,[†] Halidan Maimaiti,[†] Gregory E. LeCroy,[†] Haijun Qian,[†] and Ya-Ping Sun*[,†]

[†]Department of Chemistry and Laboratory for Emerging Materials and Technology, Clemson University, Clemson, South Carolina 29634-0973, United States

[‡]Institute of Advanced Materials and Technology, University of Science and Technology Beijing, Beijing 100083, China

[§]Department of Natural Sciences, Northwest Missouri State University, Maryville, Missouri 64468, United States

S Supporting Information

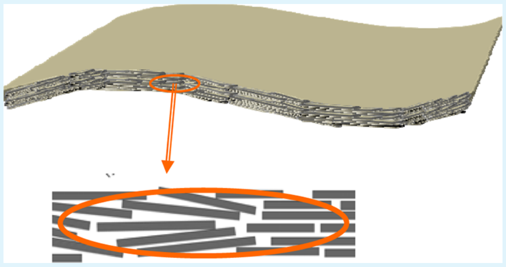

ABSTRACT: Graphene is known for high thermal and electrical conductivities. In the preparation of neat carbon materials based on graphene, a common approach has been the use of well-exfoliated graphene oxides (GOs) as the precursor, followed by conversion to reduced GOs (rGOs). However, rGOs are more suitable for the targeted high electrical conductivity achievable through percolation but considerably less effective in terms of efficient thermal transport dictated by phonon progression. In this work, neat carbon films were fabricated directly from few-layer graphene sheets, avoiding rGOs completely. These essentially graphene–graphene composites were of a metal-like appearance and mechanically flexible, exhibiting superior thermal and electrical transport properties. The observed thermal and electrical conductivities are higher than 220 W/m·K and 85000 S/m, respectively. Some issues in the further development of these mechanically flexible graphene–graphene nanocomposite materials are discussed and so are the associated opportunities.

KEYWORDS: *thermal conductivity, electrical conductivity, graphene, composite film, flexible composite, graphene oxide*

INTRODUCTION

Light-weight materials of superior thermal and/or electrical transport properties have received much attention for their variety of technological applications, from the rapidly increasing demand in effective thermal management systems to the enabling technology for high-performance electronics.[1−4] Graphene nanosheets (GNs) are ideally suited for these materials, with the all-carbon two-dimensional configuration and delocalized π-electronic network for excellent thermal and electrical conductivities.[1−3,5−7] For thermal transport, both theoretical and experimental results have suggested in-plane thermal conductivity up to thousands of W/m·K units at the individual graphene sheet level.[5,6,8−10] Therefore, these nanosheets, including especially the few-layer ones, have been widely pursued as fillers in polymeric nanocomposite materials for much enhanced thermal conductivity.[1,11−17] For example, Haddon and co-workers dispersed graphite nanoplatelets into epoxy matrixes to obtain composites of thermal conductivity up to 6.44 W/m·K at 25 vol % filler loading.[11] Veca et al. fabricated flexible nanocomposite films of epoxy polymer with few-layer GNs, with the observed in-plane thermal conductivity close to 80 W/m·K at 33 vol % filler loading.[13] GNs have also been used as filler in polymeric nanocomposites for electrically conductive properties, although the filler loading in these nanocomposites has often been at the lower side. This is probably due to the fact that mechanistically the electrical conductivity is dictated by percolation while the thermal conductivity is associated with phonon propagation (vibrational motion propagating through condensed matter).

The concept and practice on graphene-based composites go beyond the polymeric systems, including also the development of all-carbon nanocomposites from GNs and their derived precursors.[18−22] In targeted thermal transport applications, these nanocomposites are often pursued as an alternative to the highly ordered pyrolytic graphite materials of ultimate performance (the in-plane thermal conductivity of 400−1800 W/m·K, for example).[12,23−26] However, the ordered graphite materials are sometimes limited by other properties, such as their brittle nature not suitable for applications that require flexible structures, and they are generally very high in cost.[24−26] There have been a number of reported strategies on the development of flexible graphene composites with nanoscale structural features.[1,18−22] For example, Xiang and Drzal prepared papers of neat graphite nanoplatelets through mechanical pressing for high thermal transport performance.[19] Further improvements in the performance were achieved by processing the papers in a combination of thermal-annealing and hot-press treatment, reaching an in-plane thermal

Received: May 14, 2014
Accepted: August 13, 2014
Published: August 13, 2014

dx.doi.org/10.1021/am502986j | *ACS Appl. Mater. Interfaces* 2014, 6, 15026−15032

conductivity of 313 W/m·K.[20] Tian et al. used exfoliated graphene oxides (GOs) for the dispersion of few-layer GNs and also as the precursor for reduced GOs (rGOs).[18] The nanocomposite films thus fabricated were thermally annealed to facilitate the GOs-to-rGOs conversion, which was accompanied by the removal of oxygen-containing groups or species to allow more intimate contacts between rGOs and the embedded few-layer GNs. The resulting essentially all-carbon films exhibited excellent thermal transport properties, with the observed thermal diffusivity (TD) higher than those in aluminum and copper metals.[18] For similar materials of high electrical conductivity, Huang et al. prepared papers from aqueous dispersed graphene sheets that were functionalized with benzenesulfonic acid groups, followed by thermal annealing to reach 44500 S/m in electrical conductivity.[27] Bi et al. fabricated similar papers with somewhat different graphene precursors, which exhibited improved electrical conductivity to 109700 S/m.[28] The use of rGOs for the same purpose has also been popular. Chen et al. prepared GO papers for subsequent chemical reduction and thermal annealing to attain electrical conductivity up to 35100 S/m.[29] The use of large GO sheets as precursors could apparently improve the performance of the resulting papers, according to Lin et al.,[30] with the observed electrical conductivity reaching 139000 S/m after the papers were annealed at a high temperature (1100 °C). However, thermal annealing of GO papers even at relatively low temperatures (such as 200 °C) could degrade their mechanical properties in terms of the paper integrity and flexibility.[29]

In the study reported here, we fabricated flexible nanocomposite films of few-layer graphene sheets directly, without the use of rGOs to avoid their known performance deficiencies in the targeted all-carbon materials. The processed graphene–graphene (GN–GN) composite films, which were of a metal-like appearance and mechanically flexible, exhibited superior thermal and electrical transport properties. The observed thermal and electrical conductivities are higher than 220 W/m·K and 85000 S/m, respectively.

■ RESULTS AND DISCUSSION

The few-layer GNs were prepared via exfoliation of commercially supplied graphite flakes in a combination of alcohol–water and oxidative acid treatments.[13,18] In the alcohol–water treatment, the as-supplied graphite sample was stirred vigorously and sonicated in an alcohol–water mixture. The sample was then dispersed in a precooled mixture of concentrated nitric acid and sulfuric acid with vigorous sonication. The post-treatment processing included dilution, filtration, and repeated washing of the sample with water until neutral pH was reached. Upon the removal of water and then drying in a vacuum oven, the sample was characterized by using powder X-ray diffraction and Raman spectroscopy. In the former (Figure 1), the diffraction pattern exhibited a broad peak centered at $2\theta \sim 26.5°$, corresponding to the (002) interlayer. According to the Scherrer equation,[31] the peak broadening was consistent with the GNs of an expected average thickness on the order of 10 nm or less. The lateral dimension for the GNs was generally a few microns edge-to-edge based on the optical microscopy results. The Raman spectrum of the GNs was featured with a strong G band and a significant D band (Figure 1), suggesting a meaningful increase of defects from those in the precursor graphite sample.

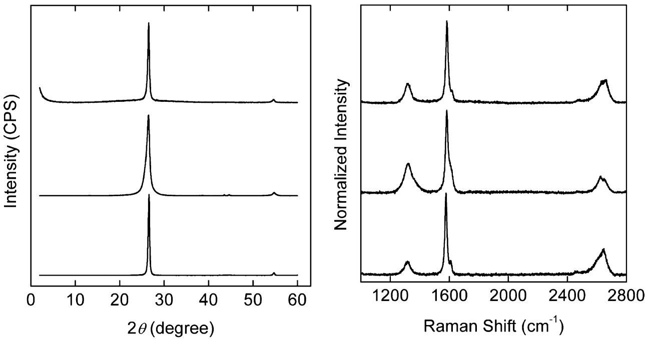

Figure 1. X-ray diffraction patterns (left) and Raman spectra (right) of precursor GNs (bottom in both figures), as-fabricated GN–GN nanocomposite films (middle), and the films post thermal annealing (top).

The GN–GN nanocomposite film fabrication was based on the vacuum filtration method, which has been popular in the preparation of various carbon-nanomaterial-derived film configurations, such as transparent conductive films and "bucky-papers" from carbon nanotubes.[32,33] A number of advantages have been discussed on the use of this method for nanotube films, including a more homogeneous distribution and improved packing of carbon nanotubes in the final films.[33−35] The homogeneity is attributed to the compensation effect naturally associated with the filtration process, such that the already deposited nanotubes reduce the flow of the nanotube suspension to have additional nanotubes deposited into other less dense areas of the film; the packing for improved contacts between nanotubes is credited to the vacuum-pressing in the filtration.[33−35] For the fabrication in this work, the GNs were dispersed in water via homogenization and sonication, and the resulting aqueous suspension was vacuum-filtered through a poly(vinylidene difluoride) (PVDF) filter (0.45 μm pore size) to form a black film on the filter surface. The film was peeled off to be free-standing and then dried in a vacuum oven at 70 °C. As shown in Figure 2, the film thus obtained (around 40 μm in thickness) was mechanically flexible, with a shiny metallic appearance. In the cycling bending test commonly used for evaluating the mechanical flexibility of film materials,[36] the film remained flexible after 50 repeated bending cycles (see also the Supporting Information, SI).

Conceptually, all-carbon films of this kind (Figure 2) are essentially GN–GN nanocomposites, although the basic nanoscale features in this case are at the level of several graphene layers (on the order of a few nanometers in thickness). These features were illustrated in the results from the cross-sectional transmission electron microscopy (TEM) imaging experiments. For TEM imaging, the GN–GN films were microtomed in the direction perpendicular to the film surface for slices of a thickness of less than 100 nm. The TEM images, with representative ones shown in Figure 3, are consistent with the expected film structures of compactly stacked GNs, each of thickness on the order of a few nanometers.

The as-fabricated GN–GN nanocomposite films were evaluated for their thermal transport properties by using a commercially acquired instrument based on the modified laser heating angstrom method,[37,38] measuring the in-plane TD in each film. The accuracy of the instrument for specimen of high TD was evaluated and validated by measuring the standard copper and silver metal films (with known TD values of 117

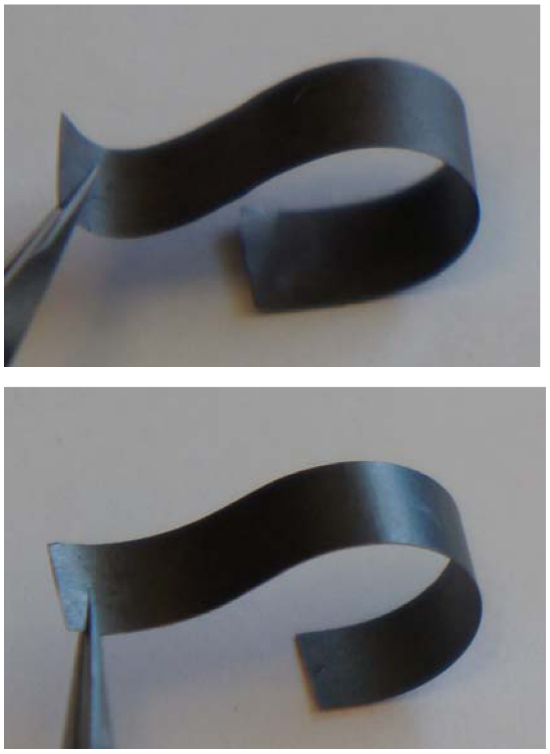

Figure 2. Photographs on a representative as-fabricated GN−GN nanocomposite film (top) and post thermal annealing (bottom). The film dimension was about 5.5 mm × 40 mm.

and 170 mm^2/s, respectively), from which the average deviations with respect to the use of different sets of instrumental parameters and in repeated measurements were generally less than 10%. For the GN−GN nanocomposite films, multiple measurements of several specimens yielded in-plane TD values of 136−174 mm^2/s, averaging 157 mm^2/s (Table 1).

Table 1. Thermal and Electrical Transport Parameters of the GN−GN Nanocomposite Films

sample	TD (mm^2/s)	electrical conductivity (S/m)
GN−GN film	157	70000
annealed GN−GN film	up to 300[a]	85000
rGO film	less than 20	~10000

[a] The value is higher than the calibrated upper limit of the experimental setup.

Theoretically, the thermal conductivity is proportional to the TD with a proportionality constant α, where α = density × specific heat. The experimentally measured density for the film was 1.68 g/cm^3. Therefore, with the commonly used specific heat value of 0.71 J/g·K for such graphitic materials, the average in-plane thermal conductivity of the as-fabricated GN−GN nanocomposite films is on the order of 187 W/m·K.

The thermal transport performance of these GN−GN films is apparently better than that of the previously reported nanocomposite films of GNs dispersed in rGOs.[18] The as-fabricated GN−GN nanocomposite films were also found to be highly electrically conductive, with a experimentally determined (by using the conventional four-probe method) electrical conductivity of about 70000 S/m (Table 1).

The film properties could be improved through thermal-annealing treatment to remove residual oxygen-containing groups and/or species carried over from the precursor GN samples used in the film fabrication. The annealing was at 1060 °C in an inert atmosphere (flowing argon gas) for about 2 h. For post thermal annealing, the shiny metallic appearance of the films was more pronounced, accompanied by a slight

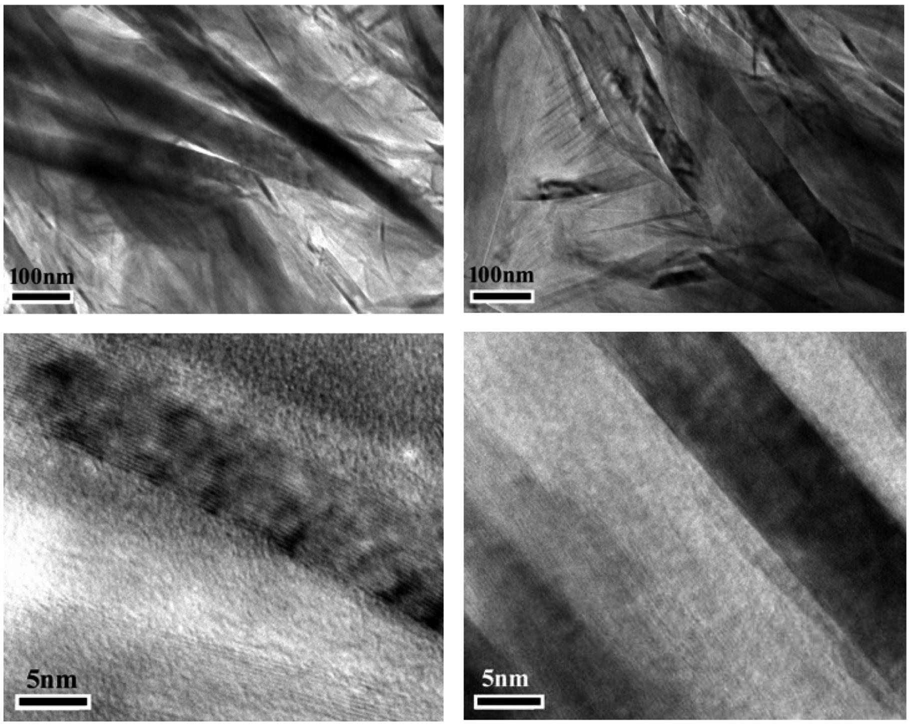

Figure 3. TEM images at lower (top) and higher (bottom) resolution on the slices from microtoming of the as-fabricated (left) and post thermal annealing (right) GN−GN nanocomposite films.

reduction in the film thickness and enhanced mechanical flexibility (Figure 2 and see also the SI). The X-ray diffraction peak of the annealed films became sharper (Figure 1), suggesting an increase (thicker) in the nanoscale features in the GN−GN films postannealing. The increase could be associated with several possible structural changes, including a partial restacking in the individual GN pieces (a reversal of the exfoliation) and an improved stacking between neighboring GN pieces. The latter, conceptually more consistent with the targeted GN−GN nanocomposite structures, should enhance the thermal and electrical transport properties. However, TEM analyses of the specimen from microtoming of the annealed GN−GN films yielded results that could not capture the nanoscale structural changes, with the observed images largely similar to those from the as-fabricated films before the annealing treatment (Figure 3). The Raman spectrum of the annealed films (Figure 1) exhibits a lower D band to G band ratio, consistent with the expected decrease of defects in the GN structures.

A piece of the GN−GN film was twisted until being fractured, and the fractured edge was examined using scanning electron microscopy (SEM). In the SEM image (Figure 4), the relatively well-ordered layer structure in the film is rather obvious.

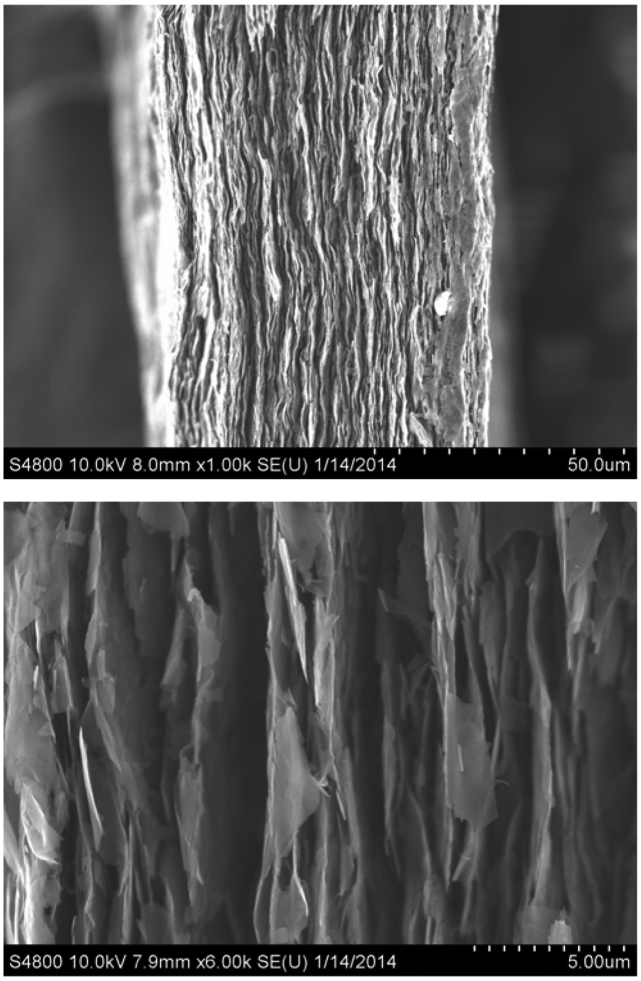

Figure 4. SEM images on the fractured edges of a representative GN−GN nanocomposite film.

X-ray photoelectron spectroscopy (XPS) results on atomic concentrations suggested that the annealed GN−GN film was purer than the graphite starting material in terms of carbon and oxygen contents, 98.3% and 1.7% in the former versus 97% and 3% in the latter, respectively. The as-fabricated film without annealing was not as pure, containing 90.4% carbon, 8.7% oxygen, and 0.9% nitrogen.

In the GN−GN films postannealing, there were indeed significant performance enhancements. The observed electrical conductivity increased more than 20% to 85000 S/m (Table 1). The enhancement in thermal transport was apparently even more substantial, with the observed in-plane TD values as high as 300 mm^2/s (Table 1). However, because the instrument was not designed specifically for such highly thermally conductive specimen (beyond the calibration with the standard silver metal film), the accuracy of the measurements and results could not be confirmed. Nevertheless, the annealed GN−GN nanocomposite films were apparently highly thermally conductive, more so than the standard silver metal film (known TD of 170 mm^2/s). Thus, the in-plane TD in the annealed GN−GN films should be in the range of 170−300 mm^2/s. The annealing also made the films more dense, with an experimentally measured density of 1.83 g/cm^3. Under the assumption of the specific heat being unchanged, which is a common practice in the literature, thermal conductivities of the annealed GN−GN films should be in the range of 220−390 W/m·K. Therefore, the thermal transport performance of these obviously flexible films is close to that found in some commercially supplied pyrolytic graphite materials (which are generally brittle with little mechanical flexibility).[24−26]

Experimentally, the film fabrication from the precursor GNs was relatively simple and stable in terms of being insensitive to unavoidable variations in duplicating preparations, with generally reproducible outcomes. The production of the precursor GNs was also insensitive to changes in the processing conditions (various lengths of sonication time, for example), which, on the one hand, provided stability in terms of yielding the precursor GNs in a relatively consistent fashion but, on the other hand, dampened the prospect of producing GNs of different nanoscale features by varying the processing conditions. In principle, thinner GNs would probably be more advantageous to further performance enhancements in the flexible GN−GN nanocomposite films, as extrapolated from the general desire for a better dispersion of lower-dimensional fillers in nanocomposite materials.[1] For such a purpose, rGOs recovered from well-exfoliated largely single-layer GOs may represent another extreme, namely, for the fabrication of rGO−rGO composite films with the nanoscale feature down to the single-layer rGO level. However, as reported previously[18,39,40] and confirmed in this study, such rGO films converted from GO films through an exhaustive processing effort, including chemical reduction, thermal annealing, etc., and their combinations, are generally poor in thermal transport performance. For example, the TD values for the rGO films with observed electrical conductivity of about 10000 S/m were less than 20 mm^2/s, considerably lower than those found in the GN−GN nanocomposite films discussed above with the few-layer GNs as precursors.

In the literature, rGO films of high electrical conductivity (139000 S/m, for example) have been reported.[30] The thermal conductivity to electrical conductivity ratios should be much lower in those films than in the GN−GN nanocomposite films obtained in this work. This is consistent with the mechanistic differences between electrical transport and thermal transport in the composite films, which are dictated by the electrical percolation and phonon progression in the filler nanostructures, respectively. The former is obviously more readily established in the conversion from GOs to rGOs; thus, high electrical conductivity in the rGO films is achieved. The GNs without their graphene structures being severely damaged like in GOs are apparently more robust precursors for highly thermally conductive films. The excellent mechanical flexibility and generally facile fabrication from inexpensive precursors make these all-carbon nanocomposite materials very competitive in many applications that demand ultrahigh thermal transport. Further performance enhancements with the use of thinner GNs, for which the production remains a challenge, may be expected.

In summary, few-layer GNs can be produced from the exfoliation of graphite in a relatively simple processing procedure, which is amenable to being scaled up because there is no meaningful bottleneck in the production. The GNs in aqueous dispersion can be fabricated directly into neat carbon films without any involvement of GOs or rGOs, and the resulting materials are essentially GN−GN nanocomposites both conceptually and practically. These unique nanocomposite materials offer superior thermal and electrical transport properties. While the observed electrical conductivity values for the GN−GN nanocomposites are no better than those achieved in well-fabricated rGO films, the thermal transport performance of the GN−GN nanocomposites is considerably more robust. In fact, the thermal conductivity in the GN−GN nanocomposites is close to that found in low-end pyrolytic graphite materials, yet the former (unlike the latter) remains mechanically flexible. Therefore, broad and significant applications of the GN−GN nanocomposites in thermal management and other systems may be envisaged.

■ EXPERIMENTAL SECTION

Materials. The graphite sample (surface-enhanced flake graphite, grade 3805) was supplied by Asbury Carbons. Sulfuric acid (93%), nitric acid (73%), ethanol, hydrogen peroxide (35%), and phosphorus pentoxide (P_2O_5) were purchased from Acros, ammonium persulfate ($(NH_4)_2S_2O_8$) was purchased from Aldrich, and potassium permanganate ($KMnO_4$) was purchased from Fisher Scientific. Poly(vinylidene difluoride) (PVDF) membrane filters (0.45 μm pore size) were acquired from Fisher Scientific, the dialysis membrane tubing (MWCO ≈ 3500) was acquired from Spectrum Laboratories, and carbon-coated copper grids for TEM analyses were acquired from SPI Supplies. Water was deionized and purified by being passed through a Labconco WaterPros water purification system.

Measurements. Powder X-ray diffraction measurements were carried out on a Scintag XDS-2000 powder diffraction system and XPS experiments on a Thermo Fisher Scientific ESCALAB 250xi system. Raman spectra were obtained on a Jobin Yvon T64000 Raman spectrometer equipped with a Melles-Griot 35 mW He−Ne laser source for 633 nm excitation, a triple monochromator, a liquid-nitrogen-cooled Symphony detector, and an Olympus BX-41 microscope. SEM images were acquired on a Hitachi S-4800 field-emission SEM system and TEM images on a Hitachi HD-2000 scanning TEM system and a Hitachi H-9500 TEM system with the specimen on a carbon- or holey-carbon-coated copper grid. In the TEM specimen preparation, a film sample was embedded in epoxy resin, followed by microtoming with the use of a Reichert-Jung Ultracut E microtome with a 30° angle diamond knife at room temperature for slices (cross-sectional with respect to the original film surface) of less than 100 nm thickness.

The in-plane TD of a free-standing thin film was determined on an Ulvac LaserPIT TD/conductivity meter operated at room temperature in a vacuum of 0.01 Pa and with the use of multiple frequencies in the measurements. The copper standard came with the instrument, and the commercially supplied (by Otto Frei Co.) silver film of 0.25 mm thickness was used as a reference sample. All of the film samples being tested were cut into rectangular pieces of 30 mm × 5 mm dimension. Commercially acquired silver paste was used as the binder to connect the specimen being tested with the sensor in the sample holder of the instrument.

The electrical conductivity of a film sample was measured by using the classical four-probe method, with the electrical current (I) and voltage (V) relationship for the film determined on the setup consisting of a multimeter (Keithley 2400 controlled by *Lab Tracer 2.0* software, both from Keithley Instruments) and a multiheight probe (Jandel). The electrical conductivity (σ) value was calculated according to the equation $\sigma = (\ln 2/\pi)(I/V)/d$, where d denotes the film thickness. Multiple spots were chosen in the measurement of each film sample, with the readings averaged for each specimen.

GN−GN Composite Films. The as-supplied graphite sample (average graphitic layer thickness on the order of 20−50 nm according to X-ray diffraction results) was processed in a combination of alcohol and oxidative acid treatments for exfoliation. In a typical experiment, the sample (1 g) was added to an alcohol−water mixture [13:7 (v/v), 400 mL], stirred at room temperature for 2 h, and then sonicated (VWR-250D, 120 W) for another 20 h. The sample was collected via filtration and then dried in a vacuum oven. A portion of the sample (250 mg) was added to a precooled (the temperature kept at less than 30 °C throughout) nitric acid−sulfuric acid mixture [1:3 (v/v), 80 mL] and sonicated in a bath sonicator for 72 h. The mixture was then transferred into water (2 L), followed by stirring at room temperature for 1 h to obtain aqueous dispersed GNs.

In the GN−GN film fabrication, an aqueous suspension of GNs (400 mL) was vacuum-filtered through a PVDF filter (0.45 μm pore size) to form a black film on the filter surface. The whole thing (film + filter) was washed repeatedly with deionized water until neutral pH was reached in the aqueous solution from washing. Then, the film was peeled off to be free-standing, followed by drying in a vacuum oven at about 75 °C.

GOs and Films. The preparation of GOs was based on the Hummers method[41] with minor modification. Briefly, concentrated H_2SO_4 (10 mL) in a 500 mL flask was heated to 80 °C, to which $(NH_4)_2S_2O_8$ (0.9 g) and P_2O_5 (0.9 g) were added. The mixture was stirred until the reagents were completely dissolved. The graphite sample (1 g) was added, and the resulting mixture was heated at 80 °C for 4.5 h. Then, the mixture was cooled to room temperature, diluted with water (250 mL), kept there for about 12 h, and filtered and washed repeatedly with water, followed by drying in a vacuum oven. The solid sample was added to concentrated H_2SO_4 (40 mL) in a 500 mL flask cooled in an ice bath. To the mixture was added slowly $KMnO_4$ (5 g over 40 min), during which the temperature was kept at lower than 10 °C. The reaction mixture, with a change in color from black to greenish brown, was heated at 35 °C for 2 h, followed by dilution with water (85 mL; ***caution!*** *the temperature must be kept at lower than 35 °C throughout*) and further stirring for 2 h. Then, the mixture was poured into a large beaker, to which water (250 mL) and then aqueous H_2O_2 (30%, 10 mL) were added. Bubbles from the aqueous mixture along with a color change to brilliant yellow were observed. After the mixture was allowed to settle for about 12 h, the clear supernatant was decanted, and the sediment was washed repeatedly with aqueous H_2SO_4 (5 wt %)−H_2O_2 (0.5 wt %) and a HCl solution (10 wt %), followed by repeated washing with water until no layer separation observed upon centrifugation. The sample was then dialyzed (MWCO ∼ 3500) against water for 7 days to yield a clean aqueous dispersion of GOs. The aqueous GOs thus obtained (acid form) were titrated by aqueous NaOH (0.1 M) until the pH was about 9. The resulting GOs (sodium form) were again dialyzed (MWCO ∼ 3500) for 7 days to reach neutral pH. Finally, the aqueous suspension of the GOs was diluted (∼0.2 wt %) and sonicated for 30 min to achieve complete exfoliation.

For the fabrication of neat GO films, the aqueous dispersed GOs (50 mg) were similarly vacuum-filtered through a PVDF filter (0.45

μm pore size) to form a dark-colored film on the filter surface. The film was peeled off to be free-standing, followed by drying in a vacuum oven at about 75 °C.

Thermal Annealing. The as-fabricated GN−GN composite films were heated in an inert atmosphere (flowing argon gas) in two steps, first slowly (2 °C/min) to 300 °C and then more quickly (7 °C/min) to 1060 °C, followed by thermal annealing at 1060 °C for 2 h. The same procedure was applied to thermal annealing of the neat GO films.

■ ASSOCIATED CONTENT

Ⓢ Supporting Information

Compiled literature data on electrical and thermal conductivities in graphene composites and details on the flexibility test. This material is available free of charge via the Internet at http://pubs.acs.org.

■ AUTHOR INFORMATION

Corresponding Authors

*E-mail: dexterquest@gmail.com.
*E-mail: meziani@nwmissouri.edu.
*E-mail: syaping@clemson.edu.

Notes

The authors declare no competing financial interest.

■ ACKNOWLEDGMENTS

Financial support from South Carolina Space Grant Consortium (SCSGC) and, in part, from the Air Force Office of Scientific Research (AFOSR) through the program of Dr. Charles Lee is gratefully acknowledged. Z.-L.H. was on leave from Beijing University of Chemical Technology in Beijing, China, and H.M. on leave from Xinjiang University in Urumqi, China, both with visiting scholarships provided by the China Scholarship Council. C.Y.K. was supported by the Excellent Young Researchers Overseas Visit Program of Japan Society for the Promotion of Science and A.A. by NASA through a Graduate Research Fellowship managed by SCSGC.

■ REFERENCES

(1) Song, W.-L.; Veca, L. M.; Anderson, A.; Cao, M.-S.; Cao, L.; Sun, Y.-P. Light-Weight Nanocomposite Materials with Enhanced Thermal Transport Properties. *Nanotechnol. Rev.* **2012**, *1*, 363−376.

(2) Yan, Z.; Liu, G.; Khan, J. M.; Balandin, A. A. Graphene Quilts for Thermal Management of High-Power GaN Transistors. *Nat. Commun.* **2012**, *3*, 827−834.

(3) Balandin, A. A. Thermal Properties of Graphene and Nanostructured Carbon Materials. *Nat. Mater.* **2011**, *10*, 569−581.

(4) Huang, H.; Liu, C. H.; Wu, Y.; Fan, S. S. Aligned Carbon Nanotube Composite Films for Thermal Management. *Adv. Mater.* **2005**, *17*, 1652−1656.

(5) Hu, J.; Ruan, X.; Chen, Y. P. Thermal Conductivity and Thermal Rectification in Graphene Nanoribbons: A Molecular Dynamics Study. *Nano Lett.* **2009**, *9*, 2730−2735.

(6) Ghosh, S.; Bao, W.; Nika, D. L.; Subrina, S.; Pokatilov, E. P.; Lau, C. N.; Balandin, A. A. Dimensional Crossover of Thermal Transport in Few-Layer Graphene. *Nat. Mater.* **2010**, *9*, 555−558.

(7) Chen, S.; Wu, Q.; Mishra, C.; Kang, J.; Zhang, H.; Cho, K.; Cai, W.; Balandin, A. A.; Ruoff, R. S. Thermal Conductivity of Isotopically Modified Graphene. *Nat. Mater.* **2012**, *11*, 203−207.

(8) Kong, B. D.; Paul, S.; Nardelli, M. B.; Kim, K. W. First-Principles Analysis of Lattice Thermal Conductivity in Monolayer and Bilayer Graphene. *Phys. Rev. B* **2009**, *80*, 033406.

(9) Balandin, A. A.; Ghosh, S.; Bao, W.; Calizo, I.; Teweldebrhan, D.; Miao, F.; Lau, C. N. Superior Thermal Conductivity of Single-Layer Graphene. *Nano Lett.* **2008**, *8*, 902−907.

(10) Ghosh, S.; Calizo, I.; Teweldebrhan, D.; Pokatilov, E. P.; Nika, D. L.; Balandin, A. A.; Bao, W.; Miao, F.; Lau, C. N. Extremely High Thermal Conductivity of Graphene: Prospects for Thermal Management Applications in Nanoelectronic Circuits. *Appl. Phys. Lett.* **2008**, *92*, 151911.

(11) Yu, A.; Ramesh, P.; Itkis, M. E.; Bekyarova, E.; Haddon, R. C. Graphite Nanoplatelet−Epoxy Composite Thermal Interface Materials. *J. Phys. Chem. C* **2007**, *111*, 7565−7569.

(12) Yu, A.; Ramesh, P.; Sun, X.; Bekyarova, E.; Itkis, M. E.; Haddon, R. C. Enhanced Thermal Conductivity in a Hybrid Graphite Nanoplatelet—Carbon Nanotube Filler for Epoxy Composites. *Adv. Mater.* **2008**, *20*, 4740−4744.

(13) Veca, L. M.; Meziani, M. J.; Wang, W.; Wang, X.; Lu, F.; Zhang, P.; Lin, Y.; Fee, R.; Connell, J. W.; Sun, Y.-P. Carbon Nanosheets for Polymeric Nanocomposites with High Thermal Conductivity. *Adv. Mater.* **2009**, *21*, 2088−2092.

(14) Liang, Q.; Yao, X.; Wang, W.; Liu, Y.; Wong, C. P. A Three-Dimensional Vertically Aligned Functionalized Multilayer Graphene Architecture: An Approach for Graphene-Based Thermal Interfacial Materials. *ACS Nano* **2011**, *5*, 2392−2401.

(15) Yavari, F.; Fard, H. R.; Pashayi, K.; Rafiee, M. A.; Zamiri, A.; Yu, Z.; Ozisik, R.; Borca-Tasciuc, T.; Koratkar, N. Enhanced Thermal Conductivity in a Nanostructured Phase Change Composite due to Low Concentration Graphene Additives. *J. Phys. Chem. C* **2011**, *115*, 8753−8758.

(16) Chu, K.; Jia, C.-C.; Li, W.-S. Effective Thermal Conductivity of Graphene-Based Composites. *Appl. Phys. Lett.* **2012**, *101*, 121916.

(17) Song, S. H.; Park, K. H.; Kim, B. H.; Choi, Y. W.; Jun, G. H.; Lee, D. J.; Kong, B.-S.; Paik, K.-W.; Jeon, S. Enhanced Thermal Conductivity of Epoxy−Graphene Composites by Using Non-Oxidized Graphene Flakes with Non-Covalent Functionalization. *Adv. Mater.* **2013**, *25*, 732−737.

(18) Tian, L.; Anilkumar, P.; Cao, L.; Kong, C. Y.; Meziani, M. J.; Qian, H.; Veca, L. M.; Thorne, T. J.; Tackett, K. N., II; Edwards, T.; Sun, Y.-P. Graphene Oxides Dispersing and Hosting Graphene Sheets for Unique Nanocomposite Materials. *ACS Nano* **2011**, *5*, 3052−3058.

(19) Xiang, J.; Drzal, L. T. Thermal Conductivity of Exfoliated Graphite Nanoplatelet Paper. *Carbon* **2011**, *49*, 773−778.

(20) Wu, H.; Drzal, L. T. Graphene Nanoplatelet Paper as a Light-Weight Composite with Excellent Electrical and Thermal Conductivity and Good Gas Barrier Properties. *Carbon* **2012**, *50*, 1135−1145.

(21) Yuan, G.; Li, X.; Dong, Z.; Westwood, A.; Cui, Z.; Cong, Y.; Du, H.; Kang, F. Y. Graphite Blocks with Preferred Orientation and High Thermal Conductivity. *Carbon* **2012**, *50*, 175−182.

(22) Lee, W.; Lee, J. U.; Jung, B. M.; Byun, J.-H.; Yi, J.-W.; Lee, S.-B.; Kim, B.-S. Simultaneous Enhancement of Mechanical, Electrical and Thermal Properties of Graphene Oxide Paper by Embedding Dopamine. *Carbon* **2013**, *65*, 296−304.

(23) Slack, G. A. Anisotropic Thermal Conductivity of Pyrolytic Graphite. *Phys. Rev.* **1962**, *127*, 694.

(24) Kastelein, B.; Vanbergen, R. D.; Postma, H.; Meijer, H. C.; Mathu, F. Thermal Conductance of Highly Oriented Pyrolytic-Graphite along the C-Direction at Very Low-Temperatures Including Magnetic-Field Effects. *Carbon* **1992**, *30*, 845−850.

(25) Wu, Z.-S.; Ren, W.; Gao, L.; Liu, B.; Jiang, C.; Cheng, H.-M. Synthesis of High-Quality Graphene with a Pre-Determined Number of Layers. *Carbon* **2009**, *47*, 493−499.

(26) Khlevnoy, B. B.; Samoylov, M. L.; Grigoryeva, I. A.; Ibragimov, N. A.; Shapoval, V. I.; Puzanov, A. V.; Ogarev, S. A. Development of High-Temperature Blackbodies and Furnaces for Radiation Thermometry. *Int. J. Thermophys.* **2011**, *32*, 1686−1696.

(27) Huang, W.; Ouyang, X.; Lee, L. J. High-Performance Nanopapers Based on Benzenesulfonic Functionalized Graphenes. *ACS Nano* **2012**, *6*, 10178−10185.

(28) Bi, H.; Chen, J.; Zhao, W.; Sun, S.; Tang, Y.; Lin, T.; Huang, F.; Zhou, X.; Xie, X.; Jiang, M. Highly Conductive, Free-Standing and Flexible Graphene Papers for Energy Conversion and Storage Devices. *RSC Adv.* **2013**, *3*, 8454−8460.

(29) Chen, H.; Mueller, M. B.; Gilmore, K. J.; Wallace, G. G.; Li, D. Mechanically Strong, Electrically Conductive, and Biocompatible Graphene Paper. *Adv. Mater.* **2008**, *20*, 3557−3561.

(30) Lin, X.; Shen, X.; Zheng, Q.; Yousefi, N.; Ye, L.; Mai, Y.-W.; Kim, J.-K. Fabrication of Highly-Aligned, Conductive, and Strong Graphene Papers Using Ultra Large Graphene Oxide Sheets. *ACS Nano* **2012**, *6*, 10708−10719.

(31) Holzwarth, U.; Gibson, N. The Scherrer Equation versus the 'Debye-Scherrer Equation'. *Nat. Nanotechnol.* **2011**, *6*, 534−534.

(32) Bahr, J. L.; Yang, J. P.; Kosynkin, D. V.; Bronikowski, M. J.; Smalley, R. E.; Tour, J. M. Functionalization of Carbon Nanotubes by Electrochemical Reduction of Aryl Diazonium Salts: A Bucky Paper Electrode. *J. Am. Chem. Soc.* **2001**, *123*, 6536−6542.

(33) Lu, F.; Wang, W.; Fernando, K. A. S.; Meziani, M. J.; Myers, E.; Sun, Y.-P. Metallic Single-Walled Carbon Nanotubes for Transparent Conductive Films. *Chem. Phys. Lett.* **2010**, *497*, 57−61.

(34) Wu, Z. C.; Chen, Z. H.; Du, X.; Logan, J. M.; Sippel, J.; Nikolou, M.; Kamaras, K.; Reynolds, J. R.; Tanner, D. B.; Hebard, A. F.; Rinzler, A. G. Transparent, Conductive Carbon Nanotube Films. *Science* **2004**, *305*, 1273−1276.

(35) Li, W. Z.; Wang, X.; Chen, Z. W.; Waje, M.; Yan, Y. S. Carbon Nanotube Film by Filtration as Cathode Catalyst Support for Proton-Exchange Membrane Fuel Cell. *Langmuir* **2005**, *21*, 9386−9389.

(36) Ha, H.-J.; Kil, E.-H.; Kwon, Y. H.; Kim, J. Y.; Lee, C. K.; Lee, S.-Y. UV-Curable Semi-Interpenetrating Polymer Network-Integrated, Highly Bendable Plastic Crystal Composite Electrolytes for Shape-Conformable All-Solid-State Lithium Ion Batteries. *Energy Environ. Sci.* **2012**, *5*, 6491−6499.

(37) Hakovirta, M.; Vuorinen, J. E.; He, X. M.; Nastasi, M.; Schwarz, R. B. Heat Capacity of Hydrogenated Diamond-Like Carbon Films. *Appl. Phys. Lett.* **2000**, *77*, 2340−2342.

(38) Takahashi, F.; Fujii, K.; Hamada, Y.; Hatta, I. Thermal Diffusivity Measurement of Chemical-Vapor-Deposited Diamond by an AC Calorimetric Method. *Jpn. J. Appl. Phys., Part 1* **2000**, *39*, 6471−6473.

(39) Yu, W.; Xie, H.; Li, F.; Zhao, J.; Zhang, Z. Significant Thermal Conductivity Enhancement in Graphene Oxide Papers Modified with Alkaline Earth Metal Ions. *Appl. Phys. Lett.* **2013**, *103*, 141913.

(40) Hwang, Y.; Kim, M.; Kim, J. Enhancement of Thermal and Mechanical Properties of Flexible Graphene Oxide/Carbon Nanotube Hybrid Films Though Direct Covalent Bonding. *J. Mater. Sci.* **2013**, *48*, 7011−7021.

(41) Hummers, W. S., Jr.; Offeman, R. E. Preparation of Graphitic Oxide. *J. Am. Chem. Soc.* **1958**, *80*, 1339−1339.

Journal of
Materials Chemistry B

RSCPublishing

FEATURE ARTICLE

View Article Online
View Journal | View Issue

Carbon "quantum" dots for optical bioimaging

Cite this: *J. Mater. Chem. B*, 2013, **1**, 2116

Pengju G. Luo,[a] Sushant Sahu,[a] Sheng-Tao Yang,[b] Sumit K. Sonkar,[a] Jinping Wang,[a] Haifang Wang,[c] Gregory E. LeCroy,[a] Li Cao[a] and Ya-Ping Sun*[a]

Received 6th January 2013
Accepted 19th February 2013

DOI: 10.1039/c3tb00018d

www.rsc.org/MaterialsB

Carbon dots, generally referring to small carbon nanoparticles with various levels of surface passivation, have emerged as a new class of quantum dot-like fluorescent nanomaterials. Since the original report in 2006, carbon dots have been investigated by many research groups worldwide, with major advances already made in their syntheses, structural and mechanistic understandings, and evaluations for biocompatibilities and potential bio-applications. In this article, representative studies responsible for these advances in the development and understanding of carbon dots are reviewed, and those targeting the use of carbon dots as high-performance yet nontoxic fluorescence agents for optical bioimaging *in vitro* and *in vivo* are highlighted and discussed.

1 Introduction

Quantum dots (QDs) are generally semiconductor nanocrystals of physical dimensions smaller than the exciton Bohr radius.[1–7] Because of the quantum-confinement effect, the electronic and optical properties of QDs exhibit characteristic dependencies on the nanoparticle sizes and composition, especially the infamous display of beautiful fluorescence colors for QDs of varying semiconductor nanoparticle sizes.[8] Among well-established semiconductor QDs are the size-wise narrowly distributed CdSe nanoparticles, whose quantum yields were found to be 10–15% with the original synthesis in a high temperature organometallic reaction by Bawendi and coworkers.[9] The capping of CdSe nanoparticles by a wide-bandgap semiconductor in later studies substantially improved both the optical performance and the photochemical stability,[10–13] with the QDs represented by CdSe–ZnS core–shell nanoparticles, now commercially available in aqueous or organic compatible versions (corresponding to different surface functionalizations), exhibiting fluorescence quantum yields of more than 50%.[10]

The high optical performance of QDs has captured the imagination of researchers in biomedical fields, with the exploration for a wide variety of potential bio-applications already producing exciting results.[14–18] The rationale for the use of QDs over organic dyes in terms of much enhanced

Pengju G. Luo has been a faculty member at Sherman College of Chiropractic since 2006 and an adjunct assistant professor at Clemson University since 2007. He received his medical degree in Clinical Medicine from Tongji Medical University (Wuhan, China) in 1997 and his Ph.D. in Microbiology from Clemson University in 2006. His current research interests are in the interdisciplinary areas of nanotechnology and biological and biomedical sciences, focusing on bioapplications of various nanomaterials such as nanoparticles, nanotubes, and carbon dots.

Sushant Sahu is a graduate student at Clemson University. He received his B.Sc. degree in chemistry from the University of Mumbai, India, in 2003 and obtained his M.Sc. degree in chemistry from the Indian Institute of Technology, Guwahati, India, in 2006. He is presently a candidate for Ph.D. at Clemson, under the supervision of Prof. Ya-Ping Sun. His research involves the development of carbon dots for energy conversion applications.

---

[a] Department of Chemistry and Laboratory for Emerging Materials and Technology, Clemson University, Clemson, South Carolina 29634-0973, USA. E-mail: syaping@clemson.edu

[b] College of Chemistry and Environment Protection Engineering, Southwest University for Nationalities, Chengdu 610041, China

[c] Institute of Nanochemistry and Nanobiology, Shanghai University, Shanghai 200444, China

performance is now generally accepted in the literature.[19] However, the obvious performance advantages of QDs for bioimaging applications are challenged by some significant shortcomings, among which the most serious is the toxicity issue. The presently dominating semiconductor QDs are limited by their containing heavy metal elements such as cadmium, whose potential health and environmental hazards are well-documented. For example, the existing data suggest that the cadmium-based QDs are toxic to vertebrate systems at relatively low concentrations,[20,21] and there may also be risks with the bioaccumulation of these toxic materials in organs and tissues.[22,23] Therefore, there has been much effort in the research community on searching for alternative QD-like photoluminescent materials.

Among more promising candidates for the alternative QDs are nanosized silicon (and germanium to some extent) particles,[24–27] though it does not appear that the development of silicon QDs is on track to compete with the cadmium-based QDs in bioimaging and related applications. Interestingly, carbon in the same group as silicon in the periodic table apparently provides a more effective solution in the development of alternatives to the semiconductor QDs, with the discovery of brightly fluorescent carbon-based QDs or carbon dots (also referred to as C-Dots).[28–30] In this article we highlight the structural characteristics and optical properties of carbon dots, and their rapid advances toward serving as high-performance yet nontoxic fluorescence agents for bioimaging and related biomedical applications.

2 Carbon dots

Carbon dots in a broad definition generally refer to small carbon nanoparticles in aqueous or other suspensions. The original hint on nanoscale carbon particles being photoluminescent could be traced back to the observation that the surface defects in both single-walled and multiple-walled carbon nanotubes became brightly emissive under some specific conditions,[31] especially when the nanotubes were functionalized for the purpose of dispersion at the individual nanotube level without bundling or aggregation.[31–36] In a conceptually and experimentally similar fashion, Sun and coworkers functionalized small carbon nanoparticles with various oligomeric species to target an effective passivation of the particle surface, resulting in bright and colorful fluorescence emissions (Fig. 1), thus the finding of carbon dots.[28] It was subsequently found that carbon dots are also strongly multiphoton fluorescent, with extremely large two-photon cross-sections on pulsed laser excitation (800–900 nm).[29,37]

Sheng-Tao Yang received his B.Sc. in 2006 and Ph.D. in 2011 at Peking University majoring in chemistry. In 2008–2009, he was a visiting graduate student in the group of Prof. Ya-Ping Sun at Clemson University. Since 2011, he has been a Lecturer at College of Chemistry and Environment Protection Engineering, Southwest University for Nationalities (Chengdu, China). His current research focuses on bio-applications and biosafety of carbon nanomaterials.

Jinping Wang received his Ph.D. from Changchun Institute of Applied Chemistry, Chinese Academy of Sciences, in 2004. He is a Full Professor in College of Chemistry and Pharmaceutical Sciences at Qingdao Agricultural University, China, and currently on leave as a visiting scholar at Clemson University. His main research interests are in the fields of biomaterials and bioanalysis, including the preparation and evaluation of nanomaterials for their interesting properties, functions, and potential applications.

Sumit K. Sonkar received his Ph.D. in chemistry from the Indian Institute of Technology Kanpur, India, in 2012. He is presently a postdoctoral scientist in the group of Prof. Ya-Ping Sun at Clemson University, focusing on the development and investigation of carbon-based quantum dots for bio- and energy-related applications.

Ya-Ping Sun earned his Ph.D. at Florida State University in 1989. After postdoctoral training at University of Texas at Austin, he joined the Clemson faculty in 1992. He has been the Frank Henry Leslie Chair Professor of Natural & Physical Sciences since 2003. His research interests are primarily in carbon-based nanomaterials.

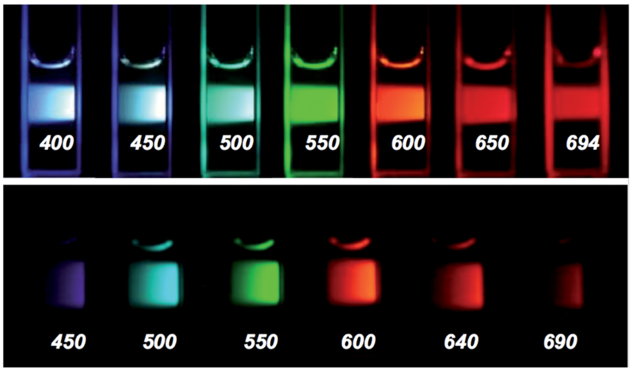

Fig. 1 Aqueous solutions of the as-synthesized carbon dots excited at the indicated wavelengths in nm and photographed directly (top), and excited at 400 nm and photographed through band-pass filters of different wavelengths as indicated (bottom) (from ref. 28).

The effective carbon particle surface passivation has apparently been a necessary condition for carbon dots of high fluorescence performance, despite the rather broad definition on carbon dots. "Naked" carbon nanoparticles without deliberate surface functionalization in relatively stable aqueous or other suspensions may also exhibit colorful fluorescence emissions, as reported by many research groups,[38–43] but with generally low to very low emission quantum yields. Since the presence of solvents around the naked particles has been necessary for the fluorescence emissions, it may be argued that the solvent molecules provide relatively weak but nevertheless meaningful surface passivation for the suspended carbon nanoparticles.[41] Therefore, there seems no need to differentiate conceptually carbon dots with and without deliberate surface functionalization (or other forms of more effective passivation effects), as the surface passivation simply alters the fluorescence performance, dramatically may be, of the various carbon dots.

The carbon nanoparticles in carbon dots may come from a variety of sources, some even from really unconventional ones. In the original study,[28] carbon soot from laser ablation of a graphitic target, which typically has a higher population of smaller carbon nanoparticles, was used as a precursor for surface passivation in the preparation of brightly fluorescent carbon dots. Since then, many different production strategies have been practiced,[44] including the use of commercially available carbon nanopowders as the starting material to harvest the desired smaller nanoparticles.[45] Among representative syntheses of carbon dots in one-pot was the work by Hu *et al.* to use direct laser irradiation of graphite powder in an organic solvent (diamine hydrate, diethanolamine, or PEG_{200N}–amine-terminated polyethylene glycol oligomers of 200 average molecular weight) under ultrasonication.[46] The carbon dots produced in the solvent diethanolamine exhibited fluorescence quantum yields as high as 7.8% at 420 nm excitation. Bourlinos *et al.* used thermal carbonization of suitable small molecule precursors, including various ammonium citrate salts, for carbon dots.[47,48] For example, the citric acid salt was heated in air at 10 °C min^{-1} until it reached 300 °C, held at that temperature for 2 h, to result in water-soluble carbon dots of 7 nm average diameter and a fluorescence quantum yield of 3% at 495 nm excitation.[47] Similarly, Wang *et al.* synthesized carbon dots *via* thermal oxidation of a molecular precursor, citric acid specifically, in a molten lithium nitrate salt in an argon atmosphere, followed by the surface passivation reaction with PEG_{1500} (polyethylene glycol oligomers of 1500 average molecular weight).[49] The surface passivation step, which was absent in the synthesis by Bourlinos *et al.*,[47,48] probably enhanced the fluorescence brightness, with the PEGylated carbon dots exhibiting an emission quantum yield of around 10%.[28,49] The same approach of thermally carbonizing polymeric nanoparticles into carbon nanoparticles was used by Sun and coworkers.[50] Upon functionalization for effective surface passivation, the resulting carbon dots were found to be similar to those with core carbon nanoparticles from another source (such as laser ablation) in terms of fluorescence performance and related spectroscopic properties.

Liu *et al.* reported a rather unusual way to harvest carbon nanoparticles in soot from smoldering candles.[38] The soot was treated with a nitric acid solution (5 M), followed by purification with polyacrylamide gel electrophoresis, and the resulting carbon nanoparticles in an aqueous suspension exhibited photoluminescent emissions over a broad color range (Fig. 2), despite their generally low quantum yields (up to 1.9% at 366 nm excitation).[38] Other carbon nanoparticles from somewhat unconventional sources for carbon dots included those from the soot produced by natural gas combustion,[51] or even from food caramels.[52] For the latter by Chattopadhyay and coworkers, amorphous carbon nanoparticles of 4–30 nm size

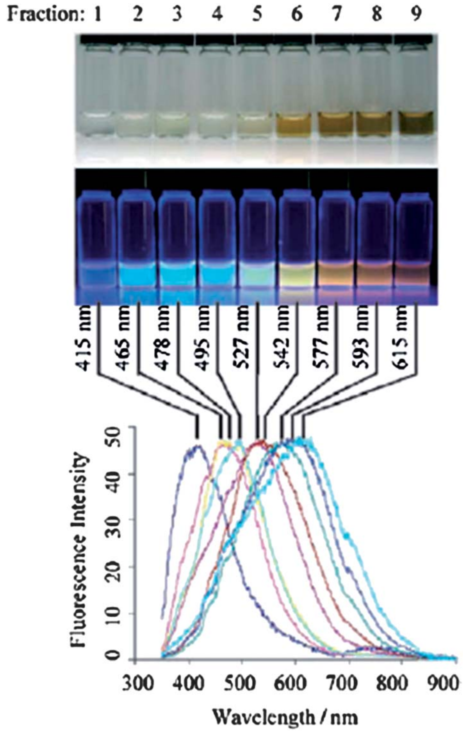

Fig. 2 Optical images of the aqueous carbon nanoparticle solutions illuminated under white light (top) and 315 nm UV light (center) with the corresponding fluorescence emission spectra (the spectral maximum indicated above each spectrum) (from ref. 38).

were obtained by heating bread, jaggery, corn flakes, or biscuits, and the nanoparticles in suspension exhibited photoluminescent emissions (quantum yield of about 1% at 365 nm excitation).[52] These results demonstrated the versatility with carbon dots in terms of their primary structure, namely the core carbon nanoparticle. In other words, photoluminescent emissions represent an intrinsic property of surface-passivated carbon nanoparticles regardless of their origins and precise structures or compositions. However, the effectiveness of the surface passivation does affect the optical performance of carbon dots in a dramatic fashion.

Wang *et al.* reported that the as-synthesized sample of carbon dots with surface functionalization by oligomeric PEG diamine (PEG_{1500N}, with 1500 denoting average molecular weight of the oligomers) was a mixture, which could be separated on a conventional gel column to obtain fractions of different fluorescence quantum yields.[53] Some of these fractions were found to be highly fluorescent, with quantum yields of 60% or higher for excitation around 450 nm (compared with the quantum yields of 16–20% in the as-synthesized mixture), and their fluorescence brightness could be appreciated by naked eyes (Fig. 3). In fact, the high fluorescence quantum yields coupled with large optical absorptivities make these carbon dots 2–3 times brighter than the corresponding commercially supplied green CdSe–ZnS QDs (Invitrogen "QD525PEG") at the individual dot level (Fig. 4). It was rationalized that the more fluorescent fractions contained carbon dots of better PEG_{1500N} functionalization and thus more effective surface passivation.[53]

The effective surface passivation to improve the fluorescence performance in carbon dots was also reflected in the work by Sun *et al.*, who doped the core carbon nanoparticle surface with inorganic salts (ZnO, ZnS, or TiO_2) in combination with the organic functionalization.[54,55] The resulting carbon dots (denoted as C_{ZnO}-Dots, C_{ZnS}-Dots, or C_{TiO_2}-Dots) exhibited much brighter fluorescence emissions than those from the corresponding carbon dots without the doping, with the observed quantum yields up to 50%. The inorganic salts must have

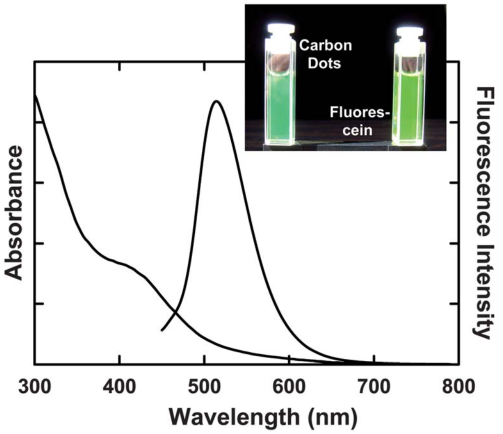

Fig. 3 The absorption and fluorescence (440 nm excitation) spectra of the ultra-bright PEGylated carbon dots. Inset: photos under sunlight for solutions of the carbon dots in water and fluorescein in ethanol with matching optical density at 440 and 490 nm, respectively (from ref. 53).

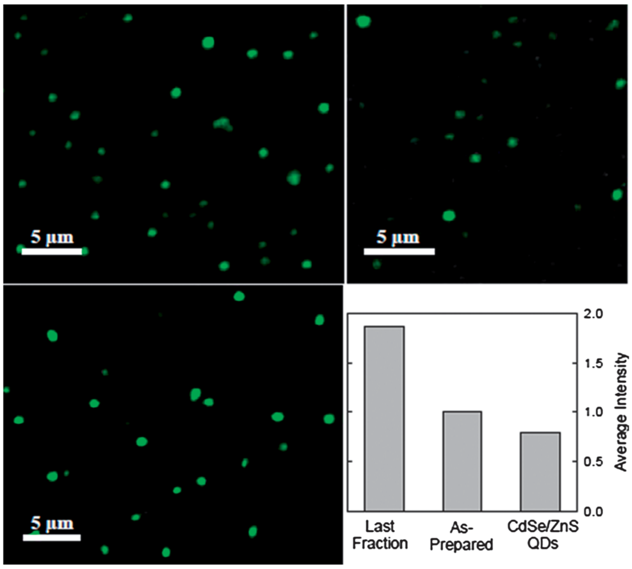

Fig. 4 Fluorescence microscopy images (458 nm excitation) of carbon dots in the "as-prepared" sample (left-top) and in the most fluorescent fraction (left-bottom), and images of Invitrogen QD525PEG CdSe–ZnS QDs (right-top). The bar-chart comparison was based on averaging the 300 most fluorescent dots in each of the three samples (from ref. 53).

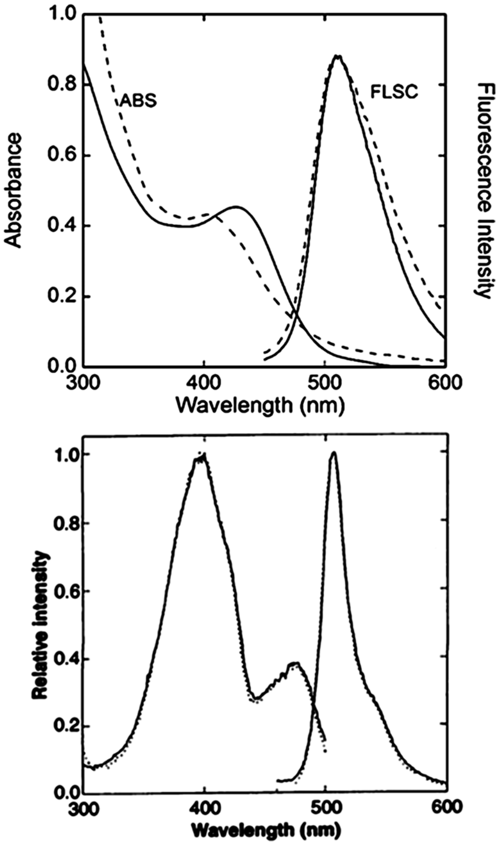

Fig. 5 Top: absorption (ABS) and fluorescence (FLSC, 440 nm excitation) spectra of the "as-prepared" (dash lines) and the most fluorescent fraction (solid lines) of the carbon dots in an aqueous solution (from ref. 55). Bottom: the excitation and emission spectra of the green fluorescent protein (*E. coli*-generated) (from ref. 56).

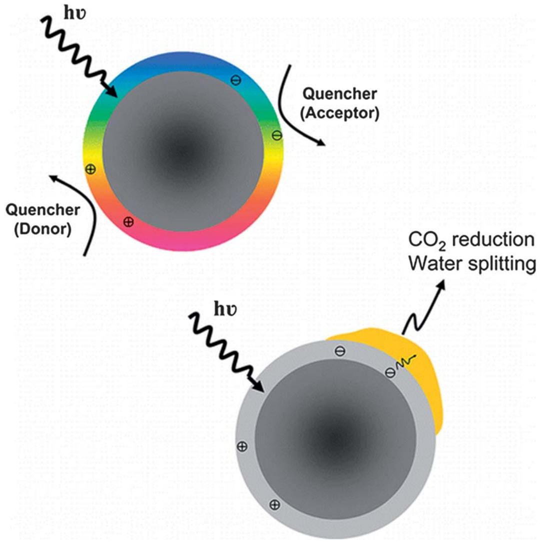

Fig. 6 Cartoon illustrations on structural features and related mechanistic implications in carbon dots (top) and those with the dot surface doped with a gold or platinum metal (bottom) (from ref. 61).

augmented the passivation effect of the subsequent organic functionalization.[55] In a further effort, Anilkumar *et al.* fractionated the as-prepared sample of C_{ZnS}-Dots on the conventional gel column to obtain carbon dots of observed fluorescence quantum yields up to 78% at 440 nm excitation. The fluorescence emissions (centered at 540 nm) cover a spectral region similar to that covered by green fluorescence proteins (Fig. 5).[56]

For the emission mechanism in carbon dots, it was proposed[28] and is now increasingly adopted in the research community[57,58] that radiative recombinations of the carbon nanoparticle surface-confined electrons and holes (Fig. 6) are responsible for the observed bright fluorescence. The electrons and holes are likely generated by efficient photoinduced charge separations in the carbon nanoparticles, and the role of surface passivation by the organic or other functionalization is probably to make the surface sites more stable to facilitate more effective radiative recombinations. Experimental evidence in support of the mechanistic framework included the fluorescence quenching results with both electron donors and acceptors, which could apparently scavenge the surface-confined holes and electrons in carbon dots, respectively (Fig. 6), to result in efficient and effective quenching of the emissions (diffusion-controlled with additional static contributions).[57] Recently, it was also demonstrated that the photogenerated electrons in carbon dots could be used for reduction purposes[59,60] and more importantly the electrons could be concentrated into the gold or platinum metal doped on the carbon particle surface (Fig. 6) for the photocatalytic conversion of carbon dioxide and also the photocatalytic splitting of water for hydrogen generation.[60,61] These results have reinforced the view that carbon dots essentially resemble nanoscale semiconductors in terms of photoinduced redox processes, in which the radiative recombinations in the absence of quenchers result in bright fluorescence emissions.

3 Optical bioimaging

Carbon dots have been evaluated for optical bioimaging applications,[28,30,62–66] including their cellular uptakes and the fluorescence brightness in the cellular environment, and their *in vivo* imaging in mice models in reference to the commercially available CdSe–ZnS QDs in the same models. The results have been very promising.[28,30,64,66] Beyond the competitive performance in cellular and *in vivo* imaging, carbon dots have also been found to be nontoxic from cytotoxicity and *in vivo* toxicity evaluations.[37,65–68]

Cellular imaging

Carbon dots have been demonstrated for successful uses in the fluorescence imaging of cells,[28,63–65] taking advantage of their visible excitation and emission wavelengths, their fluorescence brightness at the individual dot level, and their high photostability. In the original study of carbon dots by Sun *et al.*,[28] the PEGylated carbon dots were incubated with *Escherichia coli* for the fluorescence staining of the bacteria cells, so were the oligomeric aminopolymer-functionalized carbon dots with Caco-2 cells for internalization (Fig. 7). The confocal microscopy imaging revealed that the endocytosed carbon dots were mostly in the cytoplasm, with only minor penetration into the cell nucleus (Fig. 7).[28] The same approach was applied in several

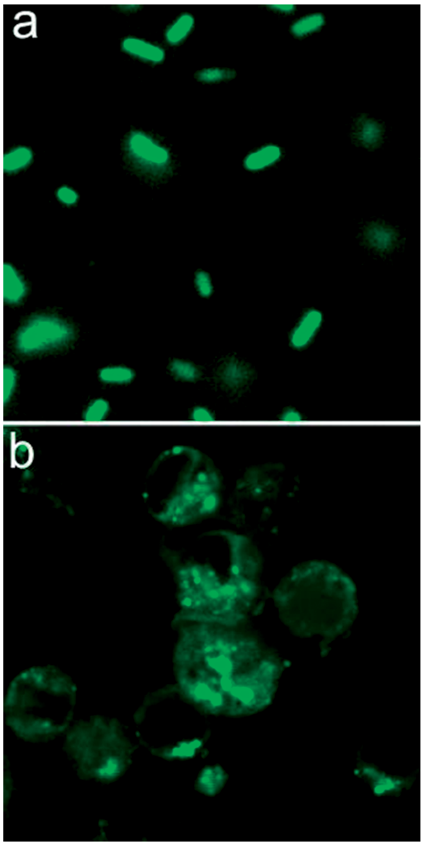

Fig. 7 Confocal fluorescence microscopy images (488 nm excitation) of (a) *E. coli* and (b) Caco-2 cells labeled with carbon dots (from ref. 28).

subsequent studies, including the one by Liu *et al.* on the labeling of *E. coli* cells and also murine P19 progenitor cells.[64]

There have been a number of other studies on using fluorescence to monitor the cellular uptake of various carbon dots.[63,65,69–72] For example, Qiao *et al.* reported the fluorescence detection of carbon dots with surface-passivation by 4,7,10-trioxa-1,13-tridecanediamine (TTDDA) in COS-7 cells.[65] After incubation of COS-7 cells with the carbon dots for 24 h, the cell membrane and cytoplasm became brightly fluorescent.[65] Similarly, Wang *et al.* incubated silica-encapsulated carbon dots with BGC823 cells for 24 h, and observed fluorescence in the cytoplasmic area due to the expected penetration of the dots into the cells but not into the nuclei.[63] Liu *et al.* incubated HepG-2 cells with the TTDDA-passivated carbon dots and examined multicolor fluorescence emissions of the dots under different excitation conditions under a laser scanning confocal microscope (LSCM). The carbon dots taken up by HepG-2 cells exhibited bright blue, green, and red emission colors at 405 nm, 488 nm, and 543 nm excitations, respectively.[69] Zhu *et al.* prepared carbon dots from graphene oxide precursors for the imaging of MG-63 cells. Bright fluorescence emissions from the cytoplasm were observed with both 405 and 488 nm excitations.[70] Yang *et al.* synthesized carbon dots by hydrothermal carbonization of chitosan.[71] In the imaging of A549 cells with the carbon dots, the fluorescence spots were observed only in the cell membrane and cytoplasmic area, with much weaker signals in the cell nucleus region. Jaiswal *et al.* used carbon dots from the microwave-mediated caramelization of PEG oligomers to label cells under UV excitation.[72] However, the magnification in the imaging was not high enough to determine the dot locations inside the cell.

The available cell imaging results generally suggest that carbon dots taken up by cells are mostly localized in the cytoplasm. However, there were a couple of reports on the internalization of carbon dots in the cell nucleus. According to Ray *et al.*,[40] small carbon nanoparticles from candle soot without any particle surface functionalization (except for the oxidation by 5 M nitric acid) could be endocytosed by EAC cells to be in both cytoplasm and nucleus. After the incubation with the carbon nanoparticles for only 30 min, the EAC cells could be lighted to bright blue-green under UV excitation and yellow under blue excitation. In the former the whole cells were lighted, while in the latter the cytoplasm was brighter than the nucleus (though it was still brighter than that in the control cells). Chandra *et al.* reported that carbon dots tagged with organic molecules (α-naphthylamine, fluorescein, and rhodamine B) were distributed in the whole human red blood corpuscles (RBC), as suggested by results from confocal microscopy.[73] For mechanistic explanations on various carbon dots targeting different compartments in cells, which are presently not available, high-resolution imaging experiments are needed to determine more precisely the intracellular distribution of the carbon dots.

Carbon dots are brightly multiphoton fluorescent, with the two-photon cross-sections in the near-IR (800–900 nm) orders of magnitude larger than those in the benchmark organic dyes.[29] Therefore, carbon dots are excellent multiphoton fluorescence agents for optical cell imaging, as demonstrated by Cao *et al.*[29] In that reported study, aminopolymer-functionalized carbon dots were taken up by MCF-7 cells after the incubation for 2 h at 37 °C (likely *via* endocytosis, as no uptake for the same incubation at 4 °C). The internalized carbon dots exhibited bright fluorescence emissions under two-photon excitation with a femtosecond pulsed laser at 800 nm (Fig. 8). Similarly in the imaging of HeLa cells by Li *et al.*,[62] carbon dots were found in lysosome and endosome of the cells.

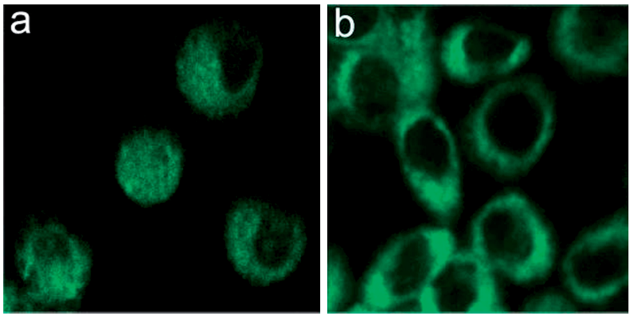

Fig. 8 Two-photon fluorescence microscopy images (pulsed femtosecond laser for 800 nm excitation) of MCF-7 cells with internalized carbon dots (from ref. 29).

The presence of surface passivation molecules on the carbon nanoparticles in carbon dots has made it easier for their

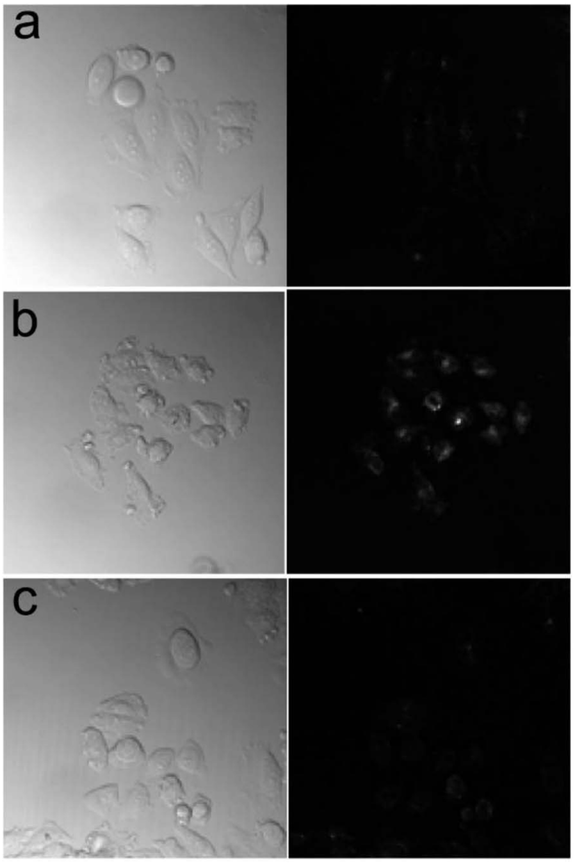

Fig. 9 (a) HeLa cells incubated with carbon dots; (b) the cells incubated with transferrin-coupled carbon dots; and (c) the cells incubated with transferrin-coupled carbon dots after transferrin pre-treatment (from ref. 74).

conjugation with bioactive species for specific applications.[74] For example, Li *et al.* coupled carbon dots with human transferrin through carbodiimide chemistry, and used the conjugates to target HeLa cells.[74] The demonstration was such that the carbon dots with the grafted PEG polymer were not able to penetrate the cell membrane, while the conjugates with transferrin exhibited selectivity toward the cancer cells (overexpressed with transferrin receptors) (Fig. 9).

Zhu *et al.* developed a carbon dot-based dual emission hybrid for imaging cellular copper ions.[75] Carbon dots were functionalized with *N*-(2-aminoethyl)-*N*,*N*,*N*′-tris(pyridin-2-ylmethyl)ethane-1,2-diamine (abbreviated as AE-TPEA) and then coated with CdSe@SiO_2 QDs. The idea was that Cu^{2+} could quench the fluorescence of carbon dots but not that of CdSe@SiO_2 QDs; thus the latter was used as an internal reference. The hybrid probe was used in the imaging of Cu^{2+} in HeLa cells. Upon the addition of Cu^{2+}, the green fluorescence from carbon dots was significantly inhibited in reference to that of the QDs.[75] Liu *et al.* used PEI-functionalized carbon dots for gene delivery and bioimaging.[76] These carbon dots were found to have positive charges on the surface, thus were polyelectrolyte-like to condense DNA. The gene expression of plasmid DNA delivered by the carbon dots was competitive to that by PEI25k in COS-7 cells and HepG2 cells.[76] Beyond the delivery, the carbon dots were also used for optical imaging. The COS-7 cells were stained by carbon dots after 3 h transfection, and the stained cells exhibited blue, green, and red fluorescence emissions with 405, 488, and 543 nm excitations, respectively. Inside the cells the carbon dots were mostly trapped in endosomal compartments, without any meaningful penetration into the cell nucleus.[76] In another drug delivery study by Lai *et al.*,[77] carbon dots with PEG functionalization were used for the delivery of the anti-cancer drug doxorubicin (DOX). The DOX loaded on the dots exhibited more toxicity to HeLa cells than free DOX, and the fluorescence imaging results seemed to suggest that the release of DOX from the carrier carbon dots occurred inside the cells.[77]

The reported studies highlighted above have demonstrated that carbon dots are amenable to various uses in optical cell imaging, with the same or similar protocols as those originally developed and validated for conventional semiconductor QDs. In fact, the brighter carbon dots already exhibited the same or better performances as those achieved by commercially available CdSe–ZnS QDs in imaging comparison at the individual dot level. More evaluations on carbon dots for potential applications such as fluorescence labeling of cells, high-resolution and/or high-sensitivity cellular imaging, drug delivery (especially for the delivery and imaging on the same platform), and single-particle tracking of live cells may be expected.

Biocompatibility and toxicity

A distinct advantage of carbon dots is their containing no heavy metal elements, unlike those in presently dominating semiconductor QDs. In fact, carbon nanoparticles have a history of being used in some commercial products, such as automobile tires. With the surface functionalization of the precursor carbon nanoparticles, the resulting carbon dots become soluble (or strictly speaking to form a solution-like dispersion), exhibiting excellent biocompatibility. The available toxicity evaluation results suggest that carbon dots are generally nontoxic or at least no more toxic than the selected oligomeric or polymeric species used as surface passivation agents in the carbon dots.[37,66–68]

Yang *et al.* performed cytotoxicity evaluations on PEGylated carbon dots and found that these dots were generally nontoxic to the selected cell lines.[37] In the evaluations, the carbon dots were introduced to HT-29 and MCF-7 cells, with the corresponding free PEG molecules as the control, and the cell proliferation, mortality, and viability were subsequently determined. No meaningful cytotoxicity was found with both carbon dots and the PEG control at relatively lower concentrations, and at higher concentrations the free PEGs were apparently somewhat more toxic to the cells than the PEGylated carbon dots (Fig. 10). The latter was explained in terms of free PEGs similar to surfactant molecules being more damaging to the cell membrane.[37] Carbon dots with the carbon particle surface functionalized by poly(propionylethylenimine-*co*-ethylenimine) (PPEI-EI) copolymers, on the other hand, were somewhat more cytotoxic than the PPEI-EI control at relatively higher concentrations.[45] In that case the carbon dots were considered more as being a delivery vehicle for PPEI-EI into the cells.[45] In the study by Liu *et al.*, the cytotoxicity of carbon dots with surface-functionalized PPEI-EI of different EI fractions was evaluated, again in terms of determining the proliferation, mortality, and viability of HT-29 and MCF-7 cells.[67] These results suggested that the cytotoxicity of carbon dots was dependent on the EI fraction in PPEI-EI on the dot surface. The significant role of the

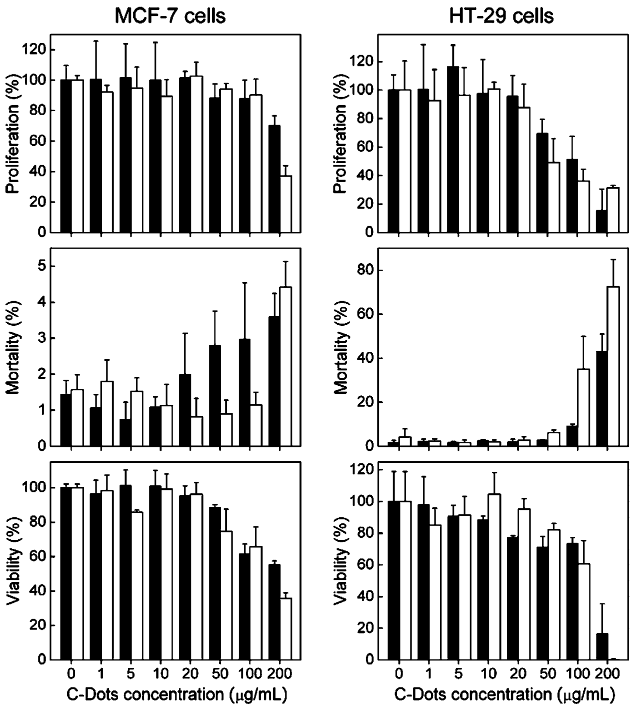

Fig. 10 Results from the cytotoxicity evaluation of PEGylated carbon dots (black) and the PEG_{1500N} control (white) (from ref. 37).

surface passivation molecules in carbon dots in the observed cytotoxicity was further confirmed in the study by Wang *et al.*, on the basis of a direct comparison between carbon dots of different surface passivation agents.[45] However, the good news from these studies is that meaningful cytotoxicity of carbon dots could only be detected at higher concentrations, much beyond those required for optical cell imaging under a conventional fluorescence microscope.

There have been a number of other studies collectively concluding that carbon dots are of no or low toxicity to various cell lines.[40,63–65,68–74] Chandra *et al.* evaluated the toxicity of carbon dots to red blood cells by measuring the hemolysis rate.[73] At a concentration of 330 μg mL^{-1}, the carbon nanoparticles with surface carboxyl groups exhibited some toxic effect, but after the coupling with organic molecules the carboxyl groups were converted into amide bonds, with the resulting carbon dots being significantly less toxic.[73] The results again support the notion that the surface functionalization of the core carbon nanoparticles plays a critical role in determining the cytotoxicity of the carbon dots.

For *in vivo* toxicity evaluation of carbon dots, Yang *et al.* used a mice model. In the experiment, an aqueous solution of the carbon dots with oligomeric PEG diamine (PEG$_{1500N}$) on the dot surface was administrated into mice *via* intravenous injection.[37] Post-administration, the carbon dots did not lead to any clinical symptoms in the mice during the observation period of up to 28 days. These PEGylated carbon dots were ^{13}C-labeled in such a way that the carbon nanoparticle core was substantially enriched with ^{13}C, which was designed to enable the quantification of carbon dots in various organs in dissected mice by using isotope-ratio mass spectroscopy.[37] Some carbon dots were found in liver, spleen, and kidneys according to the experimentally determined ^{13}C/^{12}C ratios, though the levels of accumulation were generally low. Serum biochemical parameters such as hepatic (ALT and AST) and renal (UA, BUN and Cr) toxicity indicators were found to be at normal levels (Fig. 11). Histopathological examinations on liver, spleen, and kidneys yielded results consistent with the conclusion that the PEGylated carbon dots are nontoxic *in vivo* (Fig. 11). At a relatively lower injection level sufficient for optical imaging *in vivo*,[30] the PEGylated carbon dots post-administration into mice (injection *via* the tail vein) were cleared *via* renal excretion within about 24 h. In the liver and kidney specimens from the dissection around that time point, essentially no fluorescent carbon dots were detected in the imaging by confocal fluorescence microscopy.[30,37]

In a more recent *in vivo* study by Tao *et al.*,[66] carbon dots synthesized from multi-walled carbon nanotubes as starting materials were radioactively labeled with ^{125}I for blood circulation and biodistribution evaluation in mice. The blood circulation of carbon dots followed a two-compartment model, with the first- and second-phase circulation half-lives around 0.1 h and 2 h, respectively. In biodistribution, the intravenously injected carbon dots mainly accumulated in the reticuloendothelial system (RES) organs such as liver and spleen. The kidney uptake of carbon dots was high at early time points, indicating that carbon dots could pass the glomerulus and be excreted by urine. These results were in general agreement with those found in the earlier *in vivo* study by Yang *et al.*[30,37]

Tao *et al.* also investigated the *in vivo* toxicology of carbon dots in female Balb/c mice over 90 days.[66] Neither death nor significant body weight change was observed in the treated group of mice, and no obvious signs of toxic effects from the carbon dots were observed at the injected dosage of 20 mg kg^{-1}. Blood biochemistry results based on liver (ALT, AST, ALP and A/G) and renal (BUN) function tests suggested that carbon dots were nontoxic to liver and kidneys in the observation period of

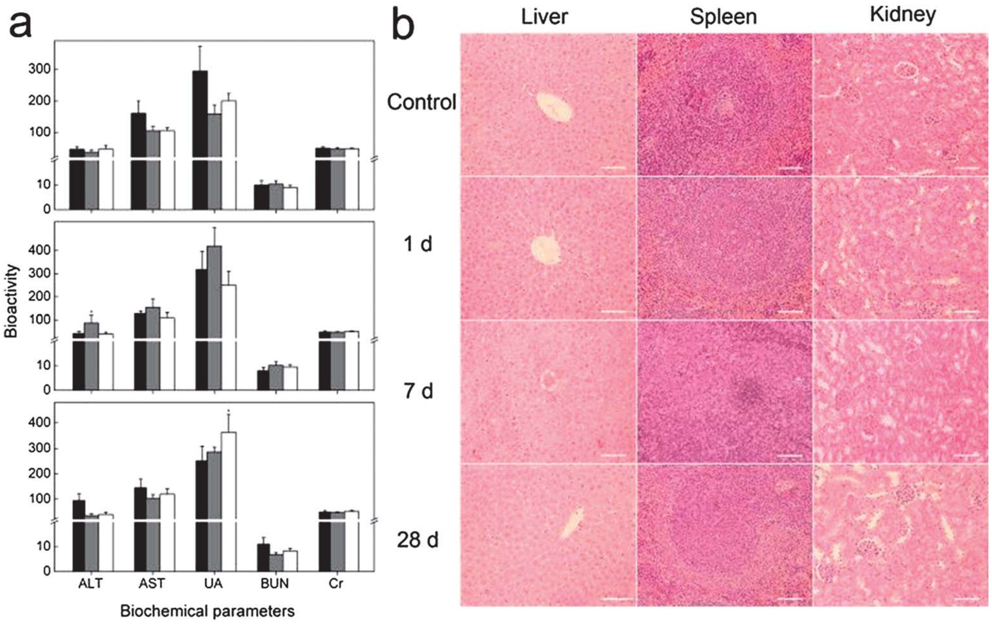

Fig. 11 Results from the *in vivo* (mice) toxicity evaluation of carbon dots: (a) serum biochemistry (the black bars for control mice; top: 1 day, middle: 7 days, and bottom: 28 days post-exposure). (b) Histopathology results (from ref. 37).

up to 90 days. Hematology analyses on various parameters (including white blood cells, red blood cells, hemoglobin, mean corpuscular volume, mean corpuscular hemoglobin, mean corpuscular hemoglobin concentration, platelet count, and mean corpuscular hemoglobin) yielded normal readings in comparison with those of the control. The nontoxic nature of carbon dots was further confirmed by histopathology analyses of liver, spleen, kidney and heart samples.

A conclusion based on the currently available toxicity data is that the intrinsic configuration of carbon dots, namely surface-functionalized small carbon nanoparticles readily aqueous soluble, is nontoxic *in vitro* and *in vivo*. Therefore, when considering toxicity issues of carbon dots for specific bio-applications, the emphasis should be on the selection of appropriate nontoxic molecules or species for the carbon particle surface functionalization, as their toxicity profile may dictate that of the resulting carbon dots.

Optical imaging *in vivo*

There have already been demonstrations of the use of carbon dots for fluorescence imaging *in vivo*.[30,62,66] Yang *et al.* were the first to explore the feasibility of carbon dots as a fluorescence contrast agent in mice.[30] In the experiment, PEGylated carbon dots in an aqueous solution were injected subcutaneously into mice, and the fluorescence images at different excitation wavelengths were collected. There was sufficient contrast for the imaging in both green and red emission colors.[30] In a more recent study, Tao *et al.* applied the same protocol to nude mice and obtained similar results.[66] More specifically, an aqueous solution of carbon dots was injected subcutaneously into the mice, followed by fluorescence imaging with excitations at seven different wavelengths from 455 nm to 704 nm. The best fluorescence contrast was found at 595 nm excitation (Fig. 12).[66]

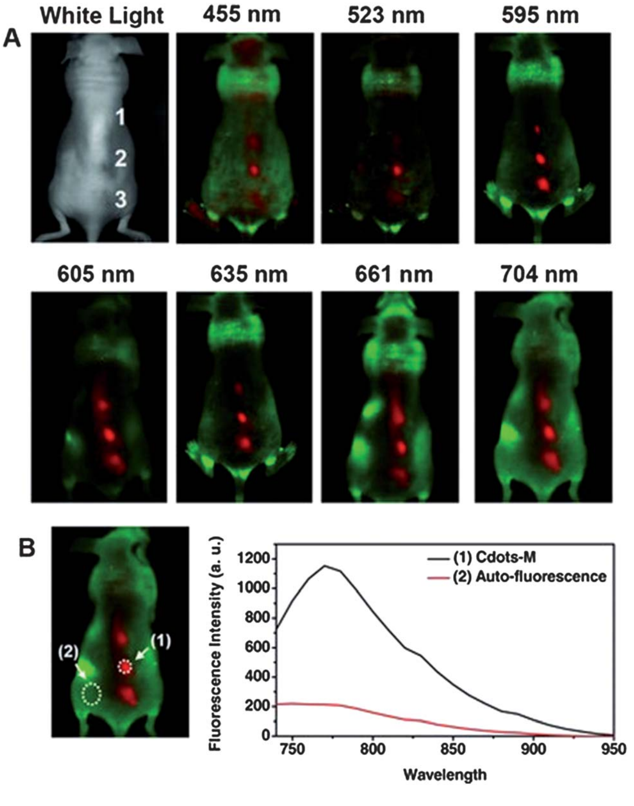

Fig. 12 Results of fluorescence imaging *in vivo* with carbon dots (from ref. 66).

Carbon dots have also been explored for fluorescence imaging in mice *via* other injection modes.[30] For the sentinel lymph node imaging, the PEGylated carbon dots were injected intradermally into the front extremity, and fluorescence images at 470 nm excitation were collected continuously. Following the injection, carbon dots migrated along the arm to the axillary lymph node (sentinel lymph node, Fig. 13). The observed migration of the carbon dots was slower in comparison with that of the semiconductor QDs, probably due to the smaller sizes of the carbon dots (around 5 nm) and/or the surface PEG functionalization. The axillary lymph nodes were harvested and dissected at 24 h post-injection, and in the specimen fluorescence from the carbon dots could readily be detected (Fig. 13).

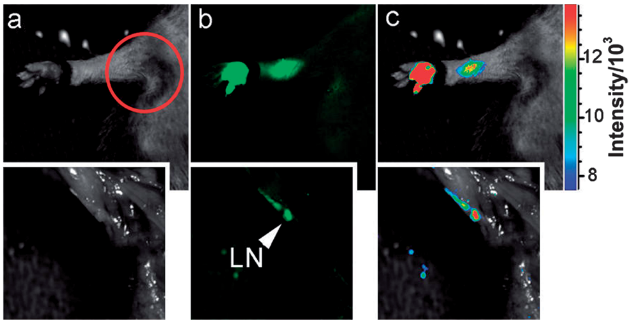

Fig. 13 Fluorescence imaging in mice with interdermal injection of the carbon dots: (a) bright field and (b) as-detected fluorescence and (c) color-coded images. Insets: images on the dissected (in the circled area) axillary lymph node (LN) (from ref. 30).

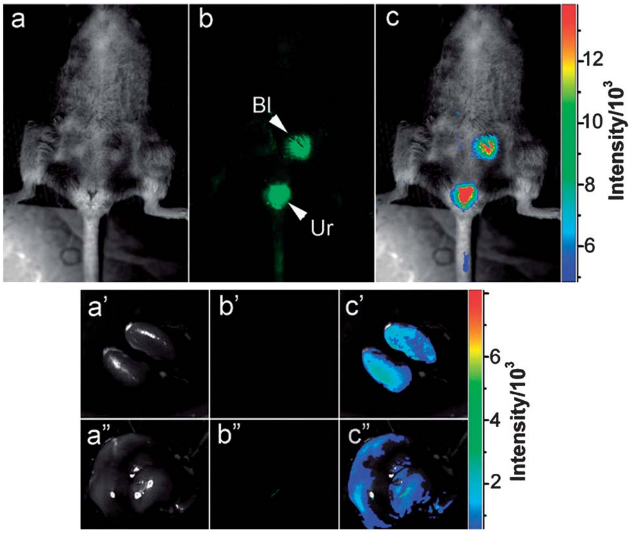

Fig. 14 Fluorescence imaging in mice with intravenous injection of the carbon dots: (a) bright field, (b) as-detected fluorescence and (c) color-coded images. Insets: the corresponding images on the dissected kidneys (a′–c′) and liver (a″–c″) (from ref. 30).

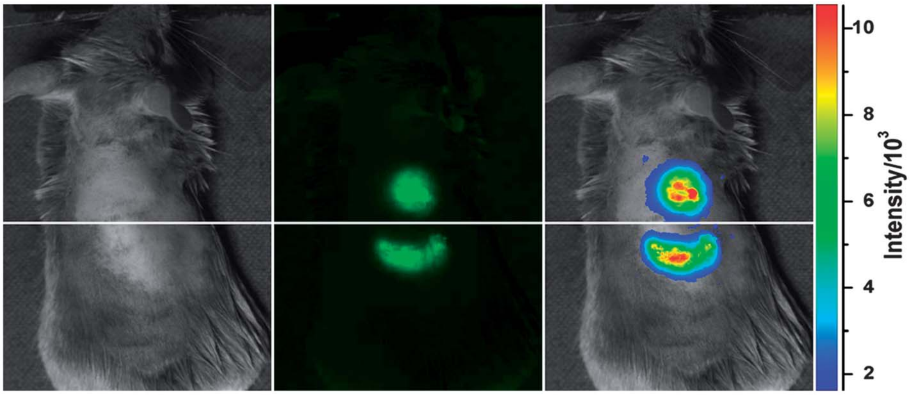

Fig. 15 A comparison of *in vivo* imaging results (subcutaneous injection on the back of mice) between the carbon dots (top) and commercial CdSe–ZnS QDs (Invitrogen, aqueous Qdot® 525 ITK™ amino (PEG) QDs, bottom), with the same number of dots under the same imaging conditions (434 nm band-pass for excitation and 474 nm cut-off filter for emission) (from ref. 78).

In the study by Yang *et al.*,[30] carbon dots were also intravenously injected into mice for whole-body circulation. The mouse abdomen was shaved for the fluorescence detection of carbon dots in organs during the circulation. The organ with bright fluorescence emissions readily observed (even by naked eyes, Fig. 14) in about an hour post-injection was the bladder, which must have accumulated a large amount of the intravenously injected carbon dots. At about 3 h post-injection, the urine became brightly fluorescent, consistent with the expected renal excretion of the carbon dots. For other organs including liver, spleen and kidneys, the fluorescence imaging was performed *ex vivo*. The organs were harvested at 4 h post-intravenous injection, in which the observed fluorescence was generally weak, suggesting a rather low accumulation level of the carbon dots. Between the dissected liver and kidneys, brighter fluorescence was detected in the latter (Fig. 14), consistent with the urine excretion pathway for the carbon dots.

Under the imaging conditions, the carbon dots were photochemically stable, without any significant signal degradation in repeated excitations for the continuous collection of fluorescence images.[30]

Li *et al.* performed a similar *ex vivo* imaging evaluation on carbon dots.[62] In the evaluation, the blue fluorescent carbon dots were detected in spleen, liver, small intestine, heart, lungs, kidneys, and also brain. The detection of carbon dots in brain was significant, suggesting that the dots might be able to cross the blood–brain barrier.

In a more recent study, Cao *et al.* made a direct comparison between carbon dots and commercially available CdSe–ZnS QDs for fluorescence imaging in mice.[78] These carbon dots were specifically prepared for relatively higher fluorescence quantum yields, about 60% at 440 nm excitation. *In vitro* under a confocal fluorescence microscope, the fluorescence brightness was similar between images of the carbon dots and the CdSe–ZnS QDs. In mice following the subcutaneous injections, the fluorescence images were also similar, as illustrated in Fig. 15, suggesting comparable performance of the carbon dots to that of the presently dominating semiconductor QDs for *in vivo* fluorescence imaging in the specific visible wavelength region.[78]

The evaluation of carbon dots *in vivo* has only had a good beginning, with much remaining to be explored. However, one conclusion from the still limited body of experimental evidence is that the optical performance of carbon dots is preserved under *in vivo* imaging conditions. Further investigations on application potentials such as the coupling of carbon dots with bioactive molecules for specific targeting *in vivo* and their uses in cancer diagnostics and angiography may be expected.

4 Summary and perspectives

Carbon dots have apparently emerged as a new class of fluorescent nanomaterials, already competitive in many respects to conventional semiconductor QDs. As fluorescence agents for optical bioimaging *in vitro* and *in vivo*, carbon dots are advantageous in terms of their ready aqueous solubility, physicochemical and photochemical stabilities, high optical performance and non-blinking, and more importantly excellent biocompatibility. A proliferation of more investigations on potential bio-applications of carbon dots in imaging and beyond may be expected. For the further development of carbon dots, the synthesis of carbon dots with bright fluorescence emissions emphasized in the red/near-IR spectral regions, thus more effective in tissue penetration, is desired. Also in need are more studies on the exploitation of the surface functionalization in carbon dots for controlled coupling with bioactive species to enable specific targeting in cellular and *in vivo* imaging and related biomedical applications. The recent effort on a more unified understanding of fluorescence emissions in carbon dots and other carbon nanomaterials, especially in modified graphene materials, is likely to continue, which should be highly beneficial to the overall development and mechanistic understanding of fluorescent carbon nanomaterials for their serving as more competitive alternatives to conventional semiconductor QDs.

Acknowledgements

Financial support from the U.S. National Science Foundation (CBET-0967423) is gratefully acknowledged. J.W. was on leave from College of Chemistry and Pharmaceutical Sciences at Qingdao Agricultural University in Qingdao, China (with a visiting scholarship provided by Shandong Provincial Education Association). G.E.L. was a research participant supported by South Carolina Space Grant Consortium, and L.C. by a *Susan G. Komen for the Cure* Postdoctoral Fellowship.

References

1 R. Rossetii and L. Brus, *J. Phys. Chem.*, 1982, **86**, 4470–4472.
2 A. I. Ekimov, A. L. Efros and A. A. Onushchenko, *Solid State Commun.*, 1985, **56**, 921–924.
3 A. Henglein, *Chem. Rev.*, 1989, **89**, 1861–1873.
4 M. G. Bawendi, M. L. Steigerwald and L. E. Brus, *Annu. Rev. Phys. Chem.*, 1990, **41**, 477–496.
5 L. E. Brus, *Appl. Phys. A: Solids Surf.*, 1991, **53**, 465–474.
6 H. Weller, *Adv. Mater.*, 1993, **5**, 88–95.
7 A. P. Alivisatos, *J. Phys. Chem.*, 1996, **100**, 13226–13239.
8 B. O. Dabbousi, J. Rodriguez-Viejo, F. V. Mikulec, J. R. Heine, H. Mattoussi, R. Ober, K. F. Jensen and M. G. Bawendi, *J. Phys. Chem. B*, 1997, **101**, 9463–9475.
9 C. B. Murray, D. J. Norris and M. G. Bawendi, *J. Am. Chem. Soc.*, 1993, **115**, 8706–8715.
10 M. A. Hines and P. Guyot-Sionnest, *J. Phys. Chem.*, 1996, **100**, 468–471.
11 X. Peng, M. C. Schlamp, A. V. Kadavanich and A. P. Alivisatos, *J. Am. Chem. Soc.*, 1997, **119**, 7019–7029.
12 D. Gerion, F. Pinaud, S. C. Williams, W. J. Parak, D. Zanchet, S. Weiss and A. P. Alivisatos, *J. Phys. Chem. B*, 2001, **105**, 8861–8871.
13 S. Kim, B. Fisher, H.-J. Eisler and M. Bawendi, *J. Am. Chem. Soc.*, 2003, **125**, 11466–11467.
14 M. Bruchez Jr, M. Moronne, P. Gin, S. Weiss and A. P. Alivisatos, *Science*, 1998, **281**, 2013–2016.
15 W. C. W. Chan and S. Nie, *Science*, 1998, **281**, 2016–2018.
16 A. P. Alivisatos, *Nat. Biotechnol.*, 2004, **22**, 47–52.
17 J. K. Jaiswal and S. M. Simon, *Trends Cell Biol.*, 2004, **14**, 497–504.
18 X. Michalet, F. F. Pinaud, L. A. Bentolila, J. M. Tsay, S. Doose, J. J. Li, G. Sundaresan, A. M. Wu, S. S. Gambhir and S. Weiss, *Science*, 2005, **307**, 538–544.
19 U. Resch-Genger, M. Grabolle and S. Cavliere-Jaricot, *Nat. Methods*, 2008, **5**, 763–775.
20 A. H. Poliandri, J. P. Cabilla, M. O. Velardez, C. C. Bodo and B. H. Duvilanski, *Toxicol. Appl. Pharmacol.*, 2003, **190**, 17–24.
21 J. Geys, A. Nemmar, E. Verbeken, E. Smolders, M. Ratoi, M. F. Hoylaerts, B. Nemery and P. H. M. Hoet, *Environ. Health Perspect.*, 2008, **116**, 1607–1613.
22 R. A. Hardman, *Environ. Health Perspect.*, 2006, **114**, 165–172.
23 S. Satarug and M. R. Moore, *Environ. Health Perspect.*, 2004, **112**, 1099–1103.
24 J. D. Holmes, K. J. Ziegler, R. C. Doty, L. E. Pell, K. P. Johnston and B. A. Korgel, *J. Am. Chem. Soc.*, 2001, **123**, 3743–3748.
25 Z. Kang, Y. Liu and S.-T. Lee, *Nanoscale*, 2011, **3**, 777–791.
26 S. Prabakar, A. Shiohara, S. Hanada, K. Fujioka, K. Yamamoto and R. D. Tilley, *Chem. Mater.*, 2010, **22**, 482–486.
27 T. N. Lambert, N. L. Andrews, H. Gerung, T. J. Boyle, J. M. Oliver, B. S. Wilson and S. M. Han, *Small*, 2007, **3**, 691–699.
28 Y.-P. Sun, B. Zhou, Y. Lin, W. Wang, K. A. S. Fernando, P. Pathak, M. J. Meziani, B. A. Harruff, X. Wang, H. Wang, P. G. Luo, H. Yang, M. E. Kose, B. Chen, L. M. Veca and S.-Y. Xie, *J. Am. Chem. Soc.*, 2006, **128**, 7756–7757.
29 L. Cao, X. Wang, M. J. Meziani, F. Lu, H. Wang, P. G. Luo, Y. Lin, B. A. Harruff, L. M. Veca, D. Murray, S.-Y. Xie and Y.-P. Sun, *J. Am. Chem. Soc.*, 2007, **129**, 11318–11319.
30 S.-T. Yang, L. Cao, P. G. Luo, F. Lu, X. Wang, H. Wang, M. J. Meziani, Y. Liu, G. Qi and Y.-P. Sun, *J. Am. Chem. Soc.*, 2009, **131**, 11308–11309.
31 J. E. Riggs, Z. Guo, D. L. Carroll and Y.-P. Sun, *J. Am. Chem. Soc.*, 2000, **122**, 5879–5880.
32 Y.-P. Sun, K. Fu, Y. Lin and W. Huang, *Acc. Chem. Res.*, 2002, **35**, 1096–1104.
33 Y. Lin, B. Zhou, R. B. Martin, K. B. Henbest, B. A. Harruff, J. E. Riggs, Z. X. Guo, L. F. Allard and Y.-P. Sun, *J. Phys. Chem. B*, 2005, **109**, 14779–14782.
34 D. M. Guldi, M. Holzinger, A. Hirsch, V. Georgakilas and V. Prato, *Chem. Commun.*, 2003, 1130–1131.
35 L. Lacerda, G. Pastorin, W. Wu, M. Prato, A. Bianco and K. Kostarelos, *Adv. Funct. Mater.*, 2006, **16**, 1839–1846.
36 B. Zhou, Y. Lin, D. E. Hill, W. Wang, L. M. Veca, L. Qu, P. Pathak, M. J. Meziani, J. Diaz, J. W. Connell, K. A. Watson, L. F. Allard and Y.-P. Sun, *Polymer*, 2006, **47**, 5323–5329.
37 S.-Y. Yang, X. Wang, H. Wang, F. Lu, P. G. Luo, L. Cao, M. J. Meziani, J.-H. Liu, Y. Liu, M. Chen, Y. Huang and Y.-P. Sun, *J. Phys. Chem. C*, 2009, **113**, 18110–18114.
38 H. Liu, T. Ye and C. Mao, *Angew. Chem., Int. Ed.*, 2007, **46**, 6473–6475.
39 J. Zhou, C. Booker, R. Li, X. Zhou, T.-K. Sham, X. Sun and Z. Ding, *J. Am. Chem. Soc.*, 2007, **129**, 744–745.
40 S. C. Ray, A. Saha, N. R. Jana and R. Sarkar, *J. Phys. Chem. C*, 2009, **113**, 18546–18551.
41 L. Cao, P. Anilkumar, X. Wang, J.-H. Liu, S. Sahu, M. J. Meziani, E. Myers and Y.-P. Sun, *Can. J. Chem.*, 2011, **89**, 104–109.
42 X. Li, H. Wang, Y. Shimizu, A. Pyatenko, K. Kawaguchi and N. Koshizaki, *Chem. Commun.*, 2011, **47**, 932–934.
43 R. Shen, K. Song, H. Liu, Y. Li and H. Liu, *ChemPhysChem*, 2012, **13**, 3549–3555.
44 H. Li, Z. Kang, Y. Liu and S.-T. Lee, *J. Mater. Chem.*, 2012, **22**, 24230–24253.
45 Y. Wang, P. Anilkumar, L. Cao, J.-H. Liu, P. G. Luo, K. N. Tackett II, S. Sahu, P. Wang, X. Wang and Y.-P. Sun, *Exp. Biol. Med.*, 2011, **236**, 1231–1238.
46 S.-L. Hu, K.-Y. Nie, J. Sun, J. Yang, N.-Q. Zhao and X.-W. Du, *J. Mater. Chem.*, 2009, **19**, 484–488.
47 A. B. Bourlinos, A. Stassinopoulos, D. Anglos, R. Zboril, M. Karakassides and E. P. Giannelis, *Small*, 2008, **4**, 455–458.

48 A. B. Bourlinos, A. Stassinopoulos, D. Anglos, R. Zboril, V. Georgakilas and E. P. Giannelis, *Chem. Mater.*, 2008, **20**, 4539–4541.

49 F. Wang, M. Kreiter, B. He, S. Pang and C.-Y. Liu, *Chem. Commun.*, 2010, **46**, 3309–3311.

50 P. Anilkumar, L. Cao, J.-J. Yu, K. N. Tackett II, P. Wang, M. J. Meziani and Y.-P. Sun, *Small*, 2013, **9**, 545–551.

51 L. Tian, D. Ghosh, W. Chen, S. Pradhan, X. J. Chang and S. W. Chen, *Chem. Mater.*, 2009, **21**, 2803–2809.

52 M. D. Palashuddin, A. Jaiswal, A. Paul, S. S. Ghosh and A. Chattopadhyay, *Sci. Rep.*, 2012, **2**, 383.

53 X. Wang, L. Cao, S.-T. Yang, F. S. Lu, M. J. Meziani, L. L. Tian, K. W. Sun, M. A. Bloodgood and Y.-P. Sun, *Angew. Chem., Int. Ed.*, 2010, **49**, 5310–5314.

54 Y.-P. Sun, X. Wang, F. Lu, L. Cao, M. J. Meziani, P. G. Luo, L. Gu and L. M. Veca, *J. Phys. Chem. C*, 2008, **112**, 18295–18298.

55 P. Anilkumar, X. Wang, L. Cao, S. Sahu, J. H. Liu, P. Wang, K. Korch, K. N. Tackett II, A. Parenzan and Y.-P. Sun, *Nanoscale*, 2011, **3**, 2023–2027.

56 M. Chalfie, Y. Tu, G. Euskirchen, W. W. Ward and D. C. Prasher, *Science*, 1994, **263**, 802–805.

57 X. Wang, L. Cao, F. S. Lu, M. J. Meziani, H. Li, G. Qi, B. Zhou, B. A. Harruff, F. Kermarrec and Y.-P. Sun, *Chem. Commun.*, 2009, 3774–3776.

58 J. Xu, S. Sahu, L. Cao, C. E. Bunker, G. Peng, Y. Liu, K. A. S. Fernando, P. Wang, E. A. Guliants, M. J. Meziani, H. Qian and Y.-P. Sun, *Langmuir*, 2012, **28**, 16141–16147.

59 J. A. Xu, S. Sahu, L. Cao, P. Anilkumar, K. N. Tackett II, H. J. Qian, C. E. Bunker, E. A. Guliants, A. Parenzan and Y.-P. Sun, *ChemPhysChem*, 2011, **12**, 3604–3608.

60 L. Cao, S. Sahu, P. Anilkumar, C. E. Bunker, J. A. Xu, K. A. S. Fernando, P. Wang, E. A. Guliants, K. N. Tackett II and Y.-P. Sun, *J. Am. Chem. Soc.*, 2011, **133**, 4754–4757.

61 L. Cao, M. J. Meziani, S. Sahu and Y.-P. Sun, *Acc. Chem. Res.*, 2013, **46**, 171–180.

62 N. Li, X. Liang, L. Wang, Z. Li, P. Li, Y. Zhu and J. Song, *J. Nanopart. Res.*, 2012, **14**, 1177.

63 F. Wang, Z. Xie, H. Zhang, C.-Y. Liu and Y.-G. Zhang, *Adv. Funct. Mater.*, 2011, **21**, 1027–1031.

64 R. Liu, D. Wu, S. Liu, K. Koynov, W. Knoll and Q. Li, *Angew. Chem., Int. Ed.*, 2009, **48**, 4598–4601.

65 Z. A. Qiao, Y. F. Wang, Y. Gao, H. W. Li, T. Y. Dai, Y. L. Liu and Q. S. Huo, *Chem. Commun.*, 2010, **46**, 8812–8814.

66 H. Tao, K. Yang, Z. Ma, J. Wan, Y. Zhang, Z. Kang and Z. Liu, *Small*, 2012, **8**, 281–290.

67 J.-H. Liu, P. Anilkumar, L. Cao, X. Wang, S.-T. Yang, P. G. Luo, H. Wang, F. Lu, M. J. Meziani, Y. F. Liu, K. Korch and Y.-P. Sun, *Nano LIFE*, 2010, **1**, 153–161.

68 Q.-L. Zhao, Z.-L. Zhang, B.-H. Huang and J. Peng, *Chem. Commun.*, 2008, 5116–5118.

69 C. J. Liu, P. Zhang, F. Tian, W. C. Li, F. Li and W. G. Liu, *J. Mater. Chem.*, 2011, **21**, 13163–13167.

70 S. Zhu, J. Zhang, C. Qiao, S. Tang, Y. F. Li, W. Yuan, B. Li, L. Tian, F. Liu, R. Hu, H. Gao, H. Wei, H. Zhang, H. Sun and B. Yang, *Chem. Commun.*, 2011, **47**, 6858–6860.

71 Y. H. Yang, J. H. Cui, M. T. Zheng, C. F. Hu, S. Z. Tan, Y. Xiao, Q. Yang and Y. L. Liu, *Chem. Commun.*, 2012, **48**, 380–382.

72 A. Jaiswal, S. S. Ghosh and A. Chattopadhyay, *Chem. Commun.*, 2012, **48**, 407–409.

73 S. Chandra, P. Das, S. Bag, D. Laha and P. Pramanik, *Nanoscale*, 2011, **3**, 1533–1540.

74 Q. Li, T. Y. Ohulchanskyy, R. Liu, K. Koynov, D.-Q. Wu, A. Best, R. Jumar, A. Bonoiu and P. N. Prasad, *J. Phys. Chem. C*, 2010, **114**, 12062–12068.

75 A. Zhu, Q. Qu, X. L. Shao, B. Kong and Y. Tian, *Angew. Chem., Int. Ed.*, 2012, **51**, 7185–7189.

76 C. Liu, P. Zhang, X. Zhai, F. Tian, W. Li, J. Yang, Y. Liu, H. Wang, W. Wang and W. Liu, *Biomaterials*, 2012, **33**, 3604–3613.

77 C.-W. Lai, Y.-H. Hsiao, Y.-K. Peng and P.-T. Chou, *J. Mater. Chem.*, 2012, **22**, 14403–14409.

78 L. Cao, S.-T. Yang, X. Wang, P. G. Luo, H.-H. Liu, S. Sahu, Y. Liu and Y.-P. Sun, *Theranostics*, 2012, **2**, 295–301.